Terms and Conditions of Use of Digitised Theses from Trinity College Library Dublin

Copyright statement

All material supplied by Trinity College Library is protected by copyright (under the Copyright and Related Rights Act, 2000 as amended) and other relevant Intellectual Property Rights. By accessing and using a Digitised Thesis from Trinity College Library you acknowledge that all Intellectual Property Rights in any Works supplied are the sole and exclusive property of the copyright and/or other IPR holder. Specific copyright holders may not be explicitly identified. Use of materials from other sources within a thesis should not be construed as a claim over them.

A non-exclusive, non-transferable licence is hereby granted to those using or reproducing, in whole or in part, the material for valid purposes, providing the copyright owners are acknowledged using the normal conventions. Where specific permission to use material is required, this is identified and such permission must be sought from the copyright holder or agency cited.

Liability statement

By using a Digitised Thesis, I accept that Trinity College Dublin bears no legal responsibility for the accuracy, legality or comprehensiveness of materials contained within the thesis, and that Trinity College Dublin accepts no liability for indirect, consequential, or incidental, damages or losses arising from use of the thesis for whatever reason. Information located in a thesis may be subject to specific use constraints, details of which may not be explicitly described. It is the responsibility of potential and actual users to be aware of such constraints and to abide by them. By making use of material from a digitised thesis, you accept these copyright and disclaimer provisions. Where it is brought to the attention of Trinity College Library that there may be a breach of copyright or other restraint, it is the policy to withdraw or take down access to a thesis while the issue is being resolved.

Access Agreement

By using a Digitised Thesis from Trinity College Library you are bound by the following Terms & Conditions. Please read them carefully.

I have read and I understand the following statement: All material supplied via a Digitised Thesis from Trinity College Library is protected by copyright and other intellectual property rights, and duplication or sale of all or part of any of a thesis is not permitted, except that material may be duplicated by you for your research use or for educational purposes in electronic or print form providing the copyright owners are acknowledged using the normal conventions. You must obtain permission for any other use. Electronic or print copies may not be offered, whether for sale or otherwise to anyone. This copy has been supplied on the understanding that it is copyright material and that no quotation from the thesis may be published without proper acknowledgement.

TRACER STUDY INVESTIGATION INTO REACTOR MIXING CHARACTERISATION

BY

ALI ELSAEH ENBAIA

DISSERTATION SUBMITTED TO THE UNIVERSITY OF DUBLIN IN PARTIAL FULFILMENT OF THE REQUIREMENTS FOR THE DEGREE OF *DOCTORATE* OF PHILOSOPHY

April 2005

Department of Civil, Structural and Environmental Engineering

Trinity College, Dublin

DECLARATION

I, the undersigned, declare that the data of this thesis has not been submitted as an exercise for a degree at this or any other University. I further declare that; except where reference is made in the text, it is entirely my own work. I agree the library may lend or copy this thesis upon request.

Ali Elsaeh Enbaia

Ali Elsaeh Enbaia

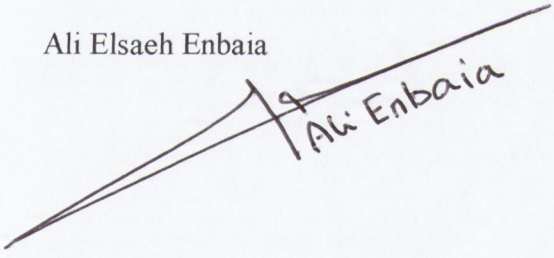

ABSTRACT

The hydraulic characterization of flow through a reactor is essential for a complete understanding of the process for which the reactor has been designed. The goal of hydraulic characterization of a continuous flow process is to track the behaviour of different portions of the fluid flow through the reactor. Most real systems have complicated hydraulic characteristics where reactors have poor inlet/outlet configurations, dead zones, internal circulations, and short circulating and/or bypassing of the fluid flow. The technique which is used to quantify the hydraulic characteristics of the fluid flow through the reactor can be divided into two main sequences.

1. An experimental tracer test, and
2. Interpretation of the data using a mathematical model.

A series of laboratory tests have been carried out using Rhodamine WT solution as a tracer in order to study the flow through various reactor configurations in the laboratory. A Self-Contained Underwater Fluorescence Apparatus (SCUFA) has been used to measure the tracer concentration at the effluent point of the total reactor configuration. The tracer is injected as a pulse or step input at the influent point and monitored at the effluent point using the SCUFA in order to get a plot the tracer concentration against time, that is referred to as a Residence Time Distribution (RTD) curve. A mathematical model is then fitted to such RTDs which enables the hydraulic characteristics of the various reactor combinations to be determined. Different hydraulic irregularities, such as short-circuits and dead zones, have been deliberately created in the experiments in order to test the validity of the technique.

The model used in this study is based on a tank in-series model using a Gamma function representation of a Continuously-Stirred Tank Reactor (CSTR). This model has been fitted to the data using the technique of minimising the sum of the differences squared on a Microsoft Excel© spreadsheet, achieved by utilising the "Solver" function built into the

spreadsheet. A series of experiments have initially been carried out on an ideal circular CSTR, followed by further experiments on a rectangular CSTR, to look at the effect of reactor geometry on mixing performance. A series of trials were then carried out on different configurations of rectangular reactors in series in the laboratory in order to characterize the efficiency of such networks and also the applicability of the modelling technique for full-scale implementation, in industrial applications. The technique has particularly been studied in relation to its ability to pick out a poorly performing reactor from a number of reactors in series.

Finally, tracer studies using Rhodamine WT were carried out on full-scale plants: a 4-tank in-series drilling fluid process with mixers in Libya and then two wastewater treatment works in Ireland; a 3 tanks in-series Activated Sludge aeration wastewater treatment process with diffused aeration; and a 2 tanks in-series extended aeration process with diffused aeration and mixers. All the trials demonstrated the ability of the mathematical model to diagnose the hydraulic characteristics of each tank in the process from the resultant RTD.

ACKNOWLEDGMENTS

In the course of researching and writing this thesis I received a lot of help in different ways from many people and I would like to take this opportunity to thank them.

Laurence Gill has provided invaluable guidance and expertise in his supervision of my research, and much of the credit for the originality of this thesis falls to him.

I would like to thank all the technical staff in the civil engineering department laboratories for their time and assistance, which they were always so willing to give. This allowed the laboratory work to run much smoother, and certainly it would not have been possible to accomplish so much without them.

I also wish to acknowledge the financial assistance of The People's Bureau of The Great Socialist People Libyan Arab Jamahiriya London who provided me with the funds to cover my research fees and living expenses.

All the staff of Alpha College of English, where I studied the English language, are due many thanks.

I would like to thank Will Beglane for the assistance he provided in the drafting of this thesis. Without his contribution this document would not have been so readily understandable.

I would like to express my sincere gratitude to my wife, *Samira*, my daughters *Weam*, *Enam*, *Bushra* and my son *Aimen* for their patience and support.

And last but not least, I wish to express my gratitude to my unselfish, ever-loving parents, who have done much more than their duty in supporting me in every possible way throughout my life.

DEDICATION

I dedicate this thesis to my wife *Samira*, my daughters *Weam*, *Enam*, *Bushra*, my son *Aimen* and to my *parents*.

SYMBOLS AND ABBREVIATIONS

RTD ..... Residence Time Distribution

PFR ..... Plug Flow Reactor

CSTR ..... Continuously-Stirred Tank Reactor

SCUFA ..... Self-Contained Underwater Fluorescence Apparatus

Q ..... Flow rate

V_R ..... Reactor volume

V_a ..... Active volume

V_m ..... Mixed volume

V_s ..... Short-circuit volume

V_d ..... Dead-zone volume

τ_{Gm} ..... Modelled retention time

τ ..... Theoretical retention time

θ ..... Normalized time

t ..... Time since the start of the tracer test

C (θ) ..... Concentration at time (θ)

n ..... Number of tanks in-series

C_0 ..... Initial concentration

C_{out} ..... Output concentration

D ..... Dispersion coefficient

$\sigma^2\theta$ ..... Variance of distribution function

G..... Mean Velocity Gradient

P..... Power requirement

μ..... Dynamic viscosity

T..... Differences in temperature

C_p..... Specific Heat

H..... Heat

ρ..... Mass density of fluid

Re..... Reynolds number (dimensionless)

P%..... Percentage of perfectly mixed flow (%)

D%..... Percentage of flow passing through dead-zones (%)

S%..... Percentage of flow short-circuiting (%)

TABLE OF CONTENTS

TABLE OF CONTENTS

Chapter 3
Model Development

Chapter 4
Preliminary Experiments (Model Development)

Chapter 5
Modifications (Dead-zones and Short-circuit Simulations)

Chapter 6
Reactor Network Laboratory Trials

Chapter 7
Reactor Diagnosis

Chapter 8
Full-scale Implementation

Chapter 9
Further Full-scale Implementation

Chapter 10
Conclusion

REFERENCES

Appendix A
SCUFA Calibration

Appendix B
Graphs for Pulse Input and Step Input Experiments

Appendix C
Graphs for Modifications (Dead-zones and Short-circuit Simulations)

Appendix D
Photograph Sequences of tracer

Appendix E
Graphs for Trials Experiments (Rectangular CSTR)

Appendix F
Codes of Computer programme

Appendix G
Graphs for Reactor Diagnosis Experiments (Rectangular CSTR)

Appendix H
Physical Properties of Water

Appendix I
Graphs for Full-scale Implementation Trials

Appendix J
Full Set of Experimental Data with the Spreadsheet Model

Appendix K
Full Set of Experimental Data with the Spreadsheet Model

Chapter 1

Introduction

Chapter 1

Introduction

1.1 Aims and Objectives of The Thesis

This thesis represents an attempt to advance our understanding in the use the Residence Time Distributions (RTD) in order to analyse a variety of reactor configurations primarily used for the treatment of water but also for other applications used in industries such as the chemical process and the oil industry. The research involves fitting such RTDs to a mathematical model in order to determine the hydraulic characteristics of the non-ideal reactor configurations under investigation. The RTD is determined experimentally by injecting an inert chemical called a tracer into a reactor at a given time, $t = 0$ and then by measuring the tracer concentration, C, in the effluent stream as a function of the time. Analysis of the RTD can then enable a determination of how long the various fluid elements have been in the reactor.

Tracers are compounds, usually dyes or salts, used for measuring, mapping, and monitoring water systems. Rhodamine WT is a fluorescent tracer that has been chosen in this study (see Section 2.3) because it can be easily and accurately measured on-site with a portable Fluorometer and it is also cost effective and safe to dispose of in the environment.

The aim of the thesis is to design and validate a mathematical model using both experimental laboratory and field data. The model is based upon the adjustment of three parameters used to describe a Gamma function, which is used to express a perfectly mixed CSTR. The model is built upon a Microsoft Excel© spreadsheet and fitted to the experimental data using a technique of minimisation of the summation of Differences Squared.

1.2 Reactor Types

A type of reactor used very commonly in industrial processes is the continuously-stirred tank reactor (CSTR) (see Figure 1.1a). In wastewater treatment a common example is the activated-sludge process where the aeration tank is normally configured as a series of CSTRs, which are usually operated so that their contents are totally mixed. However, in

many plants (as in other industrial processes) the degree of mixing is often non-ideal, and the assumption of a well-mixed tank is inadequate. Hence, in such cases, RTD modelling can be used in an attempt to understand the system.

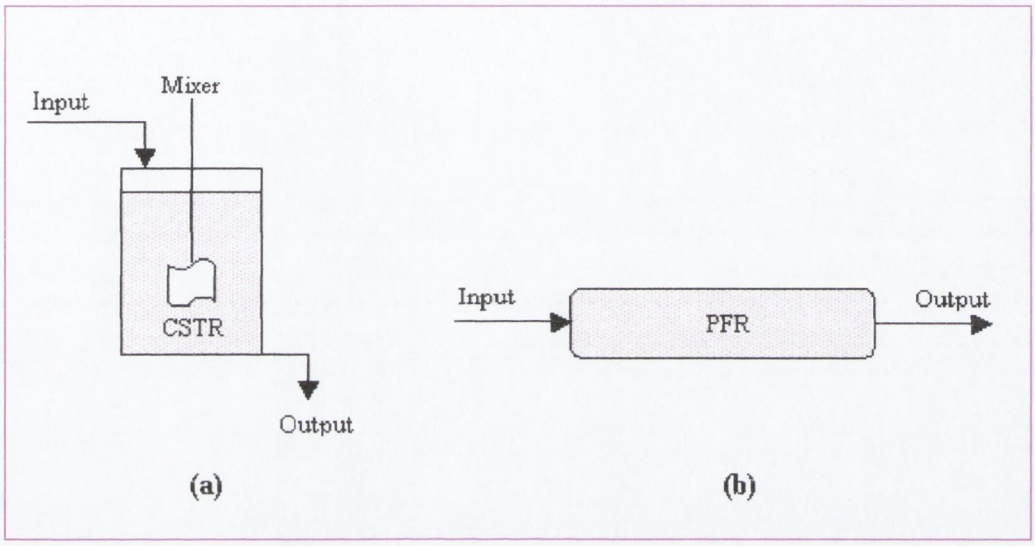

Figure1.1 (a) Continuously-stirred tank reactor (CSTR) and (b) Plug-flow reactor (PFR)

In addition to the CSTR, another type of reactor commonly used in industry is the plug-flow reactor (PFR) or tubular/piston reactor (see Figure 1.1b). In this type of the reactor, the flow could be anything from highly turbulent to laminar (plug flow with no radial variation in concentration) depending on the hydraulic conditions. In such situations the concentration varies continuously in the axial direction through the reactor.

In addition to these two principle types of reactor, other generic reactor types exist including Batch, Fluidised Bed and Packed Bed reactors, which are discussed in more detail in Section 2.4.

1.3 Contents Of The Thesis.

This Thesis is divided into ten chapters, a brief description of which is outlined here.

Chapter 2:

In this chapter the concept of Residence Time Distribution (RTD) and mean residence time are defined. The determination of RTD functions from tracer study data and the RTD

functions for ideal CSTRs is also determined. In addition, the following topics are described: reactor types; reactor configurations; mixing and type of mixers and mass balance analysis. A review of the literature is also presented, describing the recent approaches that have been taken to improve the understanding and interpretation of tracer studies including several examples of tracer studies used in industrial applications.

Chapter 3:

In this chapter, the tank in-series and one-parameter dispersion model is described, including an explanation of how to obtain the mean residence time and variance in order to calculate the number of tank in-series and the Peclet number (Pe). The concept of using combinations of ideal reactors to model a non-ideal reactor and the use of tracer data to determine such model parameters are also described.

Chapter 4:

In this chapter, the laboratory apparatus and equipment including the Self-Contained Underwater Fluorescence Apparatus (SCUFA) used in this study to evaluate the tracer concentration is described, including the experimental design.

Chapter 5:

This chapter describes the modifications which were required to the experimental apparatus in order to simulate hydraulic irregularities such as dead-zone areas and short circuits.

Chapter 6:

In this chapter, the results from a series of trials on a tanks in-series model are presented to indicate the validity of the mathematical model with respect to the hydraulics of the reactor network. A variety of reactor configurations are also analysed.

Chapter 7:

In this chapter further experimental trials in the laboratory are presented which concentrate on the identification of hydraulic irregularities introduced into a single reactor in the network.

Chapter 8:

This chapter describes a full-scale trial of the modelling technique on a 3 tanks in-series activated-sludge plant in Ireland. In addition a comparison of the full-scale parameters with a scale model in the laboratory is presented.

Chapter 9:

The results from two other full-scale trials are described: one on an oil drilling mud mixing reactor in Libya, the other at an extended aeration wastewater treatment plant in Ireland.

Chapter 10:

The conclusions from the research and recommendations for future work are outlined.

Chapter 2

Literature Review

Chapter-2

Literature Review

2.1 Introduction.

Residence Time Distributions (RTD) of reactors, involving the introduction of a tracer into a reactor as a pulse or as a step input, have been studied in many previous projects and are reviewed in this chapter. The shape of the characteristic curve of the tracer concentration in the reactor outlet versus time, indicating the mixing characteristics in the reactor, is featured in several standard textbooks of chemical engineering [Fogler, 1992; Levenspiel, 1999].

The idea of using the distribution of residence times in the analysis of chemical reactor performance was apparently first proposed by MacMullin and Weber (1935). The residence time of a substance represents the mean amount of time that a molecule or particle of the substance would stay or "reside" in a system. It is defined for a steady state, constant-volume system as,

$$\tau = \frac{V}{Q} \qquad \text{----------(2.1)}$$

Where: τ = the residence time of the substance

V = reactor Volume.

Q = volumetric flow rate.

When carrying out a test, the tracer is injected at the inlet of the reactor into the fluid flow according to some definite time sequence. The concentration of tracer is then monitored against time at the outlet. This data is converted to a RTD that indicates how much time each fraction of the tracer has spent in the reactor. An RTD, however, does not represent the mixing behavior in the reactor uniquely. For example, several different physical arrangements within the reactor may give the same tracer response, involving series of reactor elements such as plug-flow or complete mixing.

With regard to the concept of reactor flushing rate, the above relationship (Eq. 2.1) is useful for understanding the general idea of residence time. Thus, depending on the

reactor's volume and its flow rate, a reactor can either be classified as a slow flusher (the volume is large and the flow is small) or a fast flusher (the volume is small and the flow is large). More importantly, from the point of view of this thesis, the RTD of a reactor also contains information from which the mixing characteristics of such a reactor can be determined.

Finally, it should be noted that an alternative, and increasingly common technique for determining the hydraulic characteristics of reactors is the use of Computational Fluid Dynamics (CFD), the description of which is outside the scope of this thesis.

2.2 Residence Time Distributions (RTD)

2.2.1 Measurement of RTD

The RTD is determined experimentally by injecting an inert chemical, called a tracer (see Section 2.3), into the reactor at some time, t=0 and then measuring the tracer concentration, C, in the effluent stream as a function of time. The input time sequence for the tracer can be carried out in many ways with the two most common methods, pulse input and step input, shown in Figure 2.1.

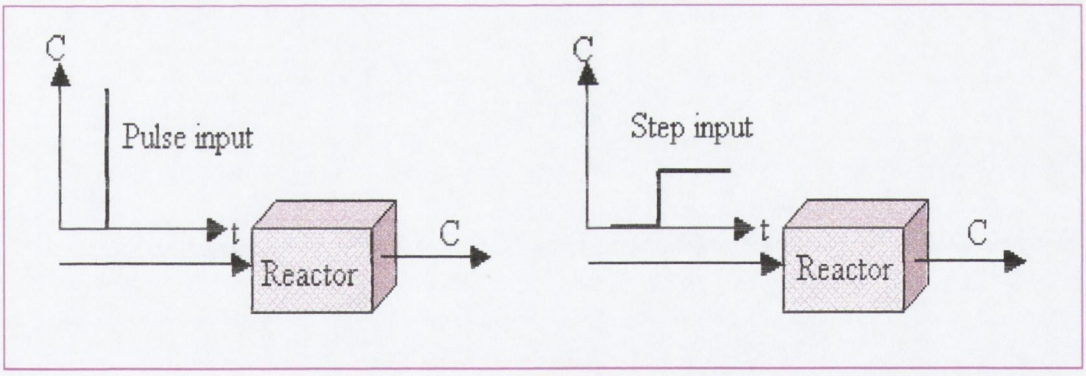

Figure 2. 1 Schematic diagram indicating the pulse and step input methods of tracer study.

2.2.1.1 Pulse Input Experiment

In the pulse input method, a known mass of tracer, M_{in} is suddenly injected in one shot into the feed stream entering the reactor in as short a time as possible (theoretically instantaneously). The outlet concentration is then measured as a function of time.

Typical concentration-time curves at the inlet and outlet of an arbitrary reactor are illustrated in Figure 2.2.

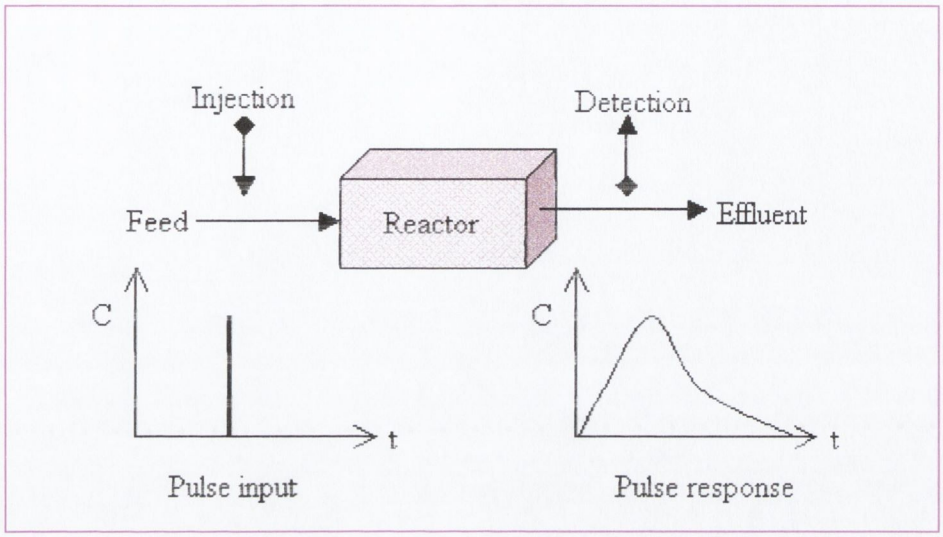

Figure 2. 2 RTD measurement for pulse input

The injection of a tracer pulse for a single-input and single-output has been mathematically analyzed [Levenspiel, 1999]. First, an increment of time Δt has been chosen sufficiently small so that the concentration of tracer, C(t), exiting between time t and t+Δt is essentially constant. Hence, the mass of tracer material, ΔM, leaving the reactor between time t and t+Δt is,

$$\Delta M = C(t)Q\Delta t \qquad \text{---------(2.2)}$$

Where:

Q = flow through the reactor

Dividing by the total amount of tracer that was injected into the reactor, M_{in}, gives,

$$\frac{\Delta M}{M_{in}} = \frac{QC(t)}{M_{in}}\Delta t \qquad \text{----------(2.3)}$$

Which represents the fraction of tracer that has a residence time in the reactor between time t and $t + \Delta t$.

For a pulse injection, $$E(t) = \frac{QC(t)}{M_{in}} \qquad \text{---------(2.4)}$$

So that, $$\frac{\Delta M}{M_{in}} = E(t)\Delta t \qquad \text{--------(2.5)}$$

The quantity E(t) is called the RTD function. This is the function which describes, in a quantitative manner, how much time different fluid elements have spent in the reactor. If M_{in} is not known directly, it can be obtained from the outlet concentration measurements by summing up all the amounts of tracer ΔM between time zero and infinity (see Eq. 2.6)

$$M_{in} = \int_0^\infty QC(t)dt \qquad \text{----------(2.6)}$$

This of course assumes that all tracer added to the reactor eventually leaves the reactor in the same form and that, for example none is lost due to settlement or reactions.

The volumetric flow rate Q is usually constant and so the E (t) can been defined as,

$$E(t) = \frac{C(t)}{\int_0^\infty C(t)dt} \qquad \text{----------(2.7)}$$

The integral in the denominator is the area under the RTD curve, which can be found using a numerical integration formula such as the Trapezoidal rule [Fogler, 1992; Bolton, 1995]. Theoretically, the fraction of all the tracer that has resided for the time in the reactor between t =0 and $t = \infty$ should be equal to unity which means it is equal to the total mass injected at the beginning, M_{in} and therefore,

$$\int_0^\infty E(t)dt = 1 = M_{in} \qquad \text{----------(2.8)}$$

2.2.1.2 Step Input Experiment

A more general relationship can formulated [Fogler, 1992] between a time varying tracer injection and the corresponding concentration in the effluent. The output concentration from a reactor in relation to the input concentration is given as,

$$C_{out}(t) = \int_0^t C_0(t)E(t)dt \qquad \text{----------(2.9)}$$

Taking a constant flow rate of tracer added to the feed, initiated at time t=0, then,

$C_0(t) = 0$ t<0 No tracer

$C_0(t) = \text{Constant}$ t≥ 0 M_{in} (µg/l) of tracer

The concentration of tracer in the feed to the reactor is kept at this level until the concentration in the effluent is indistinguishable from that in the feed. A typical outlet concentration curve for this type of input is illustrated in Figure 2.3.

This expression gives,

$$\left[\frac{C_{out}}{C_0}\right]_{step} = \int_0^t E(t)dt = F(t) \qquad \text{----------(2.10)}$$

Which can then be differentiated to obtain the RTD function E(t),

$$E(t) = \frac{d}{dt}\left[\frac{C(t)}{C_0}\right]_{step} \qquad \text{----------(2.11)}$$

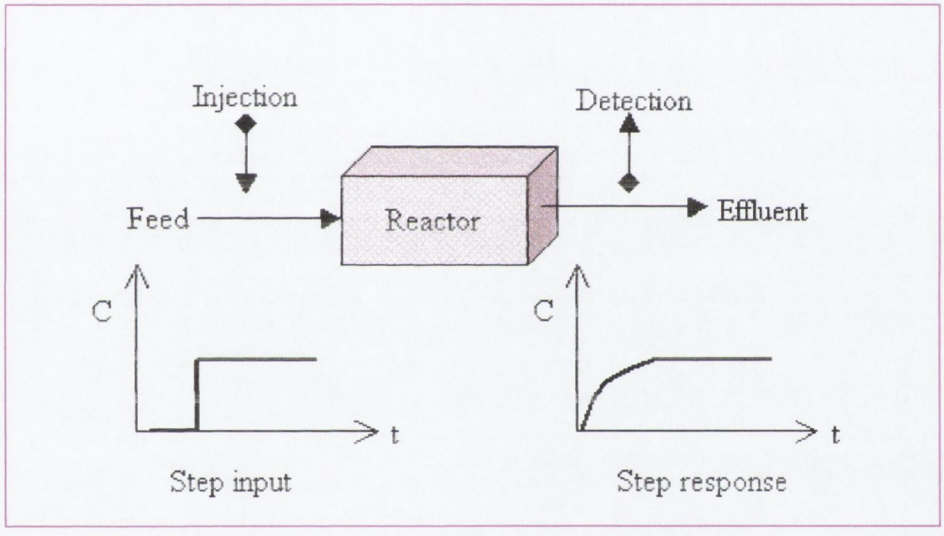

Figure 2. 3 RTD measurement for step input

2.2.1.3 The F-diagram Curve

A useful concept when considering the analysis of tracer experiments in a mixing tank is F-Diagrams or Age-distribution Functions. The output F curve from a series of **n** ideal stirred tanks, in its various forms, is given by Eq 2.14 and its associated graphical form (Figure 2.4) shows that as the number of tank-in-series increase, the system will tend towards behaving as a plug flow system [Danckwerts, 1959; Buffham and Kropholler, 1970,73].

$$F = 1 - e^{-n\theta}\left[1 + n\theta + \frac{(n\theta)^2}{2!} + \ldots + \frac{(n\theta)^{n-1}}{(n-1)!} + \ldots\right] \qquad \text{------(2.14)}$$

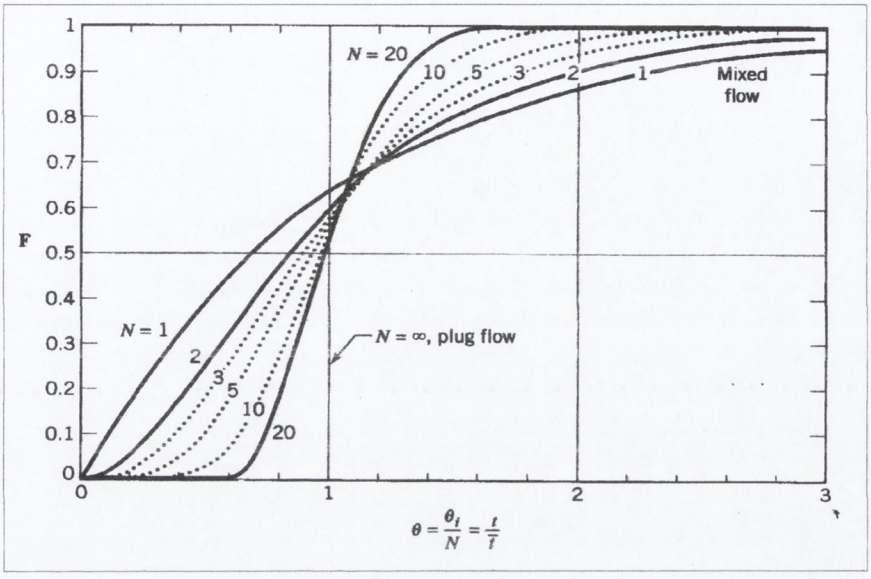

Figure 2. 4 The F-curve for the tank in series model [after Danckwerts, (1959)]

The F(t) has been defined as a cumulative distribution function and can be calculated at various times from the area under the curve of an E(t) versus time plot. In effect, F(t) represents the amount of tracer that has been in the reactor for less than any particular time and hence can be used to indicate the percentage of tracer leaving the reactor at any given time.

2.2.2 Characteristics of the RTD

It is evident that elements of fluid taking different routes through the reactor may take different lengths of time to pass through the reactor. As discussed previously the distribution of these times for the stream of fluid leaving the reactor is called the exit age distribution E(t), or the Residence Time Distribution of the fluid. It is convenient to represent the RTD in such a way that the area under the curve is unity, and therefore equal to the total mass injected at the beginning, M_{in} (see Eq 2.8) by normalizing the distribution (see Figure 2.5). One restriction on the E curve is the assumption that the fluid only enters and leaves the reactor one time, meaning that there should be no flow diffusion or up-flow eddies at the entrance or at the reactor exit. This is called the

"Closed Vessel Boundary Condition" [Levenspiel, 1999]. Conversely, where elements of fluid can cross the reactor boundary more than one time, it is called the "Open Vessel Boundary Condition".

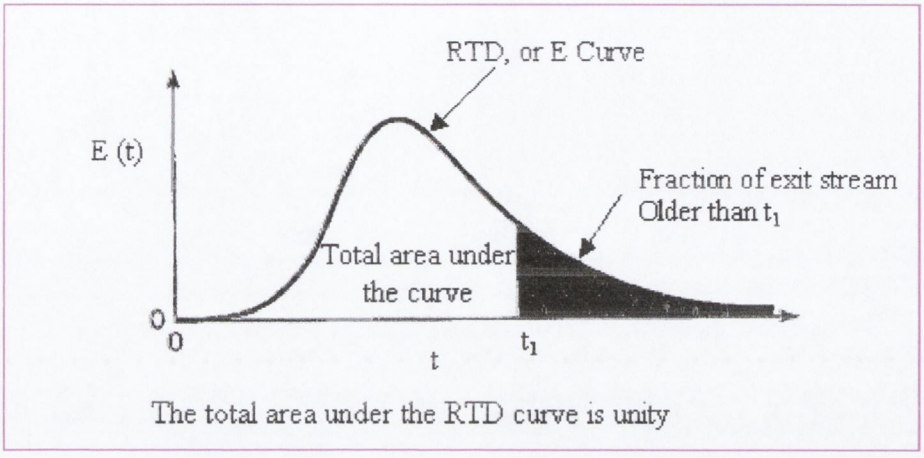

Figure 2. 5 The exit age distribution curve E for fluid flowing through a vessel, RTD [after Levenspiel, (1999)]

2.2.2.1 Boundary Conditions

A "closed" system can be described as a system in which there is a clear change in flow regimes at both the injection point and the output detection point. For example, a CSTR reactor with narrow bore inlet and outlet pipes may be described as a closed system, as illustrated in Figure 2.6. An open system has undisturbed flow regimes as it passes the injection and detection point, an example being unrestricted pipe the flow in the pipe as illustrated in Figure 2.6.

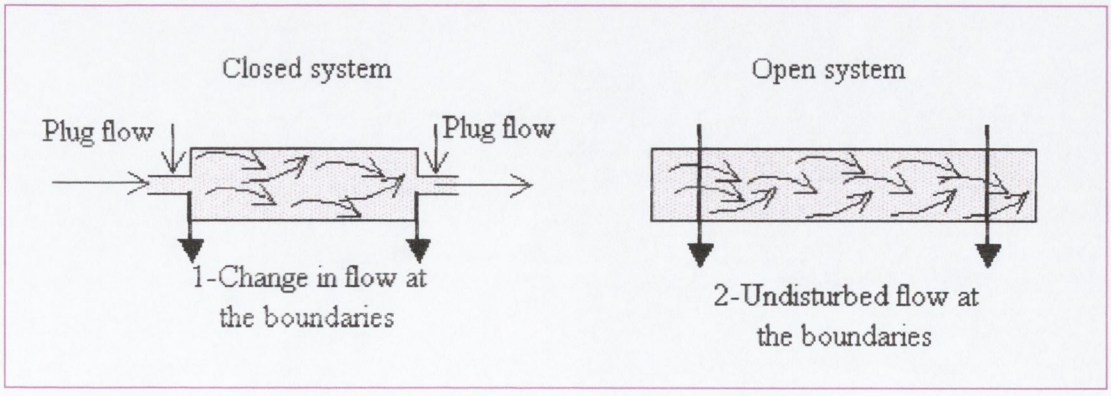

Figure 2. 6 System boundary conditions [after Levenspiel, (1999)]

The boundary condition of the reactor is an important factor to be considered in any tracer study. Indeed, the boundary condition can have a direct affect on the shape of the F curve which can be clearly seen by comparing the following graphs in Figure 2.7(a) & (b). The shape of the curves depends on the Peclet number (D/ul) (see Section2.6.1) and the boundary conditions. When the boundary conditions are closed such as in a CSTR, the tracer is dispersed inside the reactor as a function of the mixer speed and hence, the Peclet numbers are relatively large as shown in Figure 2.7(b). However, when the system has open boundary conditions such as in a plug-flow systems, the tracer dispersed is not high and the peclet numbers are much smaller, as shown in Figure 2.7(a).

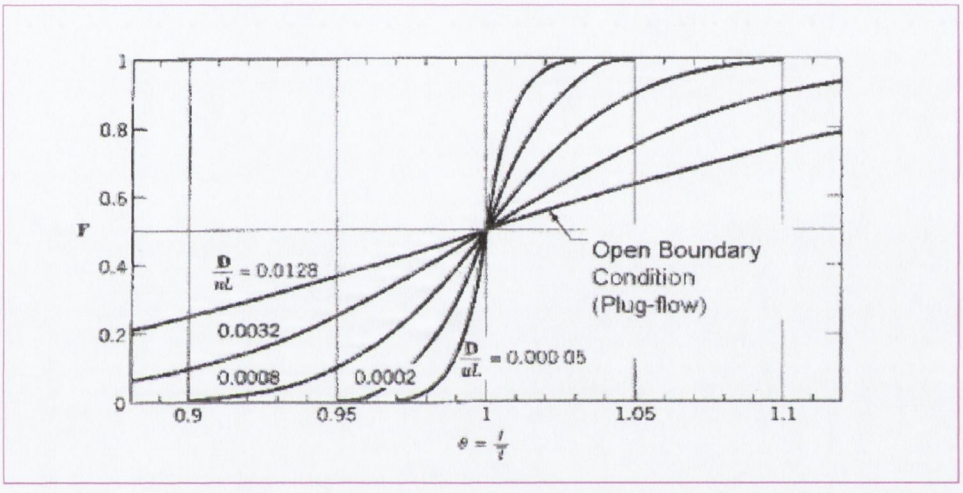

(a) Open boundary condition

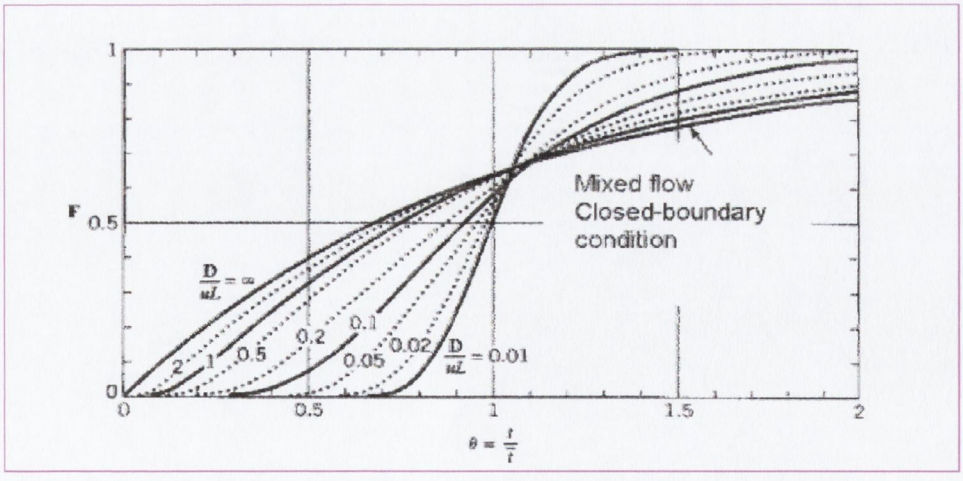

(b) Closed boundary condition

Figure 2. 7 Step response curve for comparison between open and closed boundary condition

2.2.3 Mean Residence Time

The mean residence time (see Eq. 2.1) represents the reactor's flushing rate and is used in this research to further the understanding of the behaviour of the hydraulic system from which the RTD curve has been generated. The mean residence for the E(t) curve is given by Eq.2.15 and illustrated in Figure 2.8.

$$\tau_m = \frac{\int_0^\infty tC(t)dt}{\int_0^\infty C(t)dt} = \int_0^\infty tE(t)dt \qquad \text{----------(2.15)}$$

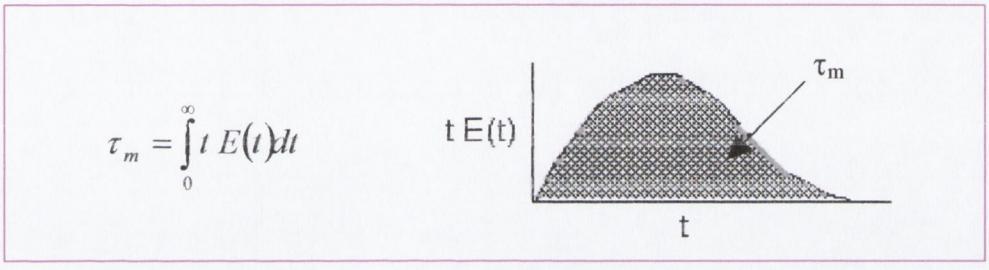

Figure 2. 8 Diagram showing the mean residence time

2.2.4 Normalized RTD function

A normalized RTD is often used instead of the function E(t) where parameter (θ) is defined as,

$$\theta = \frac{t}{\tau} \qquad \text{----------(2.16)}$$

A dimensionless function E(θ) can be defined as,

$$E(\theta) = \tau E(t)$$

The quantity θ essentially represents the number of reactor volumes of fluid, based on the entrance conditions, which have flowed through the reactor in time t. The purpose of creating this normalized distribution function is that it allows the flow performance inside reactors of different sizes to be compared directly. If the normalized function E(θ) is used, all perfectly mixed CSTRs numerically have the same RTD. If the simple

function E(t) is used, the numerical value of E(t) can differ substantially for different CSTRs. For a single perfectly mixed CSTR,

$$E(t) = \frac{1}{\tau} e^{-t/\tau} \qquad \text{----------(2.17)}$$

and therefore,

$$E(\theta) = \tau E(t) = e^{-\theta} \qquad \text{----------(2.18)}$$

2.2.5 RTD of a single CSTR

In an ideal CSTR, the concentration of any substance in the effluent stream is identical to the concentration throughout the reactor. Consequently, it is possible to obtain the RTD from conceptual considerations based on a mass balance of an inert tracer that has been injected as a pulse at time t=0 into a CSTR as follows:

$$Input - Output = Accumulation$$

$$0 - QC = +V\frac{dC}{dt} \qquad \text{---------(2.19)}$$

Assuming that the reactor is perfectly mixed, C in this equation is the concentration of the tracer in the effluent and also within the reactor where,

$$C(t) = C_0 e^{-\frac{t}{\tau}} \qquad \text{----------(2.20)}$$

This relationship gives the concentration of tracer in the effluent at any given t, (illustrated in Figure 2.9), as denoted by the normalized RTD function E(θ), described previously.

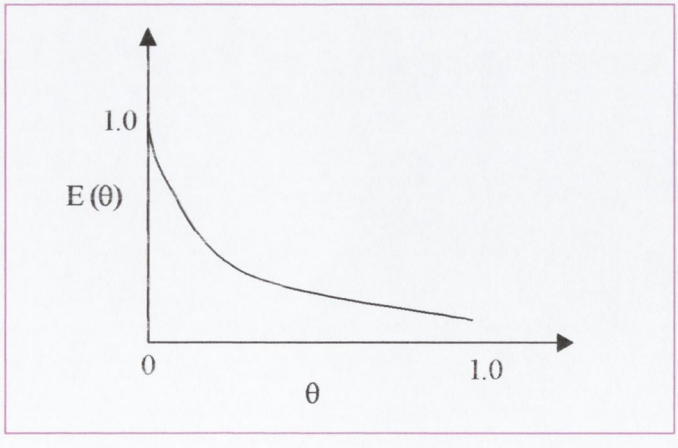

Figure 2. 9 CSTR responses to pulse tracer input [after Fogler, (1992)]

2.2.6 RTD of PFR and CSTR in series

In some stirred tank reactors, there can be a highly agitated zone in the vicinity of the impeller [Fogler, 1992] that can be modeled as a perfectly mixed CSTR. However, depending on the location of the inlet and outlet pipes, the reacting mixture may follow a somewhat tortuous path before entering or leaving the perfectly mixed zone which may be modeled as a plug-flow reactor. Thus, this type of tank reactor may be modeled as a CSTR with a PFR either preceding or following the CSTR in series. Considering first the situation where the CSTR is followed by the PFR (as shown in the Figure 2.10) the residence time in the CSTR is denoted by τ_{CSTR} and the residence time in the PFR by τ_{PFR}. If a pulse of tracer is injected into the entrance of the CSTR, the CSTR output concentration as a function of time C(t) is defined according to,

$$C(t) = C_0 e^{-t/\tau_{CSTR}} \qquad \text{----------(2.21)}$$

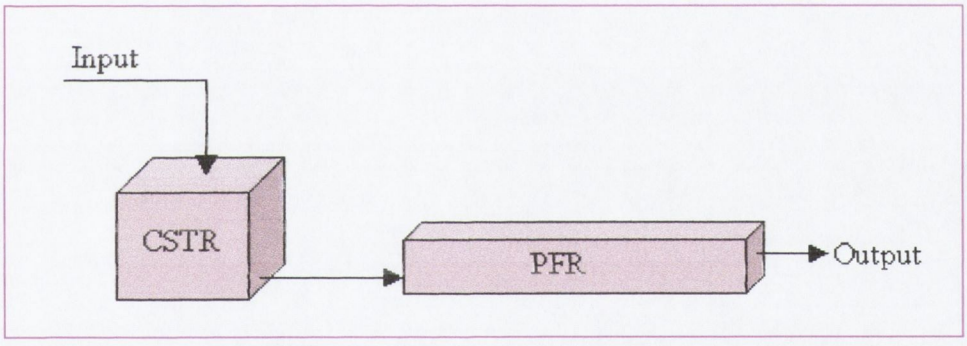

Figure 2. 10 Reactor modeled as a CSTR followed by PFR

However, this output will be delayed from exiting the overall reactor by τ_{PFR} at the output of the plug-flow section of the reactor system. Thus the RTD of the reactor system is,

$$E(t) = \begin{cases} 0 & t < \tau_{PFR} \\ \dfrac{e^{-(t-\tau_{PFR})/\tau_{CSTR}}}{\tau_{CSTR}} & t \geq \tau_{PFR} \end{cases} \qquad \text{----------(2.22)}$$

This response of Eq 2.22 is illustrated in Figure 2.11 below

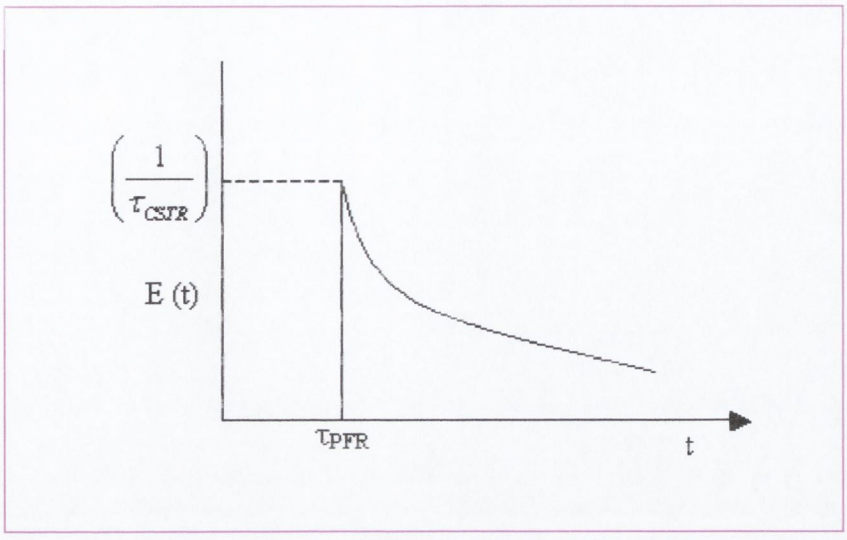

Figure 2. 11 The responses to pulse tracer input of CSTR followed by PFR [After Fogler, (1992)]

Alternatively, if the reactor system is represented by a CSTR is preceded by the PFR (as shown in Figure 2.12), then the input of the same pulse will appear at the entrance of the perfectly mixed section τ_{PFR} seconds later, meaning that the RTD of the reactor system can again be defined using the same equation (Eq 2.22) and the E(t) tracer represented by Figure 2.11.

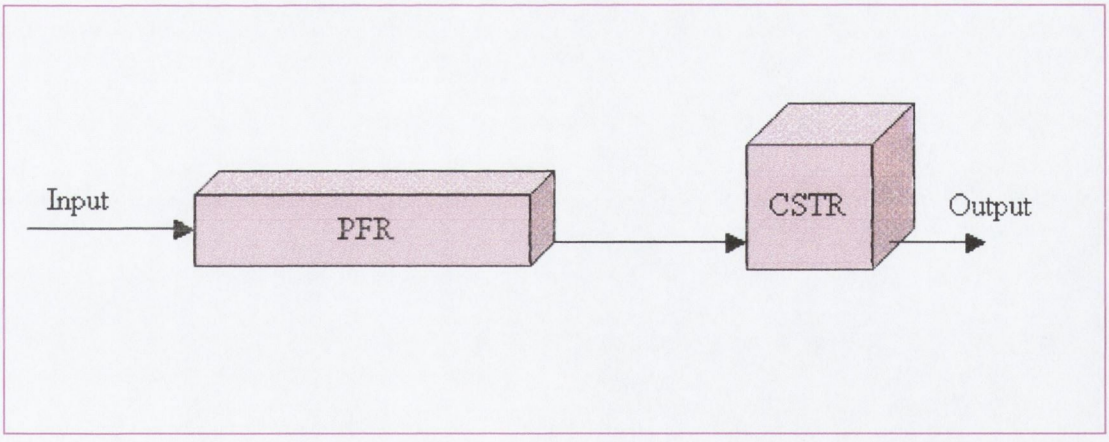

Figure 2. 12 Real reactor modeled as a CSTR is preceded by PFR

The analysis of RTDs from different reactors is considered in much more details in Section 2.6.

2.3 Tracers

Tracers are stable, nonreactive substances which are readily soluble. The most useful tracers are those which can be used in small concentrations and that can easily be detected by analysis [Perry, 1984]. The various substances chosen as tracers are selected for their properties which provide ease of detection at low concentrations. The ideal properties of the tracer are: soluble in water, not absorbed by suspended solid sediments or sample containers, stable in dilute solution in natural waters under the influence of light and temperature, not chemically reactive with any of the surfaces, and not harmful to human health. The three main generic types of tracer currently in use are chemical, fluorescent and radioactive tracers.

2.3.1 Chemical Tracers

The commonly used tracers are sodium chloride, in the form of common salt, sodium dichromate, lithium chloride, sodium nitrate, manganese sulphate and bromide. The cheapest and most convenient tracer to use in many countries is fine-grained table salt (NaCl) that dissolves quickly. Common salt has a solubility of 3.6 Kg to 10 liters at 15^0C but under field conditions not more than 2.5Kg is generally used in 10 liters of water [Clark, and William, 1977]. Such tracers are often measured by continuous conductivity measurements since there is a fixed relationship between salt concentration and electrical conductivity, (for example for sodium chloride whereby (mS/cm)*0.64 = mg/l NaCl).

2.3.2 Fluorescent Tracers

Fluorescent dyes, particularly the green dye Fluorescein, are used both as visual indicators of mixing and as a tracer for time of travel, retention or dispersion studies. Fluorescein was the first fluorescent dye used for water tracing work, and is still used for qualitative (visual) studies, for example the underground contamination of wells. It has a brilliant green fluorescence, and is therefore easy to visualize during the progress of an experiment. However, recently, Fluorescein has been replaced by other dyes, principally Rhodamine WT, due to the following drawbacks:

- It is rapidly destroyed by sunlight over a long term.
- Many naturally occurring fluorescent materials have similar characteristics and thus interfere with measurement.

- Fluorescein is more pH-sensitive than Rhodamine dyes

Rhodamine WT is the tracer that has been used in this study and is discussed in much greater detail in Section 4.2.

2.3.3 Radioactive Tracers

Radioactive tracers have considerable advantages when high discharges are required to be measured. The injection solution may range in concentration up to tens of curies per litre and most isotopes are accurately detectable down to tens of picocuries per litre, so that significant dilutions are possible as well as flexibility with regard to injection techniques. The commonly used radioactive tracers are bromine-82, which may be obtained as irradiated potassium bromide tablets, and tritium in the form of triturated water (HTO) [Clark and William, 1977].

2.3.4 Tracer Applications

Tracer techniques have been widely used in different studies. Several studies have used NaCl as a tracer to characterise the hydraulics of reactor systems [Cholette and Cloutier 1959; Bello-Mendoza and Sharratt, 1999] as well as lithium chloride [Clark and William, 1977] and bromide [Geary, 2004]. In surface waters they have commonly been used for dye dilution gauging [Cobb and Bailey, 1965], in particular for calibration of instrumentation for flow measurement [Kilpatrick, 1968] and especially where current metering is difficult, for instance, in steep rocky channels [Church and Kellerhals, 1970]. Tracers have also been used for time of travel studies [Buchanan, 1964] and for dispersion experiments in rivers [Yotsukura *et al.*, 1970] and in marine/estuarine environments [Pritchard and Carpenter, 1960]. Another application has been the tracing of karst groundwater carried out by using fluorescent tracer [Drew, 1968; Brown *et al.*, 1969], or in other aquifers associated with oilfields [Sturm and Johnson, 1950]. Tracers have also been employed for point dilution studies in wells [Lewis *et al.*, 1966] and for tracing soil water [Reynolds, 1966] while [Robinson and Donaldson 1967] have studied water uptake in plants, using fluorescent tracers. Of the commonly used fluorescent tracers, Fluorescein (Colour Index (CI) 45350 [Society of Dyers and Colourists, 1971] has been used since the end of the nineteenth century [Dole, 1906]. It is visibly detectable in low concentrations but has very poor stability under sunlight. Thus in the early 1960s, when workers in the United States and Japan

were assessing fluorescent tracers for quantitative tracing work in surface waters, they adopted the equally fluorescent tracer Rhodamine B (CI 45170) [Pritchard and Carpenter, 1960]). However, it became apparent that Rhodamine B was readily adsorbed onto sediments, and subsequently, Sulpho Rhodamine B (CI 45100) was introduced. Although this tracer was resistant to adsorption, it was comparatively expensive and was later replaced by the cheaper tracer Rhodamine WT, which was developed specifically for tracing work. Reynolds, [1966] used the green tracer pyranine (CI 59040) for tracing percolation water because it was very resistant to adsorption. A group of blue fluorescent tracers, known as optical brighteners because of their use in whitening paper and textiles, etc, have also been applied to water tracing [Glover, 1972; Buffam, and Gibilarol, 1968 and Teefy, 1996]. The use of tracer studies in the water industry has been fairly widespread involving a variety of fluorescent tracers on digesters [Bello-Mendoza and Sharratt, 1999], waste stabilistion ponds [Pedahzur *et al.*, 1993; Marais, 1974], chlorine contact tanks [Falconer and Tebbutt, 1986; Falconer and Liu, 1987; Louie and Fohrman, 1968; Marske and Boyle, 1973; Trussell and Chao, 1977 and Hart, 1979], flocculation tanks [Ives and Hoyer, 1998], constructed wetlands [King *et al.*, 1997; Bowmer, 1987; Breen, and Chick, 1995; Kadlec, 1993; Kadlec, 1994 and Kadlec and Knight, 1996] vortex separators [Higgins *et al.*, 1999] and infiltration measurements in foul water sewers [Smith and Kepple, 1972].

2.4 Consideration of Reactor Types

The principal types of reactors used for both water and wastewater treatment are the batch reactor, the plug-flow reactor (PFR), the complete-mix reactor, also known as a continuously-stirred tank reactor (CSTR), the arbitrary-flow reactor, the packed- bed reactor; and the fluidized-bed reactor. Reactors can be classified according to their hydraulic characteristics, descriptions of which are represented below.

- *The Batch Reactor*

The liquid contents are mixed completely in this type of reactor as illustrated in Figure 2.13, but there is no input or output. Hence, there is a change in concentration of the reactant with time. An example of this is the Sequencing Batch Reactor used for secondary wastewater treatment.

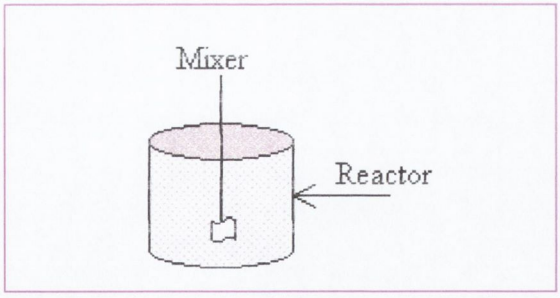

Figure 2. 13 The batch reactor

- *The Plug-Flow Reactor*

Fluid particles pass through the tank and are discharged in the same sequence in which they enter. The particles retain their identity and remain in the tank for a time equal to the theoretical retention time. This type of flow is approximated in long tanks with a high length-to-width ratio in which longitudinal dispersion is minimal or absent (see Figure 2.14). An example of this type of reactor is a chlorine contact tank in a water treatment plant.

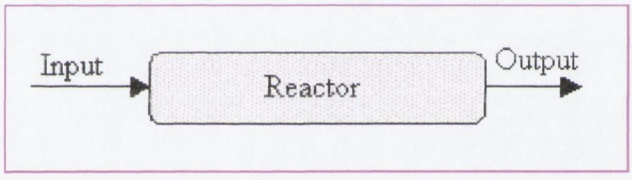

Figure 2. 14 The plug flow reactor

- *Continuously-Stirred Tank Reactor (CSTR)*

Complete mixing occurs when the particles entering the tank are dispersed immediately throughout the tank. Hence, the particles leave the tank in proportion to their statistical population. Complete mixing can be accomplished in any shaped tanks as long as the contents of the tank are uniformly and continuously redistributed (see Figure 2.15).

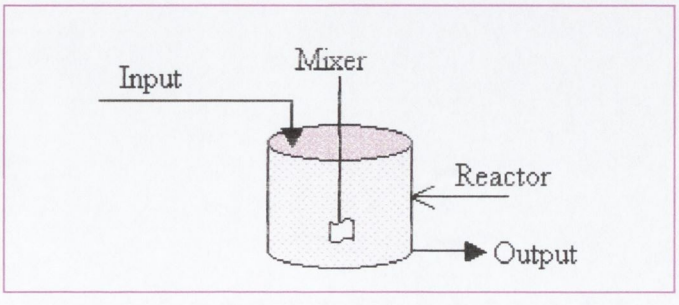

Figure 2. 15 The CSTR

- *Arbitrary-Flow Reactor*

Arbitrary flow is any degree of partial mixing between plug-flow and complete-mixing, as shown in Figure 2.16.

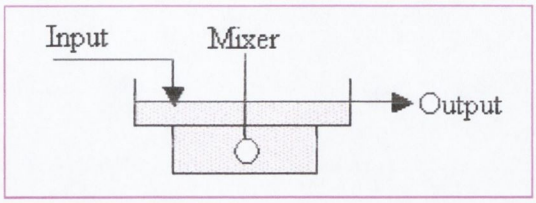

Figure 2. 16 Arbitrary-flow

- *Packed-Bed Reactor.*

Packed-bed reactors (see Figure 2.17) are filled with some type of packing material, such as rock, slag, ceramic, or plastic. With respect to flow, it can be operated in either a down flow or an up flow mode as shown in Figure 2.17 (a) & (b) respectively. An example of this reactor is the Biological Aerated Flooded Filters (BAFF) secondary treatment unit, high rate wastewater treatment process.

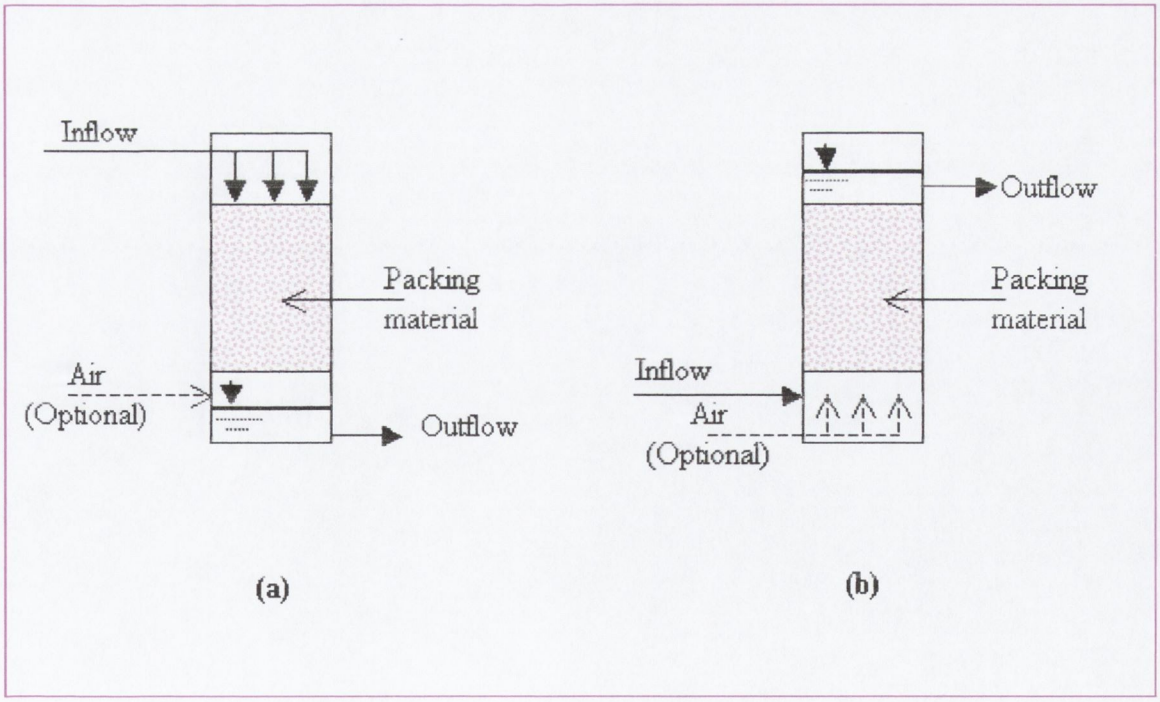

Figure 2. 17 Packed-bed reactor

- *Fluidized-Bed Reactor*

The Fluidized-bed reactor is similar to the packed-bed reactor in many respects, but the packing material is expanded by the upward movement of fluid (air or water) through the bed (see Figure 2.18). Controlling the flow rate of the fluid can vary the expanded porosity of the fluidized-bed packing material. An example, of fluidized-bed reactors in the water industry are again BAFF processes and also reactors used for air stripping.

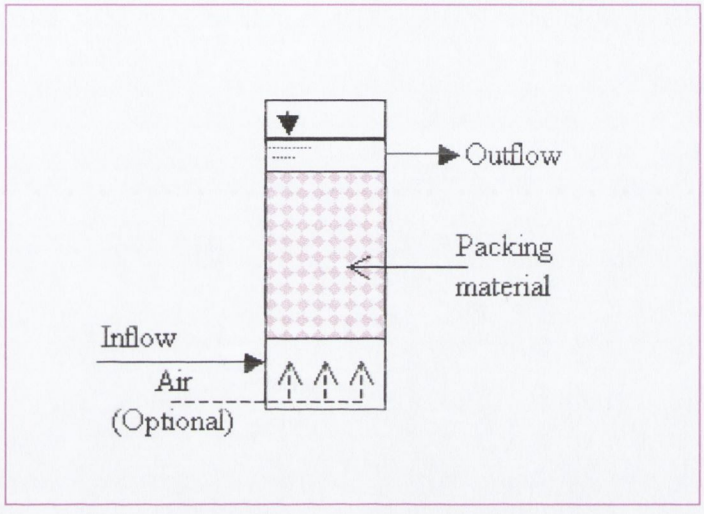

Figure 2. 18 Fluidized-bed

2.4.1 Reactor Regimes and Configuration

The combination and /or modifications of ideal reactors (PFR and CSTR) have been used to represent real reactors. Some of the more common alternative flow regimes and reactor combinations are shown schematically in Figure 2.19. Figure 2.19(b) shows a direct input with bypass flow used to achieve intermediate levels of treatment by blending various amount of treated or untreated wastewater. Figure 2.19(c) is a direct input but with a recycle flow this time, often adopted to achieve greater process control. Figure 2.19(d) is a step input with or without recycle (PFR, recycle type 1), and Figure 2.19(e) is a step input with recycle (PFR, recycle type 2) both of them are used to reduce the loading applied to the head of a plug-flow reactor. A series of complete-mix reactors can be used to model the flow regime that exists in a reactor network. If the series is composed of one reactor, then a completely mixed regime prevails. If the series consists of an infinite number of reactors in series (as shown in Figure 2.19(a)) then plug-flow conditions prevail.

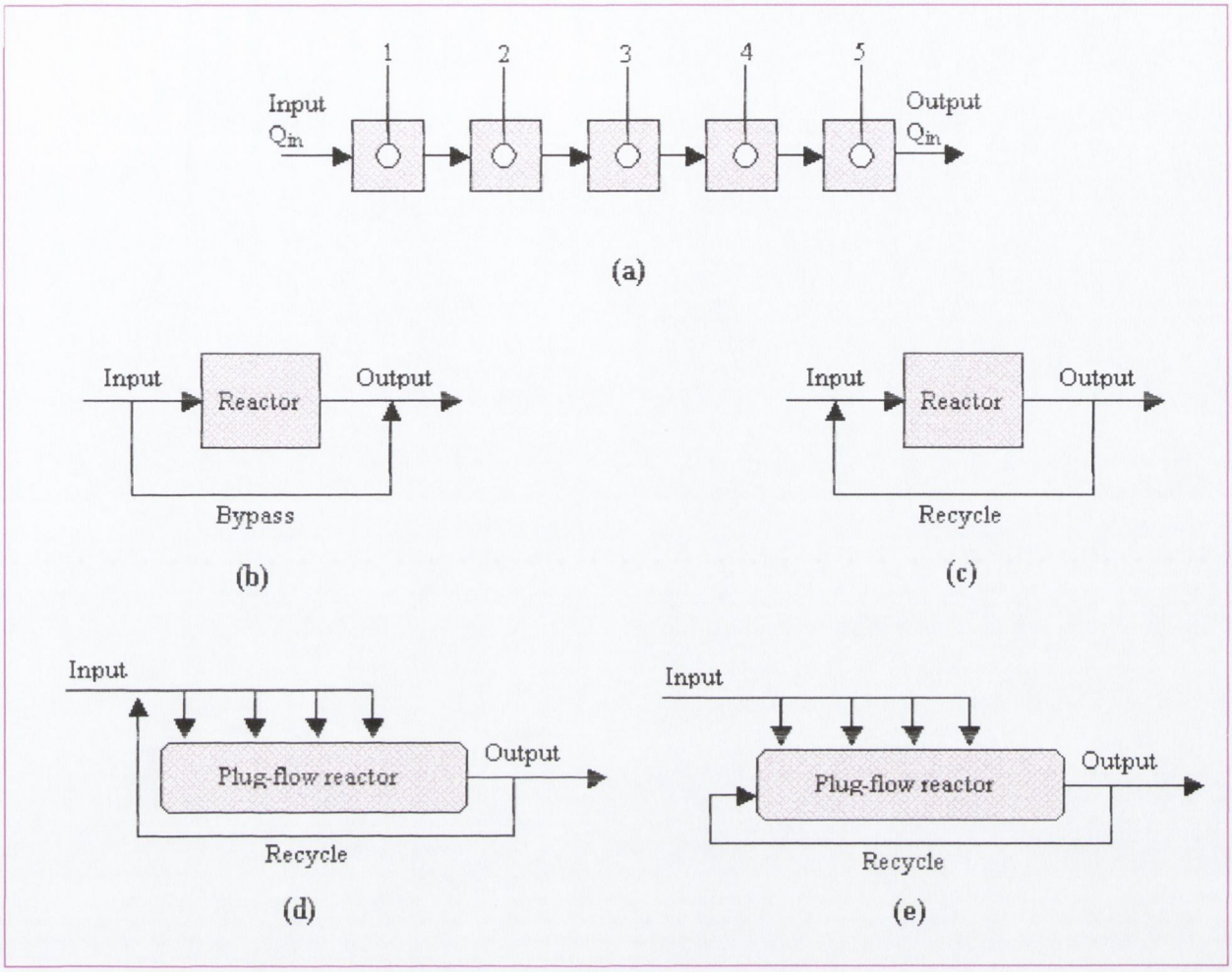

Figure 2. 19 Flow regimes and reactor configurations commonly used in the water industry

2.5 Mixing and Type of Mixers

Mixing is an important unit operation in many phases of industrial treatment, including: the mixing of one substance completely with another, the mixing of liquid suspensions, and the blending of miscible liquids, flocculation and heat transfer. In wastewater treatment works, mixing is predominantly used in suspended growth biological treatment systems in order to maximize the contact between the substrate and biomass. In water treatment applications mixing is typically used to disperse chemicals (coagulants, disinfectants etc) rapidly into the process flow

Most mixing operations in industry can be classified either as continuous rapid mixing (generally taking 30 seconds or less) or continuous mixing. When two miscible liquids are introduced into a batch reactor, a perfectly homogeneous mixture can be obtained by

agitation (with the help of diffusion if necessary) if maintained for a long enough period of time [Fu *et al.*, (1971)]. In a continuous flow system, however, it may be that perfect mixing can never be attained. There can be stagnant regions in the reactor (dead-zones) or part of the feed may be go directly to the outlet in the form of plug-flow (short-circuits). In order to study the behavior of such a system and the efficiency of mixing, one can consider the reactor or reservoir to act as a damper to variations in feed composition [Chiang and Cholette, 1971]. There are three factors in actual mixing conditions that should be taken into account. For a given agitator, only part of the total tank contents may be well mixed with the rest residing in stationary or stagnant dead zones. The part of the total volume where mixing is complete is referred to as the "effective volume of mixing": it is this part which acts as a damper to balance out any variations in feed composition. Depending on the relative position of the inlet with respect to the outlet, part of the feed may go directly to the latter without being mixed, causing channeling or a short-circuit. Only the remaining portion is thus available for mixing. Channeling is often observed in the course of experimental determinations, especially at low levels of agitation [MacDonald and Piret, 1951]. Short-circuiting is a problem for industry, because some of the input material will go directly to the output without mixing and reacting with the other substances in the reactor. Equally, any part of the feed that stays stable without mixing with the other substances in the reactor in dead-zones, reduces the overall process efficiency, particularly since it reduces the effective volume of the reactor.

2.5.1 Continuous Rapid Mixing of Chemical

In continuous rapid mixing the principle objective is to mix completely one substance with another in a period from a fraction of a second up to about 30 seconds. The rapid mixing of chemicals in a liquid can be carried out in a number of different ways, including: hydraulic jumps in open channels, venturi flumes, pipelines, pumping, static mixers and mechanical mixers. In the first four of these ways, mixing is accomplished as a result of turbulence that exists in the flow regime. In static mixers, turbulence is induced through the dissipation of energy. In mechanical mixing, turbulence is induced through the input of energy by means of rotating impellers such as propellers, turbines, and paddles. The most common form of mechanical mixing is using a vertical shaft

impeller in a tank with stator baffles (which reduce vortexing about the impeller shaft) as used, for example, for the dispersion of chemicals into water.

2.5.2 Continuous Mixing in Reactors

In continuous mixing, the principle objective is to maintain the contents of a reactor or holding tank in a completely mixed state in suspension, for example the flocs in an activated sludge aeration tank. Continuous mixing can be accomplished in a number of different ways, including; mechanical mixers, pneumatically (with air diffusers), static mixers and by pumping. In mechanical mixing, turbulence is induced through the input of energy by means of rotating impellers such as propellers, turbine, and paddles. Pneumatic mixing, an important factor in the design of aeration tanks in biological wastewater treatment processes, involves the injection of gases (normally air or oxygen) to promote turbulent conditions. Finally, an example of a static mixer is a baffled over–and-under flow channel used for flocculation.

2.5.3 Energy Dissipation in Mixing

The power input per unit volume of liquid can be used as a rough measure of mixing effectiveness, based on the reasoning that more input power means greater turbulence, and greater turbulence leads to better mixing. The following concept of a mean velocity gradient (G) can be used for the design and operation of mixing system whereby,

$$G = \sqrt{\frac{P}{\mu V}} \qquad \text{----------(2.23)}$$

Where: G = mean velocity gradient
P = power requirement
μ = Dynamic viscosity of fluid
V = Volume

Multiplying both sides of Eq.2.23 by the theoretical detention time (τ = V/Q) yields,

$$Gt_d = \frac{V}{Q}\sqrt{\frac{P}{\mu V}} = \frac{1}{Q}\sqrt{\frac{PV}{\mu}} \qquad \text{--------(2.24)}$$

Where: τ = Theoretical retention time
Q = flow rate

Typical values for G for various mixing operations are reported in the Table 2.1

Process	Range of values	
	Theoretical time	G (s^{-1})
Mixing		
Typical rapid mixing in wastewater treatment	5-20s	500-1500
Rapid mixing in contact filtration processes	<1-5s	1500-7500
Flocculation		
Typical flocculation processes used in wastewater treatment	10-30 min	20-80
Flocculation in direct filtration processes	2-10 min	20-100
Flocculation in contact filtration processes	2-5 min	30-150

Table 2. 1 The velocity gradient G for various mixing operations [Fair *et al.*, 1966].

2.5.4 Power Requirements for Mixing

The power requirements for mixing using the various types of mixers are discussed in the following sections.

2.5.4.1 Propeller and Turbine Mixers

Figure 2.20 shows a typical propeller mixer and turbine mixer used in water treatment plants. Mixing in water treatment processes usually occurs in the turbulent flow regime in which inertial forces predominate. As a general rule, the higher the velocity and the greater the turbulence, the more efficient the mixing. On the basis of inertial and viscous forces, the following mathematical relationships for power requirements for laminar and turbulent conditions have been developed [Clark and William, 1977].

Laminar: $P = k\mu\, n^2 D^3$ ---------- (2.25)

Turbulent: $P = k\, \rho\, n^3 D^5$ ---------- (2.26)

Where:
P= power requirement,
K= constant (see Table 2.2 below),
μ= Dynamic viscosity of fluid,
ρ= mass density of fluid,
D= diameter of impeller,
n= revolution per second.

Equation 2.25 applies if the Reynolds number is less than 10, and Eq. 2.26 applies if the Reynolds number is greater than 10,000. Values of K, are presented in Table 2.2.

Impeller	Laminar range (Equation 2.25)	Turbulent range (Equation 2.26)
Propeller, square pitch, 3 blades	41	0.32
Propeller, pitch of two, 3 blades	43.5	1
Turbine, 6 flat blades	71	6.3
Turbine, 6 curved blades	70	4.8
Fan turbine, 6 blades	70	1.65
Turbine, 6 arrowhead blades	71	4
Flat paddled, 6 blades	36.5	1.7
Shrouded turbine, 2 curved blades	97.5	1.08
Shrouded turbine with stator (no baffles)	172.5	1.12

Table 2. 2 Values of (K) for mixing power requirements [Rushton, 1952]

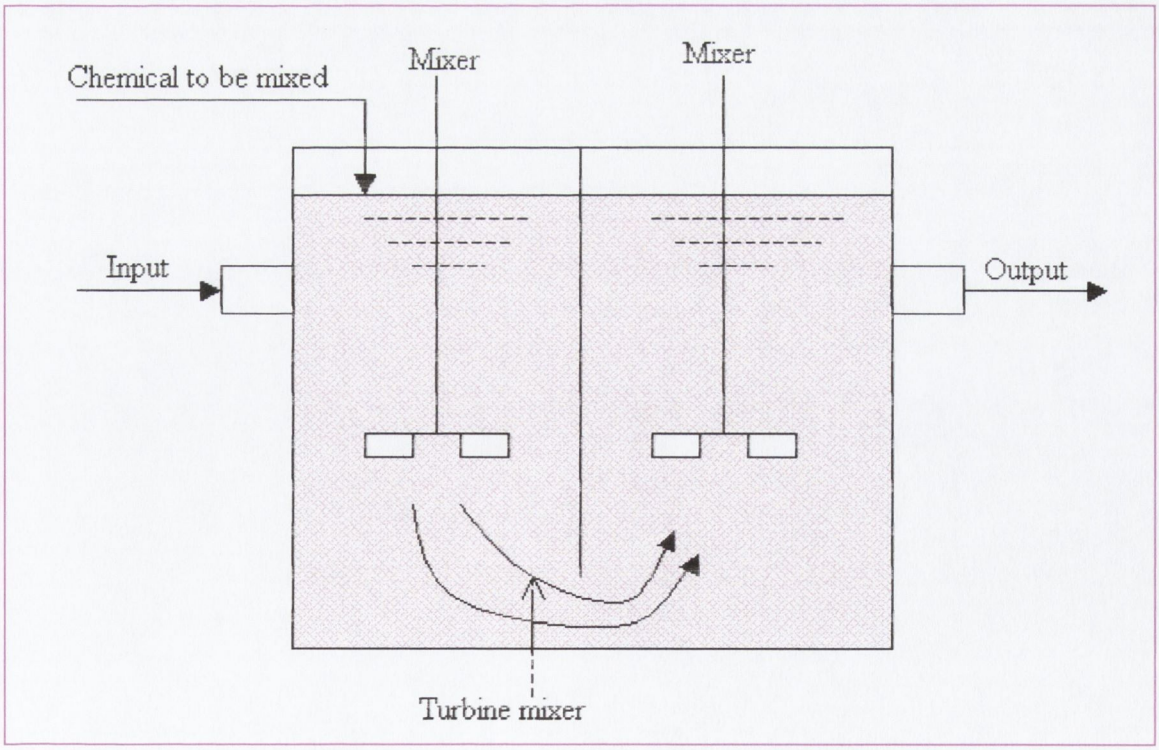

Figure 2. 20 Typical propeller and turbine mixer used in the water industry.

Vortexing, or mass swirling of the liquid, must be restricted with all types of impellers. Vortexing causes a reduction in the difference between the fluid velocity and the impeller velocity and thereby decreases the effectiveness of mixing [Douglass, 1964 and DeNevvers, 1991]. If the mixing vessel is fairly small, vortexing can be prevented by mounting the impellers off-center or at an angle with the vertical, or by having them enter the side of the basin at an angle. The usual method [Metcalf and Eddy, 2001] in both circular and rectangular tanks is to install four or more vertical baffles extending approximately one-tenth the diameter out from the wall. These effectively break up the mass rotary motion and promote vertical mixing.

2.5.4.2 Paddle Mixers

Paddle mixers generally rotate slowly, as they apply a large surface to the liquid. Paddles are often used as flocculation devices when coagulant, such as aluminum or ferric sulfate, and coagulant aids, such as polyelectrolytes are added to wastewater or sludges. Mechanically, flocculation is promoted by gentle stirring with slow-moving paddles. The action is sometimes aided by the installation of stationary slats or stator blades, located between the moving blades, that serve to break up the mass rotation of the liquid and promote mixing, the increased particle contact promoting floc growth. However, if the agitation is too vigorous, the shear forces that are set up will break up the flocs into smaller particles.

Equipment manufacturers and plant operators have performed numerous experiments to determine the optimum configuration of paddle size, spacing, and velocity and it has been found [Metcalf and Eddy, 2001] that a paddle-tip speed of approximately 0.6 to 0.9 m/s achieves sufficient turbulence with out breaking up the floc. Power in a mechanical paddle system can be related to the drag force on the paddles as follows,

$$F_D = \frac{C_D A \rho V_p^{\,2}}{2} \qquad \text{----------(2.27)}$$

$$P = \frac{F_D A \rho V_p^{\,3}}{2} \qquad \text{----------(2.28)}$$

Where: F_D = Drag force, (n)
C_D = Coefficient of paddle drag moving perpendicular to fluid
A = cross-sectional area of paddles
ρ = mass fluid density

V_p = Relative velocity of paddles with respect to the fluid, (m/s), usually assumed to be 0.6-0.75 times the paddles-tip speed.

P = power requirement

2.5.4.3 Static Mixers

Static mixers are principally identified by their lack of moving parts. A typical example is the in-line static mixer used for mixing chemicals, as illustrated in Figure 2.21, which contains elements that bring about sudden changes in the velocity patterns as well as momentum reversals. Another example, used more for flocculation, is a channel with closely spaced over and under baffles. The power consumed by static-mixing devices can be computed using the following equation.

$$P = \gamma Q h \qquad \text{---------- (2.29)}$$

Where: P = power dissipated,
γ = specific weight of water of water,
Q = flow rate,
h = head loss dissipated as liquid passes through device

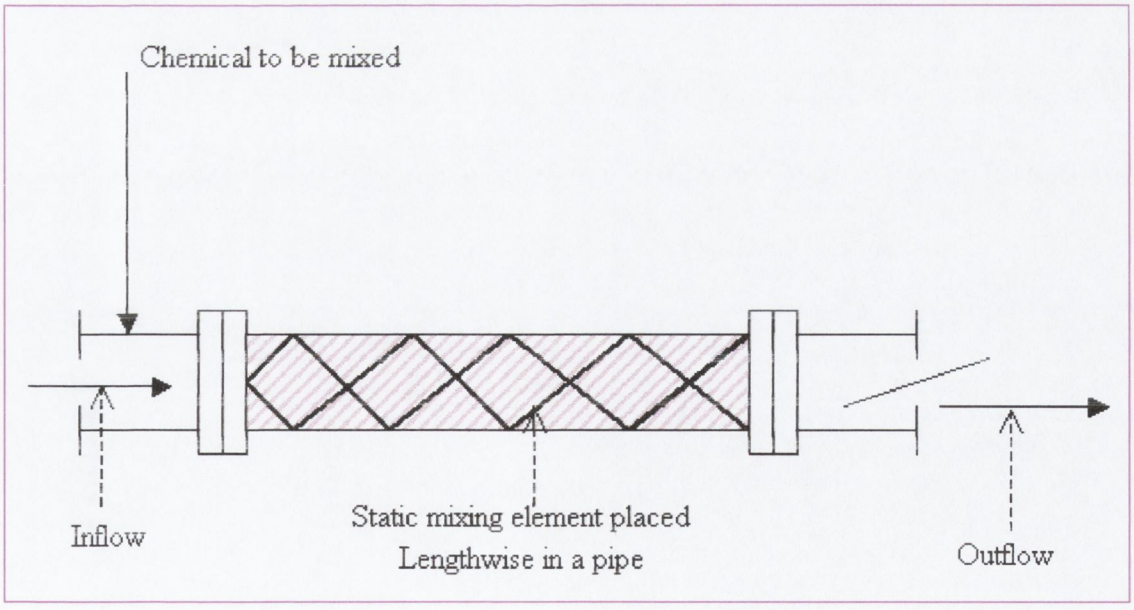

Figure 2. 21 Static in-line mixer

2.5.4.4 Pneumatic Mixers

In a mixing tank, flocculation tanks and aerated basins, mixing can be achieved by introducing air bubbles into the bottom of the tank. The power dissipated by the rising air bubbles can be estimated with the following equation [Masschelein, 1991] derived from a consideration of the work done when the volume of air released under compressed conditions, expands isothermally.

$$P = \frac{p_a V_a \ln p_c}{p_a} \qquad \text{----------(2.30)}$$

Where: P = power dissipated
p_a =atmospheric pressure
V_a = volume of air at atmospheric pressure
p_c = air pressure at the point of discharge

This can also be expressed as:

$$P_w = \frac{WRT_1}{29.7ne}\left[\left(\frac{p_2}{p_1}\right)^n - 1\right] \qquad \text{----------(2.31)}$$

Where:

P_w= Power requirement for each blower
n= 0.283 for air
29.7= constant for SI units conversion
e= Efficiency (usual range for compressors is 0.70 to 0.90)
W= weight of flow of air
R= engineering gas constant
p_1= absolute inlet pressure
p_2= absolute outlet pressure
T_1= absolute inlet temperature

Hence, the velocity gradient G, achieved in pneumatic mixing, can be obtained by substituting P_w from Eq, 2.31 into Eq. 2.23.

2.5.5 Analysis of reactor networks using Mass Balance

Reactors are normally analysed using the principle of a mass balance to define what occurs within treatment units as a function of time. For a simple CSTR, as illustrated in Figure 2.22 the system boundary must be established so that all the flows of mass into and out of the system can be identified. The proper selection of the system boundary is extremely important because, in many situations, it can be possible to simplify the

mass-balance computations. The general equation for a mass-balance analysis of to the liquid contents of the reactor is given (Eq. 2.32) where it is assumed that,

- the volumetric flow rate into and out of the reactor is constant;
- the liquid within the reactor is not subject to evaporation (isothermal condition);
- the liquid within the reactor is completely mixed;
- a chemical reaction involving the reactant C is occurring within the reactor;
- the rate of change in the concentration of the reactant C occurring within reactor is governed by a first-order reaction ($r_c = -kC$).

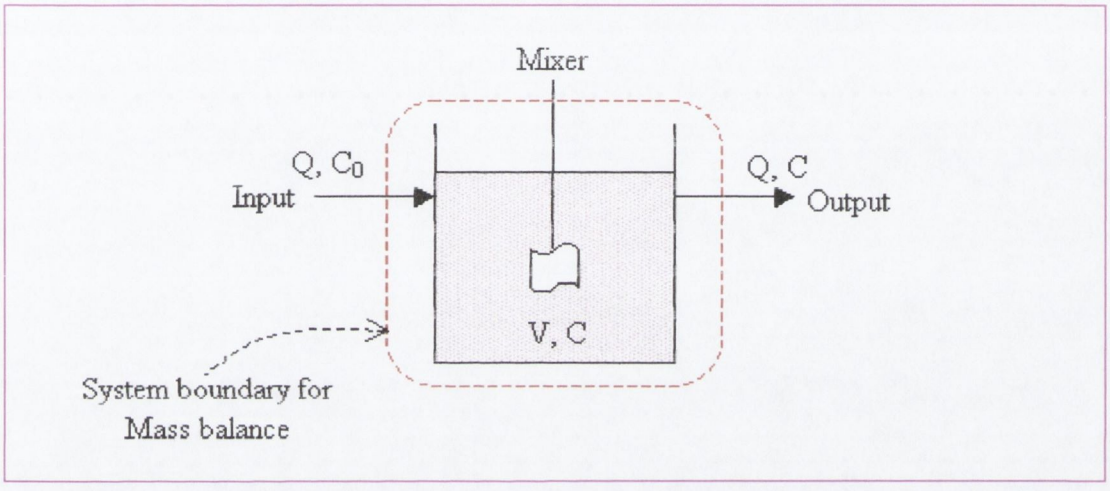

Figure 2. 22 Schematic diagram for a mass balance analysis for a CSTR

Accumulation = loading – outflow –reaction –settling ----------(2.32)

It should be noted that for tracer studies, the tracer is assumed to be non-reactive and non-settling and so the total balance can be expressed as follows,

$$V\frac{dc}{dt} = QC_0 - QC \qquad ----------(2.33)$$

In some situations, the use of a series of CSTRs may have certain treatment advantages: operational (sludge bulking), nitrification/denitrification, phosphorus removal, to save power on aeration) etc. In such situations, assuming that a slug of tracer is placed into the first reactor of a series of equally sized reactors (see Figure 2.23) so that the resulting concentration of tracer in the first reactor is C_1, and the total volume of all the reactors is V, the following material balance can be written for the reactor (which ignores changes due to settling or any reaction).

$$\frac{V}{n}\frac{dC_2}{dt} = QC_1 - QC_2 \qquad \text{----------(2.34)}$$

The generalized expression [Fogler, 1992] for the effluent concentration for i^{th} reactor in a series of n reactors is,

$$C_i = \frac{C_0}{(i-1)}(n\theta)^{i-1}e^{-n\theta} \qquad \text{----------(2.35)}$$

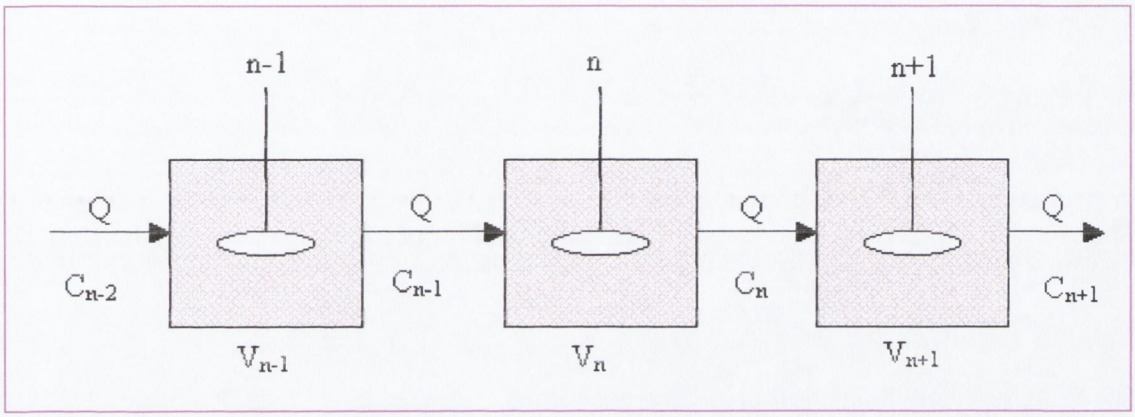

Figure 2. 23 Complete-mix reactors in series

This basic way, in which CSTRs are connected is normally termed "feed-forward" reactors [Chapra, 1997] in which water never flows through the same reactor twice (see Figure 2.24). The mass balance for feed-forward networked reactors of different volumes can be expressed as follows,

$$V_1\frac{dC_1}{dt} = QC_0 - Q_{12}C_1 \qquad \text{-------(2.36)}$$

$$V_2\frac{dC_2}{dt} = Q_{12}C_1 - Q_{23}C_2 \qquad \text{--------(2.37)}$$

Reactors can also be configured as "feedback" reactors and in this design water can flow through the same reactor twice (see Figure 2.25). The mass balance for feedback networked reactors of different volumes can be expressed as follows:

$$V_1\frac{dC_1}{dt} = QC_0 - Q_{12}C_1 + Q_{21}C_2 \qquad \text{-------(2.38)}$$

$$V_2\frac{dC_2}{dt} = Q_{12}C_1 - Q_{21}C_2 - Q_{23}C_2 \qquad \text{--------(2.39)}$$

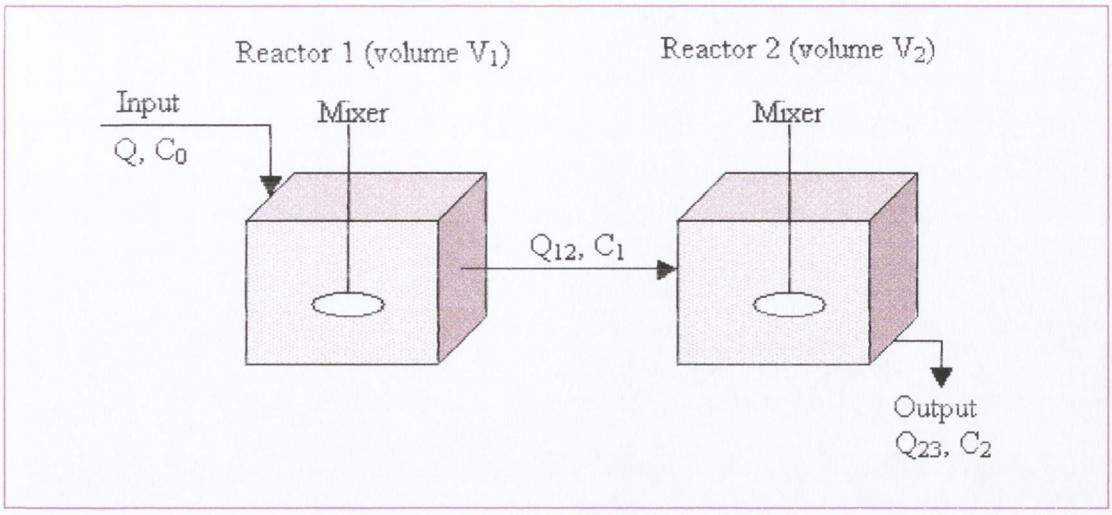

Figure 2. 24 Feed-forward system of reactors in series

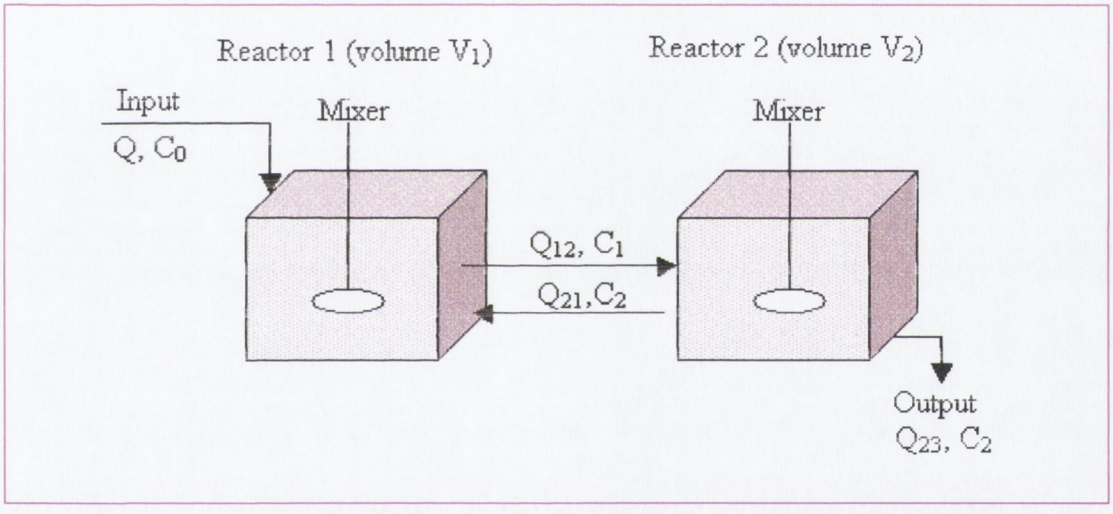

Figure 2. 25 Feedback system of reactor in series

2.6 Modelling Reactor Hydraulics

The hydraulic characterization of reactors is of fundamental importance with regards to the unit processes used in both water and wastewater treatment plants. As discussed, mixing is a common process used to reduce the degree of non-uniformity (such as concentration, viscosity, or temperature), to promote heat and mass transfer (often where a system is undergoing a chemical or biological reaction) and also to prevent settlement of solids. An analytical study of the behavior of perfectly mixed systems for CSTRs in series was first presented by MacMullin and Weber (1935) Denbigh (1944)

and Weber (1953), started to use the term "short-circuit" or " mathematically by-pass" to denote conditions involving probability considerations, applicable to well agitated tanks, in which the contents are substantially homogenous, whereby some of the molecules in the feed stream appear almost immediately in the effluent as a result of good agitation. However, this was confusing because, as pointed out by Colburn, (1935) the term "short-circuit" should refer rather to the flow pattern in a reactor where some of the input is channeled to the output, reaching the latter without being mixed. It later occurred to MacMullin (1953) that such short-circuit or canalized flow between the input and output would alter conditions in a reactor.

In any flowing system, fluid seldom moves in a (piston) plug-flow manner. There is usually a degree of longitudinal mixing with part of the fluid passing through more quickly and part lagging behind. Two models are commonly used to describe the hydraulic dispersion of such a system the dispersion model and the tank-in-series model [Levenspiel, 1999].

2.6.1 Dispersion Model

The dispersion model as was applied in different studies [Babcock *et al.*, 1966; Cairns and Perlmutter, 1960; Gunn, 1971; Pryce and Gunn, 1969] is more applicable to flow in pipe or channel where a sharp front or band of dye being injected can be envisaged. As the fluid passes along the pipe, the sharp band disperses into a fuzzy smear. Ideally, the concentration of the dye follows a statistically normal distribution with the median, being at the mean residence time point, defined by the volume divided by the flow. Levenspiel (1999) gives the following equation relating concentration versus time for the dispersion model:

$$C_\theta = \frac{1}{2\sqrt{\pi\left(D/ul\right)}} \cdot \exp\left[-\frac{(1-\theta)^2}{4D/ul}\right] \qquad \text{----------(2.40)}$$

Where: C_θ = normalized tracer response,

θ = normalized time (unit less),

D = coefficient of axial dispersion,

u = fluid velocity,

l = characteristic length.

The group D/ul is known as the dispersion number or Peclet number, comprising D (a measure of the rate of mixing), the velocity, u and the length of the path, L (assuming a pipe or channel configuration). These parameters have little significant meaning in a homogeneous fully mixed (or back mixing) tank where a tank in-series model is more appropriate. Such a number represents the ratio of the mass transport brought about by advection and dispersion. If the Peclet number is significantly greater than 1, advection is the dominant factor in mass transport. If the Peclet number is significantly less than 1, dispersion is the dominant factor in mass transport. It can also be shown that the number of CSTRs in series required to simulate a plug-flow reactor with axial dispersion is approximately equal to Peclet number divided by 2 [Metcalf and Eddy, 2001]. When dispersion is large, the output curve becomes increasingly nonsymmetrical, and the problem becomes much more sensitive to the boundary conditions (see Section 2.2.2.1).

2.6.2 Tank in-series Model

In such a conceptual model the assumption is made that a set of perfectly mixed reactors in series flow into each other. If the number of tanks is **n**, the following equation may be applied in place of Eq. 2.40 for the tank in- series model.

$$C = \frac{\theta^{(n-1)} n^n}{(n-1)!} e^{-n\theta} \qquad \text{--------(2.41)}$$

For value of n between about 5 and 20, D/uL is approximately equivalent to 1/2n, but when n is above 20, the tank in-series factorial (n-1) becomes unmanageably large for computation. If n=1 then D/uL is infinite and the relationship no longer holds. Thus, for computing purposes, the equations used are changed at an intermediate point, say between n=10 and 20, without any apparent discontinuity [Stevenson, 1995]. The Equations 2.40 and 2.41 may be integrated to give a cumulative curve, which represents the F(t) curve (see Section 2.2.1.3) for the output feed composition. The 16^{th} and 84^{th} percentiles in these cumulative curves (the times at which the change is 16% and 84% complete) are two standard deviations (2σ) apart [Levenspiel, 1999], which provide a simple way of analyzing tracer experiments used to calibrate tanks. The statistical variance σ^2 of the distribution curve is simply 1/n, where the standard deviation σ is merely the square root of the variance.

2.7 RTD Studies of Single and Multi-stage Reactor Systems

Several tracer studies have been carried out on single CSTRs and on multi-stage systems in order to study the hydraulic characterization of such networks where reactors are connected either in parallel or in series. Various theoretical frameworks have been proposed as a result of such studies, some of which are reviewed in the following section.

2.7.1 Case Study [after Cloutier and Cholette, 1968]

This series of studies derived a differential equation, which took into account the effective volumes of mixing and eventual short-circuits, in order to define the mixing conditions in a continuous flow system. The basis of the model for the study was on a normal rectangular CSTR tank as shown in Figure 2.26.

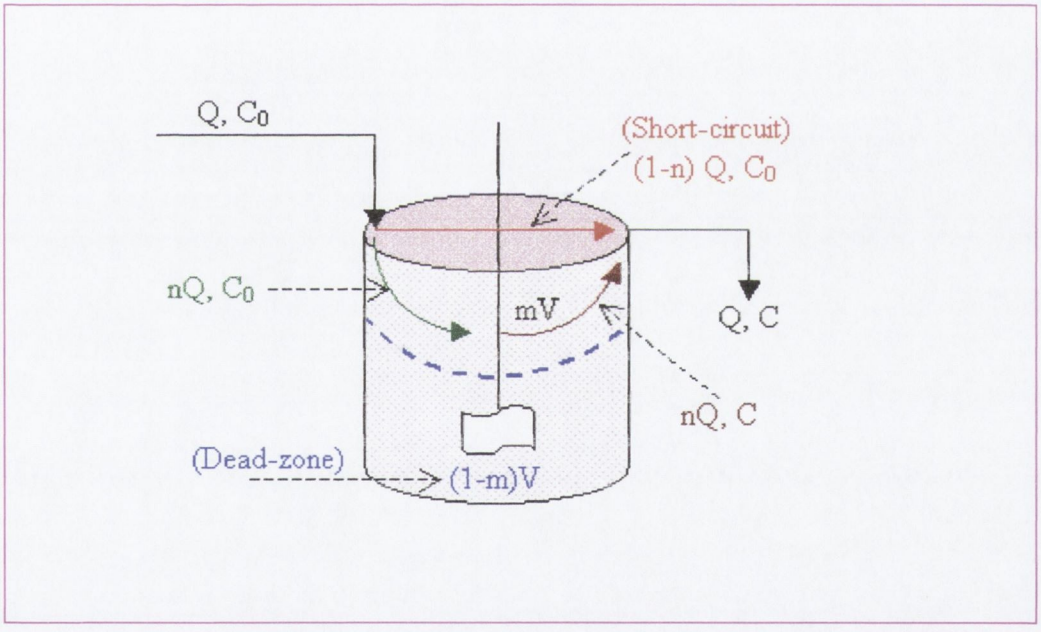

Figure 2. 26 The proposed model to study partial mixing and short-circuit [after Cholette, and Cloutier, 1959]

Different cases were studied theoretically, involving partial mixing and short-circuits, and then laboratory experiments were carried out using NaCl as the tracer on an experimental CSTR to validate the model. In this case, the CSTR was initially full of NaCl solution and water was suddenly injected at a known rate and the effluent concentration measured. Theoretical assumptions were made on whether the system

was behaving as a CSTR, based on Eq. 2.42 below to give a straight line when plotted on semi-log paper (see Figure 2.27).

$$qC_0dt = qCdt + d(VC) \qquad \text{----------(2.42)}$$

$$\frac{C}{C_0} = e^{-\frac{q}{V}t} \qquad \text{----------(2.43)}$$

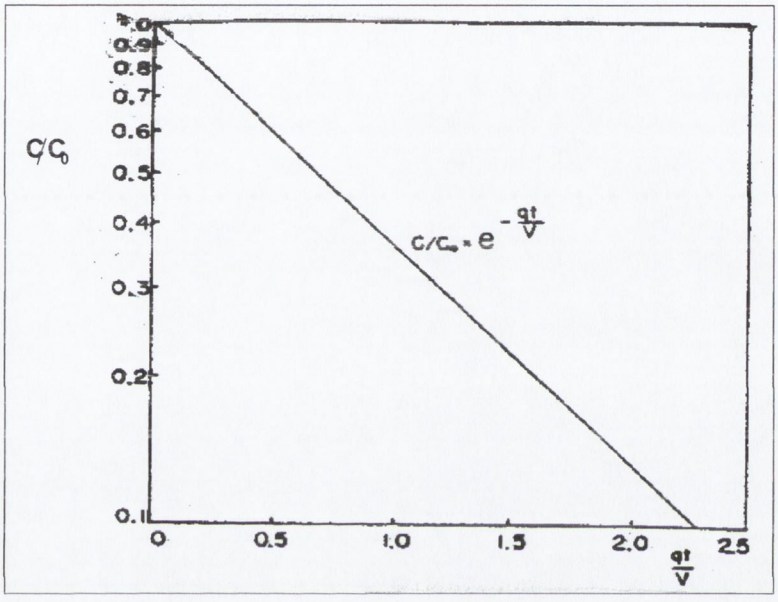

Figure 2. 27 The CSTR model on semi-log paper [Cholette and Cloutier, 1959]

With the reactor behaving as partially mixed and short-circuiting an assumption was made that only a fraction, m of the total volume was assumed to be well agitated (see Figure 2.26). A fraction, n of the feed enters the zone of perfect mixing while the other fraction (1-n) is assumed to short-circuit directly to the outlet giving the following Eq. 2.44.

$$\ln\frac{C}{C_0} = \ln n - \frac{nq}{mV}t \qquad \text{----------(2.44)}$$

Hence, by plotting C/C_0 vs. qt/V on semi-log paper (see Figure 2.28), a value of n can be read directly on the concentration ratio axis at t=0. The straight line has a slope of $-n/m$, after which m can also be derived.

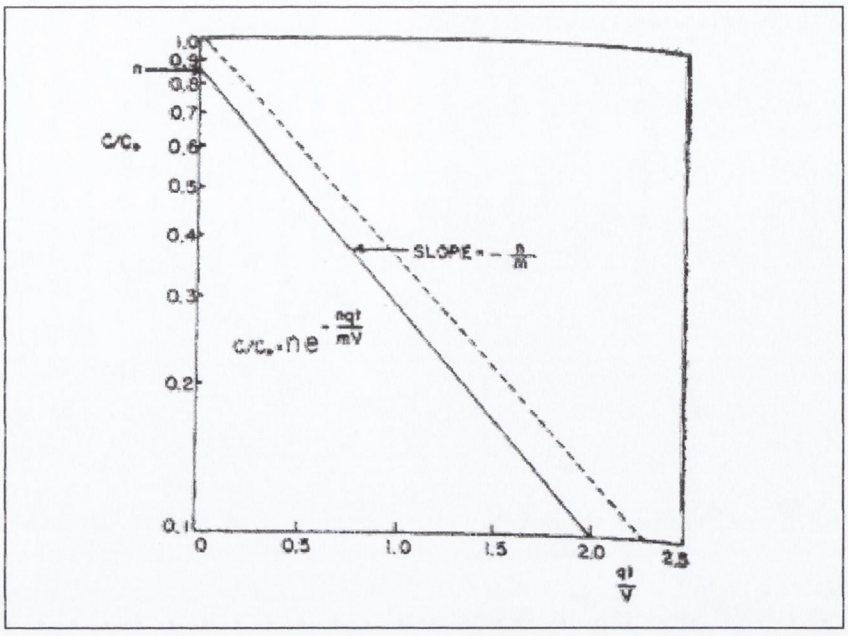

Figure 2. 28 The CSTR model with partial mixing and short-circuiting [Cholette and Cloutier, 1959]

The experimental results obtained were plotted (see Figure 2.29) enabling straight lines to be drawn through the experimental points at different levels of agitator speed (designated as N) ranging from 0 to 210 rpm. Values of m and n were then determined for each agitator speed by the theoretical method described.

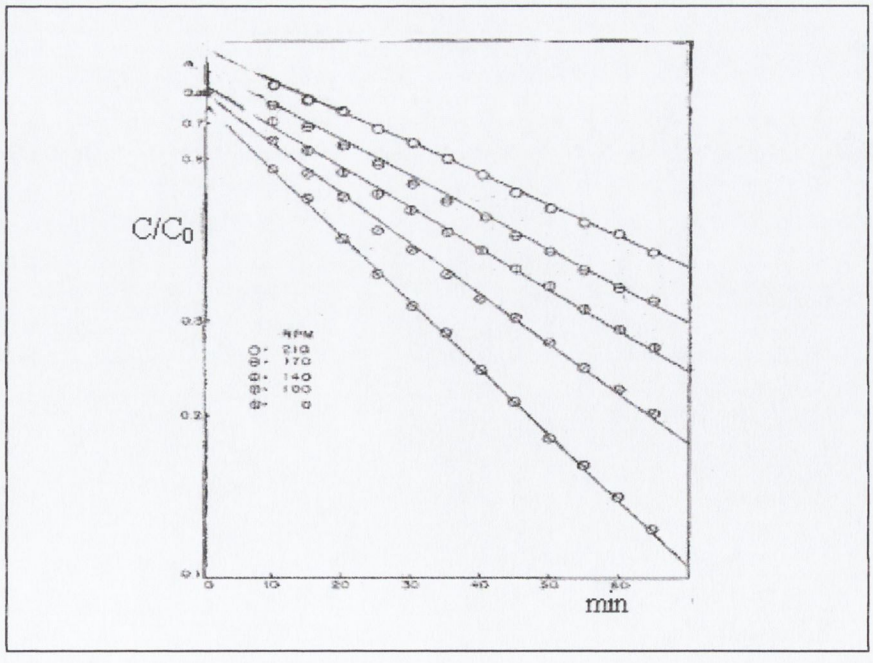

Figure 2. 29 Experimental results: relative concentration vs. time [Cholette and Cloutier, 1959]

Values of m and n were obtained with the agitator at rest (0rpm), designated as m_0 and n_0. Thus, for any given value of N, the value of $(m-m_0)$ could represent the contribution of the agitator to the level of mixing. It was found when plotting $(m-m_0)$ vs. N on semi-log paper, (see Figure 2.30 (a)) that a straight line of slope 2 is obtained which can be represented by the equation

$$(m - m_0) = an^2 \qquad \text{---------(2.45)}$$

where: a = constant, relating effective volume to agitator speed.

For the particular system studied, the constants m_0 and a were found to be 0.38 and 1.25×10^{-5} respectively. Hence, the value of 0.38 for m_0 indicated the level of mixing obtained when the agitator was at rest through the agitation produced by the introduction of the feed. As the value of m reaches 1 when the agitator speed is increased, a maximum value of $(m-m_0)$ is reached. This value remains constant, therefore, even if the agitator speed is increased because the reactor is behaving as one perfectly mixed system.

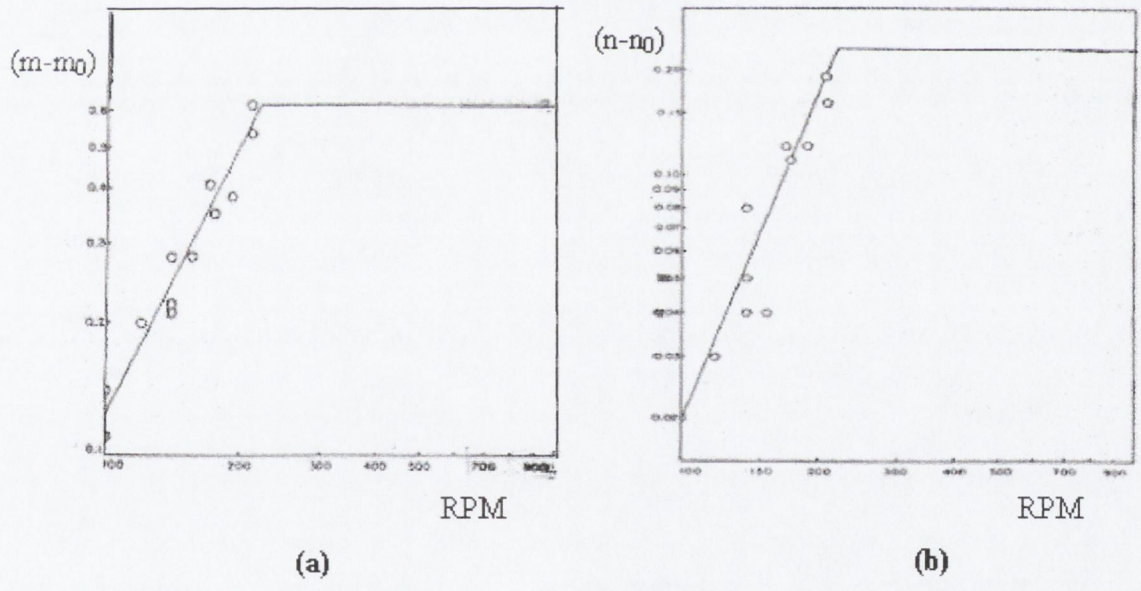

Figure 2. 30 (a) Effective volume of mixing vs. agitator speed, (b) Short-circuit effect vs. agitator speed [Cholette and Cloutier, 1959]

Proceeding in a similar way, the values of $n-n_0$ vs. N (agitator speed, rpm) were plotted on log-log paper (see Figure 2.30 (b)) as a straight line of slope 3. The values of n are thus related to the agitator by the equation;

$$n - n_0 = bn^3 \qquad \text{----------(2.46)}$$

where: b= constant, relating short-circuit effect to agitator speed.

When plotted on a linear scale, (see Figure 2.31), both variables (m and n) were found to reach a maximum value of 1 at a speed of approximately 220 rpm, indicating that at this point the system is behaving as perfectly mixed.

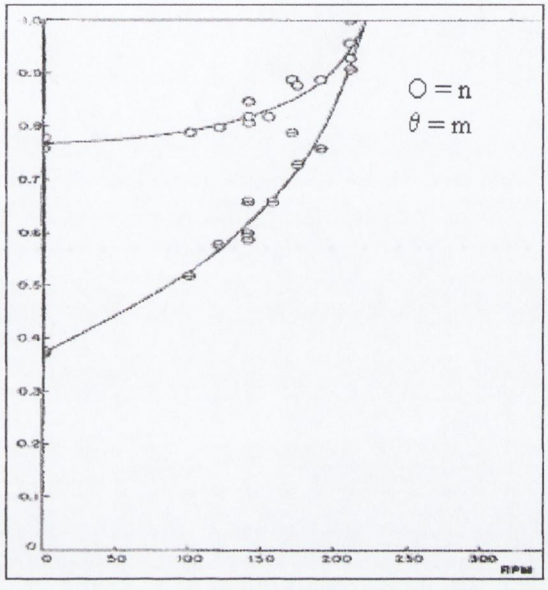

Figure 2. 31 Variations of m and n with agitator speed N [after Cholette, and Cloutier, 1959]

Variations of the level of mixing in continuous flow systems were then investigated further using the same model [Cloutier and Cholette, 1968] as a function of the following parameters: diameter, shape and speed of the agitator, feed rate and position of the feed inlet. They found that at agitator speeds less than a critical value, a minimum level of mixing was observed which depended on the position of the feed inlet. At speeds greater than to the critical value, the level of mixing increased linearly with agitator speed, at a given feed rate until conditions of perfect mixing were reached. The critical agitator speed and the position of each straight line depended on the agitator size. It was observed that the same minimum level of mixing, m_0 was displayed for each agitator at low values of rpm even when the agitator was at rest, due to the level of mixing created by the action of the feed. The value of m was seen to remain constant at m_0 for an agitator of a given size, as long as the speed of rotation was less than a certain critical value. In addition it was observed that different values of m were obtained as

the size of the agitator and the speed of the rotation increased, as illustrated in Figure 2.32.

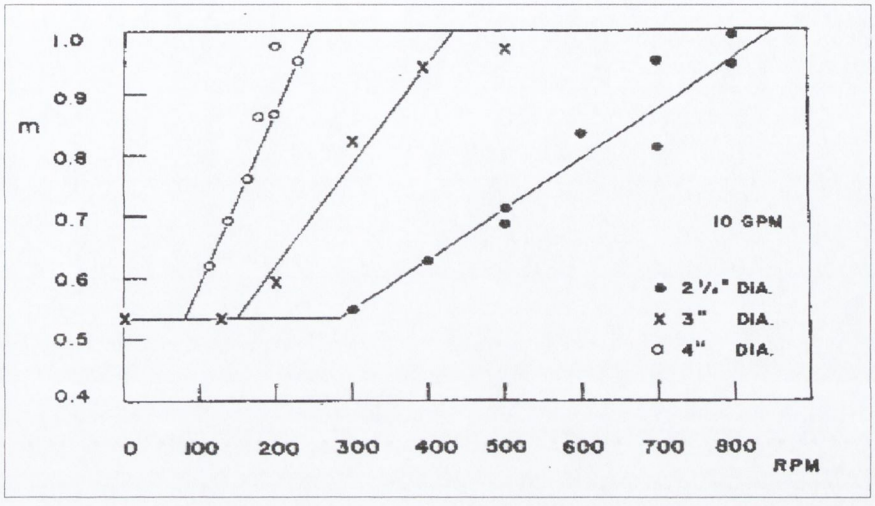

Figure 2. 32 Variation of the level of mixing with agitator speed [Cloutier and Cholette, 1968].

The second factor investigated was the effect of feed position on the hydraulic performance of the reactor. The feed position was denoted by the parameter, h, which indicated the relative distance between the inlet and the mixer. Families of curves were obtained when plotting the value of m as a function of mixer speed N; each family characterized by the feed rate and the size of the agitator. Typical curves for a given family (see Figure 2.33(a)) were similar in shape but showed a definite effect of the parameter h on the value of m. It was noted that the break in each curve occurred at a speed which was just about the same for all the curves of a given family, and was denoted as N_0 (mixer at rest). When the speed of the agitator becomes larger than N_0, the values of m were seen to increase more and more above the minimum m_0, until a maximum value of 1.0 is reached. The parallel straight lines in this region indicated that as long as conditions were limited to this region, corresponding increases in the value of m will result from increases in the value of N, no matter what the value of h. Equally it was shown that when the mixer was at rest, the position of the feed does not affect the hydraulic behavior of the reactor (see Figure 2.33 (b)). A single straight line was obtained when plotting $m-m_0$ versus N (see Figure 2.34(a)), which confirms that as the agitator speed increases more and more above N_0, the liquid recirculation reaches further and further into the reactor, as illustrated in Figure 2.34(b).

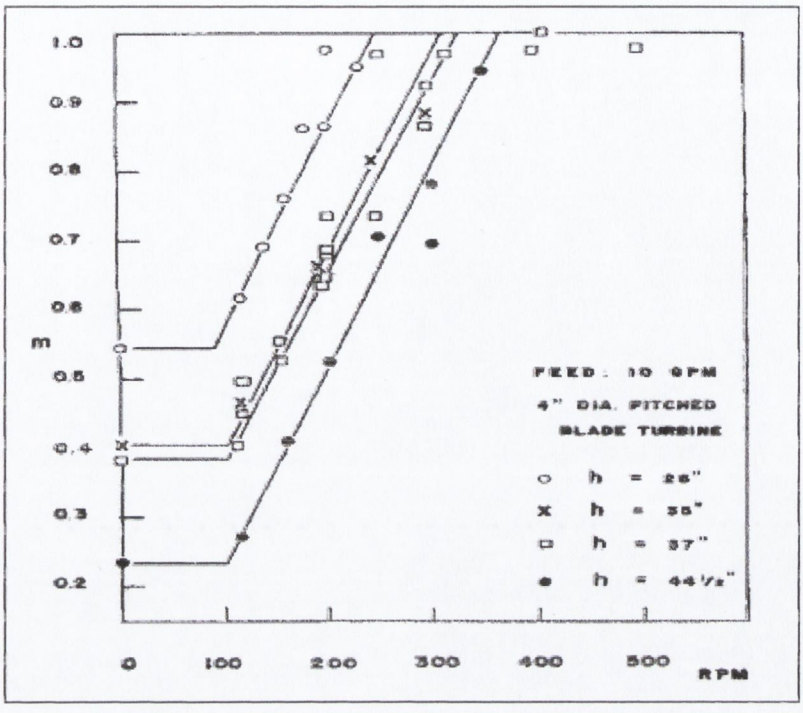

(a)

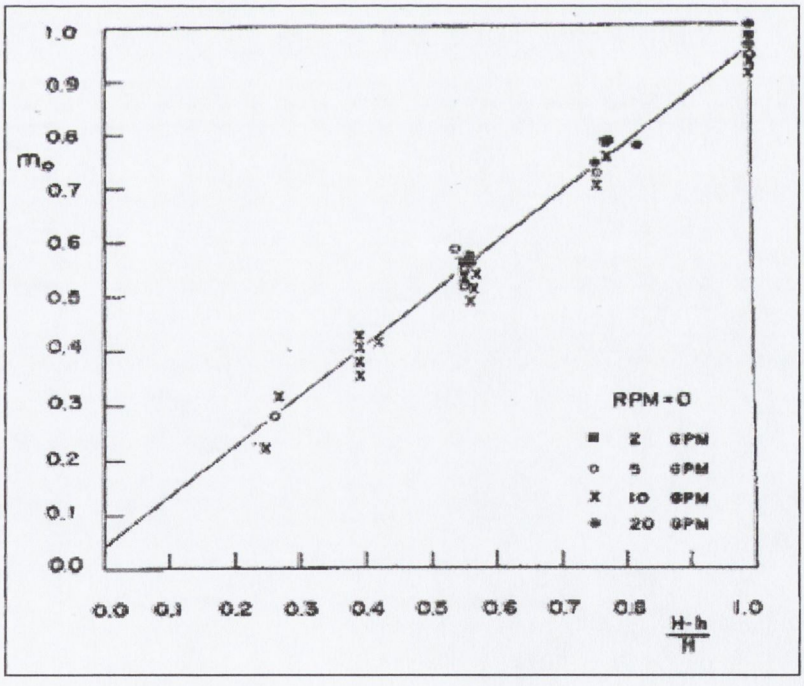

(b)

Figure 2. 33 (a) Variation of the level of mixing with agitator speed, (b) Variation of the minimum level of mixing with agitator speed at rest [Cloutier and Cholette, 1968]

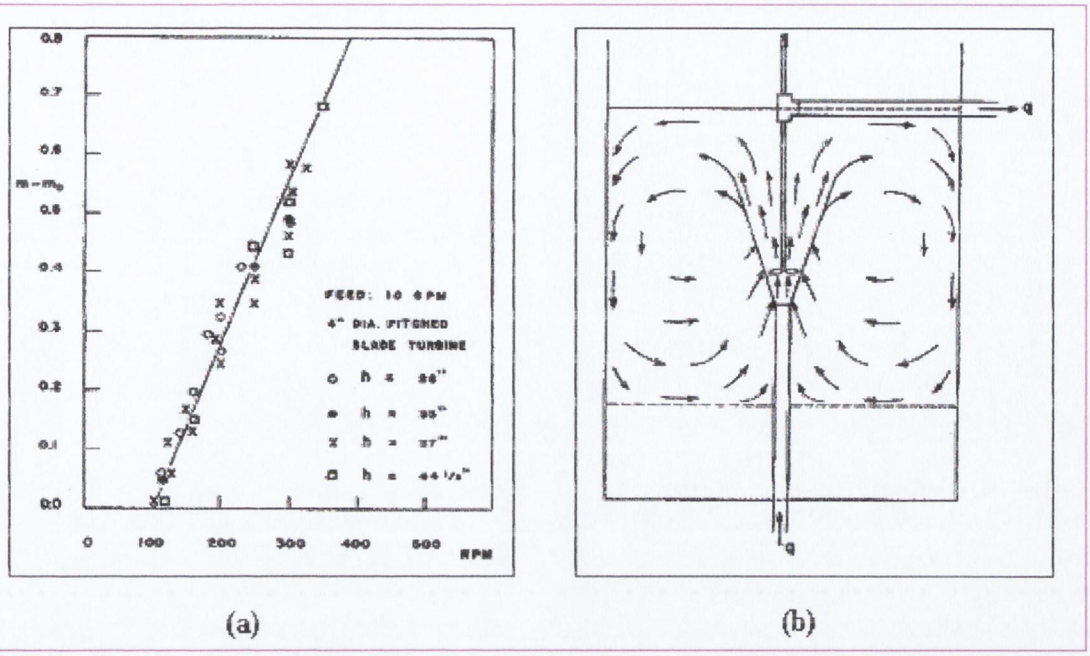

Figure 2. 34 (a) Variation of the parameter ($m-m_0$) as a function of agitator speed, (b) Flow pattern showing how the speed of agitator works [Cloutier and Cholette, 1968]

The third factor investigated was the effect of feed rate on the variation of the mixing against agitator speed for three different feed rates that is shown in Figure 2.35. Although the results were obtained from trials made with the same agitator, the values of N_0 corresponding to each feed rate were seen to increase with the increasing values of the latter. As the speed of the agitator increased above its critical value of N_0 for a given feed rate, the value of m increased with N as shown, separate curves being obtained for each feed rate. This also demonstrated that for a given speed in this region, the level of mixing decreases as the feed rate increases.

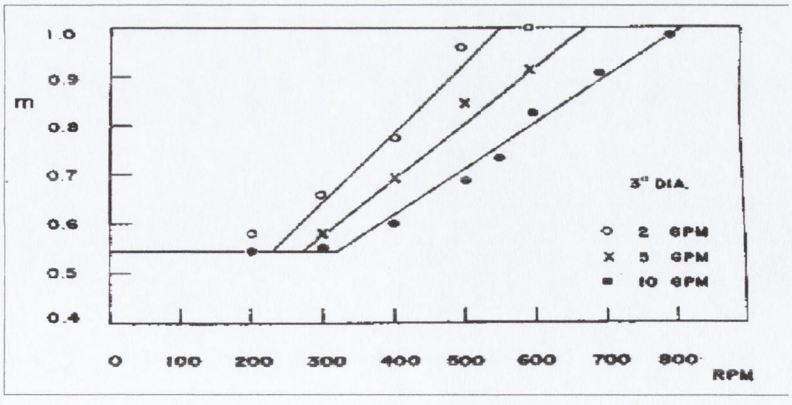

Figure 2. 35 Effect of feed rate on the variation of the level of mixing with agitator speed [after Cloutier and Cholette, 1968]

The fourth factor which also was investigated was the effect of the shape of the agitator on hydraulic mixing performance. Figure 2.36 clearly shows that with agitator speeds less than N_0, the effect is hardly noticeable since the value of m_0 is influenced more by the position of the feed inlet. However, as the speed of rotation of an agitator increases above N_0, the shape effect is more pronounced indicating that the flow pattern set up inside the reactor differs from one agitator to the other, reflecting the degree of mixing attained.

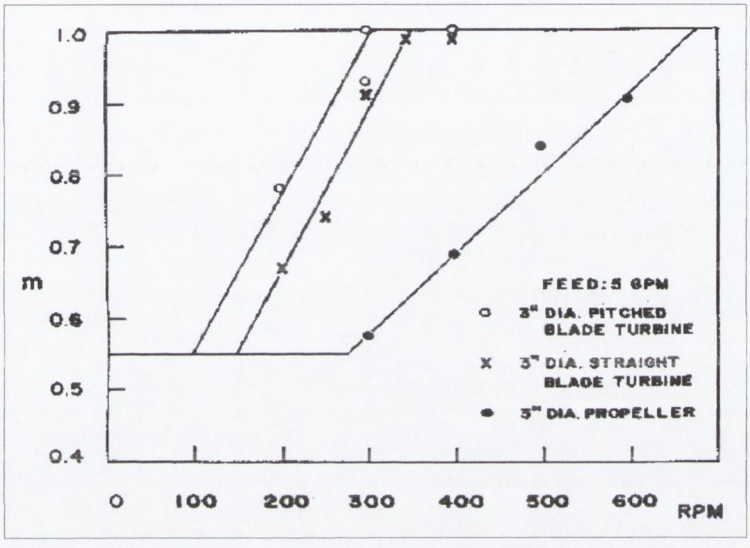

Figure 2. 36 Effect of agitator shape on the variation of the level of mixing with agitator speed [Cloutier and Cholette, 1968]

The model developed by Cholette and Cloutier, (1959) seems to be a useful tool in evaluating the actual performance of mixers in a single CSTR. However, from the point of view of this thesis the method described only focuses on the fraction of short-circuit and perfect mixing. The method has not been applied to a network of reactors, particularly in terms of the diagnosis of individual reactors within the network, which is one of the aims of this work.

2.7.2 Case Study [after Haddad and Wolf, 1967]

A three-parameter model has been suggested for expressing the RTD in multistage systems [Haddad and Wolf, 1967; Raghurman and Varma, 1970] in which it is assumed that each stage comprises an active back mix region and a dead region with cross flow of the material between the two regions. It is also assumed that a fraction of the feed short-circuits the reactor.

In models previous to this [Kafarov *et al.*, 1971; VanSwaaij *et al.*, 1969] any exchange of material between the active and dead regions was either not considered or else the major discrepancies to ideal mixing (such as bypass and the dead volume in the system) were not included. The assumption of an inert dead volume is not appropriate and, in practice, there is bound to be an exchange of material between the mixing and dead regions. The model was evaluated for different values of the parameters and then was compared with experimental data reported for RTDs of solids in multistage fluidised beds. The proposed model, shown in Figure 2.37, assumes an instantaneous bypass of fraction, X of the feed to each stage, which consists of an active back mix region and a dead region with a short-circuit ratio, P between the two regions. Consequently, unlike the earlier models [Kafarov *et al.*, 1971; VanSwaaij *et al.*, 1969] the dead region is not totally inert, but contributes to the overall mixing.

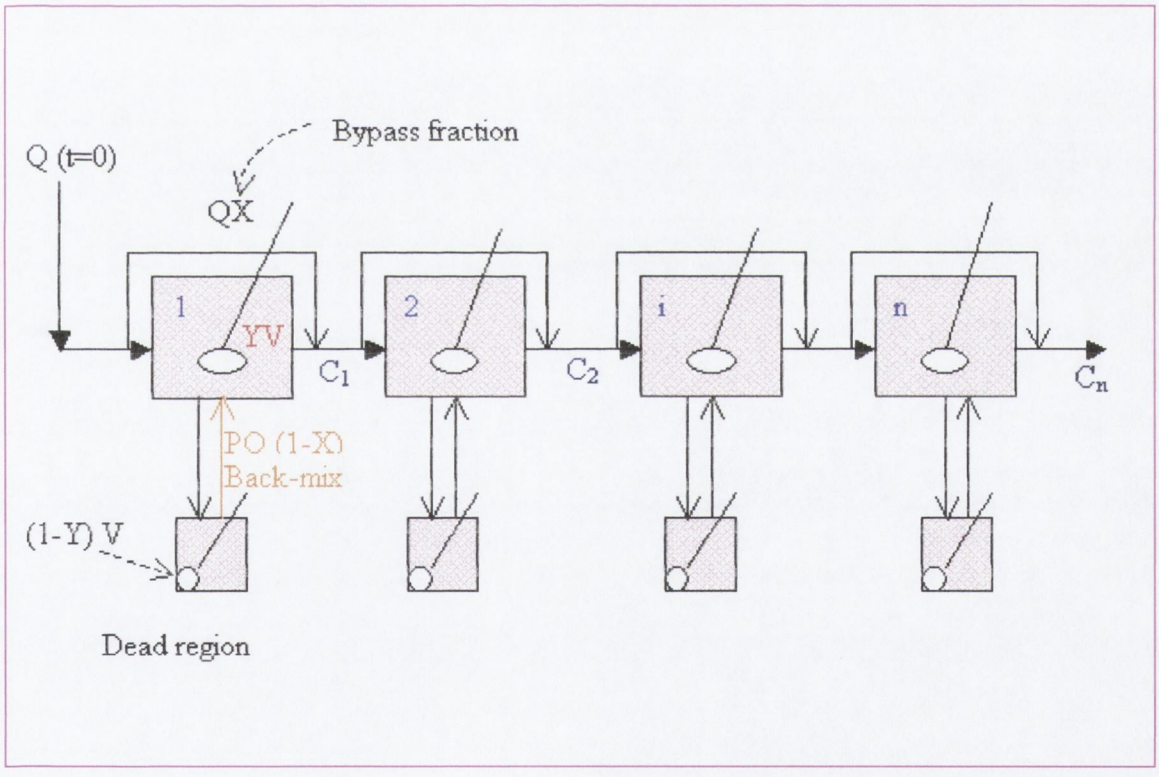

Figure 2. 37 Schematic diagram of the proposed model for RTD in multi-stage systems [after Haddad and Wolf, 1967]

The effect of the fraction of the feed entering the stage that exchanges between the inert and active regions, P (internal short-circuit) on the RTD is shown in Figures 2.38 (a) & (b) for a dead volume fraction of 0.5 and 0.1. The fractions of the dead volume and the short-circuit are closely interrelated; the dead volume reduces the effective volume

compared to that assumed for the mean residence time whereas the short-circuit promotes mixing within the stage leading to a dynamic rather than an inert dead volume. Figure 2.38(b) presents the conditions corresponding to a small value of the dead space, equal to 0.9, wherein it can be seen that the short circuit affects the RTD with decreasing influence until P=0.1. Overall the figures show that an increase in cross-flow leads to a greater degree of mixing within each stage, resulting in a broader RTD spectrum and a faster convergence of the tail to zero. This condition, which corresponds more realistically to experimental evidence than the distribution with an unusually long tail, was obtained from the assumption of inert dead volume. Comparison of Figures 2.38 (a) & (b) also show that with decreased dead volume, other conditions being equal, the RTD spectrum broadens and the peak of the distribution moves towards $\theta = 1$, indicating that the effective volume of the system increasingly corresponds to that given by the mean residence time.

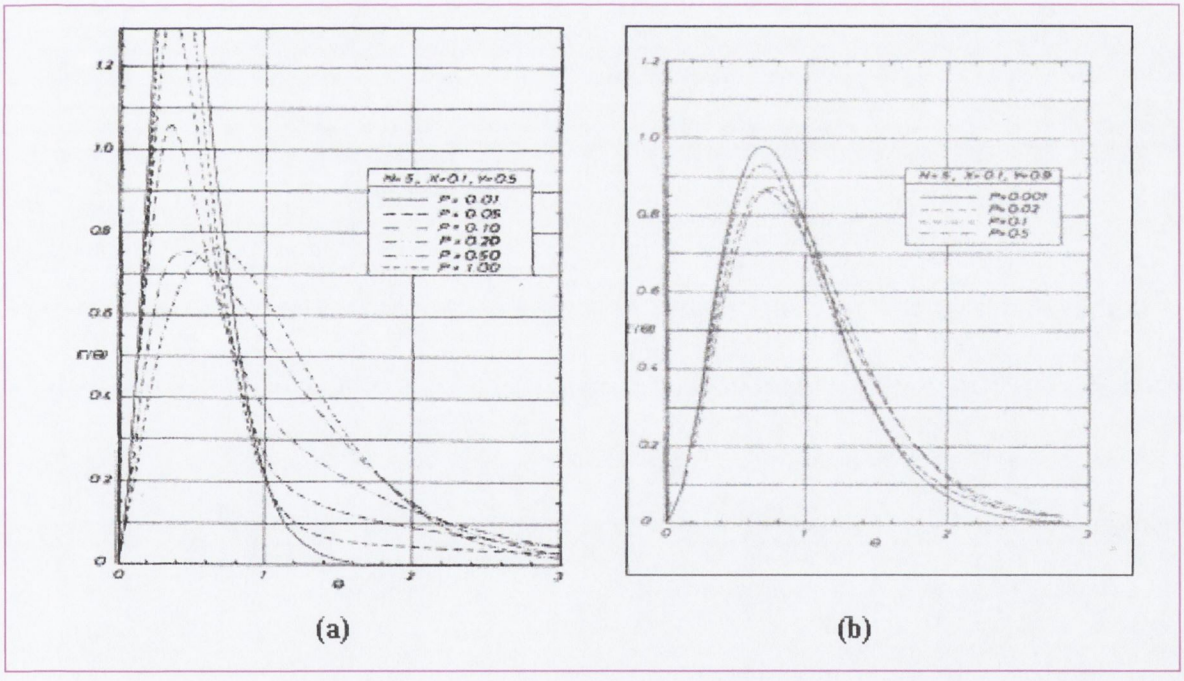

Figure 2. 38 Effect of internal short-circuits on RTD (a) 50% dead volume, (b) 10 % dead volume [Haddad and Wolf, 1967]

The RTD spectrum narrows with increased number of stages (if these stages are CSTRs) (see Figure 2.39) leading to the uniformity in residence times of the elements

with the limiting condition of plug flow at an infinite number of stages [Raghuraman and Varma, 1972] as discussed previously in Section 2.6.

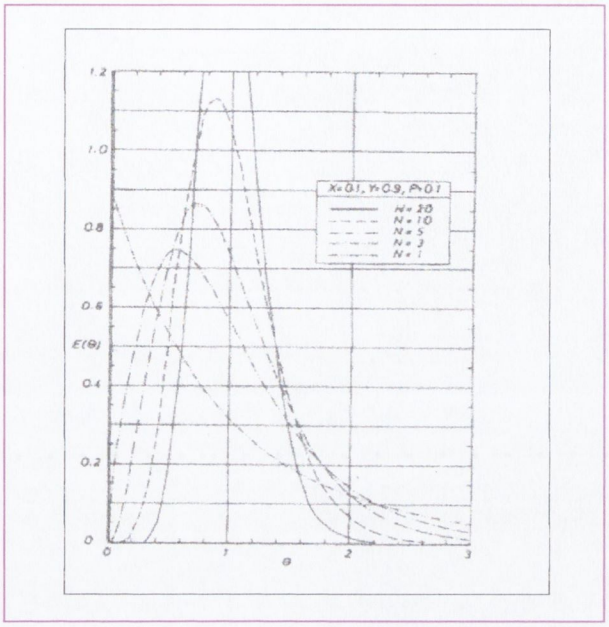

Figure 2. 39 Effect of number of stages on RTD [Haddad and Wolf, 1967]

Alternatively, an increased fraction of the feed by-passing each stage, X (ie. short-circuit) reduces the fraction of the material entering the stage and results in a broad RTD spectrum with a lower peak value indicating a wide distribution of residence times for the material of the mixing zone (see Figure 2.40).

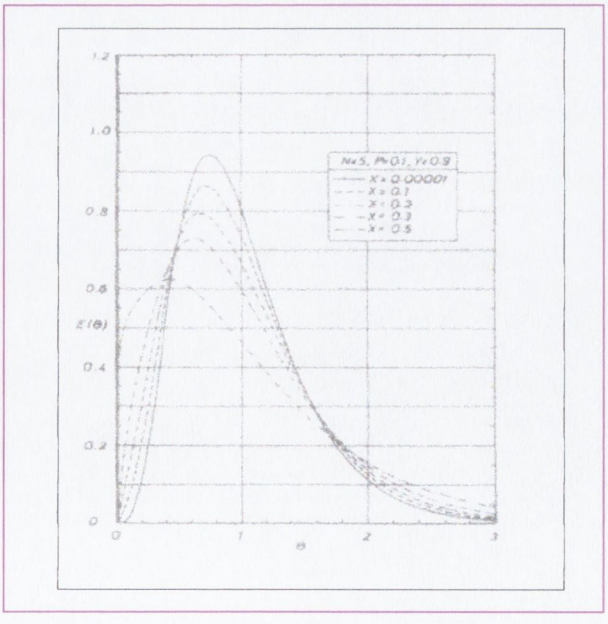

Figure 2. 40 Effect of Short-circuit on RTD [Haddad and Wolf, 1967]

Hence, this model introduced the concept of dead-zones, the internal short-circuit (between the well mixed volume and the dead-zone volume) and the short-circuit all of which are obviously critical factors to be investigated in order to understand the behaviour of any hydraulic system. However, it does not appear that the model has been used for a study at full-scale in order to check its validity outside the laboratory. In addition, it has not been shown that its application could be used in order to diagnose which one of a series of networked reactors could be exhibiting hydraulic discontinuities.

2.7.3 Case Study [after Chiang and Cholette, 1971]

Another model describing the RTD for **n** imperfectly mixed reactors in series was developed by Chiang and Cholette (1971) as shown in Figure 2.41.

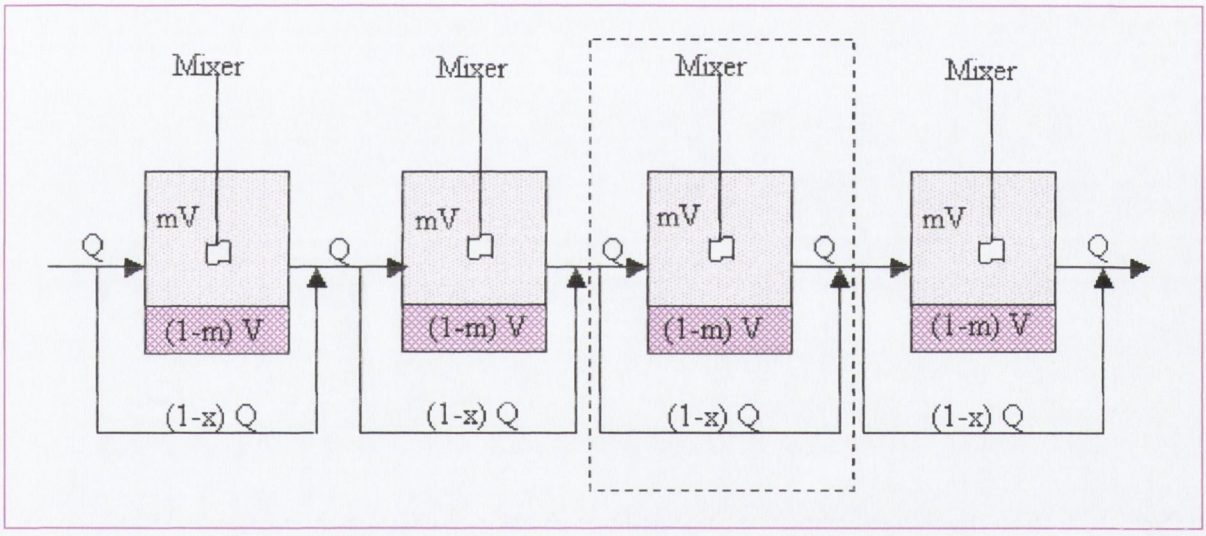

Figure 2. 41 Schematic representation of the system of a fluid in non-ideal stirred tanks in series [after Chiang and Cholette, 1971]

The parameters which characterize the mixing in each reactor are the same as those originally proposed by Cholette (Section 2.7.1) where m represents the fraction of the volume V of the reactor which is perfectly mixed, while x is the fraction of the feed which enters the zone of perfect mixing; (1-x) is thus the fraction of the feed which goes through as short-circuit while (1-m) represents the fraction of the volume of the reactor dead-zone. An expression for the above model was developed as follows,

$$C_N = 1 - \sum_{j=1}^{N} \binom{N}{j} x^j (1-x)^{N-j} \sum_{i=1}^{j} e^{-\frac{xqt}{mV}} \frac{\left(\frac{xqt}{mV}\right)^{i-1}}{(i-1)!} \qquad \text{---------(2.47)}$$

The variation of the above expression (Eq. 2.47) as a function of reducing the effective time is illustrated by five graphs in Figure 2.42, where each graph is characterized by a given degree of channeling.

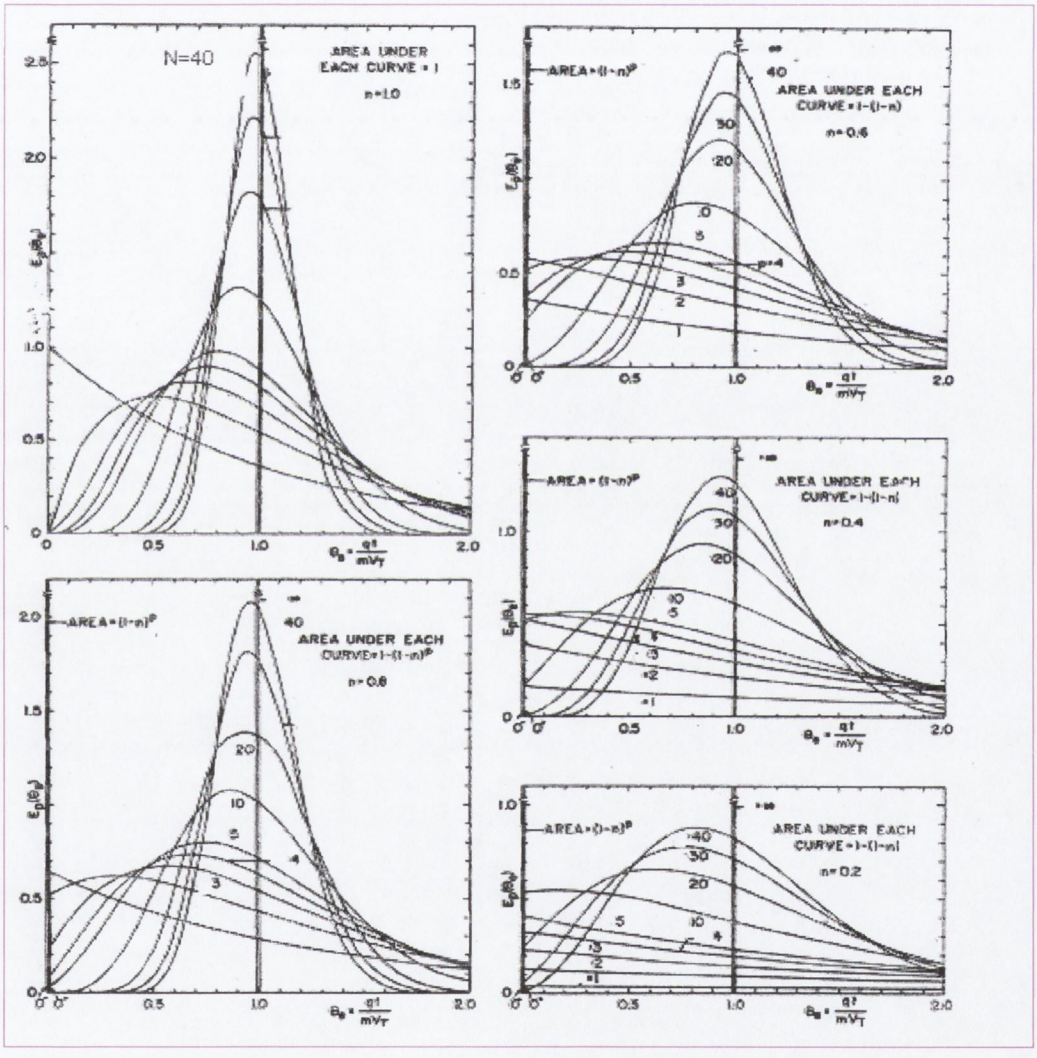

[Note (1,2,.....∞=N (number of tank in

Figure 2. 42 Residence time distributions as a function of the reduced effective time for different cascades of a given total volume [Chiang and Cholette, 1971].

The curves, similar to those obtained for the dispersion model [Levenspiel, 1999] indicate that the model can represent the mixing condition extending all the way from an imperfectly mixed reactor to plug flow. Each graph in Figure 2.42 is used to represent a family of curves obtained for a given value of x, equal to 1.0, 0.8, 0.6, 0.4 and 0.2 respectively. In the graph for x=1, the curves represent the case of perfect mixing when m is also taken as equal to only. In this case, the curve for a single reactor, n=1, represents what should be expected from one CSTR. Also, as N increased, the curves show their tendency in moving towards the plug flow condition, represented at the limit by an infinite number of reactors in series.

Again this model has been used essentially in order to understand the hydraulic system in the laboratory, where the concepts of such irregularities (dead-zones and short-circuit) were introduced, but does not appear to have been trialed under full-scale process conditions.

2.7.4 Case Study [after Rehakova and Novosad, 1968]

An alternative mathematical model for expressing the RTD in a multi-stage system with back mixing between stages and non-ideal mixing in each stage has been suggested Rehakova and Novosad (1968). This non-ideal behavior has been taken into account by assuming that each stage of the reactor consists of a series of ideally mixed, internal reactors with back mixing between the internal reactors and adjacent reactors as illustrated in Figure 2.43. The following mathematical model gave the mass balance of the tracer in dimensionless form used for the study.

$$\frac{1}{NS}\frac{dc_{1j}}{d\theta} = (1+r)C_{S(j-1)} + bC_{2j} - (1+b+r)C_{1j} \qquad ----------(2.48)$$

The mathematical model has three parameters; the number of ideally-mixed, internal reactors, S, the coefficient of back mixing between the internal reactors, b, and the coefficient of back mixing between stages, r. Calculation of the RTD curve to an instantaneous or pulse tracer injection corresponding to a given set of parameters was performed by setting up mass balance differential equations across the individual reactors.

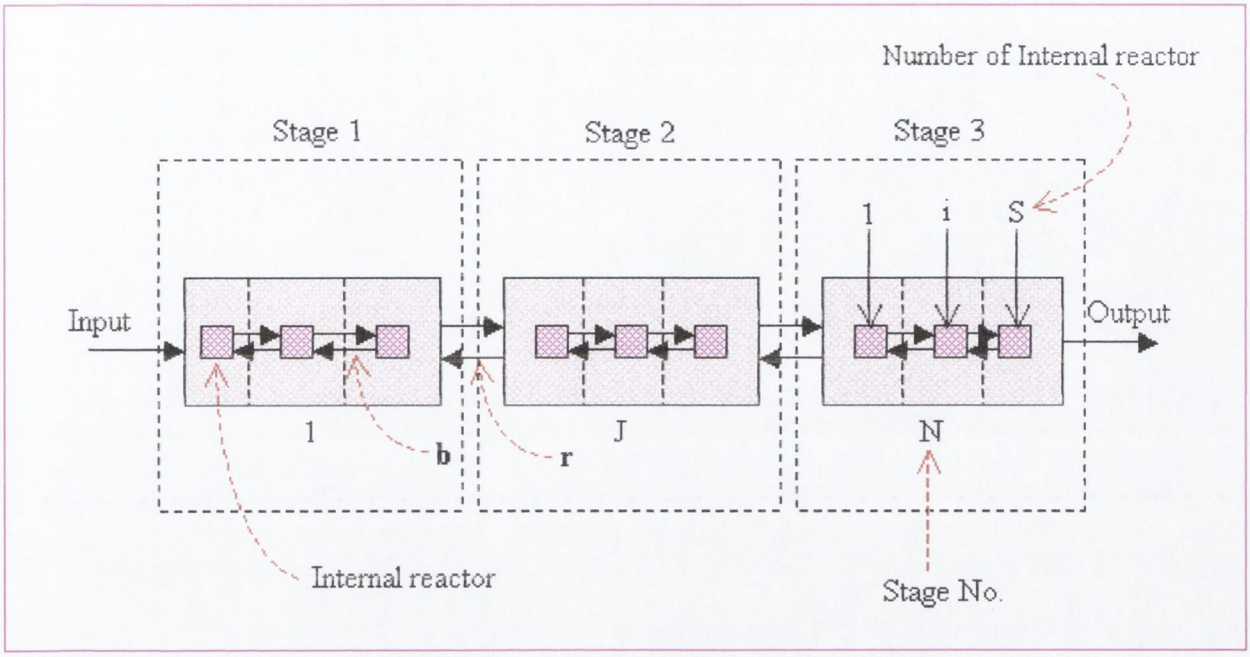

Figure 2. 43 Schematic representation of mathematical model [after Rehakova and Novosad 1968]

It was also shown that for a mechanically agitated multistage column with stage height to diameter ratio of 1, the best fit to experimental curves was obtained for a value of S=3, indicating that the parameter S depends only on the geometry of the system. The model has also been described as analogous to the circulation model proposed by Van de Vusse (1962) as shown on Figure 2.44 where the coefficient of back mixing is b and can be calculated by using the following equation.

$$b = const.\frac{nd^3}{Q} \qquad --------(2.49)$$

where: d = the stage diameter

The parameters of the Rehakova and Novosad model were compared with the Van de Vusse circulation model revealing that the parameter S seems to be analogous with parameter n_v (Eq 2.50) which expresses the diffusivity inside the circulation loop by the number of ideally mixed reactors in-series. Similarly, this parameter n_v also depends only on the geometry of the system and not on the other variables.

$$r_v = \frac{S(S - n_v - 2n_v b) + 2n_v(b + b^2)\left(1 - \exp\left(-S \ln \frac{b+1}{b}\right)\right)}{Sn_v(1 + 2b - S) - 2n_v(b + b^2)\left(1 - \exp\left(-S \ln \frac{b+1}{b}\right)\right)} \qquad \text{---------(2.50)}$$

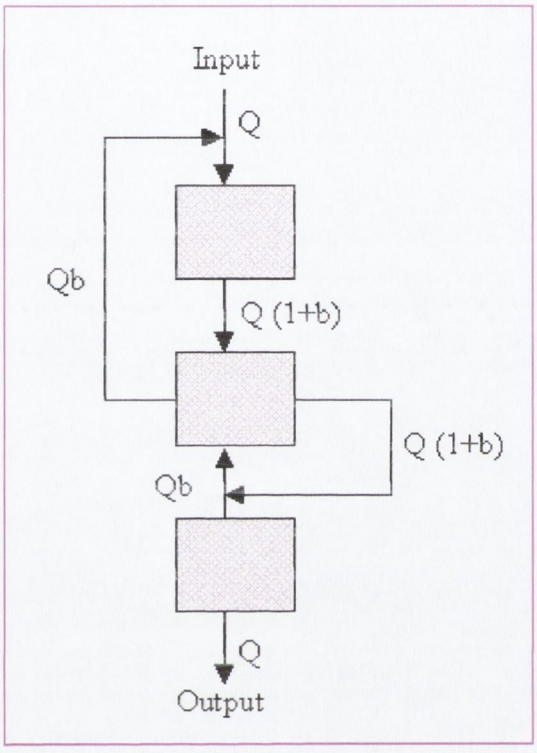

Figure 2. 44 Circulation model [after Van de Vusse, 1962].

Hence, the Rehakova and Novosad model introduced the concept of how a series of ideally mixed internal reactors with back mixing between each other can be used in order to understand the behaviour of such a system. There is also an interesting comparison between the numbers of ideally mixed internal reactors with the diffusivity inside the circulation loop proposed by Van de Vusse. This study does provide an analysis of any hydraulic irregularities that could occur inside such a system but does not appear to provide any further diagnosis concerning which reactor in the net work is exhibiting such problems and thus needs to be corrected.

2.7.5 Case Study [after Falconer and Tebbutt, 1986]

A significantly different and more practical method of studying the RTD was taken by Falconer and Tebbutt (1986) when studying the hydraulic performance of circular, rectangular and other shaped chlorine contact tanks. It was found from analysis of the

general RTD curve (see Figure 2.45) that the parameters took the form of various dimensionless hydraulic ratios involving a comparison with the theoretical retention time, T. These dimensionless time ratios, originally interpreted by Villemonte and Rohlich (1962) as criteria for hydraulic characteristics, are defined as follows,

t_i/T : a measure of the most severe short circuiting with a value of 1.0 for ideal plug flow and zero for complete mixing;

t_p/T : a measure of the average short circuiting with a value of 1.0 for ideal plug flow and zero for complete mixing;

t_{90}/T : the dispersion index, a ratio of a mixing function to a short circuiting function, with a value of 1.0 for ideal plug flow and 21.9 for complete mixing;

t_a/T : a value of 1.0 for both ideal plug flow and complete mixing;

$(t_{90} - t_p)/(t_p - t_i)$: a measure of the symmetry of the dispersion curve about the time t_p/T. If greater than 1.0, the curve has a tail which suggests mixing and recirculation. If less than 1.0, the tail is reversed and indicates short-circuiting. It is indeterminate for ideal plug flow and infinite for complete mixing.

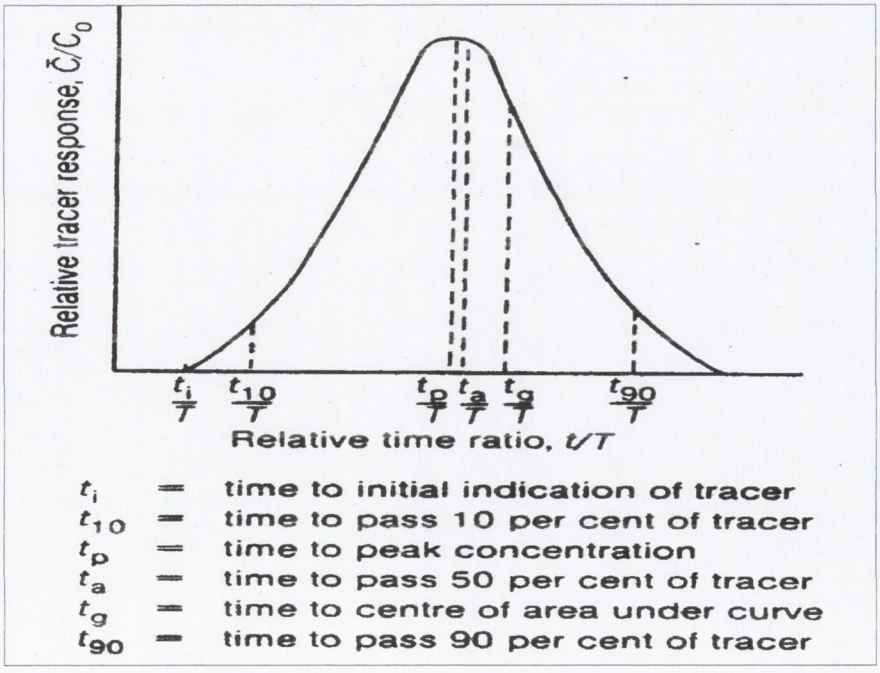

Figure 2. 45 Conventional parameters used for the flow through curve of a real basin [Falconer and Tebbutt, 1986]

The chlorine contact tank used in the study consisted of two independent chambers, the north and south tanks. The aim of the study was to attempt to reduce the degree of short-circuiting and the area of dead space by obtaining retention times which would be in closer agreement with the theoretical values. A schematic representation of the model used for this study is illustrated in Figure 2.46. Rhodamine (B) solution was introduced into the inlet supply by way of an aspirator jar and the tracer concentration was then continually monitored at the output point. The outlet RTD curve and the results obtained from the model are shown in Figure 2.47 and Table 2.3.

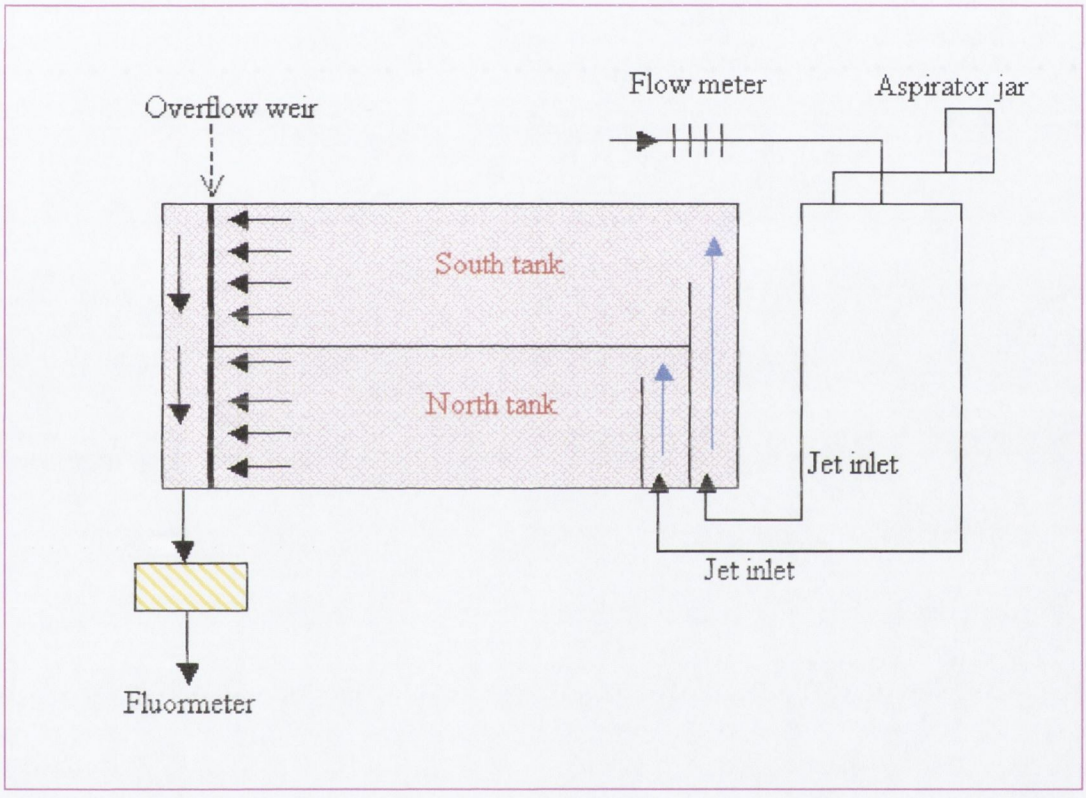

Figure 2. 46 Schematic representation of the model [after Falconer and Tebbutt, 1986]

Configuration	Time ratio						
	t_i / T	t_{10} / T	t_a / T	t_p / T	t_{90} / T	t_{90} / t_{10}	$(t_{90}-t_p) / (t_p-t_i)$
North tank	0.38	0.55	0.85	0.62	4.8	8.73	17.42
South tank	0.42	0.55	0.8	0.69	1.7	3.09	3.74
Theoretical North and South	0.60	0.80	≥1.0	1.00	1.20	1.50	0.50

Table 2. 3 The results from chlorine contact tank

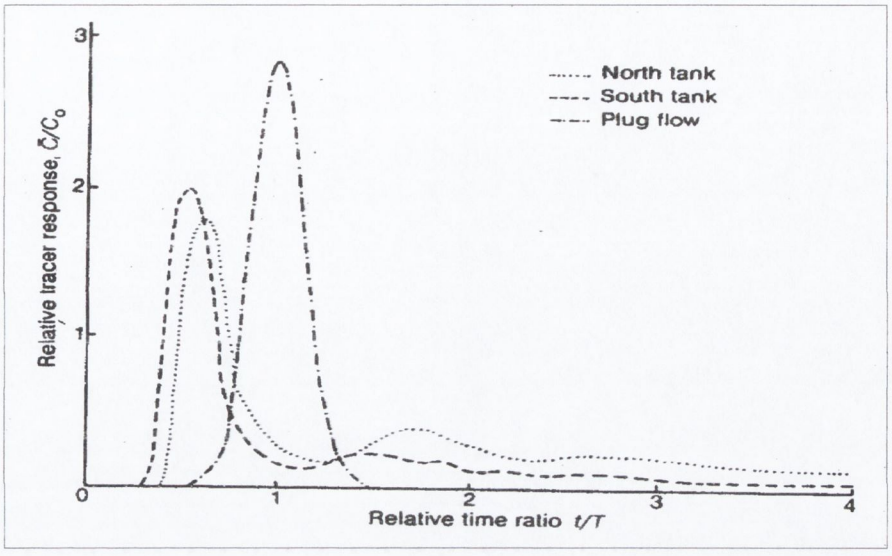

Figure 2. 47 The RTD curve for chlorine contact tank [Falconer and Tebbutt, 1986]

The results confirmed that both tanks exhibited short-circuiting, because t_i / T was less than the ideal value of 0.6 in both cases. The time ratio t_a /T is indicative of the mean retention time in the tank and ratios slightly greater than unity would have been preferable for such process rather than values of 0.85 and 0.8. The model retention time index t_p / T also confirmed the occurrence of short-circuiting, with values of about 0.6 and 0.7 for the north and south tanks respectively, which also suggested that an undesirable degree of recirculation and mixing occurred. The dispersion index t_{90} / t_{10} confirmed that both tanks were exhibiting mixing since the evaluated time ratios were larger than the theoretical plug flow value of approximately 1.5. Finally, the apparent high degree of asymmetry of the dispersion curve for the north tank in particular was substantiated by the value of approximately 17 for the time ratio, $(t_{90}-t_p)/ (tp- t_i)$. Such a high value was close to the theoretical value of 21.9 for ideal mixing, as compared with the theoretical value for plug flow, conditions of about 0.5. In summary, these results obtained using this model technique confirmed that the hydraulic characteristics exhibited in both tanks were not particularly close to the desired plug flow conditions, because of pronounced short-circuiting and, to a lesser extent, dead-zones.

The method described provides a good guide to characterising the RTD curve. The results presented are reasonable, but do not provide any method for how one can find out the comparative magnitude of the hydraulic irregularities. In addition, this method

has been used for just two stand alone chlorine contact tanks and there is no indication as to whether this method can be used in networked reactors or not.

2.7.6 Case Study [after Higgins *et al.*, 1999]

A series of laboratory experiments were used to assess the efficiency of a hydrodynamic vortex separator (HDVS) as a mixing device for tertiary treatment applications in the water industry [Higgins *et al.*, 1999] (see Figure 2.48). The device investigated was a 750-mm dia. HDVS. A horizontal pipe (about 24-pipe diameters in length) directs the flow into the device, and at approximately 12-pipe diameters a dosing point is located for the RDT pulse injection. Inlet flow control was provided by a gate valve and flow was measured by a calibration turbine-style flowmeter. The macromixing within the HDVS was characterized by investigating the RTD obtained experimentally by a pulse input of lithium chloride in a tracer study. The experimental RTD was then compared with the theoretical mixing regimes of plug-flow and complete-mix, and any differences investigated as a result of non-ideal mixing.

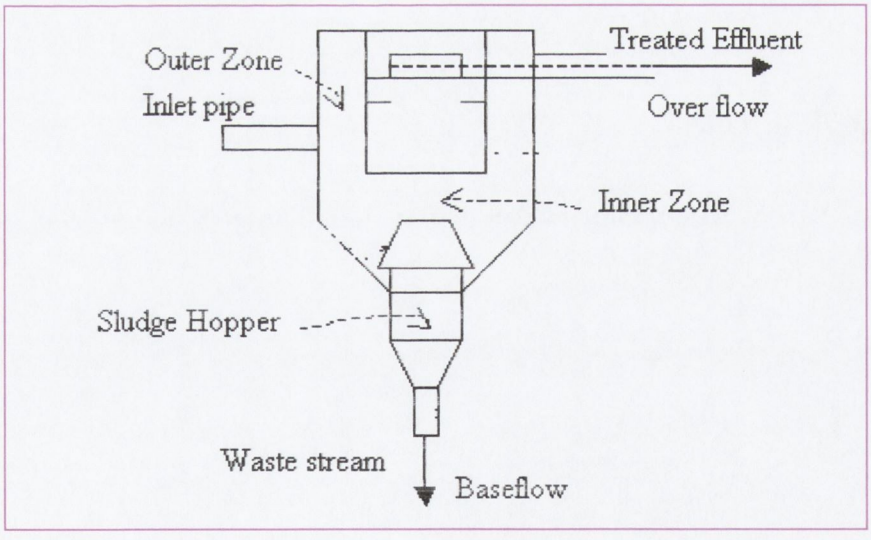

Figure 2. 48 Configuration of hydrodynamic vortex separator [after Higgins *et al.*, 1999].

Experiments were conducted with zero baseflow for range of flow-rates (0.25-8.0 l/s), providing theoretical retention times of 1-30min. The normalized exit-age distribution function for the range of flow rates investigated is shown in Figure 2.49.

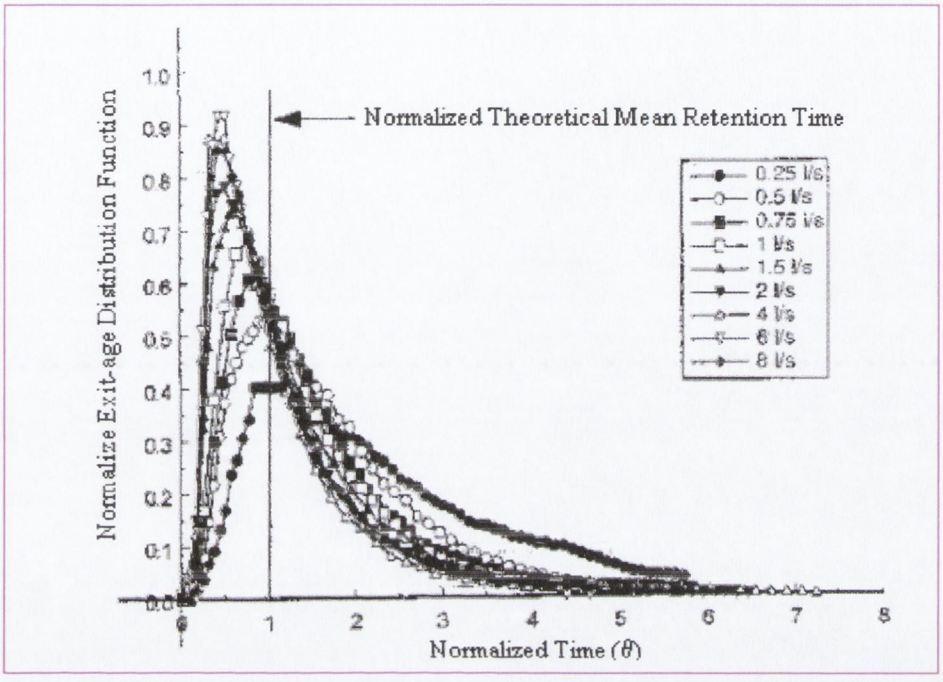

Figure 2. 49 Comparison of normalized distribution curves for different flow rate [after Higgins *et al.*, 1999].

These curves illustrate plug-flow mixing (evidenced by a significant peak on the curve) with a degree of non-ideal flow behavior. There was also a significant tailing effect of the curve, with tracer detected at approximately 6 times the theoretical retention time which demonstrated that stagnancy was present, resulting in dead spaces and some degree of short-circuiting within the device. The curves also were classified into two sets of curves with the transition point at approximately 1.5 l/s. The first set of curves (2-8l/s) illustrated an early sharp peak indicating some short-circuit. The second set of curves, at low flow rates (<1.5 l/s) showed that the largest fraction of tracer left close to the theoretical retention time, and hence the total volume is active in the mixing process.

The first and second moment of each RTD was calculated using the method of moments [Charles, 1996; Levenspiel, 1999] that was described previously (see Section 2.2.1.1) across the full experimental data for flow-rates as shown in Table 2.4. The estimated experimental mean retention time was significantly greater than the theoretical mean

retention time, with the largest error at lower flow-rates and longer contact times (+44%). For all experiments, the HDVS was operated with zero baseflow and under this condition it was suggested that the sludge hopper (see Figure 2.48) behaved as a stagnant zone. As shown in Table 2.4 the mass balance associated with a flow-rate of 1.5 l/s illustrated that some background concentration of tracer must have existed.

Flow-rate	Theoretical mean retention time	Mean retention time	Variance	Mean retention time error	Mass balance
(l/s)	(min)	(min)	(min^2)	(%)	(%)
0.25	30.9	67.4	1645	44	67
0.50	15.4	26.5	246.8	42	71
0.75	10.3	15.8	108.5	35	82
1	7.7	10.6	45.8	27	96
1.5	5.1	7.9	30.2	35	106
2	3.8	4.6	12.5	18	90
4	1.9	2.2	3.8	15	92
6	1.2	1.5	1.3	15	100
8	0.9	1.2	0.9	20	99

Table 2. 4 Comparison of RTD first and second moments [after Higgins *et al.*, 1999].

In addition, Table 2.5 displays the two model parameters from the method of moments (the number of tanks in-series and peclet number) and normalized variance, which was given as an indication of the flow regime relative to the extremes of perfect plug-flow and complete-mix.

Flow-rate	Normalized Variance	Peclet Number	No. of CSTR
(l/s)			(n)
0.25	0.36	4.24	2.76
0.50	0.35	4.42	2.84
0.75	0.43	3.25	2.30
1	0.40	3.63	2.48
1.5	0.48	2.72	2.07
2	0.57	1.98	1.75
4	0.75	0.98	1.33
6	0.58	1.91	1.72
8	0.59	1.84	1.69

Table 2. 5 Comparison of model parameters calculated using moments [after Higgins *et al.*, 1999].

The Peclet number indicates a perfectly mixed regime and high dispersion, which concurs with the results reported by Levenspiel (1999) (see Section 2.6.2). The HDVS was found to be equivalent to 1.7 to 2.8 CSTRs depending upon the flow-rate. The two parameters for the model decreased as the flow-rate increased, which implies that the flow regime more closely approximated plug-flow at lower flow-rates as dispersion and mixing effects decreased. The model parameters also support the first observations that there are two sets of curves, with the transition at approximately 1.5 l/s.

The study also provided a comparison of the experimental exit-age distribution, to the tank in-series model and axial dispersion model [Levenspiel, 1999] using the experimental moments for 4 and 0.5 l/s (see Figures 2.50 (a) and (b)) respectively. The curves were compared visually, which indicated that the axial dispersion appears to more closely approximate the experimental RTD than the tank-in-series model.

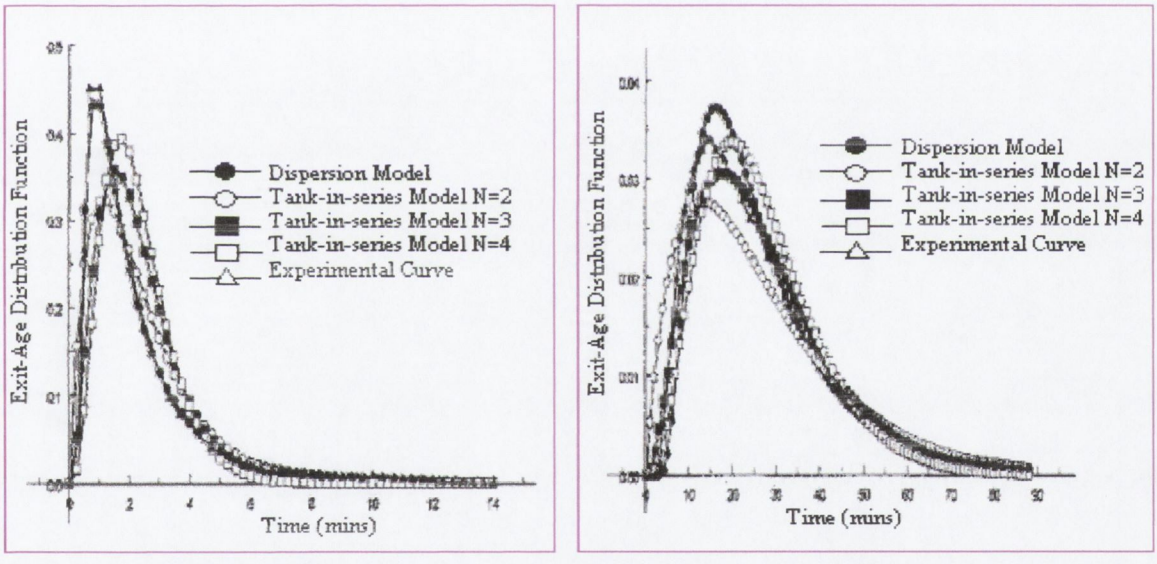

Figure 2. 50 Comparison of experimental and model E(t) curves (a) 4 l/s, (b) 0.5 l/s [after Higgins *et al.*, 1999].

In this case study, previously described formulae were applied and the concepts of the method of moments were reviewed. The research has provided a useful interpretation of the results, which could be used as guide to characterize the RTD although the comparisons were only made visually and are therefore not robust in all cases.

2.7.7 Case Study [after Shilton *et al.*, 2000]

Rhodamine WT was chosen as the tracer for this study to assess the hydraulic performance of a waste stabilisation pond in New Zealand to use it to highlight the severe impact that hydraulic short-circuiting has on treatment efficiency. This study is similar to several other studies on pond hydraulics achieved by the use of tracer studies [Mangelson and Watters, 1972; Chapple, 1985; Macdonald and Ernst, 1986; Moreno, 1990; Uluatam and Kurum, 1992; Pedahzur *et al.*, 1993 Frederick and Lloyd, 1996]. The pond system consisted of a single facultative pond 145m by 140m in size with a small 2.2Kw aerator/mixer located in one corner directly at the end of the inlet pipe. Two separate tracer runs were undertaken on the pond each one over a period of 48 days. The method of moments described previously (Levenspiel, 1999) for analysis non-ideal flow, was used to calculate treatment efficiencies from the tracer data. In order to allow direct comparison of the runs, the tracer data was normalized so that the area under the RTD curve was equal to unity, as illustrated in Figure 2.51. Both runs recorded the tracer arriving at the outlet within the first three hours. The data displayed a very rapid rise to a high peak, followed by a slow, steady decrease with a long tail, which would be expected, from a CSTR suffering from short-circuiting. The mean retention times were 18.6 days for Run 1 and 17.7 days for Run 2. The tails represent the tracer becoming well mixed and then slowly being diluted and washed out of the pond.

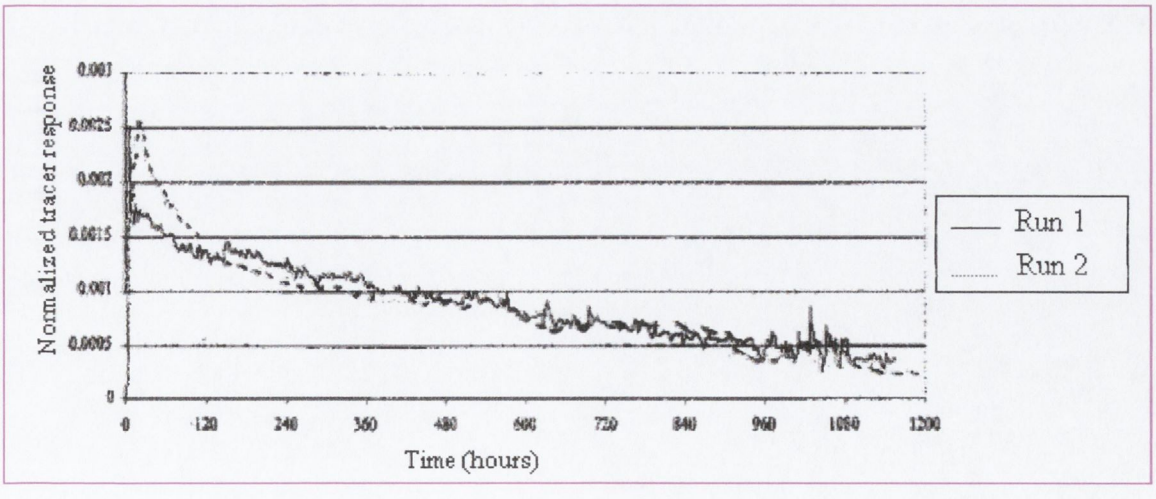

Figure 2. 51 Normalized hydraulic retention time distributions-full data [after Shilton *et al.*, 2000]

Some variation between the two runs can, however, be seen at the beginning of the runs with an enlargement of the first five days of data shown in Figure 2.52, whereby Run 1 reached an earlier peak whilst Run 2 showed a greater overall recovery of tracer (area under the curve). This could have been due to the background concentration from Run 1 that may have had a direct affect on the beginning of the RTD curve on Run 2 (see Figure 2.52) and should have been taken into account in the analysis. The shape of the RTD curve would also point to the effect of dead-zones, which may be the cause of an increase in the area under the RTD curve in Run 2. This case study demonstrated the existence of short-circuiting through the pond which was causing low treatment efficiencies. More generally, it illustrated the importance of hydraulic pond design in order to avoid the effluent being discharged before its required retention period. It was also illustrated that any change to the pond shape (by baffling for example) or the inlet/outlet configuration that could delay the arrival of tracer at the outlet, for even a short period, had the potential to significantly improve the water quality of the discharge.

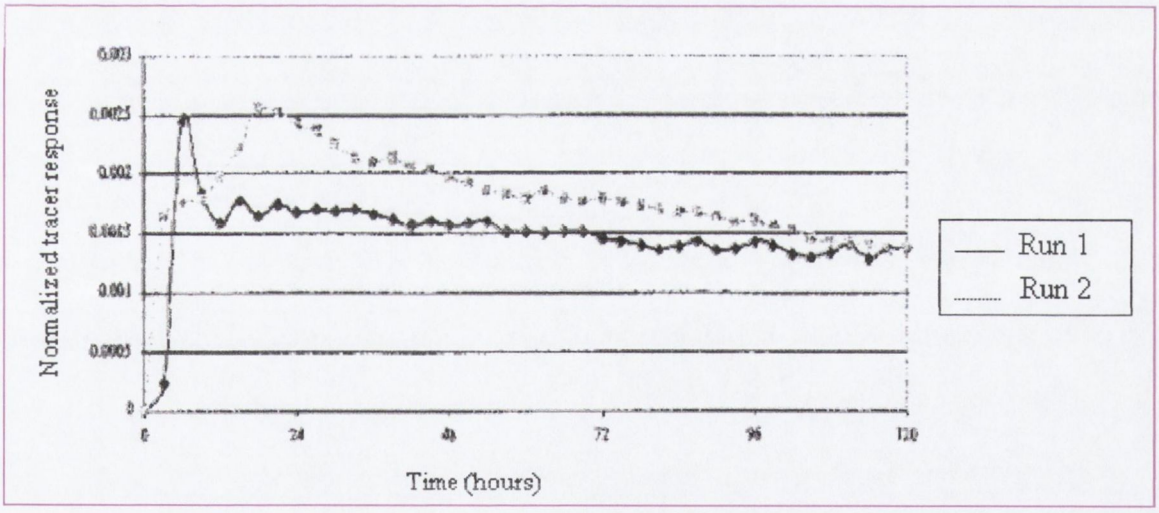

Figure 2. 52 Hydraulic retention time distributions-first five days of data [after Shilton *et al.*, (2000)]

2.7.8 Case Study [after Joel *et al.*, 2001]

The integrated disinfection design framework IDDF is an approach to determine disinfection requirements for drinking water treatment facilities [Bellamy *et al.*, 2000]. by more accurate analysis of the disinfection process. The IDDF model was created

with three components that collectively determine site-specific disinfection requirements: disinfection contactor hydraulics, disinfection demand and decay rate and pathogen inactivation kinetics. The approach relies on the accurate hydraulic characterization of the disinfection contactor, which can be described exclusively by the open form of the plug flow dispersion (PFD) model. This model was assumed when the T_{10}/HRT ratio is less than 0.5, a condition that is relatively common, where HTR is the mean hydraulic residence time and (T_{10}) is the time in which 10% of the fluid parcels will have reached the effluent. The hydraulic characterization module for generating the RTD data, was broken down into three levels for data input/collection techniques:

- Basic: dispersion coefficient **D** for input into the PFD model, number of tanks **n** for input to the complete mix tanks-in-series model.
- Standard: Full-scale experimental tracer study using a neutrally buoyant tracer chemical.
- Advanced: a Computational Fluid Dynamics model.

As discussed previously the plug flow dispersion PFD model assumes that mixing occurs in the flow direction caused by velocity gradients and that lateral or radial mixing is negligible. Environmental systems where PFD models work best include long narrow channels, packed beds, fluidised beds, and any system where a majority of the dispersion occurs in one dimension [Levenspiel, 1999; Clark, 1996]. A pulse input tracer test using fluoride was conducted through a group of six filters in series at Alameda County Water District [Bellamy *et al.*, 2000]. The tracer was injected in an open channel up-stream from the filters and then collected in the combined effluent channel. The data was fitted with the open form PFD (Eq.2.40) model and the Gamma extension n-tank in series model (Eq. 2.41). The parameters **n**=4.05 (number of tank-in-series) and **D**=0.147 (dispersion number) were determined by minimizing the sum of the differences squared between the data and the model residence time density.

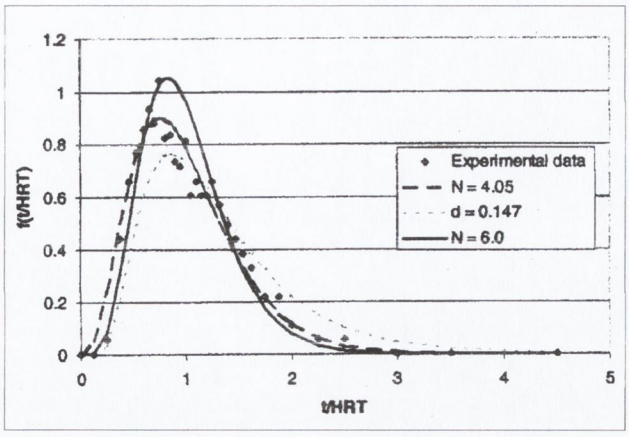

Figure 2. 53 Comparison between experimental and direct numerical model RTD curve: complete mix tanks in series (n) and PFD model (d)

[Bellamy *et al.*, 2000]

As shown from the results in Figure 2.53 above, the n-tanks in series model provided a better fit to the experimental data than the PFD model.

Other research has shown similar results using single-parameter models on chlorine contactor tanks and also that multi-parameter models fit the experimental tracer data better [Crozes *et al.*, 1998]. In this case the **n** or **D** values were determined by using the process length to width ratio, (L/W), as illustrated by the data in Figure 2.54 from a series of tracer experiments in different contactors. Each tracer test RTD curve was then fitted with the n-tanks in series model to develop the relationship between **n** and L/W.

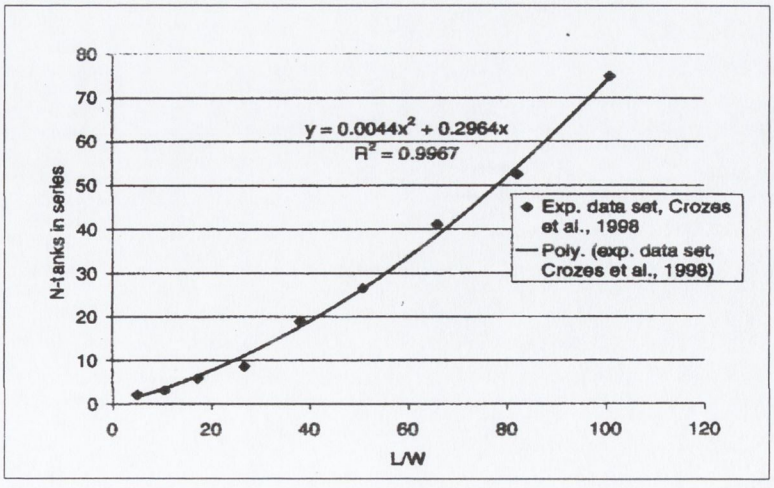

Figure 2. 54 Data conversion for reactor length to with to n for n-tanks in series model [Bellamy *et al.*, 2000]

A step-input tracer study using fluoride was conducted on the disinfection contact basin at the Marston WTP [Haas *et al.*, 1997] as shown schematically in Figure 2.55. The experimental tracer tests were conducted at three target flow rates (20, 40 and 80 MG/d), which corresponded to theoretical residence times of 257, 129, and 67 minutes, respectively. The resulting RTD curves from the tracer tests are illustrated in Figure 2.56 as a function of dimensionless time that was normalized by the theoretical time for each respective flow rate. The curves show that the Marston contactor had a high hydraulic efficiency with T_{10}/HRT greater than 0.8. In the 40 and 80 MG/d experiments the T_{10}/HRT factors are so close to 1 that the shape of F(t/HRT) more resembles that of a plug-flow reactor. The 40 and 80 MG/d experiments showed that there was some dispersion, as seen by the amount of time it takes the RTD function to reach a value of 1. It was found that the results in Figure 2.56 suggest that the dimensionless time for the 40 and 80 MG/d trials could be incorrect which was checked by analyzing the F(t/HRT) using the non-linear least squares method NLLS.

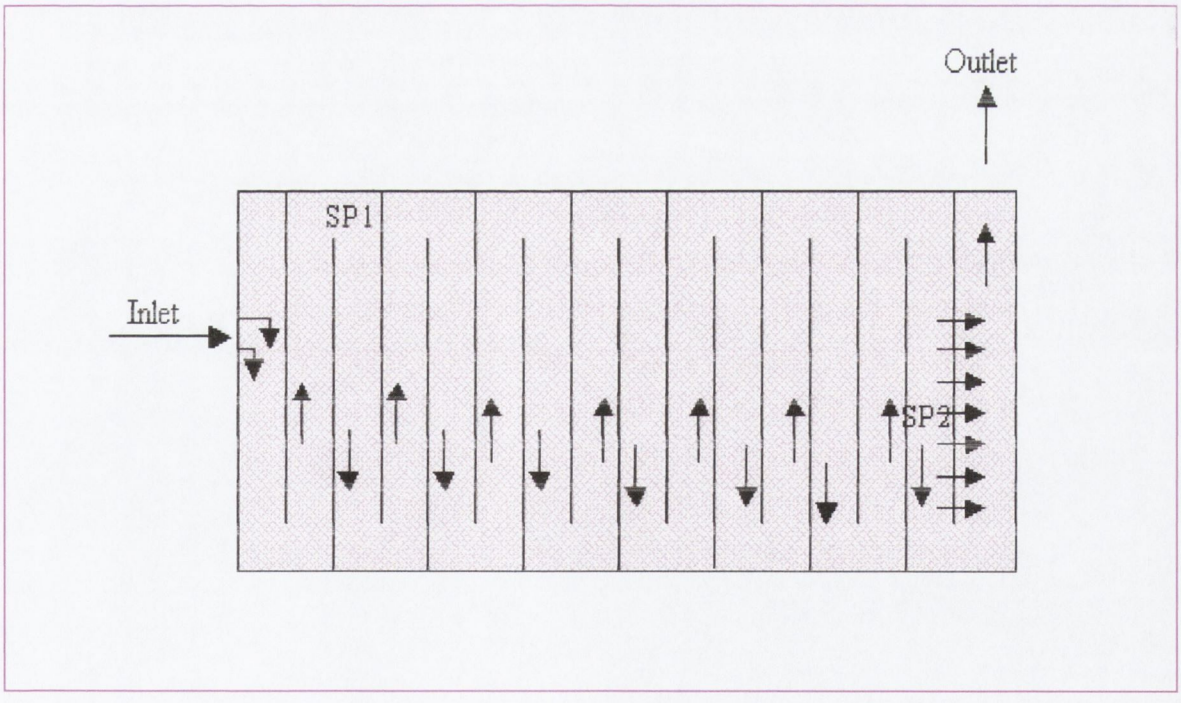

Figure 2. 55 Schematic of Marston WTP contactor [after Haas *et al.*, 1997]

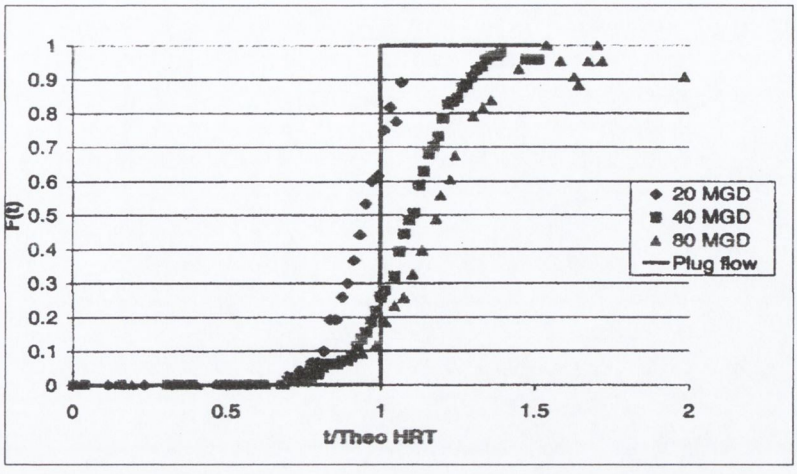

Figure 2. 56 Experimental RTD function for Marston Contactor; time normalized with theoretical HRT [after Haas *et al.*, 1997]

The NLLS method consists of fitting a non-linear function to the experimental residence time density data and minimizing the following objective function:

$$SSR = \sum_{i=1}^{N} \left(f(t_i)_{EXP} - f(t_i)_{NLF} \right)^2 \qquad \text{----------(2.51)}$$

Where: SSR=sum of the squares error;

$f(t_i)_{\exp}$ = experimental residence time density data at time t_i ; and

$f(t_i)_{nlf}$ = non-linear residence time density function value at time t_i

The non-linear residence time density function used in the NLLS method is the Nauman / Buffham (1983) extension of the dispersion model and is described as,

$$f(t) = \sqrt{\frac{HRT}{2\pi t^3 \sigma^2}} \exp\left[-\frac{(t - HRT)^2}{2HRTt\sigma^2} \right] \qquad \text{----------(2.52)}$$

where σ^2 is the dimensionless variance and HRT and σ^2 were used as the fitting parameters.

Haas *et al.*, (1997) compared the NLLS method with the traditional method of moments to compute the experimental HRT and found that the NLLS method was more accurate. The NLLS analysis for the 20 MGD data set is displayed in Figure 2.57, which determined the experimental HRT to be 252 minutes. Although F(t/HRT) did not reach

"1" during the tracer test at the 20MG/d level, the NLLS method was shown to accurately determine the experimental HRT value with a maximum F(t/HRT)=0.75. The NLLS analysis predicted that the experimental HRT would be 144 and 81 minutes for the 40 and 80-MG/d RTD functions, respectively, which are higher than the theoretical values (of 129min and 67 min).

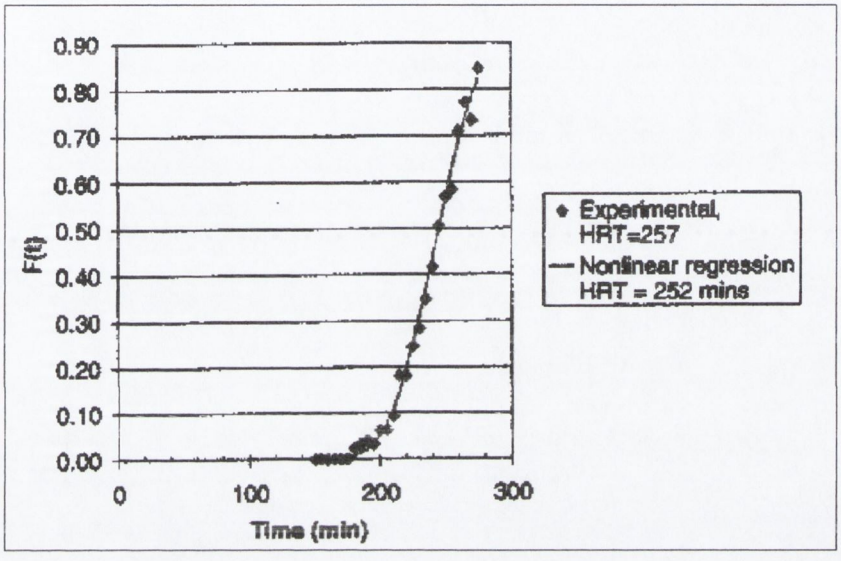

Figure 2. 57 Non-Linear least square analysis of experimental tracer teats at 20 MG/d [Haas *et al.*, 1997]

Finally, the study also showed how a CFD package was used to reduce the cost of chlorine in wastewater plant by 66% [Sanjay *et al.*, 2001]. However, as discussed earlier the use of CFD in terms of reactor characteristic is outside the scope of this thesis.

2.8 Conclusion

Numerous models of multistage reactor networks have been investigated and various theoretical frameworks have been considered in this chapter. Several of these models have been tested by carrying out tracer studies on multi-stage systems where reactors were connected either in parallel or in series. Each of these studies has provided an individual perspective on how to study the hydraulic behaviour of different treatment process, which encourages an originality of approach for any new researcher to investigate areas that have not been explored in sufficient detail. In particular, with

regard to this research, a major deficit seems to be a method for the identification of a specific reactor in a network which may be causing the problem and thus needs to be corrected. The relative percentages of fluid flow passing through dead-zones, short-circuits and perfectly mixed zones existing in the reactors also need to be quantified.

Another consideration and motivational force behind this research has been its economic implications. In both the Water and Oil industries, an understanding of how fluids mix within a reactor is essential. This applies whether the desired outcome is a homogeneous product or, an optimum volume within the reactor that is necessary for the required reaction. The focus of this study is the problem of obtaining such hydraulic performance in an industrial process so that in the future such inefficiencies in the process can be identified and eradicated. The aim is therefore to develop a simple cost effective technique to identify such problems, which can then be corrected once the inevitable economic implications to operational and production costs have been reached.

Chapter 3

Model Development

Chapter 3

Model Development

3.1 Introduction

As described in Chapter 2 the two basic models commonly in use to describe the hydraulic behaviour of a system are the dispersion model and the tank-in-series model. The different kind of model generally used in hydraulic flow characterization depends on whether the flow is considered to be plug, mixed, or somewhere between the two. The aim of this research is to show how to use the concept of RTD in order to analyse a variety of reactor networks comprising of several tank in-series as commonly used in process industries.

3.2 Reactor Modelling using RTD

There are many situations where the fluid in a reactor is neither well mixed nor approximates to plug-flow [Levenspiel, 1999]. Consequently, real reactors can be modelled in a number of ways. Each model can be classified according to the number of adjustable parameters that are extracted from the RTD data. The RTD (see Section 2.1) enables us to determine how long the various fluid elements have been in the reactor, but does not enable us to learn anything about the exchange of matter between the fluid elements. Mixing is therefore one of the major factors controlling the behaviour of the reactor.

The combination and /or modification of an ideal reactor (see Section 2.4.1) has been used to represent real reactors and, with this technique, a model has been classified as being either a one-parameter model (the tank in-series model or dispersion model) or a two-parameter model (a real reactor modeled as a combination of ideal reactors).

3.2.1 One Parameter Models

Single parameter models are often used to account for the non-ideality of reactors [Fogler, 1999]. Examples of one-parameter models are the CSTR and PFR models, as discussed in Chapter 2. In a tank in-series model, the parameter that is determined is the number of tanks, **n.** In the dispersion model, the equivalent parameter of interest is the

dispersion coefficient, **D**. These parameter values can be evaluated using measured effluent concentrations for the reactor by means of an RTD from tracer studies.

When analyzing ideal tubular reactors, for example, it has been assumed that the fluid moves through the reactor in a piston-like manner, PFR, whereby every molecule takes an identical length of time. Hence, the velocity profile is flat and there is no axial mixing. Both of these assumptions are false to some extent in real tubular reactors and frequently they are sufficiently false to warrant some modification. The more popular tubular reactor models need to have some means whereby failure in the plug-flow model is allowed for, as well as the allowance for some axial mixing assumptions. Examples include the unpacked laminar flow tubular reactor, the unpacked turbulent flow, and packed bed reactors. One approach involves modeling the non-ideal tubular reactor as a series of identically sized CSTRs. The other approach (the dispersion model) involves a modification of the ideal reactor by imposing axial dispersion on plug-flow.

3.2.1.1 Dispersion Model

The dispersion model is used to describe non-ideal tubular reactors in which axial dispersion of the tracer is assumed [Levenspiel, 1999; Ostergaard and Michelsen, 1969].

To characterize this dispersal (as shown in Figure 3.1), a diffusion-like process is superimposed on the plug-flow model. A dispersion coefficient, **D** represents this spreading process, whereby,

- Large **D** means rapid spreading of the tracer curve.
- Small **D** means slow spreading.
- **D** = 0 means no spreading, hence plug-flow.

Also, a dimensionless group $\left(\frac{D}{ul}\right)$ is used to characterise the spread in the whole reactor. The mathematical representation of this model was given in Section 2.6.1.

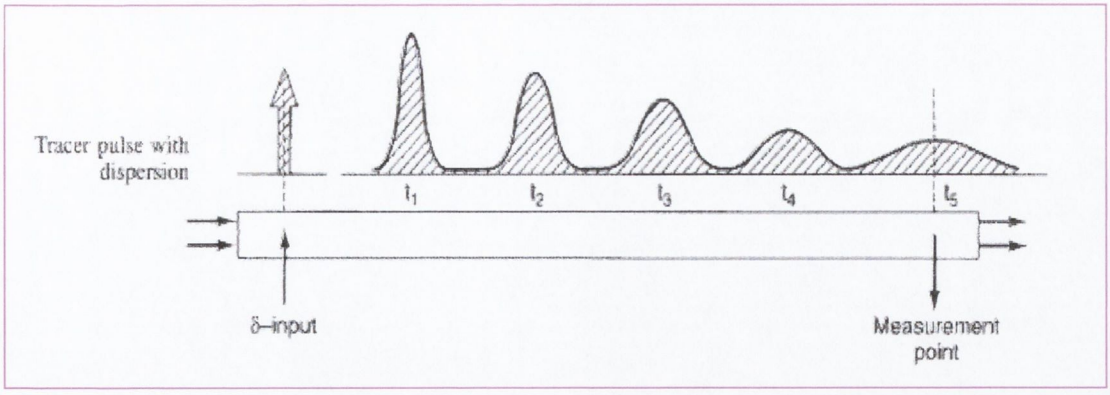

Figure 3. 1 The spreading of tracer according to the dispersion model [Levenspiel, 1999].

3.2.1.2 Tank In-Series Model

In a tank in-series model the RTD can be analyzed so as to determine the number of ideal tanks in-series that will give approximately the same RTD as the non-ideal reactor. For example, an RTD is analysed from a tracer pulse injected into a first reactor of three equally sized CSTRs in series (see Figure 3.2) from which a generic equation for **n** tanks-in-series is derived.

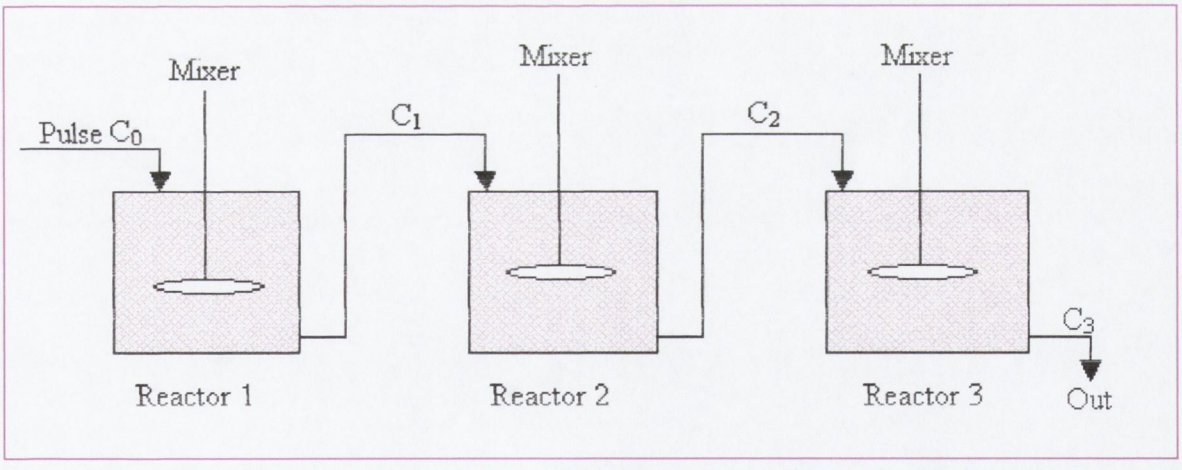

Figure 3. 2 Tank-in-series model

Using the definition of the RTD presented in Section 2.2.1, the fraction of material leaving the overall system of the three reactors (i.e., leaving the third reactor), which has been in the system between times (t) and (t+Δt) is,

$$E(t) = \frac{C_3(t)}{\int_0^\infty C_3(t)dt} \qquad \text{----------(3.1)}$$

A mass balance on the first CSTR gives,

$$V_1 \frac{dC_1}{dt} = -QC_1 \qquad \text{----------(3.2)}$$

which is integrated to give the expression for the tracer concentration in the effluent from the first reactor.

$$C_1 = C_0 e^{-\frac{Qt}{V_1}} = C_0 e^{-\frac{t}{\tau_i}} \qquad \text{----------(3.3)}$$

If the volumetric flow rate is constant, $Q = Q_0$ and all the reactor volumes are identical $V_1 = V_2 = V_i$, it follows, therefore that all the residence times of the individual reactors are identical $\tau_1 = \tau_2 = \tau_i$.

Thus, the concentration of the tracer in the effluent from the second reactor is given as,

$$C_2 = \frac{C_0 t}{\tau_i} e^{-\frac{t}{\tau_i}} \qquad \text{----------(3.4)}$$

Equally, the concentration of tracer in the effluent from the third reactor is given as

$$C_3 = \frac{C_0 t^2}{2\tau_i^2} e^{-\frac{t}{\tau_i}} \qquad \text{----------(3.5)}$$

Therefore, the generalized expression for the effluent concentration for **n** reactors in series is,

$$C_n = \frac{C_0}{(n-1)!}\left(\frac{t}{\tau_n}\right)^{n-1} e^{-\frac{t}{\tau_n}} \qquad \text{----------(3.6)}$$

Thus, a series of **n** CSTRs gives the RTD, E(t) as,

$$E(t) = \frac{t^{n-1}}{(n-1)!\tau_i^n} e^{-t/\tau_i} \qquad \text{----------(3.7)}$$

Because the total reactor volume is nV_1, then $\tau_i = \tau/n$, where τ represents the total reactor volume divided by the flow rate Q,

$$E(\theta) = \frac{n^n(\theta)^{n-1}}{(n-1)!} e^{-n\theta} \qquad \text{----------(3.8)}$$

Where $\theta = t/\tau$.

Figure 3.3 illustrates the structure of the physical model for the tank in-series model. The RTDs of various numbers of CSTRs in series are shown in Figure 3.4 (a and b), and in a three-dimensional plot as shown in Figure 3.5. As the number of CSTRs becomes very large, the behavior of the system approaches that of a plug-flow reactor.

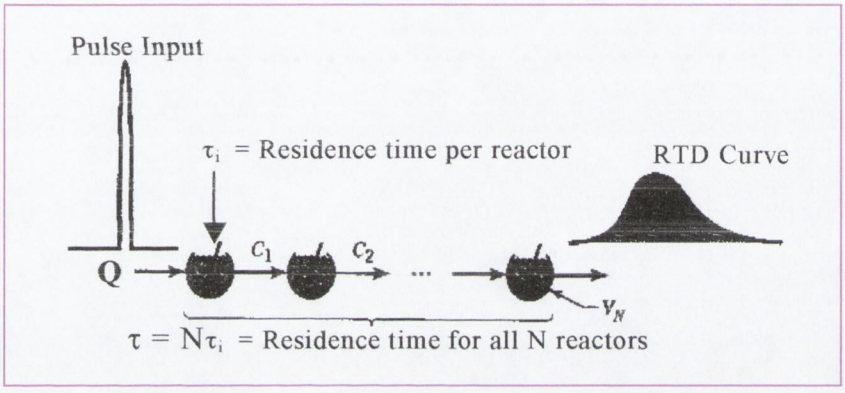

Figure 3. 3 The tank in-series model with its response [Levenspiel, 1999]

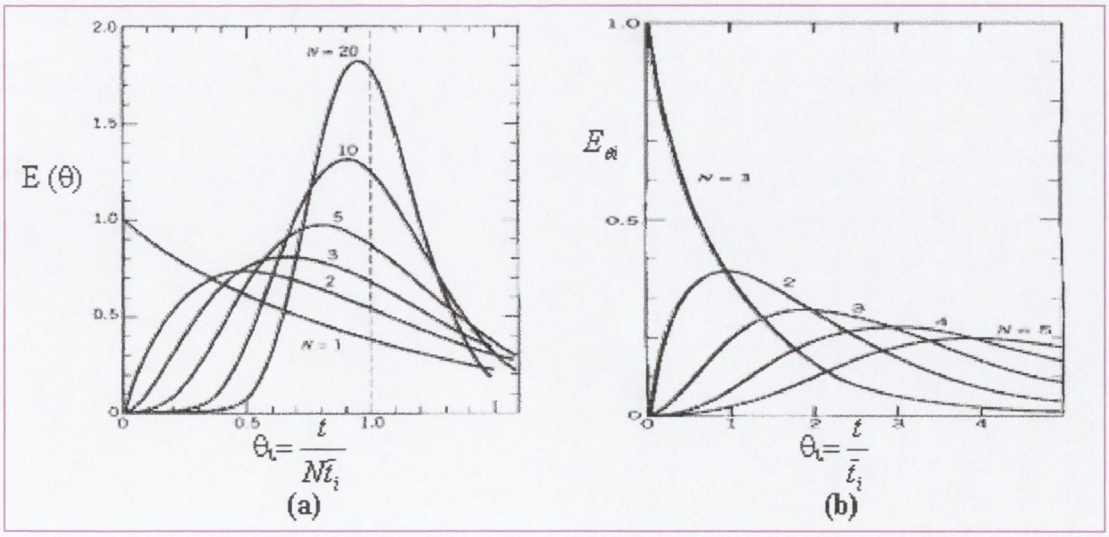

Figure 3. 4 RTD curves for tank in-series model for (a) 20 reactors and (b) 5 reactors [Levenspiel, 1999]

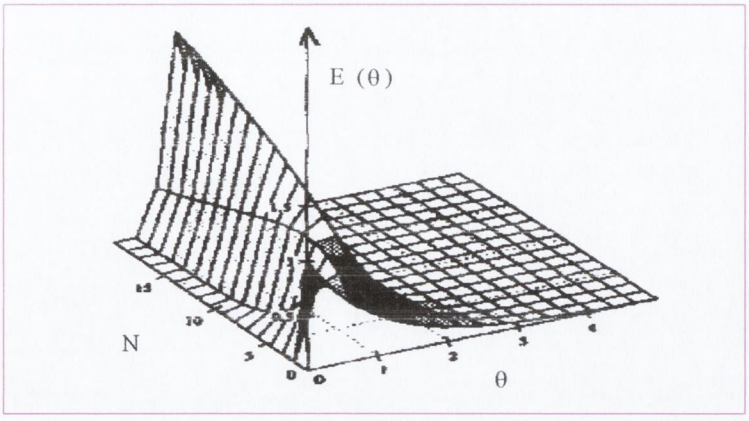

Figure 3. 5 Tank in-series response to a pulse tracer input for different numbers of tanks [Fogler, 1992]

The number of tanks in-series can be determined by calculating the dimensionless variance σ_θ^2 from the tracer experiment and is given as,

$$\sigma_\theta^2 = \frac{1}{n} \qquad \text{----------(3.9)}$$

Equation 3.9 shows that as the number of the tanks increase, the variance decreases.

Therefore, the number of ideal tanks in-series is;

$$n = \frac{1}{\sigma_\theta^2} = \frac{\tau^2}{\sigma^2} \qquad \text{----------(3.10)}$$

The tank in-series model was chosen as the basic model for this study over the dispersion model, since the performance of the plug-flow reactors with axial dispersion as discussed in Section 3.2.1.1 can be modelled as a series of complete-mix reactors in series. An example of this is the comparision of the RTD curves obtained for a plug-flow reactor with a dispersion number **D**=0.05, with the RTD curves obtained for 6, 8 and 10 CSTRs in-series (see Figure 3.6). As shown, all three of the CSTRs curves are fairly close and could be used to simulate a plug-flow reactor with a dispersion number of 0.05 [Metcalf and Eddy, 2001].

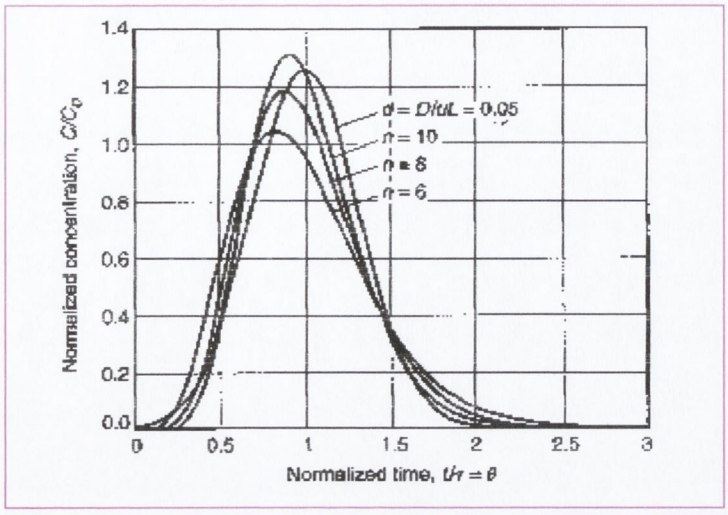

Figure 3. 6 Comparison of effluent response curves for a plug-flow and tank in-series models [Metcalf and Eddy, 2003].

3.2.1.2.1 Gamma Distribution

The Gamma distribution can be used to describe random variables bounded at one end. The Gamma probability density function is described mathematically as,

$$f(\theta,\alpha,\beta)=\frac{1}{\beta^{\alpha}\Gamma(\alpha)}\theta^{\alpha-1}e^{-\frac{\theta}{\beta}} \qquad \text{----------}(3.11)$$

where (in terms of a tank in-series model),

θ= normalized time ($\frac{t}{\tau}$)

t = time since start of tracer test

τ = theoretical retention time of reactor network

α= a parameter of the distribution which represents the number of tank in-series.

β = a parameter of the distribution which represents the dispersion of the tracer (or variance).

$\Gamma(\alpha)$= the gamma function, $=\int_0^{\infty}\theta^{\alpha-1}e^{-\theta}d\theta$

Note: $\Gamma(\alpha)=(\alpha-1)!$ when α is a positive integer and in such situations the Gamma distribution is also known as the Erlang distribution. In particular, the distribution is a reverse J-shaped curve for $\alpha \le 1$ and is single peaked, with the peak at $\theta=(\alpha-1)/\beta$ for $\alpha>1$. The effect of changing β for constant α is illustrated in Figure 3.7(a). Varying β does not change the form of distribution, only its scale. Plots of the Gamma probability density function for various values of α and a constant β are shown in

Figure 3.7(b), in which the shape of the distribution is seen to change. Consequently, α and β can be considered to be shape and scale parameters respectively and also represent the rate of distribution (i.e. the reactor's flushing rate) (see Section 2.1). The similarity between the mathematical presentations of the Gamma property function and the tank in-series model mean that the Gamma function based model can thus be used to mimic the curves for CSTRs in-series as shown in Figures 3.4 (a) & (b).

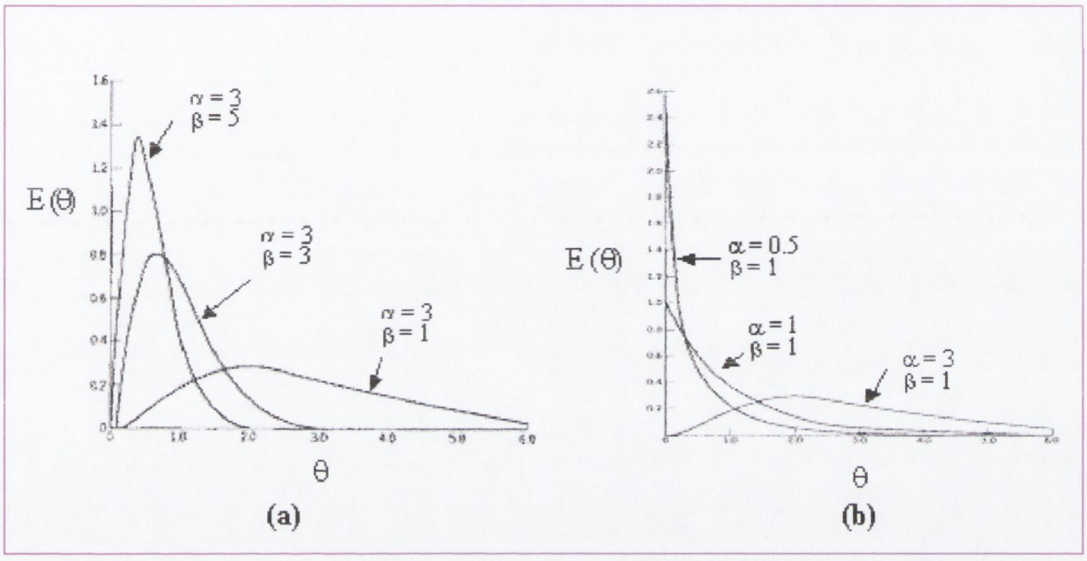

Figure 3. 7 Gamma distribution with (a) α=3 and various values of β and (b) β=1 and various values of α [Hahn, 1994]

The estimation of gamma distribution parameters can be achieved using the following equations [Hahn, 1994],

$$\beta = \frac{\bar{\theta}(n-1)}{\sum_{i=1}^{n}(\theta_i - \bar{\theta})^2} \text{----------} (3.12)$$

where, $\bar{\theta}$ is the mean, calculated as: $\bar{\theta} = \frac{\sum_{i=1}^{n}\theta_i}{n}$

θ_i, $i = 1,2,\ldots\ldots\ldots\ldots\ldots n$

$$\sigma^2{}_\theta = \frac{n\sum_{i=1}^{n}\theta_i{}^2 - \left(\sum_{i=1}^{n}\theta_i\right)^2}{n(n-1)} \text{----------} (3.13)$$

Where, $\sigma^2{}_\theta$ = the variance of the distribution function

An estimate of α is,

$$\alpha = \frac{\bar{\theta}^2 (n-1)}{\sum_{i=1}^{n} (\theta_i - \bar{\theta})^2} \qquad \text{----------(3.14)}$$

and therefore, $\alpha = \beta\bar{\theta}$ ----------(3.15)

3.3 Model Description

A tank in-series model based on the Gamma distribution was used in this research to fit the experimental data by using the optimisation technique of minimising the summation of the differences squared. The model enabled the reactor network to be characterised according to its observed retention time and apparent number of tanks in-series.

3.3.1 Model Structure

When carrying out the tracer studies, the tracer was generally injected as a pulse input and the tracer concentration was monitored at the effluent point. The reactor volume and its flow rate were also measured. The following mathematical model was formulated on an Excel© spreadsheet (Eq. 3.16) and then the model was fitted to the experimental data, from which the Gamma model retention time (modelled retention time), τ_{Gm} can be obtained.

$$C(\theta) = \left\{ M_{in} \times \frac{1}{\beta^{\alpha}\Gamma(\alpha)} \theta^{\alpha-1} e^{-\frac{\theta}{\beta}} + M_{back} \right\} \text{--------(3.16)}$$

where,
$C(\theta)$ = concentration at normalized time (θ)
$M_{in\,(\theta)}$ = mass added in to the system at any normalized time (θ)
M_{back} = background mass entering the system at any normalized time (θ)
α, β = parameters for Gamma distribution (see Section 3.2.1.2.1)

Note: the dispersion of the tracer or variance $\beta = \frac{1}{\alpha}$, the number of tanks-in-series $\alpha = \frac{1}{\sigma^2_{\theta}}$ and σ^2_{θ} = variance of distribution function.

As discussed previously in Section 2.6.1 the Peclet number represents the dispersion of tracer inside a reactor and hence the shape of the RTD curves depends on it as well as the boundary conditions. When the boundary conditions are closed such as in a CSTR, the tracer is dispersed inside the reactor as a function of the mixer speed and hence the

Peclet numbers are relatively large. Therefore the Peclet number can be used to evaluate the variance in both CSTR model and PFR model [Levenspiel, 1999]

$$\sigma^2{}_\theta = 2(P_e) - 2(P_e)^2\left[1 - e^{-(1/P_e)}\right] \qquad ----------(3.17)$$

where,

P_e = the dispersion number or Peclet number (see Section 2.6.1)

Substitution of the above parameters into Eq. 3.11 gives,

$$f(\theta, n) = \frac{n^n \theta^{(n-1)}}{(n-1)!} e^{-n\theta} \qquad ----------(3.18)$$

The model was fitted to the experimental RTD data obtained from the tracer study at each normalized time step, C(θ) by using the optimization process of summation of the difference squared (Eq 3.19) and the optimization was carried out using the "Solver" function on Excel©. The resultant best fit against the experimental data for the overall system represents a hydraulic characterization of the whole system based on a network of perfect CSTRs in series from the following parameters: α (the number of tanks in-series **n**), β the variance of distribution function ($\sigma^2{}_\theta$ characterizing the dispersion of the tracer through the reactor) and τ (the hydraulic retention time).

$$Differences\ Squared = [Exit\ Conc - C(\theta) fraction]^2 \qquad ----(3.19)$$

where, $C(\theta) fraction = C(\theta)$ concentration at time $(\theta) \times$ total fraction

The $C(\theta)$ *fraction* is used to scale the model curve to the RTD data without changing the shape.

The structure of the above model is shown in Figure 3.9 in the framework of an Excel© spreadsheet. The use of a spreadsheet-based model was chosen since it is easy to use and is time saving since basic spreadsheets can be created with the formula and functions and then altered to the individual specification of each trial. The numerical and alphabetical data can be portrayed clearly and succinctly. The Gamma distribution mathematical function, used in the model, is built into Excel© spreadsheet. The above

model (Eq 3.16) was introduced into the Excel© spreadsheet (as shown in Figure 3.8) as shown in the following formula,

$$C(\theta) = \left\{ Sum(\$C\$15 : C15 \times Gammdist(F15, \$G\$5, \$G\$6, false)) + \left(\frac{C11}{1000} \right) \right\} \text{------} (3.20)$$

Where,

F15, G5 and G6 cell references represent θ, α and β respectively.

C11 and C15 cell references represent the background and input mass of tracer.

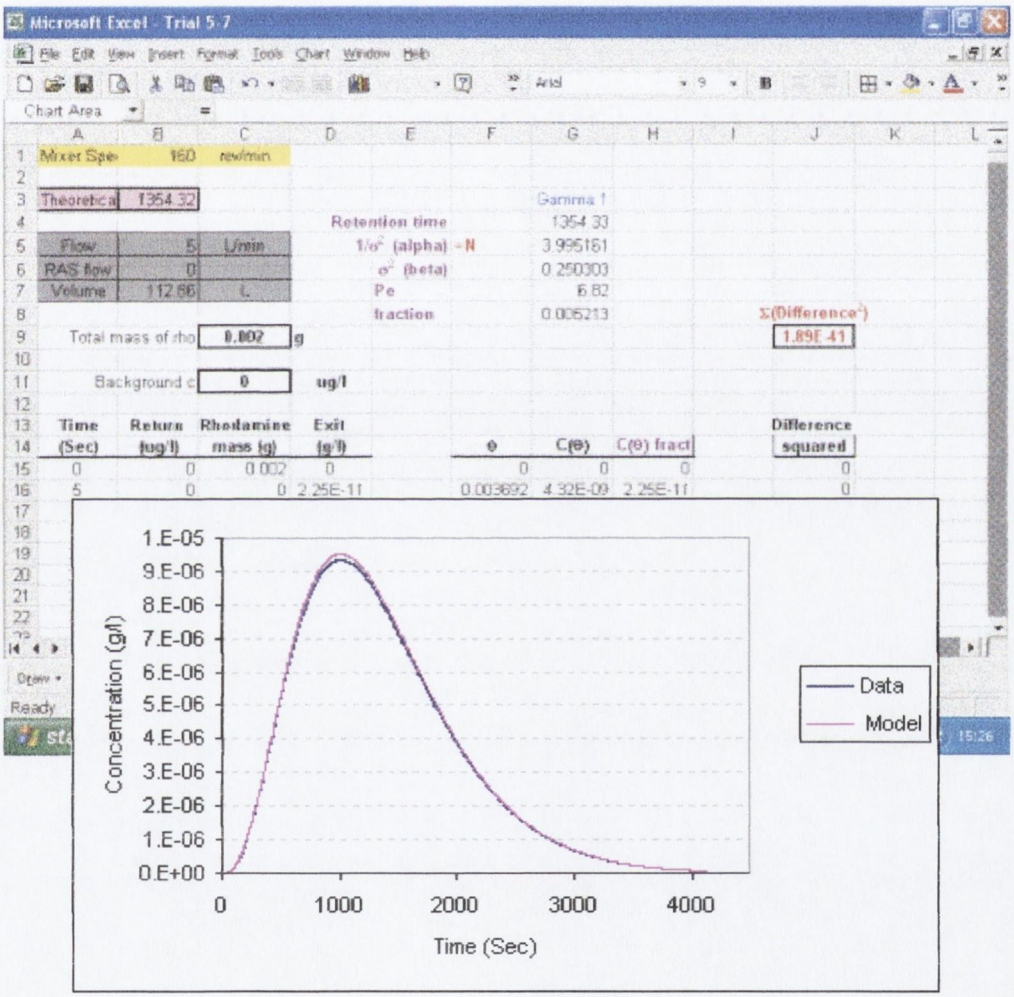

Figure 3. 8 The structure of the model on an Excel© spreadsheet

The basic structure of the spreadsheet (Figure 3.8) is arranged in a time sequence, moving down each row according to each sampling interval result as follows:

Column A (starting at A15) represents the time since start of tracer test, **column B** represents the concentration of the tracer in any return flow, **column C** represents the

concentration of mass injected at an interval time step, **column D** represents the effluent concentration of the tracer measured at each sampling interval, **column F** represents the normalized time, **column G** represents the concentration at each normalized time step, **column H** represents the fraction of the tracer at each normalized time and finally **column J** represents the difference squared between the effluent data and the model. The "Solver" function can handle problems that involve many variable cells and can help to find combinations of variables that minimize a target cell. In this model the objective was to minimize a cell which represents the sum of the differences between the model and data squared, which is cell reference J9 on Figure 3.8. In order to do this, three pieces of information must be identified for the "Solver": -

- The objective or target cell
- The variables or changing cells
- Any constraints or "conditions"

The variable cells in this case represent the following parameters: the retention time, the Peclet number (Pe) and the total tracer fraction which correspond to cell references G4, G7 and G8 respectively on Figure 3.8.

3.3.2 Model interpretation

The data that is obtained from injecting a tracer into a reactor often exhibits a significant degree of error or "noise," (see Figure 3.10(a)) from which an approach is needed to derive a single curve that represents the general trend of the data. Hence, the difference-squared method gives a best-fit model curve designed to follow the general trend of the points taken as a group, but does not necessarily intersect every point. As described previously, the mathematical model parameters (**n**, β, t and c) are used to characterise the reactor hydraulics and are determined according to the best fit between the model and the observed data. The sensitivity of the model to these parameters can be clearly seen by considering the following graphs (Figure 3.9). Figure 3.9(a) shows that β (dispersion of tracer) is extremely sensitive when the number of CSTRs is less than 4. Conversely, when the system has more than 4 CSTRs, **n** becomes extremely sensitive to changes in β. For example, changing of **n** from 10 to 50 CSTRs in-series only gives a small change in β equivalent to 0.08. In addition, the sensitivity of the model RTD curves with respect to **n** can be seen in Figure 3.9(b). When the system

contains a very high number of tanks in-series the concentration gradient is very high with respect to time. Conversely, when the system contains a low **n** the concentration is less sensitive with respect to time. Hence, the shape of the curve is very sensitive to the **n** parameter (α in Eq.3.16).

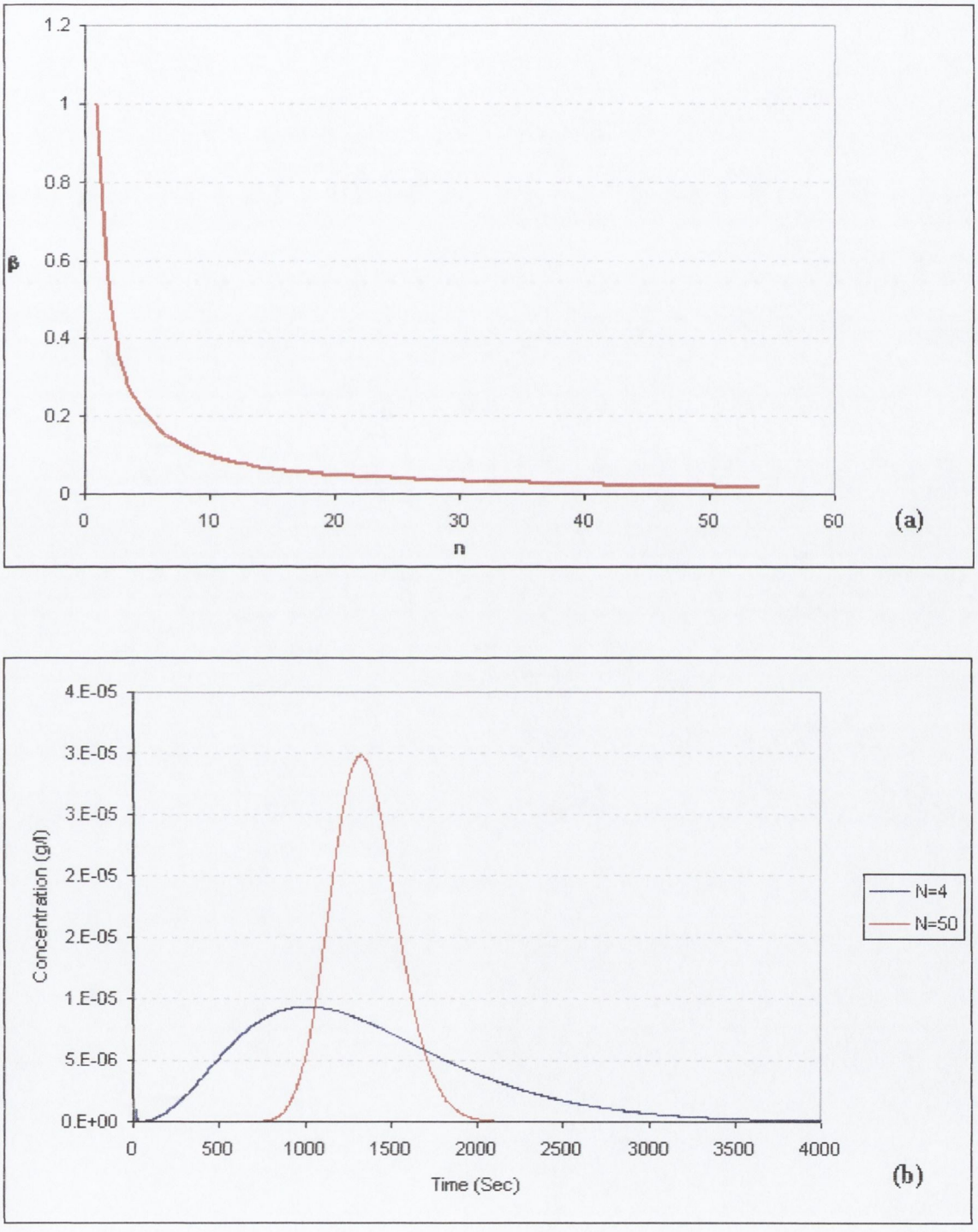

Figure 3. 9 Graphs showing the sensitivity of the model for (a) changing n against β and (b) changing t and c with constant n

3.3.2.1 Curve Fitting

The collected RTD data is a set of discrete values onto which a continuous model curve is fitted using the summation of differences squared technique. This method has produced very good fits in most situations where mixing is occurring or where there are several CSTRs in-series. However, there are certain situations when the RTD data collected are fairly erratic, for example when the mixers are switched off in a network reactor, which promotes short-circuiting and consequential erratic noise in the trace as shown in Figure 3.10(a). Where such noise exists the model still appear to produces a single curve that represents the general trend of the data since, the individual extreme data points are only very infrequent compared to the majority of points, which conform to the general trend. However, they do have a small effect on slightly elevating the curve above the general trend as can be seen in Figure 3.10(b) which could be an argument for removing such erratic values in this situation. This problem may be attributed to certain factors, which directly affect the Solver when searching for the optimum solution. There are three main factors that govern how the Solver reaches the solution: the mathematical relationships between the objective and any constraints and the decision variables; the size of the model (number of decision variables and constraints); and how dispersed the data is. In addition, the use of integer variables (used as a constraint for example) will make the memory and solution time rise exponentially as more integer variables are added. These factors are technical defaults within the computer hardware that make the Solver go off in one direction to seek a solution but may result in a mathematical dead end. In this case the Solver may have to be run again using different values for the initial parameters in order to get the true overall optimum solution.

In order to get an accurate RTD curve a sufficiently small increment of time (Δt=5sec) has been chosen which makes the curve appear as a continuous line on the full RTD plot. The first part of the RTD curve has been expanded allowing the error or "noise" to be seen clearly in Figure 3.10(b). The following Figure 3.11(a) and (b) show these problematical factors (error or "noise") being progressively diminished or virtually eliminated in the case of Figures 3.12(a) and (b) as the quality of the effluent trace improved due to increased mixing being applied to the reactors.

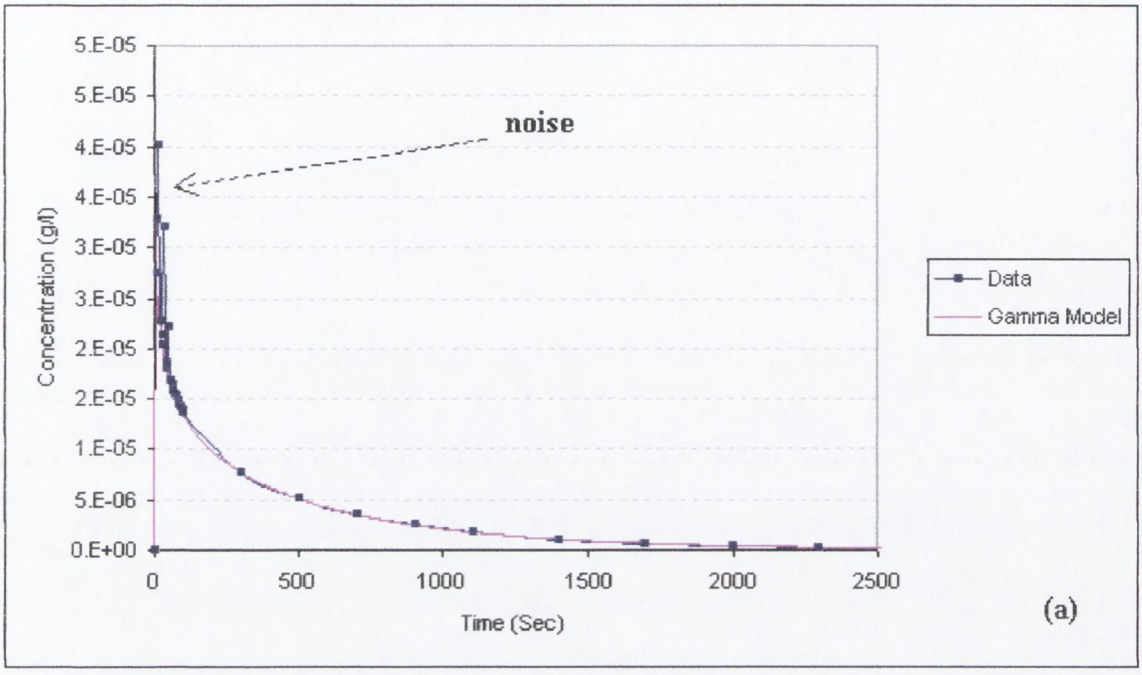

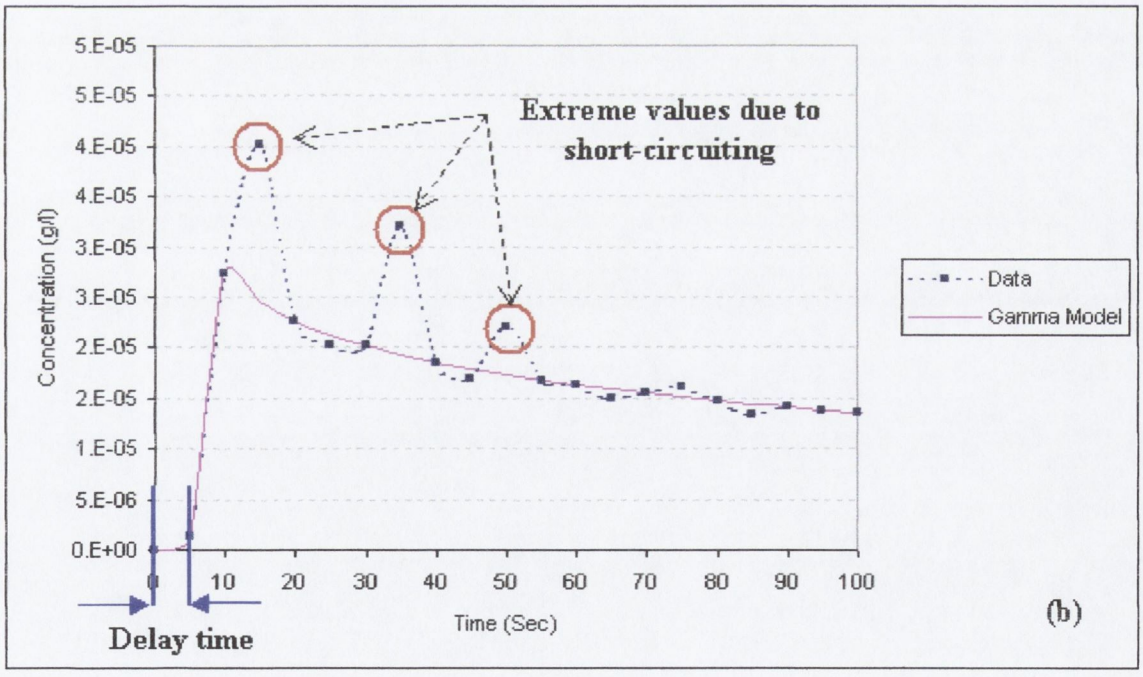

Figure 3. 10 Graphs showing the goodness of fit achieved by using the technique of summation of differences squared for 1 CSTR mixer off (a) the full RTD curve (b) expansion of the first 100 seconds

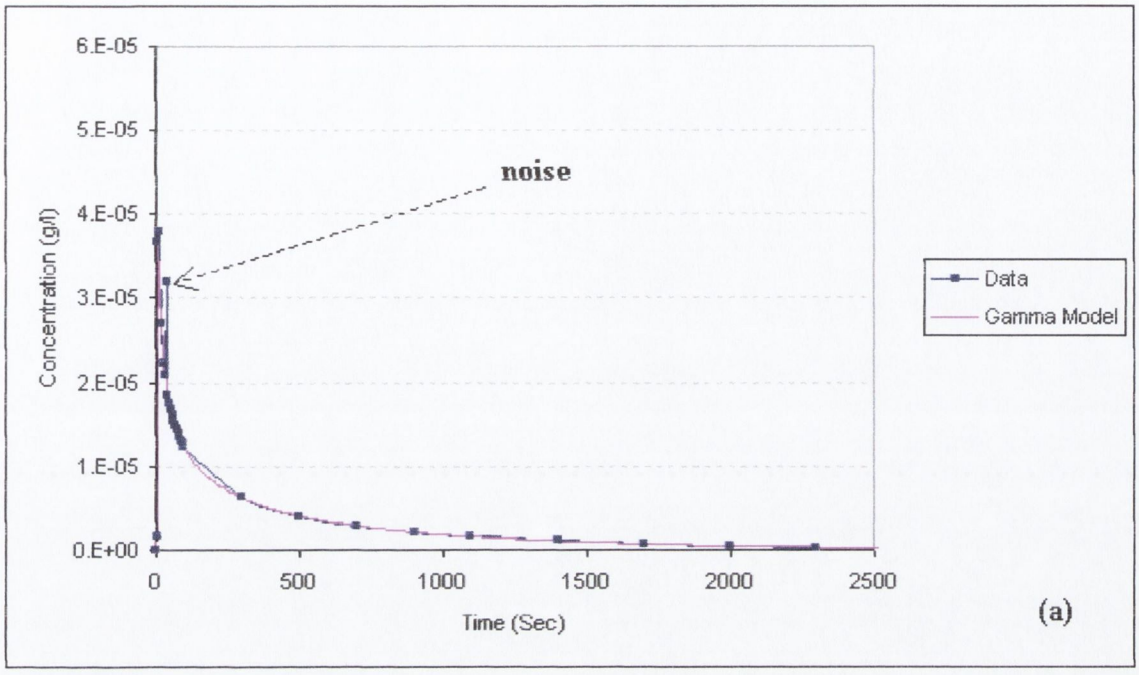

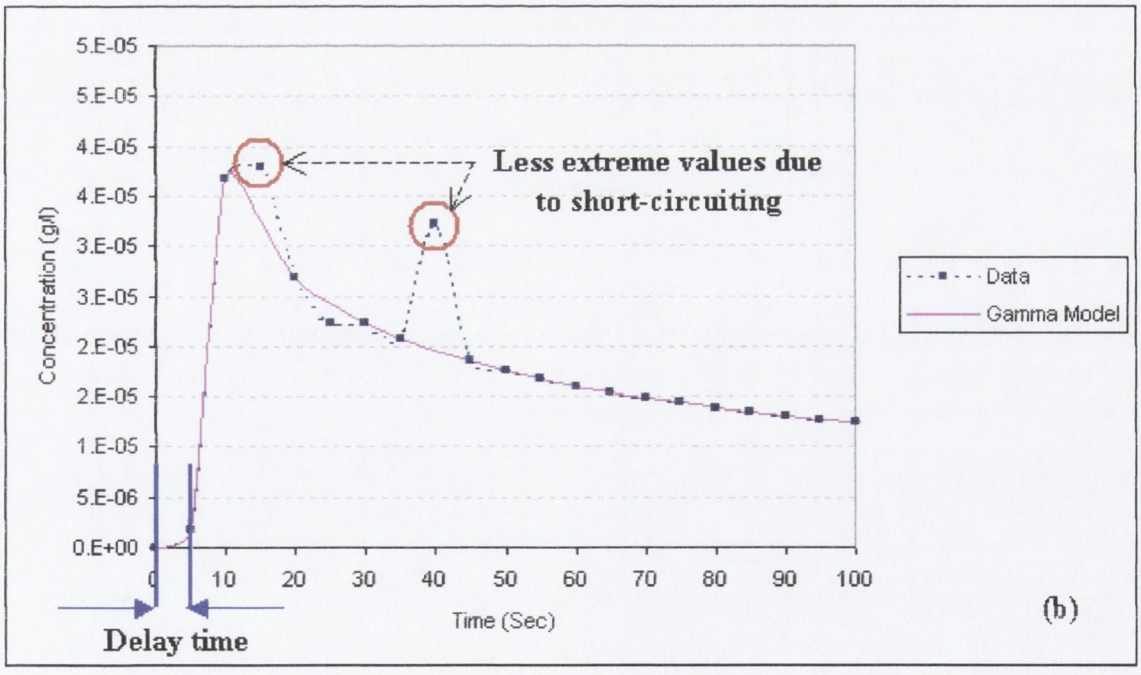

Figure 3. 11 Graphs showing the goodness of fit achieved by using the technique of summation of differences squared for 1 CSTR mixer 40 rpm (a) the full RTD curve (b) expansion of the first 100 seconds

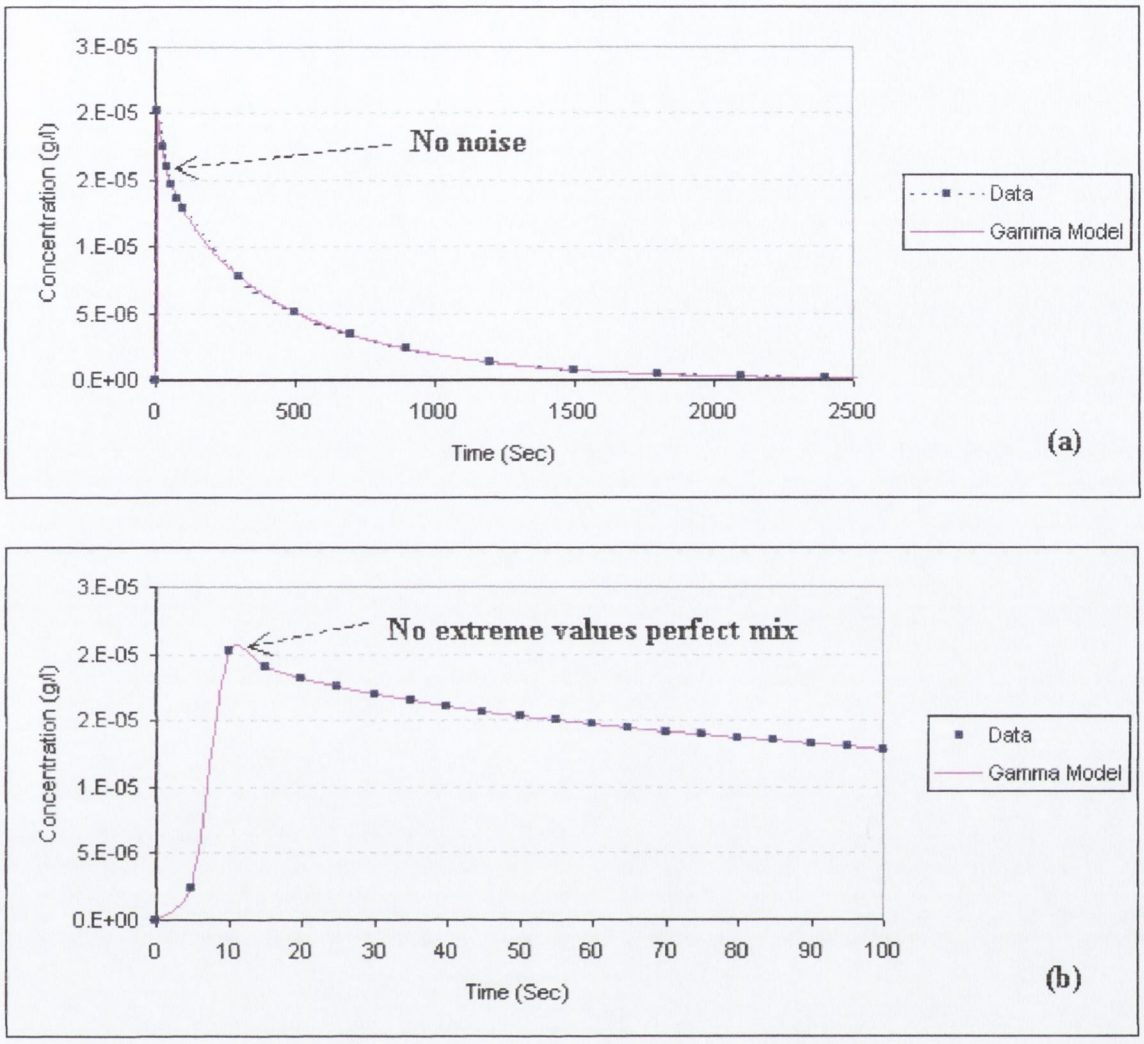

Figure 3. 12 Graphs showing the goodness of fit achieved by using the technique of summation of differences squared for 1 CSTR mixer 200 rpm (a) the full RTD curve (b) expansion of the first 100 seconds

The graphs also illustrate the delay time for the tracer to travel from the inlet point to the outlet point. This delay time can be seen to be a combination of the time for the tracer to travel across the reactor network (which in theory, is instantaneous in a CSTR) and the short time take for the tracer to flow down the 20cm outlet pipe to the SCUFA. This, which is very small, less than 5 Sec for one reactor as illustrated in Figure 3.10(b). This delay time is also shown in Appendix K and is less than 20 Sec for 2 CSTR in-series, less than 30 Sec for 3 CSTR in-series and about 40 Sec for 4 CSTR in-series. In addition, two experiments were carried out by injecting the tracer into the 1cm pipe connected directly to the SCUFA, 20cm and 50cm downstream (Appendix K) which shown the assumed δ-function in real condition (Appendix K).

3.4 Testing the Model

Different conceptual approaches in the use of the mathematical model were attempted in order to analyze the RTD data and thereby determine the hydraulic characteristics of the reactor and in particular any undesirable problems such as dead-zones and short-circuiting. A full description of these different approaches is provided in the following sections.

3.4.1 First Approach

The first approach used was to apply three mathematical models in parallel to fit the models jointly to the RTD data, as shown in Figure 3.13. The premise was that one function would identify the fraction of flow pass through perfectly mixed zone, another function would identify the fraction of flow passing through a dead-zone and the final function would identify the fraction of flow passing through the reactor in short-circuit. The overall fit is achieved by fitting the overall model curve (the addition of the three models) to the experimental data as shown in Figure 3.14.

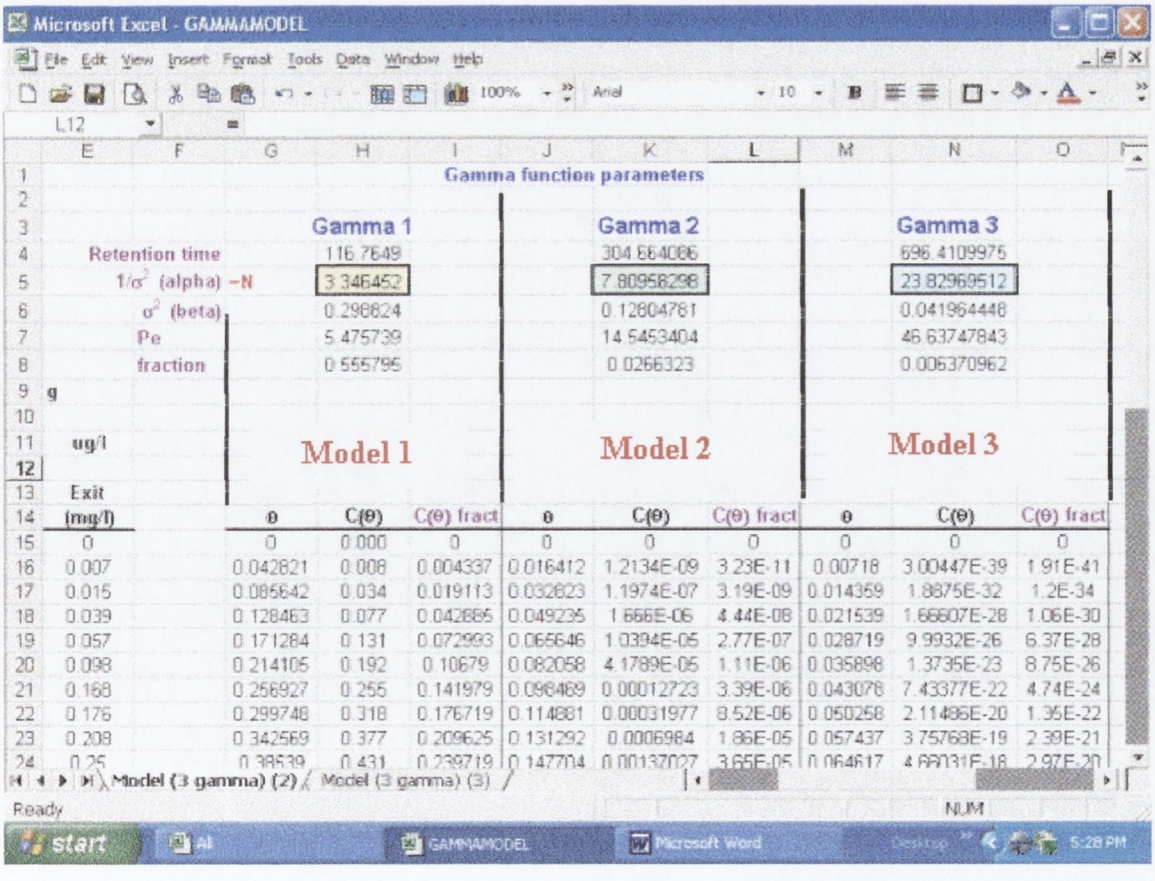

Figure 3. 13 The Excel© spreadsheet used for the three-gamma model in parallel without constraints.

This first approach was used for an extended period in order to obtain an understanding of the different hydraulic systems. The use of three mathematical models in parallel did provide a very close best fit to experimental RTD data as shown in Figure 3.14. However, the three functions could not provide a uniform approach, where it could always be guaranteed that the first mathematical model picked up the completely mixed flow, the second mathematical model picked up the dead-zone flow and the third mathematical model picked up the short-circuit flow. This can be seen from the results that were obtained from different reactor configurations shown in Table 3.1.

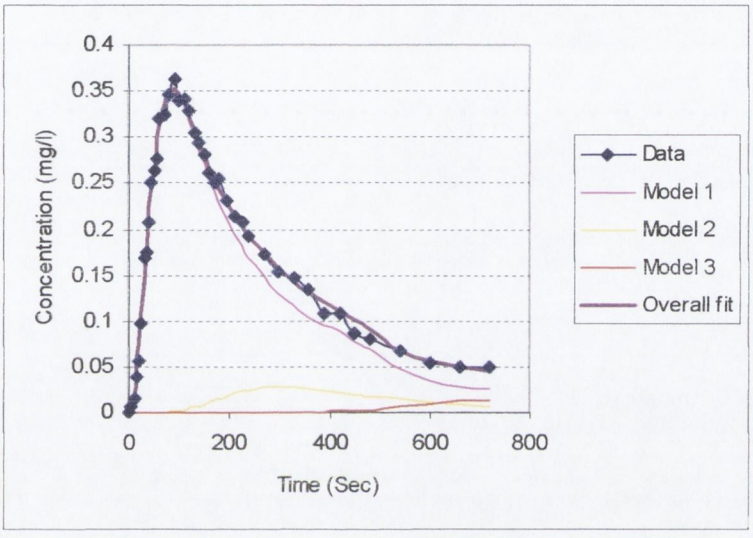

Figure 3. 14 Example of using three-gamma function models in parallel fitted to experimental RTD results (without constraints on the solver)

Experiment No.	Actual No. CSTRs	Mixer Speed	Model 1		Model 2		Model 3	
	(n)	(rpm)	(n)	Fraction	(n)	Fraction	(n)	Fraction
1	1	0	2.4	0.09	7.8	0.86	1.6	0.04
2	1	200	3.2	0.94	1.7	0.05	4.2	0.01
3	2	0	3.4	0.63	2.4	0.06	2.6	0.31
4	2	200	6.2	0.09	1.2	0.68	3.4	0.23
5	3	0	3.6	0.22	2.9	0.31	3.6	0.47
6	3	200	3.6	0.46	12.3	0.23	5.6	0.31
7	4	0	4.3	0.62	3.1	0.35	10.2	0.04
8	4	200	3.3	0.21	7.8	0.41	23.8	0.37

Table 3. 1 The results obtained from different system configurations by using the three-gamma function models in parallel

In general, when the mixer speed is at 200 rpm, the reactors should behave as perfect CSTRs. Hence, Model 1 in each experiment should show **n** equal to the exact number of CSTRs that physically make-up the system accounting for almost all the fraction of flow. Alternatively when the mixer speed is at 0 rpm, then you should expect the short-circuiting and dead-zone fractions to predominate accounting for a high fraction of overall flow. The short circuit should be typified by high numbers of CSTRs, as discussed previously for plug flow conditions. The presence of dead-zones act to reduce the perfect-mixed volume in the reactor and thereby reduce the actual retention time to a value less than the theoretical retention time. Table 3.1 therefore reveals the ability of the mathematical model to pick up these hydraulic differences when configured as three-gamma function models in parallel. For example, when the actual system was only 1 CSTR and the mixer speed was set at rest (0 rpm) the first mathematical model indicated 2.4 CSTRs in-series companied with only 0.09 fraction of flow as perfectly mixed and the second mathematical model provided 7.8 CSTRs in-series with 0.86 fraction of flow indicating plug-flow short-circuiting as may be expected. However, when the mixer speed was set at 200 rpm the mathematical model, that should provide 1 perfectly mixed CSTR in-series gave 3.2 tanks in-series with 0.94 fraction of flow which is obviously not acceptable.

The same indefinable results can be seen looking at the multiple reactor configurations. In the case when the system has 4 CSTRs in-series for example, (Experiment 8 in Table 3.1) when the mixers are working at 200 rpm, the Model 1 provides 3.3 CSTRs for 0.21 fraction of flow which again is much smaller than it should be for this case, whereas 0.37 fraction of the flow is behaving as 23.8 CSTRs in-series which again makes no physical sense. Equally, in Experiment 5 it can be seen that Model 1 and Model 3 both define 3.6 CSTRs in-series for 0.22 and 0.47 fraction of the flow which again confuses any physical interpretation of these results. Hence, it seems that the combination of 3 gamma functions running free without any constraints are able to provide a very close fit to the RTD curves, but can not be used to provide any consistent interpretation of hydraulic characteristics of the reactor networks.

3.4.2 Second Approach

The second approach was also based on the first-approach but this time some constraints were applied to the "Solver". This time, the first function was set to minimize the summation of differences squared between the data and the model with an extra constraint that forced the first mathematical model to be equal to the number of CSTRs in-series in the system (for example n=4) as shown in Figure 3.15, cell reference H5. In the second and third function the premise was to run the "Solver" to minimize the differences squared between the data and the model without any constraints so that one model would identify the fraction of flow passing through dead-zones and the other model would identify the fraction of flow passing in short-circuit through the reactor. The overall fit is again achieved from the addition of the three models as shown in Figure 3.16.

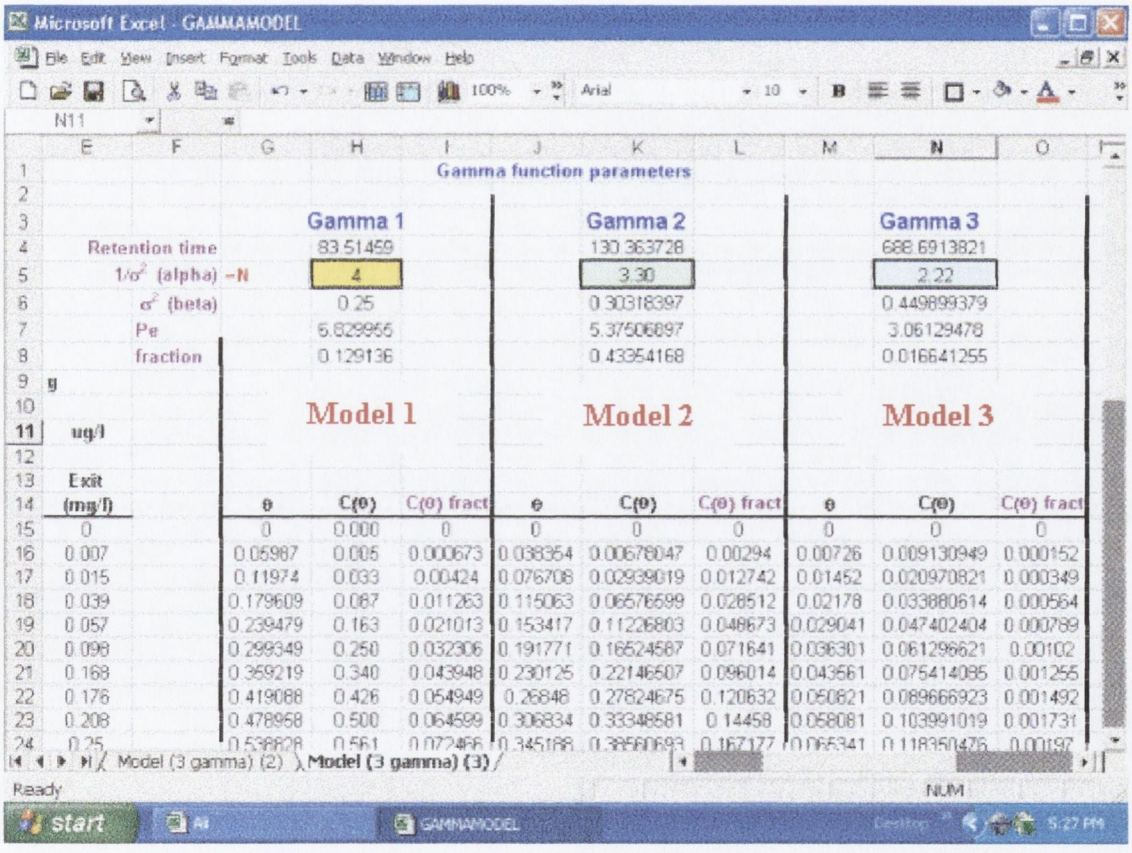

Figure 3. 15 The Excel© spreadsheet used for the three-gamma model in parallel with some constraints

Again, the use of three functions in parallel with some constraints did not provide a uniform approach, where it could always be guaranteed that one function picked up the

completely mixed flow, the other function picked up the dead-zone flow and the third function picked up the short-circuit flow. As shown in Figure 3.15 the use of three mathematical models in parallel with the single constraint successfully provided a good fit to the data. However, the results obtained from different reactor configurations, as shown in Table 3.2 were not consistent for each configuration. It was felt that the model is not reliable since the use of certain constraints to force the first mathematical model to be equal to an integer number may force the Solver to move off in a specific direction and therefore not necessarily find the optimum solution, as discussed previously. In addition, when the system is perfectly mixed the mathematical model retention time must equal exactly the theoretical retention time which does not always appear to be the case.

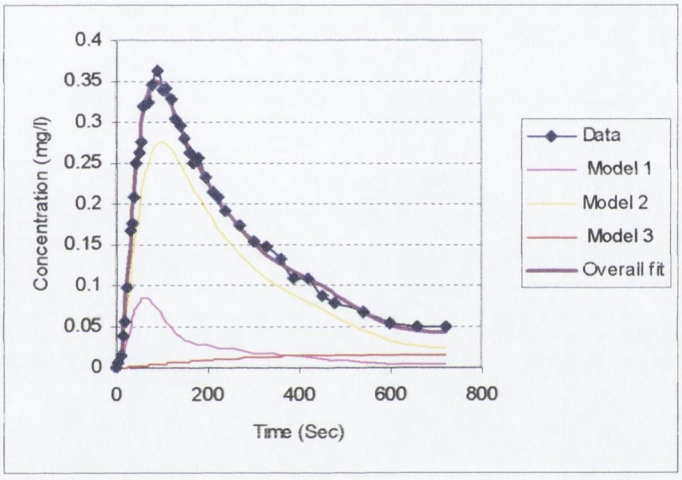

Figure 3. 16 Example of using three-gamma function models in parallel fitted to experimental RTD results (with a single constraint)

Experiment No.	Mixer Speed	Actual No. CSTRs	Theoretical retention time	Model 1 retention time	Model 1		Model 2		Model 3	
	(rpm)	(n)	(Sec)	(Sec)	(n)	Fraction	(n)	Fraction	(n)	Fraction
1	0	1	342.9	211.9	1	0.99	11.3	0.01	2.3	0.01
2	200	1	342.9	560.2	1	0.02	1	0.01	6.2	0.97
3	0	2	846.5	400.1	2	0.03	2.7	0.34	2.9	0.63
4	200	2	846.5	679	2	0.33	1.1	0.46	4.2	0.21
5	0	3	1128.6	952.7	3	0.50	3.1	0.01	4.2	0.50
6	200	3	1128.6	1125.4	3	1.00	2.9	0.00	3.1	0.00
7	0	4	1354.3	463.3	4	0.44	4.2	0.56	11.5	0.00
8	200	4	1354.3	118.8	4	0.28	8.9	0.72	14.5	0.00

Table 3. 2 The results obtained from different system configuration by using the three-gamma function models in parallel with a single constraint

Hence, it could not always be taken for granted that the second model will pick up the dead zones and the third model will pick up the short-circuit (or vice versa). The best fit that was obtained (shown in Figure 3.16) indicated that the mathematical model is working to fit the data but no constant method could be followed in order to interpret the results. As shown in Table 3.2 when the system is a perfectly mixed single CSTR, the theoretical retention time should be 342.9s which the mathematical model should provide if the system is working efficiently. However, in this case (Experiment 2) when the mixer was working at 200 rpm (which has been proven to be sufficient to promote a good mix) the model gives a retention time of 560.2s that is unacceptable. In addition, the second model and the third model show confusing results, which appear to make no physical sense. For example, in Experiment 1, when the mixer was at rest, the second model shows 11.3 CSTRs in-series which would indicate short-circuits but only associated with 0.005 fraction of flow which actually that means the short-circuits are hardly present in the system. The model should also be able to pick up the flow passing through any dead-zones. In Experiment 2 with the mixer set at 200 rpm the results show exactly 1 CSTR with only 0.018 fraction of the flow and the third model shows 6.2 CSTRs in-series with 0.972 fraction of flow which is obviously confusing in terms of any physical interpretation. There was one time where the mathematical model seemed to work exactly as had been hoped in Experiment 6 when the system contained 3 CSTRs in-series with the mixers at 200 rpm. The first mathematical model was forced to pick up 3 perfectly mixed CSTRs which gave a retention time exactly the same as the theoretical retention time (1128.6s) as well as accounting for almost all the fraction of flow 0.996. The second mathematical model showed 2.99 CSTRs in-series and the third model showing 3.1 CSTRs in-series but only with 0.001 and 0.003 fraction of the flow respectively which matches the reality. However, it could not be guaranteed that this approach would work all the time and for this reason another approach was used to interpret the results.

3.4.3 Third Approach

The third approach used just a single mathematical model to minimize the summation of differences squared as shown previously in Figure 3.8.

Once the best fit has been reached, the following results can be obtained,

- The mathematical model retention time
- The tracer mass that has left the system at $\theta = 1$
- The area under the RTD curve
- The fraction of tracer remaining in the system at any time θ
- The amount of tracer that has been resident in the reactor at any time θ

The model works to minimise the sum of the differences squared by adjustment of the retention time, the Peclet number (see Section 2.6.1) and the fraction of the tracer. In order to analyse the RTD data obtained using this single mathematical based model approach, some fundamental parameters were required.

- The mass of tracer that had passed out of the reactor too quickly.
- The percentage of the flow passing through dead-zones, $Q_d\%$.
- The percentage of the flow short-circuiting, $Q_s\%$.
- The percentage of the flow passing through completely mixed zones, $Q_m\%$.

The reactor volume and the flow through it have been considered as follows,

$$\text{Total reactor volume } (V_R) = \begin{cases} V_s = \text{Short-circuit volume (plug-flow volume)} \\ V_m = \text{Mixed volume} \\ V_d = \text{Dead-zone volume} \end{cases}$$

$$\text{Total flow rate } (Q) = \begin{cases} Q_a = \text{Active flow} \\ \\ Q_d = \text{Flow through the dead-zones} \end{cases}$$

where,

Active reactor flow (Q_a) = Mixed flow (Q_m) + Short-circuiting flow (Q_s)

3.4.3.1 Short-circuit Determination

Fundamentally, the area under the RTD curve should be equal to the total mass injected into the reactor, M_{in}. Since the theoretical retention time means the average time of the tracer molecules resident in the reactor, this point was taken as a reference to analyse the RTD data shown in Figure 3.17 below. Hence, the area to the left of the theoretical

retention time is equal to the area to the right of the theoretical retention time, whereby each area should equal half the initial tracer mass $\left(\frac{M_{in}}{2}\right)$.

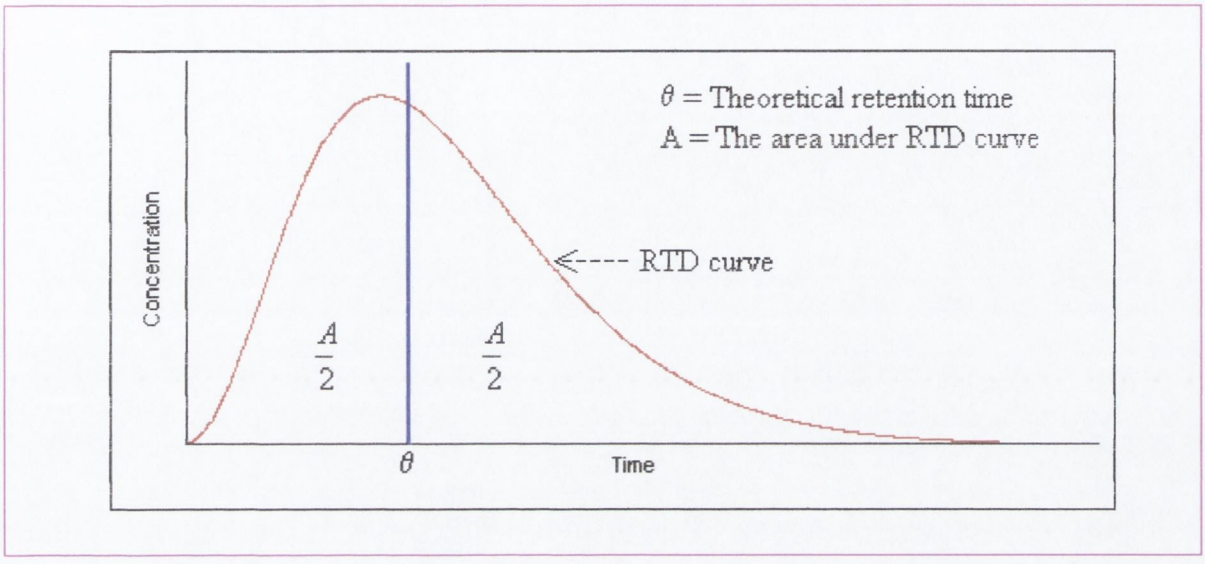

Figure 3. 17 Analysis of RTD curve

The fraction of flow short-circuiting can be evaluated by using the following formula. At the theoretical retention time (θ=1), in a perfect CSTR, the mass of tracer passed out in the effluent must be equal to half the input mass,

$$TM_{\theta=1} = MM_{\theta=1} \text{ --------(3.21)}$$

where,

$TM_{\theta=1}$ = mass passed out at the theoretical residence time

$MM_{\theta=1}$ = mass which should have passed out at the exact theoretical residence time (if the system is behaving as totally mixed)

M_{in} = mass injected at the beginning of the experiment

However, this expression is only valid if the reactor is working at the optimum level that it is designed for. If more tracer has passed out of the reactor at the theoretical retention time, then it implies that there must be some form of short-circuit operating in the reactor. As demonstrated in Eq. 3.21, the flow short-circuiting can only be determined by a prior knowledge of the initial mass of the tracer injected into the reactor and the mass that has passed out of the reactor at the theoretical retention time (θ=1), therefore,

$$Q_s = \frac{\left|(TM_{\theta=1} - MM_{\theta=1})\right|}{M_{in}} \times Q \qquad \text{-------(3.22)}$$

3.4.3.2 Dead-zone Determination

The mathematical model (Eq 3.16) is fitted to the experimental data using the developed model. The model effectively obtains the actual retention time of the RTD (cell reference G4 in Figure 3.8), which can be compared to the theoretical retention time (cell reference B3 in Figure 3.8) to determine whether the system has dead-zone problems or not. Hence, the fraction of flow passing through dead-zones can be evaluated as follows,

$$Q_d = \frac{\left|(\tau_{Gm} - \tau_T)\right|}{\tau_T} \times Q \qquad \text{----------(3.23)}$$

where,

τ_T = theoretical residence time
τ_{Gm} = modelled retention time
Q = flow rate

Consequently, the flow passing through perfectly mixed zones can be determined by,

$$Q_m = Q - \left|Q_d + Q_s\right| \qquad \text{----------(3.24)}$$

By using the above equations, the behavior of the flow entering the reactor can be considered by using the following assumptions.

Scenario 1

- If $M_{out\,at\,\tau} \leq \frac{M_{in}}{2} \Rightarrow$ there is no short-circuit problem

In this case, the assumption is that the system is either perfectly mixed or has dead-zone problems, depending on the modeled retention time. *It should be recognized that, theoretically, there could be some situations where a small short-circuit operating within the system could act to cancel out some dead-zones and thus achieve the above criteria. However, this would be very hard to recognize and also very uncommon.*

From a theoretical point of view, the dead-zone works as a tool either to reduce or increase the reactor retention time. For example, if the volume of the system is less than the assumed volume (due to siltation in the corners for example) then the retention time should be smaller than the theoretical value. Conversely, if the system is the correct volume but the mixers are not good enough to create a good enough mix, the retention time will be greater than the theoretical value. Hence, if the absolute value of the differences between the theoretical retention time and the modeled retention time is equal to the reactor's theoretical retention time, then the reactor can be considered to be perfectly mixed.

If the modelled retention time is greater or less than the reactor's theoretical retention time, with a long tail response curve (as shown in Figure 3.18), this indicates that the system is suffering from dead-zones.

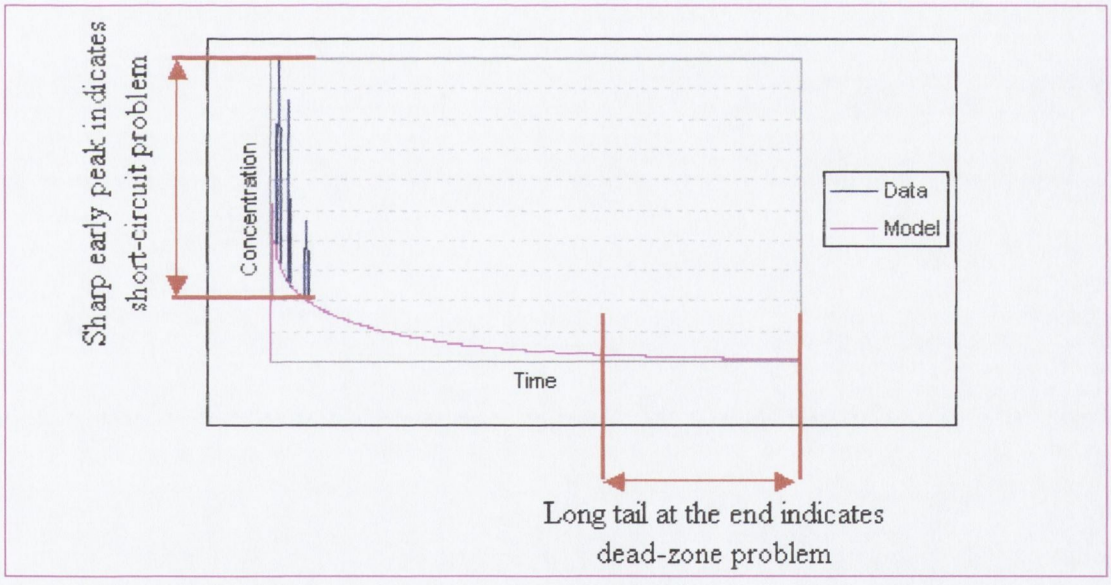

Figure 3. 18 The effect of short-circuits and dead-zones on the RTD response curve

Such dead-zones could occur due to the differences of the temperature caused by the density currents [Metcalf and Eddy, 2001] if the water entering the reactor is colder or warmer than the water in the reactor. For example, if the local temperature in the reactor is higher than the incoming flow temperature, a portion of the water can travel to the outlet along the bottom of the reactor as shown in Figure 3.19 without mixing completely.

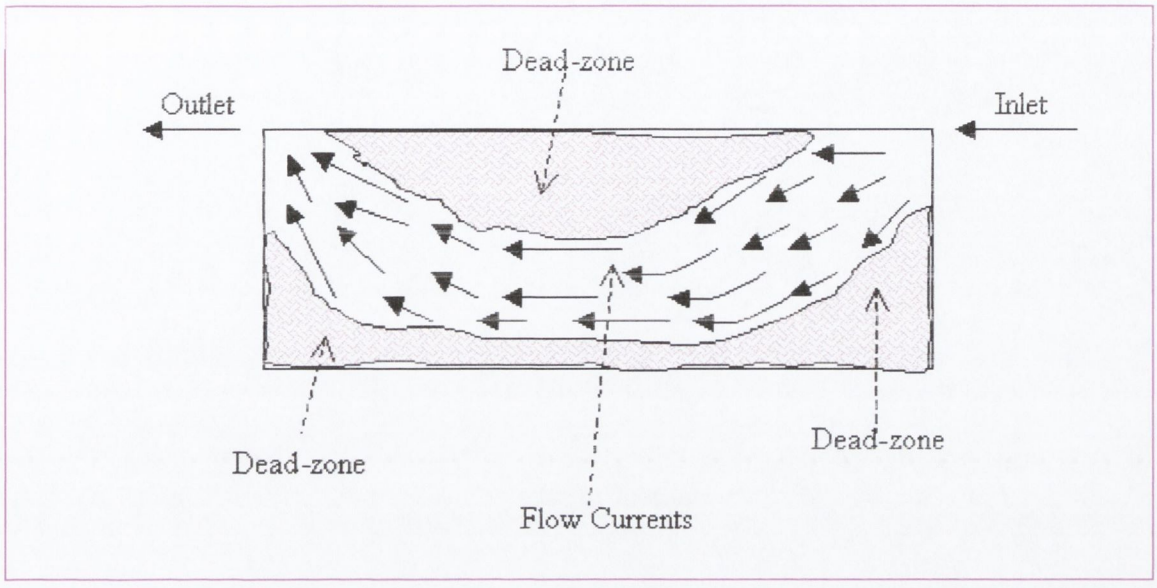

Figure 3. 19 A definition sketch for dead-zones caused by density currents caused by temperature differences

Scenario 2

- If $\sum M_{out\,at\,\tau} > \frac{M_{in}}{2} \Rightarrow$ there are short - circuit problems indicated by a sharp early peak (as shown in Figure 3.16).

Again, if the model retention time is equal to the theoretical retention time the assumption is that no dead-zones are present in the system.

Scenario 3

- Often systems will have both dead-zones and short-circuits at the same time, which is indicated if $\sum M_{out\,at\,\tau} > \frac{M_{in}}{2}$ and the model retention time is less than or greater than the theoretical retention time indicated by a sharp early peak and long tail together.

The above formulae will allow the percentage of the flow that passes through the perfectly mixed zones, any short-circuiting and/or dead-zones to be evaluated as follows and has been used to analyze the data for this research.

$$Perfectly\ \ mixed\ \ flow\ \% = \frac{Q_m}{Q} \times 100 \qquad \text{--------(3.25)}$$

$$Dead\ \ zone\ flow\ \% = \frac{Q_d}{Q} \times 100 \qquad \text{--------(3.26)}$$

$$Short\ \ circiut\ flow\ \% = \frac{Q_s}{Q} \times 100 \qquad \text{-------(3.37)}$$

Chapter 4

Preliminary Experiments (Model Development)

Chapter 4

Preliminary Experiments (Model Development)

4.1 Introduction

In this chapter the experimental equipment and apparatus that were used to carry out this research are described, and then the results of a series of laboratory experiments are presents which were carried out to determine the validity and the sensitivity of the model on a single CSTR reactor.

4.2 Rhodamine WT Tracer.

Rhodamine WT is a fluorescent tracer which has been developed specifically for environmental applications (Smart and Laidlaw, 1977) since it is non-toxic (Little and Lamb, 1973) and shows a low tendency to stain inorganic or organic matter in either fresh or salt water (Pedahzur *et al.*, 1993; Macdonald and Ernst, 1986; Mangelson and Watters, 1972; Chapple, 1985), a particularly important characteristic when used in any analysis founded on the principle of a rigorous mass balance. It can be detected at 0.01 µg/l with a state-of-the-art fluorometer, although its detectability decreases in polluted water towards more realistic levels in the 0.1 µg/l range. The chemical structure of Rhodamine WT is as shown Figure 4.1.

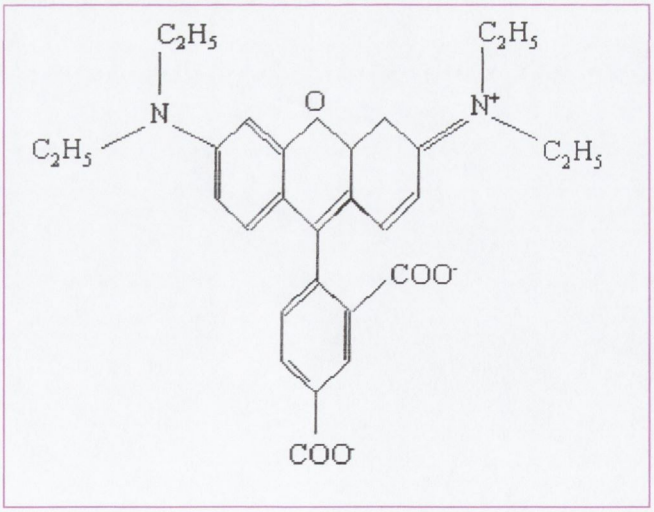

Figure 4. 1 Chemical structure of Rhodamine WT

However, studies have shown that Rhodamine WT can behave non-conservatively in certain situations, either by sorbing to sediments (Trudgill, 1987; Shiau *et al.*, 1993;

Everts and Kanwar, 1994), or by photochemical or biological degradation (Smart and Laidlaw, 1977; Tai and Rathbun, 1988). It has been reported that typically only 7.5% of Rhodamine WT can be absorbed by inorganic sediments (for example a pure limestone clay or kaolinite) and typically only 8% by organic sediments (humus, heather roots and stems, bacteria or sawdust) after a 2 hours contact time (Smart and Laidlaw, 1977). In addition, it has been reported that the Bentonite has the highest resistance to adsorption of the tracer dyes especially Rhodamine WT, where typically only 0.2-1.2% is adsorbed. This property makes the Rhodamine WT highly recommended for example for use as a tracer to study the mixing efficiency of processes used when drilling for oil (see Section 8.4). It has been reported Yotsukura *et al.* (1970) that adsorption losses onto equipment surfaces (such as glass, plastic bottles and Perspex) were not encountered when Rhodamine WT was used. They have also emphasized the clear advantages in term of recovery that Rhodamine WT has as a tracer over Rhodamine B in time of travel and dispersion measurements. Kilpatrick *et al.* (1967) reported losses of 49% for Rhodamine B, 25% for Sulpho Rhodamine B, and 7% for Rhodamine WT for gauging tests made in a wastewater secondary treatment process. They also reported average losses of 5.4% for Sulpho Rhodamine B and 1.1% for Rhodamine WT in the laboratory under the same conditions. Smart and Smith (1976) tested a number of dyes in a river in Jamaica and concluded that Rhodamine WT gave high recovery (typically 98.2%), while the other dyes such as Rhodamine B experienced large losses in surface water and ground water tests, with recovery values being under 50%. With regard to toxicity Little and Lamb, (1973) recommended that Rhodamine B should not be used as a water tracer, but Rhodamine WT does not cause any ill effects to aquatic life. Hansen *et al.*, (1958) studied the effects of Rhodamine B, Sulpho Rhodamine B, and Rhodamine WT in oral feeding studies at 100µg/l in drinking water in rats which showed that all test animals showed a loss of body weight compared to a control group and that Rhodamine B and Sulpho Rhodamine B caused the greatest liver enlargement. Subcutaneous injections of 50µg/l of Sulpho Rhodamine B caused inflammatory sores at the injection site and a marked loss in body weight, whereas Rhodamine WT appeared to cause no traumatic ill effects even after 56 days of this treatment. Long-term feeding studies (Wright and Collings, 1964) also indicated that Rhodamine WT appeared to have no toxicity levels, while Rhodamine B and Sulpho Rhodamine B appear to be slightly higher.

4.3 SCUFA Submersible Fluorometer

The Self-Contained Underwater Fluorescence Apparatus SCUFA (as shown in Figure 4.2 (a) and (b) is an accurate, simple-to-use and versatile submersible fluorometer for dye tracing applications and has been designed to operate in a wide range of concentrations and environmental conditions. It can be used in a moored or profiling mode, with or without a host computer/data logger. The SCUFA can also be used with or without a flow through cap. When used without the flow through cap (as shown in Figure 4.2 (c)), the SCUFA must be mounted with the optics facing down into the flow. However, if the flow through cap is used, then the SCUFA should always be mounted with the cap facing up (as shown in Figure 4.2 (d)) to minimize any potential air bubble effects and distortion of the optical readings.

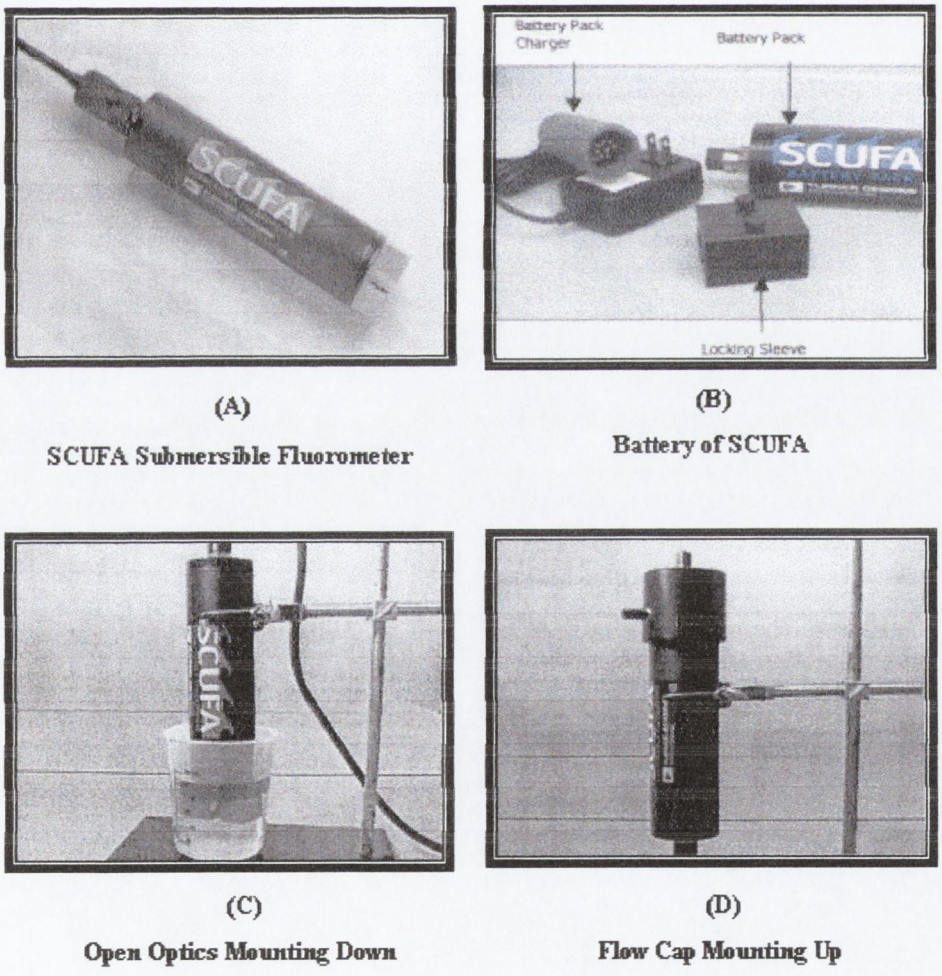

(A)

SCUFA Submersible Fluorometer

(B)

Battery of SCUFA

(C)

Open Optics Mounting Down

(D)

Flow Cap Mounting Up

Figure 4. 2 SCUFA Submersible Fluorometer

The windows based SCUFAsoft software is used to configure the SCUFA Fluorometer quickly and easily for profiling or moored applications. The interface software has up to six control screens depending on the instrument configuration that represent and control the current status of the instrument's function. The Internal Data Logging (IDL) window allows the sampling rate of the instrument to be set and the internal data logger to be programmed for up to four sampling blocks per calendar day or to run continuously. The Internal Data Logger Clock, a real-time clock in the SCUFA, is set by synching with the PC clock, set sampling rate, Data Logger and Daily Record Time. Finally, the SCUFAsoft software has the Data Screen, allowing the logged data to be downloaded, or previously logged data to be looked at, erased or exported. In addition, a graph can be displayed on the Screen. The data was exported from SCUFAsoft into an Excel© spreadsheet (using the Excel transfer function) from which it was then incorporated into the RTD model (see Section 3.3).

4.4 Experimental Procedure

Essentially, the laboratory system investigated is indicated in Figure 4.3. The reactor under investigation was fed from a constant head tank to maintain a constant flow rate throughout the experiment. The reactor had a diameter of 29cm and a height of 32cm; an impeller with 2-blade pitch pointing upward (3cm from bottom, 7cm in diameter); and a motor located at the top of the tank which controlled the speed rate of the tank's impeller. The flow inlet to the reactor was connected to a constant head tank located in the hydraulics laboratory at the highest point which had the essential function to keep the input flow rate constant whilst adjustment of outlet valve kept the volume level in the reactor during the experimental period. In order to get a more accurate flow rate, a flow meter was placed in line at the influent point, as shown in Figure 4.3. The outlet for the reactor was connected to the SCUFA device that was already connected to the computer enabling a reading of the Rhodamine WT concentration to be measured. The tracer to be injected was introduced into the reactor at the input injection point. A photograph of the apparatus in the laboratory is shown in Figure 4.4.

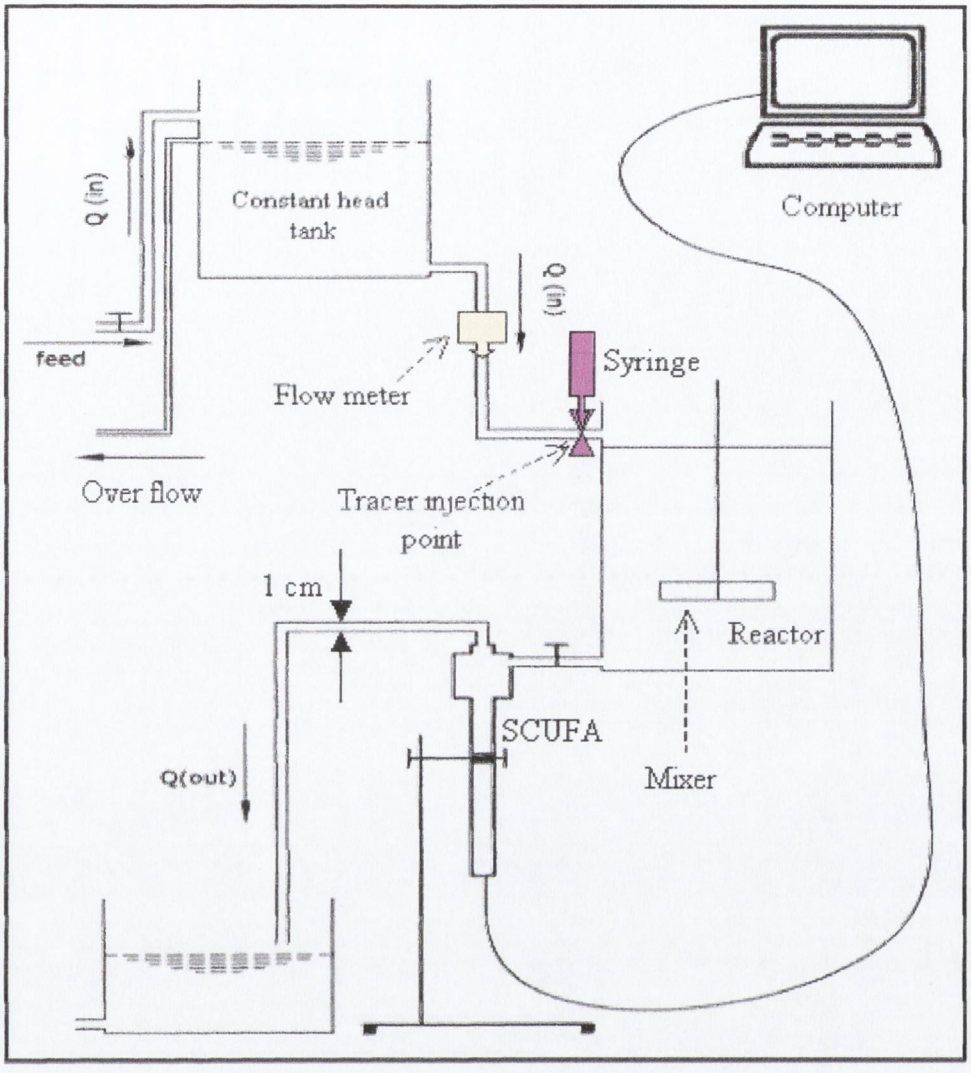

Figure 4. 3 Schematic diagram of laboratory experimental apparatus

Figure 4. 4 Photograph showing the apparatus of lab experiment

A series of pulse input and then step input tracer experiments were carried out on the simple single CSTR reactor in order to assess the basic model.

4.4.1 Pulse Input Experimental Procedure

At the start of each experiment the equipment was checked to be in good working order and each part was connected as outlined in Figure 4.3. The SCUFA was then calibrated with a standard concentration of Rhodamine WT solution (see Appendix A). The reactor was filled with water to the desired volume and adjusted until the input and output flows were equalized. At this point, the impeller stir rate was selected, the speed of rotation being proportional to the degree of mixing. The concentrated Rhodamine WT tracer was injected as close to instantaneously as possible into the inlet stream just before entrance to the reactor via a syringe as a pulse input (estimated in the order of 1/5 second), as illustrated in Figure 4.5 (a). The input was as close as possible to the inlet of the reactor to ensure a closed system as for as possible and hence limit any diffusion up stream as illustrated in Figure 4.5 (b). 10ml of Rhodamine WT at 200ppm concentration was added for each experiment. The SCUFA read the concentration of Rhodamine WT at each time step during the experiment. The data was then downloaded at the end of the experiment and exported into an Excel© spreadsheet.

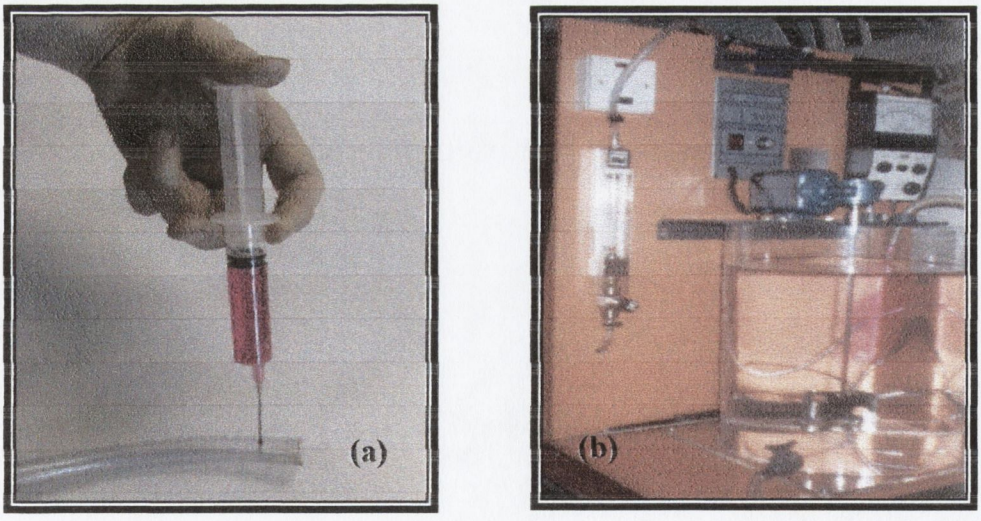

Figure 4. 5 Photograph showing the pulse input of tracer

The pulse input experiment was run many times in the laboratory, each time at a fixed flow rate and different mixer speeds to characterise the CSTR reactor. The different experimental conditions for the pulse input experiments are shown in Table 4.1.

4.4.1.1 Pulse Input Results

The experimental data were exported to the Excel© spreadsheet, and the resultant concentration against time, RTD curve was plotted. The RTD curve was then analysed and fitted to the mathematical model built on the Excel© spreadsheet, as explained in Chapter 3, by adjustment of a three parameters: retention time, Pe (Peclet number) and fraction. The model revealed the number of tanks in-series **n** which gives the best fit to experimental data using the Gamma distribution extension. Examples of the full spreadsheet data with the model results are given for experiments 1 and 5 in Appendix J. The full set of the results obtained from the experiments is shown in Table 4.2. In addition, some of the graphs for the experiments are shown in Figure 4.6 as an example. For all the rest of the graphs see Appendix B.

Experiment No.	Reactor Volume	Flow rate	Mixer speed	Rhodamine Mass
	(L)	(l/min)	(rpm)	(g)
1	20	3.50	0	0.002
2	20	3.50	20	0.002
3	20	3.50	40	0.002
4	20	3.50	80	0.002
5	20	3.50	120	0.002
6	20	3.50	160	0.002
7	20	3.50	200	0.002

Table 4. 1 Pulse input experiments – configurations

Experiment No.	Mixer speed	Mass passed out at the theoretical retention time	Theoretical retention time	Modelled retention time	P%	D%	S%	No. Of CSTR
	(rpm)	$(g)*10^{-3}$	(Sec)	(Sec)	(%)	(%)	(%)	(n)
1	0	1.26	342.85	505.18	39.7	47.3	12.9	0.72
2	20	1.19	342.85	497.56	45.5	45.1	9.4	0.75
3	40	1.13	342.85	436.38	66.4	27.3	6.4	0.75
4	80	1.04	342.85	356.54	93.9	4.0	2.1	1.00
5	120	1.04	342.85	380.58	87.2	11.0	1.8	0.96
6	160	1.05	342.85	399.19	81.3	16.4	2.3	0.92
7	200	1.00	342.85	419.38	77.7	22.3	0.0	0.89

Table 4. 2 Pulse input experiments – model results

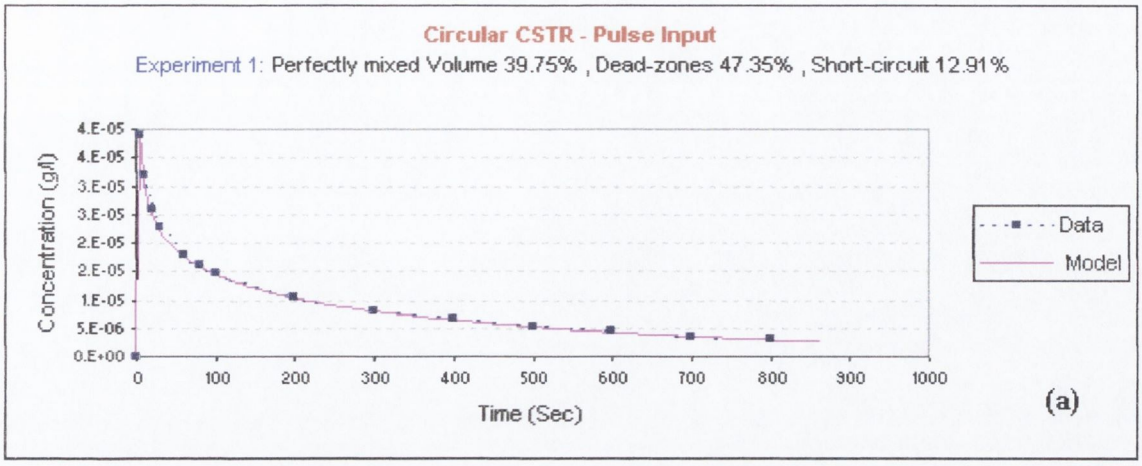

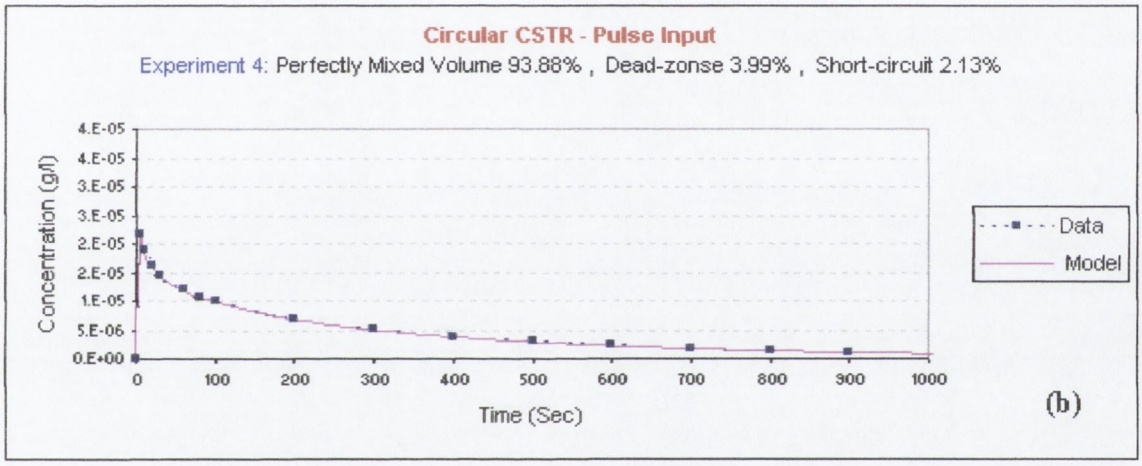

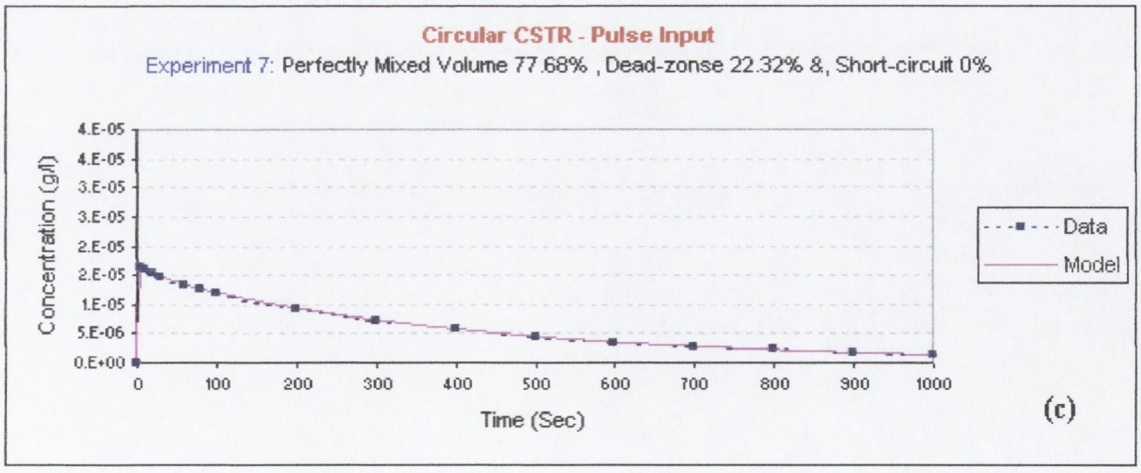

Figure 4. 6 Graphs showing laboratory results and model curves for a pulse input into a circular CSTR for (a) Experiment 1 (b) Experiment 4 and (c) Experiment 7

4.4.2 Step Input Experimental Procedure

The same experimental configuration shown in Figure 4.3 was used to carry out a series of step input experiments. Rhodamine WT solution was prepared at the desired concentration but this time was introduced into the reactor as step input (see Figure 4.7) using a burette tube calibrated to a known flow rate, as illustrated in Figure 4.8.

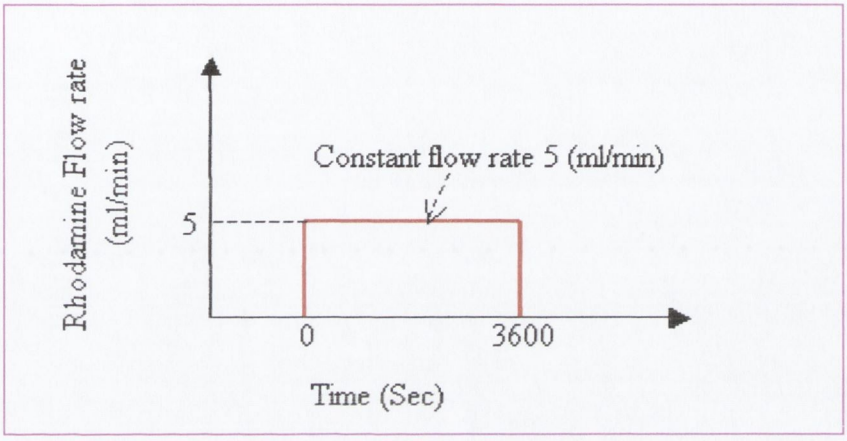

Figure 4. 7 Graph of step input of Rhodamine used for the experiments

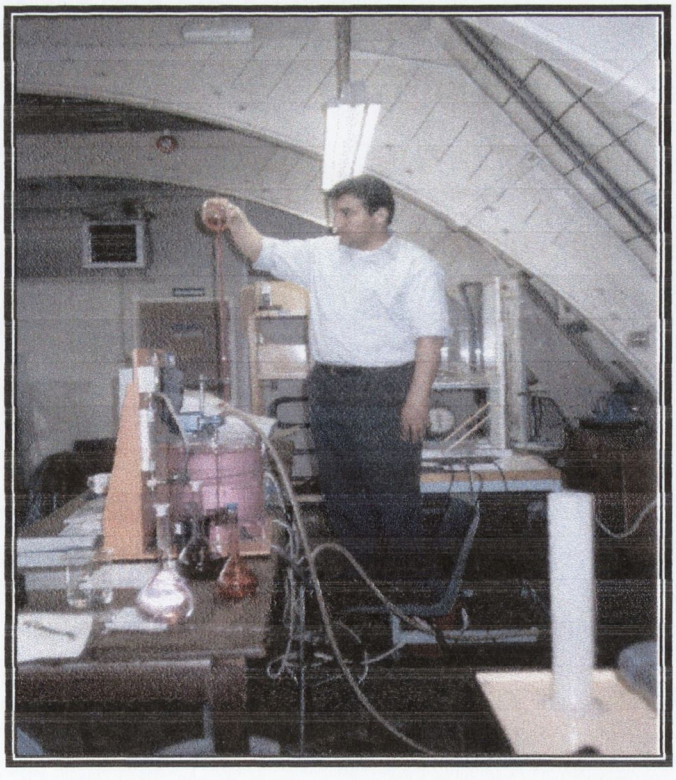

Figure 4. 8 Photograph showing maintaing the level of Rhodamine in the burette tube during the step-input experiment

The experiment was carried out several times at fixed flow rates and at different mixer speeds as shown in Table 4.3.

4.4.2.1 Step Input Results

The experimental data were exported to an Excel© spreadsheet and the tracer concentration against the time was plotted to obtain each RTD curve. The RTD curves were analysed and fitted to the mathematical model as explained in Chapter 3. The full set of the results obtained from the experiment is shown in Table 4.4. In addition, an example of some of the graphs for the experiments are shown in Figure 4.9; the rest of the graphs are in Appendix B.

Experiment No.	Reactor Volume	Flow rate	Mixer speed	Rhodamine Mass
	(L)	(l/min)	(rpm)	(g)
1	20	1.5	20	0.009
2	20	1.5	40	0.009
3	20	1.5	80	0.009
4	20	1.5	120	0.009
5	20	1.5	140	0.009

Table 4. 3 Step input experiments – configurations

Experiment No.	Mixer speed	Mass passed out at the theoretical retention time	Theoretical retention time	Modelled retention time	P%	D%	S%	No. Of CSTR
	(rpm)	$(g)^{*}10^{-3}$	(Sec)	(Sec)	(%)	(%)	(%)	(n)
1	0	4.68	800	1009.4	36.5	45.6	17.9	0.69
2	20	4.63	800	1005.95	43.5	39.5	17.0	0.84
3	40	4.54	800	974.66	68.2	29.5	2.3	0.84
4	80	4.52	800	944.72	92.1	3.2	4.8	1.00
5	120	4.52	800	898.07	85.6	10.6	3.8	0.93

Table 4. 4 Step Input experiments – model results

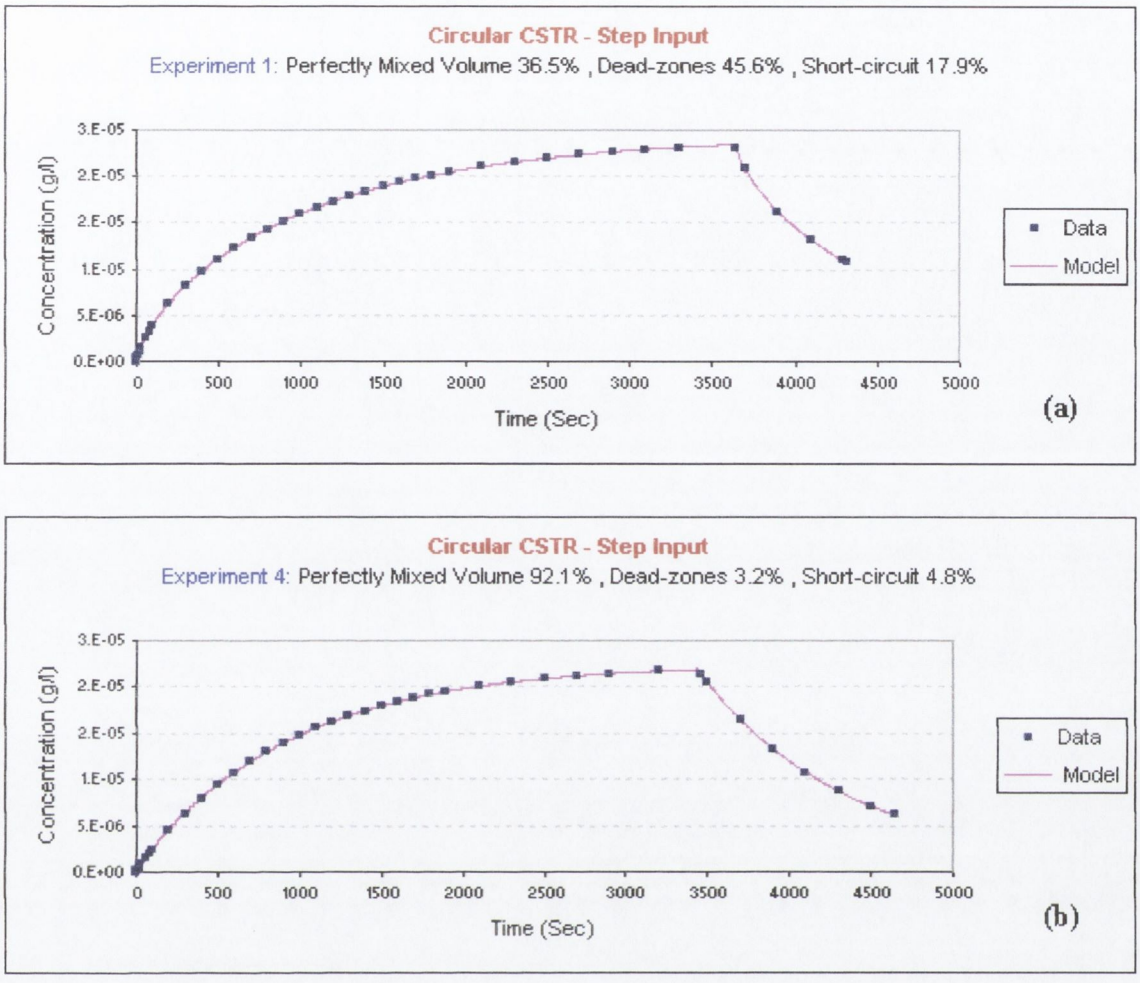

Figure 4. 9 Graphs showing laboratory results and model curves for step input method into a circular CSTR for (a) Experiment 1 and (b) Experiment 4

4.5 Results Analysis

Each run was carried out using the same flow rates but different mixer speeds. As the tracer was injected into the reactor it began spreading inside the reactor according to the mixer speeds: the faster the mixer speed, the more rapid the tracer dispersion. In addition, as the mixer speed increased, the results show that the percentage of the perfectly mixed flow increased up to a maximum level at 80rpm for both the pulse input and step input methods, as shown in Table 4.5 below and graphically as illustrated in Figure 4.10. At higher mixer speeds the percentage of perfectly mixed flow (and thus efficiency of the reactor) decreased again, due to the onset of vortexing in the reactor at high speeds. The vortex zone is the area inside the reactor that is created as the flow

begins to move round in the same direction as the mixer itself in a more plug flow manner without mixing properly with the rest of the reactor volume, as illustrated in Figure 4.11.

Experiment No.	Mixer Speed	Pulse Input	Step Input
	(rpm)	The percentage of flow passing through a perfectly mixed zone	The percentage of flow passing through a perfectly mixed zone
1	0	39.75%	36.50%
2	20	50.72%	43.50%
3	40	66.36%	68.20%
4	80	93.88%	92.10%
5	120	87.16%	85.60%
6	160	81.29%	=
7	200	77.68%	=

Table 4. 5 Comparison of pulse input and step input results

Although the step input method of injecting the tracer into the reactor is different from the pulse input method, it is clear that the results obtained from both methods (Table 4.5) provide more or less exactly the same conclusions, indicating potentially that the model is working correctly and that either method can be used in order to characterise the behaviour of the hydraulic system.

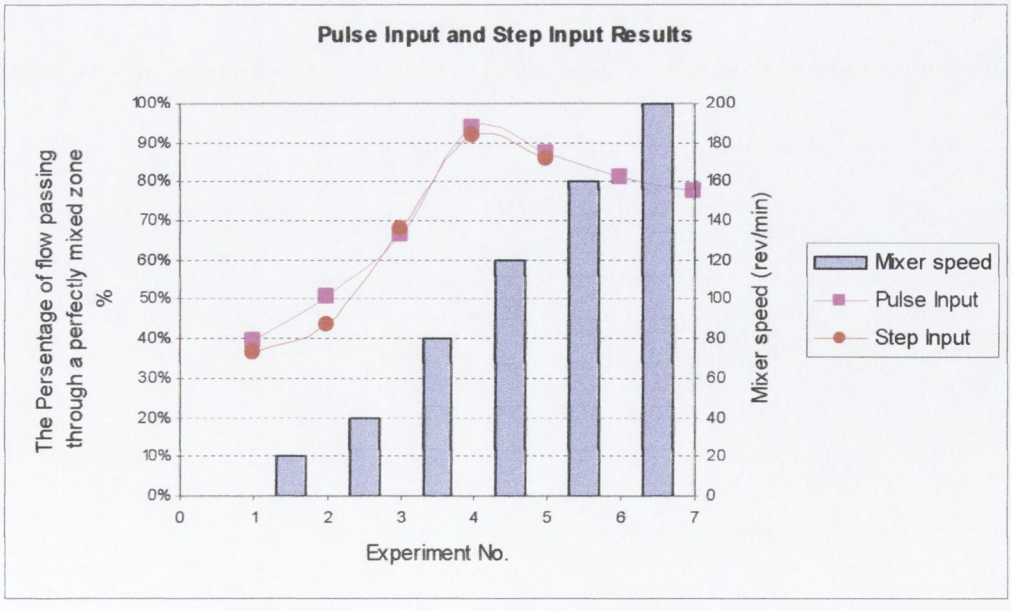

Figure 4. 10 Graph showing the effect of mixer speed on the system's behaviour

As shown in Figure 4.11(a) and Figure 2.12 below, the vortex starts away from the center of the reactor and as the speed of the mixer is increased the vortex becomes more centralized within the reactor. The vortex is a body of fluid contained in a reactor that is rotating about a vertical axis with uniform angular velocity that eventually reaches relative equilibrium and rotates with the same angular velocity as the reactor, forming a forced vortex. The vortex is an undesirable situation inside a reactor while mixing. In this case, the fluid inside the reactor will move around the mixer in a cone shape, taking the radius at the top of the fluid surface; this radius will start to decrease towards the bottom of the reactor until this radius equals 0 (see Figure 4.11). This kind of problem operates as a dead zone area which can be clearly seen from the results Tables 4.2 and 4.4. The vortex starts to form when the mixer speed is increased above 80 rpm at which point the percentage of dead-zones starts to increase correspondingly. In order to prevent gross vortexing, which is obviously detrimental to mixing, particularly in low viscosity systems, baffles are often fitted to the walls of the reactor (see Figure 4.11 (b)) which take the form of thin strips of about one-tenth of the reactor diameter typically positioned as four equally spaced baffles [Douglas, 1964; DeNevers, 1991]. In some cases, the baffles are mounted flush with the wall, although occasionally a small clearance is left between the wall and the baffle to facilitate fluid motion in the wall region. Baffles are, however, generally not required for high viscosity liquids because the viscous shear is then sufficiently great to damp out the rotary motion. The problem of vortexing can also sometimes be circumvented by mounting impellers off-center [Douglas, 1964; DeNevers, 1991].

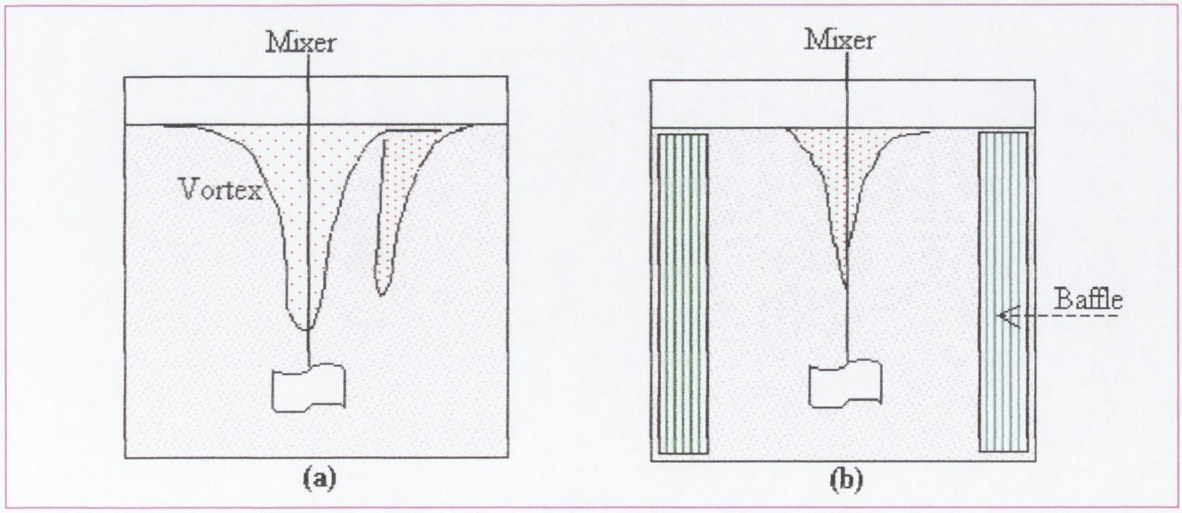

Figure 4. 11 Photograph diagram illustrating the vortex inside the circular reactor (a) without and (b) with baffle plates.

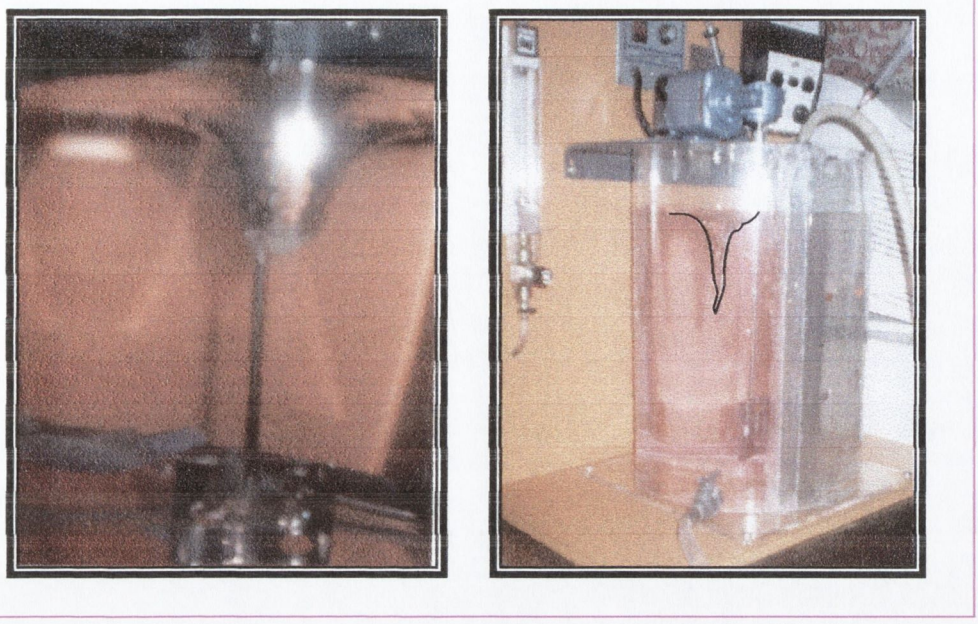

Figure 4. 12 Photograph showing the vortex area inside the reactor

4.6 Conclusion

The experiments show that the model produces similar results using either tracer input method. The advantage of the pulse input method over the step input method is primarily in the use of smaller quantities of tracer and this can be very important in terms of cost. Furthermore, the total duration of the pulse input measurement will always be shorter than that of a step input measurement and in addition, the step input method, requires more sophisticated equipment for the injection of tracer, whereas the pulse input method by contrast, requires no complex injection equipment, constituting an important advantage, particularly when highly active tracer solutions are to be injected. Hence, for these reasons, the pulse input method was used throughout the rest of this research.

The simple experiments have also shown the effectiveness of the model since it appears to have picked up the inefficiencies in the mixing caused by the onset of vortexing at high mixer speeds.

Chapter 5

Modifications

(Dead-zones and Short-circuit Simulations)

Chapter 5

Modifications (Dead-zones and Short-circuit Simulations)

5.1 Introduction

After completing a number of test runs on the single, circular tank discussed in Chapter 4 it was decided to model more complicated hydraulic anomalies and hence, modifications were needed to artificially create dead-zones and short-circuit in the reactor.

5.2 Dead-zones

Dead-Zones are areas inside a reactor that, for whatever reason or problem, are stable and do not mix with the main reactor material. As discussed in Chapter 3, if dead- zones are present, they can reduce the process efficiency. They are typically picked up on an RTD plot of a single CSTR as a long tail whereby they release the tracer only very slowly. In the case of the pulse input method, the experimental time has to be prolonged, as it necessary to continue measurements until all the tracer retained in the dead water zones has passed through the SCUFA output point.

5.2.1 Dead-zone Experiment Apparatus

In order to artificially create dead zones in the circular CSTR, a series of experiments were carried out by a variety of plates inserted into the reactor with a varying of number of 2cm diameter holes drilled in. The plate was of fixed width 20cm and length 35cm (see Figure 5.1(a)), which was inserted into the reactor of fixed volume 20 litres and effectively segregated off a volume of 5.63 litres (see Figure 5.1(b)). The plate was inserted into the reactor as illustrated in Figure 5.2 and the flow rate was adjusted to the desired flow rate, 4 l/min. For all the experiments, the reactor volume was stable at 20 litres and the mixer speed was set at, M_X rpm. The Rhodamine WT was injected as a pulse input at the side of mixed section of the reactor and the RTD data collected by the SCUFA. Certain experiments were repeated three times (Table 5.1) to ascertain the repeatability of the

experiments-these showed that the results obtained are very close indicating the validity of the model.

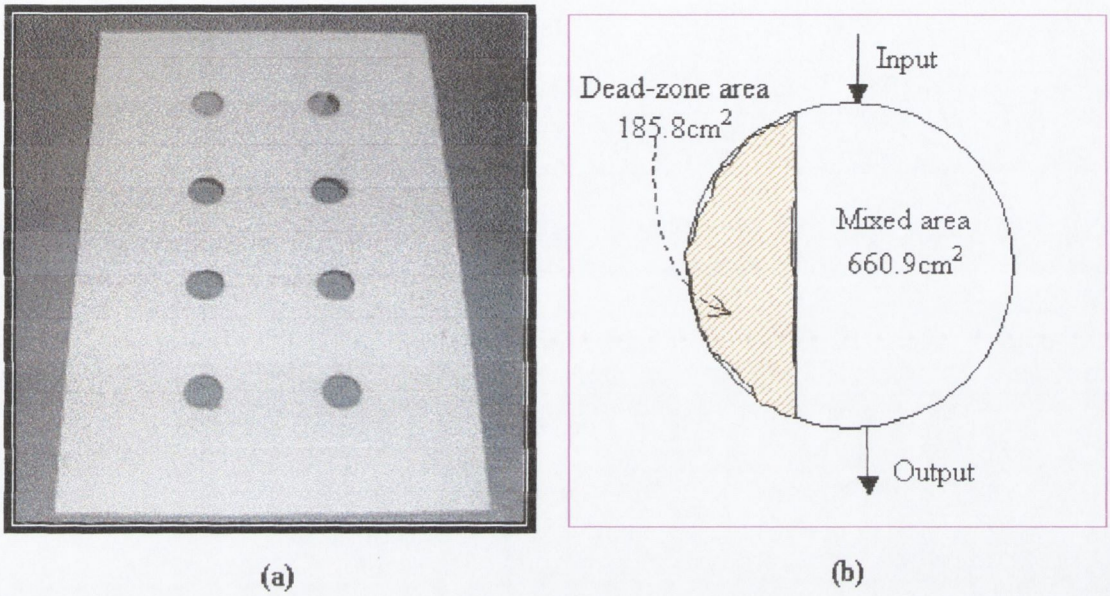

Figure 5. 1 (a) the plate with its holes and (b) schematic diagram (plan) for the mixed and separated area

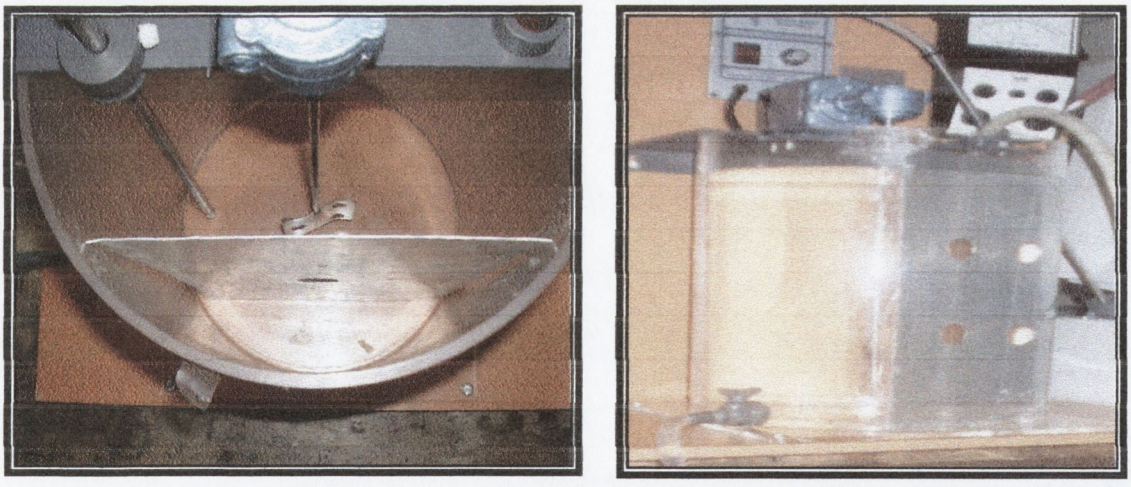

Figure 5. 2 Photos illustrating the plate inside the reactor

The experiment was run several times using different conditions to see whether the model could accurately estimate the dead zones in the system. Each experiment was carried out at a constant flow rate 4 l/min, but using different mixer speeds and with different number of

holes (1,2,4,8 and 10) in the plate. The full schedule of laboratory experiments is shown in Table 5.2.

Group 1 Experiment No.	Mixer speed	Mass passed out at the theoretical retention time	Theoretical retention time	Modelled retention time	P%	D%	S%	No. Of CSTR
	(rpm)	(g)	(Sec)	(Sec)	(%)	(%)	(%)	(n)
4 (a)	160	0.001	300	293.2	95.6	2.3	2.1	0.99
4 (b)	160	0.001	300	292.8	95.5	2.4	2.1	0.98
4 (c)	160	0.001	300	294.0	95.9	2.0	2.1	1.00

Table 5. 1 Validity of the model

Group No.	Experiment No.	Reactor Volume	Number of Holes	Total Areaa	Flow rate	Mixer speed	Rhodamine Mass
		(L)	(hole)	(cm^2)	(L/m)	(rpm)	(g)
Group 1	1	20	1	3.14	4	20	0.002
	2	20	1	3.14	4	80	0.002
	3	20	1	3.14	4	120	0.002
	4	20	1	3.14	4	160	0.002
	5	20	1	3.14	4	200	0.002
Group 2	1	20	2	6.28	4	20	0.002
	2	20	2	6.28	4	80	0.002
	3	20	2	6.28	4	120	0.002
	4	20	2	6.28	4	160	0.002
	5	20	2	6.28	4	200	0.002
Group 3	1	20	4	12.56	4	20	0.002
	2	20	4	12.56	4	80	0.002
	3	20	4	12.56	4	120	0.002
	4	20	4	12.56	4	160	0.002
	5	20	4	12.56	4	200	0.002
Group 4	1	20	8	25.12	4	20	0.002
	2	20	8	25.12	4	80	0.002
	3	20	8	25.12	4	120	0.002
	4	20	8	25.12	4	160	0.002
	5	20	8	25.12	4	200	0.002
Group 5	1	20	10	31.40	4	20	0.002
	2	20	10	31.40	4	80	0.002
	3	20	10	31.40	4	120	0.002
	4	20	10	31.40	4	160	0.002

Table 5. 2 Dead-zone experiments - configurations

5.2.2 Dead-zone Results

The experimental data were exported to an Excel© spreadsheet and plotted to obtain the RTD curve. The RTD curve was analysed and fitted to the mathematical model as explained in Chapter 3, by adjustment of three parameters: retention time, Peclet number and fraction. This model matched the number of tanks in series **n**, to give the best fit to the experimental data using the Gamma distribution model. The full set of the results obtained from the experiments is shown in Tables 5.3. In addition, an example of the graphs (one graph for each group) is shown in Figure 5.3 with the rest of the graphs in Appendix C.

Group No.	Experiment No.	Mixer speed	Mass passed out at the theoretical retention time	Theoretical retention time	Modelled retention time	P%	D%	S%	No. Of CSTR
		(rpm)	$(g)^{*}10^{-3}$	(Sec)	(Sec)	(%)	(%)	(%)	(n)
Group 1	1	20	1.20	300	518.24	17.3	72.7	9.9	0.56
	2	80	1.19	300	510.26	20.5	70.1	9.4	0.58
	3	120	1.13	300	505.67	25.1	68.6	6.4	0.61
	4	160	1.04	300	488.21	35.1	62.7	2.1	0.64
	5	200	1.04	300	473.14	40.2	57.7	2.1	0.72
Group 2	1	20	1.16	300	509.03	22.2	69.7	8.1	0.63
	2	80	1.11	300	496.37	29.1	65.5	5.5	0.73
	3	120	1.10	300	490.82	31.2	63.6	5.2	0.73
	4	160	1.04	300	470.03	41.2	56.7	2.1	0.75
	5	200	1.03	300	439.69	52.2	46.6	1.3	0.84
Group 3	1	20	1.16	300	463.76	37.3	54.6	8.1	0.75
	2	80	1.11	300	436.16	49.2	45.4	5.4	0.77
	3	120	1.11	300	430.19	51.3	43.4	5.3	0.81
	4	160	1.04	300	421.40	57.3	40.5	2.2	0.84
	5	200	1.04	300	411.43	60.7	37.1	2.2	0.87
Group 4	1	20	1.15	300	389.96	62.3	30.0	7.7	0.84
	2	80	1.10	300	372.80	70.5	24.3	5.2	0.85
	3	120	1.10	300	370.13	71.4	23.4	5.2	0.87
	4	160	1.06	300	361.67	76.6	20.6	2.9	0.89
	5	200	1.04	300	353.23	80.1	17.7	2.2	0.90
Group 5	1	20	1.15	300	358.16	72.9	19.4	7.7	0.87
	2	80	1.08	300	331.01	85.6	10.3	4.1	0.90
	3	120	1.08	300	303.80	94.9	1.3	3.8	0.99
	4	160	1.04	300	306.83	95.5	2.3	2.2	1.00

Table 5. 3 Dead-zone experiments – model results

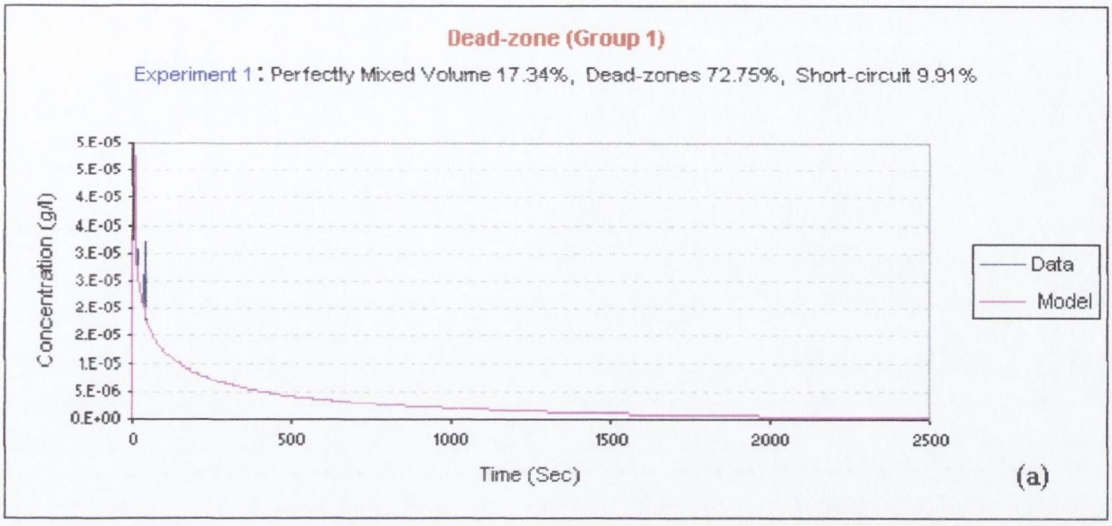
Dead-zone (Group 1)
Experiment 1: Perfectly Mixed Volume 17.34%, Dead-zones 72.75%, Short-circuit 9.91%
Concentration (g/l)
5.E-05
5.E-05
4.E-05
4.E-05
3.E-05
3.E-05
2.E-05
2.E-05
1.E-05
5.E-06
0.E+00
0
500
1000
1500
2000
2500
Time (Sec)
Data
Model
(a)

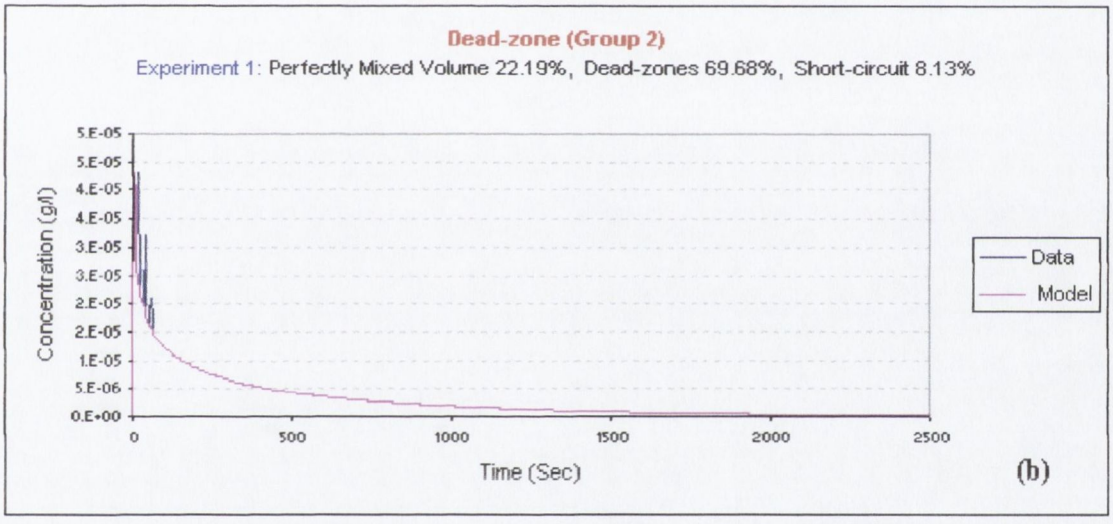
Dead-zone (Group 2)
Experiment 1: Perfectly Mixed Volume 22.19%, Dead-zones 69.68%, Short-circuit 8.13%
Concentration (g/l)
5.E-05
5.E-05
4.E-05
4.E-05
3.E-05
3.E-05
2.E-05
2.E-05
1.E-05
5.E-06
0.E+00
0
500
1000
1500
2000
2500
Time (Sec)
Data
Model
(b)

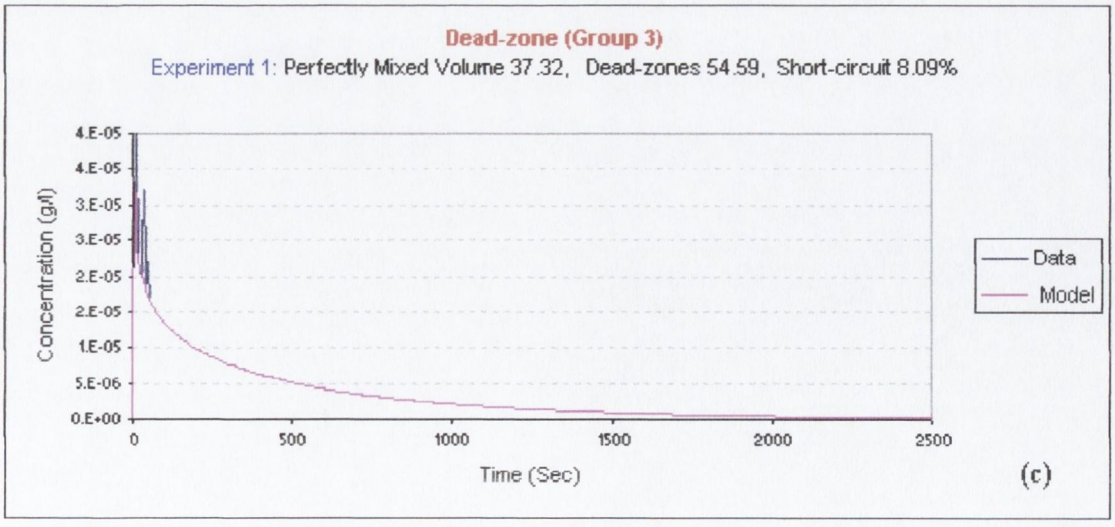
Dead-zone (Group 3)
Experiment 1: Perfectly Mixed Volume 37.32, Dead-zones 54.59, Short-circuit 8.09%
Concentration (g/l)
4.E-05
4.E-05
3.E-05
3.E-05
2.E-05
2.E-05
1.E-05
5.E-06
0.E+00
0
500
1000
1500
2000
2500
Time (Sec)
Data
Model
(c)

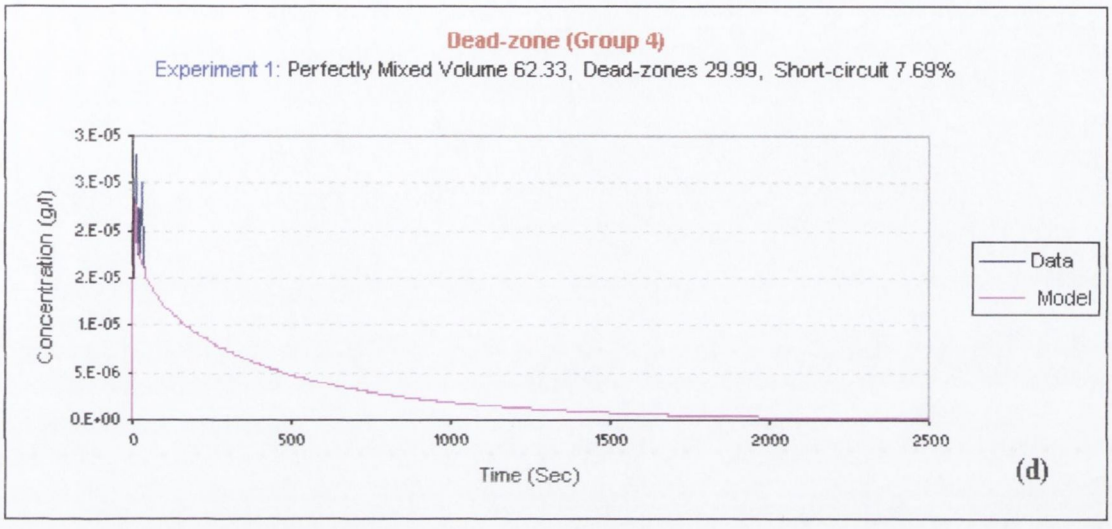

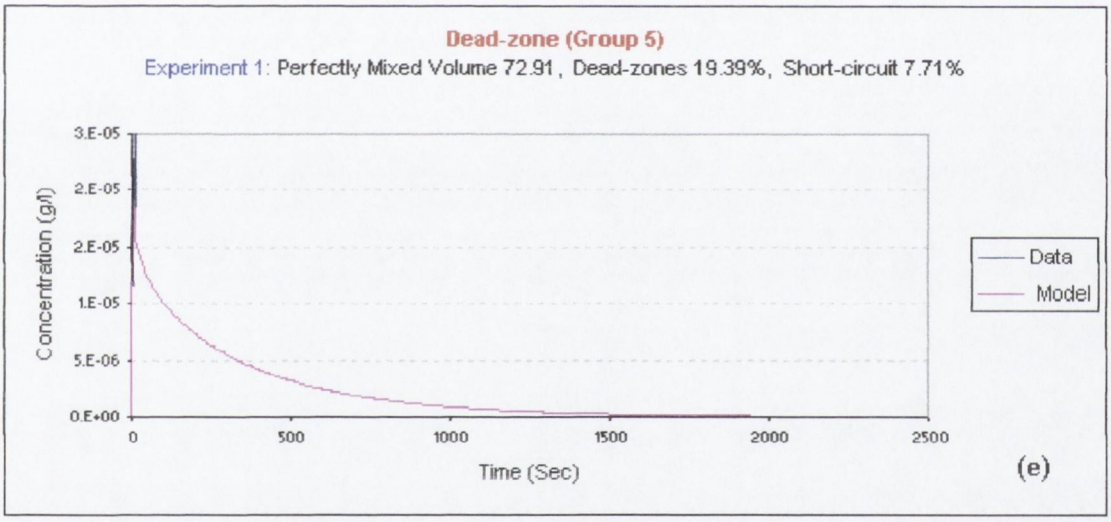

Figure 5. 3 Graphs showing laboratory results and model curves for dead-zones, Experiment 1 for (a) Group 1, (b) Group 2, (c) Group 3, (d) Group 4 and (e) Group 5

In general, as shown in Table 5.4, as the number of the holes increased, the percentage of flow passing through the perfectly mixed zone increased, as expected. In addition, the percentage of perfectly mixed flow also increased as the agitator speed increased which is more evident from the plotted data (see Figure 5.4). This shows that the dead zones acted to reduce the effective reactor volume, so that the active reactor volume was smaller than expected and also acted either to increase or decrease the theoretical retention time (refer to Section 3.4.3.2). The modelled retention time can be seen to be either greater or smaller

than the theoretical retention time indicating the existence of dead-zones and Table 5.4 shows that when the mixer speed was in the range 20 to 120 rpm with 1 or 2 holes in the plate, the flow passing through the perfectly mixed zone was very small (for example, Group 1: 17.3% to 25.1%) due to the relative strength of the dead-zone. Referring to Figure 5.4, it is very evident how the percentage of the perfectly mixed flow increases in direct ratio to the mixer speed. However, the more determining factor is the area of interface between the mixed volume and dead-zone (number of holes) because, as can be seen from Table 5.4, increasing the mixer speed from 20 to 200 rpm does result in an increased percentage of perfectly mixed flow, but only by a relatively small margin (for example Group 2: 22.2% to 52.2%). A more significant increase however comes about by the steady increase in the number of holes from one to ten holes representing an open area of 3.1 to 31.4 cm^2 (for example, from 17.3% to 72.9% in Experiment 1). It should be remembered that in all experiments the only variable is the number of holes used in each category, since the flow rate, and the volume remain constant. Finally, it should be noted that there did not appear to be any vortexing in the experiments even when the mixer speed was increased to 200rpm. This is due to the shape of the reactor effectively changing by the insertion of the plate and thus losing its circular symetry as was the case in the experiments in Chapter 4.

Group No.		1	2	3	4	5
No. of Holes		1	2	4	8	10
Experiment No.	Mixer speed (rpm)	Perfectly mixed flow (%)				
1	20	17.34	22.19	37.32	62.33	72.91
2	80	20.50	29.06	49.18	70.53	85.56
3	120	25.07	31.22	51.33	71.44	94.95
4	160	35.14	41.22	57.33	76.58	95.54
5	200	40.15	52.16	60.69	80.05	=

Table 5. 4 Conclusion of the results obtained from dead-zone experiments

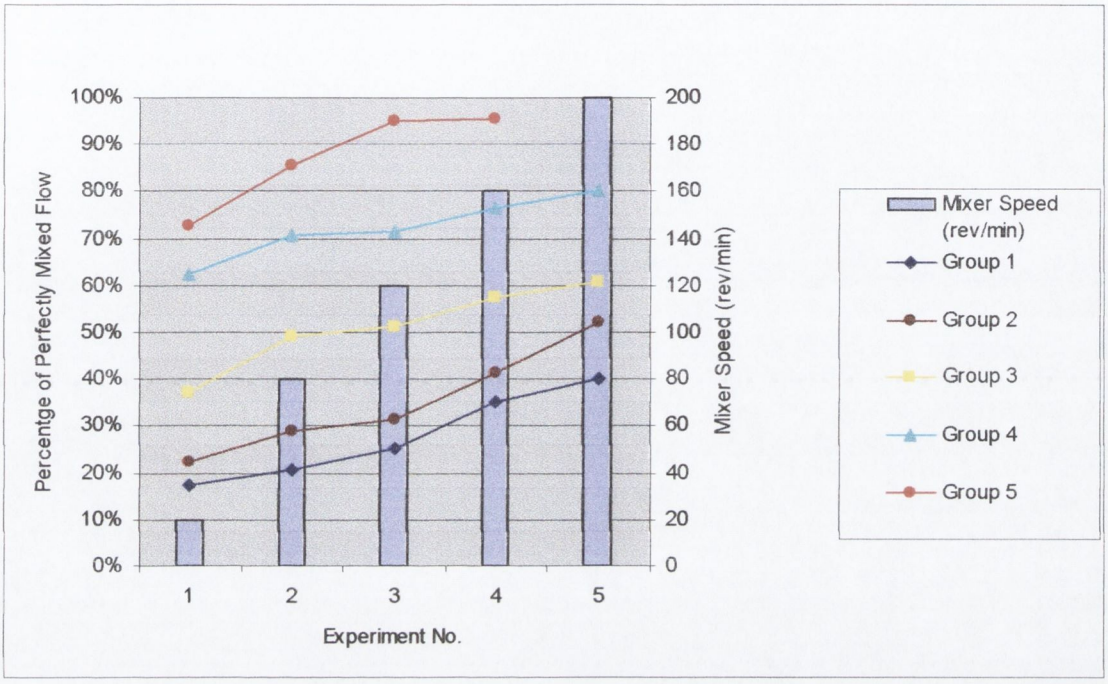

Figure 5. 4 Graph showing the effect of area of interface between the dead-zone and CSTR and mixer speed on the system's behaviour

5.3 Short-circuit

Short-circuiting is a phenomenon whereby the flow into a reactor may pass directly to the output (for whatever reason or problem) without being mixed with the reactor material. Hence, only the remaining portion of the influent is available for mixing, which again leads to process inefficiencies. As discussed in Chapter 3, in such a situation the measured mass of tracer at the theoretical retention time will be greater than half the total mass injected into the reactor at the beginning.

5.3.1 Short-Circuit Experiment Apparatus

In order to create a short-circuit zone deliberately in the circular CSTR, a hose with a diameter of 10 cm and a length of 36 cm was connected between the influent and effluent points in the reactor, as illustrated in Figure 5.6. The hose had random holes of diameter 1cm drilled along its length as illustrated in Figure 5.5. The flow rate was adjusted to a

flow rate of 2.5 l/min for all experiments and the reactor volume was kept stable at 20 litres. Each experiment was carried out at a different mixer speed and the Rhodamine WT was injected as a pulse input. As the Rhodamine was introduced through the hose, some could be seen to pass directly towards the output point while some could be seen to pass through the holes in the hose into the main reactor volume. The full data of the laboratory experiments is shown in Table 5.5.

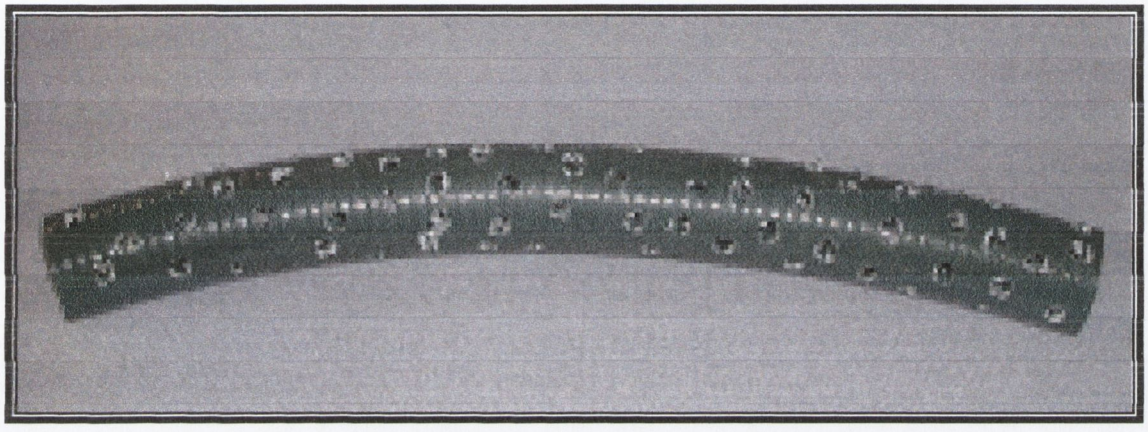

Figure 5. 5 The "short-circuit" hose with its holes

Figure 5. 6 The hose in the reactor

Experiment No.	Reactor Volume	Flow rate	Mixer speed	Rhodamine Mass
	(L)	(L/min)	(rpm)	(g)
1	20	2.50	20	0.002
2	20	2.50	40	0.002
3	20	2.50	80	0.002
4	20	2.50	120	0.002

Table 5. 5 Short-circuit experiments - configurations

5.3.2 Short-circuit Results

As before, the effluent concentrations were measured by the SCUFA and exported to an Excel© spreadsheet to obtain the RTD curve. The RTD curve was analysed and fitted to the mathematical model on the spreadsheet. The full set of the results obtained from the experiment is shown in Table 5.6 and the graphs for each experiment are shown in Figure 5.7.

Experiment No.	Mixer speed	Mass passed out at the theoretical retention time	Theoretical retention time	Modelled retention time	P%	D%	S%	No. Of CSTR
	(rpm)	$(g)^{*}10^{-3}$	(Sec)	(Sec)	(%)	(%)	(%)	(n)
1	20	1.67	480	497.87	62.58	3.72	33.70	0.69
2	40	1.37	480	495.42	78.31	3.21	18.48	0.78
3	80	1.27	480	483.65	85.97	0.76	13.27	0.88
4	120	1.18	480	487.86	89.20	1.64	9.16	0.96

Table 5. 6 Short-circuit experiments - model results

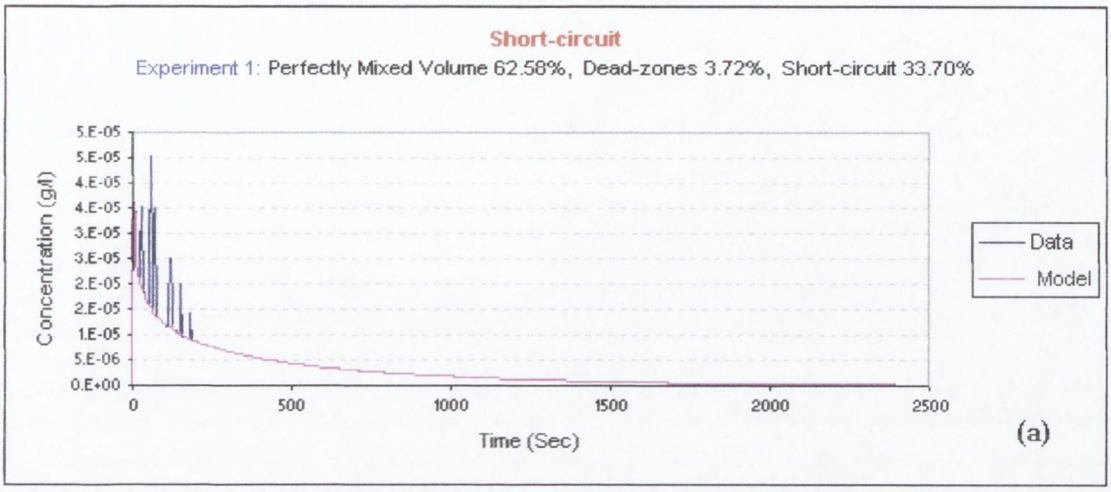
Short-circuit
Experiment 1: Perfectly Mixed Volume 62.58%, Dead-zones 3.72%, Short-circuit 33.70%
Concentration (g/l)
5.E-05
5.E-05
4.E-05
4.E-05
3.E-05
3.E-05
2.E-05
2.E-05
1.E-05
5.E-06
0.E+00
0
500
1000
1500
2000
2500
Time (Sec)
Data
Model
(a)

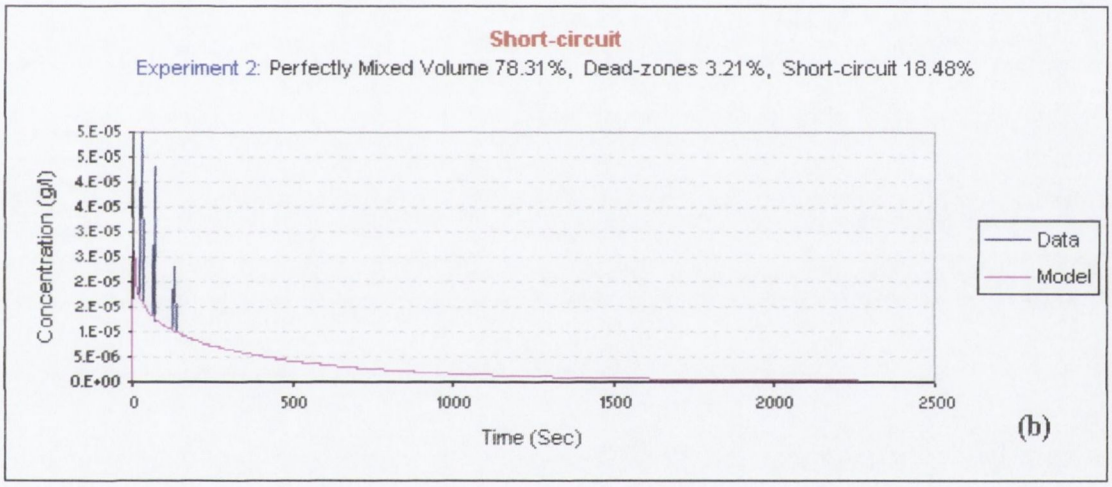
Short-circuit
Experiment 2: Perfectly Mixed Volume 78.31%, Dead-zones 3.21%, Short-circuit 18.48%
Concentration (g/l)
5.E-05
5.E-05
4.E-05
4.E-05
3.E-05
3.E-05
2.E-05
2.E-05
1.E-05
5.E-06
0.E+00
0
500
1000
1500
2000
2500
Time (Sec)
Data
Model
(b)

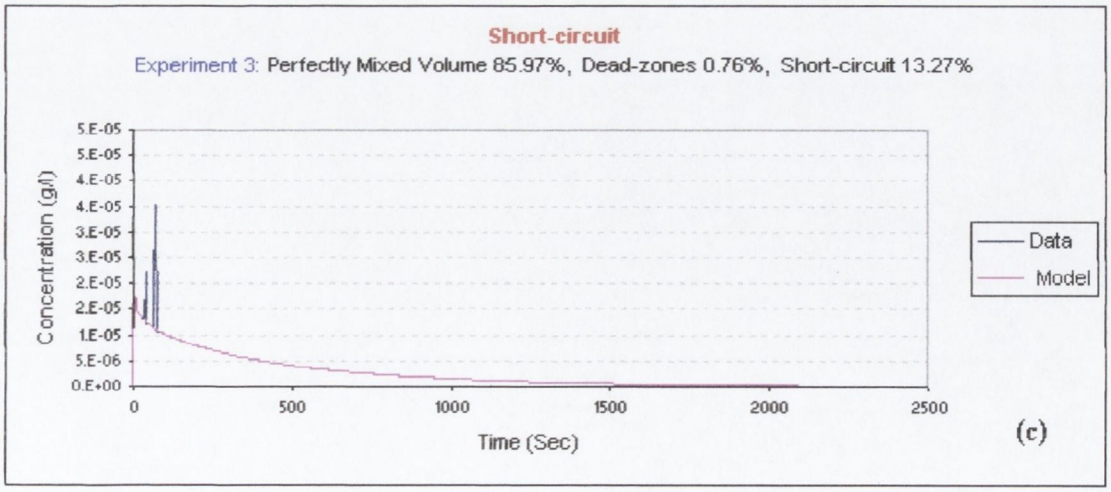
Short-circuit
Experiment 3: Perfectly Mixed Volume 85.97%, Dead-zones 0.76%, Short-circuit 13.27%
Concentration (g/l)
5.E-05
5.E-05
4.E-05
4.E-05
3.E-05
3.E-05
2.E-05
2.E-05
1.E-05
5.E-06
0.E+00
0
500
1000
1500
2000
2500
Time (Sec)
Data
Model
(c)

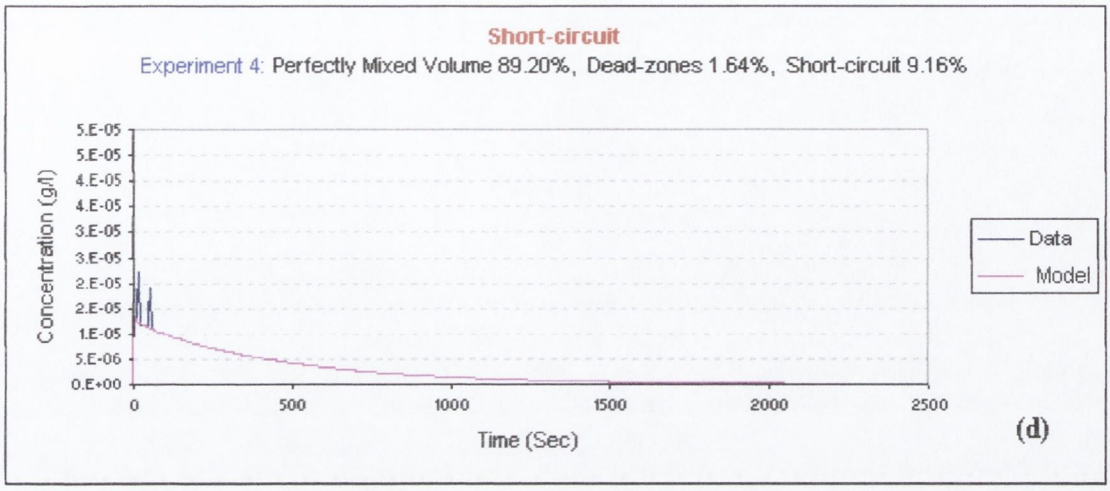

Figure 5. 7 Graphs showing laboratory results and model curves for short-circuit in a circular CSTR for (a) Experiment 1, (b) Experiment 2, (c) Experiment 3, and (d) Experiment 4

The results were collated (see Table 5.7) and plotted on a graph (see Figure 5.8) which revealed that as the mixer speed increased, the percentage of flow in the short-circuit decreased as expected. This is due to the fact that when the mixer was operating at low speeds such as 20 rpm, the velocity gradient (which is analogous to the degree of mixing) was quite small ($22.41s^{-1}$) and therefore unable to prevent the short-circuiting; when the mixer was operating at higher speeds such as 120 rpm, the velocity gradient ($329.31s^{-1}$) was sufficient to create a good mix and hence reduce the size of the short-circuit.

Experiment No.	Mixer Speed (rpm)	Velocity Gradient G (s^{-1})	Percentage of flow Short-circuiting (%)
1	20	22.41	33.70%
2	40	63.40	18.48%
3	80	179.31	13.27%
4	120	329.42	9.16%

Table 5. 7 Conclusion of the results obtained from the short-circuit experiments

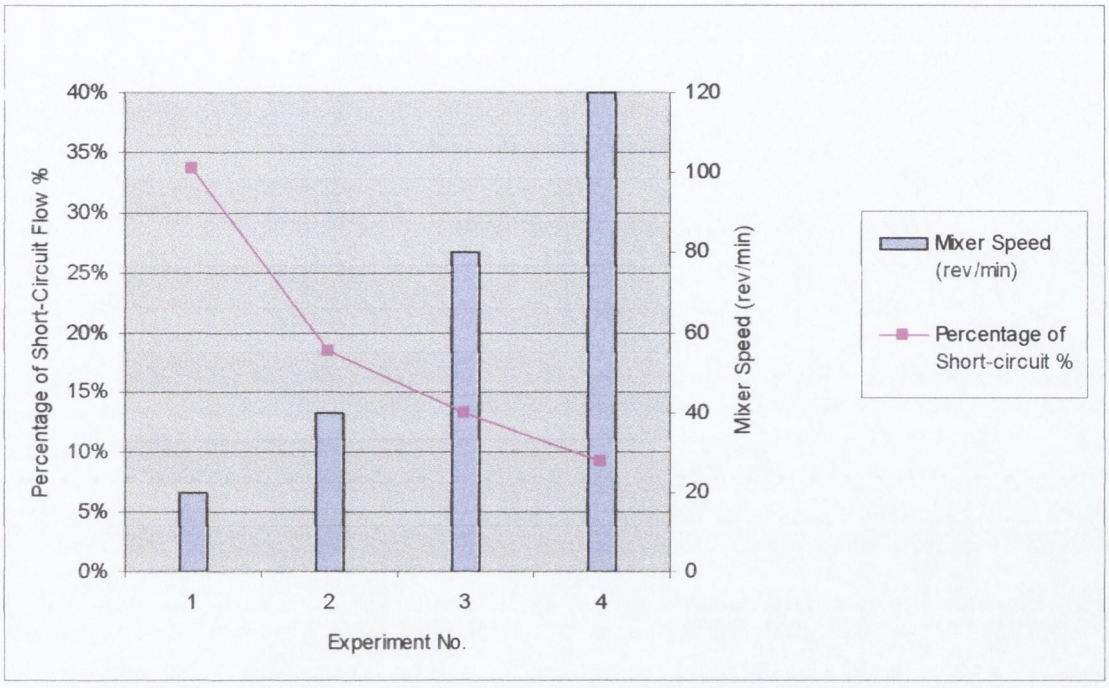

Figure 5. 8 Graph showing the effect of mixer speed on the size of the short-circuit

5.4 Combination of Dead-Zone and Short-Circuit

In order to create both short-circuit and dead zones conditions in the same reactor, a series of experiments were carried out whereby the hose used in the short-circuit experiments was again attached between the influent and effluent points, in addition to the plate used in the dead zone experiments with a single hole drilled into the centre of the plate of 2cm diameter (see Figure 5.9).

The flow rate was adjusted to 3 l/min and the reactor volume was stable at 20 litres. The Rhodamine WT was injected as a pulse input and again some could be seen to pass directly towards the output point while some could be seen to pass into the reactor through the holes in the hose to mix into the main volume. The data from the laboratory experiments is shown in Table 5.8 and the full set of the results shown in Table 5.9, with the graphs for each experiment shown in Figure 5.10.

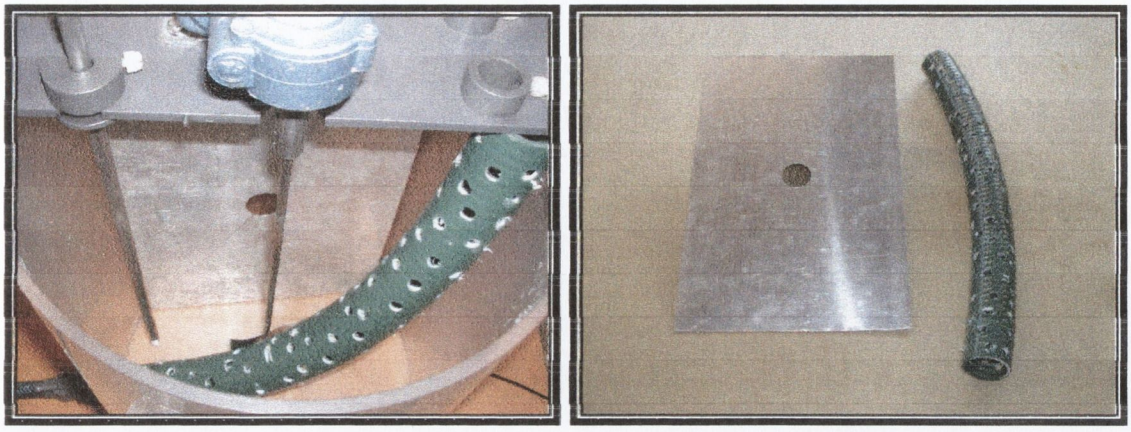

Figure 5. 9 Combination dead zone and short circuit

Experiment No.	Reactor Volume	Number of Holes (plate)	Total area	Number of Holes (Hose)	Flow rate	Mixer speed	Rhodamine Mass
	(L)	(hole)	(cm2)	(hole)	(l/min)	(rpm)	(g)
1	20	1	3.14	Random	3.00	20	0.002
2	20	1	3.14	Random	3.00	40	0.002
3	20	1	3.14	Random	3.00	80	0.002
4	20	1	3.14	Random	3.00	120	0.002

Table 5. 8 Combination dead-zone & short-circuit experiments – configurations

Experiment	Mixer speed	Mass passed out at the theoretical retention time	Theoretical retention time	Modelled retention time	P%	D%	S%	No. Of CSTR
No.	(rpm)	$(g)^{*}10^{-3}$	(Sec)	(Sec)	(%)	(%)	(%)	(n)
1	20	1.54	400	554.9	34.26	38.73	27.01	0.66
2	40	1.26	400	504.7	60.62	26.18	13.20	0.75
3	80	1.18	400	488.6	69.03	22.15	8.82	0.80
4	120	1.11	400	478.5	74.76	19.63	5.62	0.98

Table 5. 9 Combination dead-zone & short-circuit experiments – model results

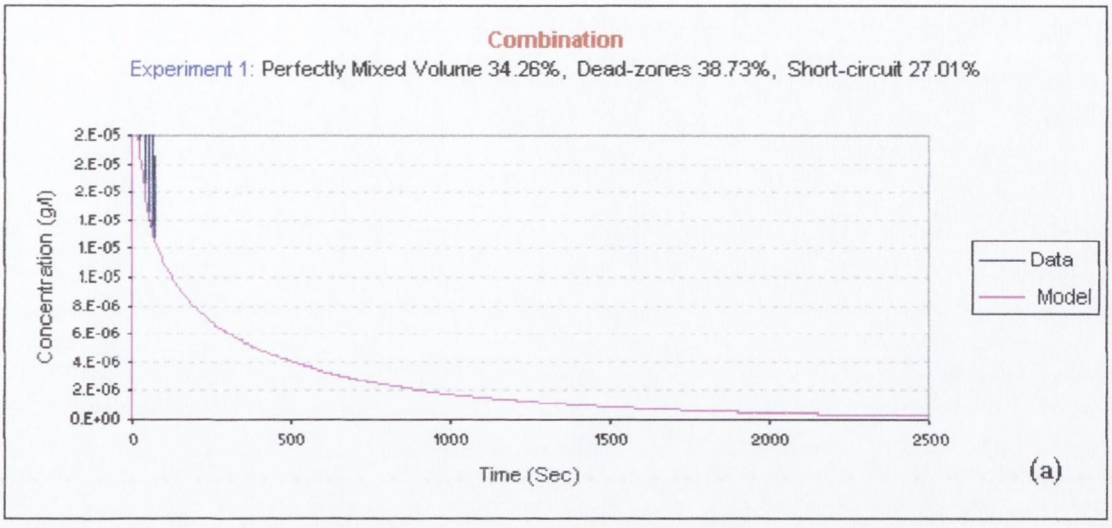
Combination
Experiment 1: Perfectly Mixed Volume 34.26%, Dead-zones 38.73%, Short-circuit 27.01%
Concentration (g/l)
2.E-05
2.E-05
2.E-05
1.E-05
1.E-05
1.E-05
8.E-06
6.E-06
4.E-06
2.E-06
0.E+00
0
500
1000
1500
2000
2500
Time (Sec)
Data
Model
(a)

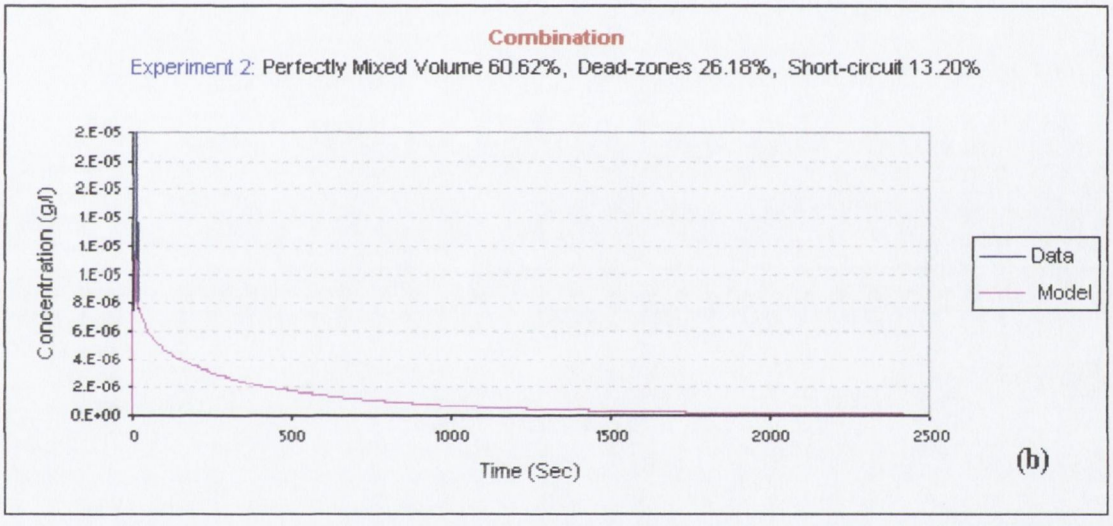
Combination
Experiment 2: Perfectly Mixed Volume 60.62%, Dead-zones 26.18%, Short-circuit 13.20%
Concentration (g/l)
2.E-05
2.E-05
2.E-05
1.E-05
1.E-05
1.E-05
8.E-06
6.E-06
4.E-06
2.E-06
0.E+00
0
500
1000
1500
2000
2500
Time (Sec)
Data
Model
(b)

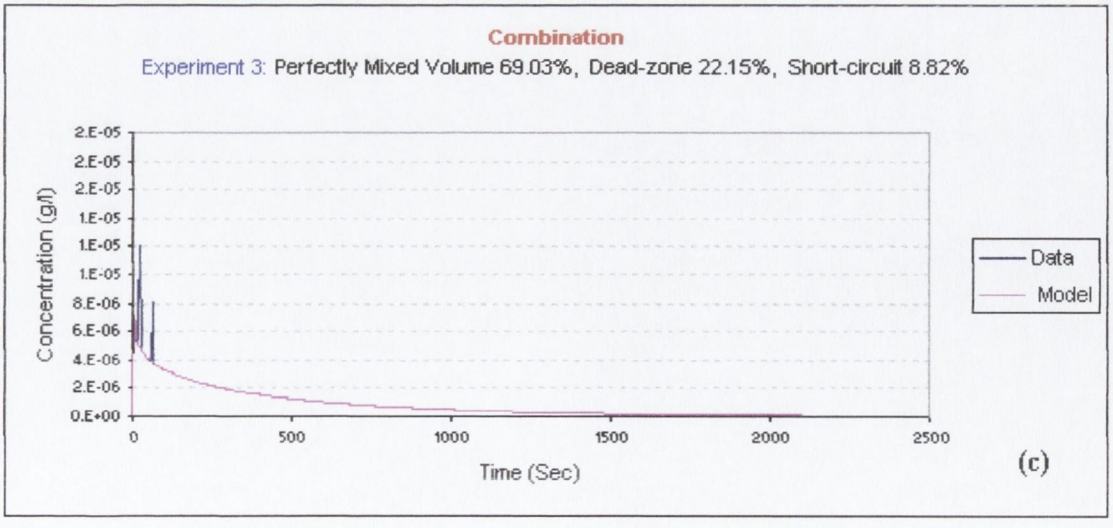
Combination
Experiment 3: Perfectly Mixed Volume 69.03%, Dead-zone 22.15%, Short-circuit 8.82%
Concentration (g/l)
2.E-05
2.E-05
2.E-05
1.E-05
1.E-05
1.E-05
8.E-06
6.E-06
4.E-06
2.E-06
0.E+00
0
500
1000
1500
2000
2500
Time (Sec)
Data
Model
(c)

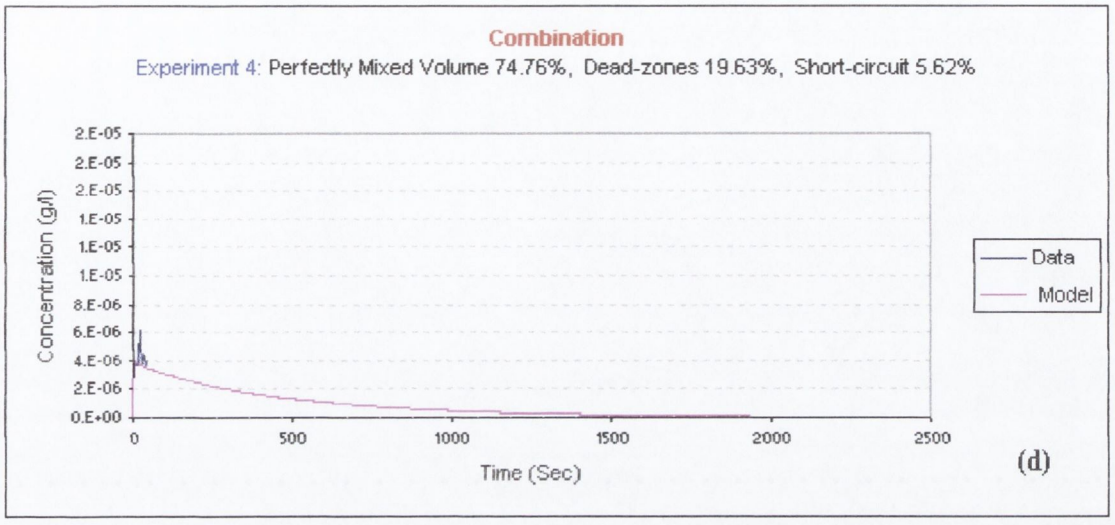

Figure 5. 10 Graphs showing laboratory results and model curves for combination experiments in a circular CSTR for (a) Experiment 1, (b) Experiment 2, (c) Experiment 3 and (d) Experiment 4

5.4.1 Combination Results Analysis

After the experiments looking at either short-circuits or the dead-zone in the circular CSTR, these results represent a more realistic scenario where both can occur at the same time. As shown in Table 5.9 when the mixer speed was low at 20 rpm, the short circuit problem appears as a relatively high figure which was verified by the results obtained in the previous short-circuit experiments. Depending on the agitation introduced by the mixer, some of the volume of the reactor can be characterised as short-circuit whilst the rest may behave as a dead-zone and a perfectly mixed volume. It is clear that as the mixer speed increased, the percentage of perfect mix increased and the undesirable problems (short-circuit and dead-zones) reduced. It is to be noted in Table 5.9 that whilst an increase in mixer speed brings about an increased percentage of perfect mix, the phenomena of dead-zones and short-circuits decrease proportionally at varying rates; namely, a sharp reduction in short-circuits (from 27.0% to 5.6%) with increased mixing (from 20 to 120 rpm). This is because there was not enough energy to remove the tracer from the short-circuit (since the tracer was effectively added into the short-circuit) when the mixer operates at low speeds. The percentage of dead-zones however, decreased at a much lower rate (from 38.5% to

19.6%) across the same mixing range. This occurs because there has to be enough energy to remove the tracer from short-circuit into the mixed area first before the tracer moves into the mixed zone and therefore has an opportunity to pass subsequently into the dead-zone area. This also leads to an increase in the reactor retention time, as shown in Table 5.9. These variants are illustrated graphically in Figure 5.11, showing the results from all four experiments which shows the short-circuits over the four experiments decreasing from 27.01% to 5.6% in proportion to mixer speed.

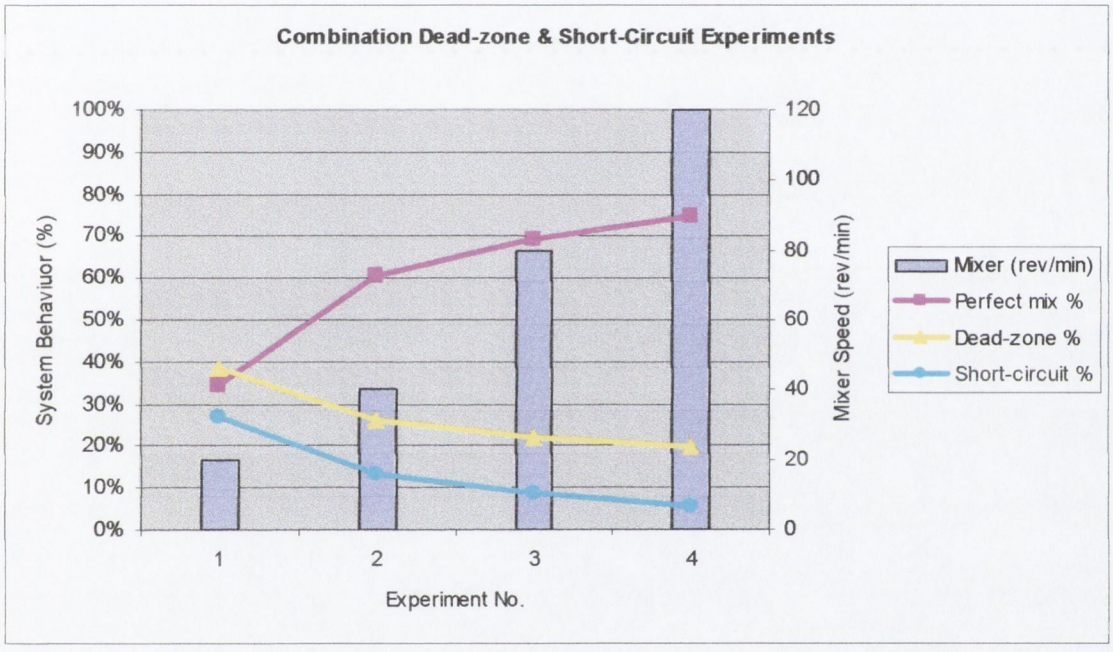

Figure 5. 11 Graph showing the effect of mixer speed on the system's behaviour

5.5 Conclusion

These simple experiments on the single CSTR in the hydraulics laboratory proved that the mathematical model could identify undesirable hydraulic characteristics in a reactor, such as the dead-zones and short-circuits, which can often create problems in real reactors in industry. The next stage was to see how the model behaved when looking at more complicated reactor networks.

Chapter 6

Reactor Network Laboratory Trials

Chapter 6

Reactor Network Laboratory Trials

6.1 Introduction

The aim of this thesis was to perform several trials on a variety of CSTR reactor configurations primarily used for the treatment of wastewater. Hence, a new physical model was built in the laboratory that allowed reactors in series to be analysed under controlled conditions in order to gain confidence in the results and hydraulic behaviour of the reactor as diagnosed by the mathematical model.

6.2 The System Apparatus

The experimental system used is indicated in Figure 6.1, which consists of a large reactor, 118.82 cm in length, 50.0 cm in height and 30.0 cm in width. The reactor was sized to these dimensions in order to get the same volume in each cell as the previous circular CSTR, allowing comparisons between the two trials to take place. The reactor has three baffles each separated by a 28.3 cm gap and each baffle is 28.5 cm high and 30.0 cm wide. The reactor with its baffles simulates four tanks in series and was fitted with an inlet pipe feed, at the top of the right hand side of the system which was connected to the constant head tank in order to keep the flow rate and water level constant in the reactors during each experiment. An outlet pipe was located at the bottom corner of the left hand side of the system, as well as four mixers, one in each tank, allowing for the perfect mixing of liquids. The mixer speed was adjusted through a variable speed reducer located at the top of each reactor, shown in Figure 6.2. The blades of each mixer were square in shape 7cm by 7cm, with a slight "S" profile, or curve, on the blades, as shown in Figure 6.1, with three holes of 2cm in diameter. Finally, the outlet pipe from the reactors was connected to the SCUFA to measure the effluent concentration of the Rhodamine WT from the reactors.

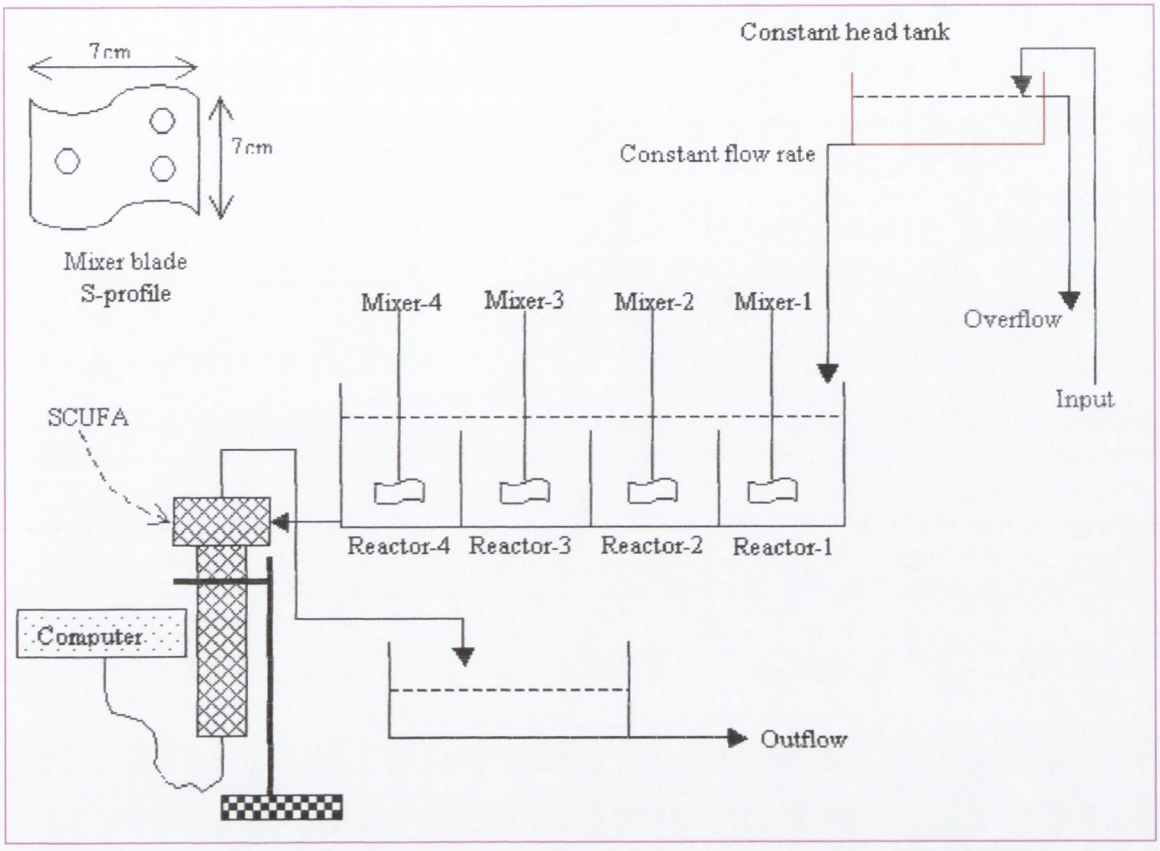

Figure 6. 1 Schematic diagram of system apparatus

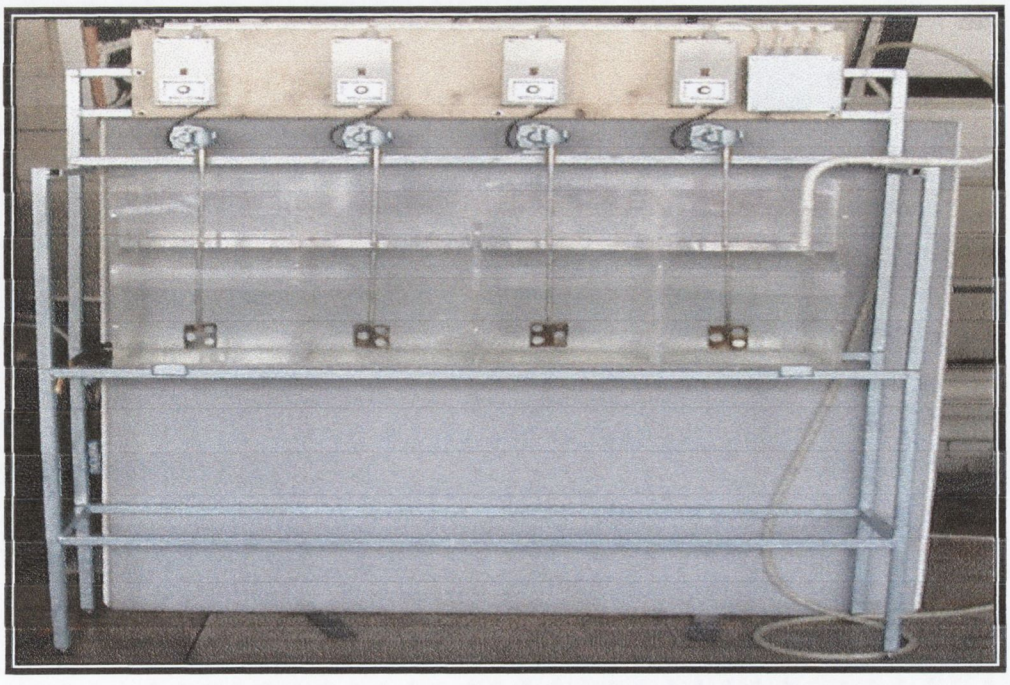

Figure 6. 2 Photograph showing the system apparatus

6.3 Procedure of Trials

Firstly, all the equipment was checked to ensure it was in good working order and that all connections had been made as outlined in the experimental design. Next, the SCUFA was calibrated with Rhodamine WT solution (see Appendix A), the reactor was filled with water and the input and output flow rates were equalized until the desired volumes in the reactors were reached. At this point, the impeller stir rate was selected. The concentrated Rhodamine WT dye was measured accurately using a pipette and then suddenly injected into the input of the system as a pulse input. The concentration of Rhodamine WT in the effluent was logged by the SCUFA during the trial and was then exported into an Excel© spreadsheet, as described previously.

6.4 Summary of Trials

A summary of each trial conducted on the laboratory model is given in the appropriate sections below. Photographic sequences of the tracer inside the reactor for each trial are presented in Appendix D.

6.4.1 Trial 1 (one CSTR model)

Trial 1 was a control trial in order to allow a comparison to be made both with the preliminary experiments carried out on the circular reactor (see Chapter 4) and also with the subsequent trials in this section to determine the behaviour of a reactor of this geometry. For this trial, the single reactor was rectangular in shape, 30.0 cm in width, 28.3 cm in length and 30.0 cm in height in order to get the same volume as the previous circular CSTR. There was no baffle in the reactor, neither had any dead-zones or short-circuit been deliberately created (Figures 6.3 (a) and (b)). This trial was run many times at different mixer speeds but always at the fixed flow rate, of 3.5l/min (the same as in circular CSTR trials).

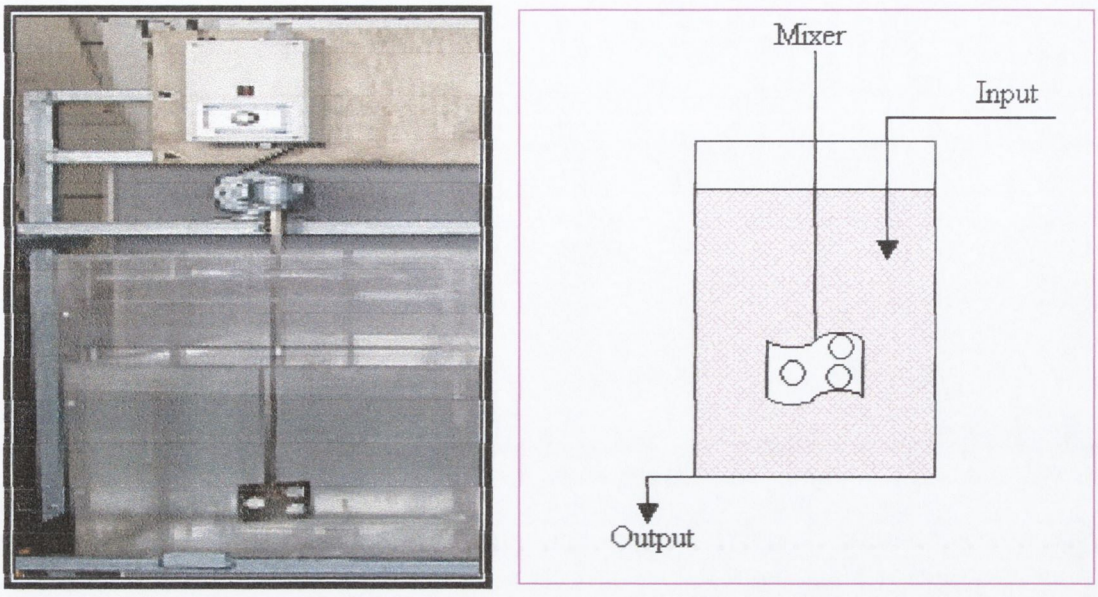

(a) (b)

Figure 6. 3 Showing one CSTR model for Trial-1 for (a) Photograph and (b) Schematic diagram

6.4.1.1 Trial 1 Data and Results

The tracer was introduced into the reactor as a pulse input at time t = 0. For the first experiment the mixer was at rest (0 rpm) and when the tracer entered the reactor it could be seen to take a vertical direction towards the bottom of the reactor (see Appendix D) due to the momentum of the influent flow. The tracer started spreading inside the reactor very slowly due to the fact that the mixer was at rest. With successive experiments the mixer speed was increased and it can clearly be seen (Appendix D) that, as the agitation introduced increased, the tracer's diffusion apparently increased as well. By following the photographic sequence in Appendix D, one can build up a broad picture of what one might expect will happen inside the reactor. Furthermore the visual observations can enable the movement of the tracer inside the reactor to be crudely ascertained including potential dead zone areas and short-circuits. The tracer concentration was measured by using the SCUFA device and discussed in Chapter 4. During trial 1, the reactor volume was controlled to a fixed volume (20L) by adjustment of the input flow rate and output flow rate (3.5 l/min). The configurations for each experiment are shown in Table 6.1 and the full set of model results can be seen in Table 6.2. An example graph for experiment 1 is shown in Figure 6.4 whilst all other graphs are shown in Appendix E. The results show that when the mixer was at rest at 0 rpm,

some of the tracer went to the output with great rapidity in short-circuit whilst much of the rest of reactor could be considered to be a dead-zone. As more agitation was introduced into the reactor from the mixer Table 6.2 shows that the short-circuits and dead-zones became smaller and disappeared at the critical mixer speed of 200 rpm. Interestingly, the problem of dead-zones slightly increased between 20 and 40 rpm which may be an indication that the mixer speed has been sufficient to break up the short-circuit but not enough to effect the dead-zones significantly. Hence, more tracer is getting trapped in the dead-zones that, at lower mixer speeds, would have passed straight through the reactor.

Experiment No.	Reactor Volume	Flow rate	Mixer speed	Power input	Velocity Gradient	Rhodamine Mass
	(L)	(l/min)	(rpm)	(Kw)	(s^{-1})	(g)
1	20.0	3.50	0	0	0	0.002
2	20.0	3.50	20	0.01	22.41	0.002
3	20.0	3.50	40	0.09	63.40	0.002
4	20.0	3.50	80	0.73	179.31	0.002
5	20.0	3.50	120	2.47	329.42	0.002
6	20.0	3.50	160	5.86	507.18	0.002
7	20.0	3.50	200	11.45	708.80	0.002

Table 6. 1 Trial 1 Experiments - configurations

Experiment No.	Mixer speed	Mass passed out at the theoretical retention time	Theoretical retention time	Modelled retention time	P%	D%	S%	No. Of CSTR
	(rpm)	$(g)^{*}10^{-3}$	(Sec)	(Sec)	(%)	(%)	(%)	(n)
1	0	1.28	342.9	473.9	47.7	38.2	14.1	0.81
2	20	1.26	342.9	395.6	71.7	15.4	12.9	0.83
3	40	1.13	342.9	409.5	74.1	19.4	6.5	0.87
4	80	1.08	342.9	396.4	80.6	15.6	3.8	0.93
5	120	1.06	342.9	354.2	93.9	3.3	2.8	0.96
6	160	1.05	342.9	351.1	95.3	2.4	2.3	0.98
7	200	1.02	342.9	343.3	99.1	0.1	0.8	0.99

Table 6. 2 Results Obtained from Laboratory Experiments for Trial 1

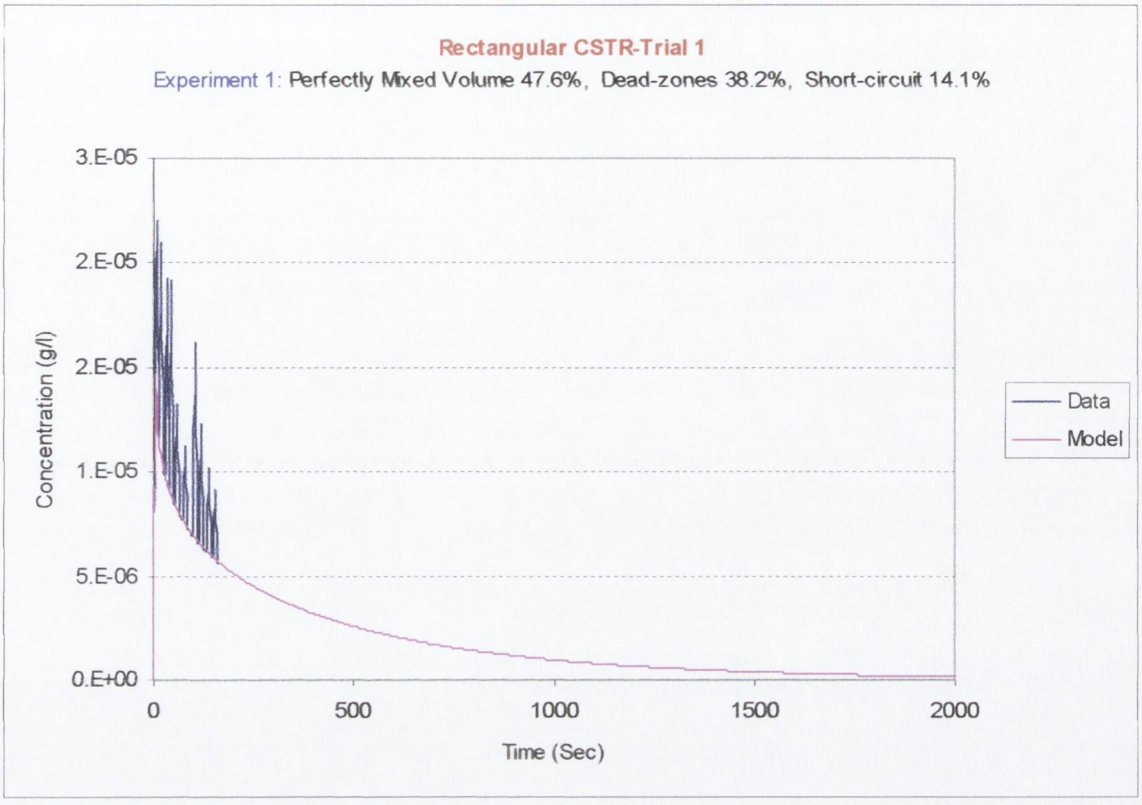

Figure 6. 4 Graph showing laboratory results and fitted model curve for a pulse input into single CSTR for Trial 1, Experiment 1.

6.4.2 Trial 2 (two CSTR in-series model)

After completing a number of experiments on the single CSTR system, trials were then carried out to study the hydraulic characteristics of multiple reactors configured in-series. For this trial two reactors in-series were modeled. In addition, the nature of the baffle between the two reactors was varied in two different ways to study the differences between the two commonly used types of baffle in the water industry. For this trial the system was rectangular in shape (30.0 cm in width, 57.0 cm in length and 50.0 cm in height), the reactor was fitted with the inlet and outlet pipes as well as two mixers as shown in Figure 6.5. A baffle was placed half-way along the system to create two equally sized reactors in-series as illustrated in Figure 6.5 and the two different baffle configurations are illustrated in Figure 6.6(a) and (b), which change the path of the flow between each reactor. Again, each trial was run many times at the different mixer speeds in order to gain representative results.

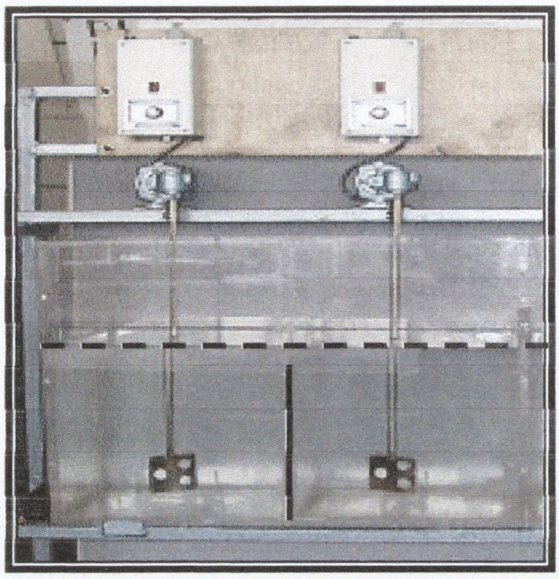

Figure 6. 5 Photograph showing two CSTR in series model

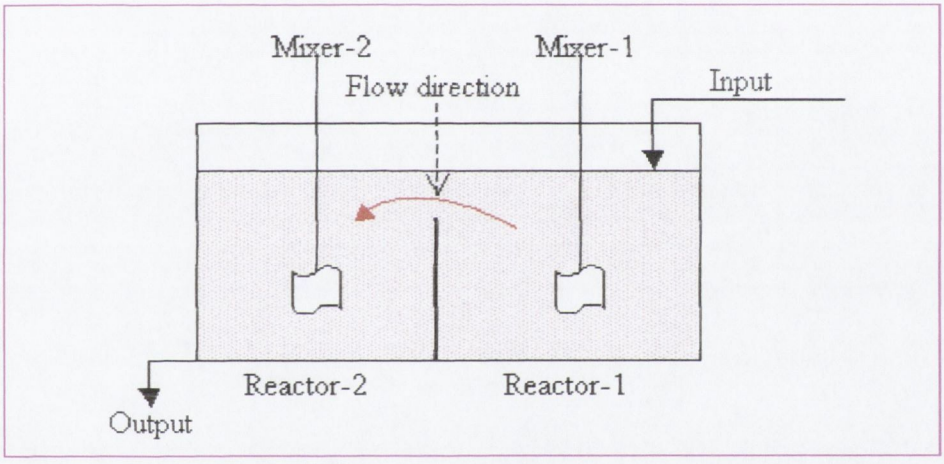

(a)

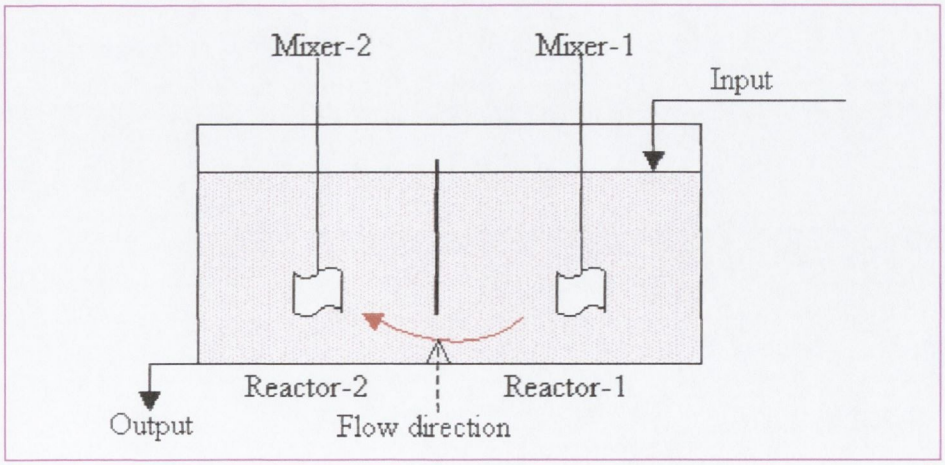

(b)

Figure 6. 6 Schematic diagram showing flow path inside the reactors for (a) Trial 2A and (b) Trial 2B

6.4.2.1 Trial 2 Data and Results

The tracer was injected into the reactor as a pulse input for all the trials. The photographic sequence of the tracer inside the reactor is illustrated in Appendix D. When the mixer speed was 0 rpm the tracer could be seen to take a vertical direction towards the bottom of the reactor and only after a period of time the tracer began to disperse. Thereafter, the tracer began to enter the second reactor and to move towards the output point with the direction of flow, as illustrated in Figures 6.6(a) and (b) above.

The photographs in Appendix D clearly identify some areas of the reactor as a short circuit whilst other areas inside the system were behaving as dead zone. The experimental configuration for both Trials 2A and 2B can be seen in Table 6.3. An example of the RTD graphs obtained for experiment 1 for each baffle configuration is illustrated in Figures 6.8(a) and (b). In addition, the full set of the results for trials (2A and 2B) can be seen in Table 6.4. This shows that the differences in mixing behaviour of the reactor were clearly ascribable to the differences in baffle configuration, the baffle being lowered in one and raised in the other. A comparison with Table 6.2 makes evident a certain pattern of behaviour, whereby the dead-zones in Table 6.4, although they appeared the same critical point of 0 rpm, did not decrease with the increase of the mixer speed at the same steady rate as in Table 6.2 but rather tended to remain at the same level (between 14.8% and 9.8%) until the mixer speed reached 200 rpm, where there was a drop-off to 6.5%. It will also be noted that the fraction of the dead-zones was considerably smaller overall in Table 6.4 compared to Table 6.2, which is related to the fact that there were 2 identical reactor in series (the residence time is higher) under the same flow conditions.

Referring to Table 6.4, the different configurations clearly produced different patterns of behaviour with regard to short-circuits and dead-zones and this may be due to the effect of the baffle position which has a direct affect on the flow path, as show in Figure 6.7(a) and (b). When the baffle was lowered, as in Trial 2A, then short-circuits disappear once the mixer speed of 40 rpm has been reached. This is due to the momentum associated with the incoming flow (4.23×10^{-7} kg.m/s). Hence, when the flow was forced to pass cross the mixer, the energy of the mixer (see Table 6.3) was sufficient to disperse the kinetic energy of the flow, as in the baffle configuration shown in Figure 6.7(a). The momentum of the flow over the central baffle was much smaller calculated at 2.2×10^{-8} kg.m/s. In Figure 6.7(b), however, although the flow momentum

was the same as in the first baffle configuration it is less interrupted by the mixer and obviously isn't being dispersed as much. This can be seen numerically in Table 6.4 for Trial-2A when the short-circuit sharply decreased. But, when the baffle is raised, as in Trial 2B, a very high percentage of short-circuits were created which only gradually declined with increased mixer speeds. The output point was also important to the direction of the flow through the reactor and hence the presence of the short-circuit had been enhanced due to the combination of inflow, baffle position and outflow points which all help to preserve the momentum of influent flow through the reactor network without forcing the flow to pass directly through a completely mixed zone (as in Trial 2A). Finally, the results show that the number of tanks in-series **n** tends towards 2 (as the mixer speeds increased) whilst the percentage of dead-zone and short-circuit flow moved towards 0%, indicating the effectiveness of the model.

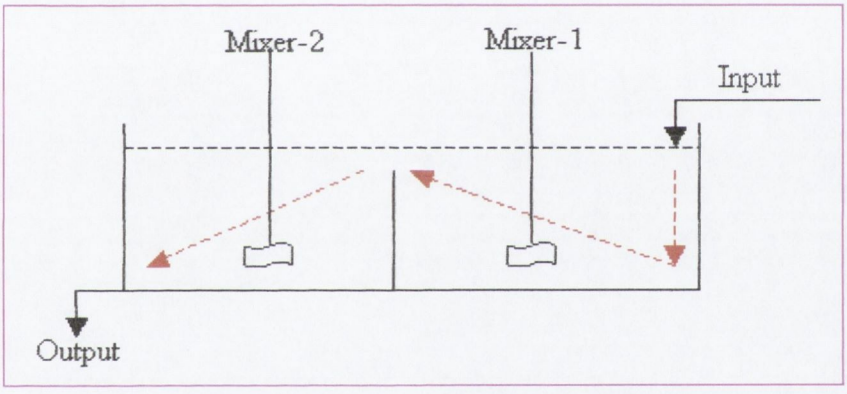

(a)

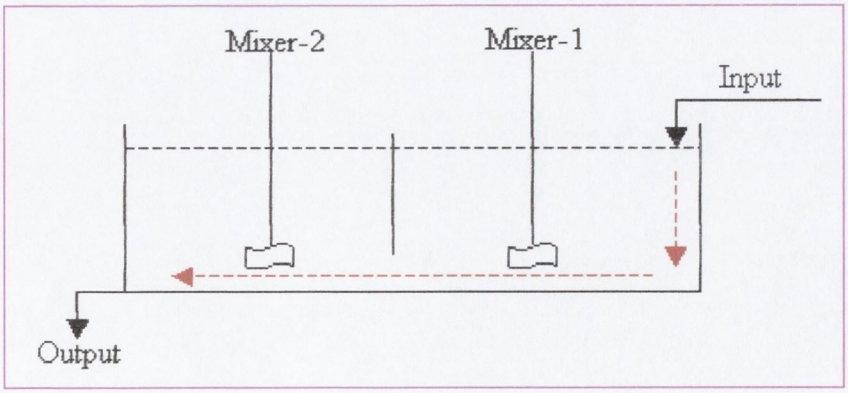

(b)

Figure 6. 7 Schematic diagram showing the flow path profile inside the reactors for (a) Trial 2A and (b) Trial 2B

Experiment No.	Reactor Volume	Flow rate	Mixer speed	Power input	Velocity Gradient	Rhodamine Mass
	(L)	(l/min)	(rpm)	(Kw)	(s^{-1})	(g)
1	56.4	4.0	0	0	0	0.002
2	56.4	4.0	20	0.02	18.87	0.002
3	56.4	4.0	40	0.18	53.38	0.002
4	56.4	4.0	80	1.47	150.97	0.002
5	56.4	4.0	120	4.95	277.35	0.002
6	56.4	4.0	160	11.73	427.01	0.002
7	56.4	4.0	200	22.91	596.76	0.002

Table 6. 3 Trials 2A and 2B experiments – configurations

Trial No.	Experiment No.	Mixer speed (rpm)	Mass passed out at the theoretical retention time $(g)^{*}10^{-3}$	Theoretical retention time (Sec)	Modelled retention time (Sec)	P% (%)	D% (%)	S% (%)	No. Of CSTR (n)
Trial-2A	1	0	1.38	846.5	1106.2	50.3	30.7	19.1	1.59
	2	20	1.32	846.5	950.5	71.6	12.3	16.1	1.61
	3	40	1.07	846.5	940.3	85.6	11.1	3.3	1.76
	4	80	1.05	846.5	931.4	87.2	10.0	2.7	1.85
	5	120	1.04	846.5	929.8	88.0	9.8	2.2	1.89
	6	160	1.03	846.5	910.4	90.8	7.6	1.7	1.97
	7	200	1.02	846.5	870.0	96.0	2.8	1.2	1.99
Trial-2B	1	0	1.50	846.5	1112.3	43.5	31.4	25.1	1.51
	2	20	1.43	846.5	970.5	63.6	14.7	21.7	1.60
	3	40	1.47	846.5	953.3	63.9	12.6	23.5	1.70
	4	80	1.39	846.5	944.4	69.0	11.6	19.4	1.80
	5	120	1.32	846.5	939.8	72.9	11.0	16.0	1.84
	6	160	1.28	846.5	920.4	77.2	8.7	14.1	1.89
	7	200	1.21	846.5	865.0	87.1	2.2	10.7	1.93

Table 6. 4 Trials 2A and 2B experiments - results

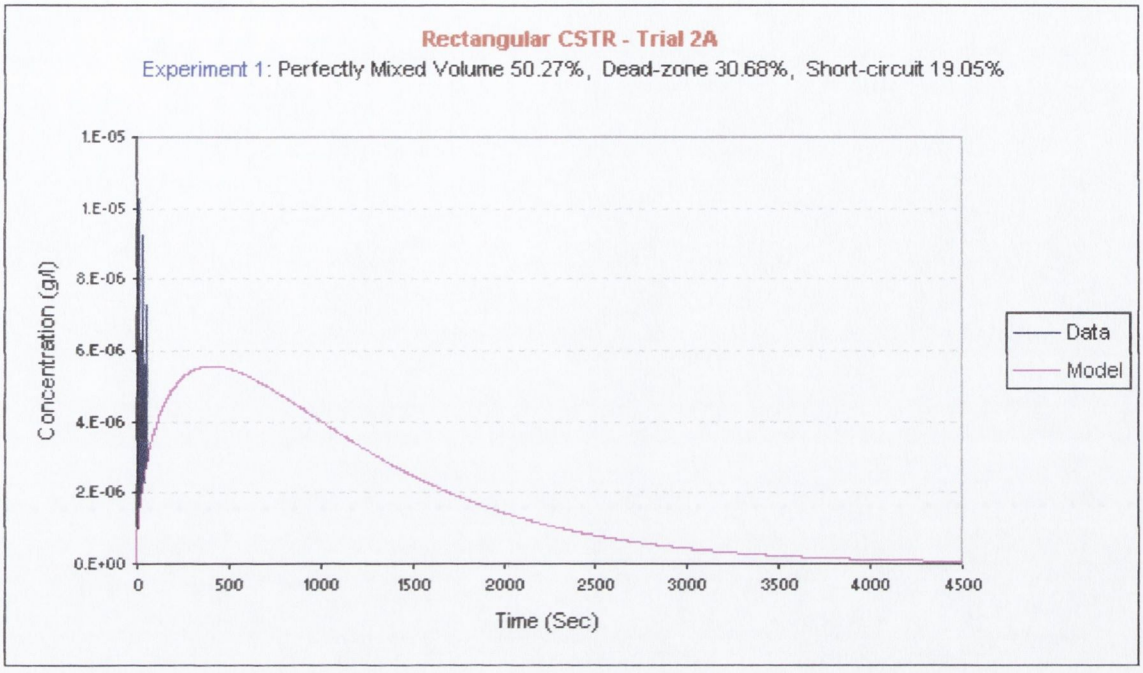

(a)

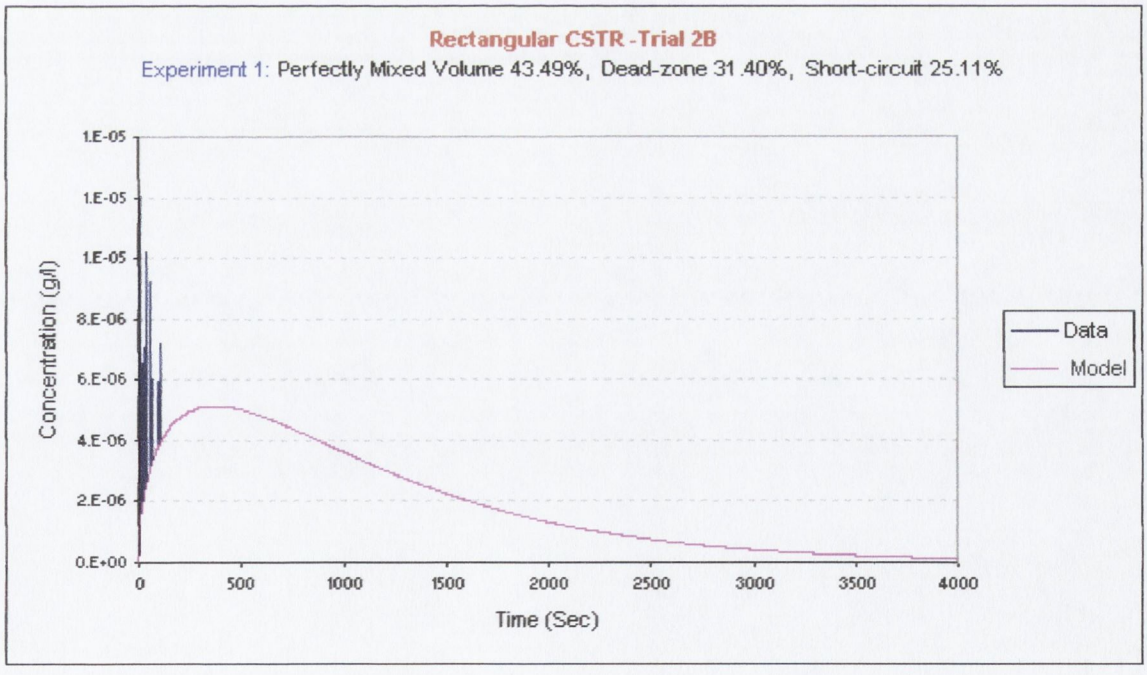

(b)

Figure 6. 8 Graphs showing laboratory results and fitted model curves for a pulse input into 2CSTR in-series for (a) Trial 2A, Experiment 1 and (b) Trial 2B, Experiment 1

6.4.3 Trial 3 (three CSTR in-series model)

In this trial, a third reactor was introduced to create a three-reactor in-series model. For this trial, the dimension of the overall system was 30.0 cm in width, 85.5 cm in length and 50.0 cm in height and baffles were introduced to divide the reactor into a three equally sized reactors in-series. The reactor was fitted with the inlet and outlet pipes as well as three mixers as illustrated in Figure 6.9. Two different baffle configurations were trialed shown on schematic Figures 6.10 (a) and (b), to analyze how the difference in flow paths might affect the hydraulic characteristics of the reactor network.

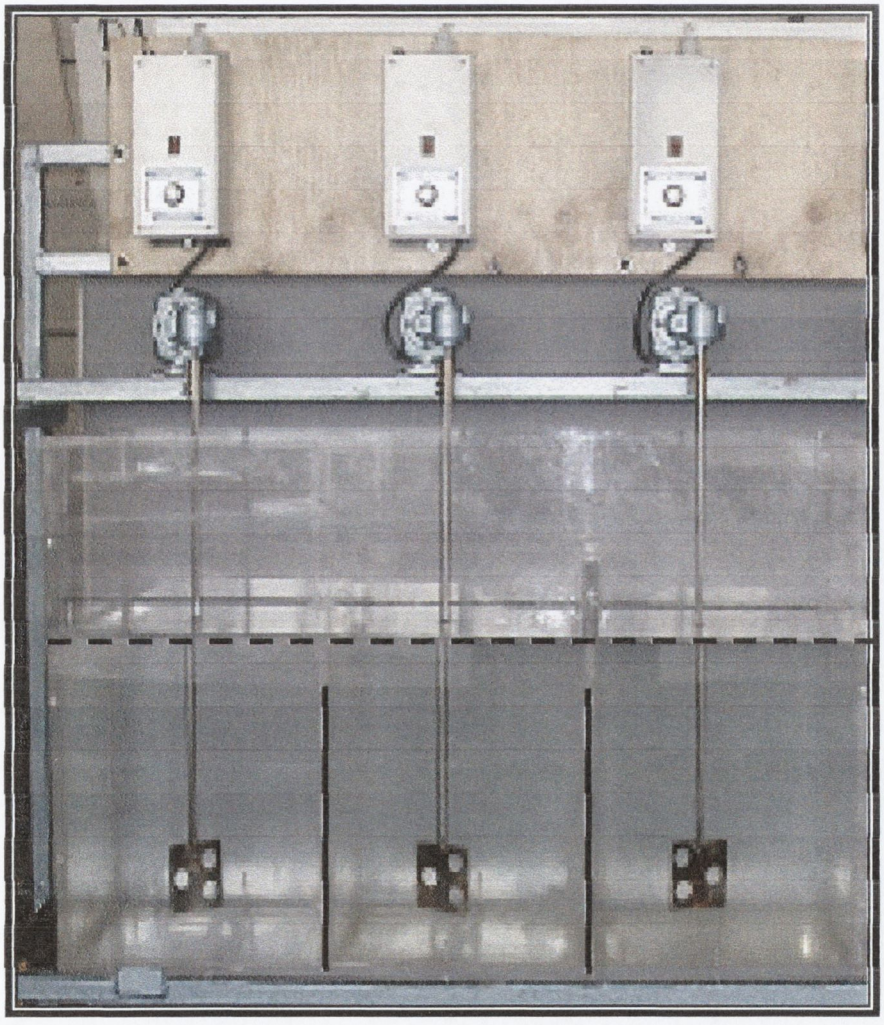

Figure 6. 9 Photograph showing three CSTR in-series model

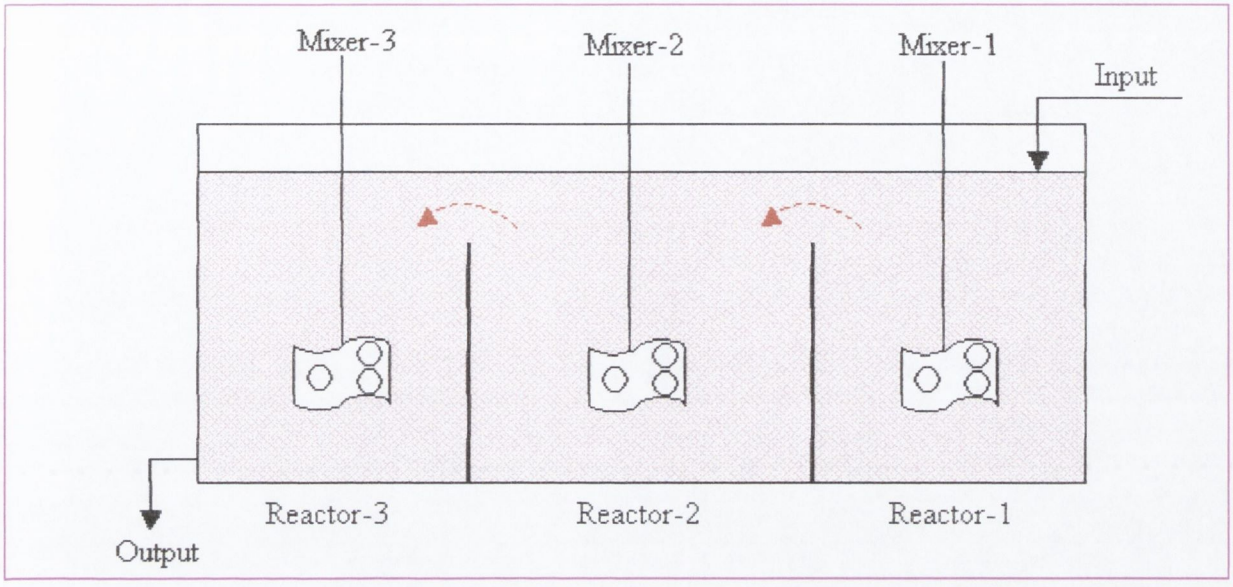

(a)

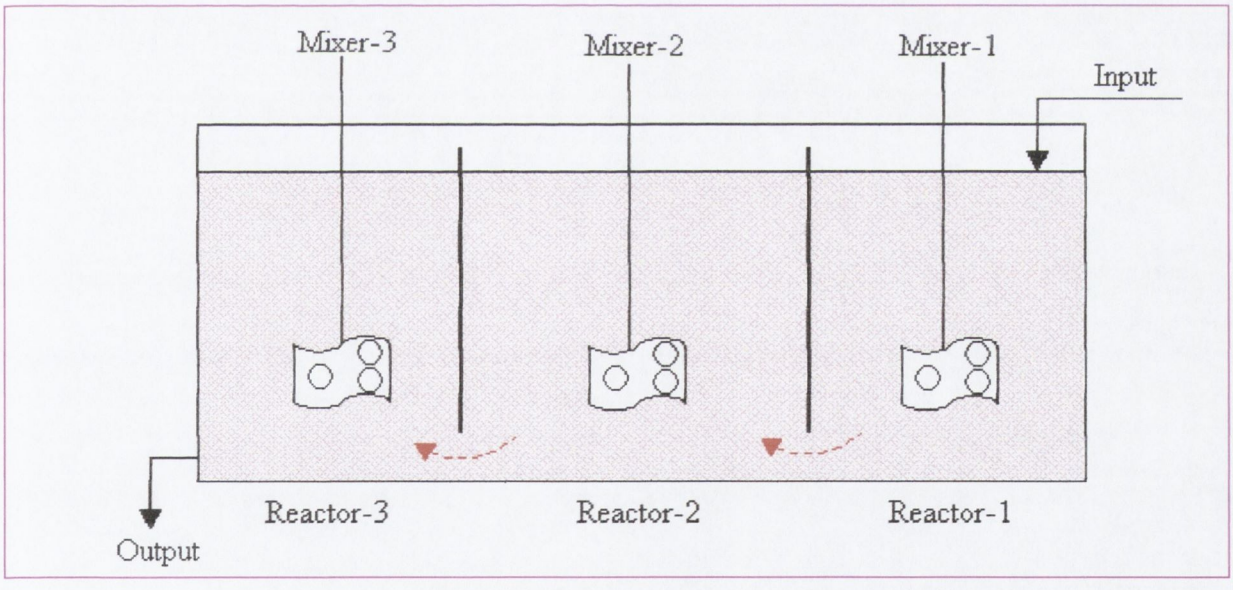

(b)

Figure 6. 10 Schematic diagram showing flow path inside the reactors for (a) Trial 3A and (b) Trial 3B

6.4.3.1 Trial 3 Data and Results

The tracer was introduced into the reactor as a pulse input as in previous experiments. The photographic sequence of the tracer inside the reactor can be seen in Appendix D, showing the tracer movement in the first experiment when the mixer speed was at rest (0 rpm), the tracer giving a visual indication of the degree of mixing short-circuits and dead-zones.

The experimental conditions and the full set of data obtained from all experiments for Trials 3A and 3B can be seen in Tables 6.5 and 6.6. An example of the RTD graphs obtained for Experiment 1 for each trial is also illustrated in Figure 6.12. In Trial 2 the differences in baffle configuration were seen to account for the appearance of dead-zones and the disappearance of any short-circuit. These trials show that in Trial 3A where both baffles were lowered, better mixing conditions were produced compared to Trial 3B where both baffle were raised. Again, as in the previous trials, the baffle position controlled the mixing behaviour as shown in Figure 6.11, which leads to the disappearance of short-circuits at relatively low mixing speeds in Trial-3A compared to the higher speeds (and hence energy input) required in Trial 3B (see Table 6.6).

Again this can be attributed to the momentum of the incoming flow (4.73×10^{-7} kg.m/s) entering the reactors. Hence, when the flow was forced to pass directly past the mixer as in baffle configuration Figure 6.11(a), the energy of the mixer was sufficient to disperse the energy of flow. In Figure 6.11(b), however, the flow momentum (2.5×10^{-8} kg.m/s) was smaller but was more uninterrupted and obviously wasn't being dispersed as much by the mixer. This can be seen numerically from the results of Trial 3A when the short-circuit sharply decreased. When the baffle was raised however, as in Trial 3B, there was a very high percentage of short-circuits which only gradually declined with increased mixer speeds. The position of the output point was also important to the direction of the flow through the reactor and hence short-circuiting had been enhanced due to the combination of inflow, baffle and outflow positions which all help to preserve the momentum of flow through the reactor network without forcing the flow to pass directly through an completely mixed zone (as in Trial 3A). In addition, the number of CSTRs in series which was recognized by the model (see Table 6.6), were less than 3 until the mixer speed have reached 200 rpm, at which point the energy input was sufficient to overcome the momentum of the incoming flow into each reactor.

In conclusion, Trial 3 confirms the results of Trial 2, whereby the percentage of both dead-zones and short-circuits are related to the baffle configuration and are shown to diminish in relation to mixer speed. The overall percentage of perfectly mixed flow in Trial 3 proved to be higher than in Trial 2 for the same mixer speeds. This is presumably due to the fact that the flow had a longer RTD in the reactor network leaving more time for dispersion and that more energy was being added into the network since there were more mixers, as shown in Table 6.5.

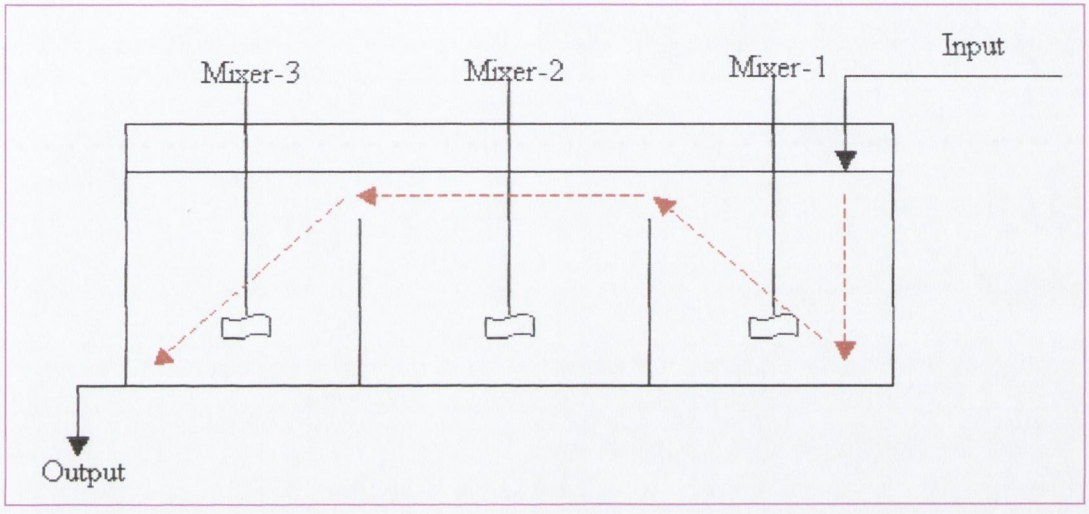

(a)

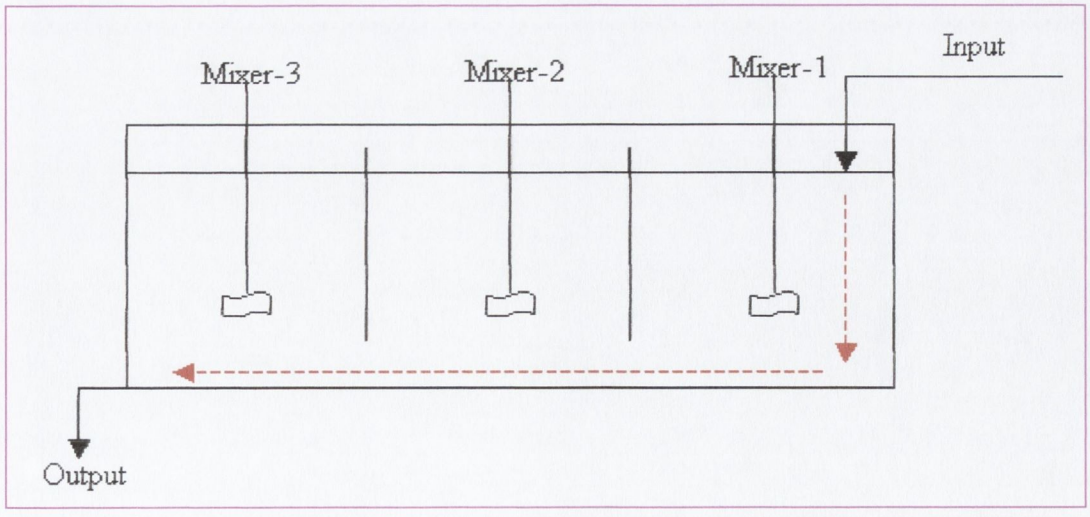

(b)

Figure 6. 11 Schematic diagram showing the flow path profile inside the reactors for (a) Trial 3A and (b) Trial 3B

Experiment No.	Reactor Volume	Flow rate	Mixer speed	Power input	Velocity Gradient	Rhodamine Mass
	(L)	(l/min)	(rpm)	(Kw)	(s^{-1})	(g)
1	84.6	4.5	0	0	0	0.002
2	84.6	4.5	20	0.03	18.87	0.002
3	84.6	4.5	40	0.27	53.38	0.002
4	84.6	4.5	80	2.20	150.97	0.002
5	84.6	4.5	120	7.42	277.35	0.002
6	84.6	4.5	160	17.59	427.01	0.002
7	84.6	4.5	200	34.36	596.76	0.002

Table 6. 5 Trials 3A and 3B experiments - configurations

Trial No.	Experiment No.	Mixer speed (rpm)	Mass passed out at the theoretical retention time $(g)^{*}10^{-3}$	Theoretical retention time (Sec)	Modelled retention time (Sec)	P% (%)	D% (%)	S% (%)	No. Of CSTR (n)
Trial-3A	1	0	1.23	1128.6	1333.9	70.4	18.2	11.5	2.69
	2	20	1.22	1128.6	1264.3	77.1	12.0	10.9	2.77
	3	40	1.19	1128.6	1233.8	81.0	9.3	9.7	2.84
	4	80	1.07	1128.6	1215.5	88.7	7.7	3.6	2.88
	5	120	1.07	1128.6	1207.7	89.7	7.0	3.3	2.95
	6	160	1.05	1128.6	1196.7	91.5	6.0	2.5	2.96
	7	200	1.00	1128.6	1191.0	94.4	5.5	0.1	2.99
Trial-3B	1	0	1.47	1128.6	1286.1	62.5	14.0	23.6	2.63
	2	20	1.44	1128.6	1261.6	66.4	11.8	21.8	2.79
	3	40	1.32	1128.6	1253.5	72.7	11.1	16.2	2.80
	4	80	1.30	1128.6	1245.8	74.5	10.4	15.1	2.84
	5	120	1.22	1128.6	1209.7	81.7	7.2	11.1	2.89
	6	160	1.09	1128.6	1207.4	88.5	7.0	4.5	2.94
	7	200	1.07	1128.6	1204.2	89.8	6.7	3.5	2.98

Table 6. 6 Trials 3A and 3B experiments - results

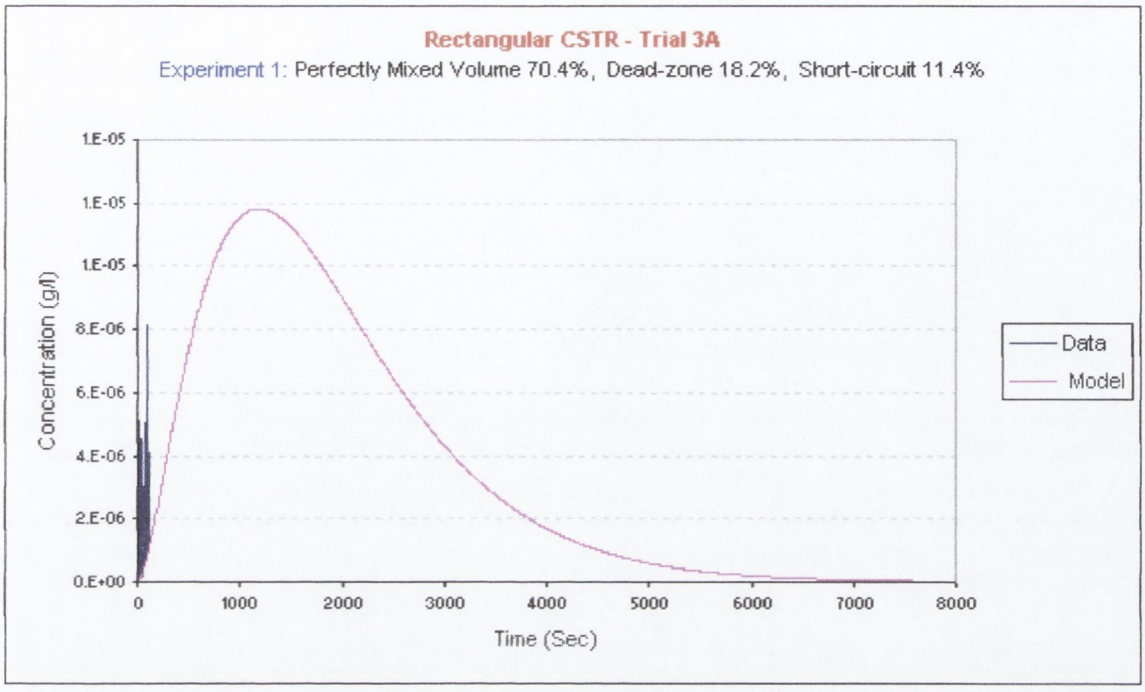

(a)

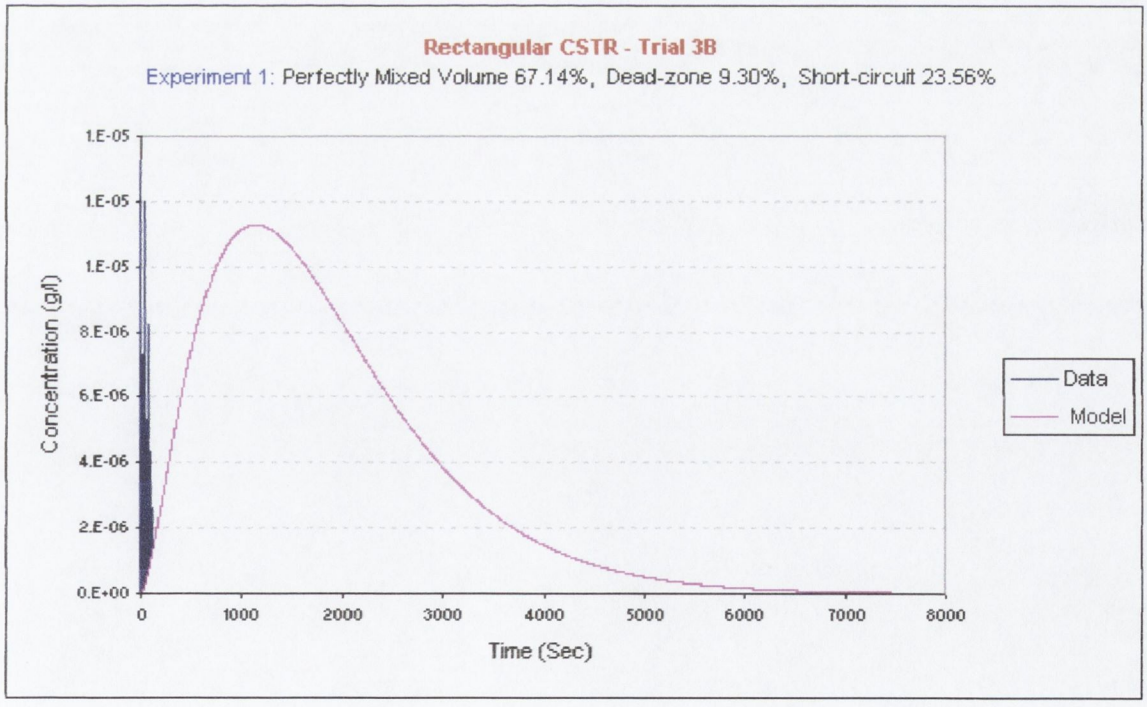

(b)

Figure 6. 12 Graphs showing laboratory results and fitted model curves for a pulse input into three CSTR in-series for (a) Trial 3A Experiment 1 and (b) Trial 3B Experiment 1

6.4.4 Trial 4 (four CSTR in-series model)

In this trial a fourth reactor was introduced to make a four CSTR in-series model as illustrated in Figure 6.13; a schematic of the flow paths is shown in Figures 6.14-6.16. Again the position of the baffles was varied. For the first set of the experiments, Trial 4A, all baffles were fixed to the base so that the flow had to move over the baffles between reactors. In the second Trial 4B the baffles between the second and the third reactors was raised so the flow had to cross through the middle of each reactor as illustrated in Figure 6.15. A third method of positioning the baffles was also studied in Trial 4C, whereby all the baffles extended above the reactor surface but a 50mm gap was left between the edge of the baffle and alternate side walls, as shown in Figure 6.16. In all these trials the same system size reactors were used as before: rectangular in shape, 30.0 cm in width, 28.33 cm in length and 30.0 cm in height. The system was fitted with the same inlet and outlet pipe as for the previous trials as well as four mixers, one in each reactor. Several experiments were run at different mixer speeds again using the pulse input method of tracer injection.

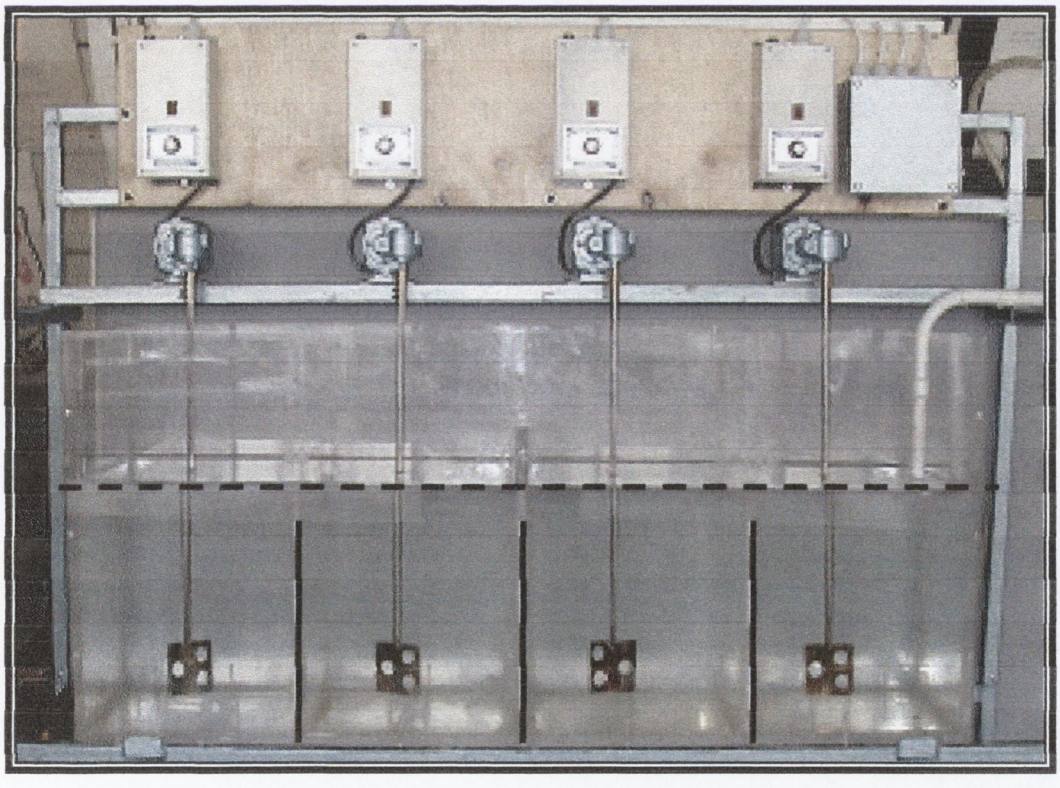

Figure 6. 13 Photograph showing four CSTR in-series model

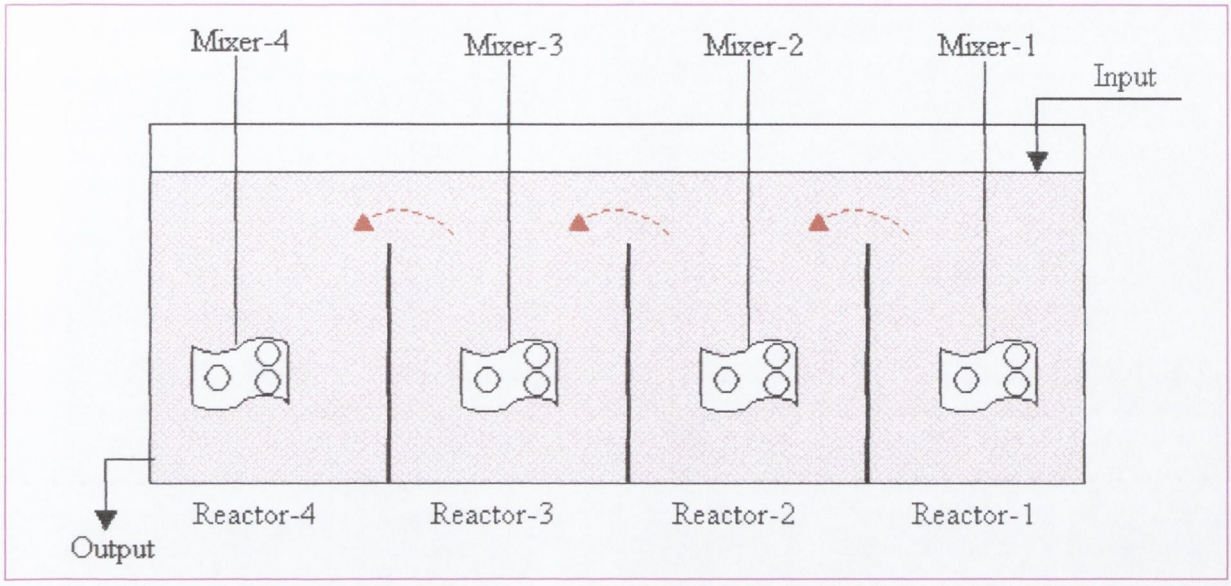

Figure 6. 14 Schematic diagram showing flow path inside the reactors for Trial 4A (over baffle flow)

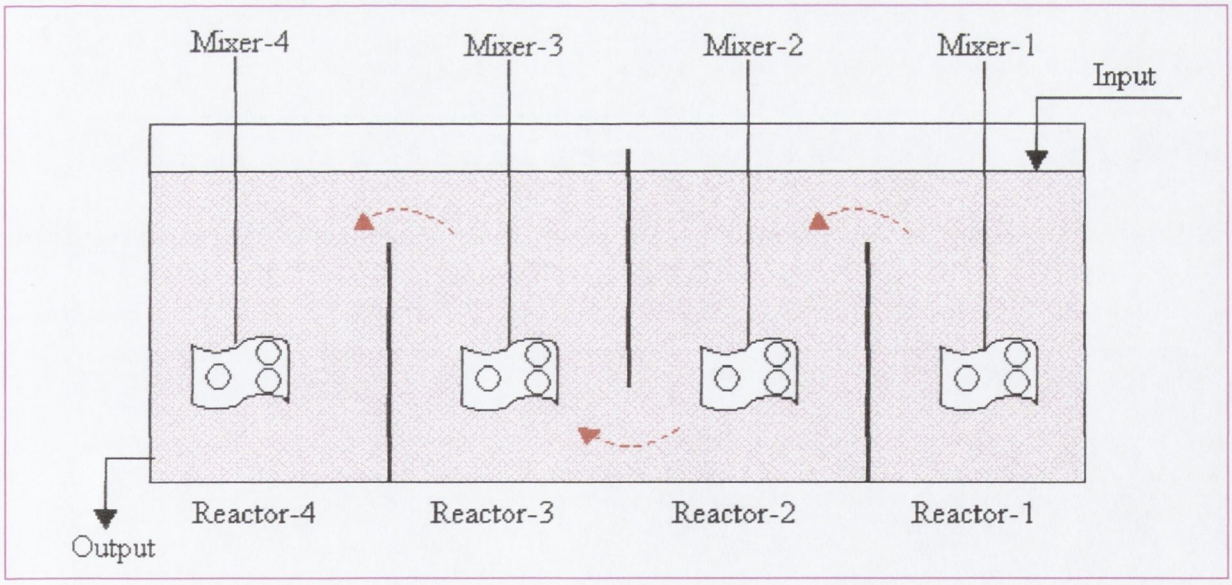

Figure 6. 15 Schematic diagram showing flow path inside the reactors for Trial 4B (vertical flow)

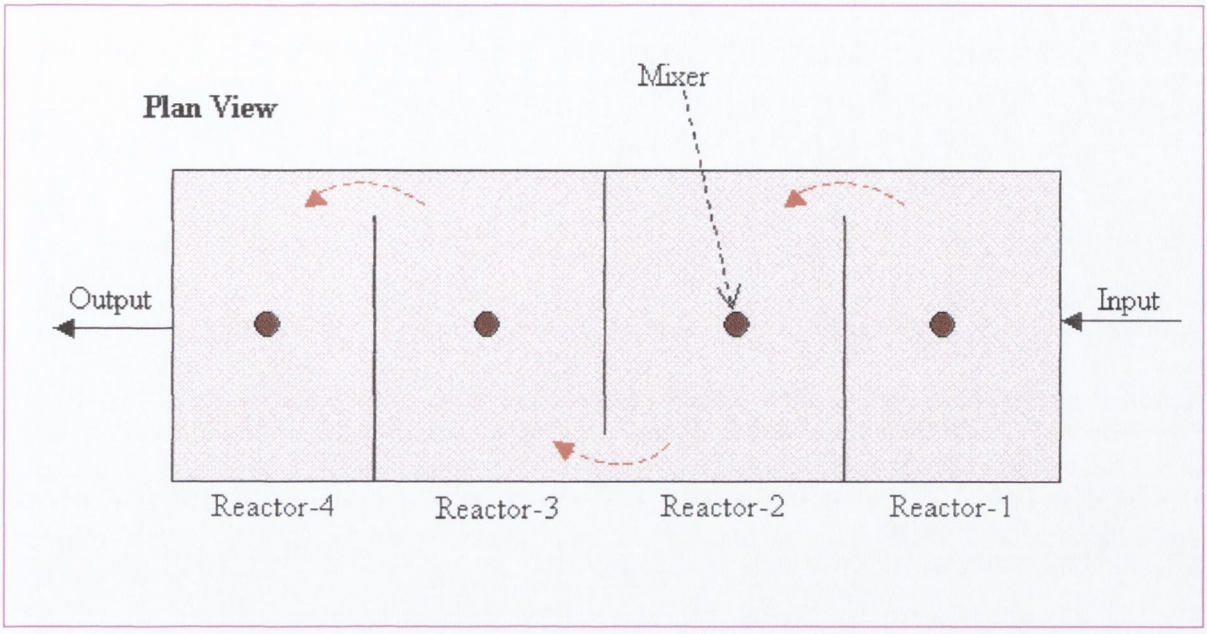

Figure 6. 16 Schematic diagram in plan showing flow path inside the reactors for Trial 4C (horizontal flow)

6.4.4.1 Trial 4 Data and Results

Again, photographic sequences of the flow path inside the reactor are shown in Appendix D, indicating the initial direction of the flow from the inlet and also the likely position of any short-circuits and dead-zones. The experimental configurations were the same for all three trials and are shown in Table 6.7. The full set of the experimental data can be seen in Table 6.7 and the results can be seen in Table 6.8. An example of RTD graphs obtained for Experiment 1 for each trial can be seen in Figure 6.19 while all other graphs are listed in Appendix E.

The results show that the mixing efficiency was better in Trial 4B where the middle of three baffles was raised compared to in Trial 4A where all four baffles were lowered. The percentage of short-circuits in Trial B was considerably lower than in Trial 4A due to the fact that the flow path was forced to cross through the middle of each reactor (where the mixer is located) as shown in Figure 6.17(b) compared to the scenario shown in Figure 6.17(a) where the flow could short-circuit over the top of reactors 2 and 3 if the energy from the mixers was not sufficient. In addition, the percentage of dead-zones in Trial 4B is much lower than in Trial 4A, resulting in an almost perfect mix.

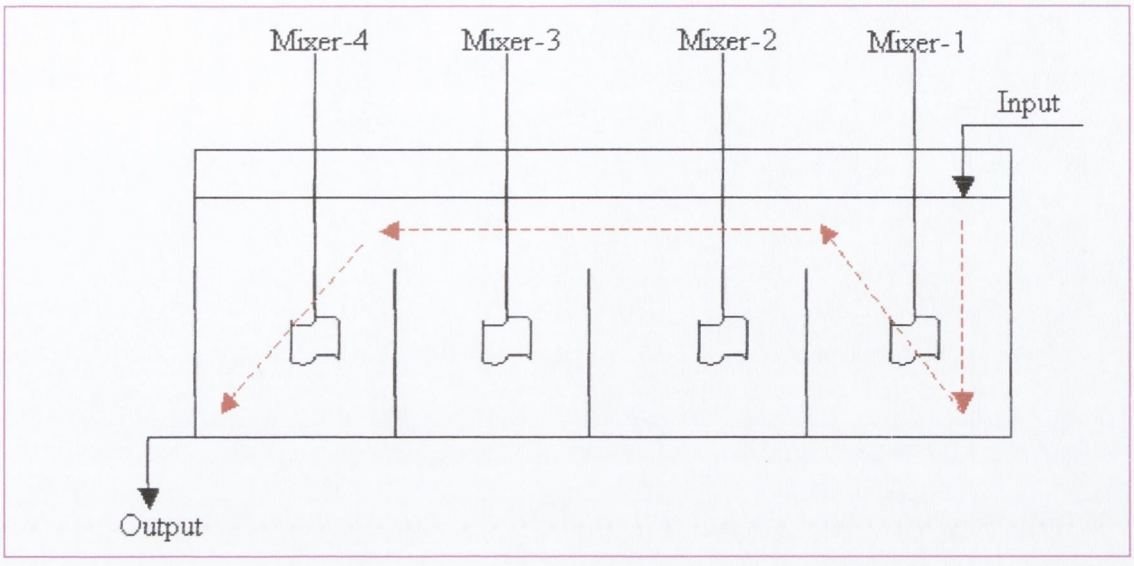

(a)

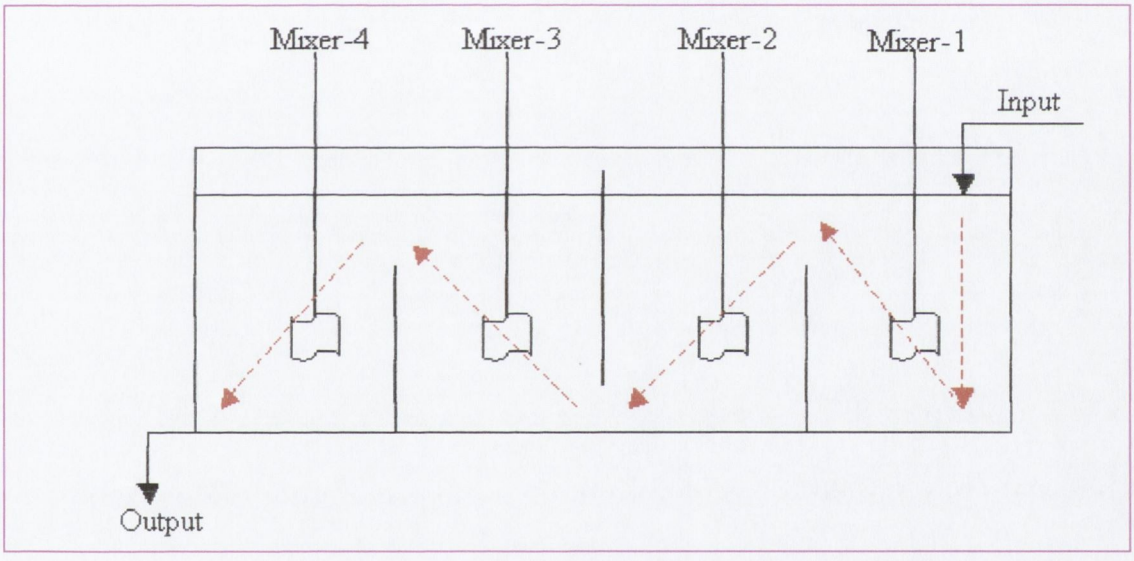

(b)

Figure 6. 17 Schematic diagram showing the flow path profile inside the reactors for (a) Trial 4A and (b) Trial 4B

The results of the analysis for Trial 4C where the flow was forced to move horizontally can be seen in Table 6.8. An example of a graph for Experiment 1 can be seen in Figure 6.19(c), while all other graphs are listed in Appendix E. As can be seen from Table 6.8, the results obtained from Trial 4C are very similar (and even slightly better) to those from Trial 4B, even though the Trial 4B baffles were arranged in a vertical configuration whilst the Trial 4C baffles were staggered in a horizontal configuration in a zigzag fashion. This demonstrates again that the mixing efficiency was created by

forcing the flow path to pass through the center of the completely mixed zone in each reactor as shown in Figure 6.18. In addition, the percentage of perfectly mixed zones achieved were better than those in the previous Trials 2 and 3, whilst the percentage of short-circuits and dead-zones were less than in previous trials. It should also be noted that the number of CSTRs in-series which was recognized by the model, was very close to 4 CSTRs, even when the mixer speed was at rest 0rpm. This was presumably due to the fact that the flow had a longer RTD in the reactor network leaving more time for dispersion and that more energy is being added into the network as shown in Table 6.7 since there were more mixers.

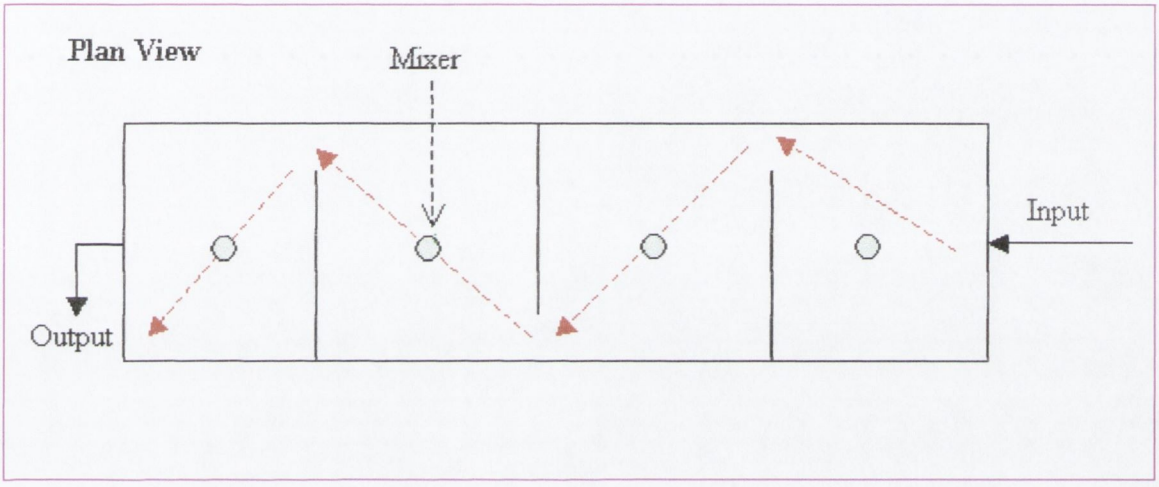

Figure 6. 18 Schematic diagram showing the flow path profile inside the reactors for Trial 4C

Experiment No.	Reactor Volume (L)	Flow rate (l/min)	Mixer speed (rpm)	Power input (Kw)	Velocity Gradient (s^{-1})	Rhodamine Mass (g)
1	112.9	5.0	0	0.00	0.00	0.002
2	112.9	5.0	20	0.05	18.87	0.002
3	112.9	5.0	40	0.37	53.38	0.002
4	112.9	5.0	80	2.93	150.97	0.002
5	112.9	5.0	120	9.90	277.35	0.002
6	112.9	5.0	160	23.46	427.01	0.002
7	112.9	5.0	200	45.82	596.76	0.002

Table 6. 7 Trials 4A, 4B and 4C experiments - configurations

Trial No.	Experiment No.	Mixer speed (rpm)	Mass passed out at the theoretical retention time $(g)^{*}10^{-3}$	Theoretical retention time (Sec)	Modelled retention time (Sec)	P% (%)	D% (%)	S% (%)	No. Of CSTR (n)
Trial-4A (Vertical Flow)	1	0	1.12	1354.3	1456.7	86.4	7.6	6.0	3.80
	2	20	1.09	1354.3	1438.4	89.2	6.2	4.6	3.85
	3	40	1.05	1354.3	1426.6	92.1	5.3	2.6	3.88
	4	80	1.04	1354.3	1397.8	94.7	3.2	2.1	3.93
	5	120	1.02	1354.3	1369.2	98.0	1.1	0.9	3.94
	6	160	1.01	1354.3	1366.4	98.5	0.9	0.6	3.98
	7	200	1.01	1354.3	1358.9	99.3	0.3	0.4	3.99
Trial-4B (Vertical Flow)	1	0	1.07	1354.3	1408.5	92.7	4.0	3.3	3.79
	2	20	1.07	1354.3	1404.6	93.0	3.7	3.3	3.90
	3	40	1.06	1354.3	1376.0	95.2	1.6	3.2	3.93
	4	80	1.05	1354.3	1375.4	96.0	1.6	2.4	3.94
	5	120	1.00	1354.3	1370.6	98.6	1.2	0.2	3.96
	6	160	1.00	1354.3	1354.5	100.0	0.0	0.0	3.99
	7	200	1.00	1354.3	1354.5	99.8	0.0	0.2	3.99
Trial-4C (Horizontal Flow)	1	0	1.03	1354.3	1381.4	96.5	2.0	1.5	3.92
	2	20	1.02	1354.3	1379.9	97.1	1.9	1.0	3.93
	3	40	1.00	1354.3	1371.9	98.5	1.3	0.2	3.93
	4	80	1.00	1354.3	1367.6	98.9	1.0	0.1	3.96
	5	120	1.00	1354.3	1357.4	99.7	0.2	0.1	3.98
	6	160	1.00	1354.3	1357.2	99.8	0.2	0.0	3.98
	7	200	1.00	1354.3	1354.3	100.0	0.0	0.0	3.99

Table 6. 8 Trials 4A, 4B and 4C experiments - results

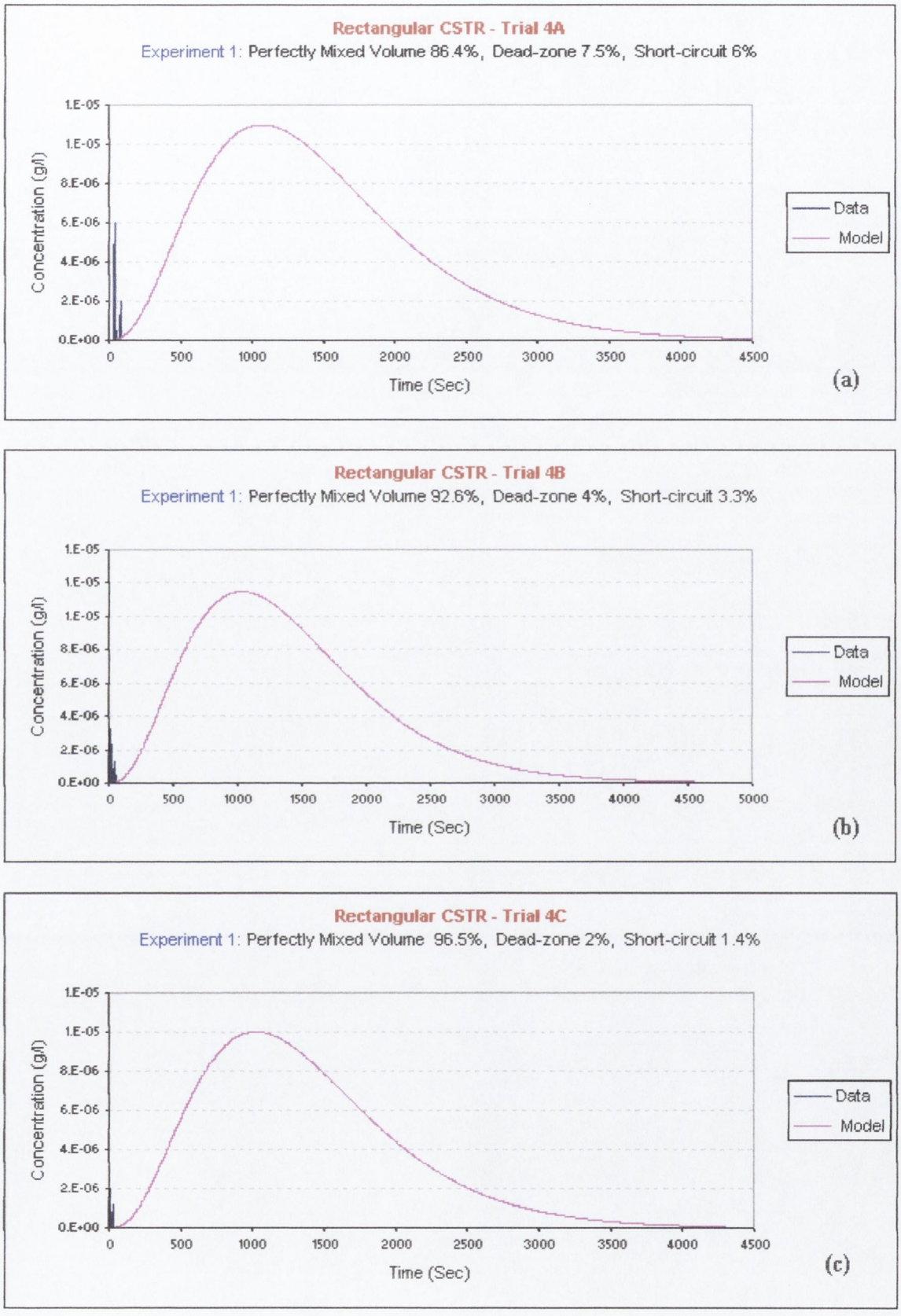

Figure 6. 19 Graphs showing laboratory results and fitted model curves for a pulse input into four CSTR in-series for (a) Trial 4A, Exp. 1, (b) Trial 4B, Exp.1 and (c) Trial 4C, Exp.1

6.5 Input and Output Variation

In order to more fully evaluate the effect of the input and output position on the performance of reactors in-series, eight different scenarios were studied as shown in Figure 6.20. The differences between each scenario were the variation in the input, the output and the baffle position. For each scenario three experiments were studied at different mixers speed 0 rpm, 100rpm and 200 rpm; a fixed flow rate of 4 l/min and fixed volume of 56.4 Litres was maintained throughout all the experiments. The scenarios were configured to allow direct comparisons to take place between the position of the influent flow and the position of the effluent flow with respect to the baffle positions as shown in Figure 6.20. In Scenarios G and H a different input technique was introduced whereby a distribution input flow line was added vertically across the whole depth for Scenario G or horizontally across the bottom of the first reactor for Scenario H, (inserted at the distance of 1 cm measured from the bottom of the system) (see Figure 6.20 H). The Rhodamine WT tracer was prepared as before and was injected at the same influent point relative to the exit nozzle as used in previous experiments. The experimental configurations can be seen in Table 6.9. An example of the RTD graphs obtained for Experiment 1 for Scenarios A and H is illustrated in Figure 6.21 while the full set of graphs from the other scenarios are shown in Appendix E. In addition, the full set of the results obtained for each scenario can be seen in Table 6.10.

Experiment No.	Reactor Volume	Flow rate	Mixer speed	Power input	Velocity Gradient	Rhodamine Mass
	(L)	(l/min)	(rpm)	(Kw)	(s^{-1})	(g)
1	56.4	4.0	0	0	0	0.002
2	56.4	4.0	100	2.83	419.44	0.002
3	56.4	4.0	200	22.91	1193.52	0.002

Table 6. 9 Input and Output experiments - configurations

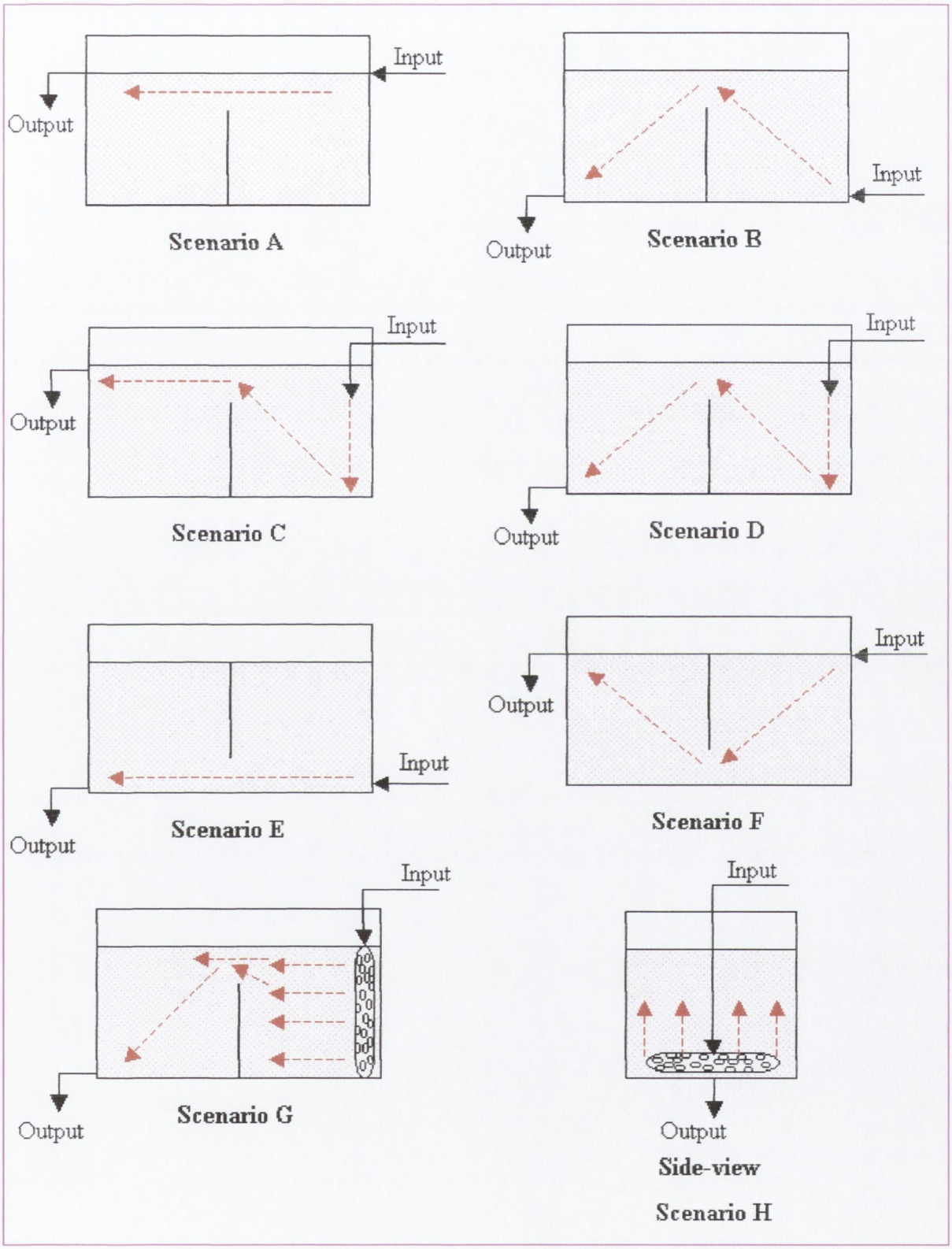

Figure 6. 20 Schematic representation of the eight experimental scenarios for inlet and outlet variations

Scenario No.	Experiment No.	Mixer speed (rpm)	Mass passed out at the theoretical retention time $(g)^{*}10^{-3}$	Theoretical retention time (Sec)	Modelled retention time (Sec)	P% (%)	D% (%)	S% (%)
Scenario (A)	1	0	1.38	846.5	1113.1	20.3	31.5	48.3
	2	100	1.32	846.5	944.6	74.9	11.6	13.6
	3	200	1.05	846.5	907.9	85.6	7.3	7.1
Scenario (B)	1	0	1.50	846.5	1147.8	53.1	35.6	11.3
	2	100	1.43	846.5	899.9	85.6	6.3	8.1
	3	200	1.37	846.5	863.5	95.6	2.0	2.4
Scenario (C)	1	0	1.50	846.5	984.8	56.4	16.4	27.3
	2	100	1.43	846.5	924.8	76.3	9.3	14.5
	3	200	1.37	846.5	883.4	86.3	4.4	9.3
Scenario (D)	1	0	1.50	846.5	1106.3	50.3	30.7	19.0
	2	100	1.43	846.5	884.5	84.5	4.5	11.0
	3	200	1.37	846.5	865.9	93.1	2.3	4.6
Scenario (E)	1	0	1.50	846.5	1109.9	19.2	31.1	49.7
	2	100	1.43	846.5	957.3	72.9	13.1	14.0
	3	200	1.37	846.5	918.4	86.8	8.5	4.7
Scenario (F)	1	0	1.50	846.5	1121.5	54.3	32.5	13.3
	2	100	1.43	846.5	907.6	86.2	7.2	6.6
	3	200	1.37	846.5	855.2	96.0	1.0	3.0
Scenario (G)	1	0	1.50	846.5	1032.9	65.6	22.0	12.4
	2	100	1.43	846.5	856.9	96.4	1.2	2.4
	3	200	1.37	846.5	846.6	99.9	0.0	0.0
Scenario (H)	1	0	1.50	846.5	967.5	77.1	14.3	8.6
	2	100	1.43	846.5	854.6	98.6	1.0	0.4
	3	200	1.37	846.5	846.5	100.0	0.0	0.0

Table 6. 10 Input and Output variation experiments - results

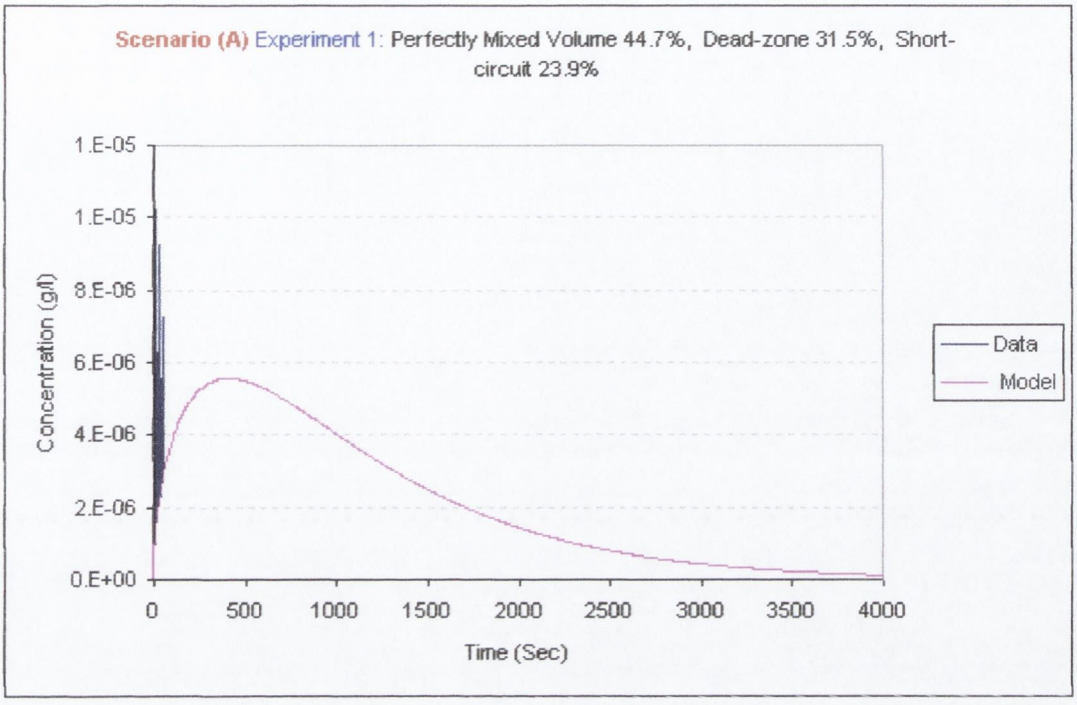

(a)

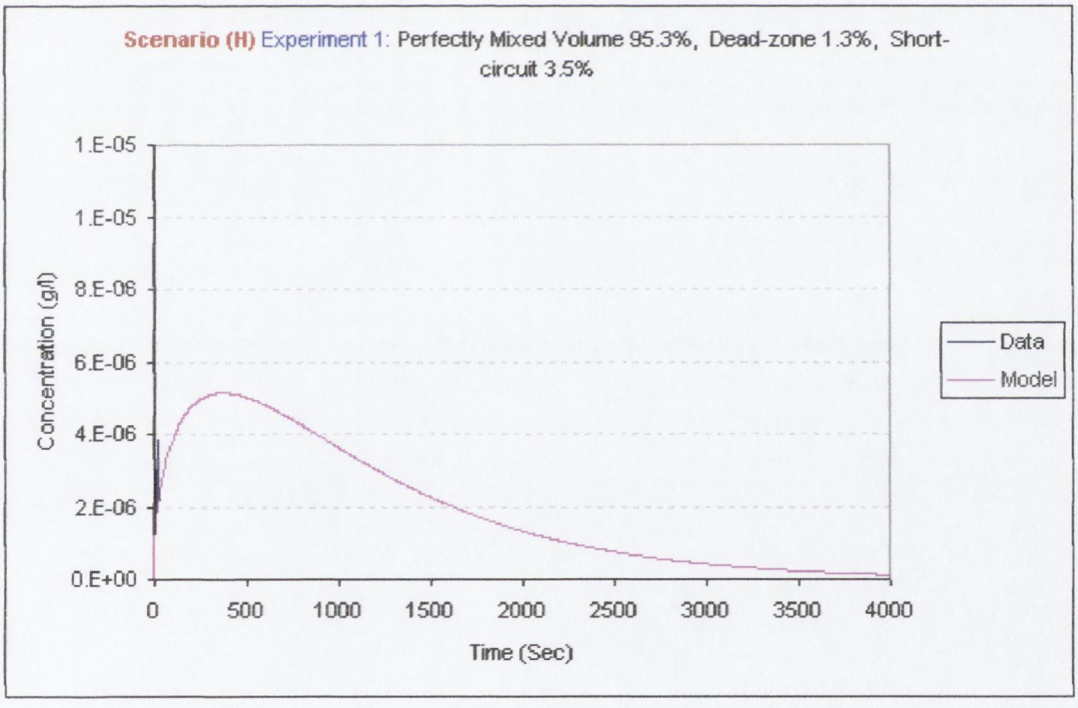

(b)

Figure 6. 21 Graphs showing laboratory results and fitted model curves for input and output variation input into two CSTR-in-series for (a) Scenario (A), Exp. 1, and (b) Scenario (H), Exp.1.

6.5.1 Input and Output variation-results

As shown in Table 6.10 the results obtained from the model indicate that the input and the output are of critical importance to be taken into an account when designing a perfect mixed system. The comparison of perfectly mixed flow, dead-zone flow and short-circuit flow for each scenarios have been compiled for ease of the comparison and can be seen in Tables 6.11, 6.12 and 6.13. In addition the differences in the performance can also be seen graphically in Figures 6.22, 6.23 and 6.24.

Experiment No.	Mixer speed	P%							
	(rpm)	Scenario (A)	Scenario (B)	Scenario (C)	Scenario (D)	Scenario (E)	Scenario (F)	Scenario (G)	Scenario (H)
1	0	20.3	53.1	56.4	50.3	19.2	54.3	65.6	77.1
2	100	74.9	85.6	76.3	84.5	72.9	86.2	96.4	98.6
3	200	85.6	95.6	86.3	93.1	86.8	96.0	99.9	100.0

Table 6. 11 Percentage of perfectly mixed flow of all scenarios

Experiment No.	Mixer speed	D%							
	(rpm)	Scenario (A)	Scenario (B)	Scenario (C)	Scenario (D)	Scenario (E)	Scenario (F)	Scenario (G)	Scenario (H)
1	0	31.5	35.6	16.4	30.7	31.1	32.5	22.0	14.3
2	100	11.6	6.3	9.3	4.5	13.1	7.2	1.2	1.0
3	200	7.3	2.0	4.4	2.3	8.5	1.0	0.0	0.0

Table 6. 12 Percentage of dead-zone flow of all scenarios

Experiment No.	Mixer speed	S%							
	(rpm)	Scenario (A)	Scenario (B)	Scenario (C)	Scenario (D)	Scenario (E)	Scenario (F)	Scenario (G)	Scenario (H)
1	0	48.3	11.3	27.3	19.0	49.7	12.4	8.6	3.5
2	100	13.6	8.1	14.5	11.0	14.0	2.4	0.4	0.4
3	200	7.1	2.4	9.3	4.6	4.7	0.0	0.0	0.0

Table 6. 13 Percentage of short-circuit flow of all scenarios

In Table 6.11 when the mixers speed were at rest the percentage of perfectly mixed flow appears to be low for all reactors ranging from 20.3% up to 77.1%. When the mixers speed were set at 100rpm the percentage of perfectly mixed flow improves ranging from 74.9% up to 98.6% and then attains even better efficiencies when the mixers speed were set at the optimum level of 200rpm. However, within the broad results the percentages were variable from one scenario to another which can be seen to be due to the input and output position of the flow into the reactor network. For example, the results that were obtained from Scenario B showed much better mixing (53.1%) than the results which were obtained from Scenario A (20.3%) when the mixers were at rest. This must be due to the initial momentum of the flow entering reactor 1 heading directly towards the outlet in Scenario A compared to the direction of the flow inside the system in Scenario B which forced the flow to cross both reactors (see Figure 6.20). This is also reflected in percentage of short-circuit flow and dead-zones as shown in Table 6.12 (48.3%) and Table 6.13 (31.5%) respectively.

This same pattern between Scenarios A and B can also be seen between Scenarios E and F as shown in Figure 6.20. Again, when the direction of flow heads straight from the inlet to the outlet (as in Scenario E) the results show a much higher degree of short-circuiting than for Scenario F, where the flow was forced to cross through the middle of each reactor by the baffles. Another interesting comparison can be seen between Scenarios A and C where both had essentially the same configurations expect that the inflow was pointed down into the reactor in Scenario C compared to across the reactor in Scenario A. This slight modification, altering the influent direction of flow, had a large effect on the efficiency of mixing and prevention of short-circuits. This initial direction of input flow was also important for Scenario D helping to promote better mixing, compared to Scenario C, by providing a good mix in the first reactor. The use of the distributed flow line as shown in Figure 6.20 was compared in two different ways: vertically in Scenario G and horizontally in Scenario H. Both configurations showed much better mixing than in the other direct input scenarios discussed above. Even when the mixers were at rest some mixing occurred due to the initial dispersion of the inlet flow over a wide area, acting to reduce its incoming momentum. Also the hydraulic irregularities disappeared which can be seen both numerically in Tables 6.11, 6.12 and 6.13 and graphically in Figures 6.22, 6.23 and 6.24.

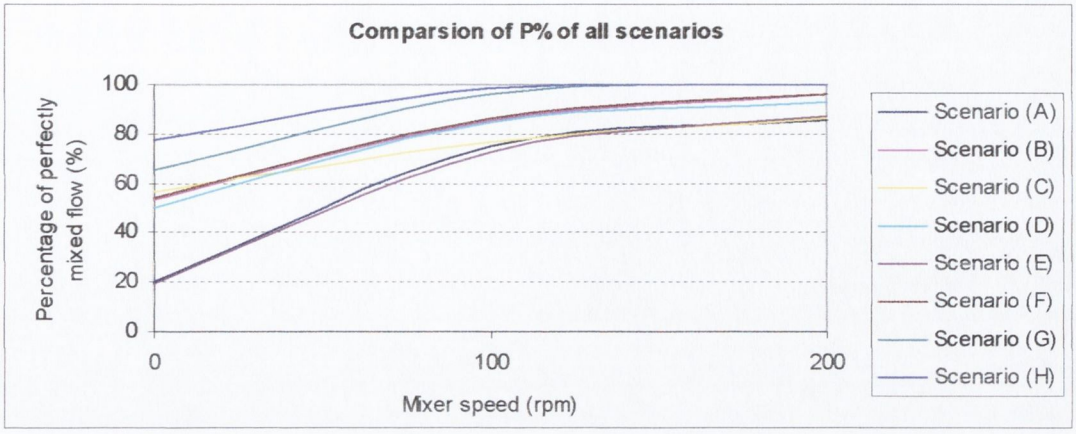

Figure 6. 22 Graph showing the percentage of the perfectly mixed flow for all scenarios

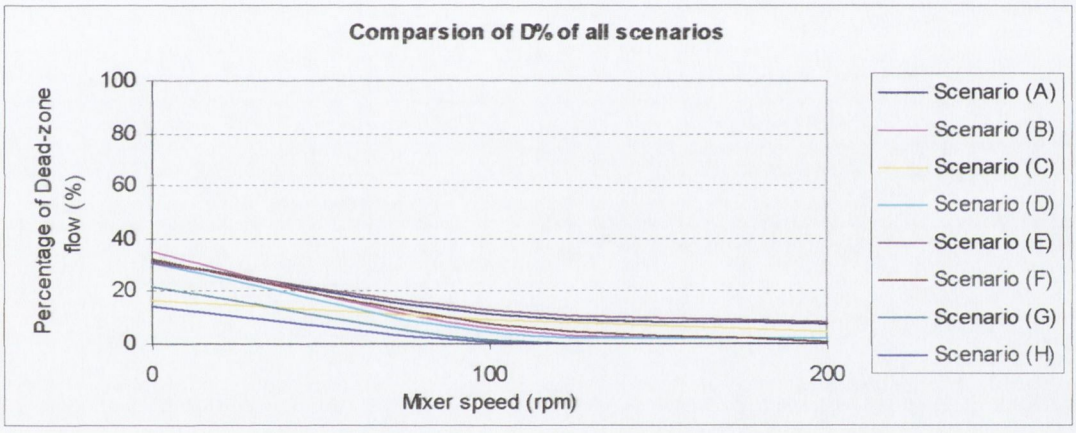

Figure 6. 23 Graph showing the percentage of the dead-zone flow for all scenarios

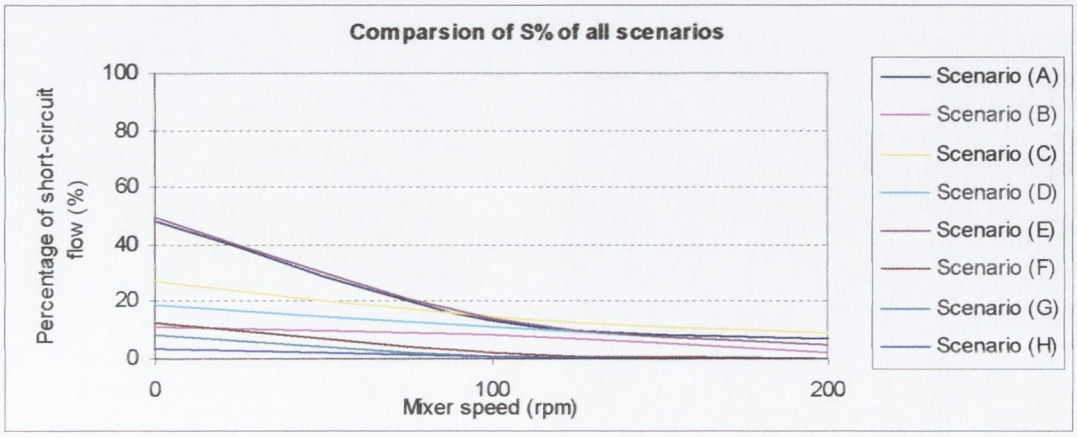

Figure 6. 24 Graph showing the percentage of the short-circuit flow for all scenarios

6.6 Results Summary

The comparison between the experiments tabulated in Table 4.2 (single circular CSTR) and Table 6.2 (rectangular CSTR) is shown in Table 6.14. All experiments were made under the same conditions of fixed flow rate (3.5 l/min) and volume (20 litres) as well as uniform mixer speed variations. Such a comparison reveals the effect that the reactor geometry has on the overall mixing efficiency of the reactor. It can be seen that as the mixer speed increased, the percentage of perfectly mixed flow increases for the rectangular CSTR model (seen graphically in Figure 6.25). However, the circular CSTR efficiency only increased up to a peak at 80 rpm, after which the onset of vortexing then acts to reduce the efficiency. Hence, the shape of the rectangular CSTR prevents the vortex problem and enables the reactor to become almost 100% fully mixed as shown in Figure 6.25. However, it can also be seen that the circular CSTR reached a higher level of mixing (per unit volume) at a optimum mixer speed of 80 rpm compared to the rectangular CSTR but in all other mixer speeds performed less favorably The shape of the reactor is thus of fundamental importance in determining mixing efficiency.

Experiment	Mixer Speed	Rectangular CSTR	Circular CSTR
No.	(rev/min)	Percentage of Perfectly mixed Flow	Percentage of Perfectly Mixed Flow
1	0	47.7%	39.8%
2	20	71.7%	50.7%
3	40	74.1%	66.4%
4	80	80.6%	93.9%
5	120	93.9%	87.2%
6	160	95.3%	81.3%
7	200	99.1%	77.7%

Table 6. 14 Summary of the results obtained from the single rectangular CSTR and single circular CSTR

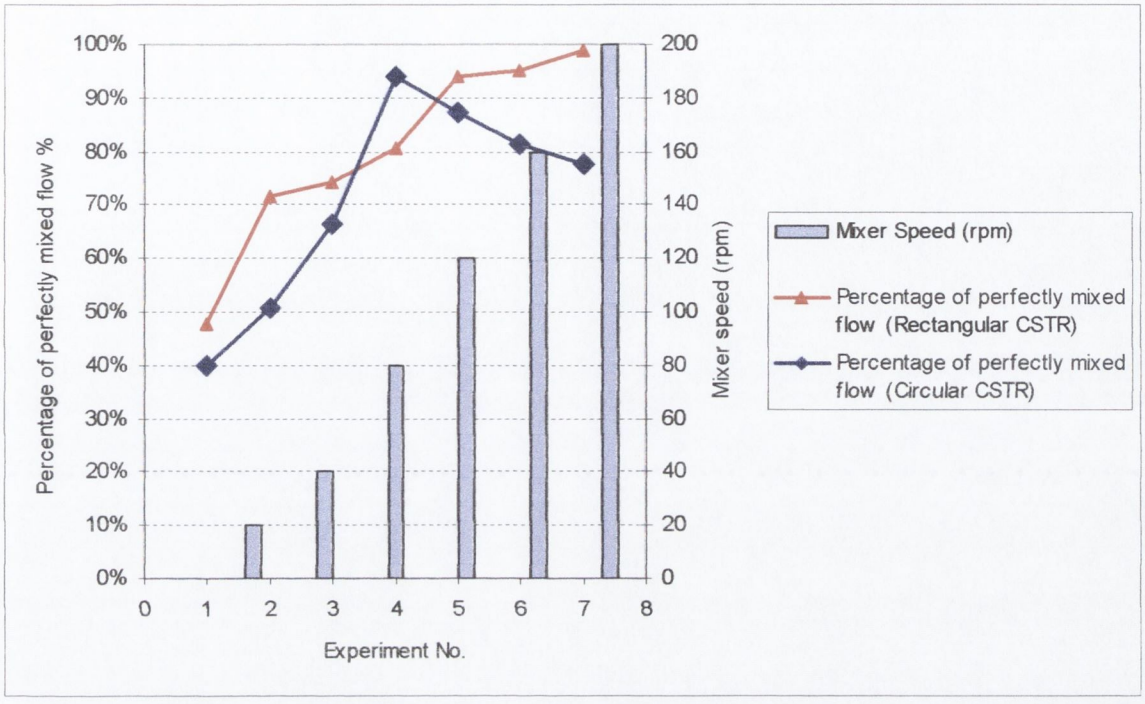

Figure 6. 25 Graph showing the effect of mixer speed on the reactor shape

One of the most important factors with regards to mixing efficiency is the power input per unit volume of fluid as has been seen in the previous laboratory trials. For example the mean velocity gradient (G) (see Appendix H) was calculated for the previous circular and rectangular CSTR experiments (see Table 6.15). The velocity gradient was then plotted against the percentage of perfectly mixed flow for each trial as illustrated in Figure 6.26 allowing direct comparison for the power input between the circular and rectangular CSTR. The velocity gradient is an important property for characterizing the mixing rate that occurs inside the reactor as shown by Figure 6.26 which also shows that the velocity gradient can be a function of the reactor shape with respect to the percentage of perfectly mixed flow. In the circular CSTR an increased power input created better mixing whereby the percentage of perfectly mixed area increased up to a maximum level at 1 Kw, but then decreased again due to the onset of vortexing in the reactor, as discussed previously.

Velocity Gradient (G)											Circular CSTR	Rectangular CSTR
Experiment No	V	n	μ	ρ	D	N_R	Q	k	P	G	P%	P%
	(m^3)	(rev/sec)	(kg/m.s)	(kg/m^3)	(m)	Non	(m^3/s)	Constant	(W)	(1/s)	(%)	(%)
1	0.02	0	0.00114	999.1	0.0989	0	0.000058	41	0	0	39.74	47.7
2	0.02	0.33	0.00114	999.1	0.0989	2857	0.000058	0.32	0.01	22.41	50.73	71.70
3	0.02	0.67	0.00114	999.1	0.0989	5715	0.000058	0.32	0.09	63.40	66.33	74.10
4	0.02	1.33	0.00114	999.1	0.0989	11430	0.000058	0.32	1	179.31	93.88	80.6
5	0.02	2.00	0.00114	999.1	0.0989	17145	0.000058	0.32	2	329.42	86.89	93.9
6	0.02	2.67	0.00114	999.1	0.0989	22859	0.000058	0.32	6	507.18	81.51	95.3
7	0.02	3.33	0.00114	999.1	0.0989	28574	0.000058	0.32	11	708.80	77.68	99.1

Table 6. 15 Velocity gradient (G) for single circular and rectangular CSTR experiments at different mixer speeds

In the case of the rectangular CSTR the same increase in power leads to increasingly better mixing with no reduction in efficiency at the higher power inputs. Hence, the energy can be used as a rough measure of mixing effectiveness, based on the fact that more input power creates greater turbulence and greater turbulence leads to better mixing.

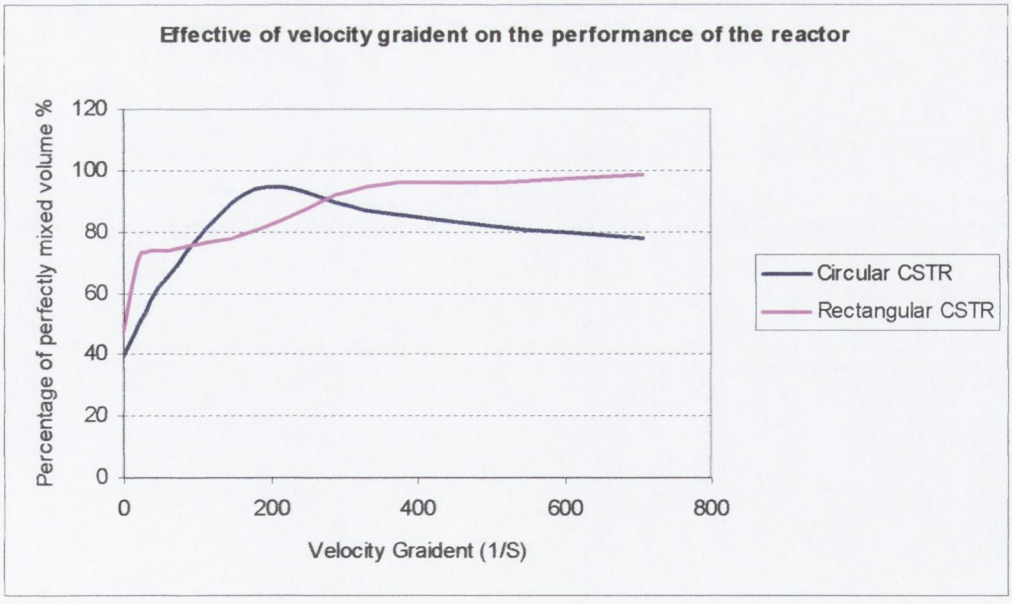

Figure 6. 26 Graph represents the differences in velocity gradient between the single circular and rectangular CSTR

The results for each pair of trials [for example, Trial 2A and Trial 2B,etc] have been outlined individually so as to allow the direct comparison in mixing efficiency based on baffle position, as illustrated previously in Figures 6.6, 6.10, 6.14, 6.15 and 6.16. A comparison of the trials has also been made in Figure 6.30. All the trials have demonstrated that the relative position of the input, output and baffles in reactors network greatly influence the efficiency of mixing (and creation of short-circuits and dead-zones) in reactor networks. The ideal scenario is to position the input, output and baffle such that the flow path is forced to pass through the center of each reactor and thus a pass as close as possible to the influence of the mixer. Another factor that can be noted from the trials is that the overall percentage of dead-zones and short-circuits decreases as the number of the reactors in the network increases, at any given mixer speed.

It is clear (see Figure 6.27) that there is a big difference in the results drawn from Trial 2A when the baffle was located at the bottom of the reactor as illustrated in previous Figure 6.6(a). In this trial the dead-zone and short-circuit problems were shown to be relatively high (30.6% and 19.1% respectively) when the mixer speed was 0 rpm. When the mixer speed increased, these problems decreased until they reached 6.9% and 0% respectively at 200rpm.

In Trial 2B the results also illustrate (Figure 6.27) what happened when the baffle was moved so that the flow passes beneath it as shown in previous Figure 6.6(b). The dead-zone and short-circuit problems were higher than those in Trial 2A, being 31.4% and 25.1% respectively with the mixer at 0rpm and 7.5% and 5.7% with the mixer at 200rpm. This difference in results between Trials 2A and 2b is a result of the baffle position.

On the other Figures 6.28 and 6.29 the dead-zone and short-circuit problems can be seen to decline sharply from Trial 3A to Trial 4C. The reasoning behind this is that these systems have more than two tanks in series which leads to an increase in the theoretical retention time which itself gives the tracer more time probabilistically move through a fully mixed zone in the reactor system .

As shown in Table 6.16 and Figure 6.30 from the comparison of all the trials there is a progressive increase in level of mixing efficiency to be seen from Trial 1 to the paired Trials 2A, 2B up to Trial 4C, as the number of reactors in-series increases. This is

presumably due to the fact that the flow has a longer residence time in the reactor network leaving more time for dispersion and also that the total energy being added into the network by the mixers is increasing with each subsequent trial.

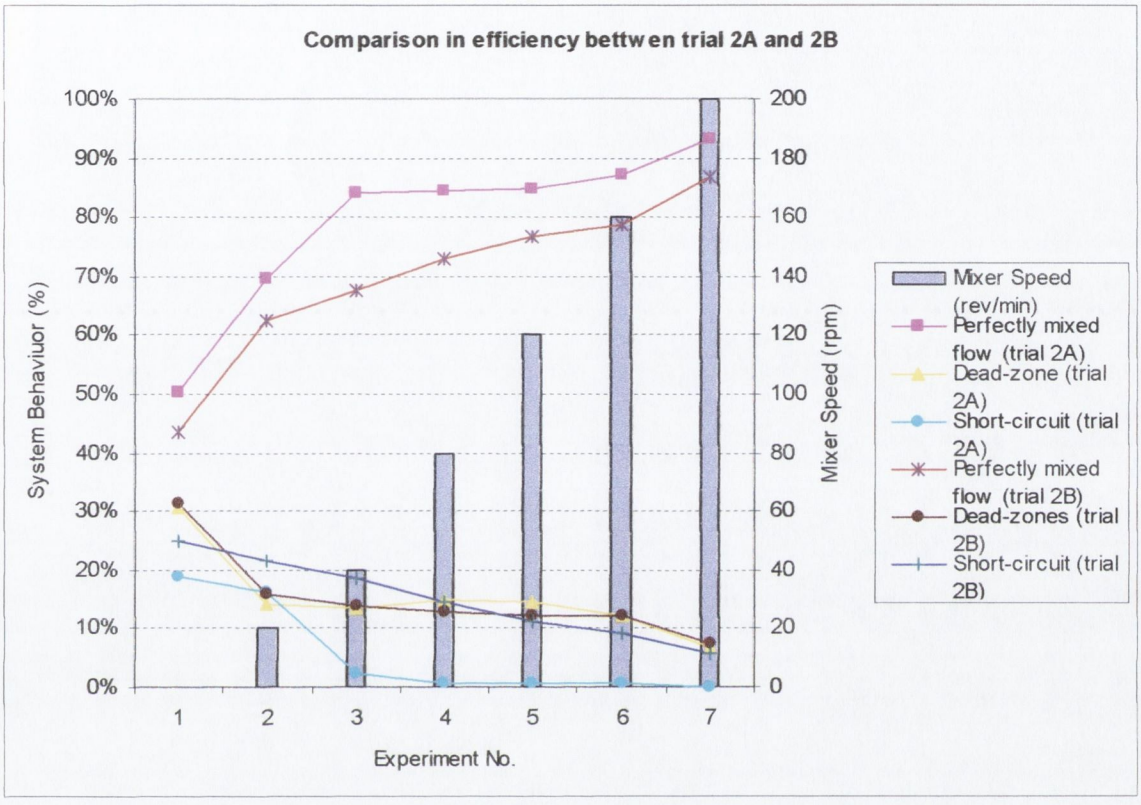

Figure 6. 27 Graph showing the effect of mixer speed on the reactor shape

Finally, the trials carried out on the input and the output positions for the 2 CSTR reactor network, have shown that careful thought in the design of the influent and effluent points can yield large differences to the hydraulic efficiency of the overall system with regards to mixing.

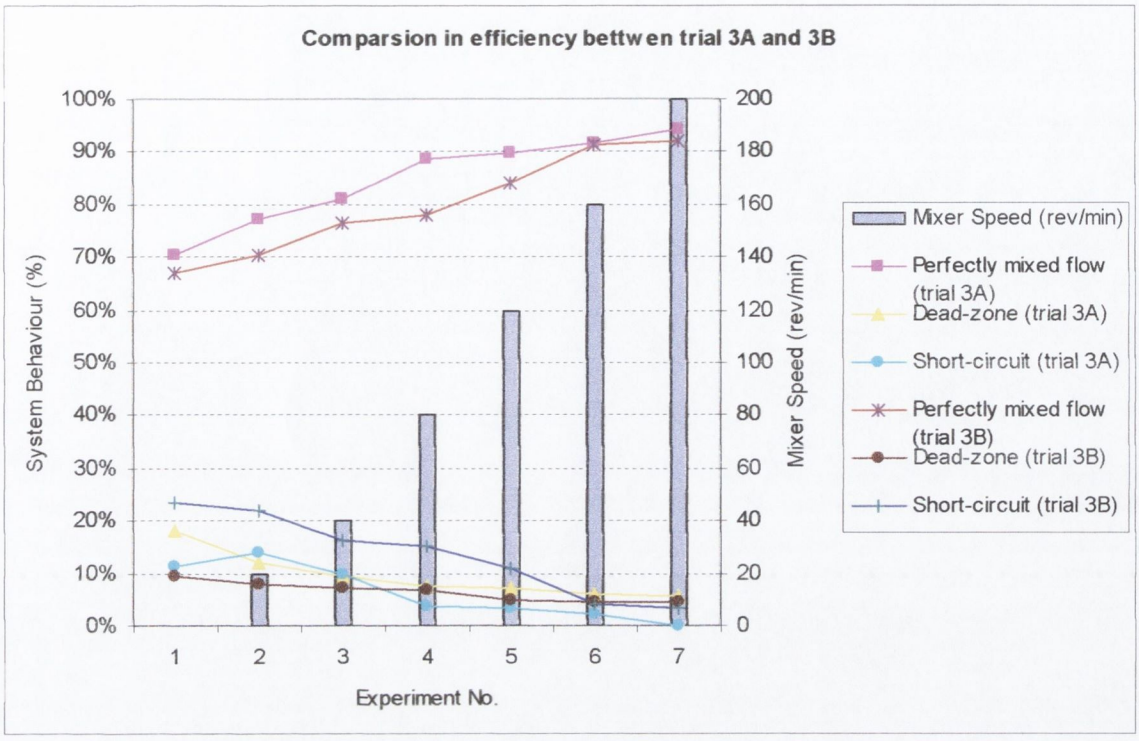

Figure 6. 28 Graph showing the effect of mixer speed on the system's behaviour (Trials 2A & 2B)

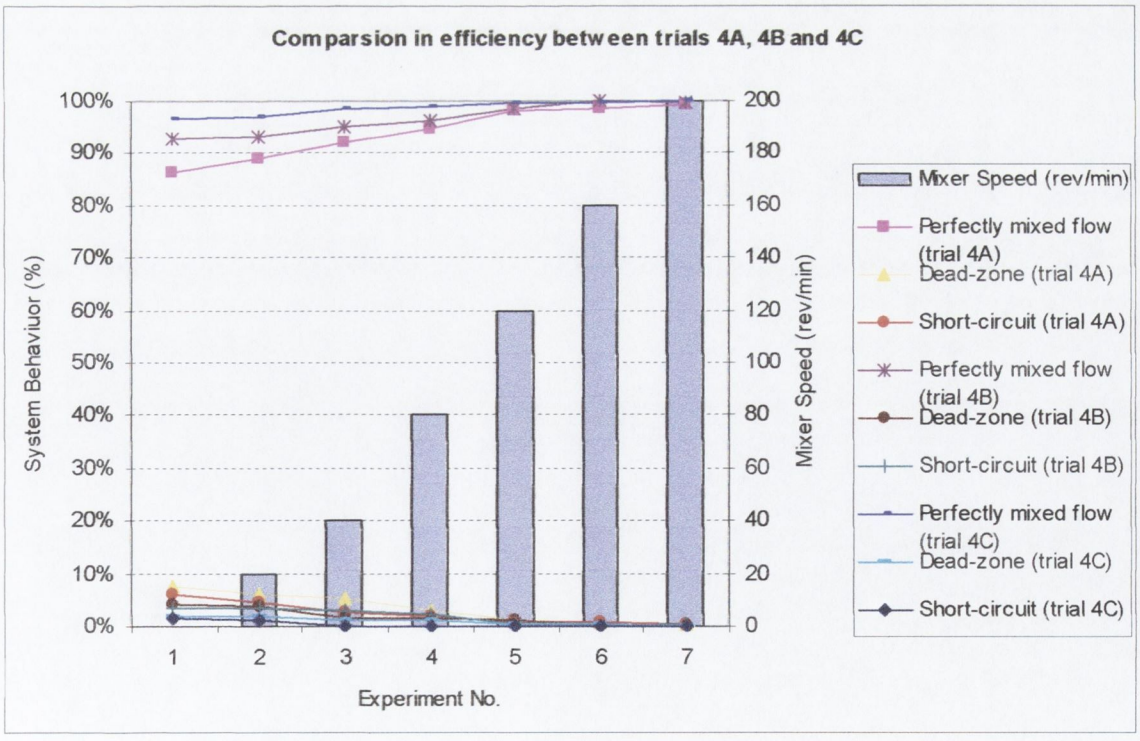

Figure 6. 29 Graph showing the effect of mixer speed on the system's behaviour (Trials 4A, 4B and 4C)

Percentage of Perfectly Mixed Flow For Each Trial									
Experiment No.	Mixer Speed	Trial [1]	Trial [2A]	Trial [2B]	Trial [3A]	Trial [3B]	Trial [4A]	Trial [4B]	Trial [4C]
1	0	47.6%	50.3%	43.5%	70.4%	62.5%	86.4%	92.7%	96.5%
2	20	71.7%	71.6%	63.6%	77.1%	66.4%	89.0%	93.0%	97.1%
3	40	74.2%	85.6%	63.9%	81.0%	72.7%	92.1%	95.2%	98.5%
4	80	80.7%	87.2%	69.0%	88.7%	74.5%	94.7%	96.0%	98.9%
5	120	94.6%	88.0%	72.9%	89.7%	81.7%	98.0%	98.6%	99.7%
6	160	96.1%	90.8%	77.2%	91.5%	88.5%	98.5%	100.0%	99.7%
7	200	98.3%	96.0%	87.1%	94.4%	89.8%	99.3%	99.8%	100.0%

Table 6. 16 Percentage of perfectly mixed volume for all trials

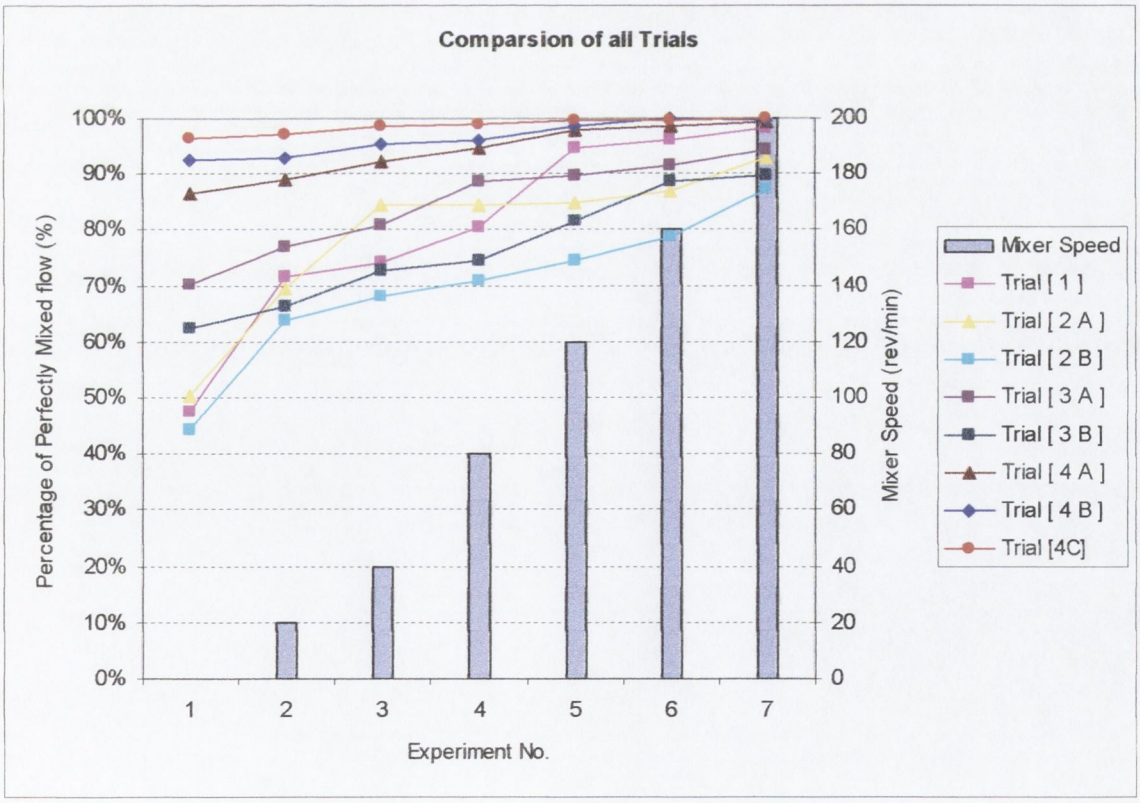

Figure 6. 30 Graph showing the efficiency of the trials on the system's behaviour

Chapter 7

Reactor Diagnosis

Chapter 7

Reactor Diagnosis

7.1 Introduction

After the numerous experiments on both single CSTRs and networks of CSTRs in-series the next stage was to develop a method in order to use the model to diagnose a reactor with hydraulic problems in the network, thus enabling further investigation to remedy the problem. As shown in the earlier chapters, certain hydraulic problems were deliberately introduced into the CSTR networks that directly affected the efficiency of the systems. The model was able to pick up the existence of dead-zones and short-circuits both of which often exist at the same time. However, the question now was whether the tracer study and the mathematical model could pick up such problems in a specific reactor in the middle of a network of CSTRs. This chapter concentrates on the identification of hydraulic problems in specific reactors that may be due to inadequate flow rate, mixer input or reactor geometry.

7.2 Theory

In some situations the use of CSTRs in-series has certain advantages with regards to treatment processes. The aim underlying this thesis is to categorise the nature and scale of any hydraulic problems by generating an effluent tracer concentration (i.e. RTD curve) from the reactors in question, which can then be fitted to the mathematical model.

In order to identify which particular reactor in a network of CSTRs in-series is causing the problem, the hydraulic theory of reactors in-series must be considered.

As discussed in Section 3.2.1.2, the generalized expression for the effluent concentration for **n** reactors in-series (see Figure 7.1) is,

$$C_n = \frac{C_0}{(n-1)!}(\theta)^{n-1} e^{-\theta} \qquad \text{----------(3.8)}$$

Where: $\theta = \frac{t}{\tau}$

t = the time at which sample was taken

τ = The hydraulic retention time for the system

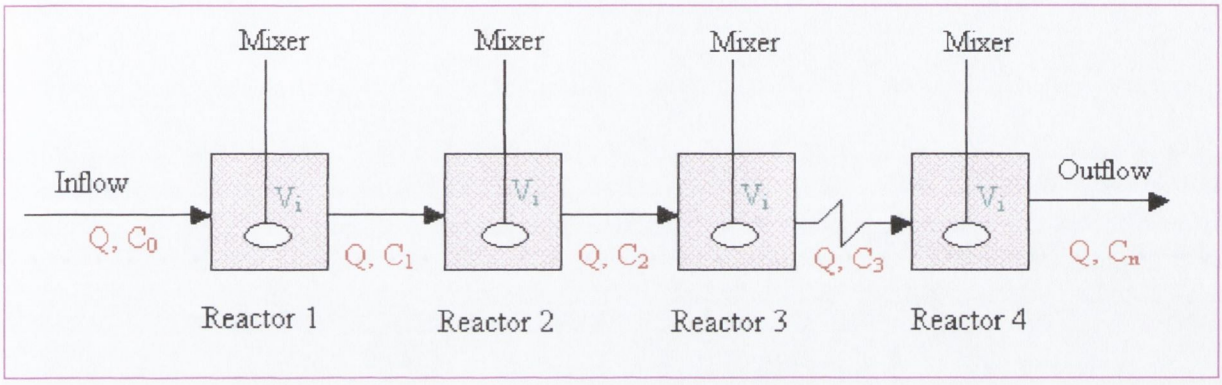

Figure 7. 1 Schematic diagram for the analysis of complete-mix reactors in series

This analysis makes the assumption that at the theoretical retention time the normalized time $\theta = 1$. If the system is perfectly mixed, homogeneous and in a steady-state condition, the relationship in the concentrations with time between the above reactors in-series (Figure 7.1) can be illustrated graphically as shown in Figure 7.2. As discussed in Section 2.2.2 the area under each RTD curve is normalized and equal to unity, which corresponds to the mass of tracer injected at the inlet point. Consequently, the individual areas under the concentration curves coming out of each reactor must all be equal and hence correspond to the mass of tracer injected at the inlet point, since the tracer must eventually pass through all reactors.

Area under RTD_1 = Area under RTD_2 = ... = Area under RTD_n = M_{in}

At time θ = 1, the following applies if the system is perfectly mixed.

$$C_1 = C_0 e^{-\theta} \qquad \text{---------(7.1)}$$

$$C_2 = C_0 \theta e^{-\theta} \qquad \text{---------(7.2)}$$

$$C_3 = \frac{C_0}{2}\theta^2 e^{-\theta} \qquad \text{---------(7.3)}$$

$$C_4 = \frac{C_0}{6}\theta^3 e^{-\theta} \qquad \text{---------(7.4)}$$

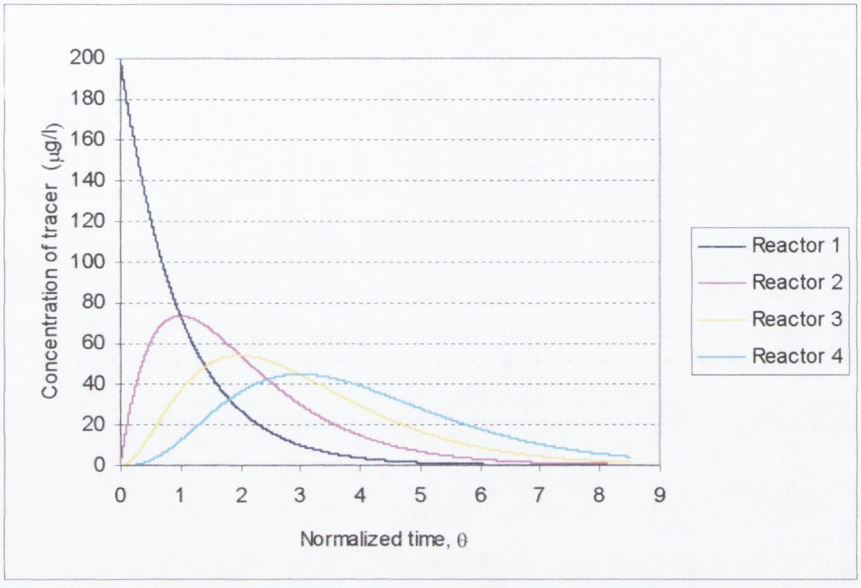

Figure 7. 2 Effluent concentration curves from four CSTRs in-series

When the system contains only one CSTR it can be broadly seen from the RTD curve whether the reactor is behaving hydraulically efficiently or whether it is not working at the optimum level it was designed for. However, if the system contains more than one reactor it is difficult to pick out a poorly performing reactor based purely on the shape of the final effluent RTD curve across the whole system. Hence, the effluent concentration for each reactor must be recorded in relation to its reactor volume and the theoretical retention time (as shown in Figure 7.3). This can be done by fitting the RTD curve to the mathematical model (Eq. 3.16) by adjustment of the three parameters as before used to describe the mathematical model function: the retention time, Peclet Number and the fraction. Once the best fit is reached, it is possible to see whether the system is working efficiently or not, by comparing the model retention time with the theoretical retention time in conjunction with the number of tanks in-series compared to how many tanks in-series the model recognized. If the theoretical retention time is equal to the mathematical model retention time and the model identifies the number of tanks in-series to be equal to the number of tanks in reality, it means that the system is working at the optimum level it was designed for. If this is not

the case, further consideration to the RTD must be given in order to identify the cause of the hydraulic discontinuity.

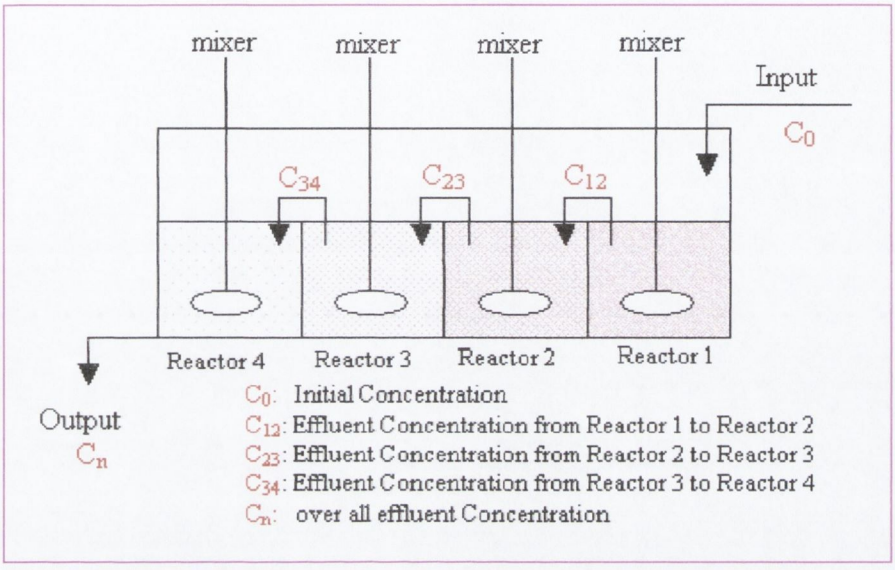

Figure 7. 3 Schematic diagram of experimental set up

This can be achieved by applying some constraints to the model in order to direct the model to predict the effluent concentration coming out of each reactor from the overall system RTD curve. This is based upon the methods described in the previous section using the theoretical retention time of the whole reactor from the overall volume and steady state flow.

For each experiment for a system of **n** reactors in series, the tracer was injected as a pulse input and the effluent concentration was recorded using the SCUFA device as before. The reactor volumes were measured and flow rate was recorded throughout each trial. The normal model was run initially in order to compare the theoretical retention time and the number of tanks in series with the outputs from the model. Then the model was directed to calculate the effluent concentration from each individual reactor, by running the mathematical model for each reactor separately on the same spreadsheet. This was achieved by running the Solver again but including constraints to direct the model according to the theoretical retention time (as shown in Figure 7.4).

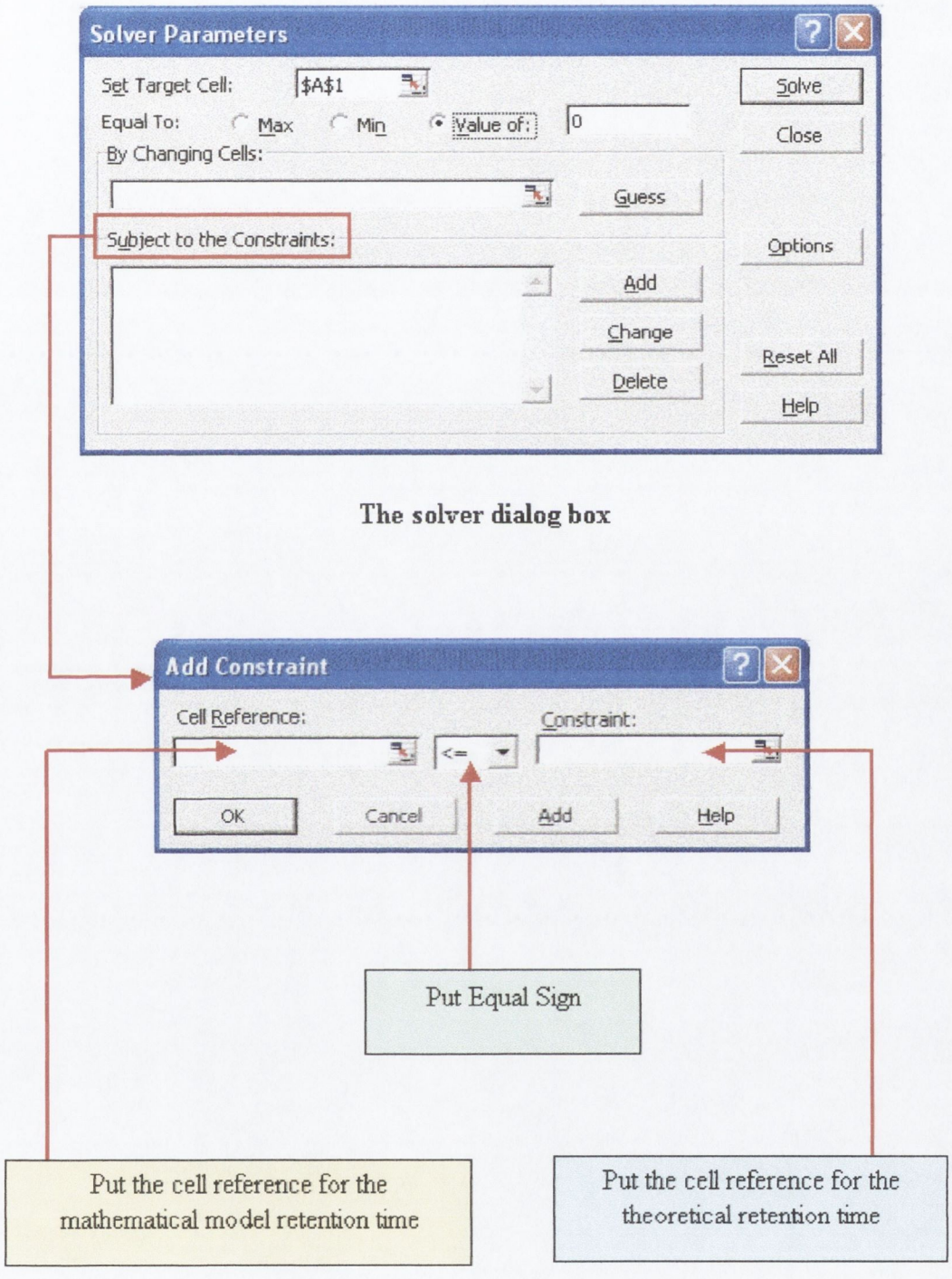

The solver dialog box

Figure 7. 4 The add constraint dialog box in solver

"Add a constraint" is a subprogram contained within a Solver programme in an Excel© spreadsheet that is used to apply some limitations to a Solver problem as described in Section 3.4.2. Constraints can be applied to adjustable (changing) cells, the target cell, or other cells that are directly or indirectly related to the target cell. It can also be used to direct the model to record the data inside the boundary of the limit. An example of this would be a recording of the effluent concentration for 0 sec up to 423.2s (as shown in Figure 7.5) cell reference G2 representing the residence time distribution for Reactor No.1 of **n** reactors in series.

How it works?

The cell reference for which the value must be constrained was entered in the Cell Reference box (as shown in Figure 7.4). In the illustrated model the cell reference was the mathematical model retention time (cell reference H4) which must be constrained to the real Residence Time Distribution (G2) (as shown in Figure 7.5).

An equal sign "=" relationship between the referenced cell and the constraint was then added (as shown in Figure 7.4) and finally the cell reference, which is the value that the model must be directed to (G4), was inserted. The following Figure 7.5 shows how two such mathematical models were arranged inside the Excel© framework. The figure shows the most important cells with its associated numbers. For this example, two mathematical models have been used on a system where both mixers are working efficiently. The first mathematical model is constrained by using the "Add constraint" built-in Solver function to record the effluent concentration C_{12} (see Figure 7.3). The corresponding curve (in pink) shows that the first CSTR has been recognized by the model, whilst the other curve shows that the trace from the two CSTRs in-series has been recognized by the model. As discussed previously, the area under each curve must be equal to the overall mass of tracer added to the system.

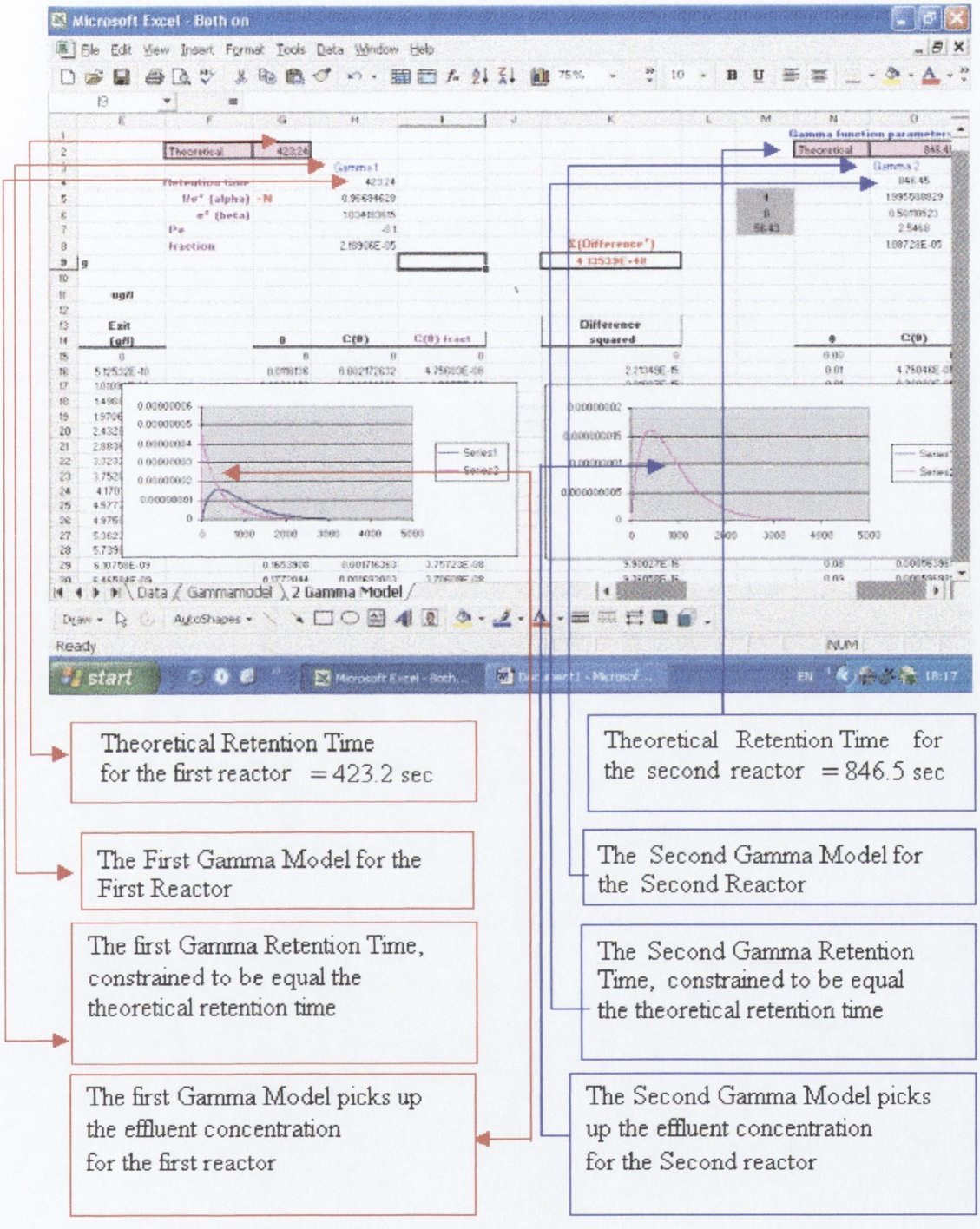

Figure 7. 5 Explanation of the mathematical model in Excel© used to predict individual reactor effluent concentrations

7.3 Model Enhancement

In order to improve the information gained from the model two Visual Basic Editor modules were inserted into the Excel© spreadsheet to enable the fraction of tracer remaining in the system at any time (θ), and the mass of tracer that has passed the system at any time (θ) to be evaluated. The Visual Basic Editor can be used to write and edit Macros attached to Microsoft Excel© spreadsheets.

7.3.1 Module 1

This programme was used to evaluate the fraction remaining (FR) in the system at any time (θ); and is based upon the following formula

$$FR(\theta) = \frac{C_1 + C_2 + \ldots\ldots\ldots\ldots + C_n}{C_0} \qquad \text{---------}(7.7)$$

Where:

FR (θ) = the fraction of tracer remaining in the system at any time (θ).

C_1= the effluent concentration of the sample taken at time, t_1

C_2= the effluent concentration of the sample taken at time, t_2

C_n= the effluent concentration of the sample taken at time, t_n

C_0=the initial tracer concentration injected at the effluent point.

The code for this module was placed into the Visual Basic Editor and can be seen in Appendix F whilst Figure 7.6 shows how this model was used in the Excel© Framework in order to get the fraction remaining in the system at any normalized time (θ). This is obtained by dividing the mathematical model retention time by the time at which the sample was taken (as discussed in Section 2.2.4).

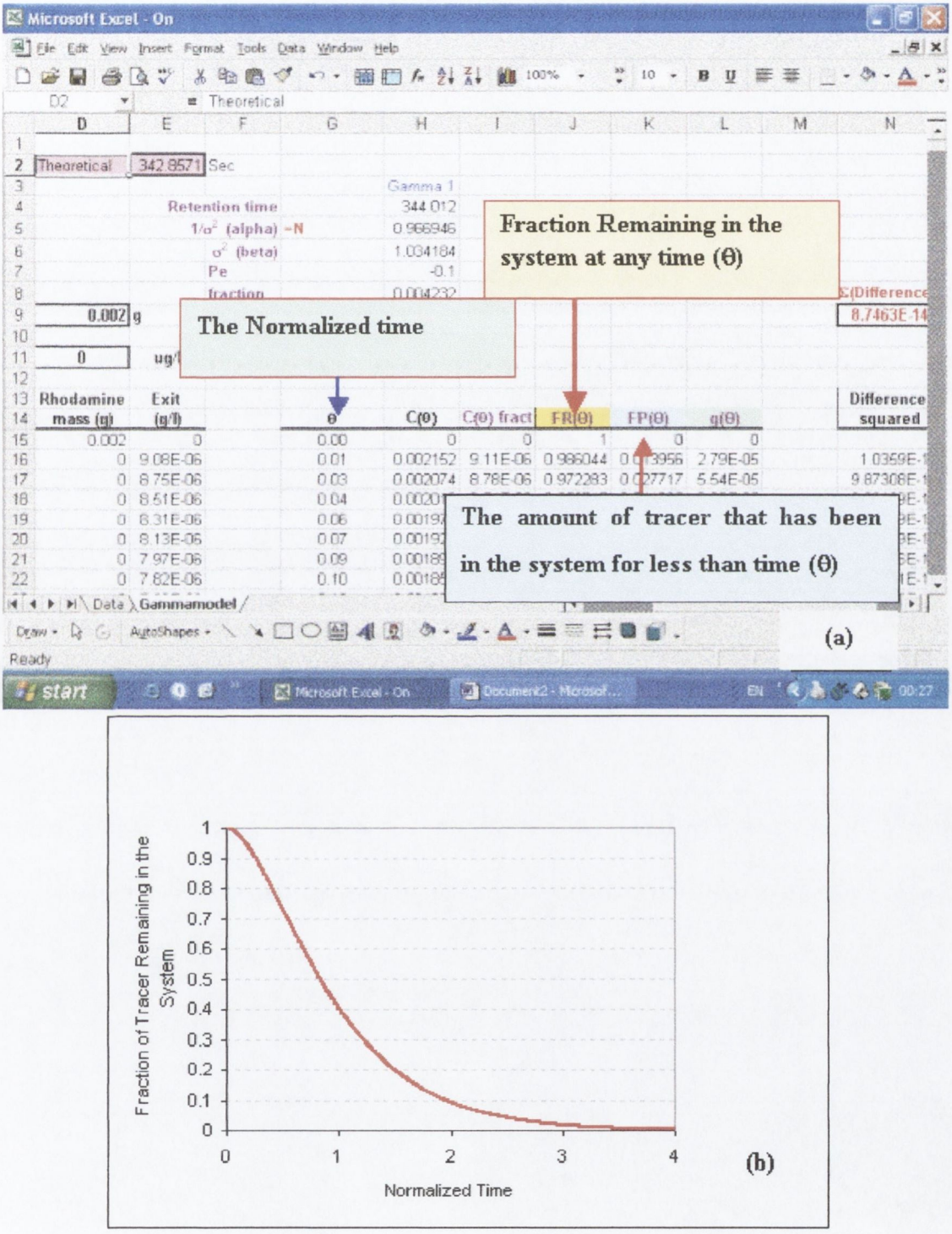

Figure 7. 6 The structure of the Module 1 (a) laid out on an Excel© spreadsheet model and (b) fraction of tracer remaining in the system vs. normalized time

7.3.2 Module 2

This programme was written to evaluate the amount of tracer that has been in the reactor for less than time (θ), and is based upon the following formula

$$FP(\theta) = 1 - e^{-\theta_i}\left[1 + \theta_i + \frac{\theta_i}{2\Gamma} + \ldots\ldots\ldots\ldots + \frac{\theta_i^{n-1}}{(n-1)\Gamma} + \ldots\ldots\right] \qquad ------(7.8)$$

Where:

FP (θ) = the amount of tracer that has been resident in the reactor for time less than time, θ.

Again the code for this module in the Visual Basic Editor is shown in Appendix F. The previous Figure 7.6(a) shows how this model was used in Excel© in order to get the fraction remaining in the system at any time), while Figure 7.7 shows graphically the fraction which was obtained by running the module versus the normalized time (θ).

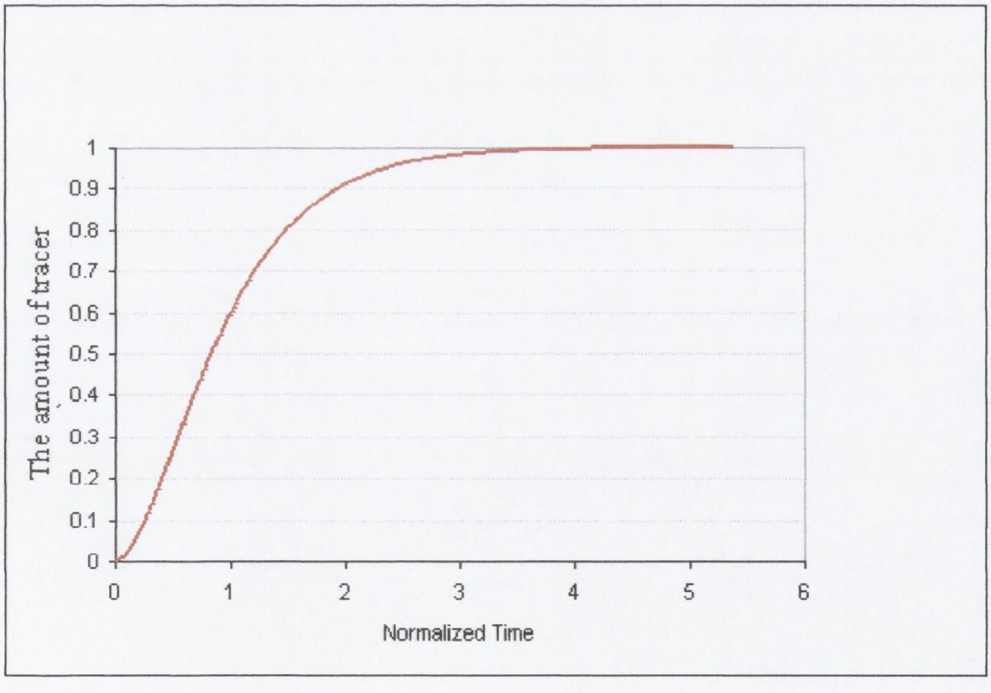

Figure 7. 7 The amount of tracer that has been left in the system for less than time θ.

7.4 Trials

The procedure for the trials was essentially the same as those described in Section 6.2. The previous trials carried out on different reactor configurations in Chapter 6 showed that it was possible to express the magnitude of the hydraulic problems as a percentage of the flow through the reactor. The following sets of trials aimed to diagnose hydraulic problems in specific reactors from looking only at the overall effluent concentration curve (RTD) from the reactor network. Hence, the trials were carried out on different reactor configurations initially starting with one reactor and then two, three and finally four in series. Different scenarios were set up whereby the mixer speed was set to its optimum level in all reactors except one in which the mixer was switched off. Other trials were set up where one mixer was set to a speed less than the optimum required for a complete mix. The purpose of the experiment was to see whether it was possible to evaluate the RTD for the reactor network across a range of mixer speeds and identify the location of the hydraulic inefficiency using the mathematical model.

The experimental apparatus was essentially the same as indicated in Section 6.2 (Figure 6.1) consisting of a large reactor, 118.82 cm in length, 50cm in height and 30cm in width with baffles simulating up to four tanks in series (three baffles each separated by a 28.3 cm gap, each baffle being 28.5 cm high and 30.0 cm wide). The inlet pipe feed was connected to the constant head tank to maintain a constant flow rate during the experiment. The outlet pipe from the reactors was connected to the SCUFA to measure and log the effluent concentration of the Rhodamine WT passing through against time.

7.4.1 Trial 1 (two CSTRs in-series)

Four different scenarios were considered with two CSTRs in-series to evaluate the model's ability to recognise whether a specific reactor is not performing correctly as shown in Figure 7.8: Scenario A, where both mixers are on; Scenario B, where both mixers are off; Scenario C, where mixer one is off; and Scenario D, where mixer two is off. The laboratory data for each scenario is shown in Table 7.1 and the results are shown in Table 7.2 with the corresponding effluent concentration graph shown in Figure 7.9. In addition, the effluent concentration RTD from each individual reactor, obtained adding constraints to the model, as discussed in the previous section, is shown in Figure 7.10.

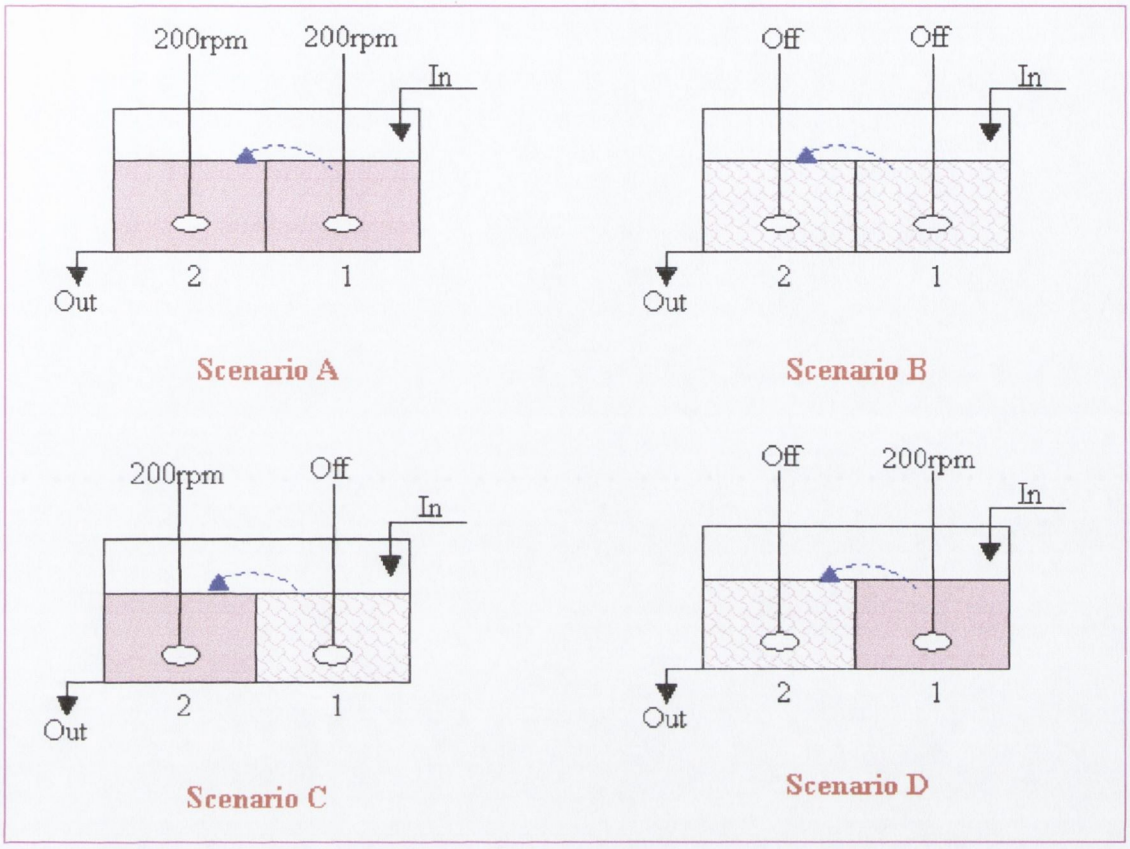

Figure 7. 8 Schematic representation of the four experimental scenarios for Trial 1

Scenario No.	Reactor volume	Flow rate	Mixer speed reactor 1	Mixer speed reactor 2	Rhodamine mass
	(L)	(l/min)	(rpm)	(rpm)	(g)
A	56.43	3	200	200	0.002
B	56.43	3	0	0	0.002
C	56.43	3	0	200	0.002
D	56.43	3	200	0	0.002

Table 7. 1 Two CSTR in-series experiments - configurations

Scenario No.	Mixer speed Reactor 1	Mixer speed Reactor 2	Reactor [1]		Reactor [2]	
			Theoretical retention time at the end of Reactor 1	No. Of CSTR	Theoretical retention time at the end of Reactor 2	No. Of CSTR
	(rpm)	(rpm)	(S)	(n)	(S)	(n)
A	200	200	564.3	0.99	1128.6	1.99
B	0	0	564.3	2.62	1128.6	5.47
C	0	200	564.3	2.53	1128.6	3.54
D	200	0	564.3	0.99	1128.6	3.84

Table 7. 2 Two CSTR in-series model laboratory experiments - results

Figure 7. 9 Graph showing laboratory result and model curve for Trial 1, Scenario A

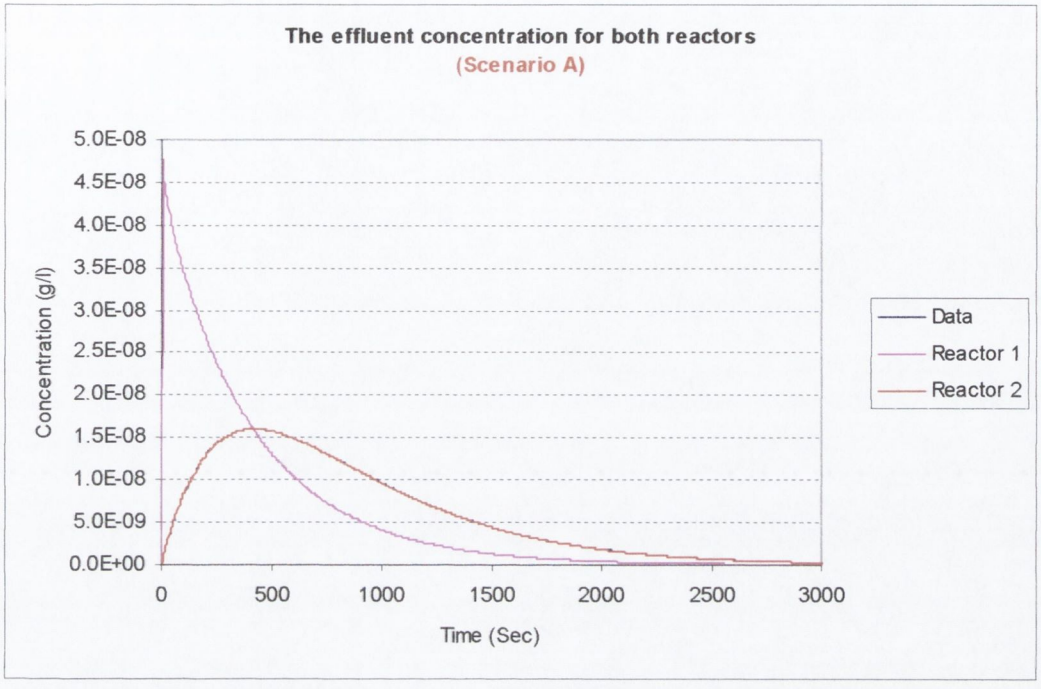

Figure 7. 10 Graph showing laboratory effluent concentration result and model curves from each reactor for Trial 1, Scenario A

7.4.1.1 Results Analysis (Trial 1)

When a system contains more than one reactor it is difficult to pick out a poorly performing reactor based purely on the shape of the single effluent concentration curve. Consequently, the effluent concentration for each reactor has been calculated from the model in relation to the reactor volume and the theoretical retention time for each individual reactor. Mathematically, if the volume in **n** reactors in-series is constant, the differences between the reactor and the following reactor must be equal to the total volume divided by **n** reactors in-series indicating that the system is equalized. As discussed previously the Gamma model function can mathematically express the effluent RTD from a perfectly mixed CSTR, and this model is able to recognize the number of **n** reactors in-series based on the reactor volume which is constant from one reactor to another.

Again, the area under the RTD curves from each reactor must be equal to the mass injected, and is thus equalized from one reactor to another. As shown in Figure 7.10 it is clear that the area under each curve is exactly the same, with the effluent concentration curve from

Reactor 2 exactly matching the effluent concentration data curve, which was obtained across the system in the experiments. In this example, the system was perfectly mixed (when all mixers were working at 200 rpm) which is also possible to see numerically as shown in Scenario A in Tables 7.2 where the differences between the number of CSTRs for any reactor and the following reactor is equal to 1 (indicating the reactor is working efficiently) and constant from one reactor to another in the network.

In the cases when the hydraulic irregularities were deliberately created in the system it may be possible to recognize that there was some sort of problem in the system from the result curves but it is not possible to pick out which reactor is promoting the hydraulic irregularities that need to be corrected. However, by applying the technique described in this chapter the poorly performing reactor can be diagnosed. Table 7.2 shows different results that were obtained from the four different Scenarios A to D. When the mixers were set at 0 rpm the model gives the number of CSTRs in the **n** networked reactor to be higher than expected and the differences between each reactor and its following reactor is not equal to 1 indicating the hydraulic irregularities are present in the system. However, for Scenario B the mathematical model picked out **n** = 2.62 for the first reactor which is obviously higher than it should be indicating that the hydraulic irregularities exist in this reactor. For the second reactor the model picked out that **n** = 5.47 which also indicates that the hydraulic irregularities exist in this reactor. The difference between the second and the first reactor is obviously not equal to 1 and the modelled high numbers of CSTRs in-series indicated the reactor is short-circuiting. In Scenarios C and D the overall amount of shear applied to each system was the same. However, in Scenario C the mixer in Reactor 1 was at rest in contrast to Scenario D where the mixer in Reactor 2 was at rest. The mathematical model picked out nearly the same number of CSTRs where **n** = 3.54 and 3.84 respectively for the effluent trace from second reactor which is obviously higher than it should be indicating that hydraulic irregularities exist in these reactors. However, the model picked out different results for the intermediate values from Reactor 1 where **n** = 2.53 and 0.99 respectively which indicated that Reactor 1 in Scenario C was not performing efficiently but it was performing efficiently in Scenario D which is acceptable and expected.

7.4.2 Trial 2 (three CSTRs in-series)

Five different scenarios were considered in order to evaluate the model's ability to diagnose the poor performance of a single reactor in the network as shown in Figure 7.11 below. Scenario A, where all mixers are on; Scenario B, where all mixers are off; Scenario C, where mixer one is off; Scenario D, where mixer two is off; and Scenario E, where mixer three is off. The experimental configurations for each scenario are shown in Table 7.3 and the results are shown in Table 7.4. The corresponding effluent concentration graphs are shown in Figure 7.12 and also the model's prediction of the respective effluent concentrations from each individual reactor, which were obtained by adding certain constraints to the model as discussed in Section 7.2, are shown in Figure 7.13. All other graphs are in Appendix G.

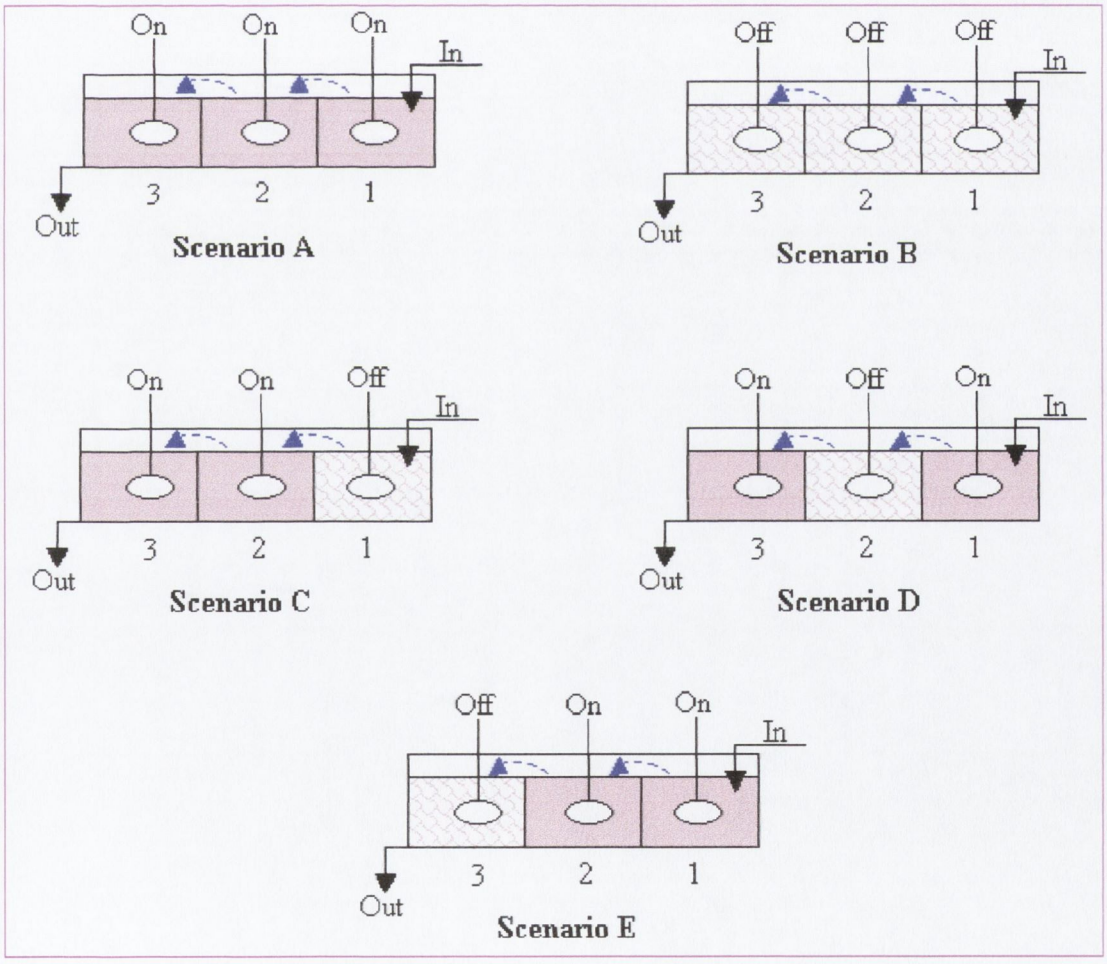

Figure 7. 11 Schematic representation of the five experimental scenarios for Trial 2

Scenario No.	Reactor volume	Flow rate	Mixer speed Reactor 1	Mixer speed Reactor 2	Mixer speed Reactor 3	Rhodamine mass
	(L)	(l/min)	(rpm)	(rpm)	(rpm)	(g)
A	84.65	3	200	200	200	0.002
B	84.65	3	0	0	0	0.002
C	84.65	3	0	200	200	0.002
D	84.65	3	200	0	200	0.002
E	84.65	3	200	200	0	0.002

Table 7. 3 Three CSTR in-series experiments - configurations

	Reactor [1]		Reactor [2]		Reactor [3]	
Scenario No.	Theoretical retention time at the end of Reactor 1	No. Of CSTR	Theoretical retention time at the end of Reactor 2	No. Of CSTR	Theoretical retention time at the end of Reactor 3	No. Of CSTR
	(S)	(n)	(S)	(n)	(S)	(n)
A	564.3	0.96	1128.6	1.99	1692.8	2.99
B	564.3	1.69	1128.6	3.48	1692.8	5.28
C	564.3	1.73	1128.6	2.75	1692.8	3.82
D	564.3	0.96	1128.6	2.98	1692.8	3.98
E	564.3	0.96	1128.6	1.96	1692.8	3.74

Table 7. 4 Three CSTRs in-series model experiments - results

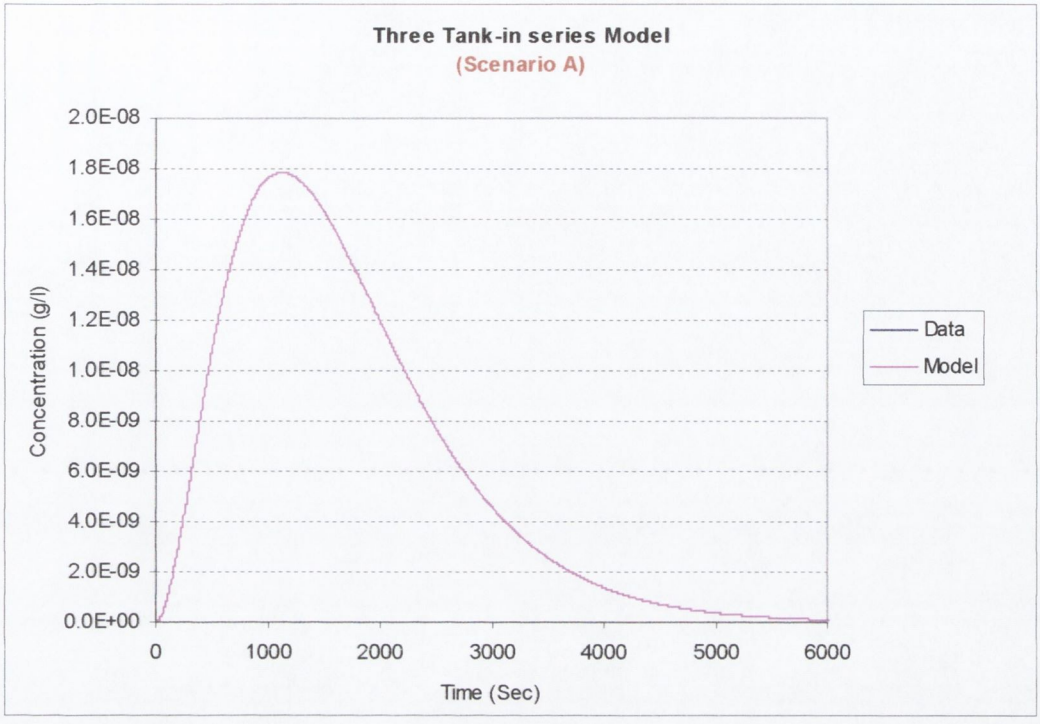

Figure 7. 12 Graph showing laboratory result and model curves for Trial 2 for Scenario A

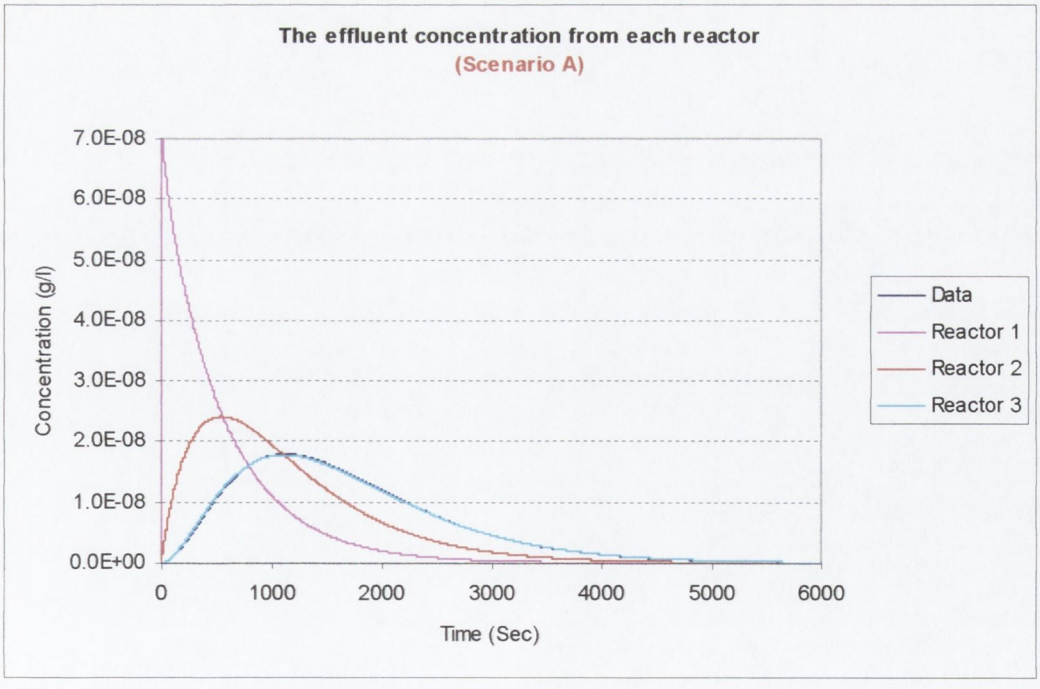

Figure 7. 13 Graph showing laboratory effluent concentration result and model curves from each reactor for Trial 2 for Scenario A

7.4.2.1 Results Analysis (Trial 2)

Again, the area under the RTD curves from each reactor must be equal to the mass injected, and is thus equalized from one reactor to another. As shown in Figure 7.13 it is clear that the area under each curve is exactly the same, with the effluent concentration curve from Reactor 3 exactly matching the effluent concentration data curve which was obtained across the system. In this example, the system was perfectly mixed (with all mixers working at 200 rpm) which is also possible to see numerically in Table 7.4 Scenario A where the differences between the number of CSTRs for any reactor and the following reactor is equal to 1 (indicating each reactor was working efficiently) and constant from one reactor to another in the network.

In the Scenarios where the hydraulic irregularities were deliberately created in the system again it may be possible to recognize that there is a problem in the system from the final effluent trace curve but it is not possible to pick out which reactor is promoting the hydraulic irregularities that need to be corrected. For example, Figure 7.14 shows that the actual effluent concentration curve measured in Scenario B does not exactly match the effluent concentration curve from Reactor 3 that was obtained by the model using the constraints subprogram, (see Section 7.2). This indicates that the system was not performing as 3 with **n** set to 3 CSTRs but at this stage it is still not possible to pick out from the graph which reactor is not working correctly.

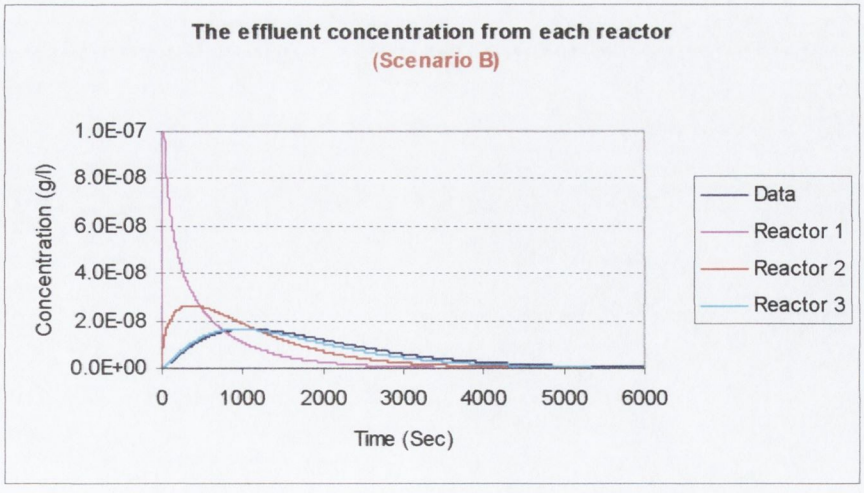

Figure 7. 14 The modelled effluent concentrations across the whole system. ***Note, the effluent concentration for Reactor 3 does not completely match the data***

However, by applying the technique described in this chapter the poorly performing reactor can be identified. Table 7.4 shows the results that were obtained from the four different Scenarios A to E. When the mixers were set at 0 rpm the model gives the number of CSTRs in **n** networked reactors to be higher than expected and it can also be seen that the differences between each reactor and its following reactor is not equal to 1 indicating the hydraulic irregularities present in the system. However, for Scenario B the mathematical model picked out **n** = 1.69 for Reactor 1 which is obviously higher than it should be indicating that the hydraulic irregularities existed in this reactor. For Reactors 2 and 3 the model picked out that **n** = 3.48 and 5.28 which also indicates that the hydraulic irregularities existed in these reactors. The difference between the second and the first reactor is not equal to 1 which, accompanied with high numbers of CSTRs in-series, indicates that the reactor was short-circuiting. In Scenarios C, D and E the same power input per unit volume was applied to the overall systems but with the variation that the mixers in Reactors 1, 2 and 3 for Scenarios C, D and E respectively were at rest. The mathematical model picked out nearly the same numbers of CSTRs where **n** = 3.82, 3.98 and 3.74 respectively for the effluent at the end of the system which is obviously higher than it should be indicating that the hydraulic irregularities existed in these reactors. However, the model picked out different results where **n** = 1.73, 0.96 and 0.96 for the effluent at the end of Reactor 1 for Scenarios C, D and E respectively which indicates that Reactor 1 in Scenario C was not performing efficiently while in Scenarios D and E they were performing efficiently which is again acceptable and expected. In addition, the model picked out the **n** =2.75, 2.98 and 1.96 for the effluent at the end of Reactor 2 for each Scenarios C, D and E respectively which is obviously higher than it should be for Scenarios C and D. This is acceptable even for Scenario C where the mixer was working at the optimum level of 200 rpm since the RTD has been affected by the Reactor 1 (which was at rest): for Scenario D this is due to the mixer being at rest.

7.4.3 Trial 3 (four CSTRs in-series)

Three main categories of baffle configuration were considered in this trial to evaluate the model with respect to the changes in the flow path as shown in Figure 7.15. Category 1, where the over-baffle flows takes place (Figure 7.15(a)). Category 2, where the baffle position between the second and the third reactors was raised in order to change the direction of flow to a vertical direction (Figure 7.15(b)) and Category 3 where the flow was moving in a horizontal direction across the reactors (Figure 7.15(c)).

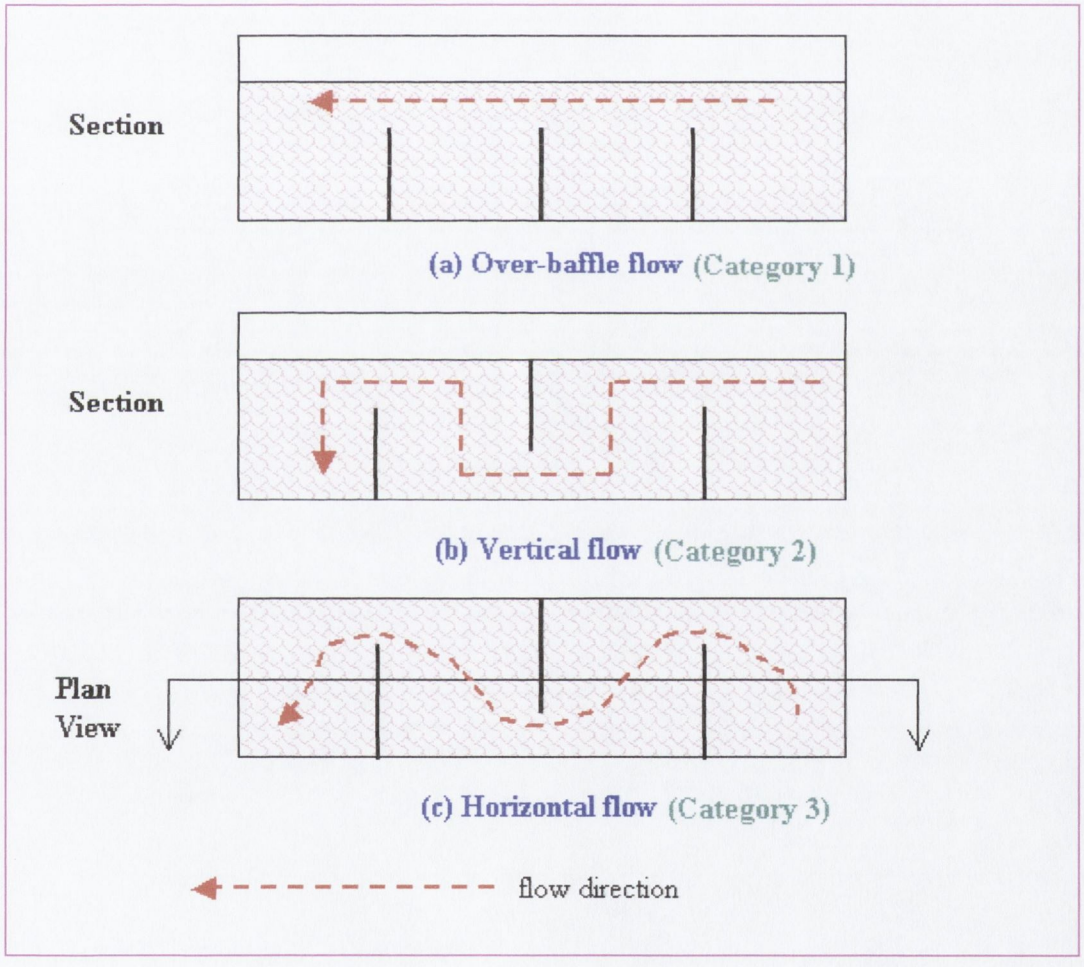

Figure 7. 15 Schematic representation showing the flow direction for (a) Category 1-Over-baffle flow, (b) Category 2-Vertical flow and (c) Category 3-Horizontal flow

For each baffle configuration category, six diagnostic scenarios (as shown in Figure 7.16) were considered to evaluate the model: Scenario A, where all mixers are on; Scenario B, where all mixers are off; Scenario C, where mixer 1 is off; Scenario D, where mixer 2 is off; scenario E, where mixer 3 is off; and Scenario F, where mixer 4 is off. The experimental configurations for each scenario are shown in Table 7.5 and the model results are shown in Table 7.6. An example of the corresponding effluent concentration graph is shown in Figure 7.17 with respective modelled concentrations from each individual reactor shown in Figure 7.18. All other graphs are presented in Appendix G.

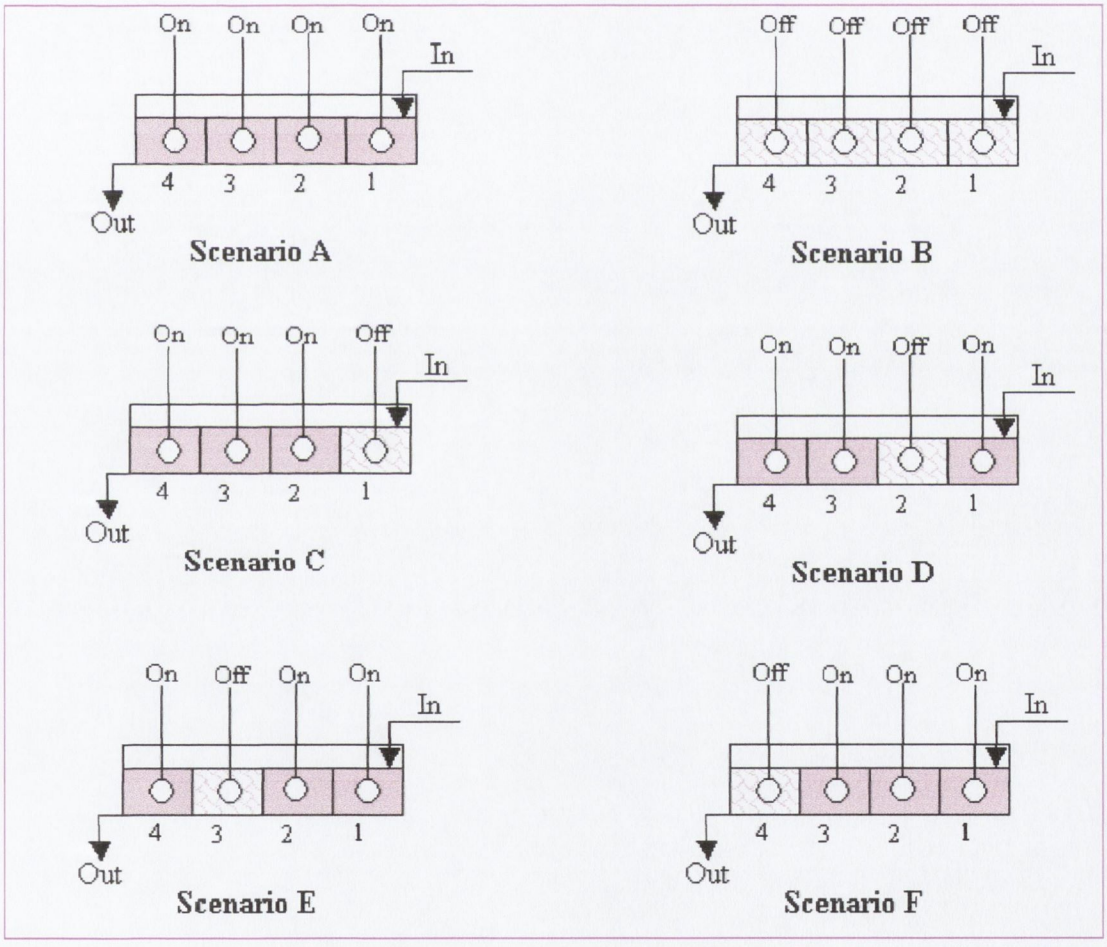

Figure 7. 16 Schematic representation of the six experimental scenarios for Trial 3

Scenario No.	Reactor volume	Flow rate	Mixer speed Reactor 1	Mixer speed Reactor 2	Mixer speed Reactor 3	Mixer speed Reactor 4	Rhodamine mass
	(L)	(l/min)	(rpm)	(rpm)	(rpm)	(rpm)	(g)
A	112.86	3	200	200	200	200	0.002
B	112.86	3	0	0	0	0	0.002
C	112.86	3	0	200	200	200	0.002
D	112.86	3	200	0	200	200	0.002
E	112.86	3	200	200	0	200	0.002
F	112.86	3	200	200	200	0	0.002

Table 7. 5 Four CSTR in-series experiments - configurations

		Reactor [1]		Reactor [2]		Reactor [3]		Reactor [4]	
Categories	Scenario No.	Theoretical retention time at the end of Reactor 1	No. Of CSTR	Theoretical retention time at the end of Reactor 2	No. Of CSTR	Theoretical retention time at the end of Reactor 3	No. Of CSTR	Theoretical retention time at the end of Reactor 4	No. Of CSTR
		(S)	(n)	(S)	(n)	(S)	(n)	(S)	(n)
Over-baffle flow direction	A	564.3	0.96	1128.6	1.96	1692.8	2.96	2257.2	4.99
	B	564.3	2.69	1128.6	4.65	1692.8	6.72	2257.2	8.96
	C	564.3	2.03	1128.6	3.02	1692.8	4.02	2257.2	5.05
	D	564.3	0.96	1128.6	2.97	1692.8	3.96	2257.2	4.95
	E	564.3	0.97	1128.6	1.99	1692.8	4.07	2257.2	5.07
	F	564.3	0.96	1128.6	1.93	1692.8	2.98	2257.2	5.20
Vertical flow direction	A	564.3	0.99	1128.6	1.99	1692.8	2.99	2257.2	4.00
	B	564.3	2.59	1128.6	3.65	1692.8	4.73	2257.2	7.52
	C	564.3	2.31	1128.6	3.36	1692.8	4.45	2257.2	5.47
	D	564.3	0.97	1128.6	3.49	1692.8	4.50	2257.2	5.51
	E	564.3	0.99	1128.6	1.97	1692.8	4.20	2257.2	5.20
	F	564.3	0.99	1128.6	1.99	1692.8	2.99	2257.2	5.52
Horizontal flow direction	A	564.3	0.99	1128.6	1.99	1692.8	2.99	2257.2	4.00
	B	564.3	2.64	1128.6	3.01	1692.8	4.74	2257.2	6.66
	C	564.3	2.1	1128.6	3.15	1692.8	4.2	2257.2	5.20
	D	564.3	0.99	1128.6	3.32	1692.8	4.32	2257.2	5.32
	E	564.3	0.99	1128.6	1.99	1692.8	4.02	2257.2	5.11
	F	564.3	0.99	1128.6	1.99	1692.8	2.99	2257.2	5.20

Table 7. 6 Four CSTR in-series model experiments - results

Figure 7. 17 Graph showing laboratory result and model curves for Trial 3, Scenario A

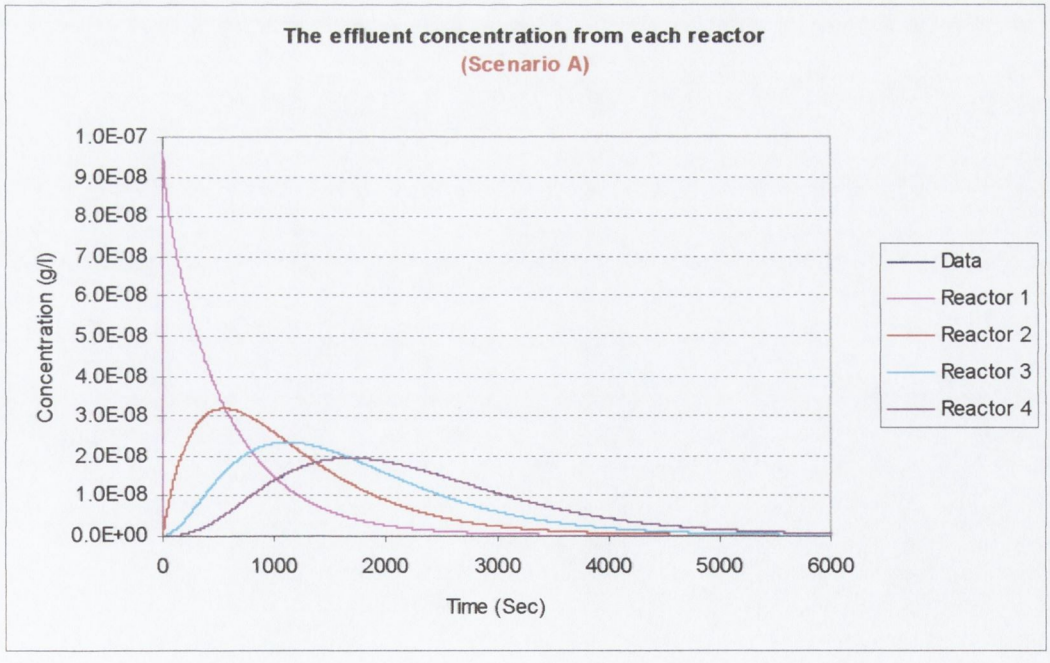

Figure 7. 18 Graph showing laboratory effluent concentration result and model curves from each reactor for Trial 3, Scenario A

7.4.3.1 Results Analysis (Trial 3)

Again, the area under the RTD curves from each reactor must be equal to the mass injected and is thus equalized from one reactor to another. As shown in Figure 7.13 it is clear that the area under each curve is exactly the same, with the effluent concentration curve from Reactor 4 exactly matching the effluent concentration data curve, which was obtained across the system. In this example, the system is perfectly mixed (with all mixers working at 200 rpm) which is also possible to see numerically in Tables 7.4 Scenario A where the differences between the number of CSTRs for any reactor and the following reactor is equal to 1 (indicating each reactor was working efficiently) and constant from one reactor to another in the network.

In the scenarios where the hydraulic irregularities were deliberately created in the system it can be generally seen that there is a problem in the system for example from Figure 7.19 which shows that the actual effluent concentration curve measured in Scenario B does not match exactly the effluent concentration curve from Reactor 4 that was obtained by the model using the constraints subprogram with **n** set to 4 CSTRs. At this stage though, it is not possible to pick out from the graph which reactor is not working correctly.

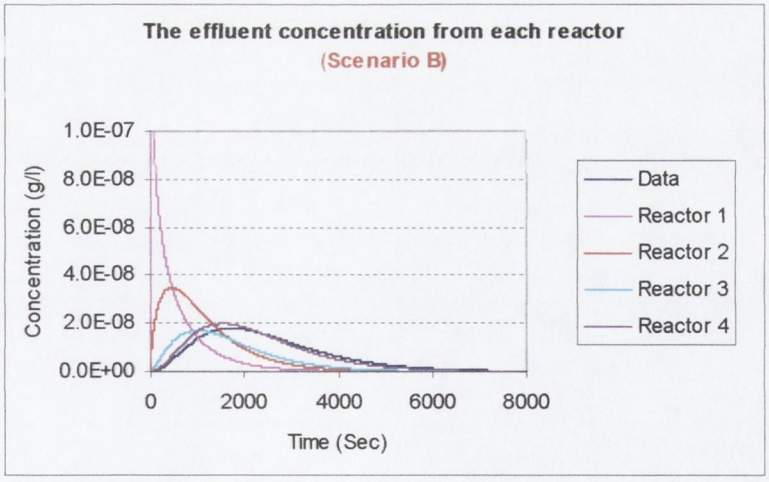

Figure 7. 19 The modelled effluent concentrations across the whole system. ***Note, the effluent concentration for Reactor 3 does not completely match the data***

However, by applying the technique described in this chapter the poorly performing reactor can be identified. Table 7.6 shows the different results that were obtained from the five different Scenarios A to F. When the mixers were set at 0 rpm the model gives the number of CSTRs in **n** networked reactors to be higher than expected and the differences between each reactor and its following reactor is not equal to 1 indicating the hydraulic irregularities present in the system. However, in Table 7.6 Scenario B for the over-baffle configuration the mathematical model picked out **n** = 1.69 for Reactor 1 which is obviously higher than it should be indicating that the hydraulic irregularities existed in this reactor. For Reactors 2, 3 and 4 the model picked out that **n** = 3.65, 5.72 and 7.96 which also indicates the presence of hydraulic irregularities in the system. The difference between the second and the first reactor is not equal to 1 which, accompanied with the high numbers of CSTRs in-series, indicates the reactor was short-circuiting. In Scenarios C, D, E and F the same power input per unit volume was applied to the overall systems but with the variation that the mixers in Reactors 1, 2, 3 and 4 for Scenarios C, D, E and F respectively were at rest. The mathematical model picked out nearly the same numbers of CSTRs where **n** = 5.13, 4.95, 5.07 and 5.20 respectively for the effluent at the end of the system which is obviously higher than it should be indicating the hydraulic irregularities in these reactors. However, for the effluent at the end of Reactor 1 the model picked out **n** = 2.03, 0.96, 0.97 and 0.96 for Scenarios C, D, E and F respectively which indicated that the Reactor 1 in Scenario C was not performing efficiently compared to Scenarios D, E and F where it was performing efficiently which was expected since this was the physical reality in the experiments. In addition, the model picked out **n** = 3.02, 2.97, 1.99 and 1.93 for the effluent at the end of Reactor 2 for each Scenario C, D, E and F respectively which is obviously higher than it should be for Scenarios C and D since the mixers in these two reactors were working at the optimum level 200 rpm. The results in Scenarios C and D have been influenced by the lack of motion in the first and second reactors respectively (which were at rest) whereas in Scenarios E and F the mixers in Reactors 1 and 2 were working fine. Again it can be noted (as for the previous results in Tables 7.2 and 7.4) that if the system is performing efficiently as in Scenario A, the differences in the modelled number of tanks in-series, **n** between the reactor and the following reactor is 1 indicating that the system is working as a CSTR. When one of the reactors is not working properly for whatever reason or problem this

difference will move away from unity. For example, in Scenario E the mathematical model picked out **n** = 0.97,1.99, 4.07 and 5.07. In this case Reactor 1 was performing efficiently and the difference between Reactors 1 and 2 is 0.98 (i.e. close to 1) indicating that Reactor 2 was performing efficiently. However, the difference between Reactors 2 and 3 is 2.23 which indicates that Reactor 3 was not performing efficiently (as was the case in the experiments). Finally the difference between Reactors 3 and 4 was 1 which indicates the Reactor 4 is also performing efficiently (which again was the case in reality).

Comparing the results that were obtained for Category 1 (over-baffle flow) with the results that were obtained for Category 2 (vertical flow) and Category 3 (horizontal flow) (see Figure 7.15) it is clear that, in general, the over-baffle flow configuration for Category 1 performed worse than the vertical flow or horizontal flow configuration in Categories 2 and 3, as expected. The mathematical model produced higher values of CSTRs in-series for Scenario A in Category 1, **n** = 4.99 than for Category 2 and 3 which produced similar results, **n** = 4.00. This is due to the direction of flow through the reactor system which heads straight from the inlet to the outlet (see Figure 7.15(a)) in Category 1 compared to the vertical and horizontal flow paths taken in Categories 2 and 3 respectively which ensures that the tracer disperses throughout the entire system hence creating perfectly mixed conditions as revealed by the results.

In another similar comparison between Categories 1, 2 and 3 using Scenario B (all mixers at rest) the mathematical model picked out higher number of CSTRs in Category 1, **n** = 2.69, 4.65, 6.72 and 8.96 compared to **n** = 2.59, 3.65, 4.73 and 6.52 for Category 3 and **n** =1.64, 3.01, 4.74 and 7.66 for Category 2. This again indicates the more efficient baffle configurations of Categories 2 and 3 compared to the over-baffle flow design in Category 1, but also indicates that the horizontal-flow baffle configuration in Category 3 appears to be more optimal than the vertical-flow baffle configuration in Category 2. This same pattern is repeated for all the different experimental Scenarios when the vertical and horizontal flow baffle configuration are compared. This is primarily due to the position of the inlet and outlet ports for the vertical-flow configuration which is discussed in Section 7.5 below in more detail.

7.5 Input and Output Variation

The input and output configurations between the reactors were considered in more detail by looking at eight further scenarios, as shown in Figure 7.20. This was necessary in order to evaluate the model's ability to recognize the poor performance of a reactor with regard to the position of the input, output and baffle positions between the reactors. Each scenario was repeated two times, one where all the mixers were set to 200 rpm, the other where all the mixers were set at rest, 0 rpm. The experimental system was essentially the same as indicated in Section 4.4, only a small change being made to the input and output or baffle position from one scenario to another, as shown in Figure 7.20. It should be noted that Scenario E was the same as Scenario D, except that a distributed flow line was inserted at the bottom of the reactor for the inflow and the output point was at the top. In Scenario H, some modifications were made to the outlet point involving a small box, 14 cm in length, 9 cm in height and 7 cm in width, which was installed inside the reactor to provide an effluent weir for the flow to pass over, creating lower local velocities at the outlet point. The box was centralized 22 cm from the bottom of the reactor and 6.8 cm from each side of the reactor (as shown in Figure 7.20).

The experimental configurations for each scenario are shown in Table 7.7, the results are shown in Table 7.8 and the corresponding effluent concentration and model graphs are shown in Figures 7.21 and 7.22.

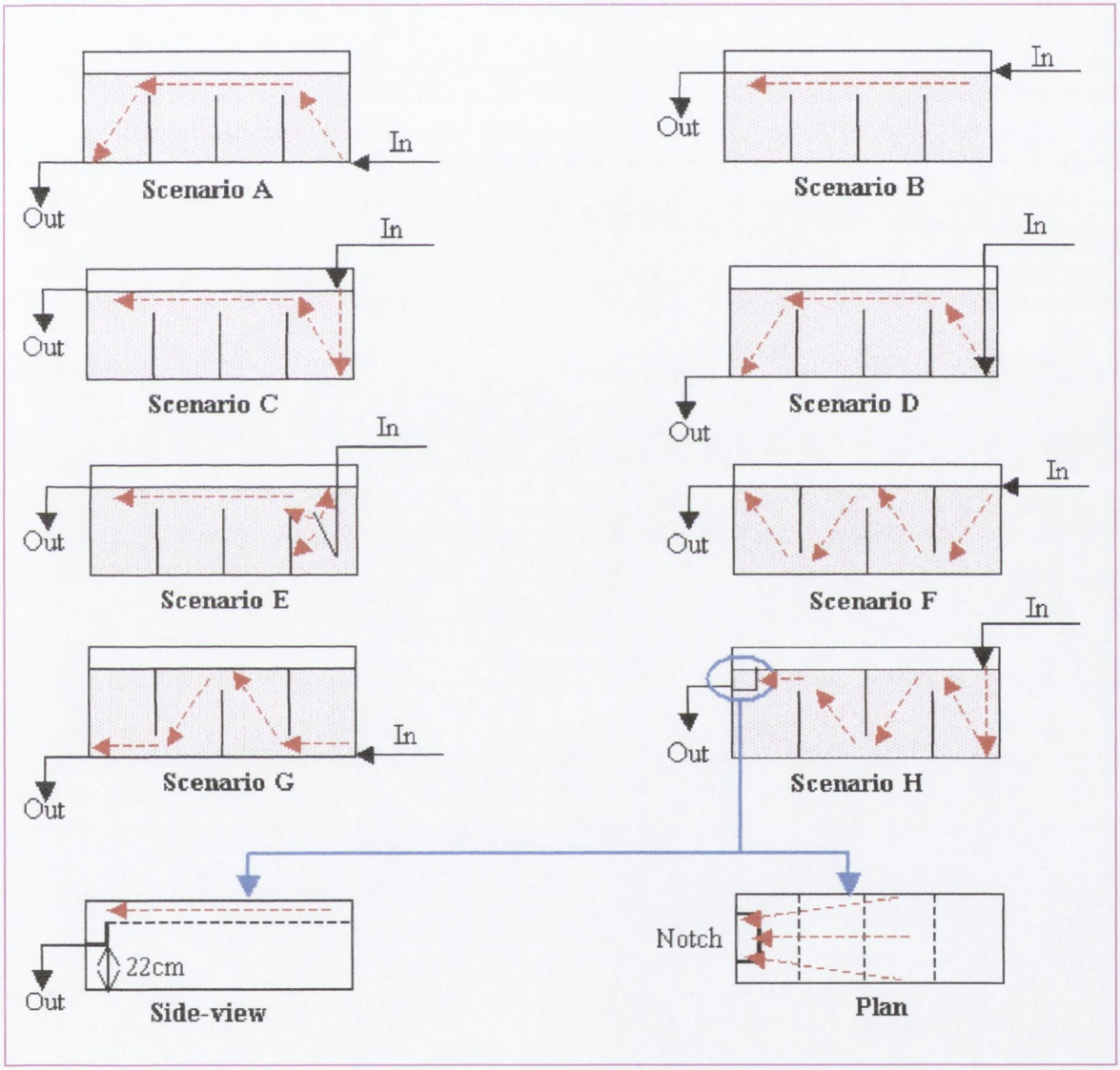

Figure 7. 20 Schematic representation of the eight scenarios for inlet and outlet variation experiments

Scenario No.	Reactor volume	Flow rate	Mixer speed	Rhodamine mass
	(L)	(l/min)	(rpm)	(g)
A	109.4	3	200	0.002
			0	
B	109.4	3	200	0.002
			0	
C	109.4	3	200	0.002
			0	
D	109.4	3	200	0.002
			0	
E	109.4	3	200	0.002
			0	
F	109.4	3	200	0.002
			0	
G	109.4	3	200	0.002
			0	
H	109.4	3	200	0.002
			0	

Table 7. 7 Input and output variation experiments - configurations

		Reactor [1]		Reactor [2]		Reactor [3]		Reactor [4]	
Scenario No.	Mixer speed	Theoretical retention time at the end of Reactor 1	No. Of CSTR	Theoretical retention time at the end of Reactor 2	No. Of CSTR	Theoretical retention time at the end of Reactor 3	No. Of CSTR	Theoretical retention time at the end of Reactor 4	No. Of CSTR
	(rpm)	(S)	(n)	(S)	(n)	(S)	(n)	(S)	(n)
A	200	547	0.99	1094	1.99	1641	2.99	2188	3.99
	0		0.94		2.85		5.41		6.53
B	200	547	0.99	1094	1.99	1641	2.99	2188	3.99
	0		1.96		4.01		5.52		7.31
C	200	547	0.99	1094	1.99	1641	2.99	2188	3.99
	0		0.99		2.96		4.80		6.99
D	200	547	0.99	1094	1.99	1641	2.99	2188	3.99
	0		0.98		2.90		5.36		6.43
E	200	547	0.99	1094	1.99	1641	2.99	2188	3.99
	0		0.99		2.90		4.91		6.83
F	200	547	0.99	1094	1.99	1641	2.99	2188	3.99
	0		1.10		2.23		3.62		4.72
G	200	547	0.99	1094	1.99	1641	2.99	2188	3.99
	0		1.32		2.59		3.65		8.71
H	200	547	0.99	1094	1.99	1641	2.99	2188	3.99
	0		0.99		2.05		3.01		4.24

Table 7. 8 Input and Output variation experiments - results

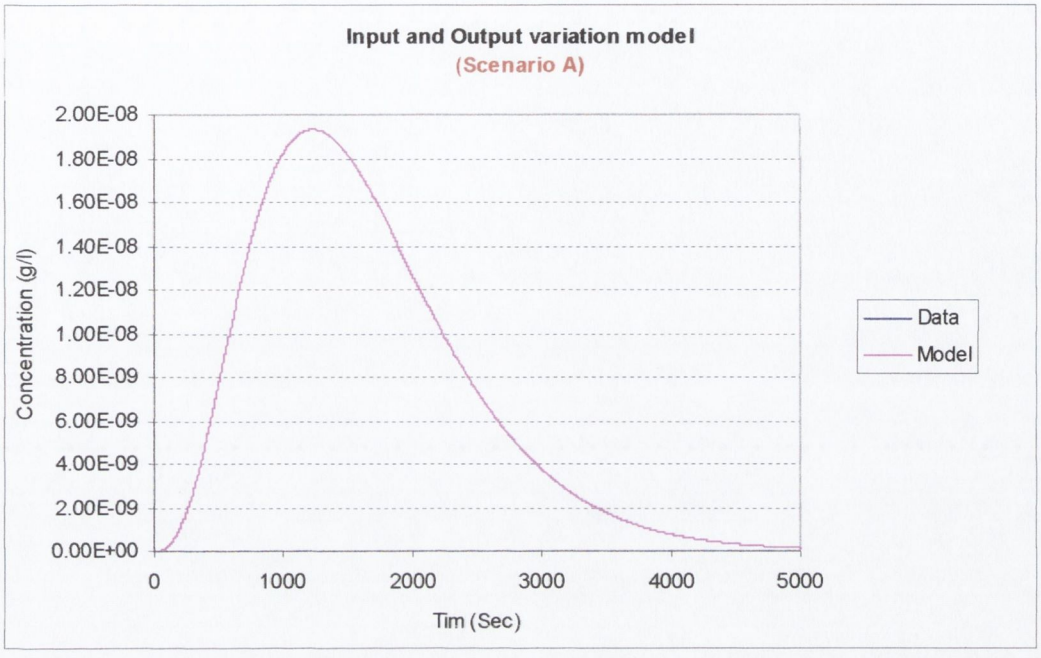

Figure 7. 21 Graph showing result and model curve for input and output variation Scenario A *(mixers on)*

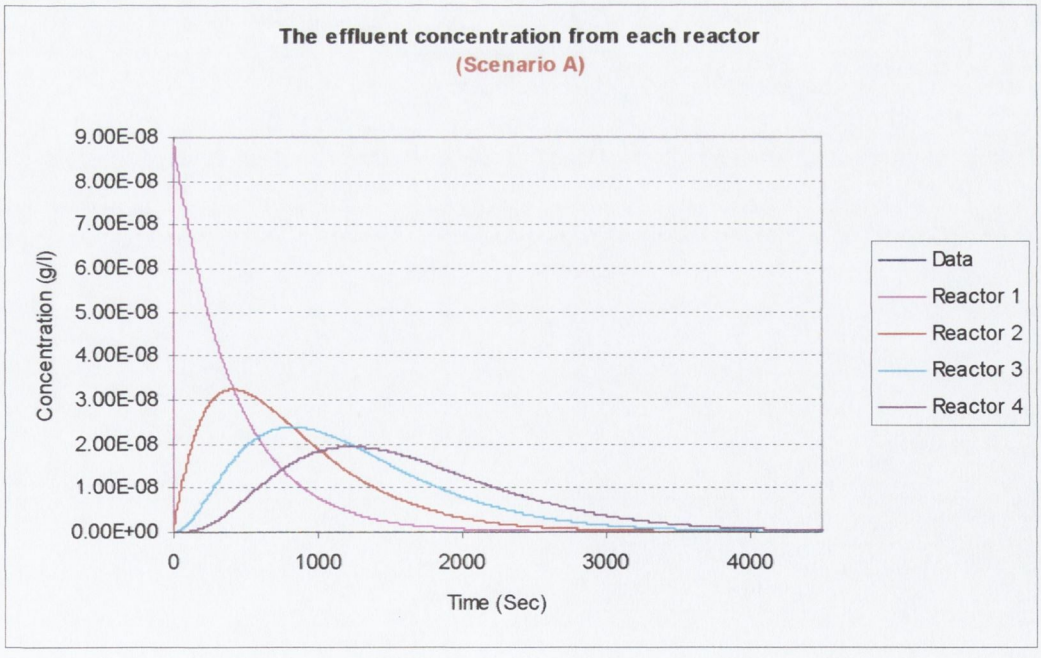

Figure 7. 22 Graph showing effluent concentration result and model curves from each reactor for input and output variation Scenario A *(mixers on)*

7.5.1 Results Analysis of Input and Output

As discussed in Section 7.5 many experiments were analysed with regard to the position of the input, output and baffles. The results obtained indicate that no difference could be discerned between the different configurations when the mixers were working at the optimum level 200 rpm. As shown in Table 7.8 the differences between each reactor and the following reactor were constant and equal to 1. This indicates that such a mixer speed (200 rpm) is sufficient to overcome any hydraulic discontinuities from the geometry of the system. However, when the mixers were at rest the results obtained were more interesting, revealing the differences that the position of the input and output can make in order to ensure the system is working hydraulically efficiently with regards to mixed reactors. In terms of the influent in each reactor, the momentum of the incoming flow has to be broken up which also has a directional component to it. For all Scenarios (except Scenario E), the momentum of flow entering Reactor 1 was 4.23×10^{-7} kg.m/s whilst the momentum of the flow passing over or under the baffles in the middle of the systems was only 2.2×10^{-8} kg.m/s. In Scenarios A and D the results show that there was quite a good mix occurring in Reactors 1 and 4 due to the fact that the flow path had to cross through the centre of the reactor to reach the outlet point (as discussed in Chapter 6). The difference in direction of the influent into Reactor 1 has been picked up by the model where Scenario A gives a slightly worse result than Scenario D [$\mathbf{n}$ = 0.94 compared to $\mathbf{n}$ = 0.98]. This would be expected since there is a vector component of the influent flow towards the outlet in Scenario A, thus promoting a slight short-circuit through the reactor. The results for Reactors 2 and 3 (when the mixers were at rest) indicated high numbers of CSTRs for these reactors $\mathbf{n}$ = 2.85, 5.41 and 6.53 for Scenario A and $\mathbf{n}$ = 2.91, 5.36 and 6.43 for Scenario D since there was no energy to disperse the incoming flow significantly into the main mixed zone of the reactor. Comparing these results with the results that were obtained for Scenario B where the only differences were the position of the input and the output being moved to the top of the reactors (see Figure 7.20) it is clear that Scenario B performed worse than Scenarios A and D as expected. The mathematical model produced higher values of CSTRs in-series for Scenario B than for Scenarios A and D which was due to the momentum of the inlet flow entering carrying straight through the reactors towards the output.

In another similar comparison between Scenarios F and G, where the input and the outputs were at the top (Scenario F: flow in a vertical direction) and at bottom (Scenario G: flow in a horizontal direction) the mathematical model recognised **n** = 4.72 CSTRs for the system in Scenario F and a higher value of **n** = 8.71 for Scenario G. Again this was due to the position of the input point, promoting short-circuits in Scenario G with the direction of the momentum of incoming flow heading directly towards the output in Reactors 1 and 4. The flow in Scenario F crosses each reactor in a diagonal direction, which helps to create some mixing (dispersion) in the reactor even without the mixers on.

In another comparison between Scenarios B, C and E the mathematical model picked out **n** = 1.96, 0.99 and 0.99 for Reactor 1 in each respective scenarios which indicated that there were good mixes for Scenarios C and E due to the inlet flow direction crossing the middle of the reactor compared to poor mixing in Scenario B since the flow headed across the top of the reactor towards the output. It should also be noted that the model did not pick up any significant difference between the point input (Scenario C) and dispersed input (Scenario E). In addition the mathematical model picked out similarly high values of CSTRs for the rest of the Reactors 2, 3 and 4 for all three Scenarios due to the momentum of inflow into Reactor 2 heading directly across the top of Reactors 2, 3 and 4 towards the output.

In the case of Scenario H the results were much better compared with the previous similar Scenarios F and G when all the mixers were at rest. The mathematical model picked out **n** = 0.99, 2.05, 3.01 and 4.24 for Reactors 1,2,3 and 4 respectively indicating that the benefits of this configuration as indicated by the model. In particular, Reactor 4 gave a reasonable results (considering the direction of flow across the reactor) because the installed box worked to reduce the localised outlet velocity of the flow, thus reducing any short-circuiting.

7.6 Results Summary

The comparison between the results tabulated in Table 7.2 (two tanks in-series), Table 7.4 (three tanks in-series), Table 7.6 (four tanks in-series) and Table 7.8 (input and output variation) is shown in Tables 7.9, 7.10 and 7.11. All experiments were made under the same conditions of fixed flow rate (3 l/min) and mixer speeds (0 rpm and 200 rpm) and provided very similar results, supporting the assumption made in the analysis that when the

system is perfectly mixed (all mixers are working at 200 rpm) the differences between the number of CSTRs for any reactor and its following reactor is equal to 1 (indicating the reactor is working efficiently) and constant from one reactor to another in the network.

Scenario No.	Mixer speed Reactor 1	Mixer speed Reactor 2	Reactor 1 No. Of CSTR	Difference between Reactors 1 and 2	Reactor 2 No. Of CSTR
	(rpm)	(rpm)	(n)	(n)	(n)
A	200	200	0.99	1.00	1.99
B	0	0	2.62	2.85	5.47
C	0	200	2.53	1.01	3.54
D	200	0	0.99	2.85	3.84

Table 7. 9 Difference between Reactor 1 and 2 for Trial 1

Scenario No.	Reactor 1 No. Of CSTR	Difference between Reactors 1 and 2	Reactor 2 No. Of CSTR	Difference between Reactors 2 and 3	Reactor 3 No. Of CSTR
	(n)	(n)	(n)	(n)	(n)
A	0.96	1.03	1.99	1.00	2.99
B	1.69	1.79	3.48	1.80	5.28
C	1.73	1.02	2.75	1.07	3.82
D	0.96	2.02	2.98	1.00	3.98
E	0.96	1.00	1.96	1.78	3.74

Table 7. 10 Differences between Reactor 1 & 2 and Reactor 2 & 3 for Trial 2

Categories	Scenario No.	Reactor 1 No. Of CSTR	Difference between Reactors 1 and 2	Reactor 2 No. Of CSTR	Difference between Reactors 2 and 3	Reactor 3 No. Of CSTR	Difference between Reactors 3 and 4	Reactor 4 No. Of CSTR
		(n)	(n)	(n)	(n)	(n)	(n)	(n)
Ove-baffle flow direction	A	0.96	1.00	1.96	1.00	2.96	2.03	4.99
	B	2.69	1.96	4.65	2.07	6.72	2.24	8.96
	C	2.03	0.99	3.02	1.00	4.02	1.03	5.05
	D	0.96	2.01	2.97	0.99	3.96	0.99	4.95
	E	0.97	1.02	1.99	2.08	4.07	1.00	5.07
	F	0.96	0.97	1.93	1.05	2.98	2.22	5.20
Horizontal flow direction	A	0.99	1.00	1.99	1.00	2.99	1.01	4.00
	B	1.64	1.37	3.01	1.73	4.74	1.92	6.66
	C	2.1	1.05	3.15	1.05	4.2	1.00	5.20
	D	0.99	2.33	3.32	1.00	4.32	1.00	5.32
	E	0.99	1.00	1.99	2.03	4.02	1.09	5.11
	F	0.99	1.00	1.99	1.00	2.99	2.21	5.20
Vertical flow direction	A	0.99	1.00	1.99	1.00	2.99	1.01	4.00
	B	2.59	1.06	3.65	1.08	4.73	2.79	7.52
	C	2.31	1.05	3.36	1.09	4.45	1.02	5.47
	D	0.97	2.52	3.49	1.01	4.50	1.01	5.51
	E	0.99	0.98	1.97	2.23	4.20	1.00	5.20
	F	0.99	1.00	1.99	1.00	2.99	2.53	5.52

Table 7. 11 Differences between Reactor 1 & 2, Reactor 2 & 3 and Reactor 3 & 4 for Trial 3

Table 7.9 shows that when the system was working at its optimum level (all mixers at 200 rpm, **n** = 0.99 for Reactor 1 and the difference between Reactors 1 and 2 is exactly 1, which indicating that the system was performing as two CSTRs. In the case where the mixers were at rest, as in Scenario B, the mathematical model picked out **n** = 1.69 and the differences between Reactors 1 and 2, equal to 1.68 (i.e. not equal to 1) indicating that neither Reactor 1 nor Reactor 2 were performing efficiently which obviously was the case because the mixers were at rest (see Figure 7.8). In the case where one reactor in the system was at rest, for example Scenario C, the mathematical model picked out **n** = 2.53 for

Reactor 1 with the difference between Reactor 1 and 2 equal to 1.01. This correctly indicates that Reactor 1 was not performing efficiently whilst Reactor 2 was performing efficiently. Conversely, in Scenario D the mathematical model picked out **n** = 0.99 for Reactor 1 with the difference between Reactor 1 and 2 equal to 2.85. This again correctly indicates that Reactor 1 was performing efficiently whilst Reactor 2 was not performing efficiently. The same pattern in the results are encountered for all the other different configurations used in Trial 2 and Trial 3 as shown in Tables 7.10 and 7.11 indicating that it is possible to use the mathematical model in order to pick out a hydraulic irregularity from a specific reactor in a network of reactors. Thus the model is suitable for use as a diagnostic tool on operational full-scale systems. The model has also shown that it is possible to distinguish between the mixing efficiencies due to the design of reactor systems with regards to baffle configuration and inlet and outlet position and structure. This can be used to design (or retrofit) the most energy efficient reactor system which uses the momentum of the incoming flow to maximum advantage.

Chapter 8

Full-Scale Implementation

Chapter 8

Full-Scale Implementation

8.1 Introduction

A number of experiments were studied in the laboratory in order to prove the mathematical model as discussed in previous chapters. The results obtained were promising, indicating that it would be worth examining the ability of this model in full-scale processes under normal operating conditions. The laboratory trials took place under controlled conditions; fixed flow rate and reactor volumes, known reactor geometries and also using clean water without any sediments in the incoming flow which could interfere with the tracer measurement. In reality most processes do not use clean water and the flow rate is often variable and in some plants (particularly wastewater treatment) is very hard to predict. Hence, the volume of the reactors can change slightly with flow rates and also the system geometry may be affected by sediment deposition for example, where these materials cannot be maintained in suspension and start to settle in the dead-zones of the reactors. Hence, the technique was trialled in three different full-scale processes in order to examine the validity and robustness of the model under real implementation conditions.

8.2 Greystones Wastewater Treatment Plant, Wicklow

8.2.1 Background

The Greystones Wastewater Treatment Works (WwTW) located in County Wicklow Ireland, is a secondary treatment plant constructed in 1993 to treat wastewater from a population equivalent of 40,000. The secondary treatment is an activated sludge process using a three tank in-series mixed aerated reactor with diffused aeration followed by a clarifier used to separate the active biomass and return the sludge to the aeration tank, as shown in Figure 8.1. The aeration tank consists of three large tanks in-series; each 11.75 m in length, 5.10 m in height and 5.37 m in width, fitted with an inlet feed at the top of the first reactor on the northern side as shown in Figure 8.2(a). An outlet pipe is located at the top of the third reactor again on the northern side (see Figure 8.2(b)); which leads to a flow splitter chamber to feed the clarifier tanks as shown in

Figure 8.3. It should be noted that over the last few years the aeration tanks have experienced continuous foaming problems whereby approximately 1 m depth of brown, viscous foam has sat on top of the three aeration tanks (see Figure 8.2 (c and d)).

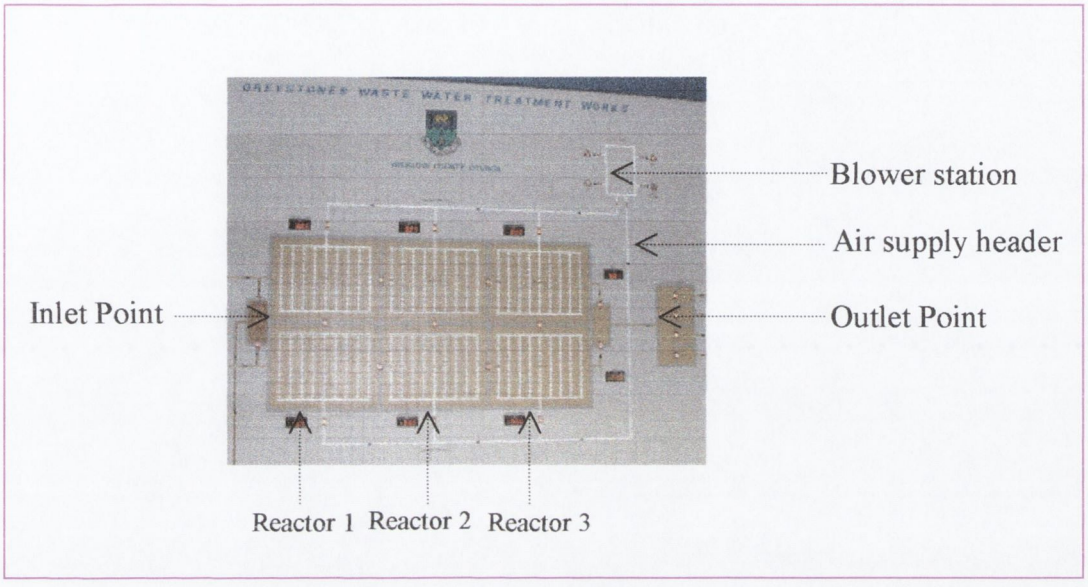

Figure 8. 1 Photograph showing the schematic process flow diagram of aeration tanks for Greystones WwTW

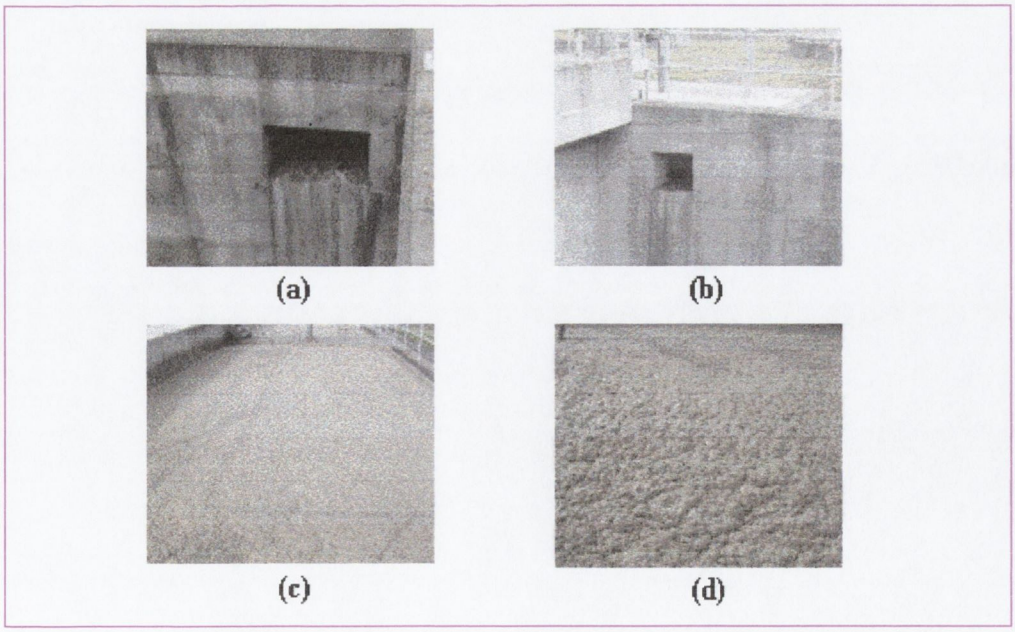

Figure 8. 2 Photographs showing (a) inlet, (b) outlet, (c) and (d) brown, viscous foaming on the aeration tanks

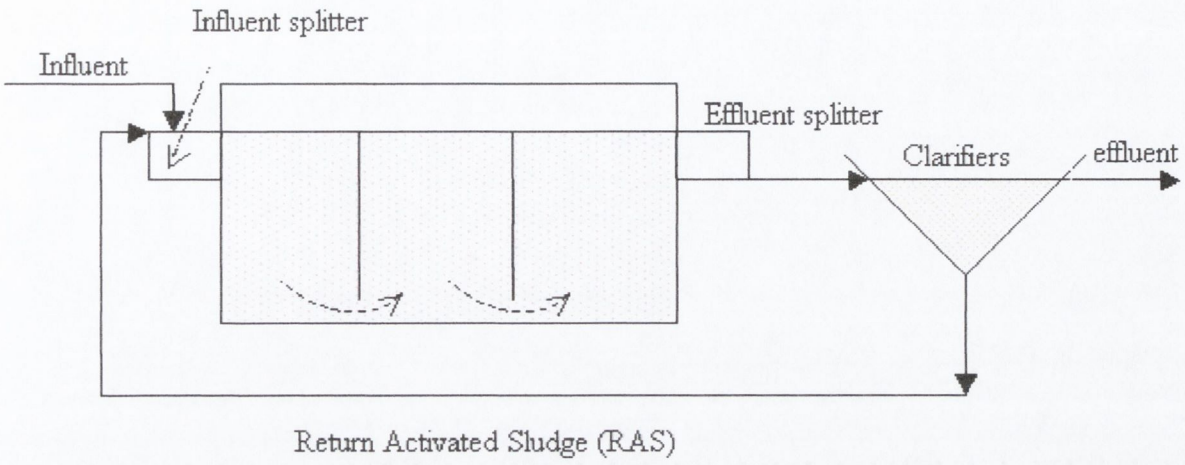

Figure 8. 3 Schematic diagram showing the Activated Sludge process

The return activated sludge (RAS) is pumped from the base of the clarifiers back to the inlet chamber in front of the first reactor where it mixes with the influent flow as shown in Figure 8.3. Two small gaps, 1m by 1m, are located in the baffles between the reactors as shown in Figure 8.4. The first gap is located in the baffle between the first and second reactor at the base, the second gap is located between the second and third reactor again at the base. In case a problem is encountered in any reactor, a valve can be used to control the penstocks to isolate the particular reactor for maintenance.

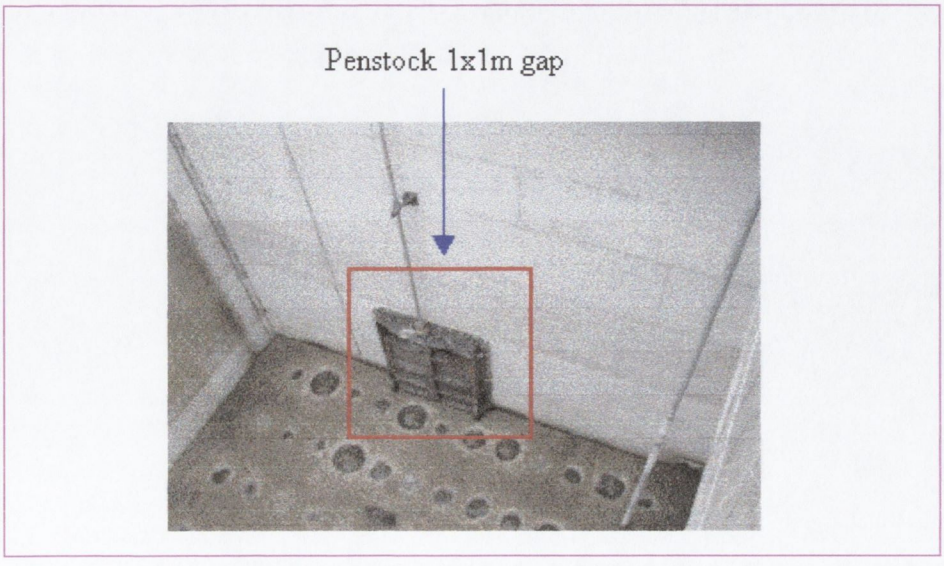

Figure 8. 4 Photograph showing the gap in the baffle between the reactors

The aeration system consists of a network of diffused aerators in the base of each reactor as shown in Figure 8.5 (a and b). The aeration system in each tank consists of 240 diffusers spaced in a 0.27m x 0.57m lattice. A common air supply header supplies a fixed airflow rate of 1240 m^3/h, which is distributed between the three tanks according to their inlet valve settings. The 90 mm diameter (HKLE 5375-12) diffusers provide both the necessary process air for the microorganisms (maintaining dissolved oxygen concentrations above 0.5 (mg/l) and have also been designed to keep the microbial flocs in a continuous state of agitated suspension in the wastewater. Hence, in principle, each pocket should behave as a Continuously Stirred Tank Reactor (CSTR) for optimal process efficiency. The aerators are connected to a blower station via an air supply header as shown in Figure 8.5 and located in a separate building.

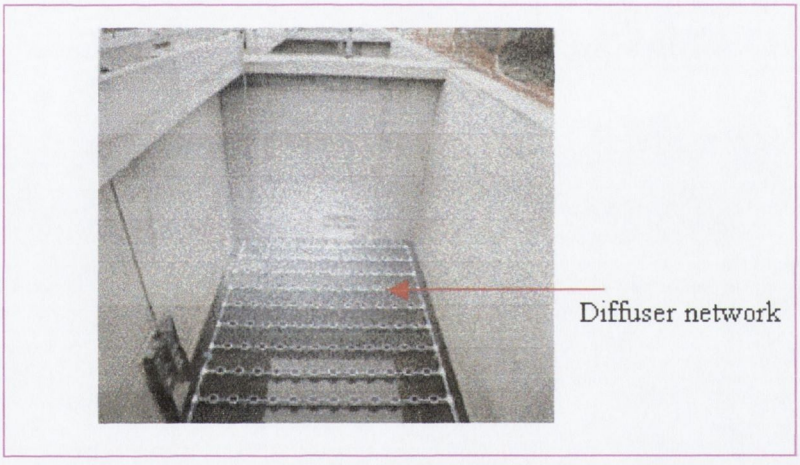

(a)

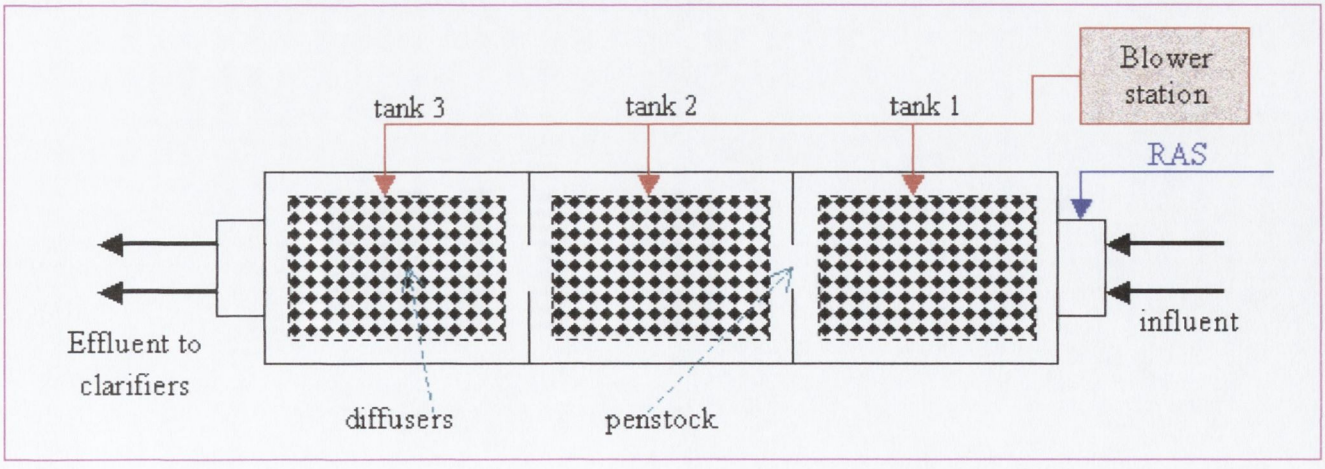

(b)

Figure 8. 5 The aeration network inside each tank (a) Photograph and (b) Schematic diagram

8.2.2 RTD Trials

Two tracer studies were carried out on the aeration reactor network; one on 3rd July 2003 and one on 12th July 2003. The water depth was measured at 5.1m, giving a corresponding volume for each aerated reactor of 322.1 m^3 and total system volume of 966.3 m^3. Therefore, a quantity of 966.3 ml of 0.2g/ml of Rhodamine WT tracer was prepared relating to the volume of the aerated reactors (see Appendix A). The SCUFA was calibrated with Rhodamine WT solution (see Appendix A), and then an initial experiment was performed to assess the SCUFA's ability to measure the tracer concentration accurately in the wastewater by using a sample of 2 litres of mixed liquor from the system. 2 ml of 0.2g/ml (200,000 mg/l) Rhodamine WT was added to the wastewater sample and well mixed and the SCUFA was then inserted into the sample. However, it was soon realised that such a method of on-line measurement of the aeration chamber effluent could not be used due to the density of flocs in the wastewater affecting the optical transmission of the instrument. The SCUFA only measured a value of 2.35 μg/l when the concentration of tracer should have been 200 μg/l. Hence, a second technique was tried whereby a sufficient amount of time was given for the bacteria to settle down to the bottom of the flask (10 minutes) as shown in Figure 8.6 and then the clear supernatant was taken to another jar and the SCUFA was inserted (with open optics pointed downwards - Figure 8.7) to take the tracer measurement. Using this method the SCUFA more successfully measured a concentration of 170 μg/l, compared to the calculated value of 200 μg/l.

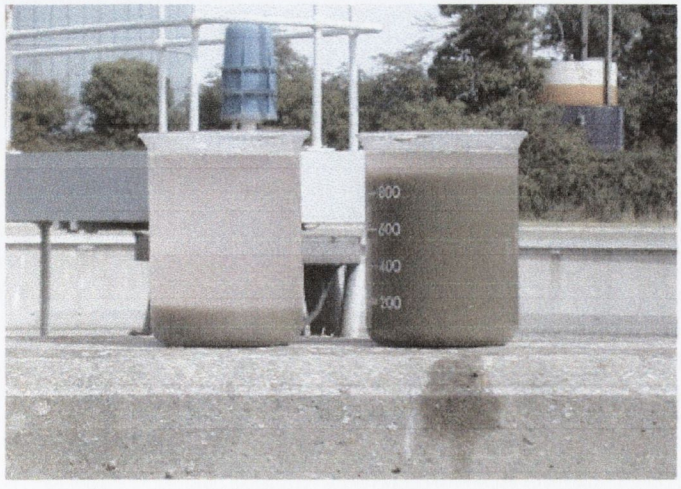

Figure 8. 6 Photograph showing the settlement of the bacteria flocs to reveal the clear supernatant

Figure 8. 7 Photograph showing the use of the SCUFA to indicate the tracer concentration

Consequently, this technique was developed such that samples were taken every 10 minutes for both the outlet and the RAS. The SCUFA was connected to the computer to export the data onto an Excel© spreadsheet as shown in Figure 8.7. The flow rate into the plant (and hence the reactors) continuously varied and was recorded on the control SCADA system that was located in a separate control room building. Equally, the RAS varied slightly throughout each trial, which was again recorded using the same SCADA system.

8.2.2.1 Trial 1

In the first trial the constant airflow from the blower station to each reactor was split evenly between the three reactors since all the controlling valves were set to 50%, as shown in Figure 8.8. Hence, the airflow rate to each reactor was 413.3 m^3/h during the trial.

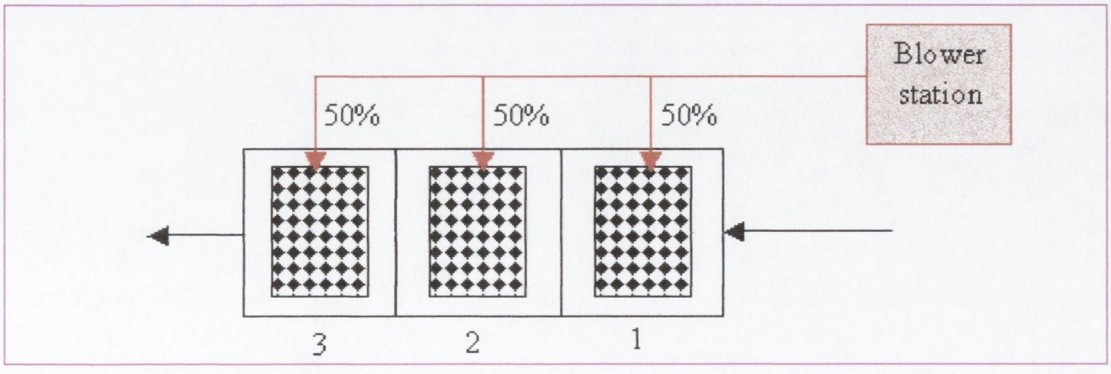

Figure 8. 8 Schematic representation showing the airflow valve settings for Trial 1

The Rhodamine WT was injected into the aerated networked reactors as a pulse input into the influent pipe, as shown in Figure 8.9 at time, t=0.

Figure 8. 9 Photograph showing the injection of the tracer into the system

A sample of effluent from Reactor 3 was taken every 10 minutes as shown in Figure 8.10 and the tracer concentration was measured with the SCUFA using the technique discussed previously. The inlet flow rate during the trial was measured by the SCADA every 10 minutes and had an average of 150.7 m^3/h with an average RAS flow rate 143.3 m^3/h. The water temperature was also measured inside the reactor and was 17°C in the incoming flow and 25°C in the aeration tank effluent throughout the trial.

Figure 8. 10 Photograph showing the sampling of the effluent

The effluent tracer concentrations as a function of time were exported into the Excel© spreadsheet for analysis. For these trials the mathematical model was adjusted to deal with varying conditions at each individual sample point incorporating the inlet and RAS flow rates, and the volume of the aerated network reactors as shown in Figure 8.11. The RAS flow rate is represented by **column B**, the flow rate through to the works represented by **column A**, the cumulative flow rate through the system represented by **column C**, the aerated networked reactors volume represented by **column D**, the theoretical retention time at each sample point represented by **column E**, the time at which each sample was taken represented by **column F**, the RAS concentration represented by **column G** and the differences between the RAS and the background concentration represented by **column H**. It should be noted that all effluent concentrations had the original background concentration (as measured by SCUFA) subtracted to give the true concentration increase as a result of the tracer addition to the system.

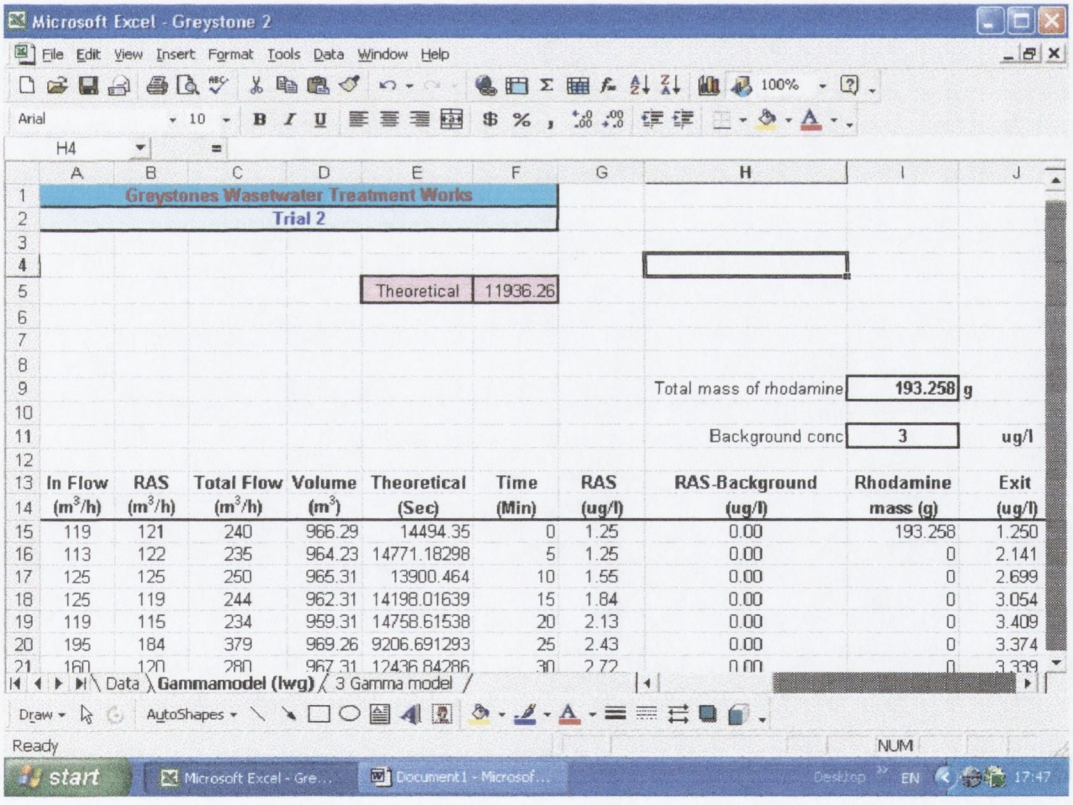

Figure 8. 11 The structure of the model laid out on an Excel© spreadsheet

The system configurations during the trials are shown in Table 8.1 and the results obtained for this trial are shown in Table 8.2. In addition, the corresponding graph for

this trial is shown in Figure 8.13 and the effluent concentration curves from each reactor generated by the model are shown in Figure 8.14.

8.2.2.2 Trial 2

A second trial was carried out on the system following identical procedures as the first trial. The only change was that a different airflow was introduced to each reactor by changing the controlling valves as shown in Figure 8.12.

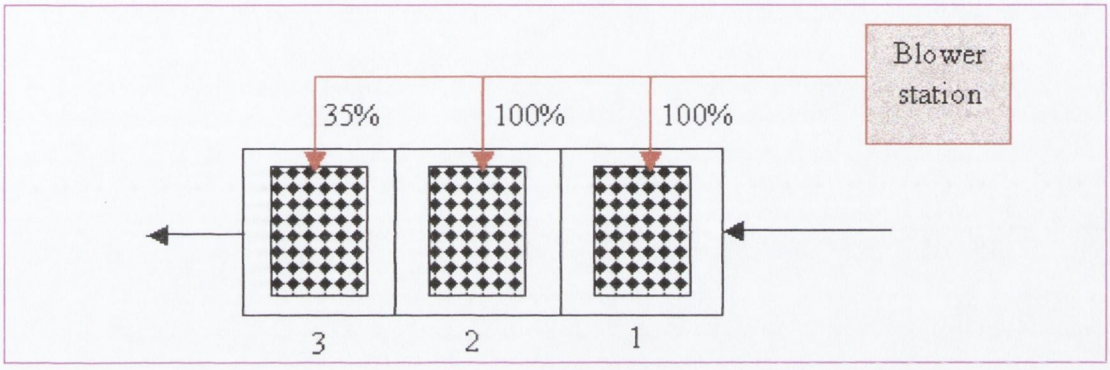

Figure 8. 12 Schematic representation of the airflow valve settings for Trial 2

Again the water temperature measured throughout the trials was 17°C in the incoming flow and 25°C in the effluent. The system configurations are shown in Table 8.1 and the results obtained for this trial are shown in Table 8.2. In addition, the corresponding graphs of effluent concentration and model curves are shown in Figures 8.13 and 8.14.

Trial No.	Reactor Volume	Average Inlet Flow Rate	Average RAS Flow Rate	Average Total Flow Rate	Aeration Supply (m^3/h)			Rhodamine Mass
	(m^3)	(m^3/h)	(m^3/h)	(m^3/h)	1	2	3	(g)
1	966.3	150.7	143.3	301.3	413	413	413	193.3
2	966.3	152.2	136.5	303.1	528	528	185	193.3

Table 8. 1 Full-scale implementation (Greystones WwTW) - trials configurations

Trial No.	Modelled retention time	Reactor [1]		Reactor [2]		Reactor [3]		Overall System Performance		
		Theoretical retention time at the end of Reactor 1	No. Of CSTR	Theoretical retention time at the end of Reactor 2	No. Of CSTR	Theoretical retention time at the end of Reactor 3	No. Of CSTR	P%	D%	S%
		(S)	(n)	(S)	(n)	(S)	(n)	(%)	(%)	(%)
1	12085.3	3979.3	1.7	7958.8	19.8	11938.2	22.1	55.7	1.5	42.8
2	12189.7	3990.1	1.5	79801.3	15.6	11970.5	19.0	61.5	2.3	36.3

Table 8. 2 Full-scale implementation (Greystones WwTW) - model results

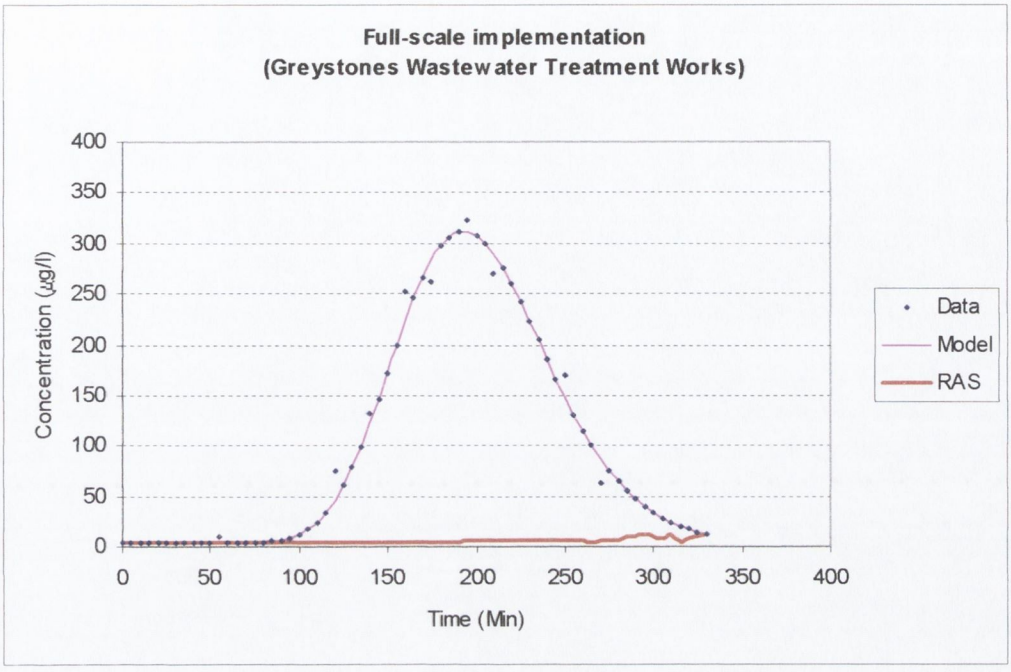

Trial 1

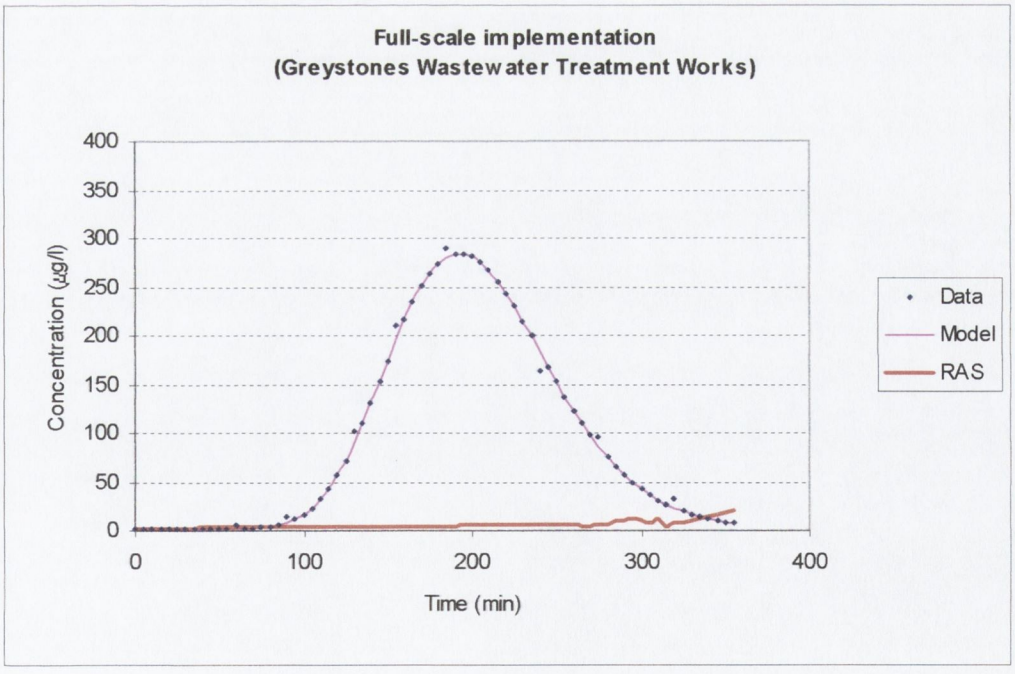

Trial 2

Figure 8. 13 The effluent concentration curve for each Trial for full-scale implementation (Greystones WwTW)

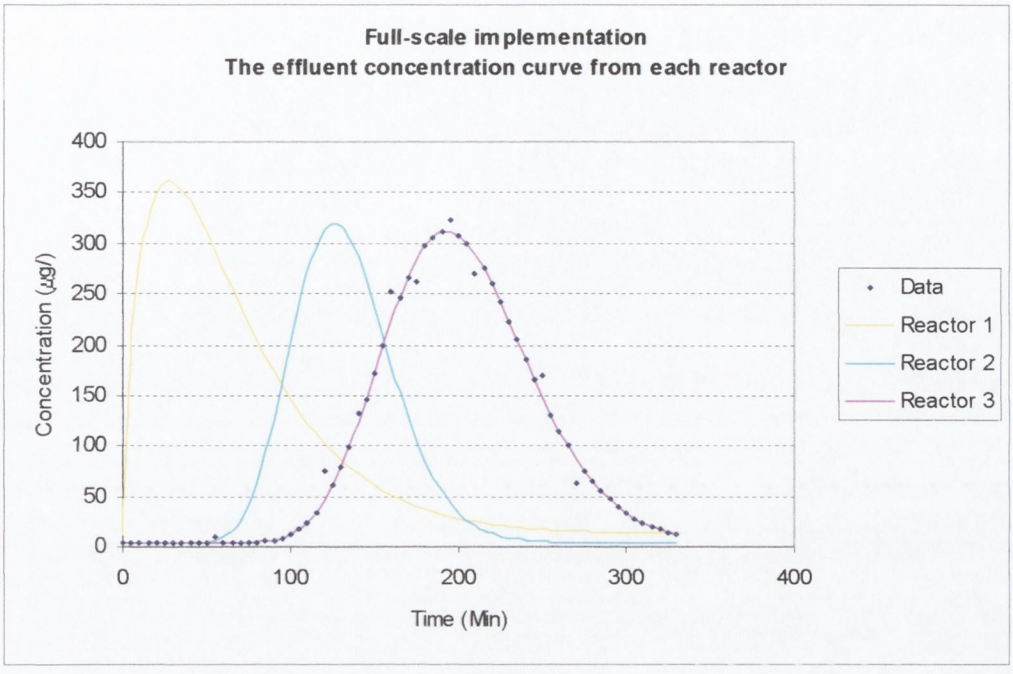

Trial 1

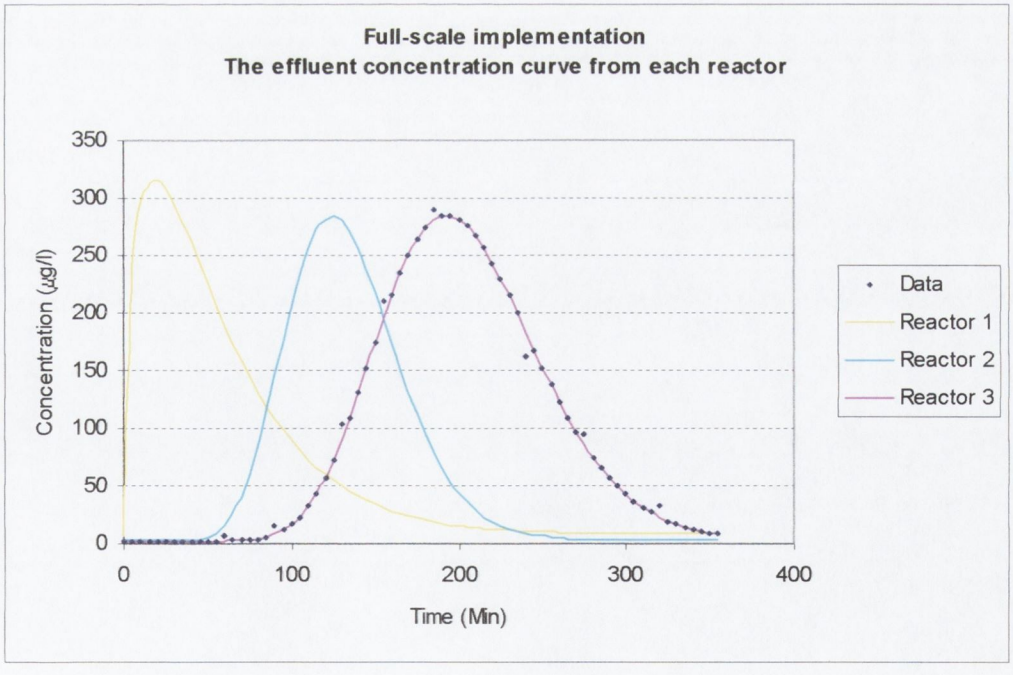

Trial 2

Figure 8. 14 The effluent concentration curve from each reactor for Trial 1 and 2 for full-scale implementation (Greystones WwTW)

8.2.3 Results Analysis

The result from the trials indicate that there is severe short-circuiting from Reactor 1 to Reactor 3 which can be seen both numerically in Table 8.2 and graphically in Figure 8.14. In Trial 1 the model gives 19.8 reactors in-series for the effluent RTD curve from Reactor 2, while in Trial 2 the corresponding number is 15.6 reactor in-series. This indicates that the flow is short-circuiting directly from Reactor 1 to Reactor 3 without mixing properly in the volume of Reactor 2. In addition, as shown in Table 8.3 the mathematical model picked out **n** = 1.7 and 22.1 for the effluent RTD curve from Reactors 1 and 3 in Trial 1. The differences between Reactors 1 and 2 is 18.05 reactors in-series and the differences between Reactors 2 and 3 is 2.33 reactors in-series which also indicates that all Reactors 1 and 3 are short-circuiting but too much lesser extent. This same pattern is also repeated in Trial 2.

Trial No.	Reactor 1 No. Of CSTR	Difference between Reactor 1 and 2	Reactor 2 No. Of CSTR	Difference between Reactor 2 and 3	Reactor 3 No. Of CSTR
	(n)	(n)	(n)	(n)	(n)
1	1.7	18.05	19.8	2.33	22.1
2	1.5	14.08	15.6	3.42	19.0

Table 8. 3 Differences between Reactor 1 & 2 and Reactor 2 & 3 for the Greystones system

This plug flow is probably due to an inadequate design of the inlet and outlet ports of Reactor 2 which are directly opposite each other (see Figure 8.3) but may also be enhanced due to the differences in incoming flow temperature compared to the water temperature in the reactors. The temperature of mixed liquor in the tanks is commonly higher than that of the incoming wastewater because of the airflow through the diffusers generating heat due to friction which warms the wastewater. Hence, this temperature difference has the potential for the formation of density currents in the aeration tanks. The density of water decreases as the temperature increases (see Appendix H) whereby the warmer water in Reactor 2 may float on top of the colder water entering at the base that will then head towards the effluent port on the base on the opposite side. Hence, both these aspects of the design would appear to encourage the short-circuiting through Reactor 2, which has been picked up by the model.

The velocity gradient, G produced by the aeration in each reactor is shown in Table 8.4.

Trial No.	Tank No.	V (m^3)	V_{tank} (m^3)	Valve open %	Fraction Per tank	Q (m^3/h)	Q_{tank} (m^3/h)	W (kg/s)	R J(mol k)$^{-1}$	T_1 (k)	P_1 (atm)	P_2 (atm)	μ (kg/m.s)	P_{tank} (W)	G_{tank} (s^{-1})	G_{tank} (s^{-1})
1	1	966.3	322.1	50	0.33	1240	413.33	0.18	8.31	305.27	1.00	1.49	0.001	9264.10	169.42	**169.42**
	2		322.1	50	0.33		413.33	0.18						9264.10	169.42	
	3		322.1	50	0.33		413.33	0.18						9264.10	169.42	
2	1	966.3	322.1	100	0.43	1240	527.66	0.23	8.31	305.27	1.00	1.59	0.001	13862.46	207.25	**179.04**
	2		322.1	100	0.43		527.66	0.23						13862.46	207.25	
	3		322.1	35	0.15		184.68	0.08						4851.86	122.61	

Table 8. 4 Velocity gradient (G) for Greystones system

The mixing energy produced by the aeration is obviously not strong enough to prevent the short-circuit through Reactor 2. The short-circuit is maybe due to the momentum associated with the incoming flow to Reactor 2 (0.02 Kg.m/s) which is obviously higher than the momentum associated with the influent into Reactor 1 (0.01 Kg.m/s). This can be compared with the results in Section 6.4.2.1 where the short-circuiting was reduced due to the momentum associated with the incoming flow being higher than the momentum of the flow over / below the central baffles.

However, the short-circuiting could also be due to the differences in temperature between influent and effluent flow. As shown previously there is a maximum 8°C difference between influent and effluent water temperature in the reactors. However, the influent flow will be heated slightly in Reactor 1 and therefore, the influent flow into Reactor 2 has been assumed to have been increased in temperature by 2°C, to 19°C. As a result a maximum temperature difference of 6°C between the flow passing through Reactor 2 and warmer fluid in the top has been used in the following calculation which shows the potential strength of stratification due to the difference in density between the cold water on the base and wormer water in the top of the reactor. The Richardson number, which describes the balance between stable density stratification and the existing shear rate to create a perfect mixed flow has been calculated using the following formula (Cengel, 2003) as shown in Table 8.5 and gives a value of 3.30. The Richardson number is used to determine whether a water body will remain stratified (if $R_i > 1$) which means that the energy input into the system transmitted into shear is smaller than the strength of stratification or whether there is enough shear applied to the

volume to break through the stratification and promote a fully mixed, turbulent system (R_i <1) (van Haren and Howarth, 2004).

$$R_i = \frac{[N]^2}{[S]^2} \qquad \text{----------(8.1)}$$

where;

R_i = Richardson number
S = existing shear rate
N = the ratio of the buoyancy frequency, in which has been calculated as,

$$N = \frac{g}{\Delta T_v} \times \frac{\delta \theta_v}{\delta Z} \qquad \text{----------(8.2)}$$

where;

g = gravitational acceleration
Z = height
θ_v = virtual potential temperature, in which has been calculated as

$$\theta_v = \theta(1 + 0.6r_l - r) \qquad \text{----------(8.3)}$$

θ = the actual potential temperature
r = mixing ratio
r_l = mixing ratio of liquid water in air
T_v = virtual absolute temperature in which has been calculated as

$$T_v = T\left(1 + r_l / \varepsilon\right) / (1 + r_l) \qquad \text{----------(8.4)}$$

ε = the ratio of the gas constants of air and water vapour 0.622

$\Delta\theta_V$	ΔT_V	Q	G	R_i
°C	°C	(m^3/h)	(s^{-1})	
1613.83	6.79	1240	169.42	**3.30**
1714.68	12.45	3500	493.01	**0.99**

Table 8. 5 Richardson number (R_i) for Greystones system

Hence, with Ri = 3.30 the existing shear rate introduced by the air is obviously not enough to break through the density current. The extra amount of shear that would need to be applied to reduce the Richardson number to 0.99 and promote a fully mixed

system and prevent the short-circuiting has been calculated as shown in Table 8.5. Therefore, the airflow rate would have to be increased to provide enough shear in the reactor whereby G = 493.01 s^{-1}. It showed be acknowledged that by increasing the airflow rate this will also increase the potential level of stratification since it is the air that is also heating the water. This has been taken into account by assuming the worst scenario whereby the temperature of the water in the top of Reactor 2 can only reach a maximum temperature of 32.12 °C (the temperature of the air coming out of the diffuser). This level of shear required (G = 493.01 s^{-1}) is more in line with the shear required for the other fully mixed systems at both in the laboratory experiments and the on-site trials in Libya.

8.2.3.1 Tracer Recovery

The principle behind these tracer studies is based on a mass balance of the tracer. Hence, one of the most important factors to look at is the recovery of the mass injected at the beginning to ensure that it has all been picked up eventually in the effluent and not been absorbed onto the equipment or organic / inorganic materials. A computer programme in Basic language attached to Excel© spreadsheet (see Appendix F) has been employed to evaluate the tracer recovery at any time during the experiment's run. The formulae that have been used are as follows,

$$g(t_i) = [t_i - t_{i-1}] \times Q \times C(t_i) \quad \text{----------(8.4)}$$

$$g_{cum} = g(t_1) + g(t_2) + \ldots\ldots\ldots\ldots + g(t_n) \quad \text{----------(8.5)}$$

$$f(t_i)\% = \frac{g_{cum}(t_i)}{M_{in}} \times 100 \quad \text{----------(8.6)}$$

$$f_{total}(t_n)\% = \frac{g_{cum}(t_n)}{M_{in}} \times 100 \quad \text{----------(8.7)}$$

where;

$g(t_i)$ = mass at any given time

t_{i+1}, t_{i-1} = time at which sample was taken

g_{cum} = cumulative mass at any given time

$f(t_i)\%$ = the percentage of the tracer recovery at any given time t_i

$f_{cum}(t_i)\%$ = the cumulative percentage of the tracer recovery at the end t_n

The tracer recovery for the all laboratory experiments was shown to be 100% indicating that there was no absorption loss onto equipment (see Figure 8.15(b)), which concurs with the research carried out by Yotsukura *et al* (1970). When the tracer was injected into Greystones WwTW it showed an average recovery of only 51.5 % as shown in Table 8.6 and graphically as in Figure 8.15(a).

However, the figures also have to be adjusted for the errors in the SCUFA measurement methodology of the effluent due to the turbidity of the supernatant. In Section 8.2.2 it was shown that the SCUFA measured 170 µg/l compared to the actual value of 200 µg/l. Therefore this gives only 85% of the true value indicating a15% under representation can be attributed to this method. Hence, the original experimental values were multiplied by (1/0.85) in order to adjust for this error and get more realistic values for the mass balance. When this measuring accuracy was taken into account it should an average recovery of 65.7% as shown in Table 8.6 and graphically as shown in Figure 8.15(a).

Location	Tracer recovery
Laboratory Trials	100%
Greystones WwTW Trial 1	50.2%
Greystones WwTW Trial 2	52.8%
Greystones WwTW Adjusted recovery Trial 1	65.1%
Greystones WwTW Adjusted recovery Trial 2	66.3%

Table 8. 6 The percentage of Tracer recovery at Greystones WwTW

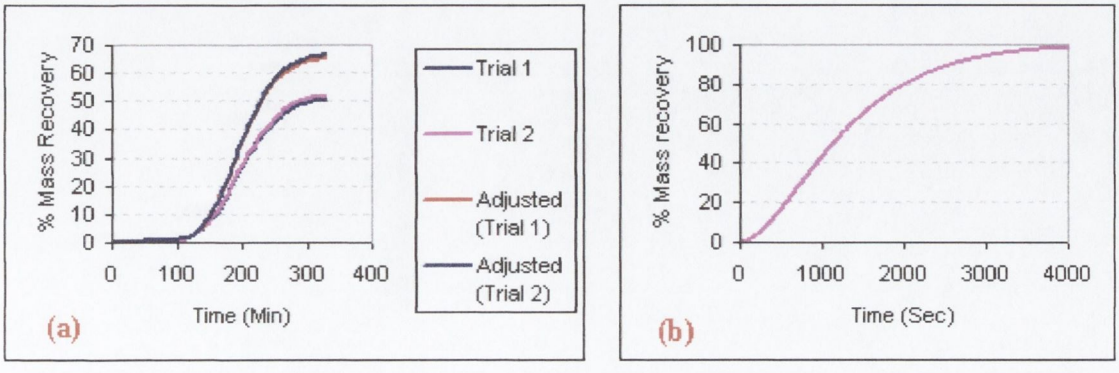

Figure 8. 15 Tracer mass recovery curves for (a) Greystones WwTW trials (in mixed liquor) and (b) laboratory trials (in clean water)

The average tracer recovery of only 65.7% indicates the extent of absorption and up take by the biomass. It was decided to scale up the RTD curve retrospectively on the assumption that the removal of Rhodamine from the solution would have been proportional to time spent in the tank but declining at an exponential rate. This decay kinetic was confirmed by the controlled batch experiment on 20 litres of MLSS whose concentration was monitored with respect to time. Hence, an exponential curve was fitted to the trial data to recreate the exact amount of Rhodamine mass recovered by the end of the trial. Each original effluent concentration data point was then scaled appropriately to obtain a readjusted data set that showed a mass recovery of 100% as shown in Table 8.8. The adjusted data was then entered into the spreadsheet and the model was run to obtain a best fit with the experimental RTD curve from each trial by adjustment of the model parameters (as discussed previously in Chapter 7). This technique enables tracer studies to be carried out on such systems as long as all inputs and outputs of tracer mass during the trial period are rigorously accounted for. When this technique was applied to the original data, the size of adjusted RTD curves increase such that the area under the RTD curve is equal to the mass injected at the beginning of each trial. The results were used to calculate the affect of the absorption of the tracer into the bacteria and also to assess the suitability of Rhodamine WT for use in such an environment, where high concentrations of organic material and biomass exist. The results obtained for these adjusted RTD curves are shown in Table 8.7. In addition, the corresponding graphs of effluent concentration and model curves are shown in Figures 8.16 (a) and (b).

Trial No.	Modelled retention time	Reactor [1]		Reactor [2]		Reactor [3]		Overall System Performance		
		Theoretical retention time at the end of Reactor 1	No. Of CSTR	Theoretical retention time at the end of Reactor 2	No. Of CSTR	Theoretical retention time at the end of Reactor 3	No. Of CSTR	P%	D%	S%
		(S)	(n)	(S)	(n)	(S)	(n)	(%)	(%)	(%)
1	12085.3	3979.3	1.5	7958.8	16.5	11938.2	21.0	58.1	2.5	39.5
2	12189.7	3990.1	1.3	79801.3	14.3	11970.5	17.6	64.7	3.2	32.0

Table 8. 7 Full-scale implementation (Greystones WwTW) – adjusted model curve results

The results showed a very similar pattern to the results obtained using the original curves. The mathematical model picked out **n** = 16.5 and 14.3 for the effluent concentration RTD curves for Reactor 2 which still indicated that the short-circuiting problem exists in the system. In addition, the tracer recovery using the adjusted data is

shown in Table 8.8, which gives value close to 100% proving the robustness of the method.

Location	Tracer recovery
Greystones WwTW Trial 1	98.99%
Greystones WwTW Trial 2	99.56%

Table 8. 8 The percentage of Tracer recovery at Greystones WwTW (adsorption adjusted data set)

The similarity in the results using the original and adjusted data sets also indicates the suitability of using Rhodamine WT as a tracer in such studies using this modelling framework.

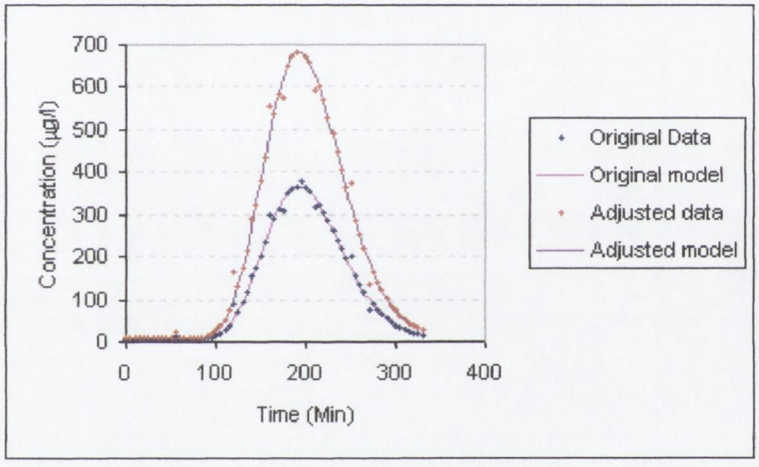

Trial 1

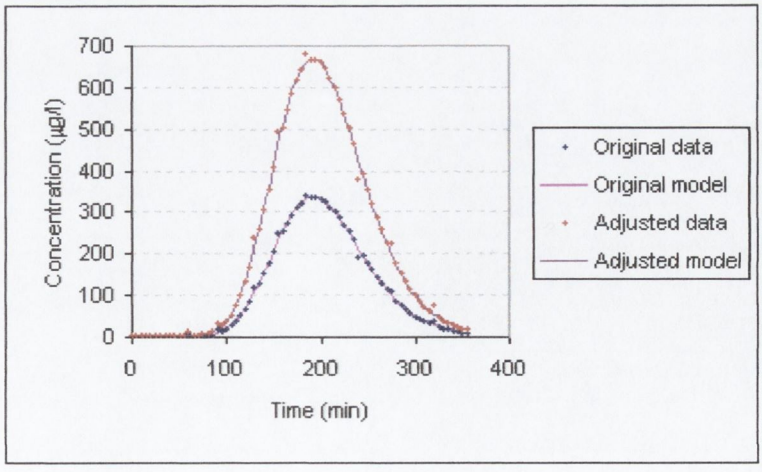

Trial 2

Figure 8. 16 The effluent concentration curve for each Trial for full-scale implementation at Greystones WwTW on original and adjusted data sets

The results from these RTD trials at Greystones WwTW maybe used to explain certain process problems that have been experienced with the activated sludge plant. The extent of foaming in the tanks has been a persistent phenomenon at the plant for several years that has always apparently defied explanation since the plant is operated at normal F: M ratios [food biomass ratio] varying from 0.35-0.4. One hypothesis, as a result of these trials, is that the extreme plug flow demonstrated in Reactor 2 means that the majority of the flow is obviously short-circuiting the tank and therefore creating stratification in the reactor forming an area of low substrate concentration in the top layers of the tank. This region would be an ideal area for the development of *Nocardia bacteria* (responsible for the brown, viscous foam) since they commonly favour environments with low F: M values and also high temperatures (Jenkins *et al.*, 2004). The heat transfer as a result of the diffused aeration in the tank would reinforce this potential, both in terms of temperature and also stratification.

8.3 Laboratory Model of Greystones WwTW

The results that were obtained from the Greystones WwTW are interesting since they indicate hydraulic problems in the middle aerated Reactor 2 and also show promise for the applicability of the model for use as a tool in real plants. An approximate scaled-down version of the Greystones system was constructed in the laboratory to see initially whether it is possibly to mimic the actual conditions in the Greystones reactors and then to study possible improvements that could be made to the system. In particular, the level of mixing in Reactor 2 was found to be a particular problem and was modelled in the laboratory using two different scenarios:

- Increasing the mixer speed in the middle reactor from 0rpm up to 200rpm while the other mixers in Reactors 1 and 3 were at the optimum level, 200rpm.
- Increasing the mixer speed in all reactors at the same mixer level.

The scaled-down version as shown in Figure 8.17 consisted of three small reactors in-series (each one 28.5 cm in length, 30 cm in width and 30 cm in height) fitted with an inlet pipe feed at the top of the first reactor and an outlet pipe located at the top of the third reactor as shown in Figure 8.17.

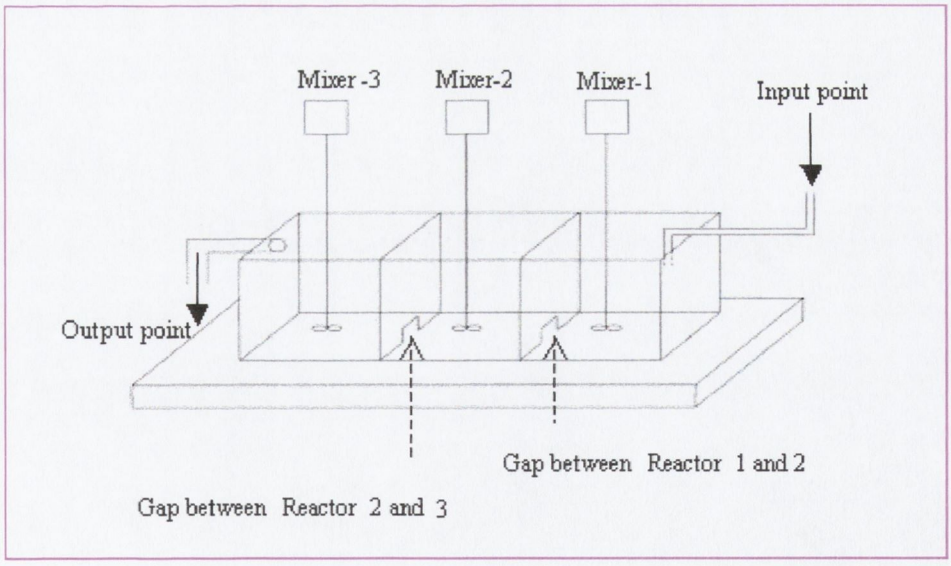

Figure 8. 17 Schematic representation of the laboratory model of Greystones WwTW

Two small gaps (5cm x 5cm) were located in the baffles between the reactors (as shown in Figure 8.18), one in the base between the first reactor and the second reactor and the

other also in the base between the second reactor and the third reactor. The two gaps were designed to be opposite each other as at Greystones WwTW.

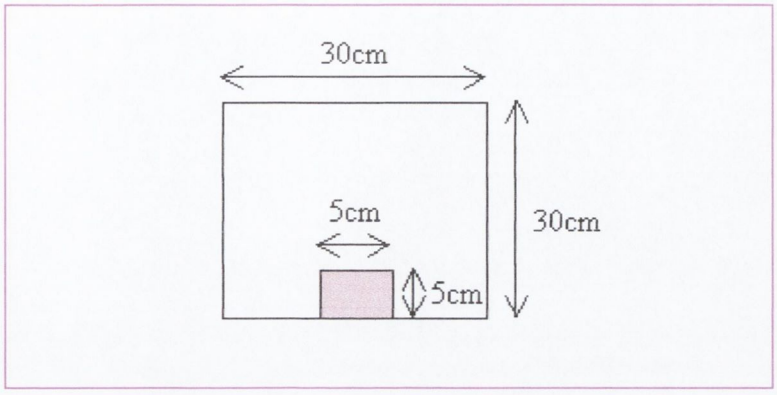

Figure 8. 18 The dimensions of the baffle and the gap between the reactors for the Greystones WwTW laboratory model

There were also three mixers, one in each reactor, to enable different degrees of mixing to be obtained using a variable speed reducer located at the top of each reactor. The blades of each mixer were square in shape (7cm x 7cm) with a slight "S" profile or curve on the blades. Three holes of 2 cm in diameter were cut out of each blade to allow the power input from each mixer to attain the full range of velocity gradients required for the experiments. The SCUFA was calibrated with Rhodamine WT solution (see Appendix A) and connected to the outlet pipe as before. The water depth was measured at 27 cm, giving a corresponding volume in each reactor of 23.08 L (and overall system volume of 69.26 L). The flow rate through the reactor was fixed at 2.4 L/min and the incoming water temperature was 15°C. 10 ml of Rhodamine WT was prepared and was introduced for each experiment into the system as a pulse input at the inlet point. The tracer concentration as a function of time was measured using the SCUFA device at the outlet point. Six experiments were undertaken for each different scenario in order to investigate and to interpret the cause of the huge plug flow found in Reactor 2 in the previous full-scale trials. All system parameters were the same for the different scenarios, the only difference between experiments being the mixer speeds as shown in Table 8.9 and Table 8.11. The results obtained from all experiments are shown in Table 8.10 (for the first scenario) and in Table 8.12 (for the second scenario) and an example of the RTD graphs and model curves for Experiment 6 of each scenario is shown in Figures 8.19 and 8.20 - the rest are presented in Appendix I.

Experiment No.	Reactor Volume	Flow Rate	Mixer Speed for Reactor 2	Mixer Speed for Reactors 1 and 3	Rhodamine Mass
	(L)	(l/min)	(rpm)	(rpm)	(g)
1	69.26	2.4	0	200	0.002
2	69.26	2.4	40	200	0.002
3	69.26	2.4	80	200	0.002
4	69.26	2.4	120	200	0.002
5	69.26	2.4	160	200	0.002
6	69.26	2.4	200	200	0.002

Table 8. 9 Laboratory model of Greystones WwTW [Scenario-1] – experimental configurations

Experiment No.	Reactor [1]		Reactor [2]		Reactor [3]	
	Theoretical retention time at the end of Reactor 1	No. Of CSTR	Theoretical retention time at the end of Reactor 2	No. Of CSTR	Theoretical retention time at the end of Reactor 3	No. Of CSTR
	(S)	(n)	(S)	(n)	(S)	(n)
1	577.1	1.06	1154.3	7.66	1731.4	8.62
2	577.1	0.97	1154.3	6.83	1731.4	7.79
3	577.1	0.98	1154.3	5.67	1731.4	6.69
4	577.1	0.99	1154.3	4.14	1731.4	5.21
5	577.1	0.99	1154.3	2.30	1731.4	3.32
6	577.1	0.99	1154.3	2.00	1731.4	2.99

Table 8. 10 Laboratory model of Greystones WwTW [Scenario-1] – results

Experiment No.	Reactor Volume	Flow Rate	Mixer Speed (all reactors)	Rhodamine Mass
	(L)	(l/min)	(rpm)	(g)
1	69.3	2.4	0	0.002
2	69.3	2.4	40	0.002
3	69.3	2.4	80	0.002
4	69.3	2.4	120	0.002
5	69.3	2.4	160	0.002
6	69.3	2.4	200	0.002

Table 8. 11 Laboratory model of Greystones WwTW [Scenario-2] – experimental configurations

Experiment No.	Reactor [1]		Reactor [2]		Reactor [3]	
	Theoretical retention time at the end of Reactor 1	No. Of CSTR	Theoretical retention time at the end of Reactor 2	No. Of CSTR	Theoretical retention time at the end of Reactor 3	No. Of CSTR
	(S)	(n)	(S)	(n)	(S)	(n)
1	577.1	4.67	1154.3	9.64	1731.4	11.70
2	577.1	3.80	1154.3	7.61	1731.4	9.32
3	577.1	3.32	1154.3	6.71	1731.4	7.65
4	577.1	2.39	1154.3	5.57	1731.4	6.59
5	577.1	0.99	1154.3	2.06	1731.4	3.05
6	577.1	0.99	1154.3	2.00	1731.4	2.99

Table 8. 12 Scaled-down model of Greystones WwTW [Scenario-2] – results

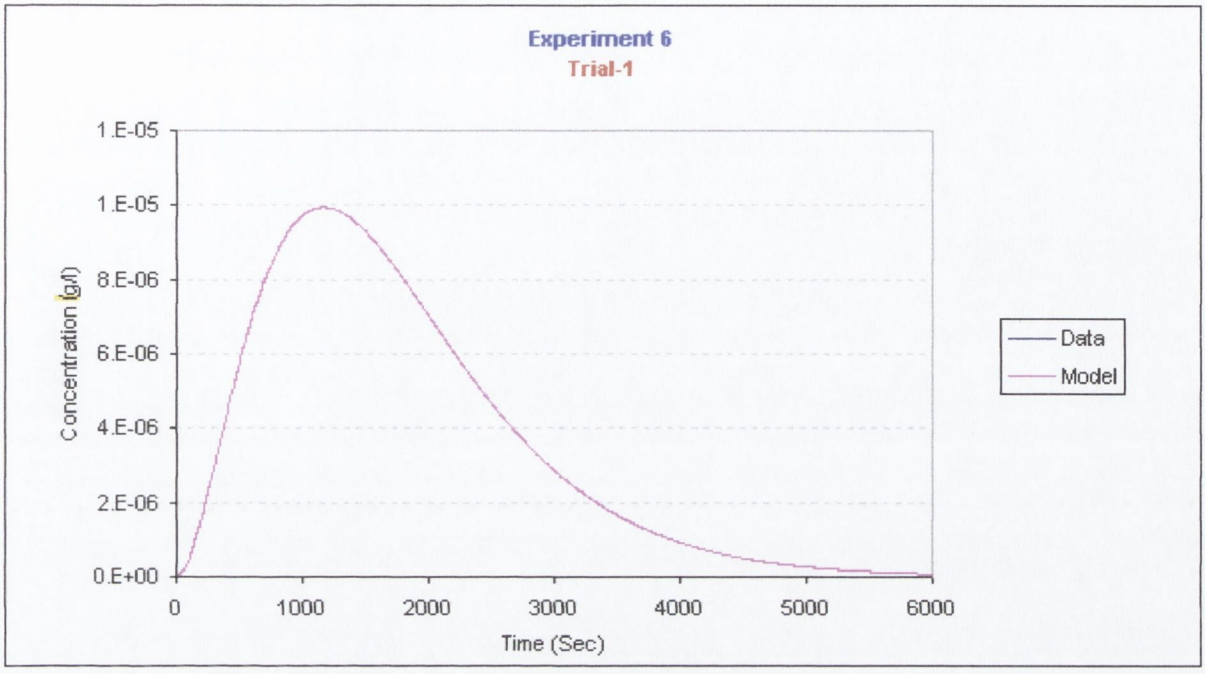

(a) Scenario-1 Experiment 6

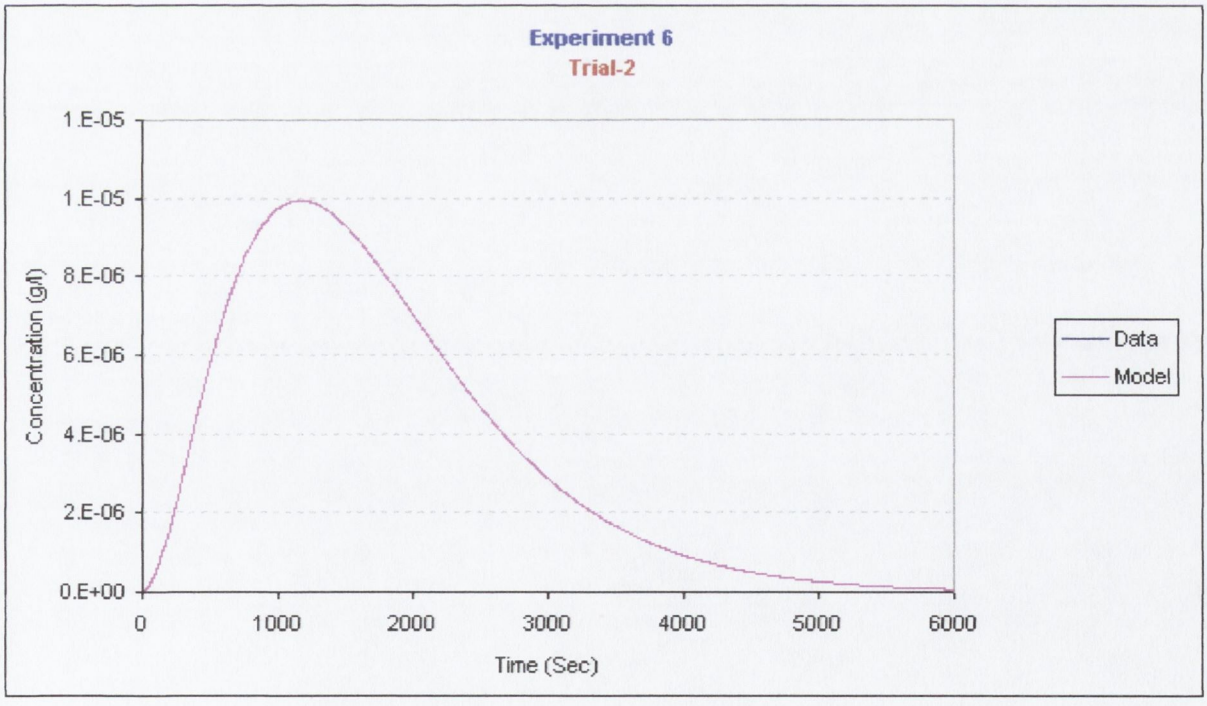

(b) Scenario-2 Experiment 6

Figure 8. 19 Graphs showing laboratory results and fitted model curves for approximated scaled-down version for (a) Scenario 1 Exp.6 and (b) Scenario 2 Exp.6

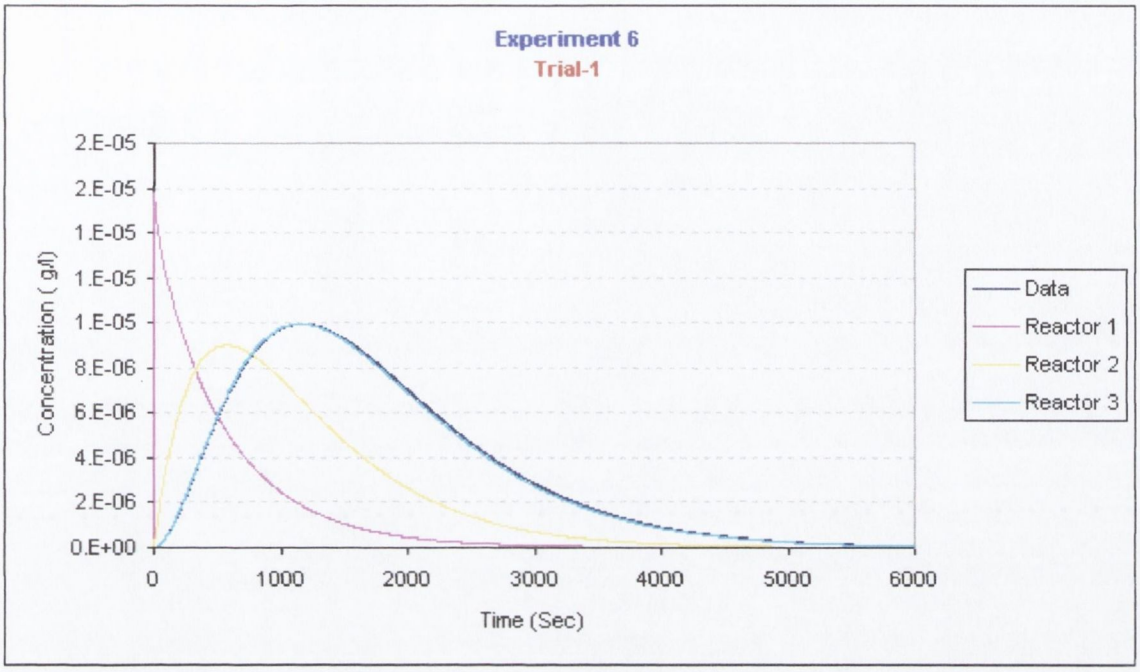

(a) Scenario-1 Experiment 6

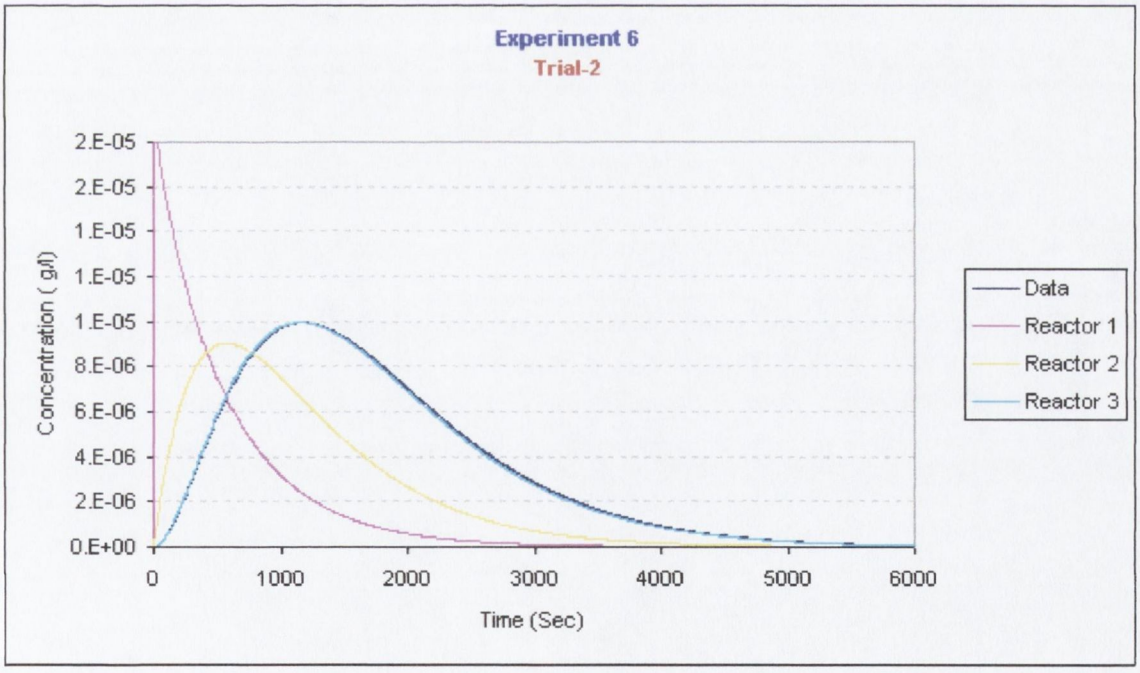

(b) Scenario-2 Experiment 6

Figure 8. 20 Graphs showing laboratory effluent concentration results and fitted model curves from each reactor for approximated scaled-down version for (a) Scenario 1 Exp.6 and (b) Scenario 2 Exp.6

8.3.1 Results Analysis

The first Scenario showed the affect of changing the mixer speed on Reactor 2 in order to see whether the position of the gaps, which were located opposite to each other, had a direct affect on the short-circuiting in the reactor. The effluent concentration curves for each experiment in this trial have been plotted on the same graph (Figure 8.21) to allow direct comparison between the experiments and allow the ideal power input per unit volume to be detected. As shown in Table 8.10, some plug flow from Reactor 1 to Reactor 3 can be seen from the mathematical model indicating the equivalent of 7.66 reactors in-series when the mixer speed was 0 rpm. This short-circuit can also be seen in the photographs that were taken in the laboratory during the experiments, as shown in Figure 8.22. As the mixer speed was successively increased to 200 rpm the short-circuit flow disappeared which can be seen from the mathematical model indicating the equivalent of 2 reactors in-series (Table 8.10). In addition, as discussed in Chapter 7 and shown in Table 8.13 the differences between the number of reactors in-series modelled for Reactor 1 and 2 is not equal to 1 indicating the presence of short-circuit flow in Reactor 2 whereas the differences between Reactor 2 and 3 are close to unity in all the experiments indicating that Reactor 3 was performing efficiently. This plug can also be seen graphically on the effluent curves as shown in Figure 8.21.

Experiment No.	Reactor 1 No. Of CSTR	Difference between Reactor 1 and 2	Reactor 2 No. Of CSTR	Difference between Reactor 1 and 3	Reactor 3 No. Of CSTR
	(n)	(n)	(n)	(n)	(n)
1	1.06	6.60	7.66	0.96	8.62
2	0.97	5.86	6.83	0.97	7.79
3	0.98	4.69	5.67	1.02	6.69
4	0.99	3.15	4.14	1.07	5.21
5	0.99	1.31	2.30	1.02	3.32
6	0.99	1.01	2.00	0.99	2.99

Table 8. 13 Differences between Reactor 1 & 2 and Reactor 2 & 3 of laboratory Scenario 1 for Greystones WwTW model

It should be noted that the short-circuit observed in these experiments is only caused by the geometry of the reactor and not any density currents since there is no difference in temperature between the influent flow and water in the reactors.

Equally, in the second Scenario, where the level of the mixer speed was increased in all three reactors together at the same time from 0 rpm up to 200 rpm, the results show how the mixing level directly affects the performance of the system, as can be seen numerically in Table 8.12. When the mixer speed was 0 rpm the model shows each reactor suffering from short-circuiting, although Reactor 2 is higher than the others due to the inadequate design of the gaps being directly opposite each other. In addition, as the mixer speeds increase the short-circuit diminishes gradually up to the point where the perfect mix has been reached across the whole system when all mixers speed were working at 160 rpm. The differences between each reactor and its neighbouring reactor can also be seen to be equal to 1 as shown in Table 8.14. It can be also seen that Reactors 1 and 3 have reached completely mixed states at 120 rpm, at which point Reactor 2 is still indicating some short-circuiting. Again this demonstrates the inefficient design of the reactor having the inlet and the outlet gaps opposite each other on the base.

Experiment No.	Reactor 1 No. Of CSTR	Difference between Reactor 1 and 2	Reactor 2 No. Of CSTR	Difference between Reactor 1 and 3	Reactor3 No. Of CSTR
	(n)	(n)	(n)	(n)	(n)
1	4.67	5.0	9.64	2.1	11.70
2	3.80	3.8	7.61	1.7	9.32
3	3.32	3.4	6.71	0.9	7.65
4	2.39	3.2	5.57	1.0	6.59
5	0.99	1.1	2.06	1.0	3.05
6	0.99	1.0	2.00	1.0	2.99

Table 8. 14 Differences between Reactor 1 & 2 and Reactor 2 & 3 of laboratory Scenario 2 for Greystones WwTW model

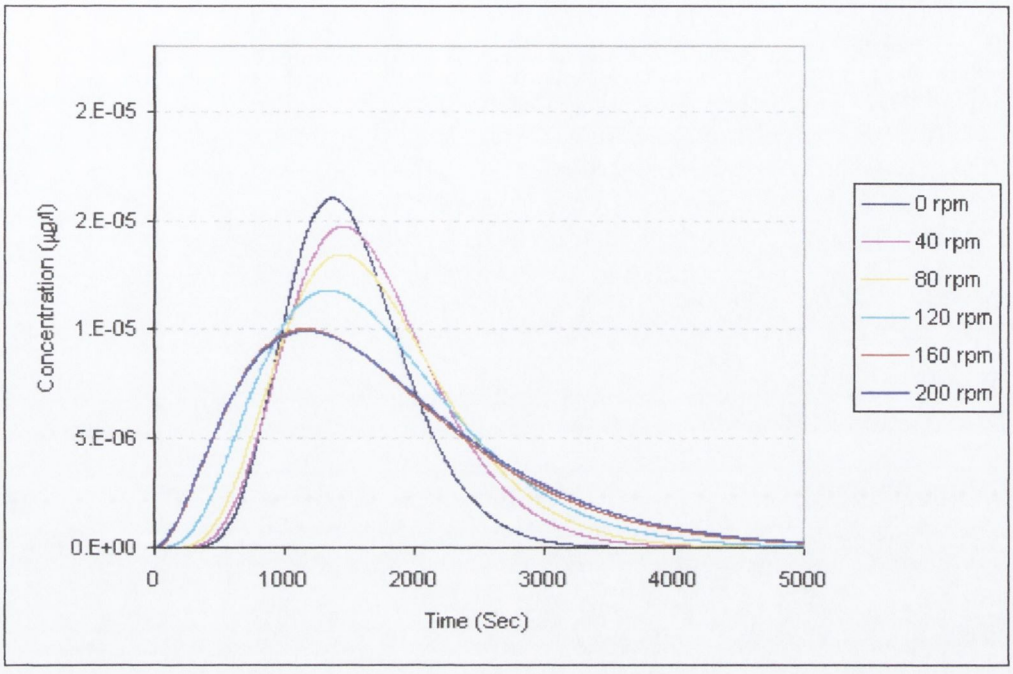

(a) The mixers in Reactor 1 and 3 working at 200 rpm while the mixer in Reactor 2 varying from 0-200 rpm

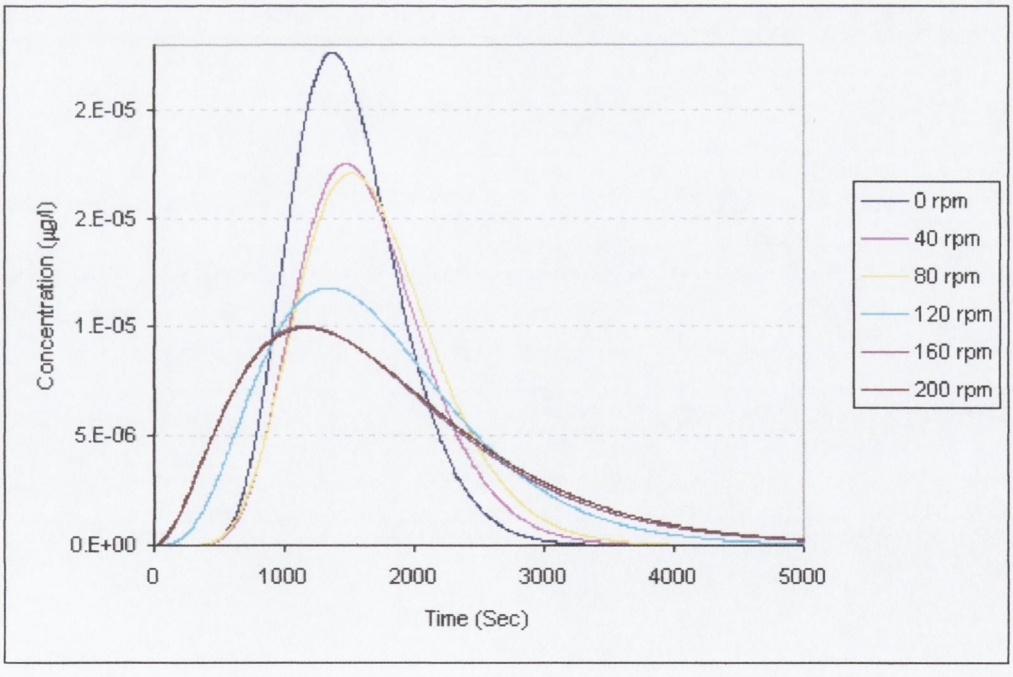

(b) All mixers varying from 0-200 rpm

Figure 8. 21 (a and b) Graphs showing the differences of the mixer level on the behavior of the hydraulic system of laboratory model for Greystones WwTW

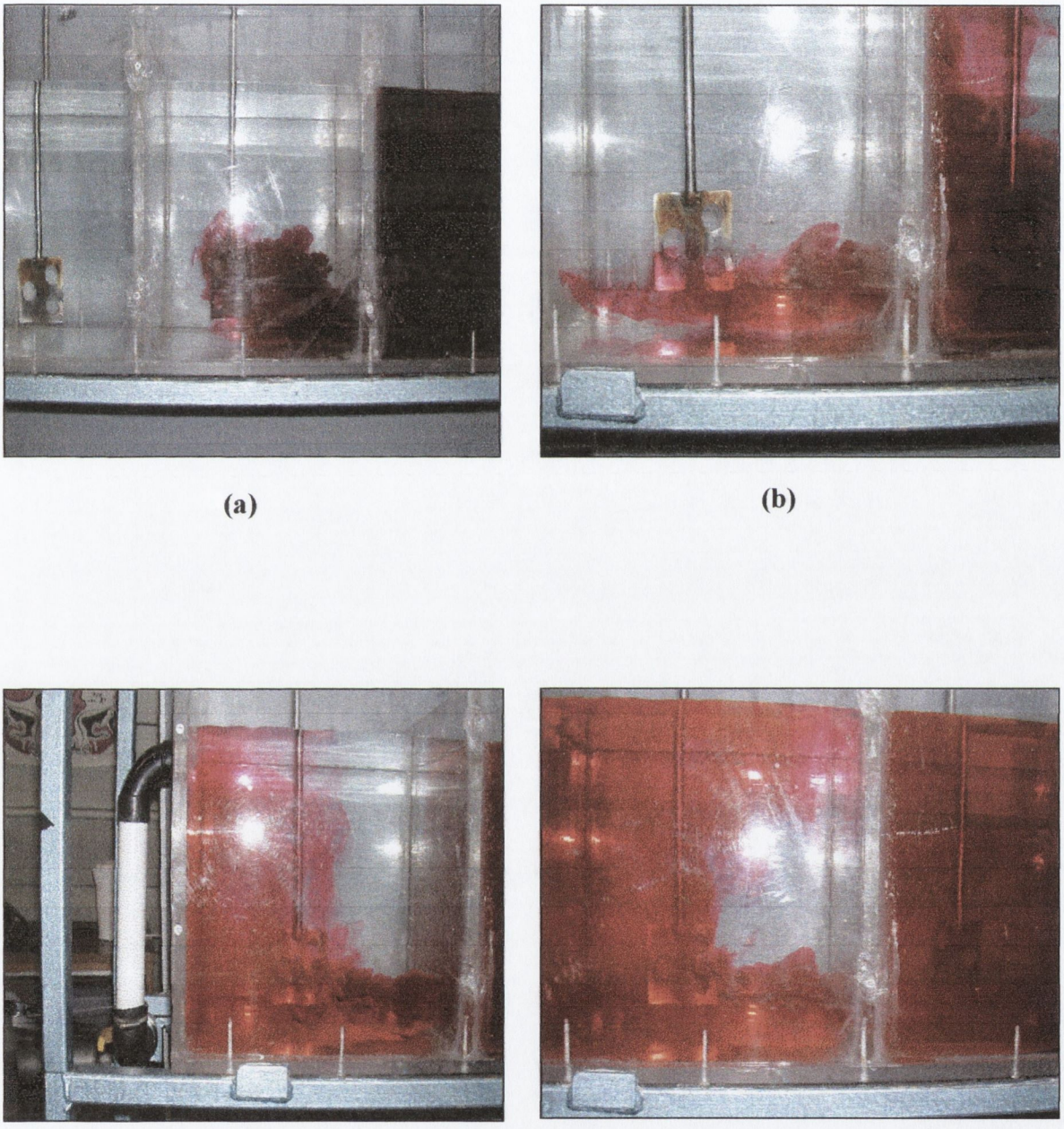

Figure 8. 22 Photographic sequences of the tracer in the scaled-down model

8.4 Modifications to Laboratory Model of Greystones WwTW

As indicated from the initial laboratory trials, it is clear that there is a large plug flow element through Reactor 2. Therefore, some modifications were made to the initial laboratory model in order to see whether the position of the gap was causing the problem and whether a solution could be found to improve the performance of the reactors in Greystones WwTW. The modification made was to change the position of the gaps between the reactors as shown in Figure 8.23, so they were not directly opposite one another.

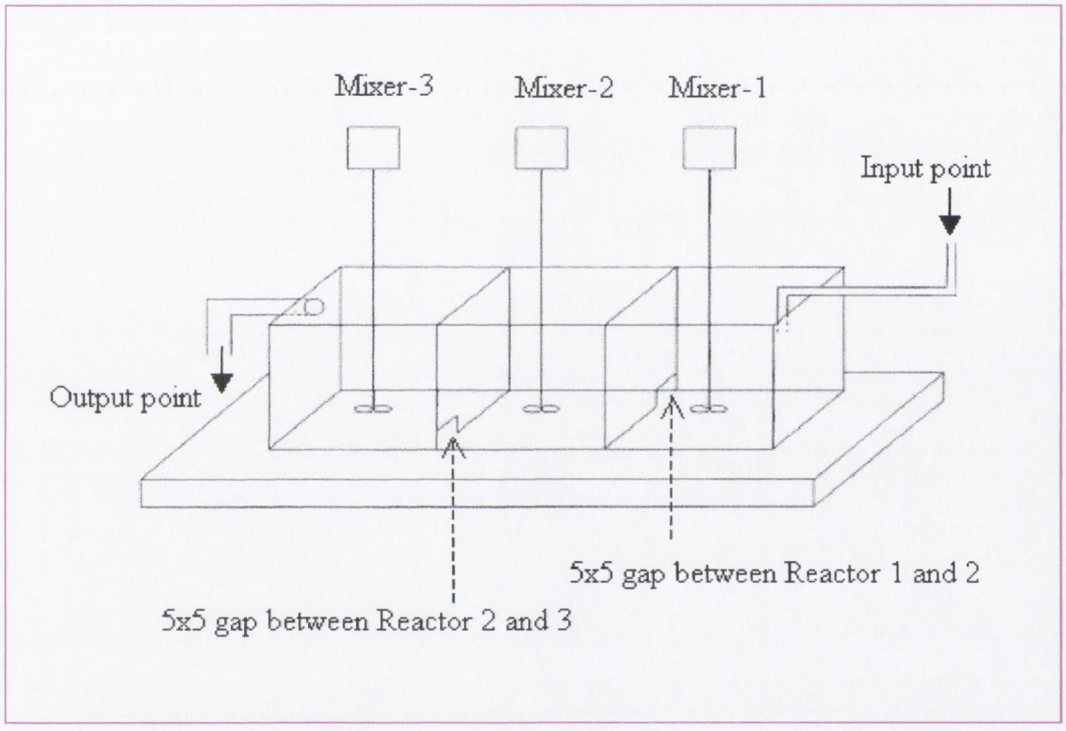

Figure 8. 23 Schematic representation of the modifications to the scale model of Greystones WwTW

Again, the same pattern of trials studying the two different mixing scenarios (see Section 8.3) were carried out. Six experiments were undertaken for each different scenario using the same system configurations as those shown in Table 8.9 and Table 8.11. The results obtained from each experiment are shown in Table 8.15 (for the first scenario) and in Table 8.16 (for the second scenario). In addition, an example RTD curve and model curves for Experiment 6 are shown in Figures 8.24 and 8.25 for each scenario while the rest are located in Appendix I.

Experiment No.	Reactor [1]		Reactor [2]		Reactor [3]	
	Theoretical retention time at the end of Reactor 1	No. Of CSTR	Theoretical retention time at the end of Reactor 2	No. Of CSTR	Theoretical retention time at the end of Reactor 3	No. Of CSTR
	(S)	(n)	(S)	(n)	(S)	(n)
1	577.1	1.02	1154.3	4.69	1731.4	5.92
2	577.1	0.97	1154.3	3.27	1731.4	4.39
3	577.1	0.99	1154.3	3.12	1731.4	4.19
4	577.1	0.99	1154.3	1.99	1731.4	2.99
5	577.1	0.99	1154.3	1.99	1731.4	2.99
6	577.1	0.99	1154.3	1.99	1731.4	2.99

Table 8. 15 Laboratory model (with modifications) of Greystones WwTW [Scenario-1] - results

Experiment No.	Reactor [1]		Reactor [2]		Reactor [3]	
	Theoretical retention time at the end of Reactor 1	No. Of CSTR	Theoretical retention time at the end of Reactor 2	No. Of CSTR	Theoretical retention time at the end of Reactor 3	No. Of CSTR
	(S)	(n)	(S)	(n)	(S)	(n)
1	577.1	3.23	1154.3	5.23	1731.4	7.20
2	577.1	1.19	1154.3	3.22	1731.4	5.21
3	577.1	1.06	1154.3	2.77	1731.4	3.82
4	577.1	0.96	1154.3	2.00	1731.4	3.12
5	577.1	0.96	1154.3	2.00	1731.4	3.00
6	577.1	0.96	1154.3	2.00	1731.4	3.00

Table 8. 16 Laboratory model (with modifications) of Greystones WwTW [Scenario-2] - results

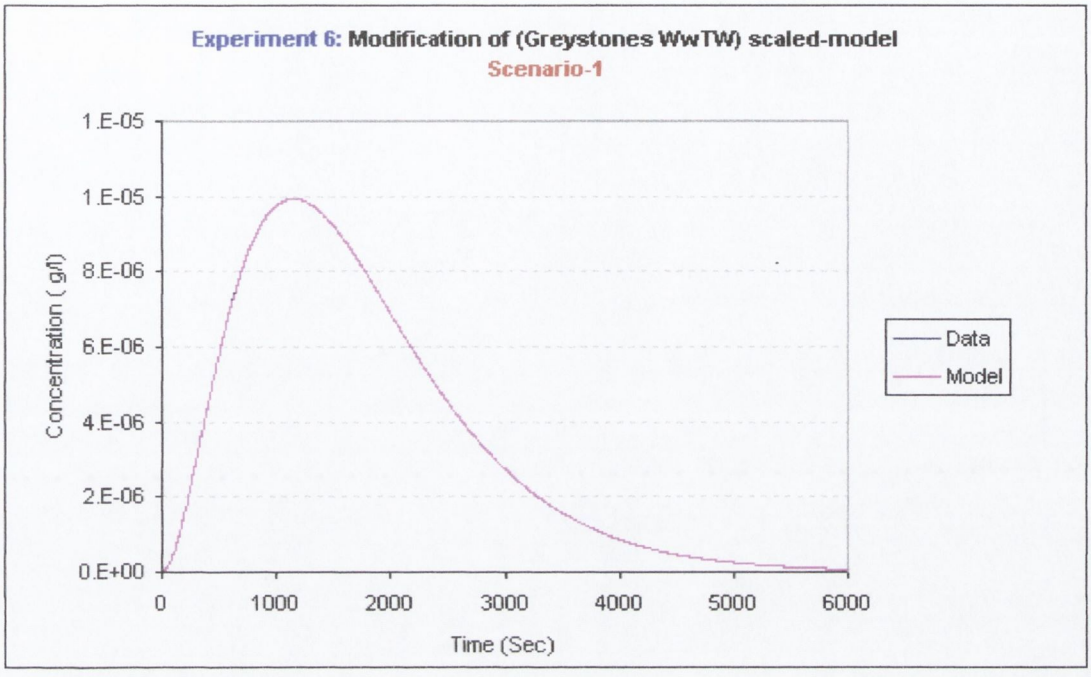

(a) Scenario-1 Experiment 6

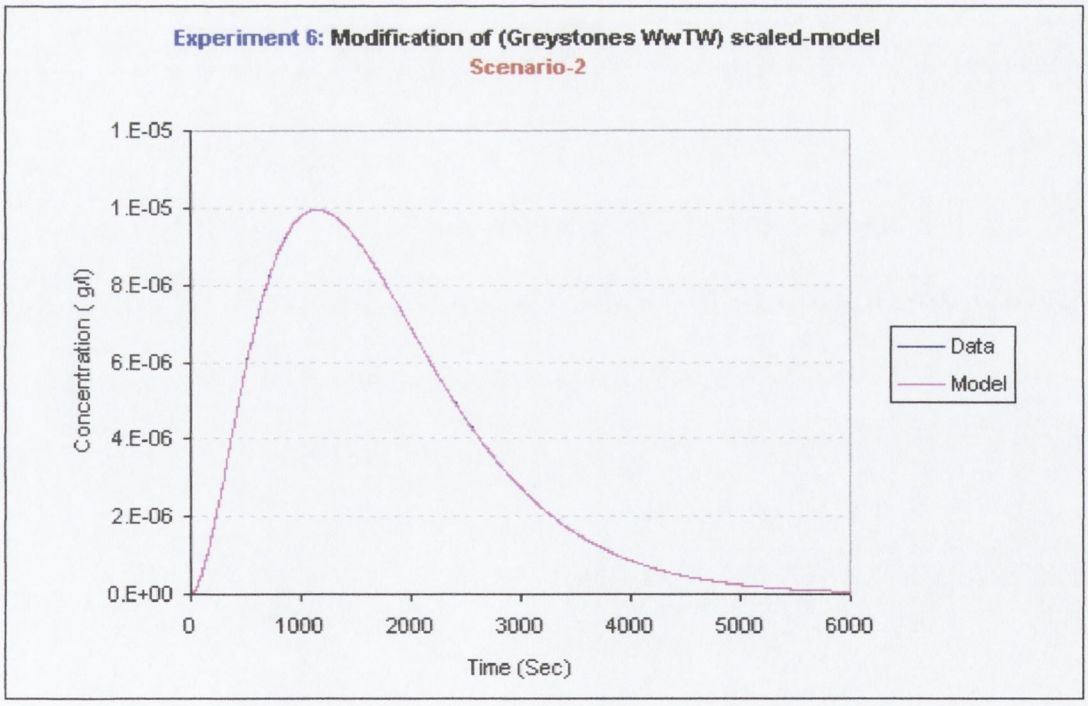

(b) Scenario-2 Experiment 6

Figure 8. 24 Graphs showing laboratory results and fitted model curves for modification scaled-down version for (a) Scenario 1 Exp.6 and (b) Scenario 2 Exp.6

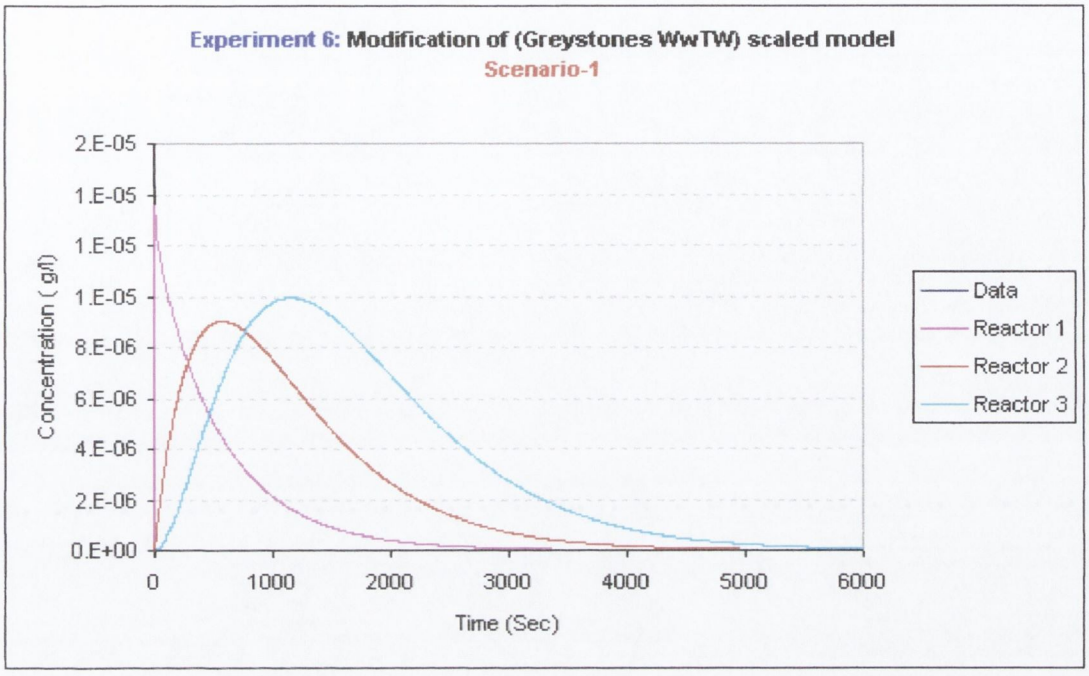

(a) Scenario-1 Experiment 6

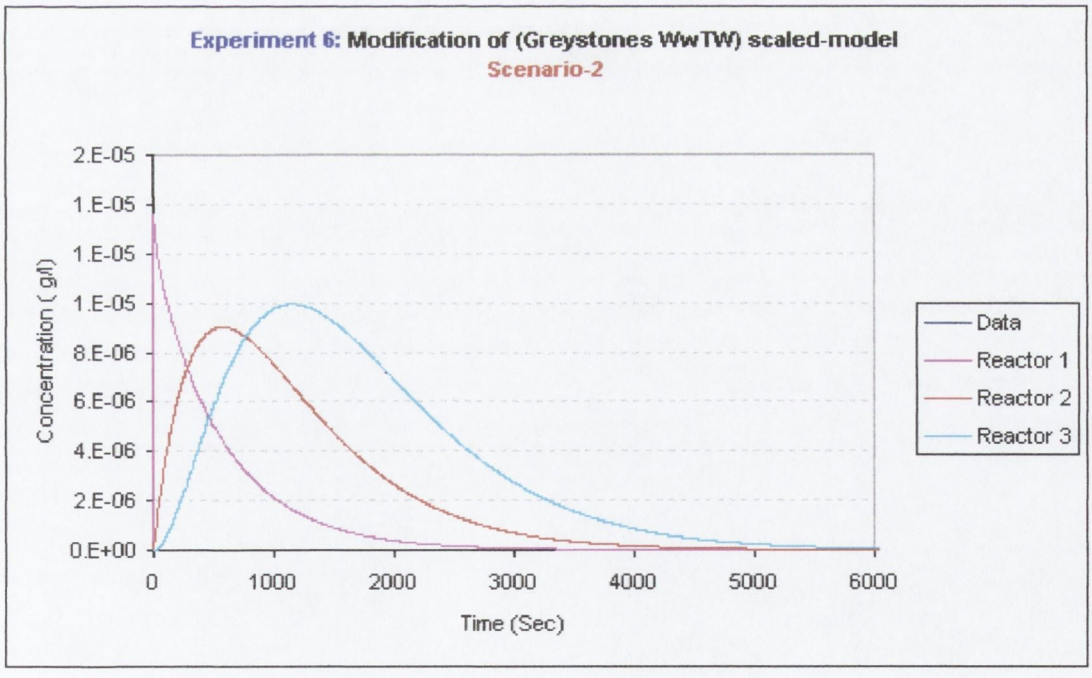

(b) Scenario-2 Experiment 6

Figure 8. 25 Graphs showing laboratory effluent concentration results and fitted model curves from each reactor for modification scaled-down version for (a) Scenario 1 Exp.6 and (b) Scenario 2 Exp.6

8.4.1 Results Analysis

The results in Table 8.15 obtained after modifying the inlet and outlets were much better, indicating that the short-circuiting is partly due to inadequate design of the gaps in the baffles of Reactor 2 located opposite each other. In the first scenario the results show that Reactor 2 was still suffering from short-circuiting when the mixer level was at 0 rpm up to 80 rpm, but did not appear to be as strong as the short-circuit in the first trial when the gaps were opposite each other. This can also be seen graphically when comparing Figure 8.21(a) with Figure 8.26(a). The graphs in Figure 8.26 illustrate what would be expected from a 3-reactor in-series model, and the perfectly mixed system was reached when the mixer in Reactor 2 was working at 120 rpm, as shown in Table 8.17. This can be compared with the first trial where the perfectly mixed system was only reached when Reactor 2's mixer was at 160 rpm.

Experiment No.	Reactor 1 No. Of CSTR	Difference between Reactor 1 and 2	Reactor 2 No. Of CSTR	Difference between Reactor 2 and 3	Reactor 3 No. Of CSTR
	(n)	(n)	(n)	(n)	(n)
1	1.02	3.67	4.69	1.23	5.92
2	0.97	2.30	3.27	1.12	4.39
3	0.99	2.13	3.12	1.07	4.19
4	0.99	1.00	1.99	1.00	2.99
5	0.99	1.00	1.99	1.00	2.99
6	0.99	1.00	1.99	1.00	2.99

Table 8. 17 Differences between Reactor 1 & 2 and Reactor 2 & 3 of laboratory modification model Scenario 1 for Greystones WwTW

Equally, for the second scenario where all mixers where set to the same level, the results indicate that the system was suffering from short-circuiting when the mixers were working at 0 rpm up to 80 rpm but this was not as strong as the short-circuit flow in the first trial. A perfect mix across the system was reached at 120 rpm as can be seen in Table 8.18 where the differences in **n** between each reactor its neighbouring reactor is equal to 1. Again, this point was only reached in the first trial when all mixers were at 160 rpm (see Table 8.14).

Experiment No.	Reactor 1 No. Of CSTR	Difference between Reactor 1 and 2	Reactor 3 No. Of CSTR	Difference between Reactor 2 and 3	Reactor 3 No. Of CSTR
	(n)	(n)	(n)	(n)	(n)
1	3.23	2.0	5.23	2.0	7.20
2	1.19	2.0	3.22	2.0	5.21
3	1.06	1.7	2.77	1.1	3.82
4	0.96	1.0	2.00	1.1	3.12
5	0.96	1.0	2.00	1.0	3.00
6	0.96	1.0	2.00	1.0	3.00

Table 8. 18 Differences between Reactor 1 & 2 and Reactor 2 & 3 of laboratory modification model Scenario 2 for Greystones WwTW

Looking at the overall systems, the results suggest that in terms of the power input per unit volume, the most energy efficient way to run the system would be to operate the mixers of CSTRs 1 and 3 at 80 rpm and Reactor 2 at 120 rpm.

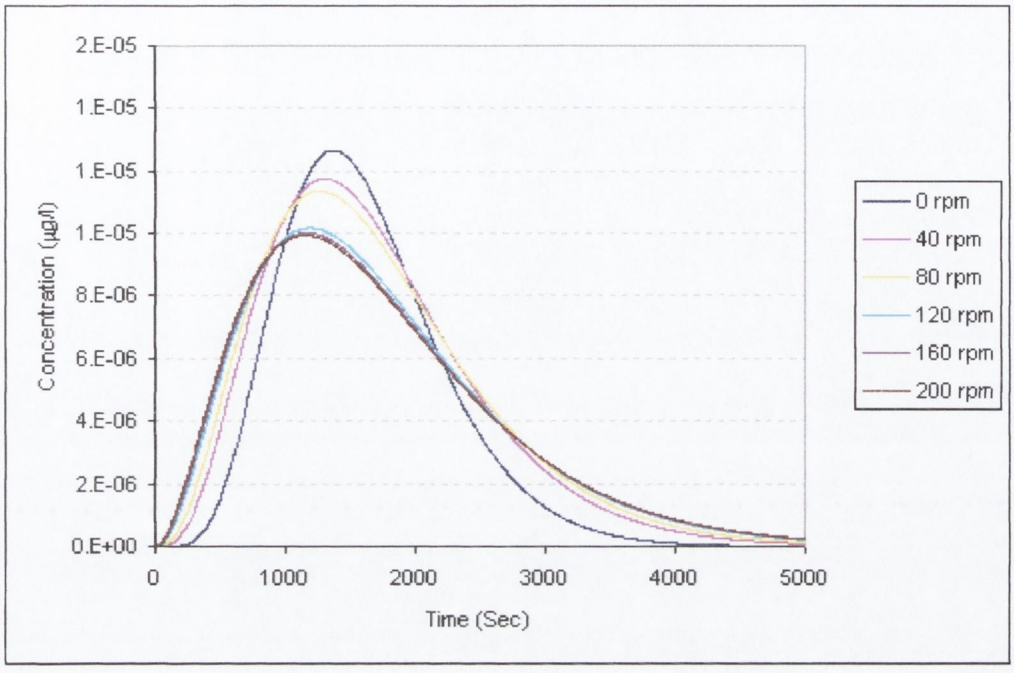

(a) The mixers in Reactor 1 and 3 working at 200 rpm while the mixer in Reactor 2 varying from 0-200 rpm

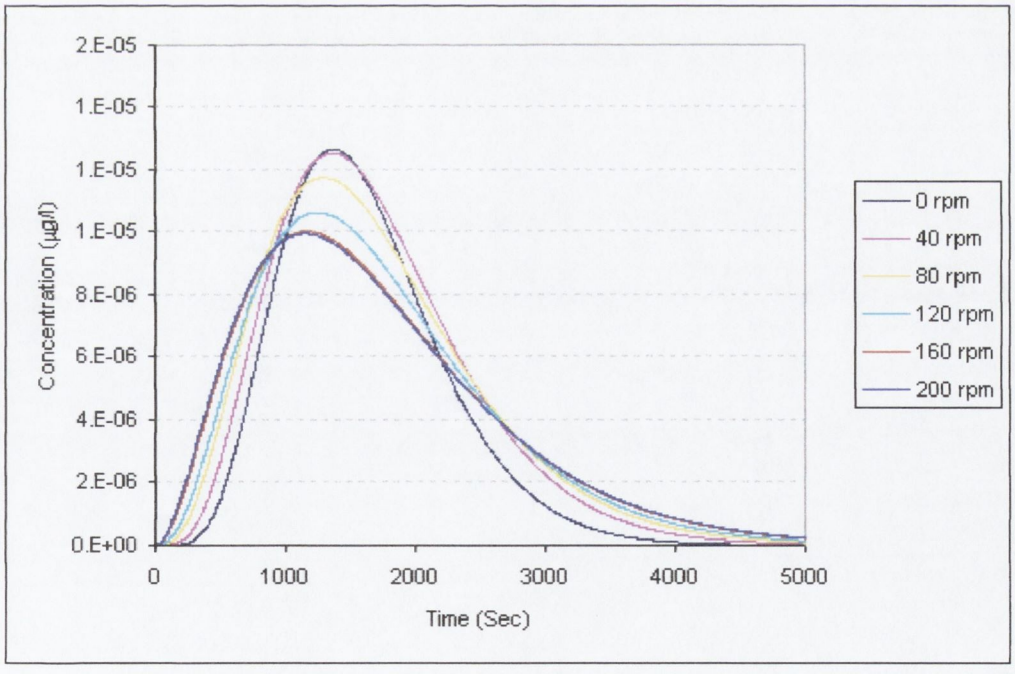

(b) All mixers varying from 0-200 rpm

Figure 8. 26 (a and b) Graphs showing the differences of the mixer level on the behavior of the Greystones model (with modifications)

8.5 Scaled-down version of Greystones System

The previous experiments on the Greystones laboratory physical model were only looking at an approximate scaled-down version (Section 8.3). A further set of scaled-down trials were carried out whereby the model was more accurately scaled-down with regards to both the velocity gradient G and the geometric area of the gaps between the reactors as detailed in Table 8.19 below. The airflow rate introduced during the full scale Trial 1, was balanced between the three reactors and equal to 413.3 m^3/h, creating an equal velocity gradient in each individual reactor of 169.42 s^{-1} (see Table 8.4). In Trial 2 the airflow rate in Reactors 1 and 2 was equal to 527.7 m^3/h and 184.7 m^3/h in Reactor 3. This gave a velocity gradient of 207.25 s^{-1} for Reactors 1 and 2 and 122.61s^{-1} for Reactor 3.

Trial No.	Tank No.	V (m^3)	V_{tank} (m^3)	Valve open %	Fraction Per tank	Q (m^3/h)	Q_{tank} (m^3/h)	P_{tank} (W)	G_{tank} (s^{-1})	$G_{average}$ (s^{-1})
1	1	966.29	322.097	50	0.3	1240	413.33	9264.10	169.42	**169.42**
	2		322.097	50	0.3		413.33	9264.10	169.42	
	3		322.097	50	0.3		413.33	9264.10	169.42	
2	1	966.29	322.097	100	0.426	1240	527.66	13862.46	207.25	**179.33**
	2		322.097	100	0.426		527.66	13862.46	207.25	
	3		322.097	35	0.149		184.68	4851.86	122.61	

Table 8. 19 Velocity gradient (G) of full-scale Greystones reactor system

In this section two different scenarios were undertaken in the laboratory to mimic the two different full-scale trials carried out at Greystones WwTW with regards to the velocity gradient. In order to get the same shear rate, some modifications were made to the blades of each mixer from the previous laboratory system. The dimensions of the blades were increased to 13.85 cm by 8.0 cm, again with a slight "S" profile in order to get the approximate diameter. To get the proper shear rate for each trial a combination of appropriate speed for each mixer (rpm) and appropriate blade diameter was selected as shown in Table 8.20 below.

Exp. No	V (m^3)	V_{tank} (m^3)	n_{tank} (rev/sec)	n_{tank} (rev/min)	μ (kg/m.s)	ρ (kg/m^3)	D (m)	N_R Non	Q (m^3/s)	k Constant	P_{tank} (W)	P (W)	G_{tank} (s^{-1})	$G_{average}$ (s^{-1})
1	0.069	0.023	2.82	169	0.00114	999.1	0.2	189807.97	0.000040	0.32	0.75	2.26	169.33	**169.33**
		0.023	2.82	169							0.75		169.33	
		0.023	2.82	169							0.75		169.33	
2	0.069	0.023	2.93	176	0.00114	999.1	0.2	197211.82	0.000040	0.32	0.84	2.53	179.33	**179.33**
		0.023	2.93	176							0.84		179.33	
		0.023	2.10	126							0.31		108.82	

Table 8. 20 Velocity gradient (G) of scaled-down Greystones WwTW model

In addition to the velocity gradient G, the other characteristic that was taken into account in terms of scale was the area of the gaps between the reactors. The proportion of the gap area to the reactor baffle area in the full-scale plant is 0.0364, which was replicated in the laboratory model as shown in Table 8.21.

Greystones system							Scaled-down version						
Baffle dimensions			Gap dimensions				Baffle dimensions			Gap dimensions			
Width	Depth	Area	Width	Depth	Area	Fraction	Width	Depth	Area	Width	Depth	Area	Fraction
(m)	(m)	(m^2)	(m)	(m)	(m^2)		(cm)	(cm)	(cm^2)	(cm)	(cm)	(cm^2)	
5.375	5.1	27.413	1	1	1	0.036	30	27	810	5.43	5.43	29.48	0.036

Table 8. 21 The scaling of the gap to the baffle area

The other characteristic that should be considered in terms of scale is the theoretical retention time of water in the reactor system. The theoretical retention time at full-scale for Greystones was about 3 hours which would have required a much larger physical model to be built in the laboratory to achieved the same retention time when the flow rate was in the range of 1 to 6 l/min. It should be noted that due to the physical constraints in the laboratory it was only possible to achieve constant flow rates between 1- 6 l/min as shown in Table 8.22. It shows that to mimic the retention time in the laboratory scaled-down version, a flow rate of 0.39 l/min was needed which was below the levels which could be accurately measured and applied (using a flow rate of 1 – 6 l/min). Conversely, a volume ranging from 180 to 1080 litres would have been needed in the laboratory to achieve correct retention time which was also above the limitation of the laboratory physical model.

Flow rate	Reactor volume	Theoretical retention time Laboratory	Theoretical retention time Greystones	Volume needed in Laboratory	Flow rate needed in Laboratory
(L/min)	(L)	(h)	(h)	(L)	(L/min)
1	69.3	1.16	3	180	0.39
2	69.3	0.58		360	
3	69.3	0.39		540	
4	69.3	0.29		720	
5	69.3	0.23		900	
6	69.3	0.19		1080	

Table 8. 22 Limitations of the flow rate and volume for laboratory scaled-down version of Greystones WwTW

The two scenarios that were undertaken to mimic the full-scale trials carried out at Greystones WwTW were as follows:

- Scenario 1 applied a mixer speed of 169 rpm in each reactor looking at a range of flow rates from 1 l/min to 6 l/min.
- Scenario 2 applied 175 rpm for Reactors 1 and 2, and 126 rpm for Reactor 3 again looking at flow rates from 1 l/min to 6 l/min.

The experimental configurations are shown in Tables 8.23 and 8.24, and the results obtained from each experiment in each trial are shown in Tables 8.25 and 8.26. In addition, an example RTD curve and model curves for each scenario of Experiment 6 is attached in Figures 8.27 and 8.28.

Experiment No.	Reactor Volume	Flow Rate	Mixer Speed	Rhodamine Mass
	(L)	(L/min)	(rpm)	(g)
1	69.3	1	169	0.002
2	69.3	2	169	0.002
3	69.3	3	169	0.002
4	69.3	4	169	0.002
5	69.3	5	169	0.002
6	69.3	6	169	0.002

Table 8. 23 Scaled-down model of Greystones WwTW [Trial 1] – experimental configurations

Experiment No.	Reactor Volume	Flow Rate	Mixer Speed for Reactors 1 and 2	Mixer Speed for Reactor 3	Rhodamine Mass
	(L)	(L/min)	(rpm)	(rpm)	(g)
1	69.3	1	175	126	0.002
2	69.3	2	175	126	0.002
3	69.3	3	175	126	0.002
4	69.3	4	175	126	0.002
5	69.3	5	175	126	0.002
6	69.3	6	175	126	0.002

Table 8. 24 Scaled-down model of Greystones WwTW [Trial 2] – experimental configurations

Experiment No.	Reactor [1]		Reactor [2]		Reactor [3]		System Performance		
	Theoretical retention time at the end of Reactor 1	No. Of CSTR	Theoretical retention time at the end of Reactor 2	No. Of CSTR	Theoretical retention time at the end of Reactor 3	No. Of CSTR	P%	D%	S%
	(S)	(n)	(S)	(n)	(S)	(n)	(%)	(%)	(%)
1	1385.0	1.0	2770.0	2.00	4155.0	3.40	88.4	11.5	0.10
2	692.5	1.0	1385.0	2.20	2077.5	3.30	91.2	6.4	2.45
3	461.7	1.2	923.3	3.90	1385.0	5.60	78.9	12.8	8.30
4	346.3	1.3	692.5	4.20	1038.8	6.50	70.0	11.4	18.62
5	277.0	1.4	554.0	7.52	831.0	8.70	68.1	8.6	23.29
6	230.8	1.4	461.7	9.30	692.5	11.02	72.7	0.2	27.15

Table 8. 25 Scaled-down model of Greystones WwTW [Trial 1] - results

Experiment No.	Reactor [1]		Reactor [2]		Reactor [3]		System Performance		
	Theoretical retention time at the end of Reactor 1	No. Of CSTR	Theoretical retention time at the end of Reactor 2	No. Of CSTR	Theoretical retention time at the end of Reactor 3	No. Of CSTR	P%	D%	S%
	(S)	(n)	(S)	(n)	(S)	(n)	(%)	(%)	(%)
1	1385.0	0.96	2770.0	2.00	4155.0	3.40	91.3	8.6	0.0
2	692.5	0.96	1385.0	2.30	2077.5	3.65	95.3	2.8	1.9
3	461.7	1.00	923.3	2.10	1385.0	3.20	91.0	1.9	7.1
4	346.3	1.00	692.5	3.20	1038.8	4.30	83.0	1.4	15.6
5	277.0	1.20	554.0	4.50	831.0	5.60	81.1	1.3	17.6
6	230.8	1.30	461.7	8.70	692.5	10.20	75.3	0.0	24.7

Table 8. 26 Scaled-down model of Greystones WwTW [Trial 2] - results

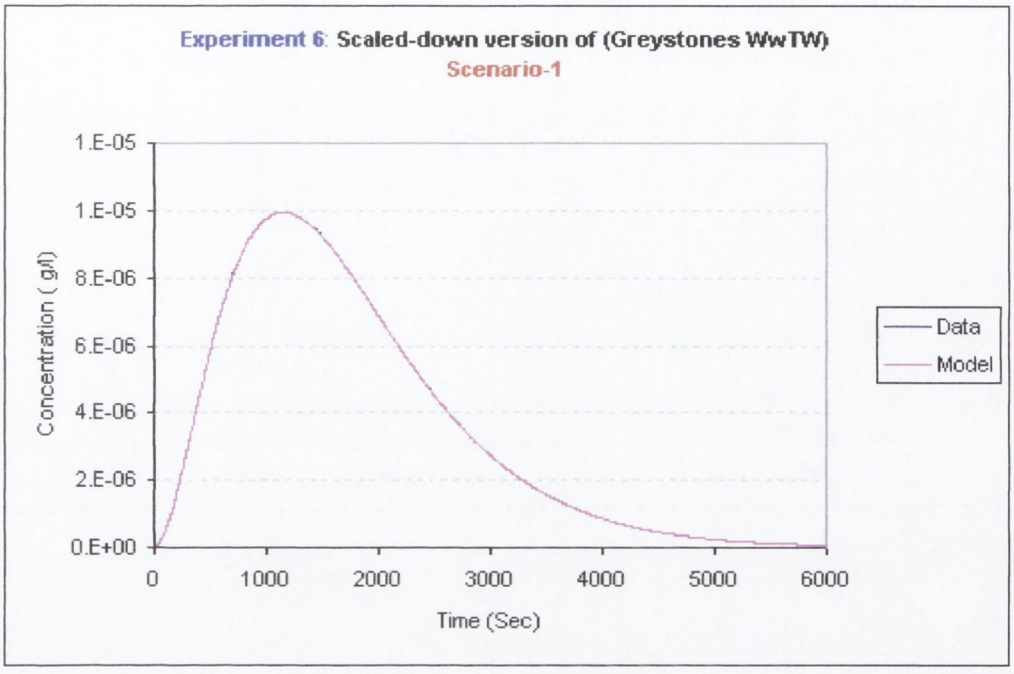

(a) Scenario-1 Experiment 6

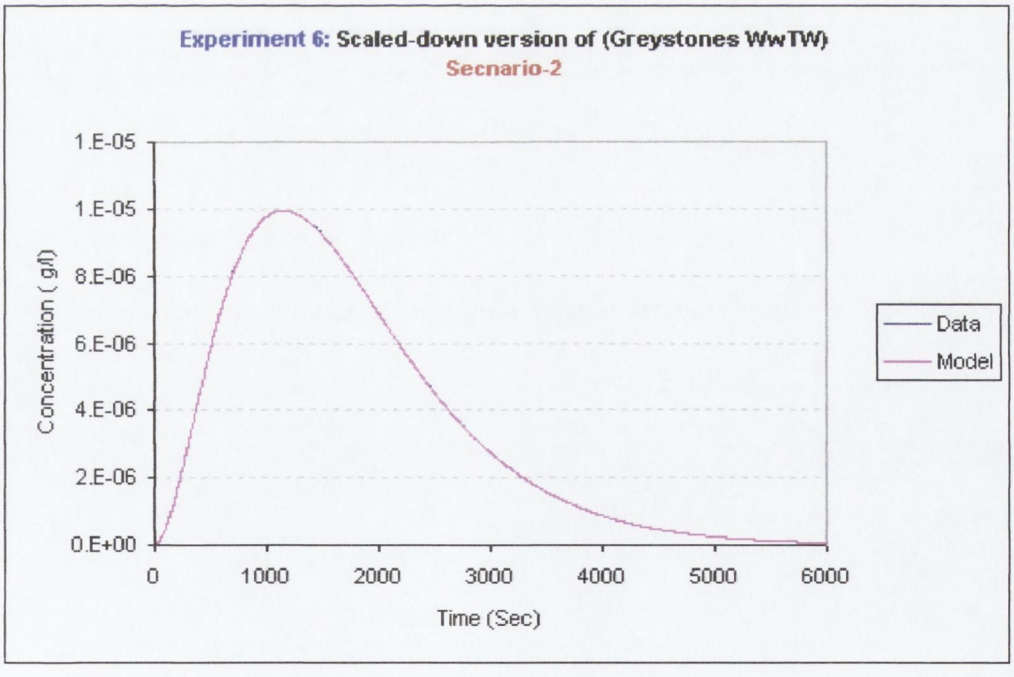

(b) Scenario-2 Experiment 6

Figure 8. 27 Graphs showing laboratory results and fitted model curves for scaled-down version for (a) Scenario 1 Exp.6 and (b) Scenario 2 Exp.6

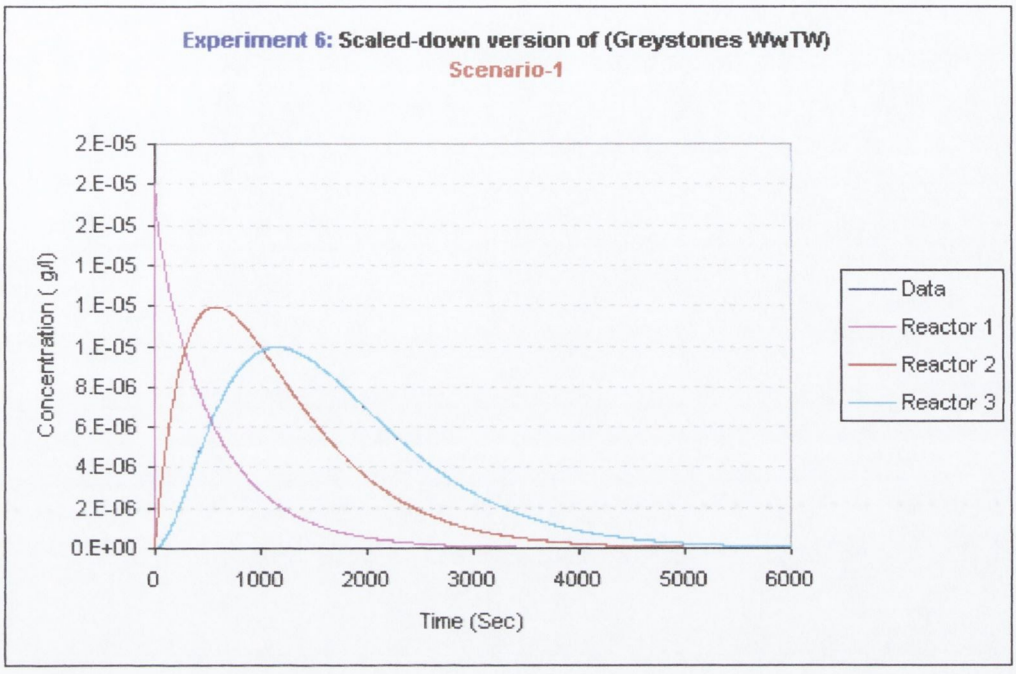

(a) Scenario-1 Experiment 6

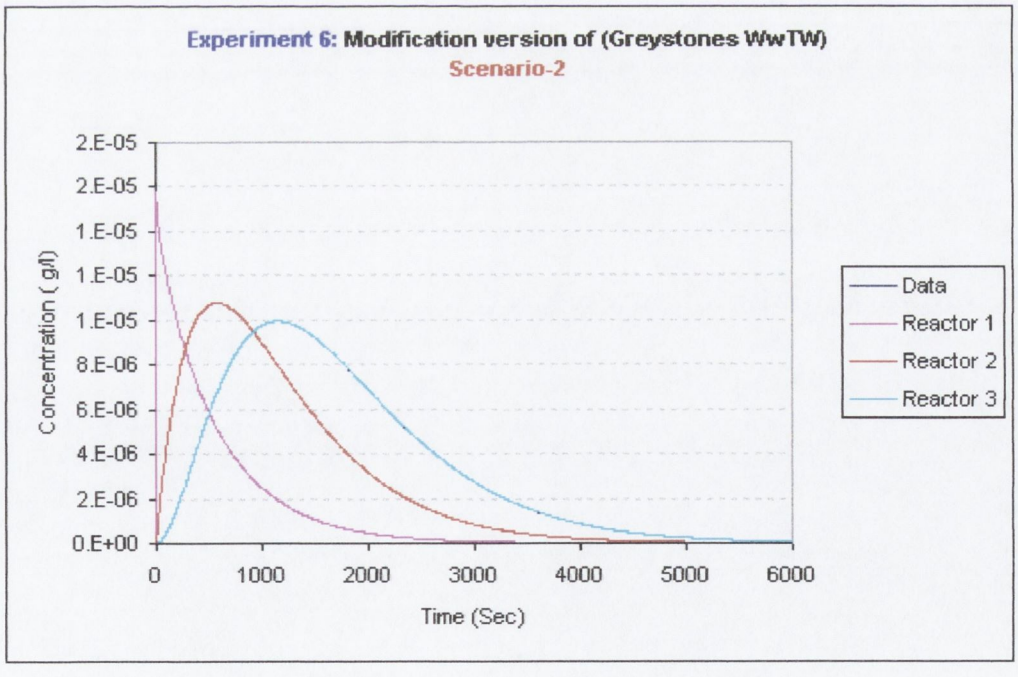

(b) Scenario-2 Experiment 6

Figure 8. 28 Graphs showing laboratory effluent concentration results and fitted model curves from each reactor for scaled-down version for (a) Scenario 1 Exp.6 and (b) Scenario 2 Exp.6

8.5.1 Results Analysis

The results from the two scenarios modelled in the laboratory indicate that there does not appear to be agreement between the scaled-down model and the full-scale situation. The differences in the temperature between the influent and mixed liquor were identified as one potential problem at full scale. However, since it was not possible to model such temperature differences, the flow rate was increased from 1 l/min to 6 l/min in an attempt to mimic the channelling possibly created by density currents at Greystones WwTW. Another reason for the disparity between the scale model and full-scale model results could be to do with the nature and position of the mixers. Although both systems had the same velocity gradient, G, applied, this was achieved by the aerator diffusers spread across the whole floor of the reactor in the full-scale plant compared to the single mechanical mixer in the laboratory model. Thirdly, the difference in retention time between the full-scale and laboratory models would have been a factor, whereby the effect of the dispersion of the tracer entering into the proportionally smaller volume in the scale model would have also contributed to a more efficiently mixed system.

It should be noted from the results in Table 8.25 that when all mixers were working at 153 rpm and a low flow rate was applied (1-2 l/min) the percentage of perfectly mixed flow appeared to be high. In this situation the shear rate was high enough to break the localised kinetic energy across the system in the influent into each reactor. Conversely, when high flow rates were applied (3-6 l/min), the percentage of perfectly mixed flow decreased respectively and the percentage of flow short-circuiting started to become significant. Hence, at these flow rates the shear rate applied by the mixers was not high enough to break through the channelling causing by the flow. This can also be seen from the mathematical model indicating the equivalent of $\mathbf{n} = 9.30$ reactors in-series from Reactor 2 to Reactor 3 when the flow rate was at 6 l/min indicating the channelling through Reactor 2 was very strong. In comparison to the results obtained during the full-scale trials at Greystones it appears that the geometry of the system may not affect the short-circuiting as significantly as thought previously which means that it could be more affected by density currents. The evidence for this is that as the flow rate increases the number of tanks in-series indicated by the mathematical model in Reactor 2 increases up to $\mathbf{n} = 9.30$ when the flow rate applied was at 6 l/min which matches the

strong short-circuiting through Reactor 2 achieved at full-scale more clearly (see Table 8.2).

In the second scenario when the mixers were set at 175 rpm for Reactors 1 and 2, and 126 rpm in Reactor 3, more or less the same results (Table 8.26) were achieved, allowing for some slight differences in the percentage of perfectly mixed flow which were higher compared to the results obtained from Scenario 1: 88.4% to 72.7% for Scenario 1 and 91.3% to 75.3% for Scenario 2. This is due to the shear rate that was applied into Reactor 2 in the second scenario being slightly higher than in first scenario. These results also match the pattern of results that were obtained from the full-scale Greystones trials where the percentage of perfectly mixed flow increased between Trial 1 and Trial 2 55.8% - 61.5% due to the shear rate in Trial 2 being slightly higher than Trial 1. However, the flow channelling problem was still evident in the system at high flow rates (6 l/min) which can also be seen from the mathematical model indicating the equivalent of **n** = 8.70 reactors in-series from Reactor 2 to Reactor 3 again indicating strong short-circuiting through Reactor 2 (but not as strong as in Scenario 1). Again this result matches the results that were obtained from Greystones where the number of tank in-series decreased in Trial 2.

8.6 Conclusion

In general, the results obtained are promising indicating that it was worth examining the mathematical model in further systems in order to prove its ability under different hydraulic environments. The results which were obtained using the model in the wastewater treatment process made physical sense though only a low recovery of the tracer was achieved. The model provided more or less the same overall result using the adjusted data which further indicates the validity of both the tracer study technique and mathematical model. In addition, the results from the scale model indicated that the short-circuiting in the second reactors at Greystones WwTW may be the combination of both poor geometrical design and also the effect of density currents due to the heating of the water by the diffused aeration systems.

Chapter 9

Further Full-Scale Implementation

Chapter 9

Further Full-Scale Implementation Trials

9.1 Waha Oil Company Trials

9.1.1 Background

The Waha Oil Company is located in Libya and one of its main functions is to drill for oil. As a part of the drilling process a mixing system is used to mix Bentonite (Montmorillonite) with fresh water, as illustrated in Figure 9.1. The Bentonite is added to the drill solids for two beneficial effects: an increase in viscosity, which improves the lifting capacity of the mud to carry cuttings to the surface (especially helpful in larger holes where the annular velocity is low); and the second benefit is the formation of a wall cake in permeable zones thus preventing fluid loss and increasing wellbore stability.

The system consists of four large reactors in-series, each one 6m in length, 3m in height and 4m in width, fitted with an inlet pipe feed at the top of the first reactor and an adjustable flow meter allowing control over the flow rate. A hopper is used to inject the Bentonite into the influent stream. An outlet pipe is located at the bottom of the fourth reactor as illustrated in Figure 9.1; the outlet point is also connected to an adjustable valved flow meter. Both inlet and outlet valved flow meters work to keep the mixture inside the system at the same level from one reactor to another. Each reactor has a mixer in the form of a propeller, with 3 square pitch blades (40 cm by 30 cm) all working at the same speed of 1010 rpm. Each reactor in the system also has four small pumps located two on each side, two of them work to suck the mixture from the bottom of the reactor and inject the mixture at high pressure into the top of the reactor, while the other pumps are working to suck the mixture from the top of the reactor and inject it at the bottom of the reactor which also promotes excellent shearing and therefore mixing. These pumps are only used for a specific type of drilling mud, such as high viscosity mud and oil base mud, in order to create a good shear rate. In the type of mud used during the RTD trials where the Bentonite had to be mixed with fresh water these pumps were not needed and were switched off. Three small gaps 50 cm by 50 cm, are located between the reactors. The first gap is located between the first and second

reactor at the bottom, the second gap is located between the second and third reactor at the top, and the third gap is located between the third and forth reactor at the bottom (Figure 9.1). In case a problem is encountered in any reactor each gap can be controlled by a penstock located at the top of the system to isolate the reactor from the system. In addition there is an emergency channel used to bypass the system if such a problem occurs.

The mixing system is connected to the circulation system at the outlet point, as shown in Figure 9.1. Therefore, the mixed mud leaving the mixing system enters the circulation system and is then pumped to the well for several functions such as cleaning the hole, removal of cuttings, control of formation pressure, maintenance of wellbore stability, cooling and lubrication of the drill bit and transmission of hydraulic power to the bit, before coming back then again to the circulation system. There is no return allowed to the mixing system, thus maintaining control of the mixing system at all times which also prevents any bacterial growth in the system.

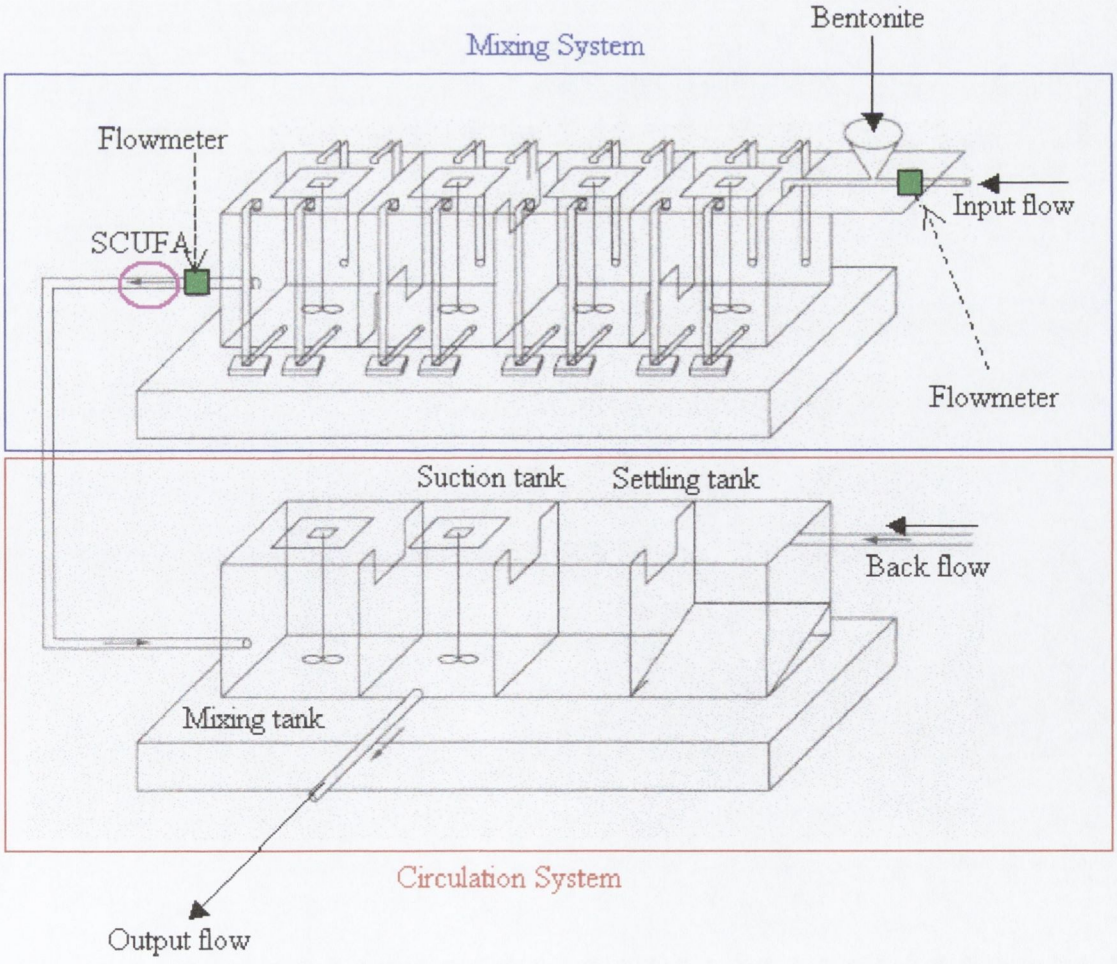

Figure 9. 1 Schematic representation of the Waha Oil Company mixing and circulation system

A circular gap was opened at the top of the outlet pipe between the mixing and circulation system. The SCUFA was calibrated with Rhodamine WT solution (see Appendix A) and was inserted with its Open Optics pointed downwards, as illustrated in Figure 9.2, to allow detection of the effluent tracer concentration. The SCUFA was connected to the computer to export the data onto an Excel© Spreadsheet, as in previous trials.

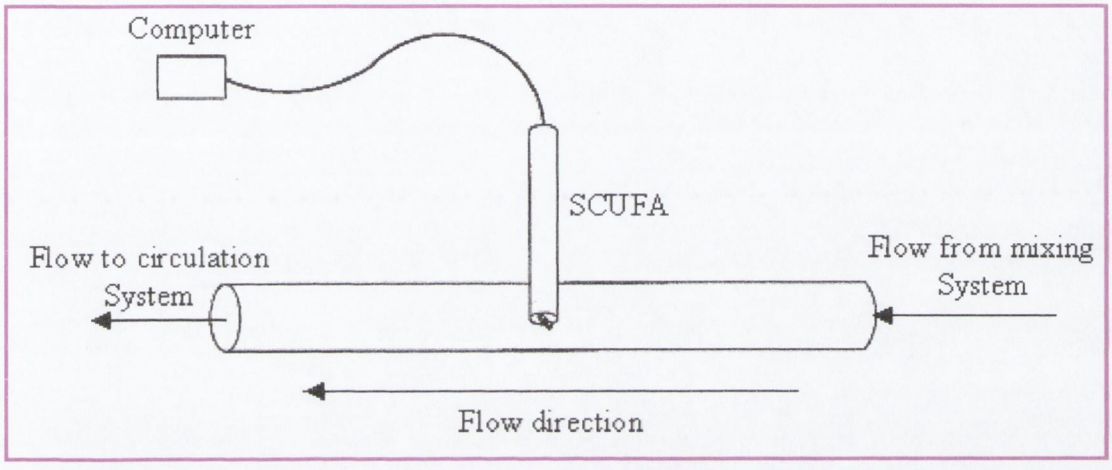

Figure 9. 2 Schematic representation of the SCUFA inside the output pipe

9.1.2 RTD Trials

Two tracer studies were carried out on the mixing reactors network, on 12th and on 13th December 2002. The mixture depth was measured in each reactor at 2m, giving a corresponding volume in each reactor of 48m^3 and total system volume of 192m^3. For both trials the measured flow rate was fixed at 5103.7 L/min, and both the influent and effluent mixture temperatures were 30°C. An initial experiment was performed to assess the SCUFA's ability to measure the tracer concentration accurately in the Bentonite mixture by using a sample of 2 litres of mixture from the system. 2 ml of 0.2g/ml (200,000 mg/l) tracer was added to the Bentonite sample and well mixed. The SCUFA was then inserted into the sample that soon showed that such a method of on-line measurement of the effluent could be used to measure the effluent tracer concentration since the SCUFA measured a concentration of 198.5 μg/l (compared to the target value of 200 μg/l). A quantity of 192 ml of (0.2g/L) Rhodamine WT was then prepared relating to the total reactor network volume (see Appendix A).

9.1.2.1 Trial 1

In this trial all mixers were working at a fixed speed of 1010 rpm as shown in Figure 9.3. The concentrated tracer Rhodamine WT was injected rapidly into the inlet stream just before entrance to the reactor relative to the nozzle as a pulse input to ensure a closed system as much as possible and hence to limit any diffusion up stream. The SCUFA measured the concentration of Rhodamine WT at each time step during the experiment as illustrated in Figure 9.2. The data was then downloaded at the end of the experiment and exported into an Excel© spreadsheet. The model was run to obtain a best fit with the experimental RTD curve from each trial by adjustment of the model parameters (as described previously). In addition, the technique described in Chapter 7 was applied to identify the poorly performing reactor in the system.

The system configurations for this trial are shown in Table 9.1 and the results obtained are shown in Table 9.2. In addition, the corresponding RTD graphs and model curves for this trial are attached in Figures 9.5(a) and 9.6(a).

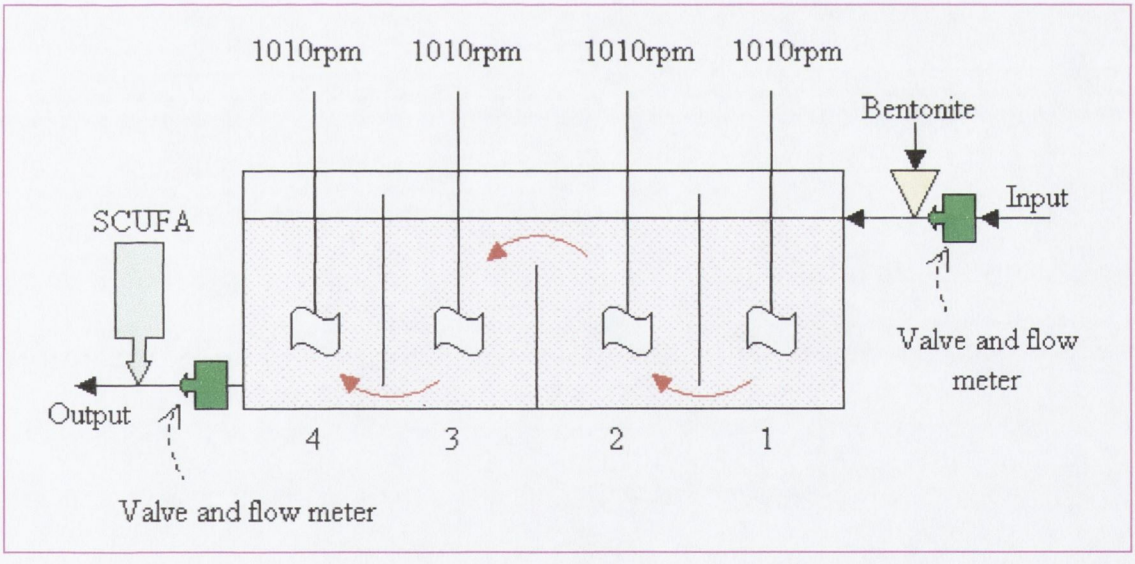

Figure 9. 3 Schematic representation of the Waha Oil Company Mixing system-Trial 1

9.1.2.2 Trial 2

The procedures carried out in the second trial were the same as for the first trial. The only change was that in this trial the mixer in Reactor 2 was deliberately switched off, in order to test the model as shown in Figure 9.4. The system configurations for this

trial are shown in Table 9.1 and the results obtained are shown in Table 9.2. The corresponding RTD graph and model curves are shown in Figures 9.5(b) and 9.6(b).

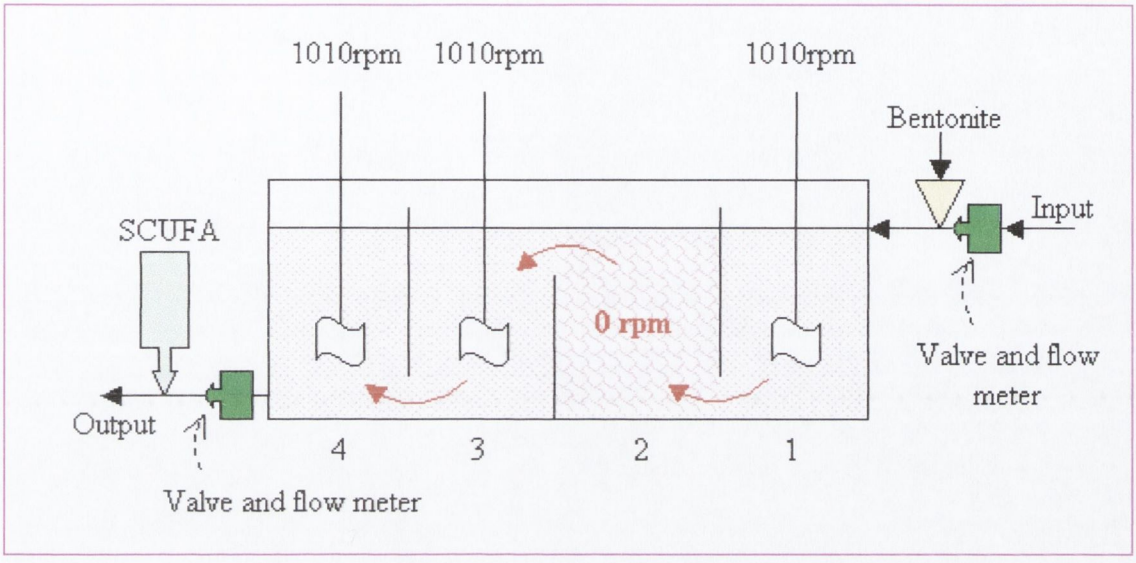

Figure 9. 4 Schematic representation of the Waha Oil Company Mixing system- Trial 2

Trial No.	Reactor Volume	Flow Rate	Mixer Speed Reactor 1	Mixer Speed Reactor 2	Mixer Speed Reactor 3	Mixer Speed Reactor 4	Rhodamine Mass
	(m^3)	(l/min)	(rpm)	(rpm)	(rpm)	(rpm)	(g)
1	192	5103.66	1010	1010	1010	1010	38.4
2	192	5103.66	1010	0	1010	1010	38.4

Table 9. 1 Waha Oil Company trials - experimental configurations

Trial No.	Reactor [1]		Reactor [2]		Reactor [3]		Reactor [4]		Overall System Performance		
	Theoretical retention time at the end of Reactor 1	No. Of CSTR	Theoretical retention time at the end of Reactor 2	No. Of CSTR	Theoretical retention time at the end of Reactor 3	No. Of CSTR	Theoretical retention time at the end of Reactor 4	No. Of CSTR	P%	D%	S%
	(S)	(n)	(S)	(n)	(S)	(n)	(S)	(n)	(%)	(%)	(%)
1	564.3	0.99	1128.6	2.01	1692.9	2.98	2257.2	4.02	99.7	0.0	0.3
2	564.3	1	1128.6	1.6	1692.9	2.5	2257.2	3.7	87.0	13.0	0.0

Table 9. 2 Waha Oil Company trials - results

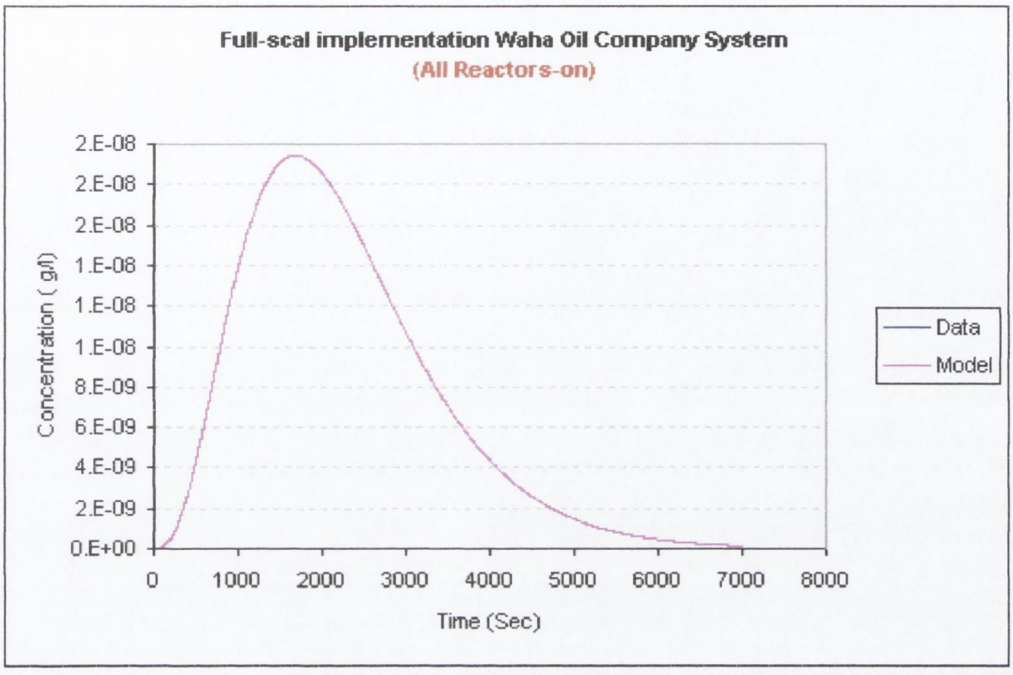

(a)

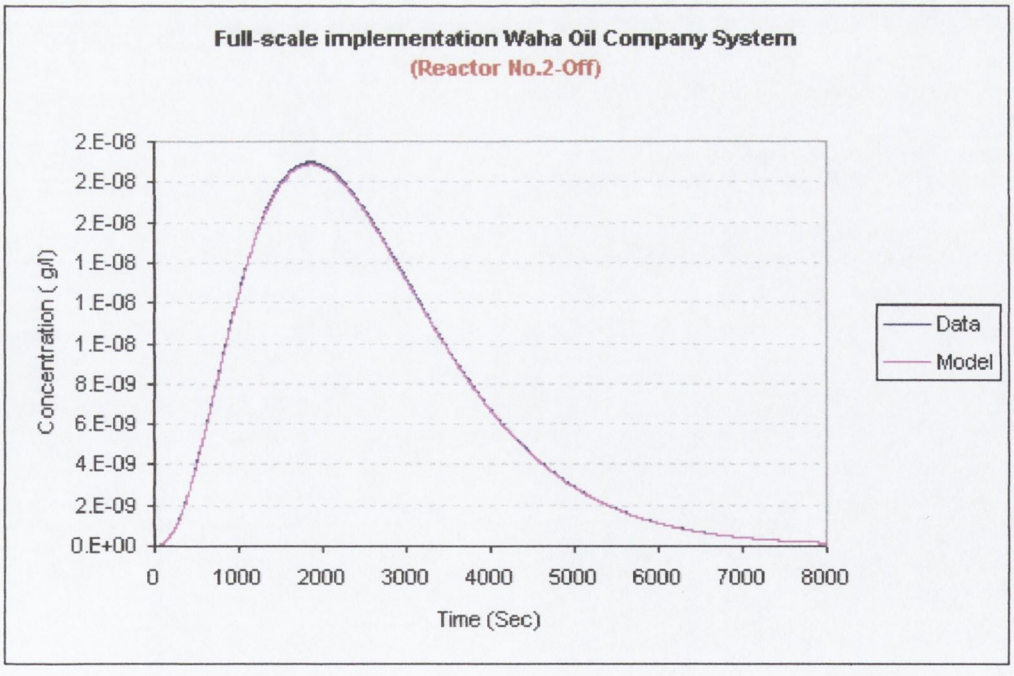

(b)

Figure 9. 5 Graphs showing trial results and fitted model curves for Waha Oil Company mixing system for (a) Trial 1 and (b) Trial 2

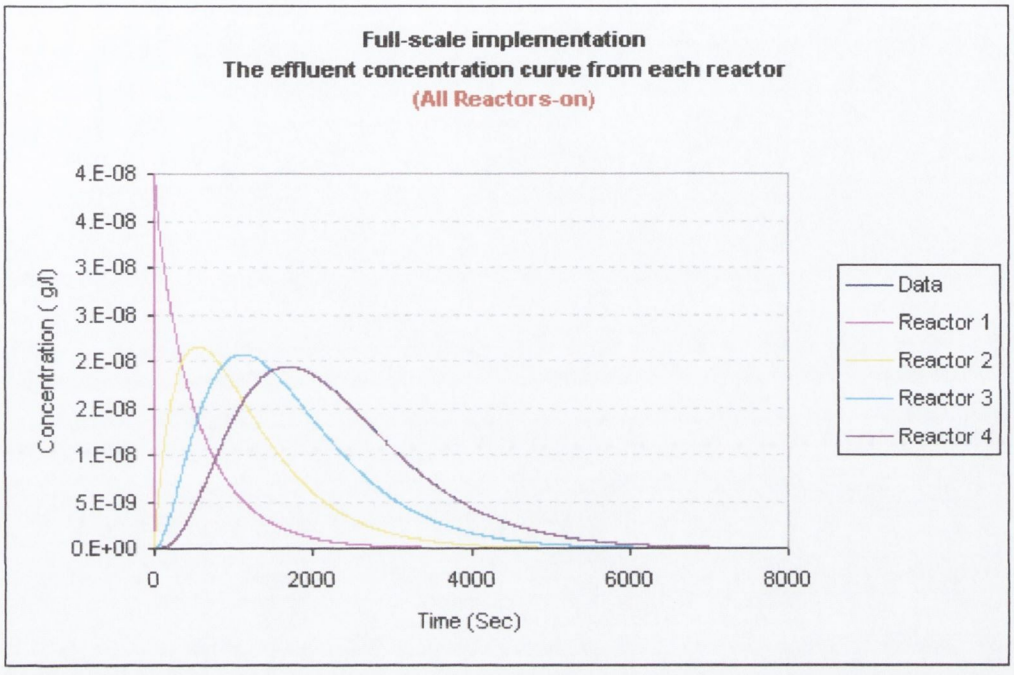

(a)

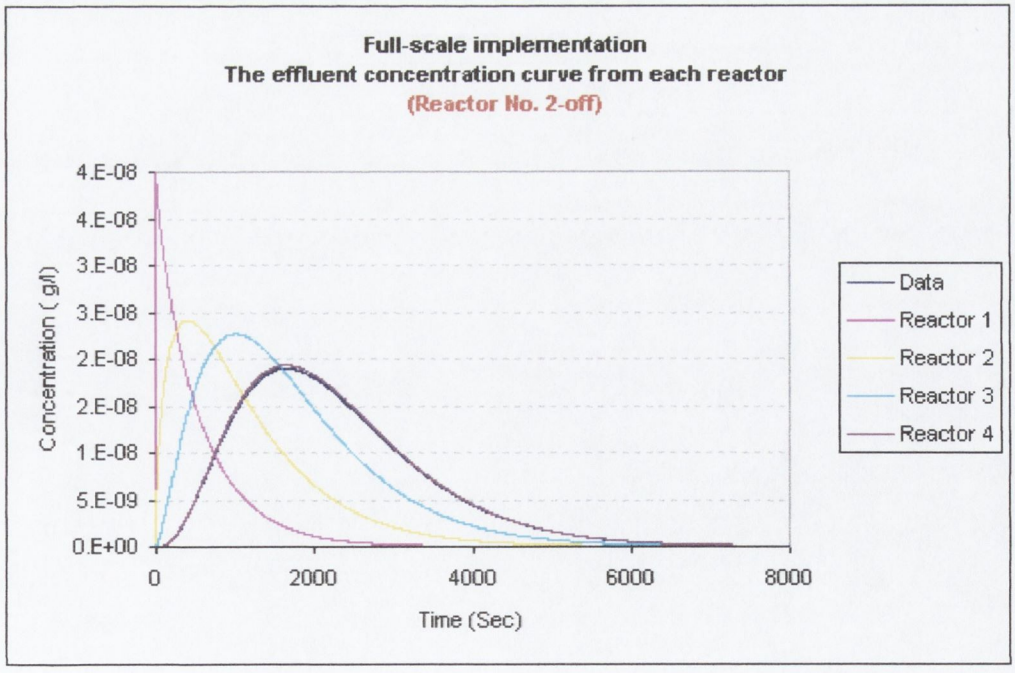

(b)

Figure 9. 6 Graphs showing trial effluent concentration results and fitted model curves from each reactor for Waha Oil Company mixing system for (a) Trial 1 and (b) Trial 2

9.1.3 Tracer Recovery

The tracer recovery for the Rhodamine WT into the Bentonite mixture was calculated for the two trials (as described in Section 8.2.3.1) giving an average value of 98.8% which is shown graphically for the two trials in Figure 9.7: this is in line with the findings of Smart and Laidlaw (1977).

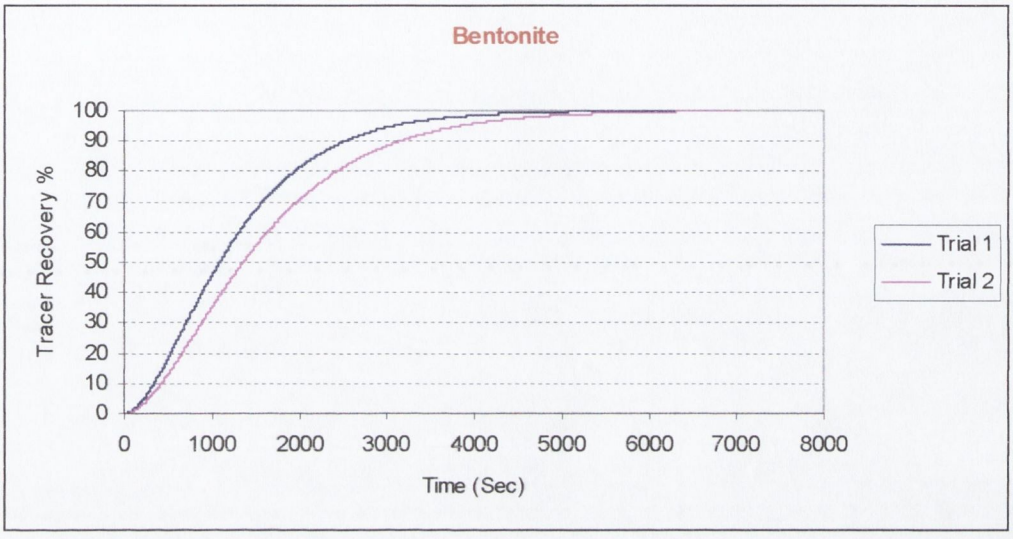

Figure 9. 7 Graph showing the tracer recovery for Bentonite

Hence, no adjustment to the effluent concentrations was required to take account of absorption, as had been the case at Greystones WwTW.

9.1.4 Discussion of Results

The tracer data was normalized so that the area under the curve is equal to the mass injected at the beginning; the resultants RTDs for both trials are illustrated in Figure 9.5. The model results are shown in Table 9.2. Both trials recorded the tracer arriving at the outlet within the same time with similar high peaks, followed by a slow, steady decrease but with different shaped tails. As shown in Figure 9.5(a) in the first trial the tail stopped after 7000 seconds while in the second trial it stopped after 8000 seconds. The long tail for Trial 2 indicates that the system was operating inefficiently and suffering from dead-zones, which would be predicted in this case because the mixer in Reactor 2 was deliberately switched off resulting in a delayed retention of the tracer. When the graphs are compared some differences in curve shape between the two runs are visible. In Trial 1 the concentration curve over the whole system matches exactly the concentration curve which was obtained by applying the **n** = 4 constraint on the

mathematical model. In Trial 2 the effluent concentration curve does not exactly match the modelled curve, with the same **n** = 4 constraint on, particularly in the tail which is significantly longer indicating that the system is not behaving as 4 perfectly mixed CSTRs. The model was also used to see whether it was possible to diagnose which reactor was not working properly. Table 9.3 shows the differences between the prediction for the number of tanks in-series **n** for Reactor 1 compared to Reactor 2. In Trial 1 the differences in **n** between Reactors 2 and 1 is equal to 1.02 that indicates that there is not a problem in Reactor 2. However, in Trial 2 the differences between Reactor 2 and 1 is only equal to 2.50 indicating that there is a problem in Reactor 2 (as discussed in Chapter 7).

Trial No.	Reactor 1 No. Of CSTR	Difference between Reactors 1 and 2	Reactor 2 No. Of CSTR	Difference between Reactors 2 and 3	Reactor 3 No. Of CSTR	Difference between Reactors 3 and 4	Reactor 4 No. Of CSTR
	(n)	(n)	(n)	(n)	(n)	(n)	(n)
1.00	0.99	1.02	2.01	0.97	2.98	1.04	4.02
2.00	1.06	2.50	3.56	1.01	4.57	1.02	5.59

Table 9. 3 Differences between Reactor 1 & 2, Reactor 2 & 3 and Reactor 3 & 4 for Waha Oil Company Trials

This change in the perfectly mixed trace from Reactor 2 has a direct affect on Reactors 3 and 4. In addition, as shown in Table 9.2 there are differences in the percentage of the perfectly mixed flow across the whole system: 99.7% in Trial 1 compared to 87% in Trial 2. This is due to the differences in the velocity gradient G, which had an average value of 718.4 s^{-1} for Trial 1 compared to only 622.6 s^{-1} for Trial 2 as a result of switching off the mixer in Reactor 2, as seen in Table 9.3.

Trial No.	V	n	μ	ρ	D	R_e	Q	k	P	G	P%
	(m^3)	(rps)	(kg/m.s)	(kg/m^3)	(m)		(m^3/s)	Constant	(W)	(s^{-1})	(%)
1	192	16.80	0.000797	995.7	0.42	11107064.73	0.085061	0.32	78979.21	718.42	99.70
2	192	16.80	0.000797	995.7	0.42	11107064.73	0.085061	0.32	59234.41	622.17	86.98

Table 9. 4 Velocity gradient of Waha Oil Company mixing system

9.2 Leixlip Wastewater Treatment Trials

9.2.1 Background

The Leixlip WwTW located in the west of Dublin, Ireland is a secondary treatment extended aeration system (activated sludge) shown in Figure 9.8 which was constructed in 1979 to treat wastewater from a population equivalent of 76648.

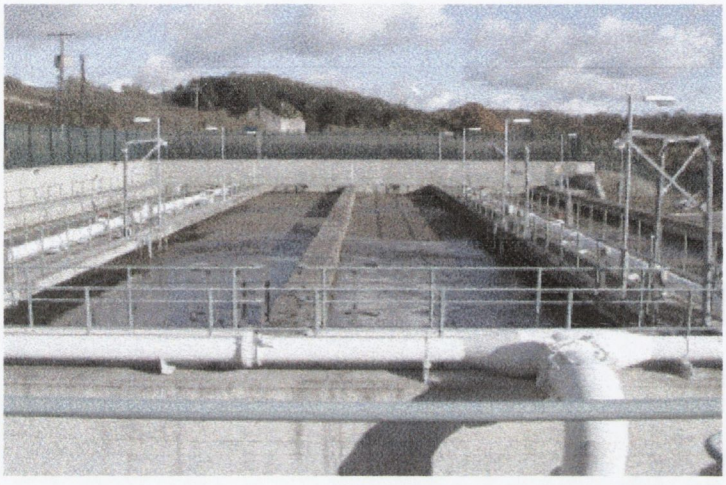

Figure 9. 8 Photograph showing the extended aeration process of Leixlip WwTW

The extended aeration basin consists of two separate systems in parallel as illustrated in Figure 9.9. Each system consists of two long channel reactors in parallel; 47.2 m in length, 6.0 m in depth and 3.0 m in width, fitted with an inlet pipe feed at the bottom of the first reactor to one side. A large gap in the central baffle wall is located at the end between the channels that allows the flow to move around to the second channel as a continuous loop. In addition, there are circulation pumps working as static mixers with flow rates 200 m^3/h and 300 m^3/h for the first and the second systems respectively located at the beginning between the channels, which enables the mixed liquor to be recirculated around the system. The outlet from the basin is located at the top of the second channel which leads to a flow splitter chamber to feed the clarifier tanks, as shown in Figure 9.10. The return activated sludge (RAS) is pumped from the clarifiers back to the inlet chamber in front of the first channel where it mixes with the influent flow.

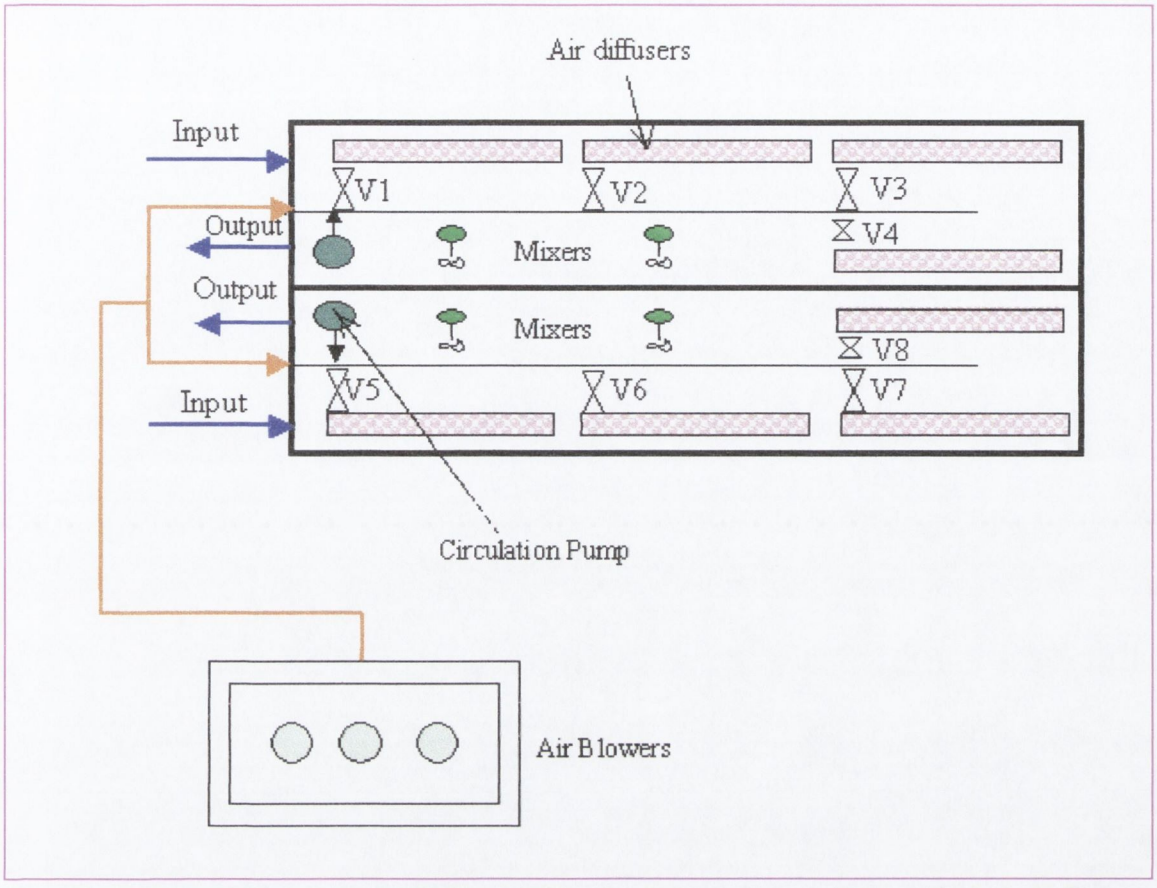

Figure 9. 9 Schematic diagram of the extended aeration process at Leixlip WwTW

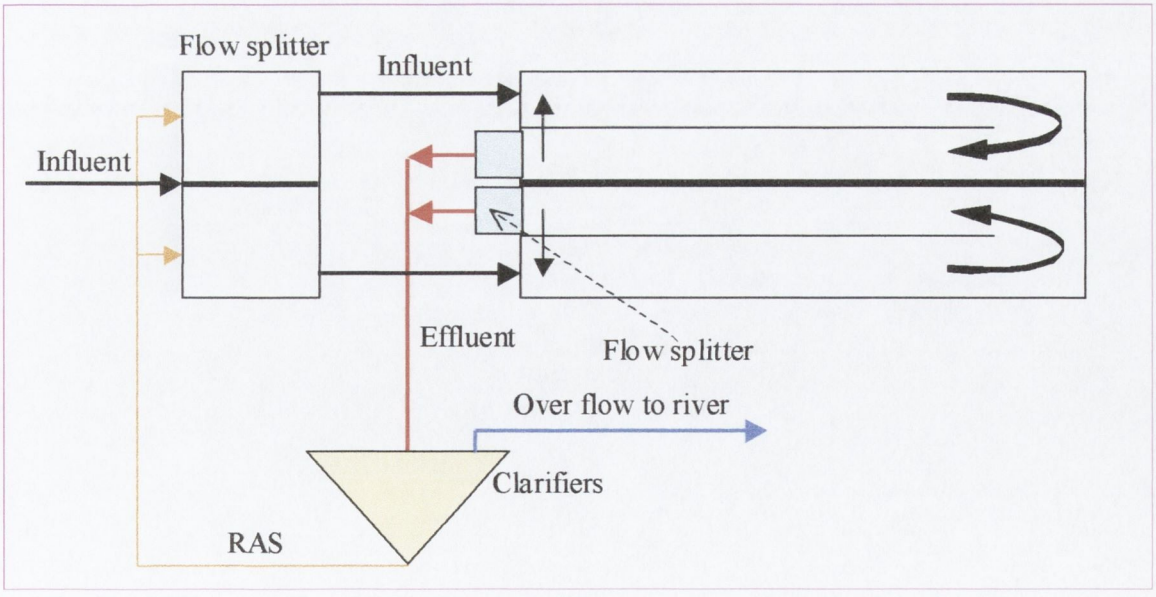

Figure 9. 10 Schematic diagram showing the Return Activated Sludge

The aeration system consists of diffused aeration networks which are connected to a blower station via an air supply header, as shown in Figure 9.9. The aeration has a dual function: to supply oxygen to the aerobic microorganisms in the reactor for respiration and to maintain the microbial flocs in a continuous state of agitated suspension, which ensures maximum contact between the surface of the floc and the wastewater. In addition, each system consists of two mixers as shown in Figure 9.9 to keep the flocs in suspension in zones where aeration is not required due to specific process requirements. Each mixer consists of three blades of square pitch 0.85 m by 0.85 m working at the same speed: 258 rpm and 492 rpm for the first and second system respectively.

9.2.2 RTD Trials

Two tracer studies were carried out, one on each extended aeration channel network on 26th October 2003. The water depth in the channels was measured at 6 m; giving a corresponding volume for each aerated system of 849.6 m^3 and total system volume of 1699.2 m^3. Therefore, a quantity of 699 ml of 0.2 g/ml of tracer was prepared relating to the volume of the aerated systems (see Appendix A). The SCUFA was calibrated with Rhodamine WT solution and the ability of the SCUFA to measure the tracer concentration accurately in the mixed liquour was again examined. As at Greystones WwTW (see Section 8.5.2), the SCUFA could not read the concentration accurately and so the technique of taking discrete samples every 10 minutes, which were then left to settle in order to measure the supernatant concentration, was adopted as before.

9.2.2.1 Trial 1

In this trial the blower station introduced 1342.1 m^3/h and varied airflow rates to each cell of the aerated network, as shown in Figure 9.11, whilst the two mixers were operating at the same speed of 258 rpm.

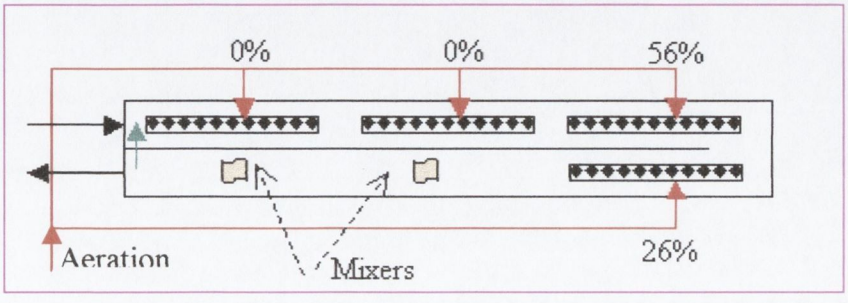

Figure 9. 11 Schematic representation for the airflow network for Trial 1

The Rhodamine WT was injected into the aerated networked channels as a pulse input at the influent chamber as shown in Figure 9.12.

Figure 9. 12 Photograph showing the injection of the tracer into the system

The sample was taken every 10 minutes from the effluent stream (see Figure 9.13) and the tracer concentration as a function of time was measured using the SCUFA device. The flow rate was also recorded every 10 minutes on the SCADA system giving an average flow of 1551.6 m^3/h. In addition, the RAS flow rate was recorded at each 10 minutes time step giving an average of 670 m^3/h and the circulation pump flow rate was fixed throughout the trial period at 200 m^3/h. The water temperature was measured both inside the system (16°C) and in the incoming flow (16°C).

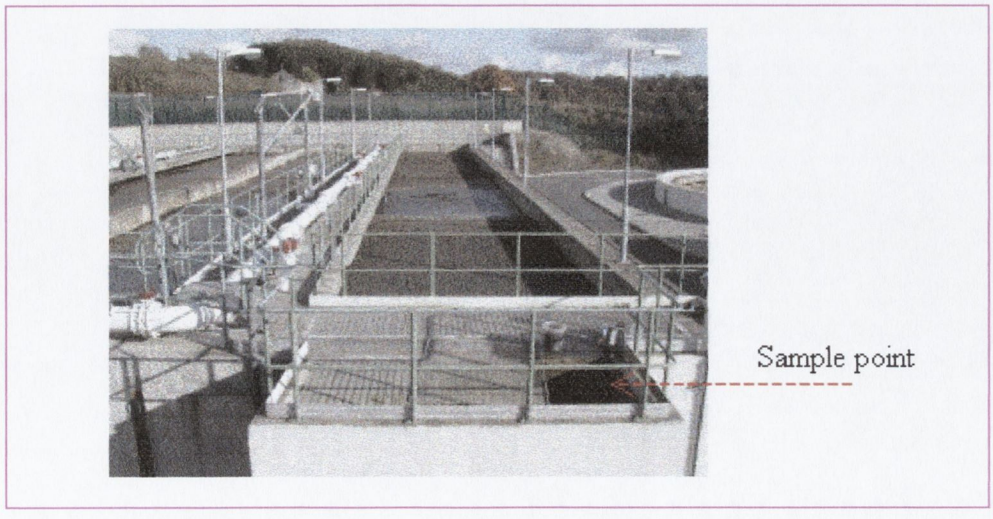

Figure 9. 13 Photograph showing the collection of the sample at the effluent stream

The tracer concentration as a function of time was exported into an Excel© spreadsheet to be analysed. The mathematical model was adjusted to deal with each individual time step for the effluent flow rate but also to include the extra input to this system from RAS flow rate and the circulation pump flow rate. The volume of the aerated network channels was also adjusted as described previously (see Section 8.5.2.1). The system configurations are shown in Table 9.4 and the model results obtained for this trial are shown in Table 9.5. In addition, the corresponding RTD graph and model curves for each trial are presented in Figures 9.15 and 9.16.

9.2.2.2 Trial 2

This trial was carried out on the second extended aeration basin following exactly the same procedures as the first trial. The only change was that the blower station introduced 2050 m^3/h and higher airflow rates to each cell in the aerated network as shown in Figure 9.14. The mixers were also operating at a higher speed of 492 rpm.

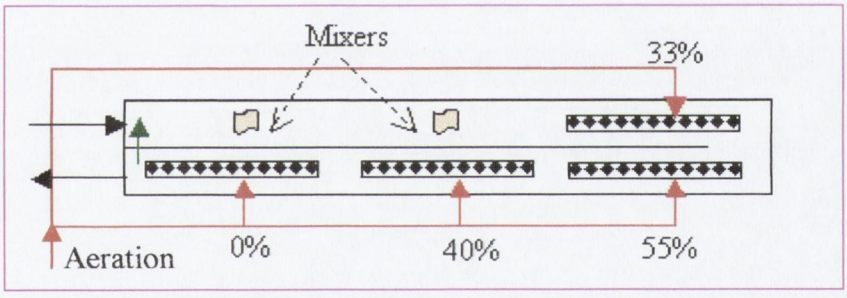

Figure 9. 14 Schematic representation for the airflow network for Trial 2

The flow rate was recorded every 10 minutes as before giving an average value of 1642m^3/h and the average RAS flow 670 m^3/h. The water temperature measured both inside the systems and in the incoming flow was stable at 16°C. The experimental configuration is shown in Table 9.4 and the results obtained for this trial are shown in Table 9.5. In addition the corresponding RTD graph for this trial and the model curves are presented in Figures 9.15 and 9.16.

System No.	Reactor Volume	Average Flow Rate	Rhodamine Mass
	(m^3)	(m^3/h)	(g)
1	1699.2	1551.6	200
2	1699.2	1642.1	200

Table 9. 5 Full-scale implementation Leixlip WwTW - experimental configuration

System No.	Theoretical retention time	No. Of CSTR	P%	D%	S%
	(Sec)	(n)	(%)	(%)	(%)
1	3956.7	7.26	42.2	40.1	17.7
2	3735.5	5.31	69.6	17.3	13.2

Table 9. 6 The results obtained from full-scale implementation model experiments Leixlip WwTW

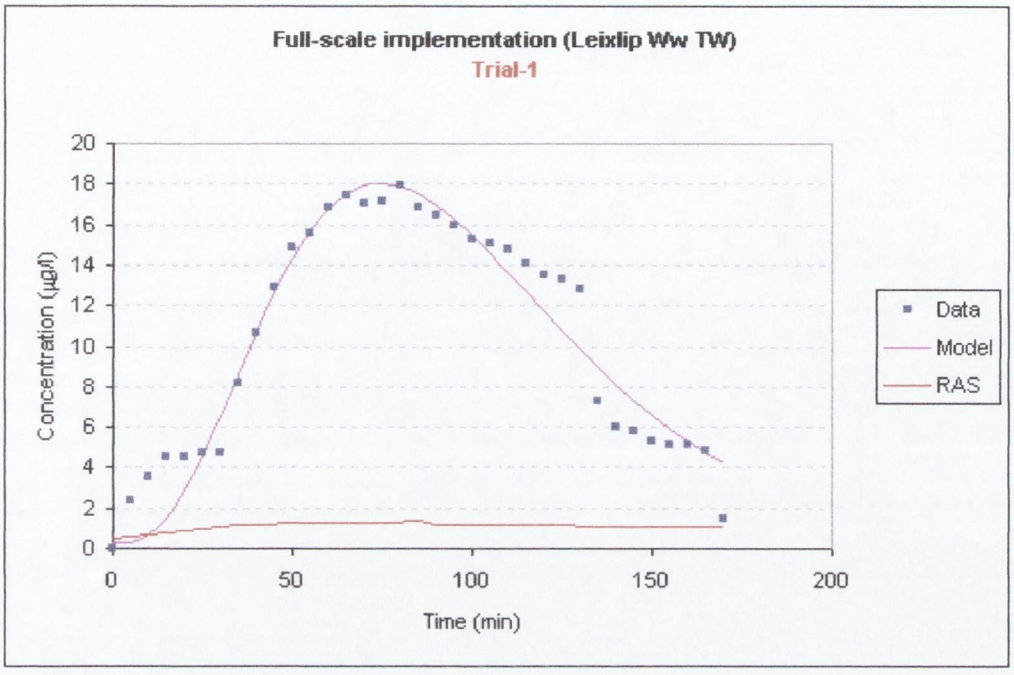

(a)

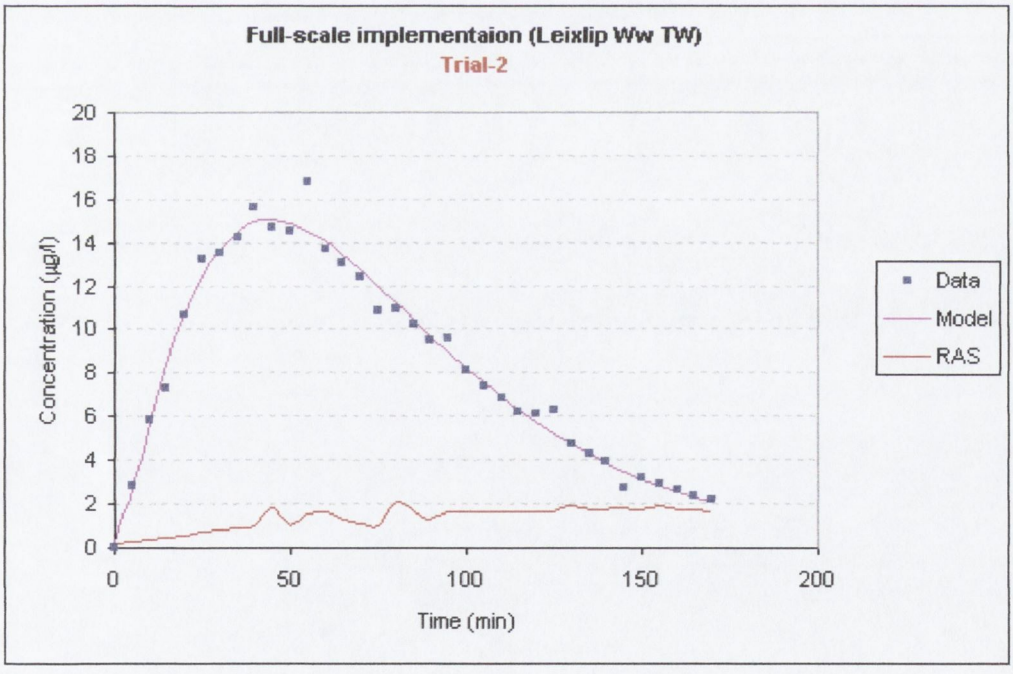

(b)

Figure 9. 15 Graphs showing trial results and fitted model curves for Leixlip extended aerated system for (a) Trial 1 and (b) Trial 2

9.2.3 Results Analysis

The RTD data from both experiments was downloaded and exported into an Excel© spreadsheet. The model was then run using the single Gamma function left to run free (without constraints) to obtain a best fit with the experimental RTD curve from each trial by adjustment of the model parameters (as described previously). For this trial it was not felt appropriate to use the technique described in Chapter 7 to identify a poorly performing reactor in the system since this extended aeration reactor system is designed to operate effectively as a continuous loop with no definable individual reactors. It should be noted that the circulation was taken into account not only in terms of the overall flow round the system (see Figure 9.16) but also in term of feedback of tracer to the inlet (see Figure 9.17). Hence, the effluent concentration of Rhodamine WT at each time step was modelled as an influent concentration due to the recirculation in addition to any other tracer coming back into the system with the RAS.

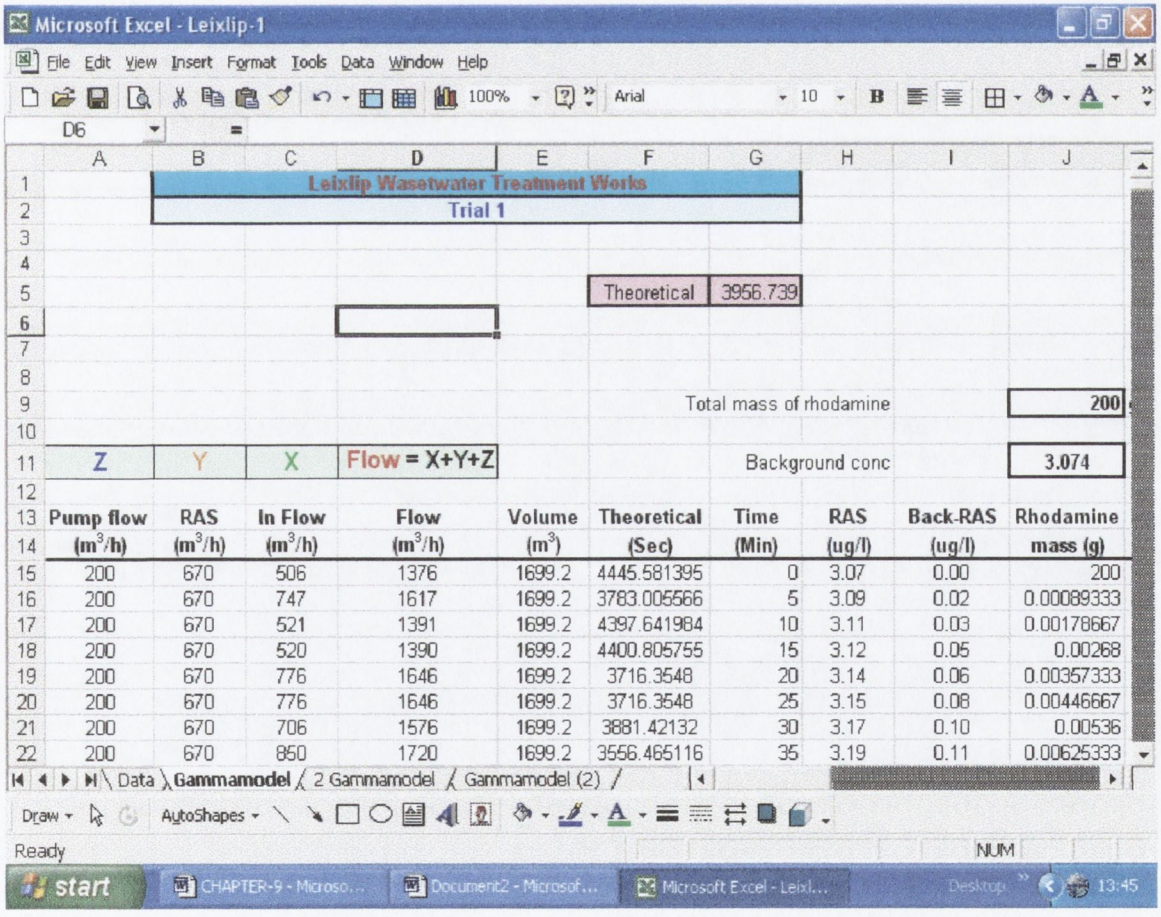

Figure 9. 16 The structure of the model on an Excel© spreadsheet highlighting the flow recirculation (Leixlip WwTW)

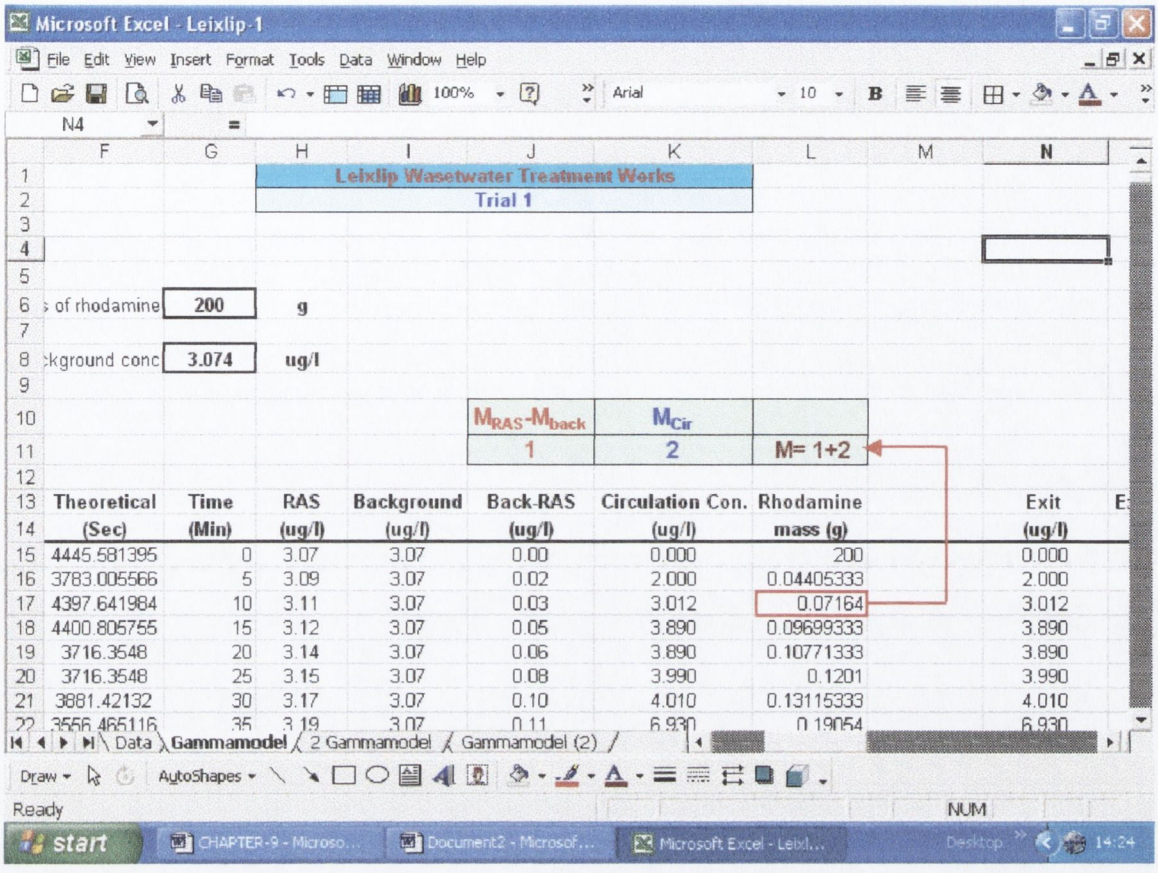

Figure 9. 17 The structure of the model on an Excel© spreadsheet highlighting the tracer mass recirculation (Leixlip WwTW)

9.2.4 Discussion of Results

The results obtained at Leixlip WwTW indicate that there is a significant difference between the two trials as displayed in Table 9.5. In System 1 the model indicates 7.26 reactors in-series whilst in System 2 the model indicates 5.31 reactors in-series. The 5 CSTRs picked out by the model seems to concur with actual system which comprises about 5 mixing zones (see Figure 9.14). The model for Trial 1 however gives 7 CSTRs whilst there only seems to be about 4 distinct mixing zones in reality (see Figure 9.11). Alternatively, the results from both systems indicate that they were behaving close to plug flow which is the general principle behind the design of extended aeration treatment systems. This difference in degree of plug flow must be due to the difference in power input per unit volume and hence the velocity gradient as shown in Tables 9.7, 9.8 and 9.9, giving an average value of 361.88 s^{-1} applied in Trial 1, compared to 804.48 s^{-1} in Trial 2. Hence, the system that had less mixing (System 1) was exhibiting conditions closer to plug-flow which was identified by the model.

System No.	V	W	R	T1	P1	P2	n	e	μ	Q	P	G
	(m^3)	(kg/s)	(kJ/k mol k)	(K)	(atm)	(atm)			(kg/m.s)	(m^3/s)	(W)	(1/s)
1	1699.2	0.327	8.314	289.150	1	1.707	0.283	0.700	0.001139	0.372803	21629.4	106.20
2	1699.2	0.499	8.314	289.150	1	1.707	0.283	0.700	0.001139	0.372803	33311.6	131.19

Table 9. 7 Velocity gradient of extended aerated system at Leixlip WwTW [Blowers]

System No.	V	n	μ	ρ	D	R_e	Q	k	P	G
	(m^3)	(rev/sec)	(kg/m.s)	(kg/m^3)	(m)		(m^3/s)	Constant	(W)	(1/s)
1	1699.2	4.30	0.001139	999.1	1.2	16294364.88	0.372803	0.32	126502.91	255.66
2	1699.2	8.20	0.001139	999.1	1.2	31072974.89	0.372803	0.32	877276.95	673.26

Table 9. 8 Velocity gradient of extended aerated system at Leixlip WwTW [Mixers]

System No.	V	μ	Q	γ	ϖ	K_{SM}	h	P	G
	(m^3)	(kg/m.s)	(m^3/s)	(KN/m^3)	(m/s)	(S^2/m)	(m)	(W)	(1/s)
1	1699.2	0.001139	0.048611	9.790	0.026222	2.50	0.001719	0.00082	0.02
2	1699.2	0.001139	0.083333	9.790	0.026222	2.50	0.001719	0.00140	0.03

Table 9. 9 Velocity gradient of an extended aerated system at Leixlip WwTW [Pumps]

9.2.5 Tracer Recovery

The tracer recovery for each trial was calculated as before *(indicating the adjustment due to the 15% measurement losses as discussed in Section 8.3.2.2)*, giving an average value of 67 % as shown in Figure 9.18, which is similar to the Greystones trials indicating the extent of absorption and up take by the biomass. Hence, the same technique of scaling up the RTD curve retrospectively on the assumption that the

removal of Rhodamine from the solution would have been proportional to time spent in the tank but declining at an exponential rate, was adopted as before.

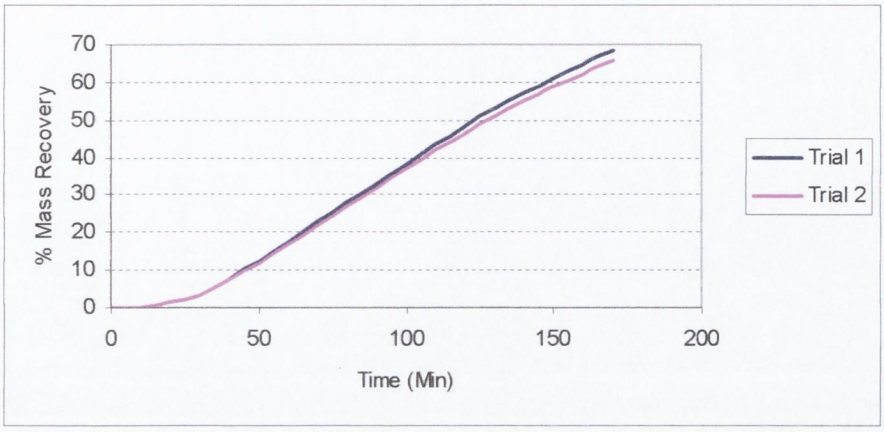

Figure 9. 18 Graph showing the tracer recovery for Leixlip WwTW trials

An exponential curve was fitted to the trial data to recreate the exact amount of Rhodamine mass recovered by the end of the trial. Each original effluent concentration data point was then scaled appropriately to obtain a readjusted data set that showed a mass recovery of 98.5% as shown in Table 9.10. The adjusted data was then entered into the spreadsheet and the model was run to obtain a best fit with the experimental RTD curve from each trial by adjustment of the model parameters (as described previously). The results obtained for these adjustable RTD curves are shown in Table 9.11. In addition, the corresponding graphs of effluent concentration and model curves are shown in Figures 9.19 (a) and (b).

	Tracer recovery
Leixlip WwTW Trial 1	98.5%
Leixlip WwTW Trial 2	99.1%

Table 9. 10 The percentage of Tracer recovery at Leixlip WwTW (modeled Trials)

System No.	Theoretical retention time	No. Of CSTR	P%	D%	S%
	(Sec)	(n)	(%)	(%)	(%)
1	3956.7	6.35	45.3	39.3	15.4
2	3735.5	4.85	73.3	15.8	10.9

Table 9. 11 Model results from adjusted data set (Leixlip WwTW)

The mathematical model picked out **n** = 6.35 and 4.85 for the adjusted effluent concentration RTD curves from System 1 and 2 respectively which still indicates that the systems were behaving close to plug-flow. The results are broadly similar to the previous results (Table 9.6), which again indicates the suitability of Rhodamine WT for such studies using this modelling technique even if the adjustment is not made for the adsorption of tracer by the biomass, as was found at Greystones WwTW.

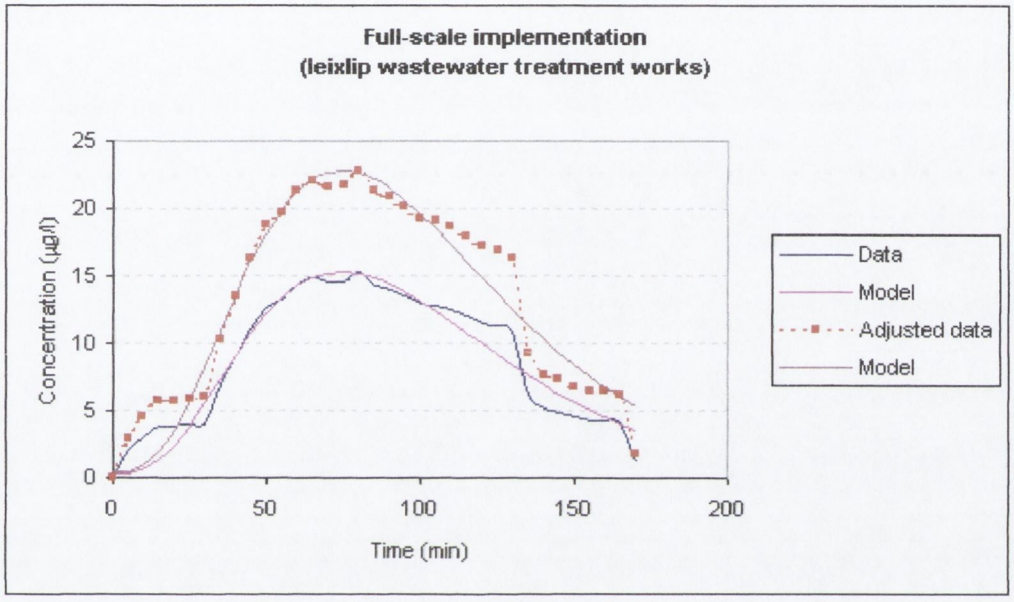

(a) Trial 1

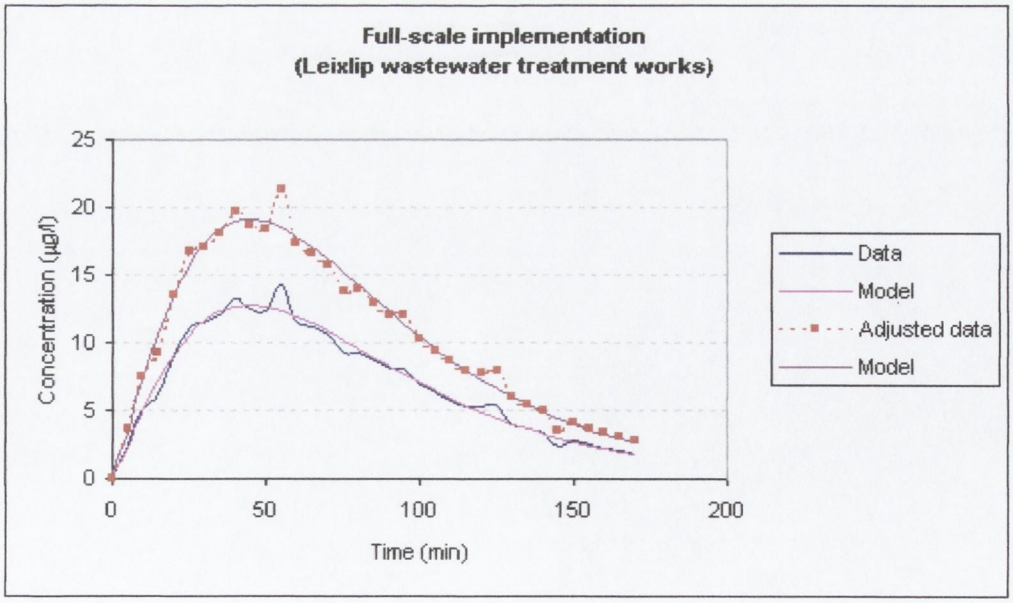

(b) Trial 2

Figure 9. 19 The effluent concentration curve for each Trial for full-scale implementation Leixlip WwTW on adjusted data set

9.3 Overall Comparison of Velocity Gradients

The velocity gradients G achieved in the individual systems located at in this thesis have been determined in the previous sections and are compared here in relation to the performance of these systems. Fundamentally G should be proportional to the degree of mixing attained although there will be variations to this trend according to the geometry of each reactor and the position and type of mixers employed. As discussed in previous sections the velocity gradient is a function of the power input per unit volume which needs to be established in the design or characterisation of any hydraulic mixing system. From the point of view of economy, however, it is important to ensure that the mixers operate at lowest power possible under such conditions, to achieve the required agitation. Table 9.12 shows a comparison of how the velocity gradient has contributed towards to a perfectly mixed environment in each system studied in this thesis. In the case of the Waha Oil Company a perfect mix was obtained with a high velocity gradient ranging from 622.2 s^{-1} to 718.4 s^{-1} a range that also concurs with the results that were reported by Fair *et al.* (1966). Equally, the results that obtained from the laboratory trials show that a perfect mix was obtained with high velocity gradients at an average value of 708.8 s^{-1}. In the case of the Greystones WwTW there was a low percentage of perfect mix due to a low velocity gradients ranging from 145.6 s^{-1} to 157.6 s^{-1}. This concurs to an extent with the results obtained for the laboratory trials which show that when lower values of G were applied, the percentage of perfectly mixed flow picked up by the model reduces. However, as illustrated in Figure 9.20, the reduction in mixing efficiency in the laboratory trials with respect to G is not as extreme as was experienced at Greystones WwTW. This indicates that other aspects of the reactor design (geometry, type and position of the mixer etc) also need to be carefully considered in addition to the gross velocity gradient in order to promote an efficiency mixing system. As shown in Figure 9.20 the perfectly mixed flow falls sharply at a high velocity gradient applied to the circular CSTR, which appears to be contrary to the overall pattern. However, this is due to the onset of vortexing at higher mixer speed as discussed previously. This specific problem has not been encountered for the rectangular shaped CSTRs which also demonstrate a high degree of mixing at relatively low velocity gradients 300 s^{-1} compared to on-site-trials. This difference is probably due to the relatively higher contribution of shear associated with the momentum of incoming flow in the laboratory reactors compared to the larger industrial trialled.

Note: that the results from Leixlip WwTW trials are not included in this comparison since the extended aeration treatment process is not designed as a series of CSTRs in-series and therefore the calculated perfectly mixed percentage is meaningless in this situation.

Comparsion of Velocity Gradient G				
Location	**No. Of CSTR (n)**	**Run No.**	**P%**	**G (s^{-1})**
Waha Oil Company	4	Run 1	99.7	718.4
	4	Run 2	86.98	622.2
Greystones Wastewater treatment works	3	Run 1	40.31	169.4
	3	Run 2	42.07	179.0
Lab		**Mixer speed (rpm)**	**P %**	**G (s^{-1})**
Laboratory [Rectangular CSTR] (R:1)	1	120	93.9	329.4
		200	99.1	708.8
Laboratory [Circular CSTR] (C:1)	1	120	87.2	329.4
		200	77.7	708.8
Laboratory [Rectangular CSTR] (R:3)	3	120	94.3	329.4
		200	99.2	708.8
Laboratory [Rectangular CSTR] (R:4)	4	120	98.5	329.4
		200	99.3	708.8

Table 9. 12 The comparison of velocity gradient G

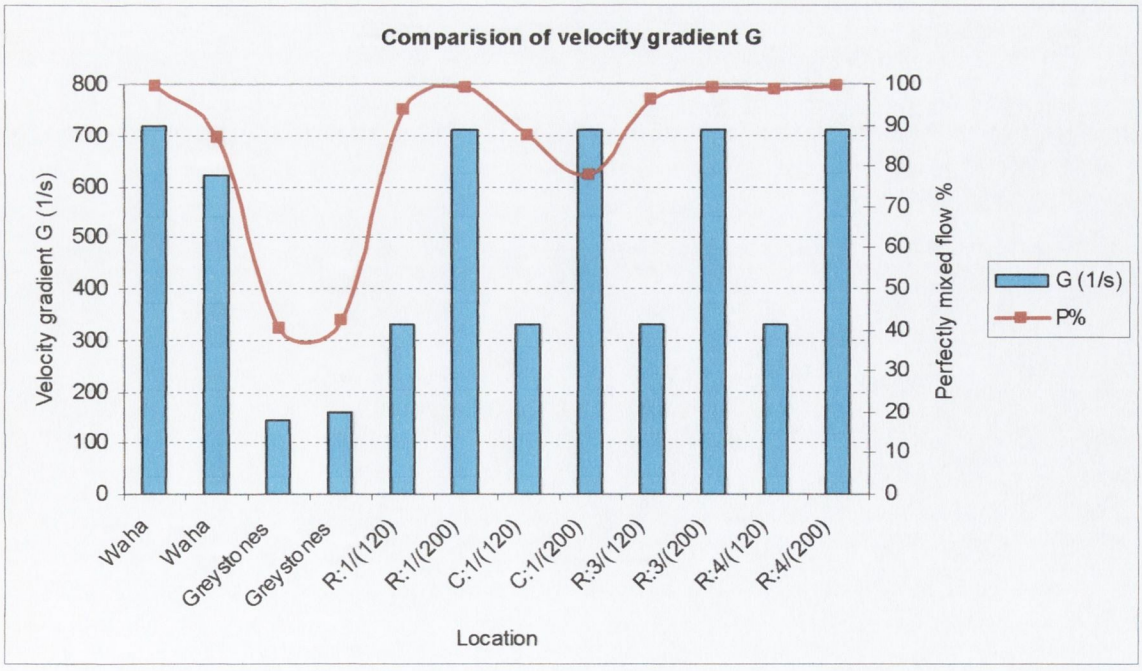

Figure 9. 20 Graph showing the comparison of velocity gradient G against mixing efficiency

Chapter 10

Conclusions

Chapter 10
Conclusions

10.1 Overall Summary

Several tracer studies have been carried out in previous studies on multistage systems where reactors are connected either in parallel or in series systems in order to study the hydraulic behaviour of the network reactors and various theoretical frameworks have been proposed, some of which are reviewed in Chapter 2. The body of scientific literature available on this subject has provided considerable help in the understanding of how such studies might be approached; although several researchers have studied the behaviour of tank hydraulics each from different perspectives, thus encouraging an impetus towards originality for any new researcher. This thesis has attempted to research those areas hitherto not covered sufficiently and, in particular, has attempted to evaluate the relative percentages of flow pass through dead-zones, short-circuits and perfectly mixed zones in reactors. It has also attempted to provide a diagnostic tool for the identification of a particular reactor in a network of reactors that may be creating a problem which can then hopefully be corrected.

From a purely academic point of view, the present research draws its motivation from a desire to see a more complete and comprehensive study made in this field. Further motivation has been found in its relevance and immediate application in the economic sphere. In the water industry and in the oil industry (especially for the drilling processes outlined in Chapter 9) an understanding of the mixing of fluids within reactor units is crucial where either a homogeneous product is required or the volume of the reactor needs to be optimally used for the specific reaction for which it was designed. The problem of obtaining such hydraulic behaviour in an industrial process is the focus of the present study so that such non-idealities may in future be effectively dealt with and eliminated. The solving of such a problem obviously leads to economic savings, for example, in production and maintenance costs.

The basic concepts and formulae relevant to residence time distributions RTD have been reviewed (see Chapter 2) in order to ensure a clear understanding of their characteristics which can be generated by the mixing processes of a chemical reactor. From these principles, a mathematical model (based upon the Gamma distribution) has been developed (see Chapter 3) to fit to the RTD curves from tracer studies carried out on reactor systems and thereby evaluate its hydraulic characteristics.

A number of experiments were run on model reactors in the laboratory to test the mathematical model. A circular CSTR was first tested (see Chapter 4) and some modifications were undertaken in order to create specific hydraulic problems (dead-zones and short-circuit) which can arise in reactors (see Chapter 5). Trials on multiple reactors (see Chapter 6) were then performed on a variety of CSTR configurations in the laboratory in order to study the validity of this model further and in addition, develop the technique in order to identify which reactor in a network was not performing as a perfect CSTR (see Chapter 7). Finally, three trials were undertaken on full-scale operating systems (in the water and oil industry) to evaluate the model's ability for such an implementation.

10.2 Conclusions

The experimental and theoretical work undertaken within the scope of this research has led to the following conclusions:

- The validity of using the pulse input method of tracer injection compared to step input method was proved. Its advantage is primarily in the use of smaller quantities of tracer, which can be very important in terms of cost. Furthermore, the total duration of the pulse input measurement will always be shorter than that of a step input procedure which also requires more sophisticated equipment for the injection of tracer to maintain a constant tracer concentration in the feed point compared to the pulse input method advantage, particularly when highly active tracer solutions are to be injected.
- The level of mixing calculated by the tracer and modelling technique when the mixer was at low speeds for the circular CSTR was 39.7% and for the rectangular

CSTR was 47.7%. This concurs with the results reported by Cloutier and Cholette (1968) who measured 38% perfect mix under similar condition one rectangular reactor. A maximum mixing level in the laboratory experiments was found to be 99% at 200 rpm which again can be compared with a level of 100% at 220 rpm reported by Cloutier and Cholette (1968).

- The modifications trials undertaken on the circular CSTR in the hydraulics laboratory (Chapter 5) have demonstrated that the mathematical model could identify undesirable hydraulic characteristics in a reactor, such as the dead-zones and short-circuits which can often create problems in real reactors in industry.
- The trials undertaken on a rectangular CSTR model, starting from one CSTR and progressing up to four reactors in series (Chapter 6) at different mixer speeds and reactor geometries affecting flow directions, have demonstrated that the model is able to pick up the differences hydraulic performance between the systems.
- A Comparison of the results obtained from the circular CSTR and those obtained from the rectangular CSTR indicates that there is an optimum mixer speed and hence energy efficiency to achieve perfect mixing for specific reactor shapes.
- The trials undertaken on both the circular and rectangular CSTRs in the laboratory have demonstrated that the velocity gradient is an important property for characterizing the mixing rate that occurs inside the reactor although efficient mixing is also a function of the reactor shape. In the circular CSTR an increased the velocity gradient led to a better mixing rate up to a maximum level at 179.31/s and then decreased again due to onset of vortexing. Conversely, in the case of the rectangular CSTR the same increase in velocity gradient led to increasingly better mixing with no reduction in efficiency at the higher velocity gradient. In addition, the results that were obtained from various input and output configurations in the laboratory and also the full-scale implementations have demonstrated that when the velocity gradient was high the appearance of the flow short-circuiting decreases. For example, the mathematical model picked out **n** = 19.8 and 15.6 tanks in-series for Trial 1 and 2 respectively in Greystones when the velocity gradient increased from 169.42 in Trial 1 to 179.33 in Trial2.

- The laboratory trials on the networked reactors revealed that the influent position, effluent position and baffle configuration within reactors can have a large affect on hydraulic performance and mixing efficiency. However, such problems in the geometric design of reactors can be overcome by increasing the energy input from the mixers.
- Several trials undertaken in multiple-reactor configurations also proved the ability of the model to pick out a specific reactor that was not performing correctly and hence demonstrated its use as a diagnostic tool to eliminate such undesirable problems. The technique has been developed which enables individual tanks to be hydraulically characterized.
- The technique has also been used successfully to diagnose the mixing problems in a full-scale operational Activated Sludge aeration tank which, in turn has also given some insight into the process problems experienced at the plant. The poor geometric design and low shear velocities from the diffused aeration seem to be responsible for the inadequate mixing.
- The trials carried out in high concentrations of bacteria with relatively long residence times have shown that Rhodamine WT is absorbed. However, the results achieved as part of this thesis have indicated that the use of the tracer in conjunction with the modelling method proposed still give an accurate hydraulic characterisation of the reactor systems.
- The results obtained so far indicate that there is a definite potential in this technique, for further implementation at full-scale plants as was shown in the successful trials on the Bentonite mixing tanks for the oil industry and the extended aeration, treatment process which was shown to be operating close to plug flow.

10.4 Recommendations for Further work

Although an attempt has been made, within the scope of the present research, to cast more light on the problems related to networked reactors, a great deal more research is required

in this area before one can fully characterise any hydraulic system. It would, therefore, be desirable to examine the following areas in further detail:

- An examination of the effect adjusting baffle spacing and gaps on multiple tank in-series-models.
- The use of dispersion models to compare against the results obtained using this tank in-series model would prove interesting.
- The use of Computational Fluid Dynamics (CFD) to model a real system in parallel and thus provide a compassion to results obtained using this tank in-series model should also be undertaken.
- It would also be important to build up the modelling application in a more suitable computer programme by using a computer language such as Visual Basic or using a package such as MATLAB so as to eliminate errors and control the functions more easily.
- More research should be undertaken into the kinetics of absorption of different tracers and tracer uptake by bacteria as found in wastewater treatment process.
- It would also be important to draw a temperature profile at same depth points and with different stages along the reactor length in real plants (for example, Greystones WwTW), which could allow the researcher to cast more light on the density differences.

After such research has been carried out the tracer technique and modelling approach could be more developed to yield more incisive levels of understanding regarding the behaviour of hydraulic systems.

REFERENCES

References

Babcock, R. E., Green, D. W. and Perry, R. H. (1966). Longitudinal dispersion mechanism in packed beds. *A. I. Ch. J.* **12**, 922-927.

Bellamy, W., Carlson, K., Pier, D., Ducoste, J. and Carlson, M. (2000). Determining disinfection needs. *J. Am. Wat. Wks Assoc.* **92** (5), 44-52.

Bello-Mendoza, R. and Sharratt, P.N. (1999). Analysis of Retention Time Distribution (RTD) curves in an anaerobic digester with confined-gas mixing using a compartment model. *Wat. Sci. Tech.* **40** (8), 49-56.

Bischoff, K. B. (1963). The general use of imperfect pulse inputs to find characteristics of flow systems. *Can. J. Chem. Eng.***41**, 129.

Bolton, W. (1995). Mathematics for engineering. 3rd Edition William, Oxford, Newness.

Bowmer, K. H. (1987). Nutrient removal from effluent by an artificial wetland: influence of rhizosphere aeration and preferential flow studied using bromide and dye tracers. *Wat. Res.*, **12,** 591-599.

Breen, P. F. and Chick, A. J. (1995). Rootzone dynamics in constructed wetlands receiving wastewater: a comparison of vertical and horizontal flow systems. *Wat. Sci. Tech.*, **32**(3), 281-290.

Brown, M. C., Wigley, T. L., and Ford, D. C. (1969). Water budget studies in karst aquifers. *J. Hydro.* **9**(1), 113-116.

Buchanan, T. J., (1964). Time of travel of soluble contaminations in streams. *Sanit. Eng. Div. Amer. Soc. Civil Eng.*, **90**(SA3), 1-12.

Buffamb. A. B and Gibilarol, G. (1968). The analytical solution of the Deans-Levich model for dispersion in porous media. *Chem. Engng. Sci.* **23**, 1399-1401.

Buffham, B. A. (1971). On the residence time distribution for a system with velocity profiles in its connections with the environment. *Chem. Eng. Sci.* **27**, 987-991.

Buffham, B. A., and Kropholler, H. W. (1970). The washout curve, residence time distribution, and F curve in tracer kinetics. *Math. Biosci.* **6**, 179-184.

Buffham, B. A., and Kropholler, H. W., (1973). Tracer kinetics: some general properties, the mean residence time distribution and applications to phase and chemical equilibria. *Chem. Eng. Sci.* **28**, 1081-896.

Cairns, E. L., and Perlmutter, D. D. (1960). Longitudinal mixing in packed beds. *Chem. Eng. Sci.* **12**, 20-34.

Camp, T.R., and P.C.Stein. (1943). Velocity and internal work in fluid motion. *J. Boston Soc. Civ. Eng.* **30**, 209.

Cengel, Yunus. A. (2003). Heat transfer: a practical approach. 2nd Edition. New York; London: McGraw-Hill.

Cha, L. C., and Fan, L. T. (1963). Age distributions for flow systems. *Can. J. Chem. Eng.* **41**, 62-66.

Chapple, L. (1985). A Study of Bacterial Kinettics and Hydraulic Shortcircuiting in Sewage Lagoons. Masterate Thesis. University of Queensland.

Chapra S. C. (1997). Surface water-quality modelling. 2nd Edition. New York, London, McGraw-Hill.

Charles, H. N. (1996). Moment analysis of trace. *J. Envir. Eng. ASCE.* **122,** 12. 1121-1123.

Chiang, D. and Cholette, A. (1971). Internal age and residence time distributions of a fluid in non-ideal stirred tanks in series. *Can. J. Chem. Engng*, **49**, 484-487.

Cholette, A. and Cloutier, L. (1959). Mixing Efficiency Determinations for Continuous flow Systems. *Cana .J of Chem. Eng* 105-112.

Church, M., and Kellerhals. (1970). Stream gauging techniques for remote areas using portable equibment. *Tech. Bull.* **25**, 90-95.

Clark, and William, J. (1977). Water supply and pollution control. 3rd Edition. New York, London: Harper.

Clark, M. M. (1996). Transport Modelling for Environmental Engineers. Wiley Interscience, New York.

Cloutier, L. and Cholette, A. (1968). Effect of various parameters on the level of mixing in continuous flow system. *The Can. Jour. of Chem. Engin* **46**, 82-88.

Cobb, E. D., and Bailey, J. F., (1965). Measurement of discharge by dye dilution methods. *Surface Water Techniques of the U. S. Geological Survey*. **1** (14), pp26.

Colburn, A. P., (1935) The theory of short-circuit. *TRANS. A. I. Ch.E* **31,** 457-458.

Cooke, M. H., and Bridgwater, J. (1952). The relationship between Variance and sample size for mixtures. *Appl. Sci. Research*, **3**, 279-296.

Crozes, G. F., Hagstrom, J. P., Clark, M. M., Ducoste, J. and Burns, C. (1998). Importing Clear well Design for CT Compliance. *American Water Works Association Research Foundation, Denver.*

Curl, R. L., and McMillin, M. L. (1966). Accuracies in residence time measurement. *AICHE J.* **12**, 819-822.

Danckwerts, P. V. (1959). The effective of incomplete mixing on homogeneous reactions. *Chem. Eng. Sci. 8* .**2**, 93.

David, R., and Villermaux, J. (1975). Micromixing effects on complex reactions in a CSTR. *Chem. Eng. Sci.* **30**, 1309-1313.

De Nevers, N. (1991). Fluid Mechanics for chemical engineers 2nd Edition. McGraw-Hill, New York.

Deaner, D. G. (1970). A producer for conducting dye tracer studies in chlorine contact chambers to determine detention times and flow characteristics. Reprint11269, 3pp., G. K. *Turner Associates, Palo, Alto, Calif.*

Denbigh, K. G. (1944). Velocity and yield in continuous reaction systems. *Trans. Faraday. Soc.* **40,** 352-373.

Doheim, M. A., and collinge, C. N. (1980). Contact time distributions in fluidised bed reactors. *Chem. Eng. Sci.* **19**, 39-56.

Dole, R. B. (1906). Use of fluorescein in the study of underground waters. In U.S. Geol. Surv. *Water Supply Pap.* **160**, edited by M.C. Fuller, 73-83.

Douglas, J. F. and Francis, J. (1917). Fluid Mechanics. 2nd Edition. London, ELBS.

Douglas, J. M. (1964) The effect of mixing on reactor design. *AICHE Symp. Ser. 48.* **60**, 1.

Drew, D. P., (1968). Tracing percolation water in karst areas. *Trans. Cave. Res. Group G. Brit.* **10**(2), 103-104.

Everts, C.J. and Kanwar, R.S. (1994). Evaluation of Rhodamine WT as an adsorbed tracer in an agricultural soil. *J. Hydrol.* **153**, 53-70.

Fair, G.M.; Geyer, J.C. and Okun, D.A. (1966). Water and wastewater engineering. New York: London: Wiley.

Falconer R. A. and Tebbutt T. H. Y. (1986). A theoretical and hydraulic model study of a chlorine contact tank. *Proc. Instn Civ. Engrs.* **81**(2), 255-276.

Falconer, R. A. and Liu, S. Q. (1987). Mathematical model study of plug flow in a chlorine contact tank. *Journal of the Institution of Water and Environmental Management.* **1**(3), 279-290.

Fogler, H. S. (1992). Elements of chemical reaction engineering. 2nd Edition. Prentice-Hall.

Frederick, G. L. and Lloyd, B. J. (1996). An evaluation of retention time and short-circuiting in waste stabilisation ponds using Serratia marcescens bacteriophage as a tracer. *Wat. Sci. Tech.* **33** (7), 49-56.

Froment, G. F., and Bischoff, K. B. (1979). Chemical reactor analysis and design. Wiley, New York.

Fu, B., Weinstein, H., Bernstein, B., and Shaffer, A. B. (1971). Residence time distribution of recycle systems- integral equation formulation. *Ind. Eng. Chem. Process design develops*. **10**,501-508.

Geary, P.M. (2004). Effluent tracing and the transport of contamination from a domestic septic tank. *Proceedings of the 1st International Conference on Onsite Wastewater Treatment and Recycling (IWA)*. Freemantle, Australia: 11-13 February 2004.

Gibilaro, L. G. (1971). The recycle flow-mixing model. *Chem. Eng. Sci*. **26**, 229-304.

Gibilaro, L. G. (1975). On the residence time distribution for systems with open boundaries. *Chem. Eng. Sci*. **33**, 1069-1047.

Gibilaro, L. G. (1977). Mean residence time in continuous flow systems. *Nature*. **270**, 47-48.

Glover, R. R., (1972). Optical brighteners-A new water tracing reagent. *Trans. Cave. Res. Group G. Brit.* **14**(2), 84-88.

Gunn, D. J. (1971). Axial dispersion in packed beds: the effect of the quality of packing. *Trans. Inst. Chem. Engrs*. **49**, 109-113.

Haas, C. N., Joffe, H. M. and Jacangelo, J. (1997). Continuous flow residence time distribution function characterization. *J. Environ. Engng ASCE 123.* **2**, 107-114.

Haddad, A. H., and Wolf, D. (1967). Residence time distribution function for multi-stage systems with back mixing. *Can. J. Chem. Eng*. **45**, 100-104.

Hahn, G. J. (1994). Statistical models in engineering. 3rd Edition. Wiley, Chichester, New York.

Hans van Haren and M. J. Howarth. (2004). Enhanced stability during reduction of stratification in the North Sea. *Continental Shelf Research* **24**. 805-819.

Hansen, W. H., Fitzhugh, O. G., and Williams. (1958) Subacute oral toxicity of nine D & C coal tar colours, *J. Pharmacol. Exp. Ther.* **122**, 29A.

Hart, F. L. (1979). Improved hydraulic performance of chlorine contact chambers. *J. Wat. Pollut. Control Fed.* **51**(12), 2868-2875.

Hersey, J. A. (1975). Ordered mixing: A new concept in powder mixing practice. *Powder Tech*. **11**, 41-44.

Hibly, J. W. (1981). Definition and measurement of the degree of mixing in liquid mixtures. *Int. Chem. Eng*. **21**, 197-204.

Higgins, P. R., Alkhadar, R. M., Phipps, D. A., and Andoh, R. Y. G. (1999). Investigation into the retention time distribution of a hydrodynamic vortex separator. J. CIWEM, **13**, 255-261.

Ives, K.J. and Hoyer, O. (1998). Tracer studies of the hydraulics of tapered flocculation. *Wat. Sci. Tech.* **37** (10), 69-77.

Jenkins, D., Richard, M.G. and Daigger, G.T. (2004). Manual on the causes and control of activated sludge bulking, foaming and other solids separation problems.3rd edn. CRC Press / IWA Publishing.

Joel, D.; Kenneth, C. and William, B. (2001). The integrated disinfection design framework approach to reactor hydraulics characterization. *Journal of Water Supply: Research and Technology- AQUA.* **50**(4), 245-261.

Kadlec, R. H. (1993). Flow patterns in constructed wetlands. In: *Hydraulic Engineering.* **1**, Shen, H. W., Su, S. T. and Wen, F. (eds). American Society of Civil Engineers, New York.

Kadlec, R. H. (1994). Detention and mixing in free water wetlands. *Ecological Engineering.* **3**, 345-380.

Kadlec, R.H. and Knight, R. L. (1996). Treatment Wetlands. Lewis, Boca Rotan.

Kafarov V. V., Arva P., Dorokhov I. N., and D. Vargane D. (1971). Analysis of a cellular model with stagnant zones for flows in packing. *Theo. Found. Chem. Engng*, **5**, 18-26.

Kan, K. M., and Greenfield, P. F. (1983). A residence –time model for Trickle-flow reactors Incorporating Incomplete Mixing in Stagnant Regions. *A. I. Ch. E. J.* **29**, 123-132.

Kappel, M. (1979). Development and application of a method for measuring the mixture quality of miscible liquids. *Int. Chem. Eng.* **19**, 196-215.

Kilpatrick, F. A. (1967). Dye-dilution discharge measurements made under ice cover in Laramie River at Laramie, Wyoming. *U.S. Geol. Surv. Water Recourse. Div. Bull.* 41-47.

Kilpatrick, F. A. (1968). Flow calibration by dye dilution measurements made. *Civil. Eng.*, **38**(2), 74-76.

King, A.C., Mitchell, C.A. and Howes, T. (1997). Hydraulic tracer studies in a pilot scale subsurface flow constructed wetland. *Wat. Sci. Tech.* **35** (5), 189-196.

Klinkenberg, A. (1966). Distribution of residence times in a cascade of mixed vessels with backmixing. *Ind. Eng. Chem. Fundamentals.* **5**, 283-285.

Klinkenberg, A., and Sjenitzer, F. (1948). Holding-time distributions of the Gaussian type. *Chem. Eng. Sci.* **5**, 258-270.

Levenspiel, O. (1999). Chemical reaction engineering. 3rd Edition. Wiley, Chichester, New York.

Lewis, D. C.; Kriz, G. J. and Bughy, R. H. (1966). Tracer dilution sampling technique to determine hydraulic conductivity of fractured rock. *Water Resour. Res.*, **2**(3), 533-542.

Lin, S. H., (1980). The residence time distribution for laminar, Non-Newtonian flow in annuls with negligible diffusion. *Chem. Eng. Sci.*, **35**, 1477-1480.

Little, L. W., and Lamb, J. C., (1973). Acute toxicity of 46 selected dyes to Fathead minnow (Pimephales promelas), in dyes and the environment. *American Manufacturers Institute, New York, 1. Chap 5.*

Louie, D. S. and Fohrman, M. S., (1968). Hydraulic model studies of chlorine mixing and contact chambers. *Journal of the Water Pollution Control Federation*. **40**(2/1), 174-184.

Macdonald, R. and Ernst, A. (1986). Disinfiction efficiency and problems associated with maturation ponds. *Wat. Sci. Tech.* **18** (10), 19-29.

MacDonald, R. W., and Piret, E. L. (1951). Continuous flow stirred tank reactor systems. *Chem. Eng. Prog.* **47**, 363.

MacMullin, R. B. and Weber, M. J. (1953). The theory of short-circuiting in continuous flow mixing vessels in series and the kinetics of chemical reactions in such systems. *Transactions of AICHE*. **31**, 409.

MacMullin, R. B., and Weber, M., J. (1935). Determining the efficiency of continuous mixers and reactor. *Chem. Met. Eng.* **42**, 254-257.

Mangelson, K. A. and Watters, G. Z. (1972). Treatment efficiency of waste stabilization ponds. *Journal of the Sanitary Engineering Division, ASCE* **SA2**, 407-425.

Mann, U., and Crosby, E. J. (1973). Cycle time distributions in circulating systems. *Chem. Eng. Sci.* **28**, 623-627.

Marais, G. V. R. (1974). Faecal bacterial kinetics in stabilization ponds. *Journal of the Environmental Engineering Division, ASCE*. **EE1**. 120-139.

Marecose do Monte, M. and Mara, D. (1987). The hydraulic performance of waste stabilisation ponds in Portugal. *Water Science Technology*. **19**(12), 219-227.

Marske, D. M. and Boyle, J.D. (1973). Chlorine contact tank design – a field evaluation. *Water and Sewage, January*. 71-77.

Masschelein, W. J. (1991). Unit Processes in Drinking Water, Marcel Dekker. New York.

Mayomo, J. A. (1971). Residence time distributions of a series of laminar stages. *Can. J. Chem. Eng.* **49,** 691-694.

Metcalf and Eddy, Inc. (2001). Wastewater Engineering Treatment and Reuse. New York; London: McGraw-Hill, 2001©.

Metcalf and Eddy. Inc. (1981). Wastewater Engineering: Collection and Pumping of Wastewater. McGraw-Hill, New York.

Michelsen, M. L., and Ostergaard, K. (1970). The use of residence time distribution data for Estimation of parameters in the axial dispersion model. *Chem. Eng. Sci.* **25**, 583-592.

Millbury, W. F., Pipes, W. O. and Grieves, R. B. (1965). Compartmentalization of aeration tanks. *Journal of the Sanitary Engineering Division, Proceedings of the American of civil Engineers*, **91**, SA3 45-61.

Moreno, M., (1990). A tracer study of the hydraulics of facultative stabilisation ponds. *Wat. Res.* **24**(8), 1025-1030.

Murphy, K. L. and Timpany, P. L. (1935). Design and analysis of mixing for an aeration tank. *Journal of the Sanitary Engineering Division, Proceeding of the American of Civil Engineers.* **93**, SA5 1-15.

Nauman, E. B. and Buffham, B. A. (1983). Mixing in continuous flow systems. New York: Wiley.

Nauman, E. B., and Buffham, B. A. (1977). Limiting forms of the residence time distribution in recycle systems. *Chem. Eng. Sci.* **32,** 1233-1236.

Nauman, E. B., and Buffham, B. A. (1979). A note on residence time distribution for recycle systems. *Chem. Eng. Sci.* **34,** 1057-1058.

Orcutt, J. C., Davidson, J. F., and Pigford, R. L. (1962). Reaction time distributions in fluidized catalytic reactors. *Chem. Eng. Prog. Symp. Ser.* **58**, 1-15.

Orth, P., and Schugerl, K. (1972). Distribution of residence times and contact times in packed reactors: Influence of the chemical reaction. *Chem. Eng. Sci.* **27**, 497-509.

Ostergaard, K., and Michelsen, M. L. (1969). On the use of the imperfect tracer pulse method for determination of hold-up and axial mixing. *Can. J. Chem. Eng.* **47,** 107-112.

Pedahzur, R., Nasser, A., Dor, I., Fattal, B. and Shuval, H. (1993). The effect of baffle installation on the performance of a single cell pond. *Wat. Sci. Tech.*, **27** (7-8), 45-52.

Peplinski, D.K. (2000). Computational fluid dynamics modelling of rectangular disinfection clear wells. MS Thesis, North Carolina State University, Raleigh.

Perry, R. H.; Editor. , Don W. Green; assistant editor, James O. Maloney. (1984). Perry's chemical engineering handbook. London, New York, McGraw-Hill.

Petho, A. (1968). Notes on the Determination of the residence time distribution in continuous-flow systems. *Chem. Eng. Sci.* **23,** 807-810.

Pinto, G., and Tadmor, Z. (1970). Mixing and residence time distribution in melt screw extruders. *Poly. Eng. Sci.***10**, 279-288.

Pritchard, D. W., and Carpenter, H. J. (1960). Measurement of turbulent diffusion in estuarine and inshore waters. *Bull. Int. Ass. Sci. Hydrol.* **20,** 37-50.

Pryce, C., and Gunn, D. J. (1969). Dispersion in Packed beds. *Trans. Inst. Chem. Engrs.* **47,** 341-350.

Raghurman, J., and Varma, Y. B. G. (1970). A model for residence time distribution in multistage systems with cross-flow between active and dead regions. *Chem. Eng. Sci.,* **28.** 585-591.

Ranade, V. R., and Ulbrecht, J. J. (1981). The residence time distribution for laminar flow of Non-Newtonian liquids through helical tubes. *Chem. Eng. Commun.* **8**, 165-176.

Rao, D. P., and Edwards, L. L. (1973). Mixing effects in Stirred tank reactors: A comparison of models. *Chem. Eng. Sci.* **28**, 1179-1192.

Rehakova. M. and Novosad. Z. (1968). Residence time distribution and fraction conversion for a multistage reactor with back mixing between real stages. *Chem. Engng. Sci.* **23**, 139-145.

Retallick, W. B. (1965). Distribution of residence times in a cascade of mixed vessels with backmixing. *Ind. Eng. Chem. Fundamentals.* **4**, 88-90.

Reynolds, E. R. C. (1966). The percolation of rainwater demonstrated by fluorescent dye. *J. Soil Sci.* **17**(1), 127-132.

Rippin, D. W. T. (1967). The recycle reactor as a model of incomplete mixing. *Ind. Eng. Chem. Fundamental.* **6,** 488-492.

Robinson, D. W., and Donaldson, D. (1967). Pontacyl brilliant pink as a tracer dye in the movement of water in phreatophytes. *Water Resour. Res.* **3**(1), 203-211.

Rubinovitch, M., and Mann, U. (1979). The limiting residence time distribution of continuous Recycle systems. *Chem. Eng. Sci.* **34,** 1309-1317.

Rushton, J. H. (1952) Mixing of Liquids in Chemical Processing, *Industrial Engineering Chemistry*, Vol. **44**, No. 12.

Rushton, J.H. (1943). Mixing of liquid in chemical processing. *Ind. Eng. Chem.* **44,** 1952.

Sanjay Reddy, P. E. (2001) Computer simulation reduces cost of chlorine in wastewater plant by 66%. *Journal Articles Fluent Software Users.* JA**115,** 1-3.

Shiau, B.J., Sabatini, D.A. and Harwell, J.H. (1993). Influence of Rhodamine WT properties on sorption and transport in subsurface media. *Ground Water* **31** (6), 913-920.

Shilton, A., Wilks, T., Smyth J. and Bickers, P. (2000). Tracer studies on a New Zealand waste stabilisation pond and analysis of treatment efficiency. *Wat. Sci. Tech.* **42** (11), 342-348.

Smart, P. L. and Laidlaw, I. M. S. (1977). An evaluation of some fluorescent dyes for water tracing. *Water Recourse Research, 13*,**1**, 15-33.

Smart, P. L., and D. I. Smith. (1976). Water tracing in tropical regions; The use of fluorometric techniques in Jamaica. *J. Hydr.* **30**, 179-195.

Smith, S. A. R., and L. G. Kepple. (1972). Infiltration measure in sanitary sewers by dye-dilution method. *Water Sewage Works.* **Jan**. 58-61

Society of Dyers and Colourists. (1971), Colour Index, 3rd ed., Bradford England.

Stevenson, D. G., (1995) The Design of Disinfection Contact Tanks, J. CIWEM, Vol. **9**, 146-152.

Stokes, R. L., and Nauman, E. B. (1970). Residence time distribution functions for stirred tanks in series. *Can. J. Chem. Eng.* **48**, 723-725.

Sturm, P. W., and Johnston, W. E. (1950). Field experiments with chemical tracers in flood waters. *Prod. Mon.* **Dec** 11-17.

Tai, D.Y. and Rathbun, R.E. (1988). Photolysis of Rhodamine WT dye. *Chemosphere* **17** (3), 559-573.

Teefy, S. (1996). Tracer Studies In Water Treatment Facilities: A Protocol And Case Studies. Catalog no 90690. American Water Works Research Foundation, Denver.

Trudgill, S.T. (1987). Soil water dye tracing, with special references to the use of Rhodamine WT, Lissamine FF and Amino G Acid. *Hydrol. Proc.* **1**, 149-170.

Trussell, R. R., and Chao, J.L. (1977). Rational design of chlorine contact facilities. *Journal of the Water Pollution Control Federation.* **April** 659-667.

Turner, J. C. R. (1971). The interpretation of residence time measurements in systems with or without mixing. *Chem. Eng. Sci.* **26**, 412-428.

Uluatam, S. and Kurum, Z. (1992). Evaluation of the wastewater stabilisation pond at the METU treatment plant. *International Journal of Environmental Studies.* **41**(1-2), 71-80.

Van De Vusse J. G. (1962) A new model for the stirred tank reactor. *Chem. Eng. SCI.* **17**, 507-521.

Vansswaaij W. P. M., Charpentierj. C. and Villermauxj. (1969). Residence time distribution in the liquid face of trickle flow in packed columns. *Chem. Engng. Sci.* **24**,1083-1095.

Veeraraghavan S. and Silveston P. L. (1971). Residence time distribution in short tubular vessels. *Can. J. Chem. Engng*, **49**, 346-353.

Viessman, Warren. (1993). Water supply and pollution control. 5th Edition. New York: HarperCollins.

Villemonte J. R. and Rohlich G. A. (1962). Hydraulic characteristics of circular sedimentation basins. Proc. 17th Industrial Waste Conference, Purdue University, 682-702.

Webb, J. M., Hansen, W. H., Desmond, A., and Fitzhugh, O. G. (1961) Biochemical and toxicological studies of Rhodamine B and 3.6-diaminofloran, *Toxical. Appl. Pharmacl.* **3**(6), 696-706.

Weber, A. P. (1953) The design of commercial continuous-reactor systems. *Chem. Eng. Prog.* **49,** 26-33.

Wehner, J. F., and Wilhlm, R. H. (1956). Boundary condition of flow reactor. *Chem. Eng. Sci.* **6**, 89.

Wein, O., and Ulrecht, J. (1972). Residence time distribution in laminar flow systems. *Collect Czech. Chem. Commun.* **37**, 412-428.

Weinstein, H., and Adler, R. J. (1967). Micromixing effects in continuous chemical reactors. *Chem. Eng. Sci.* **22**, 65-75.

Wolf. D. and Resnick. W. (1965). Experimental study of residence time distribution in a multistage fluidised bed. *Ind. Engng. Chem. Fundls.* **4**, 77-81.

Worrel, G. R., and Eagle ton, L. C. (1964). An Experimental study of mixing and segregation in a stirred tank reactor. *Can. J. Chem. Eng.* **42**, 254-258.

Wright, R. R., and Collings, M. R. (1964). Application of fluorescent tracing technique to hydrologic studies. *J. Amer. Water Works Ass.* **56**, 748-754.

Yotsukura et al. (1970). Measurement of mixing characteristics of Missouri River between Sioux City, Iowa and Plattsmouth, Nebraska. *U.S. Geol. Surv. Water. Supply. Pap.* **29**.

Zwietering, T. N. (1959). The degree of mixing in continuous flow systems. *Chem. Eng. Sci.* **11**, 1-15.

Appendix A

SCUFA Calibration

Appendix A
SCUFA Calibration

A1. Introduction

The SCUFA was calibrated using Rhodamine WT solution, prepared in the laboratory.

The linear range of the SCUFA is: $0 \rightarrow 100 ppb \rightarrow 100 \mu g / l$. The SCUFA was therefore calibrated to 100ppb=0.1ppm.

A2. Calibration Procedure

The concentration of Rhodamine WT used to calibrate SCUFA was prepared step by step as illustrated below (Figure A.1) where,

1. 1 ml of original Rhodamine (20% powder of Rhodamine per weight) was dissolved into 999 ml of distilled water = 200mg/l Rhodamine concentration,
2. 1 ml of 200ppm solution was dissolved into 999 ml distilled water = 0.2ppm and,
3. 500ml of 0.2ppm was dissolved, into 500ml distilled water = standard of 0.1ppm = 100ppb.

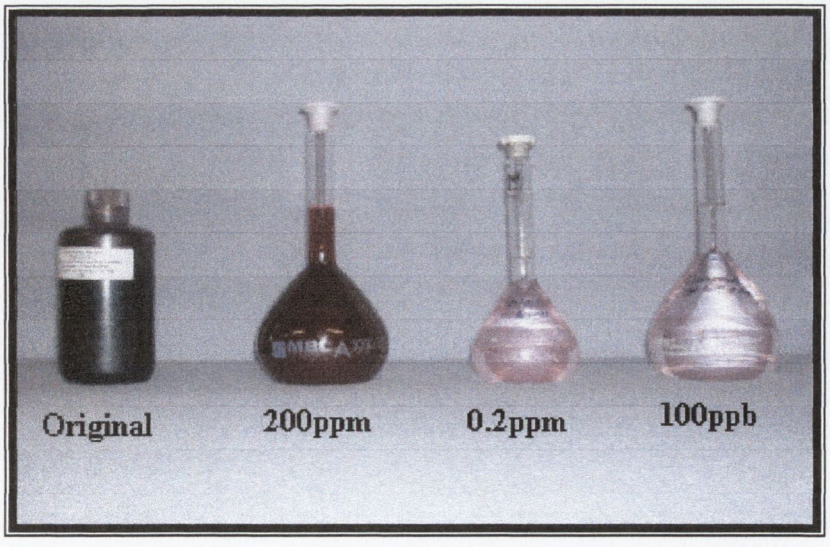

Figure A. 1 Rhodamine WT solution at different concentrations

The first time the SCUFAsoft program is started; a communication screen automatically appears which allows the appropriate communication to be designated for the SCUFA and communication is established. The SCUFA real-time output can be seen on the right hand side of the tool bar (see Figure A.2).

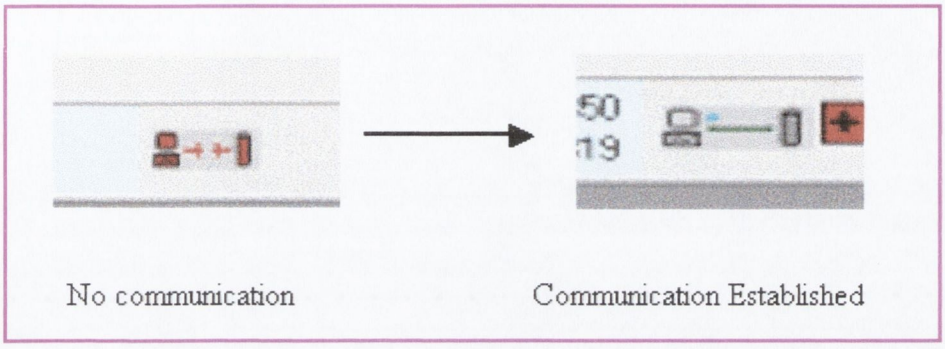

Figure A. 2 Communication Icons tool bar

The output is updated at a rate of 1 Hz. This real-time output will always override any programmed sampling intervals when the instrument is communicating with SCUFAsoft. The SCUFA Fluorometer can be calibrated to convert the fluorescence output into a direct concentration. To perform this, a blank sample, a primary calibration standard and / or a secondary, solid standard will be needed. The calibration procedure is a 7-step process that must be conducted through the interface software.

Step-1 Channel.

Choose the appropriate channel, Fluorescence, which is configured for Rhodamine WT.

Step-2 Calibration Standard Concentration.

Set the standard concentration value. The calibration standard value must be between 0.001 and 999.9 µg/l. A value of 100 µg/l was generally chosen for these studies.

Step-3 Blanking.

Check the Subtract Blank Box in order to have the blank signal automatically subtracted from sample readings using a sample of clean water as the blank.

Step-4 Calibration.

The SCUFA optics are then submerged with the optics downwards into a known concentration of 100µg/l Rhodamine WT, prepared previously, and the Calibration

button was clicked. The standard is read over a 15 seconds period and an average reading appears.

Step-5&6 Confirmation and Finish.

Steps 5 and 6 transfer and store the calibration data into the SCUFA.

Step-7 Solid Standard

In addition, a solid secondary standard can be used as a reference to the initial calibration. The solid standard was snapped onto the optical head of the SCUFA and adjusted until the desired signal was reached. The Record Button is clicked; the solid standard is measured and averaged over a 15 second period.

A.3 Original Rhodamine Concentration Calculation

The calculation of the amount of Rhodamine WT to inject into each RTD study is calculated as follow, based on the volume of the reactor and SCUFA detection range. In these studies the target peak effluent concentration was chosen to be 100µg/l. The original concentration of Rhodamine WT required for a pulse input experiment (and hence also the volume of Rhodamine WT to be added to each experiment) was calculated using Equation A.1, (see worked example).

$$C_0 = \frac{(C * V)}{V} = \frac{(\overline{C} * X)}{V} \qquad ----------(A1)$$

Where:

X= Original volume of Rhodamine to be added to the experiment (ml).

$\overline{C}$ = Original concentration of Rhodamine (µg/l)

C_0= Initial concentration of Rhodamine (µg/l)

Worked Example:

Original concentration of Rhodamine =200,000 µg/l

Initial concentration of Rhodamine =100µg/l

Reactor volume=20L

X=??

The volume of Rhodamine WT to be added to the experiment in order to get 100μg/l peak is:

$$X = \frac{100\frac{\mu g}{l} \times 20l \times 1000\frac{ml}{l}}{200{,}000\frac{\mu g}{l}} = 10ml$$

Equally, the Rhodamine WT mass added to the reactor can be evaluated as follows:

$$M = 0.0002g/ml \times 10ml = 0.002g$$

Appendix B

Graphs for Pulse Input and Step Input Preliminary Experiments (Circular CSTR)

Appendix B
Graphs for Pulse Input and Step Input Experiments

B.1 Pulse Input Graphs

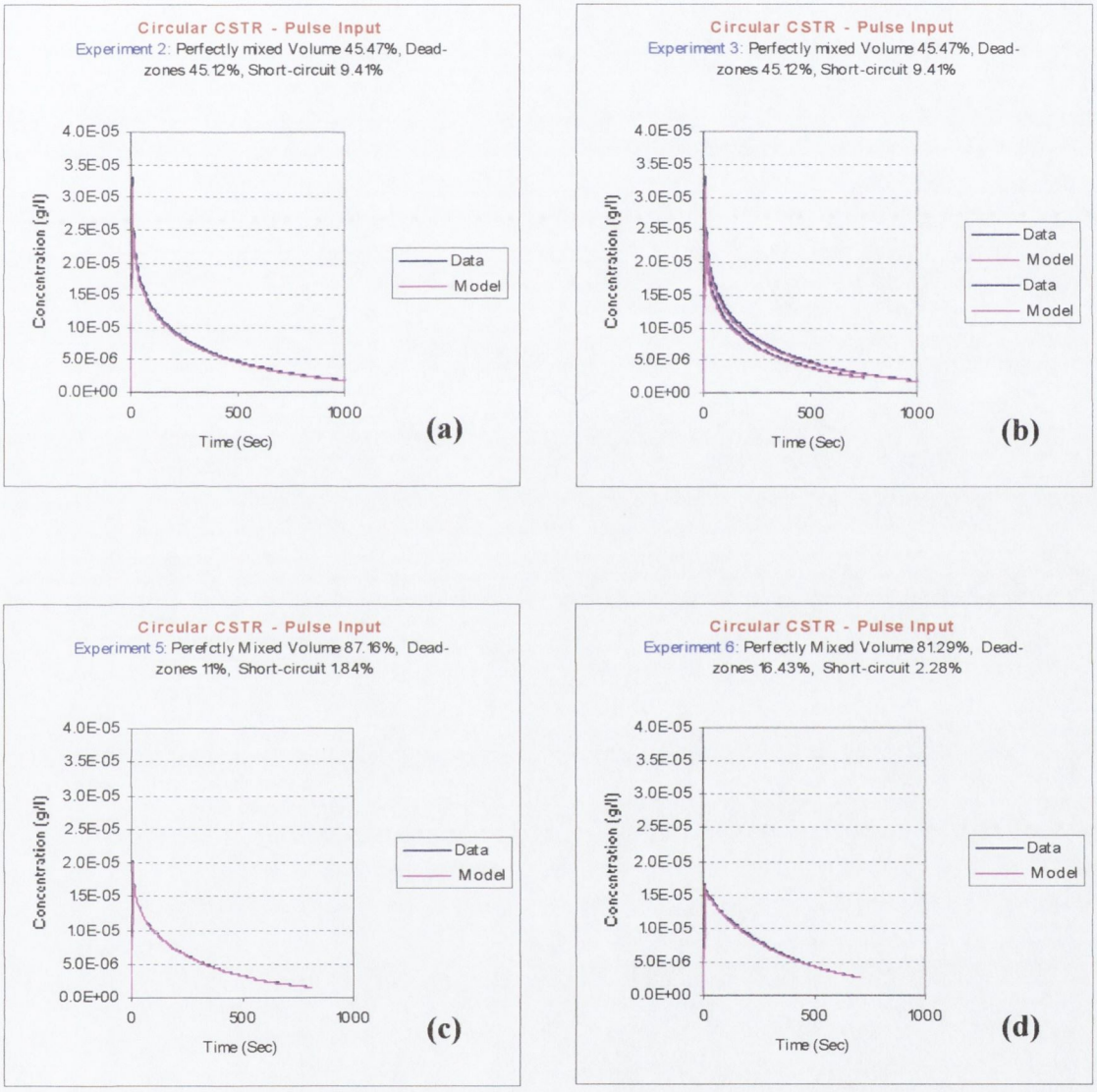

Figure B. 1 Graphs showing laboratory results and model curves for a pulse input method into a circular CSTR for (a) Experiment 2, (b) Experiment 3, (c) Experiment 5 and (d) Experiment 6

B.2 Step Input Graphs

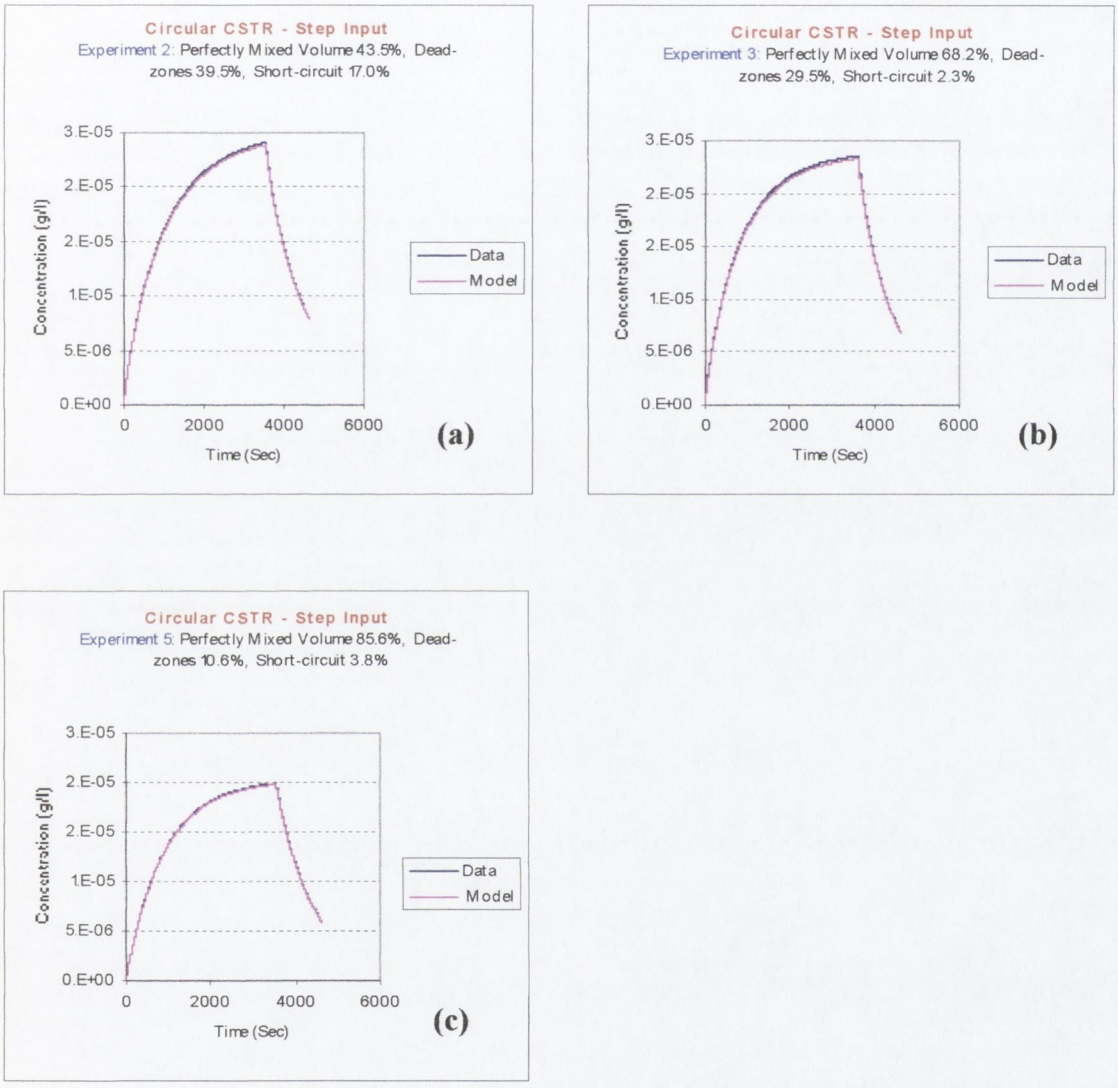

Figure B. 2 Graphs showing laboratory results and model curves for a step input method into a circular CSTR for (a) Experiment 2, (b) Experiment 3 and (b) Experiment 5

Appendix C

Graphs for Experiments with Modifications-

Dead-zones and Short-circuit Simulations (Circular CSTR)

Appendix C

Graphs for Modifications (Dead-zones and Short-circuit Simulations)

C.1 Dead-zone Graphs (Group 1)

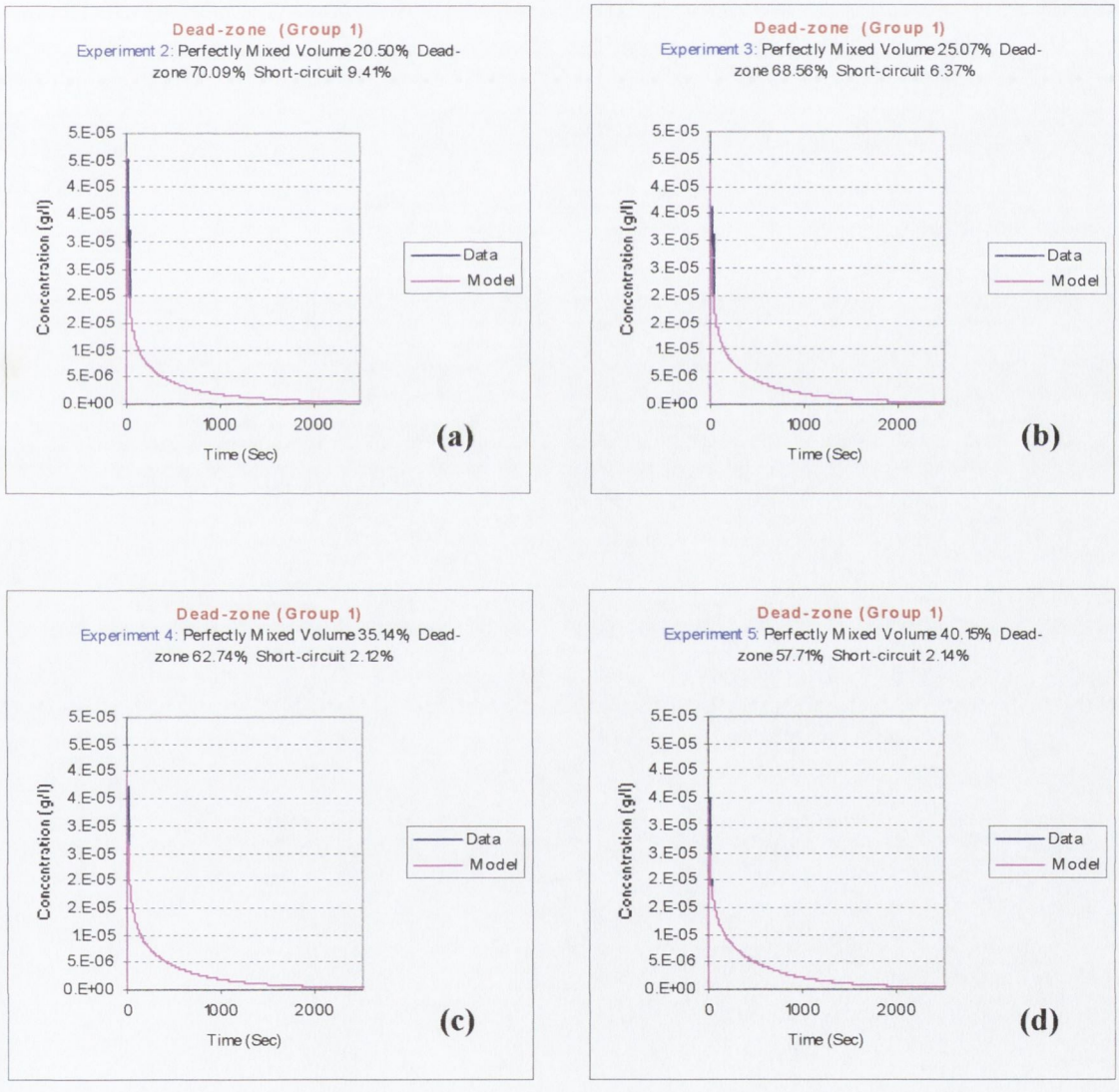

Figure C. 1 Graphs showing laboratory results and model curves for dead-zones into a circular CSTR for group1 for (a) Experiment 2, (b) Experiment 3, (c) Experiment 4 and (d) Experiment 5

C.2 Dead-zone Graphs (Group 2)

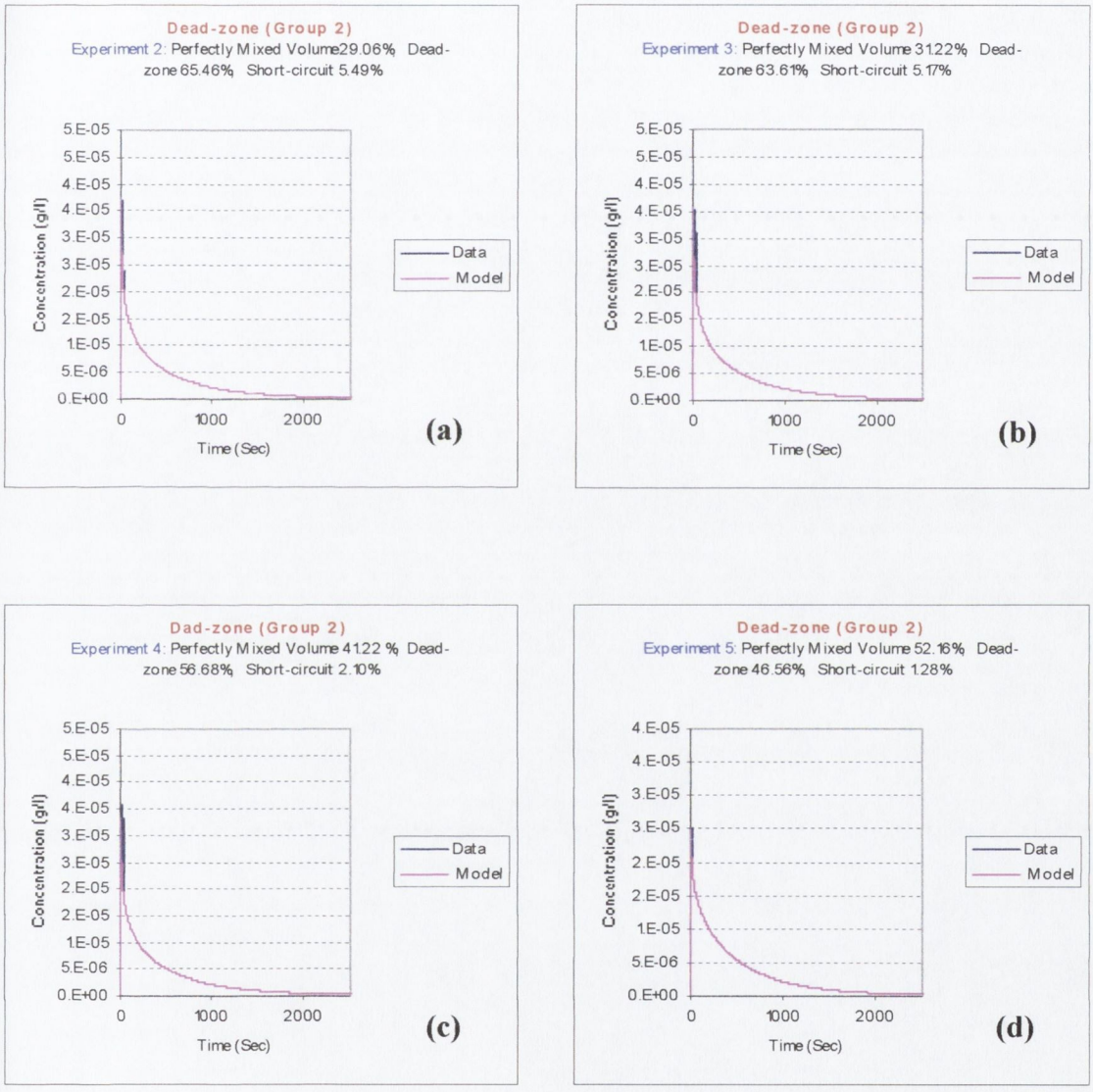

Figure C. 2 Graphs showing laboratory results and model curves for dead-zones into a circular CSTR for group 2 for (a) Experiment 2, (b) Experiment 3, (c) Experiment 4 and (d) Experiment 5

C.3 Dead-zone Graphs (Group 3)

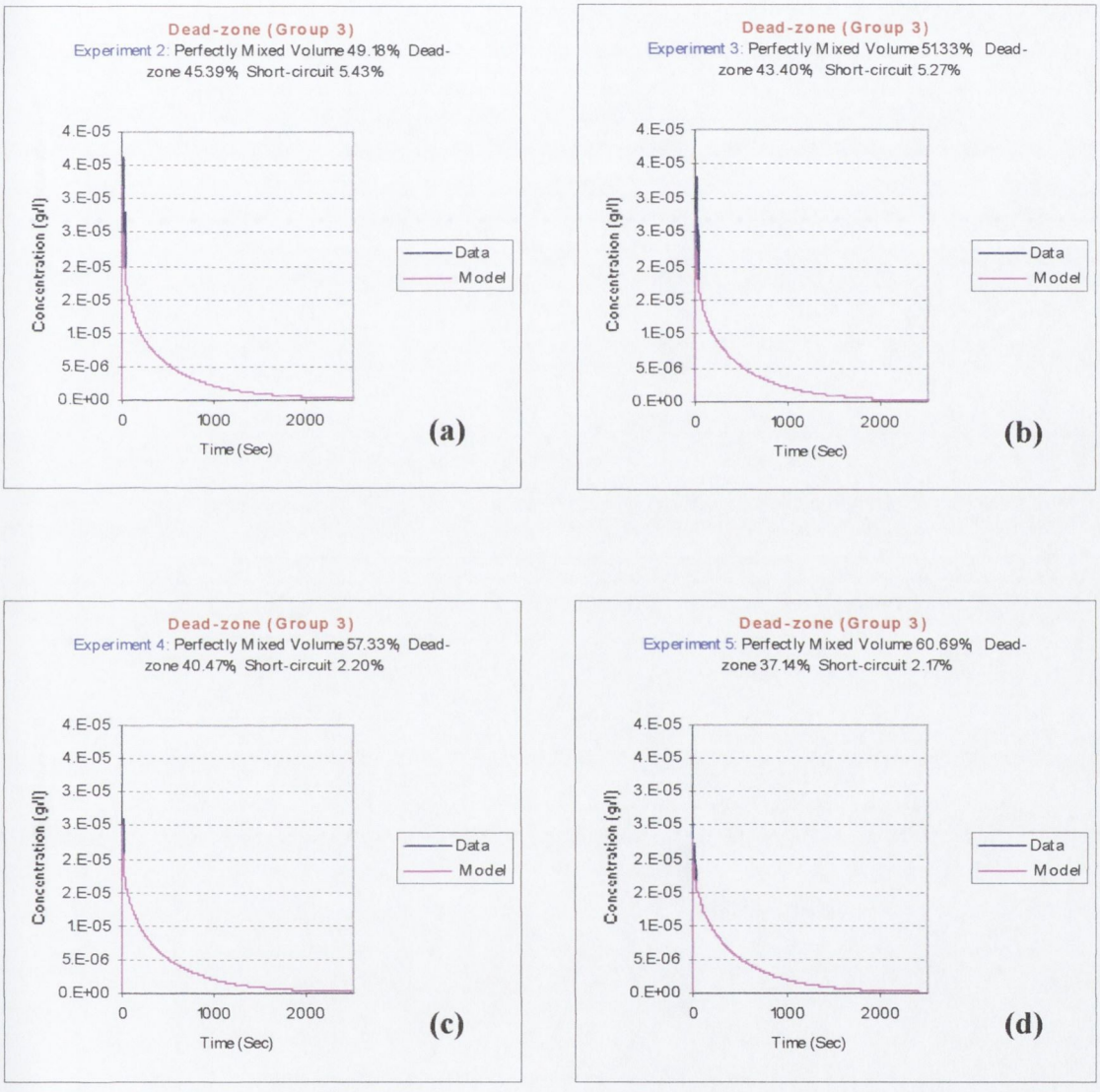

Figure C. 3 Graphs showing laboratory results and model curves for dead-zones into a circular CSTR for group 3 for (a) Experiment 2, (b) Experiment 3, (c) Experiment 4 and (d) Experiment 5

C.4 Dead-zone Graphs (Group 4)

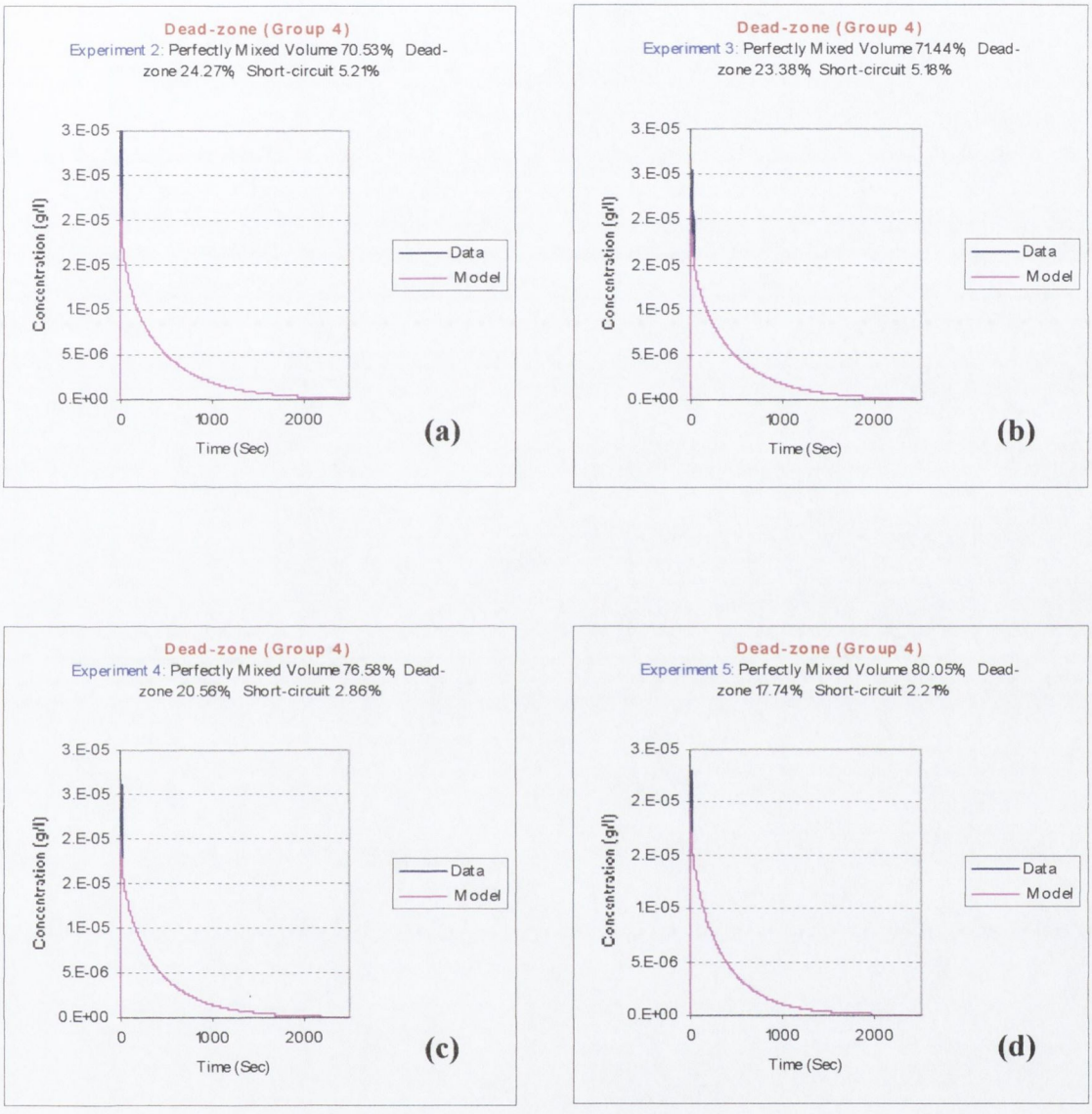

Figure C. 4 Graphs showing laboratory results and model curves for dead-zones into a circular CSTR for group 4 for (a) Experiment 2, (b) Experiment 3, (c) Experiment 4 and (d) Experiment 5

C.5 Dead-zone Graphs (Group 5)

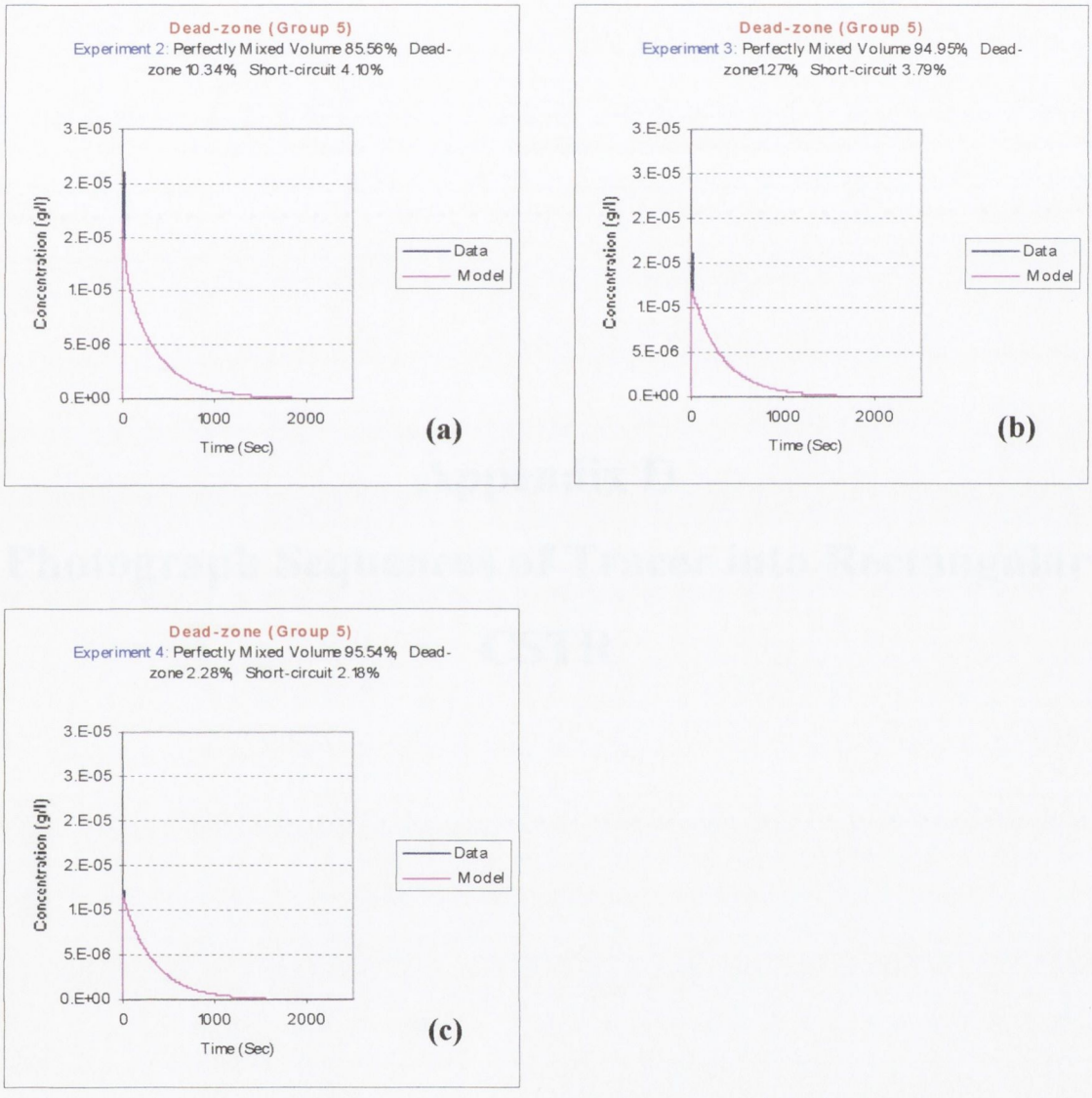

Figure C. 5 Graphs showing laboratory results and model curves for dead-zones into a circular CSTR for group 5 for (a) Experiment 2, (b) Experiment 3 and (c) Experiment 4

Appendix D

Photograph Sequences of Tracer into Rectangular CSTR

Appendix D

Photograph Sequences of Tracer into Rectangular CSTR

D.1 Photograph Sequences of Tracer into One CSTR Model [Trial 1]

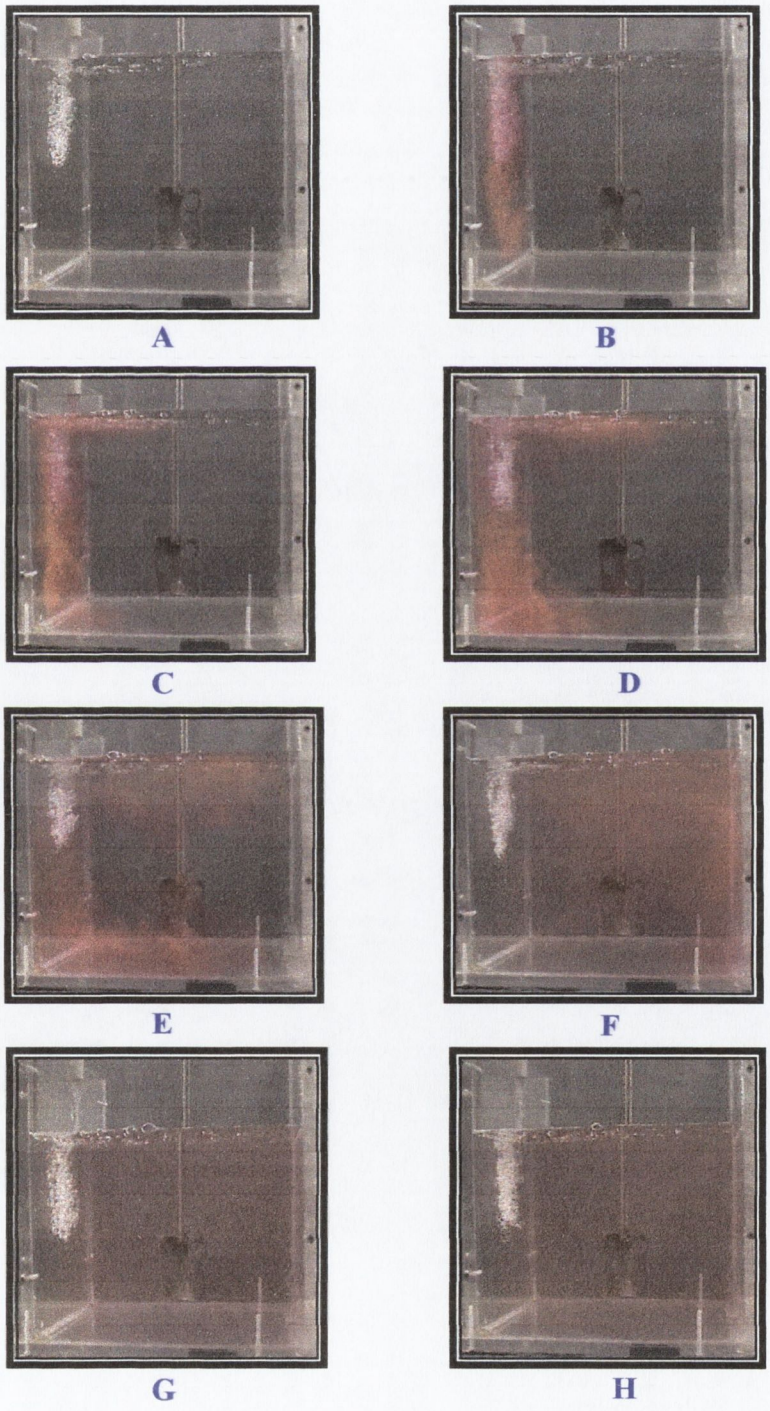

D.2 Photograph Sequences of Tracer into Two CSTR Model [Trial 2A]

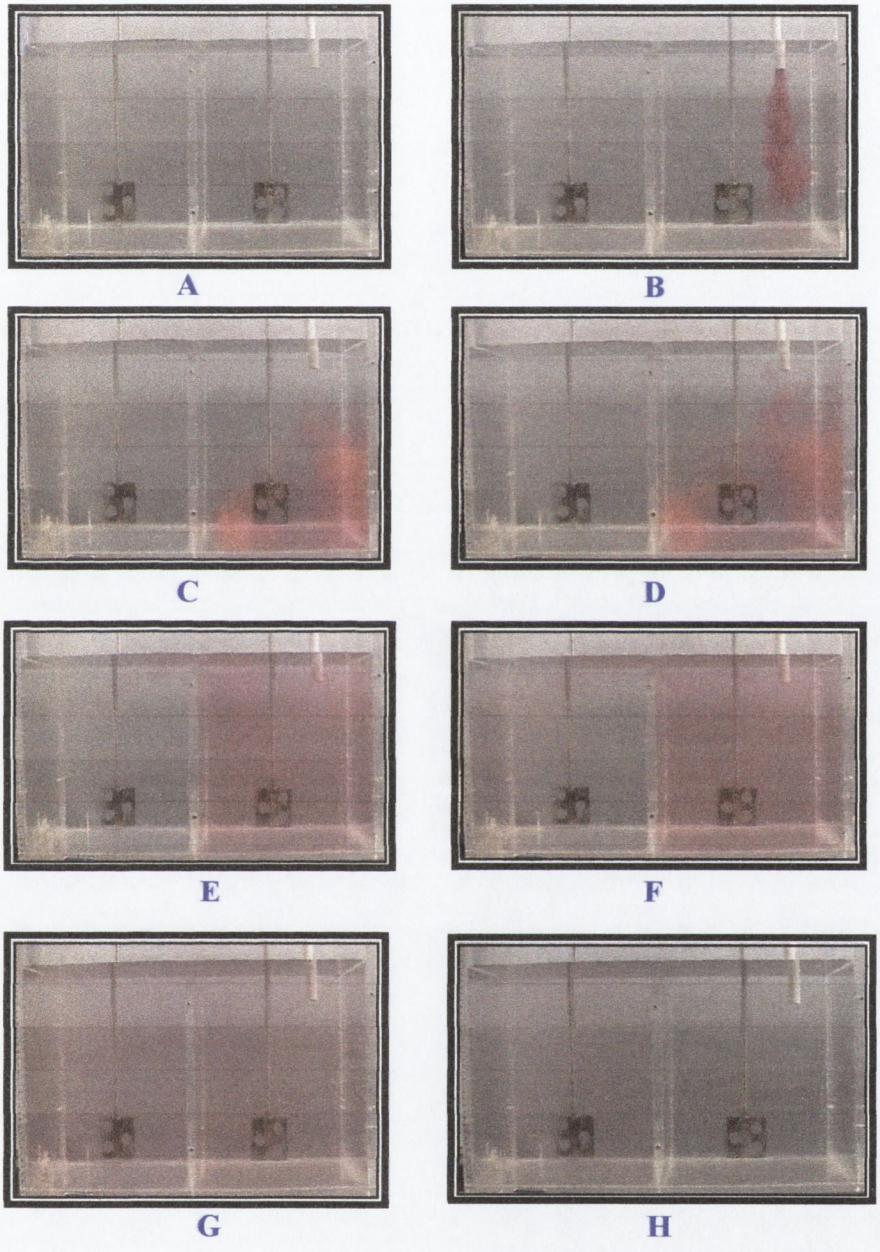

D.3 Photograph Sequences of Tracer into Two CSTR Model [Trial 2B]

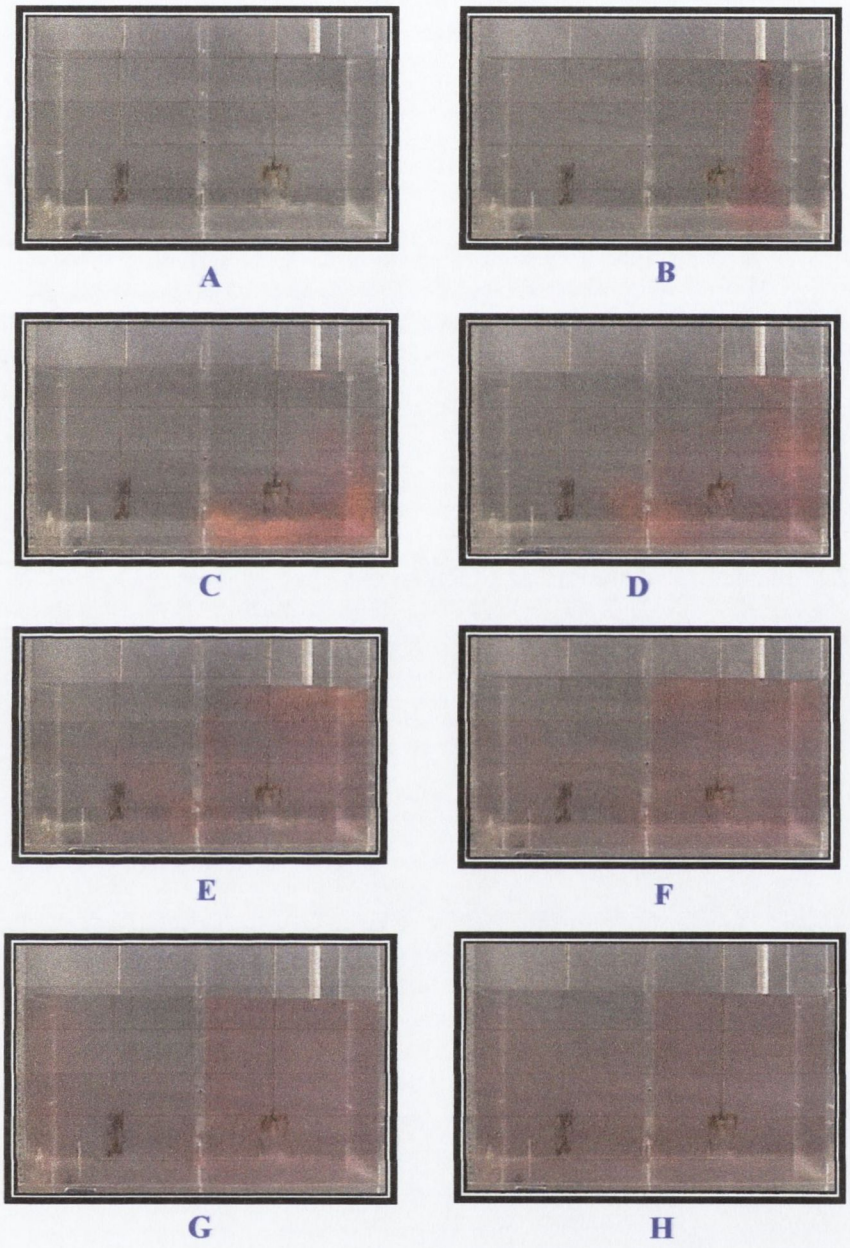

D.4 Photograph Sequences of Tracer into Three CSTR Model [Trial 3A]

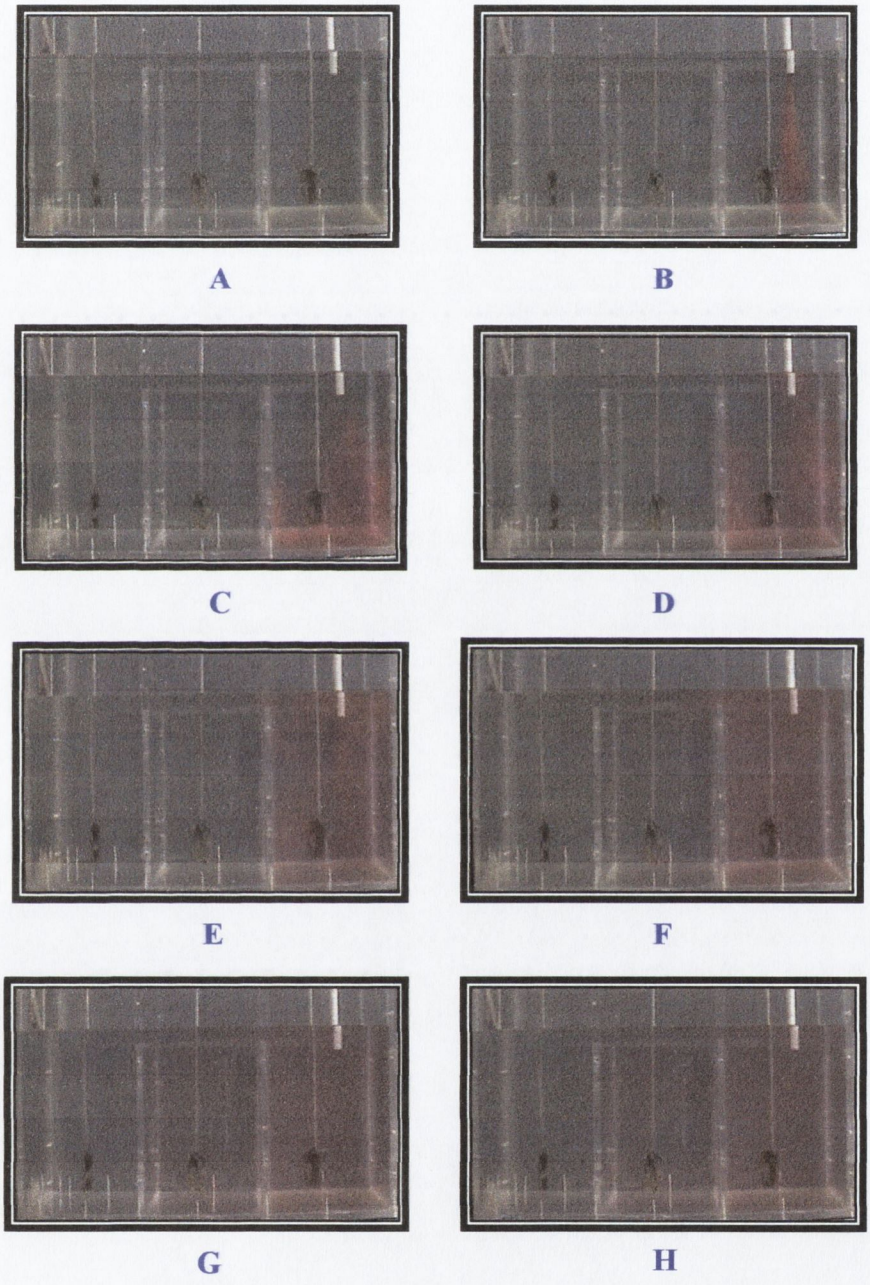

D.5 Photograph Sequences of Tracer into Three CSTR Model [Trial 3B]

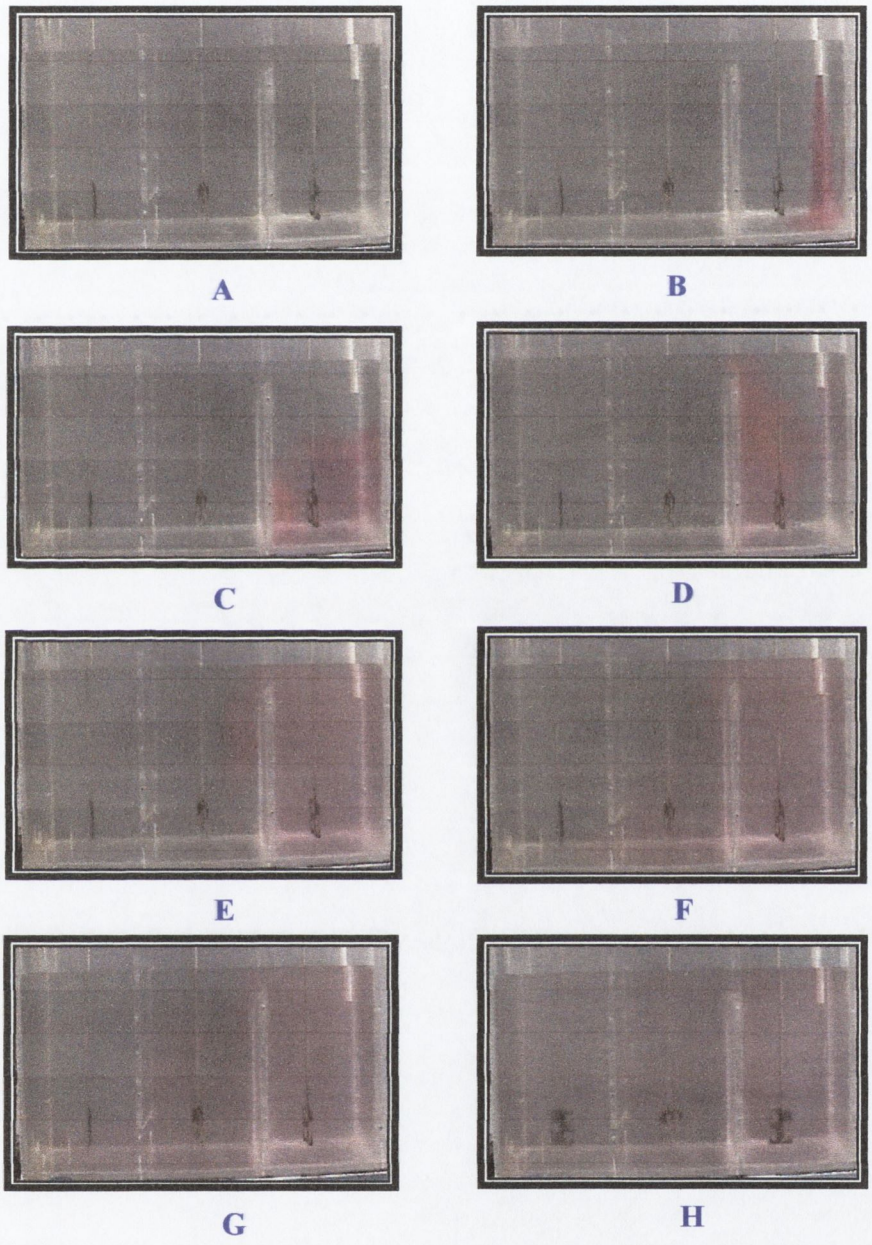

D.6 Photograph Sequences of Tracer into Four CSTR Model [Trial 4A]

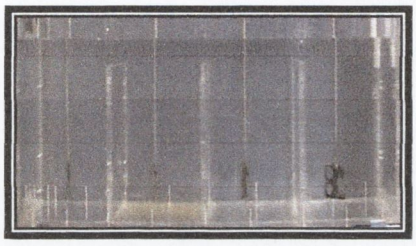

A

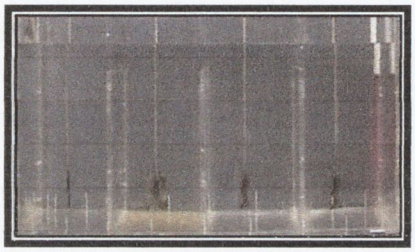

B

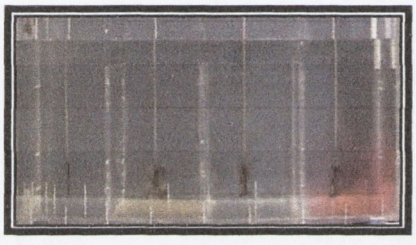

C

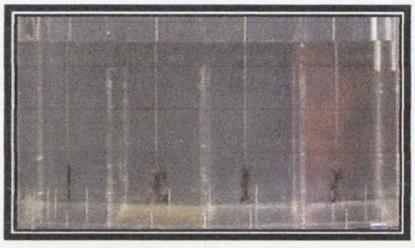

D

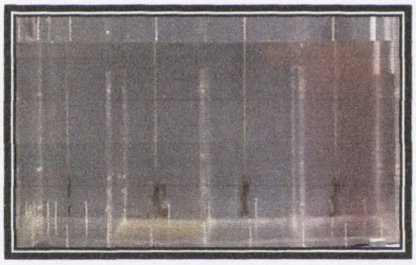

E

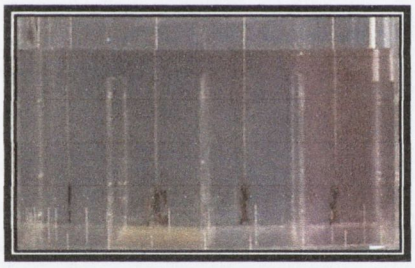

F

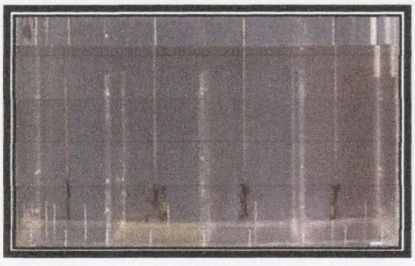

G

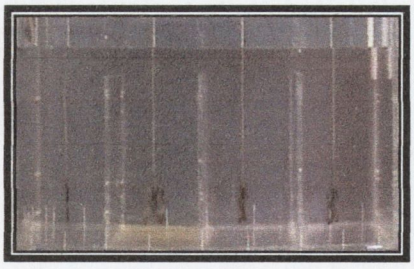

H

D.7 Photograph Sequences of Tracer into Four CSTR Model [Trial 4B]

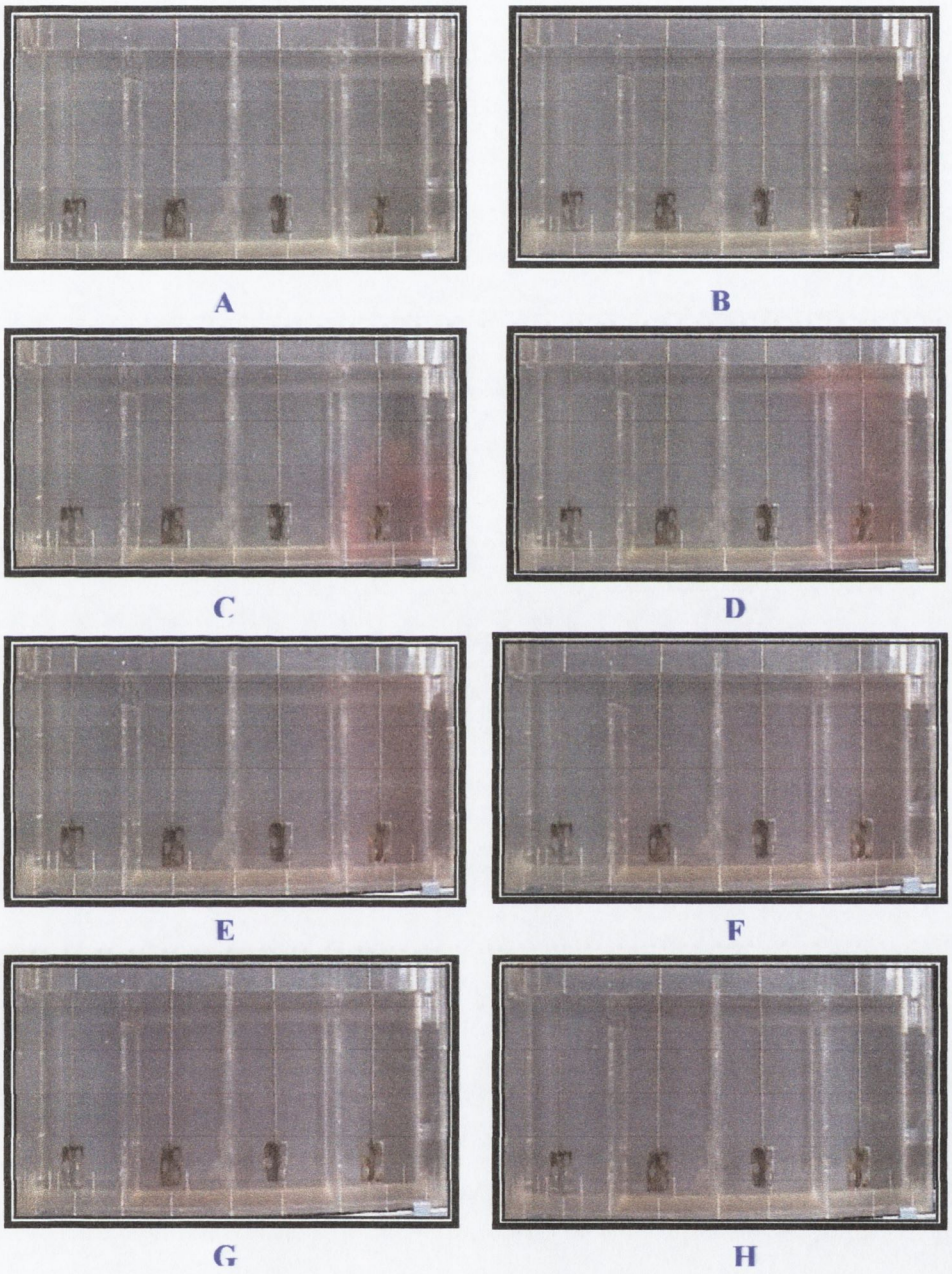

D.8 Photograph Sequences of Tracer into Four CSTR Model [Trial 4C]

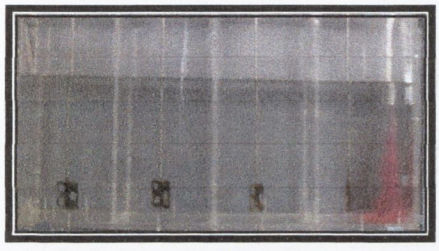

A

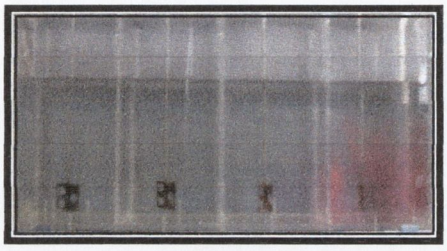

B

C

D

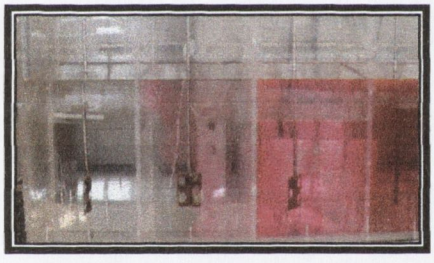

E

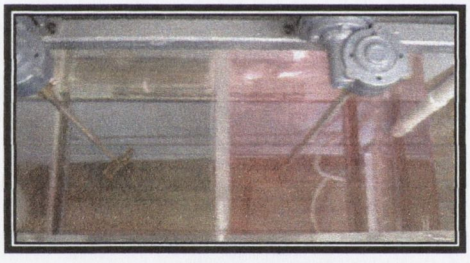

G

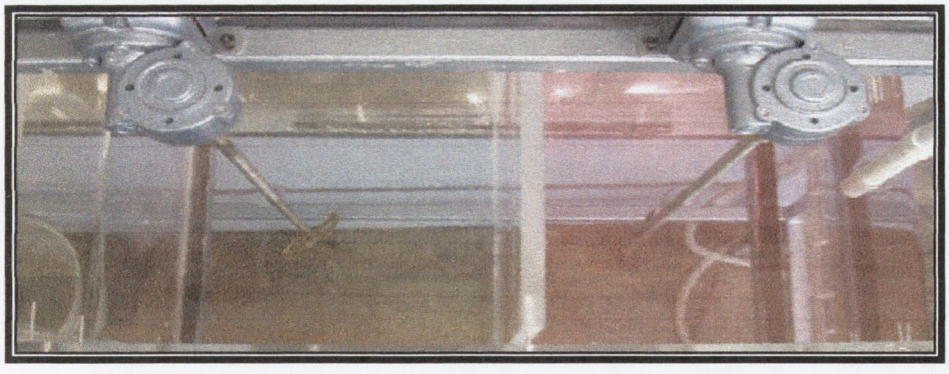

F

Appendix E

Graphs for Tank-in-series Trials

(Rectangular CSTR Network)

Appendix E

Graphs for Trials Experiments (Rectangular CSTR)

E.1 Trial-1 (One CSTR)

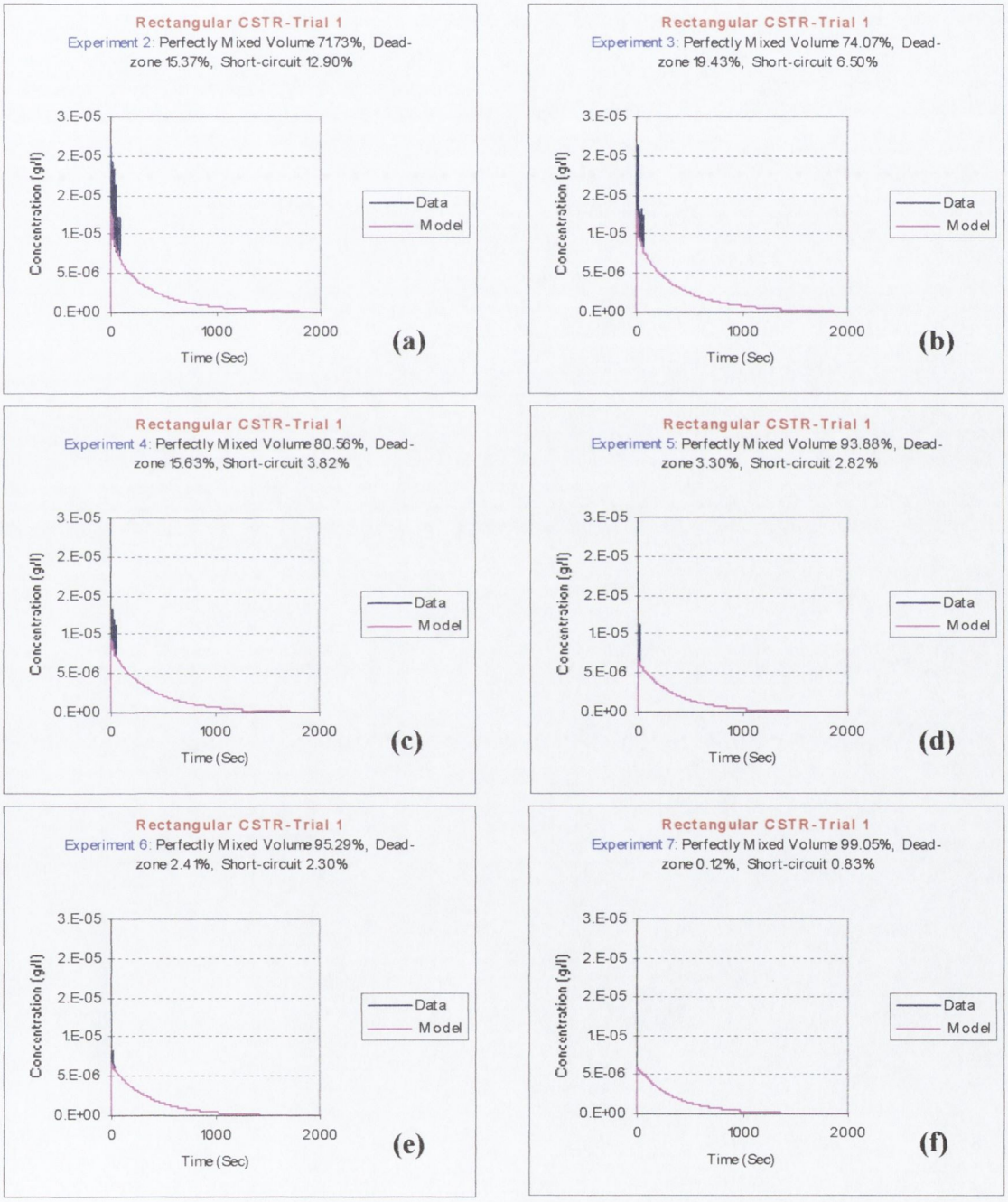

Figure E. 1 Graphs showing laboratory results and fitted model curves for Trial-1 experiments into single CSTR for (a) Exp.2, (b) Exp.3, (c) Exp. 4, (d) Exp. 5, (e) Exp. 6 and (f) Exp. 7

E.2 Trial-2A (Two CSTR-in-Series)

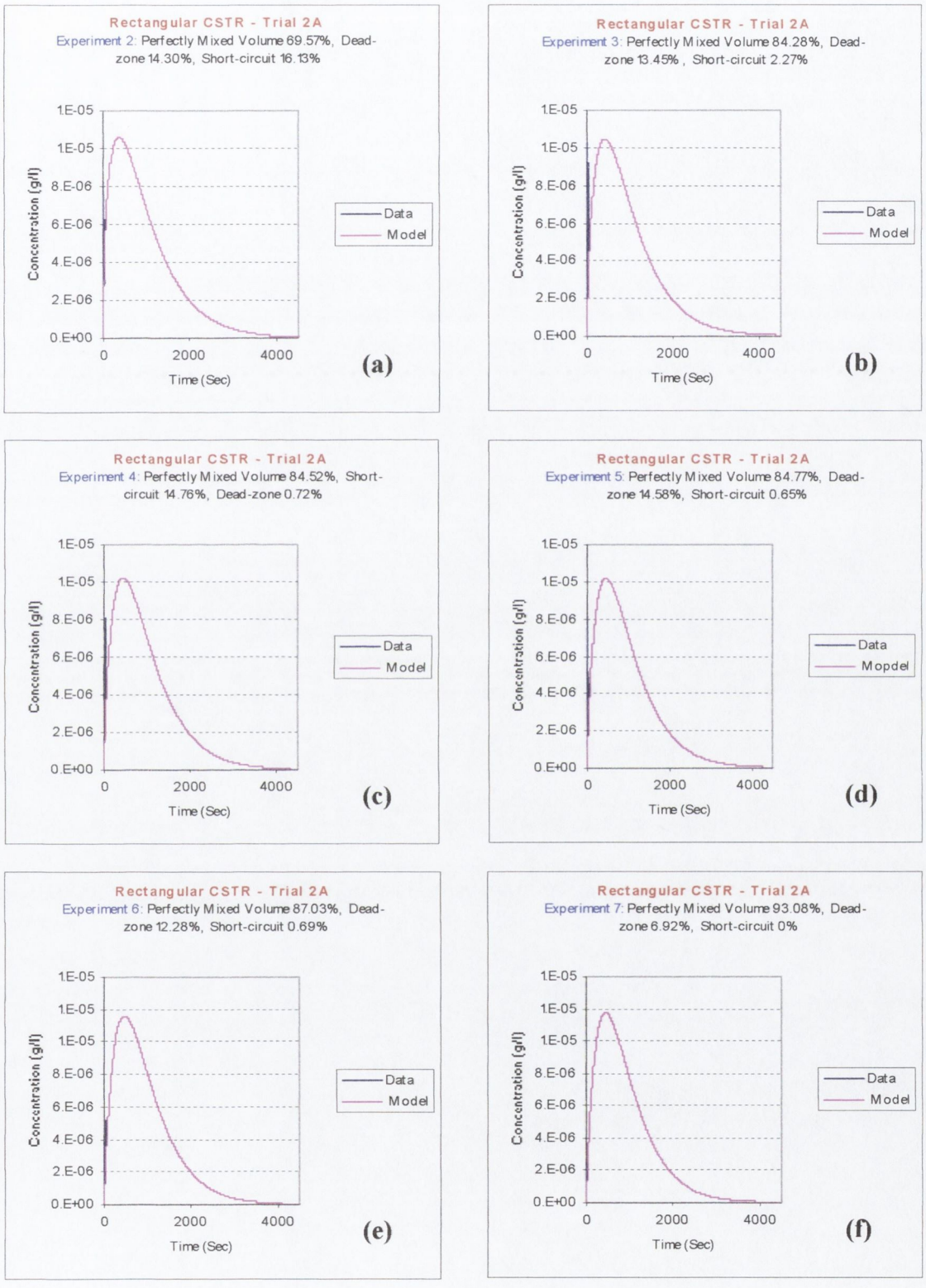

Figure E. 2 Graphs showing laboratory results and fitted model curves for Trial-2A experiments into two CSTR in-series for (a) Exp.2, (b) Exp.3, (c) Exp. 4, (d) Exp. 5, (e) Exp. 6 and (f) Exp. 7

E.3 Trial-2B (Two CSTR-in-Series)

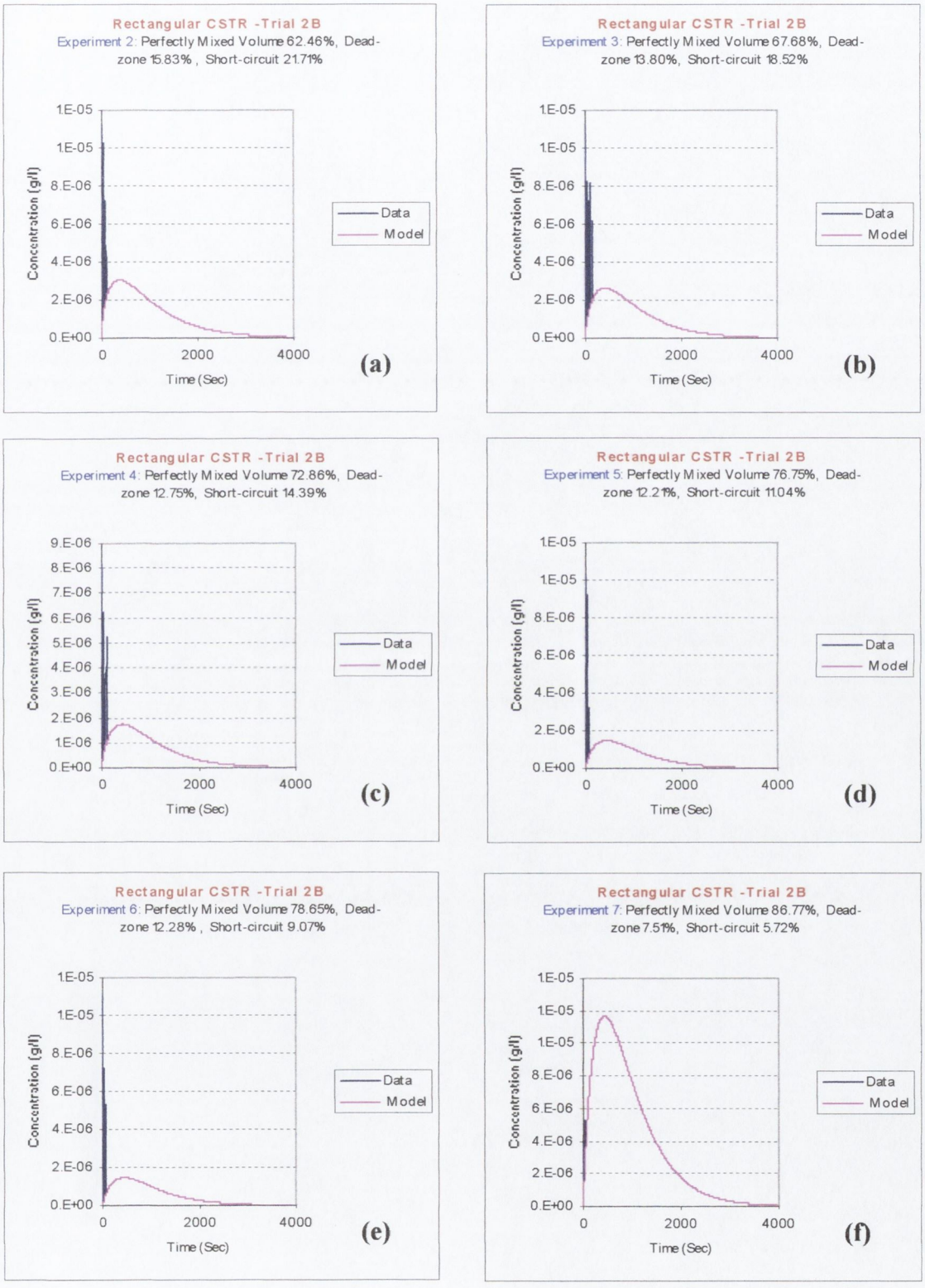

Figure E. 3 Graphs showing laboratory results and fitted model curves for Trial-2B experiments into two CSTR in-series for (a) Exp.2, (b) Exp.3, (c) Exp. 4, (d) Exp. 5, (e) Exp. 6 and (f) Exp. 7

E.4 Trial-3A (Three CSTR-in-Series)

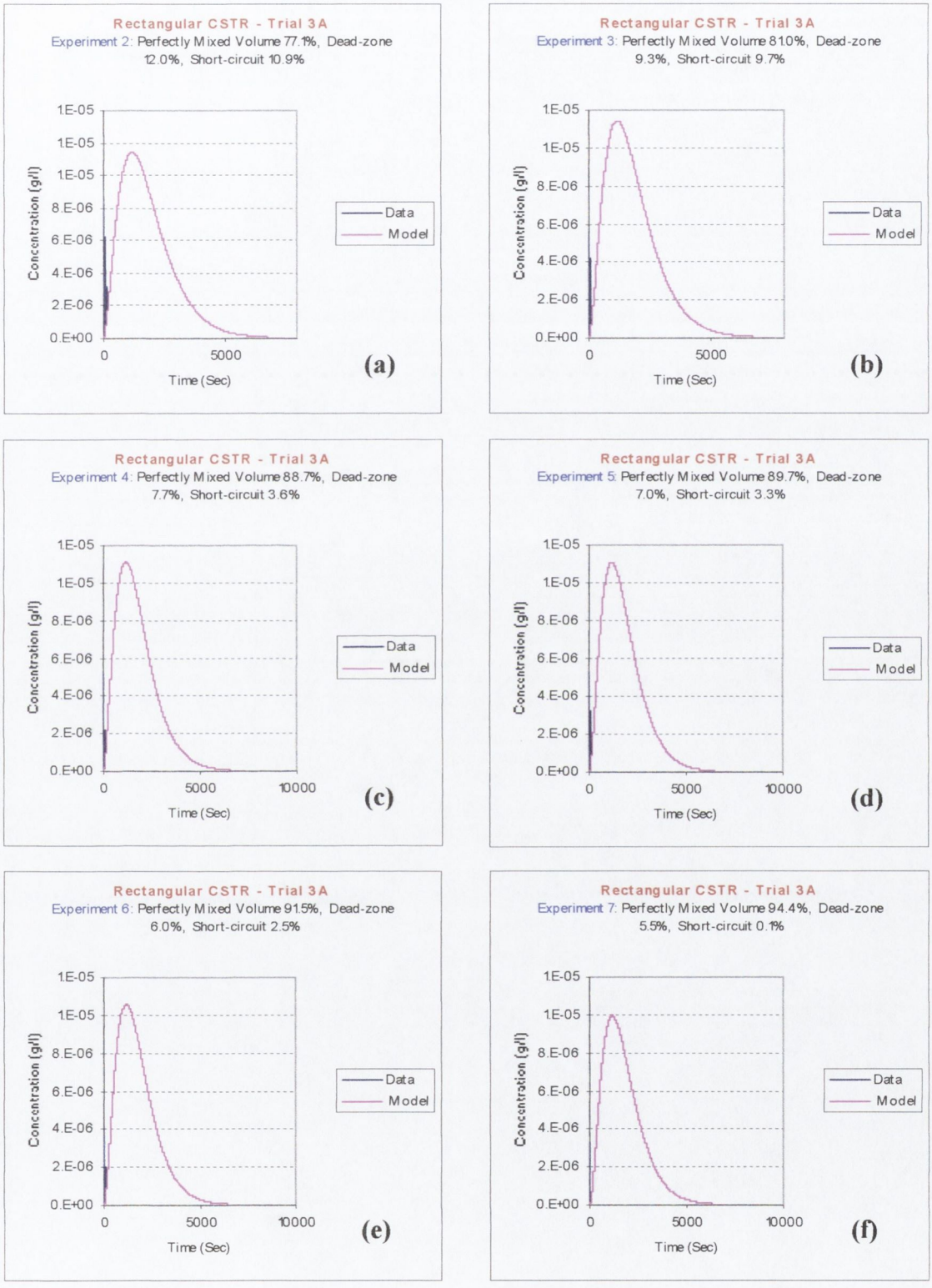

Figure E. 4 Graphs showing laboratory results and fitted model curves for Trial-3A experiments into three CSTR in-series for (a) Exp.2, (b) Exp.3, (c) Exp. 4, (d) Exp. 5, (e) Exp. 6 and (f) Exp. 7

E.5 Trial-3B (Three CSTR-in-Series)

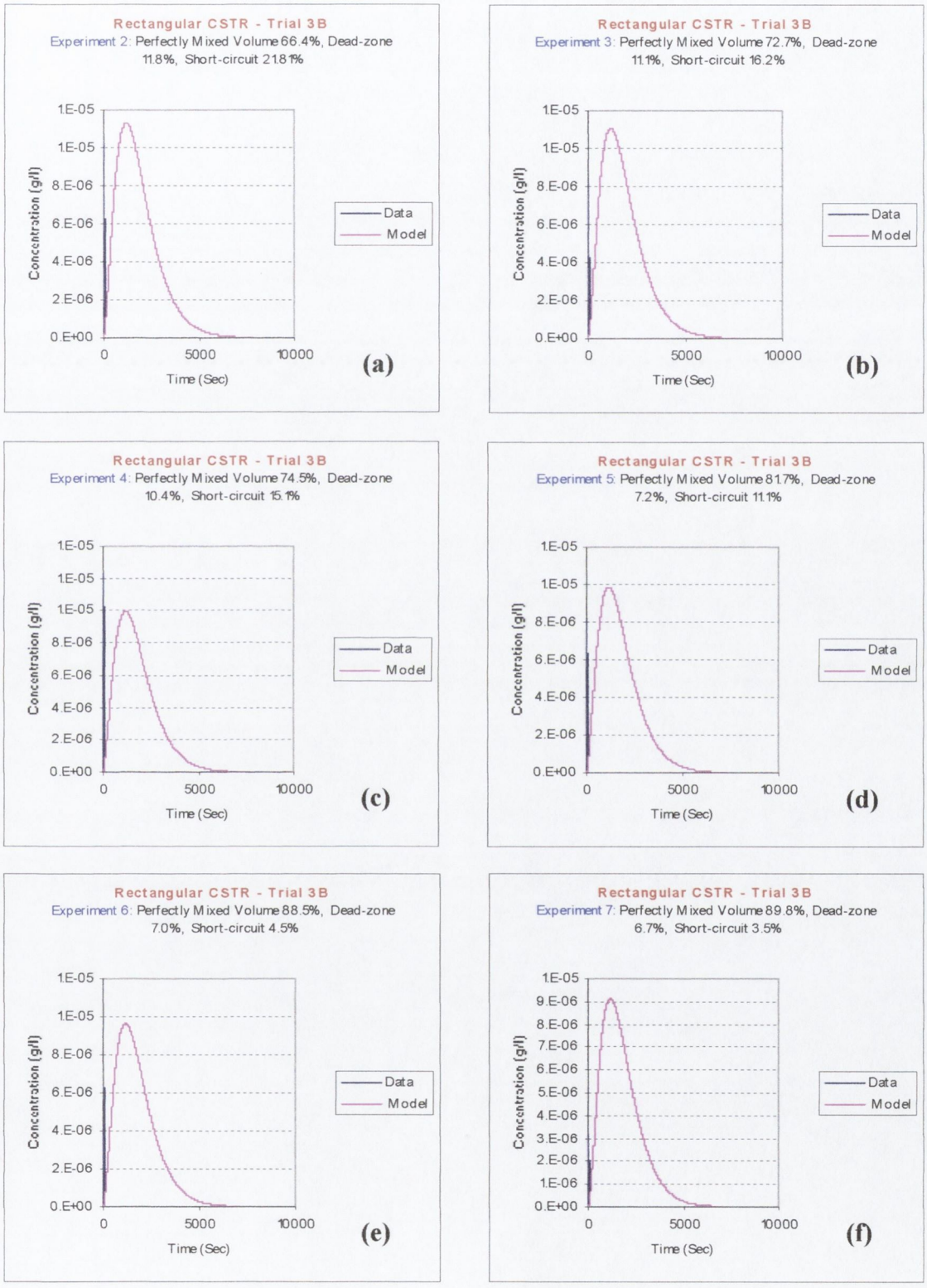

Figure E. 5 Graphs showing laboratory results and fitted model curves for Trial-3A experiments into three CSTR in-series for (a) Exp.2, (b) Exp.3, (c) Exp. 4, (d) Exp. 5, (e) Exp. 6 and (f) Exp. 7

E.6 Trial-4A (Four CSTR-in-Series)

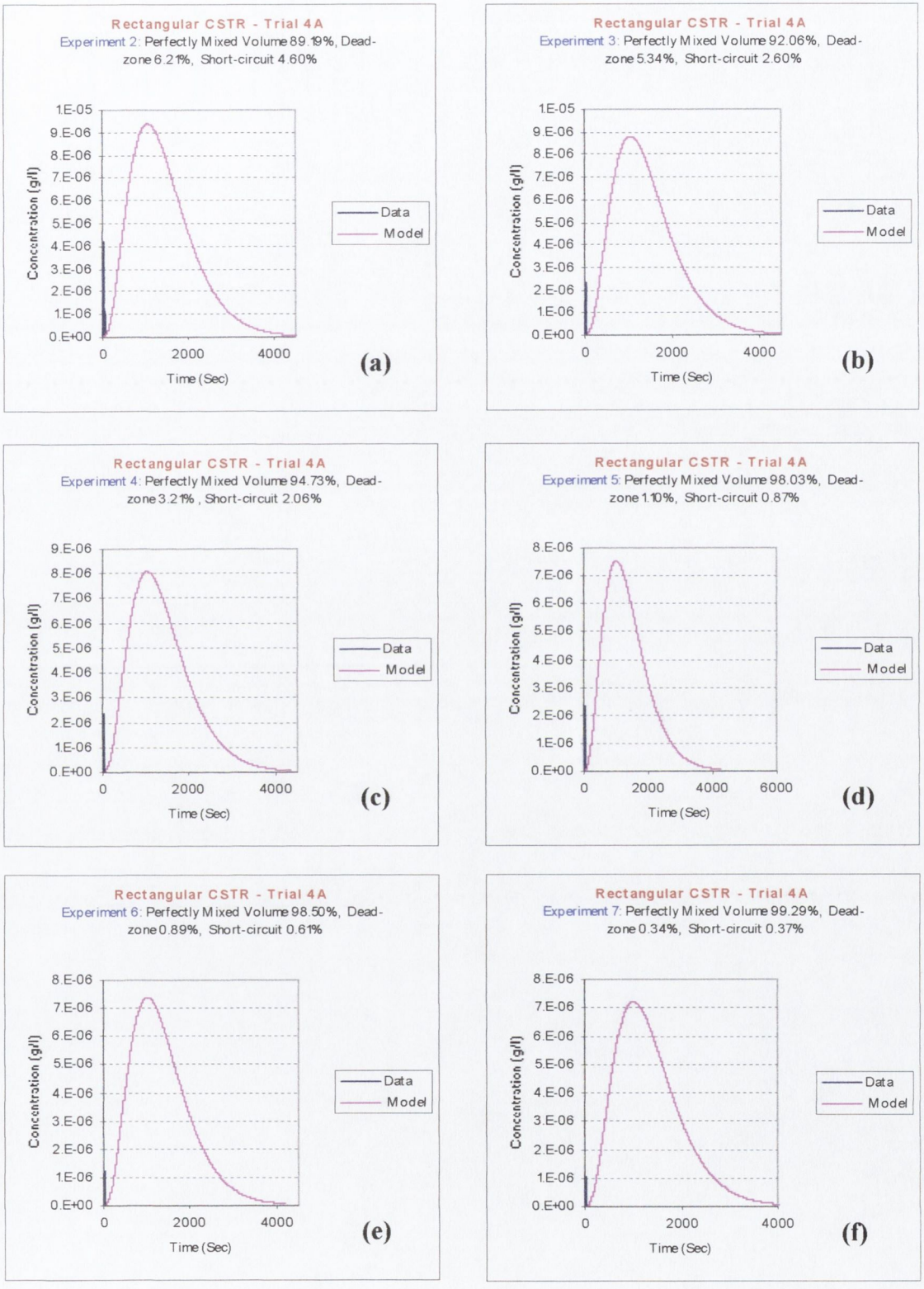

Figure E. 6 Graphs showing laboratory results and fitted model curves for Trial-4A experiments into four CSTR in-series for (a) Exp.2, (b) Exp.3, (c) Exp. 4, (d) Exp. 5, (e) Exp. 6 and (f) Exp. 7

E.7 Trial-4B (Four CSTR-in-Series)

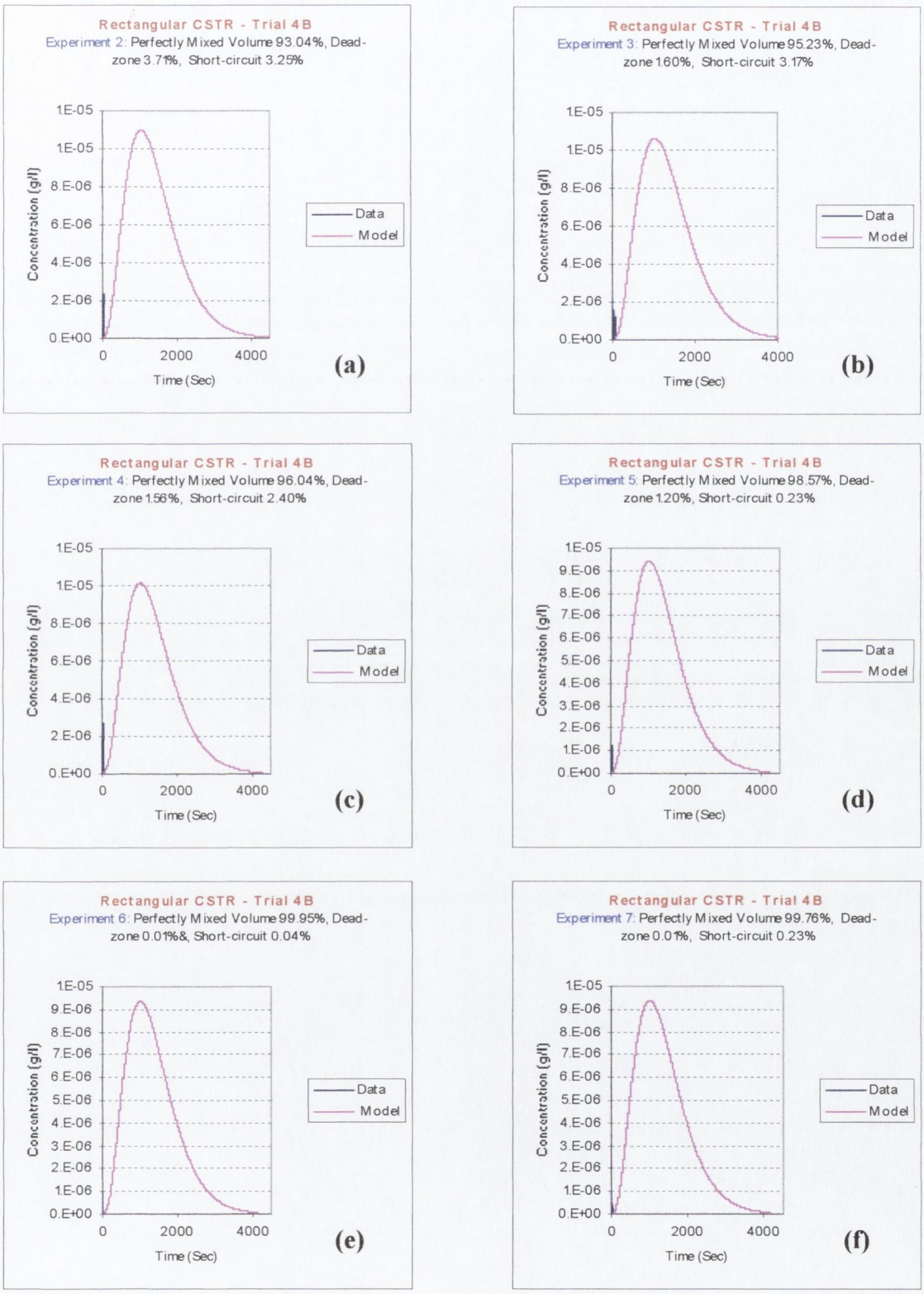

Figure E. 7 Graphs showing laboratory results and fitted model curves for Trial-4B experiments into four CSTR in-series for (a) Exp.2, (b) Exp.3, (c) Exp. 4, (d) Exp. 5, (e) Exp. 6 and (f) Exp. 7

E.8 Trial-4C (Four CSTR-in-Series)

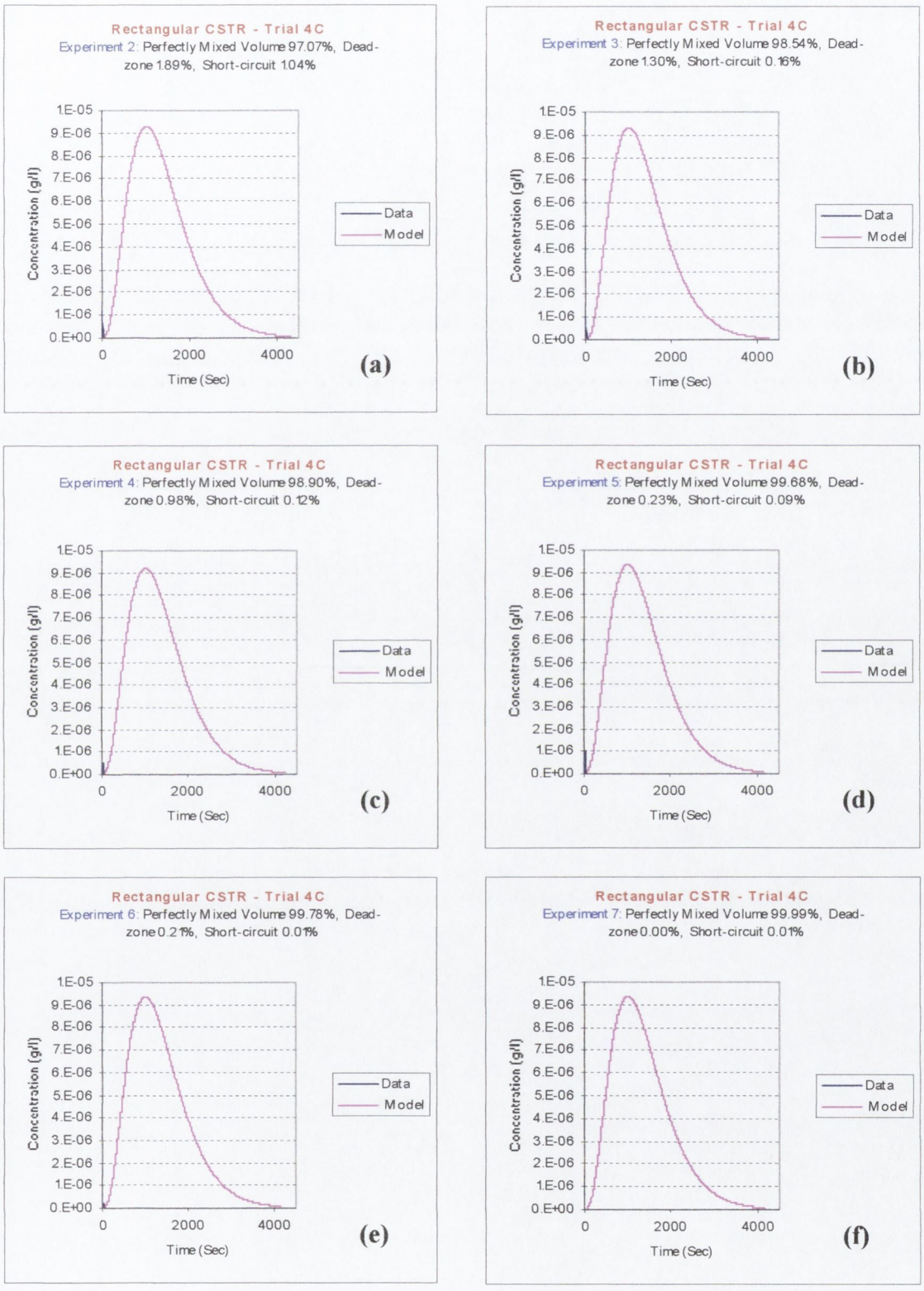

Figure E. 8 Graphs showing laboratory results and fitted model curves for Trial-4C experiments into four CSTR in-series for (a) Exp.2, (b) Exp.3, (c) Exp. 4, (d) Exp. 5, (e) Exp. 6 and (f) Exp. 7

E.9 Input and Output Variation

E.9.1 Scenario (A)

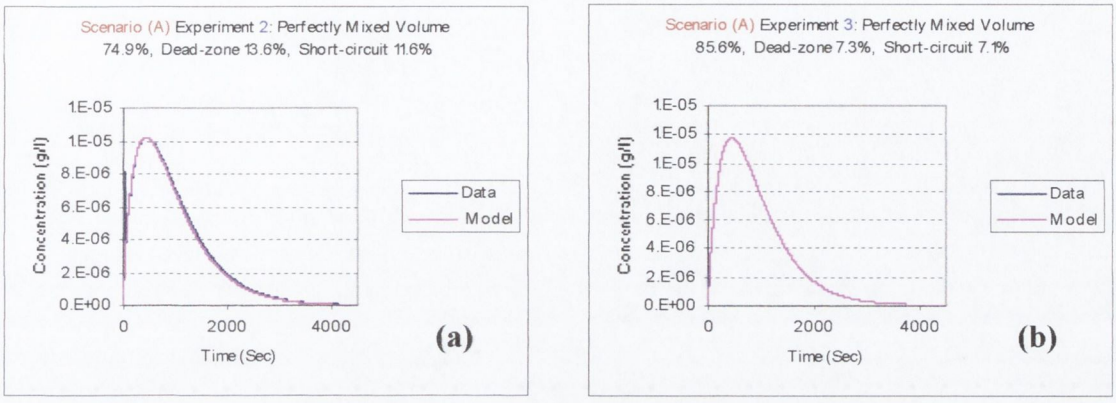

Figure E. 9 Graphs showing laboratory results and fitted model curves for Input and output variation scenario (A) into two CSTR in-series for (a) Exp.2 and (b) Exp.3.

E.9.2 Scenario (B)

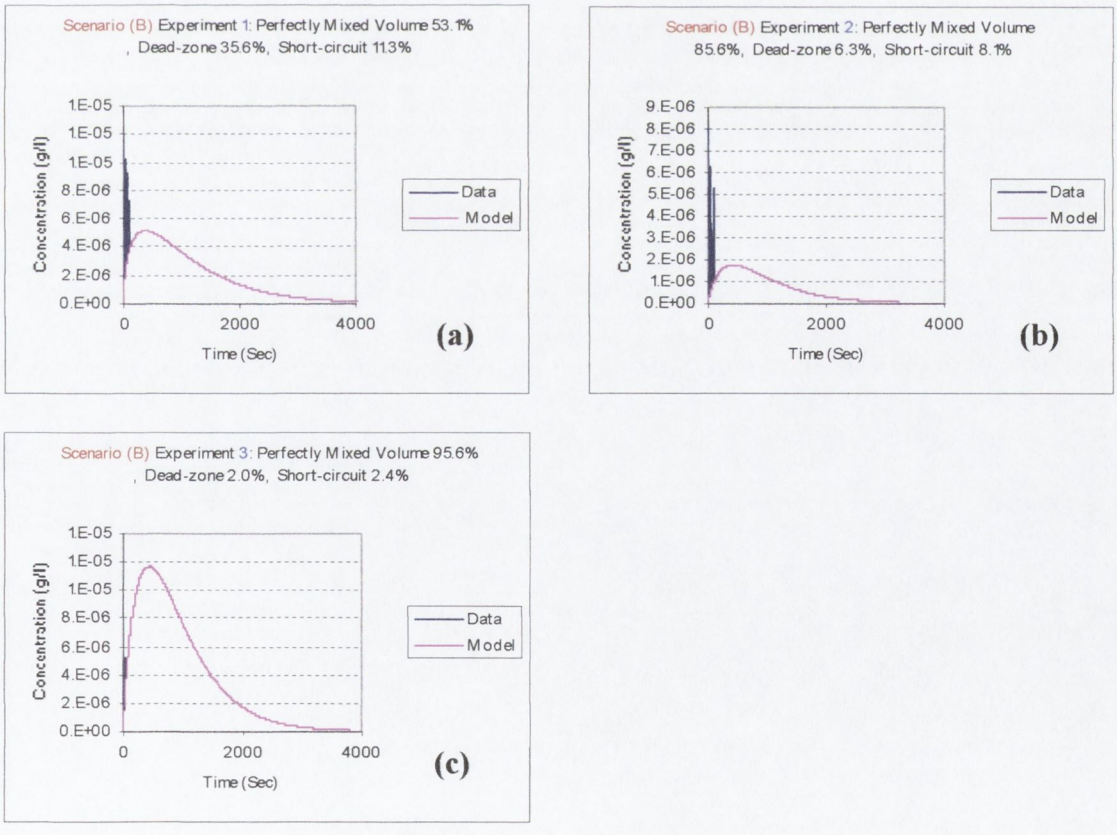

Figure E. 10 Graphs showing laboratory results and fitted model curves for Input and output variation scenario (A) into two CSTR in-series for (a) Exp.1, (b) Exp.2 and (c) Exp.3

E.9.3 Scenario (C)

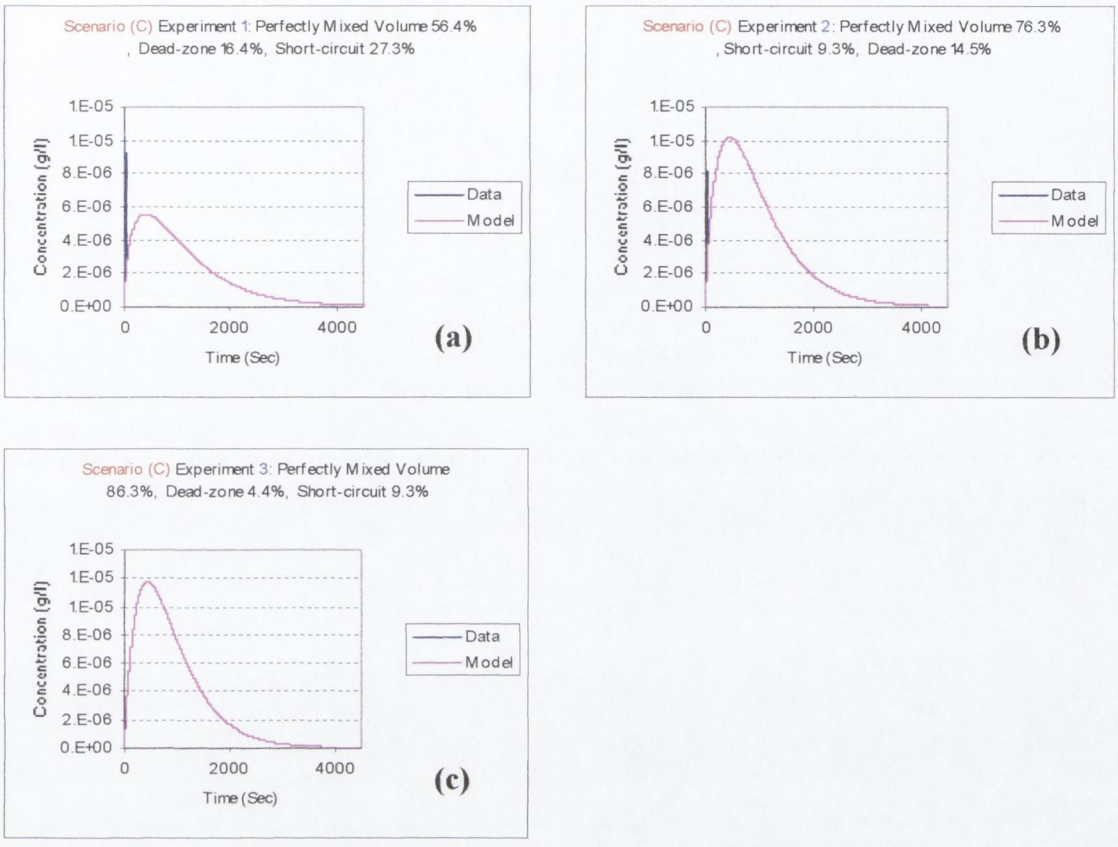

Figure E. 11 Graphs showing laboratory results and fitted model curves for Input and output variation scenario (C) into two CSTR in-series for (a) Exp.1, (b) Exp.2 and (c) Exp.3

E.9.4 Scenario (D)

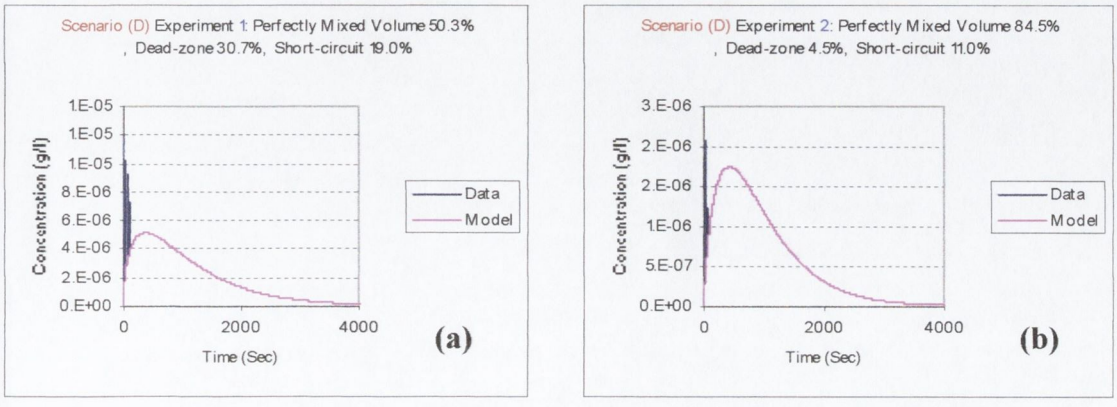

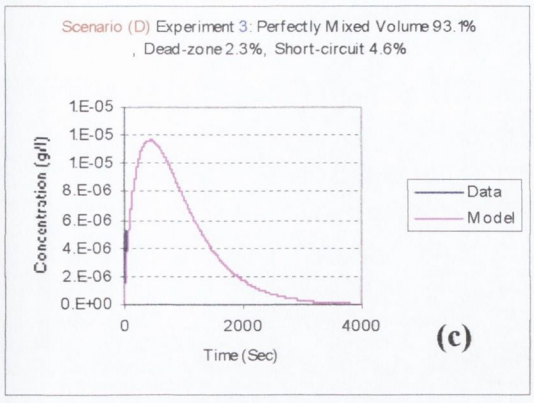

Figure E. 12 Graphs showing laboratory results and fitted model curves for Input and output variation scenario (D) into 2 CSTR in-series for (a) Exp.1, (b) Exp.2 and (c) Exp.3

E.9.5 Scenario (E)

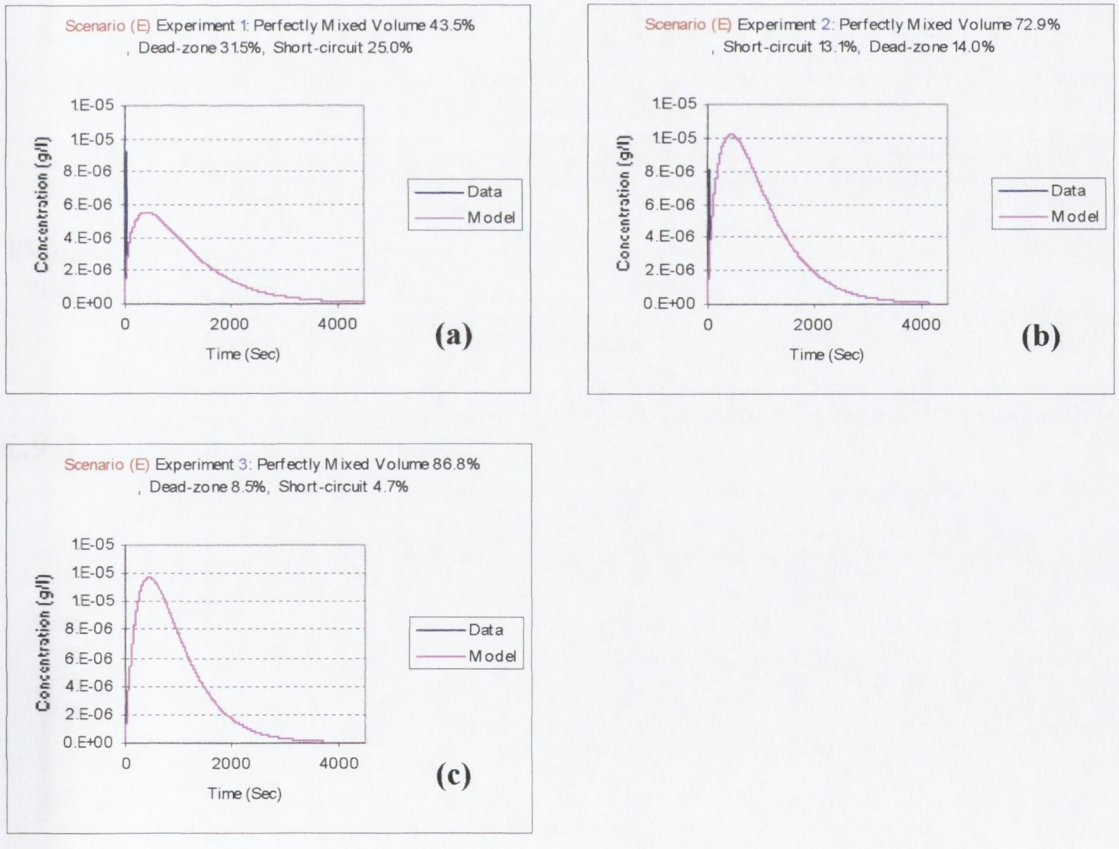

Figure E. 13 Graphs showing laboratory results and fitted model curves for Input and output variation scenario (E) into 2 CSTR in-series for (a) Exp.1, (b) Exp.2 and (c) Exp.3

E.9.6 Scenario (F)

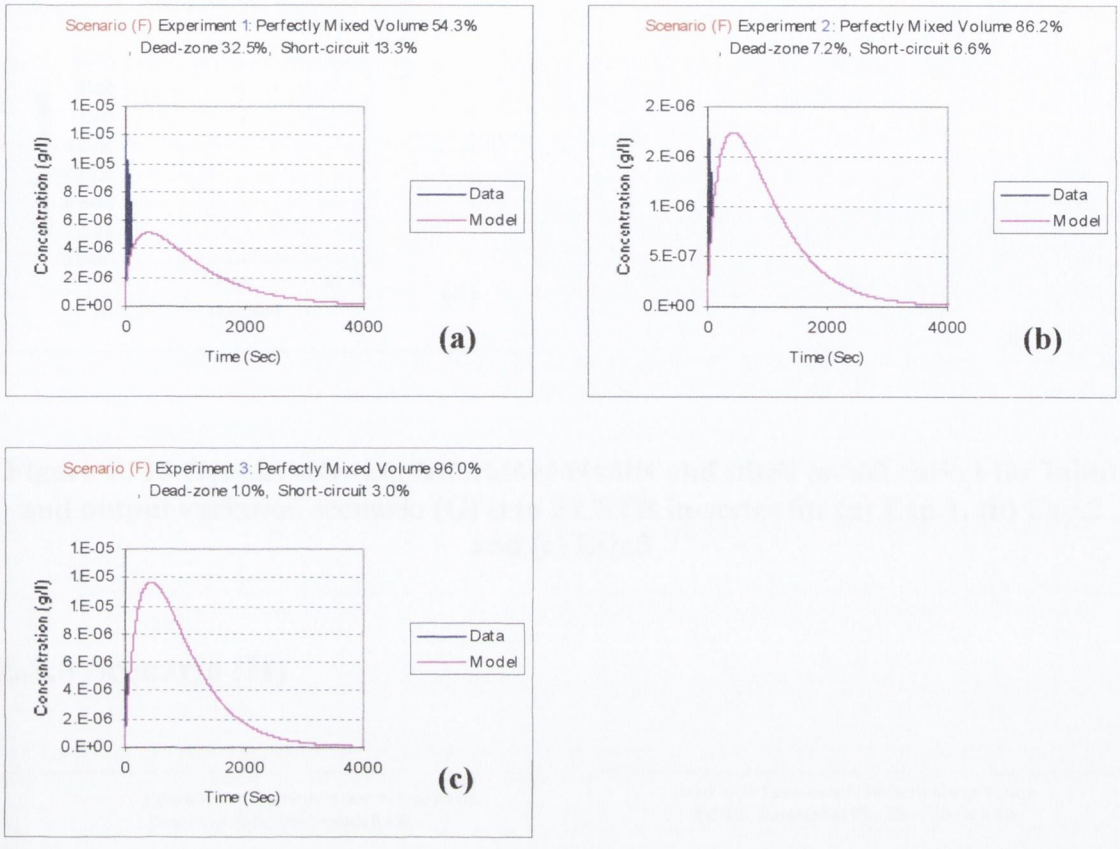

Figure E. 14 Graphs showing laboratory results and fitted model curves for Input and output variation scenario (F) into 2 CSTR in-series for (a) Exp.1, (b) Exp.2 and (c) Exp.3

E.9.7 Scenario (G)

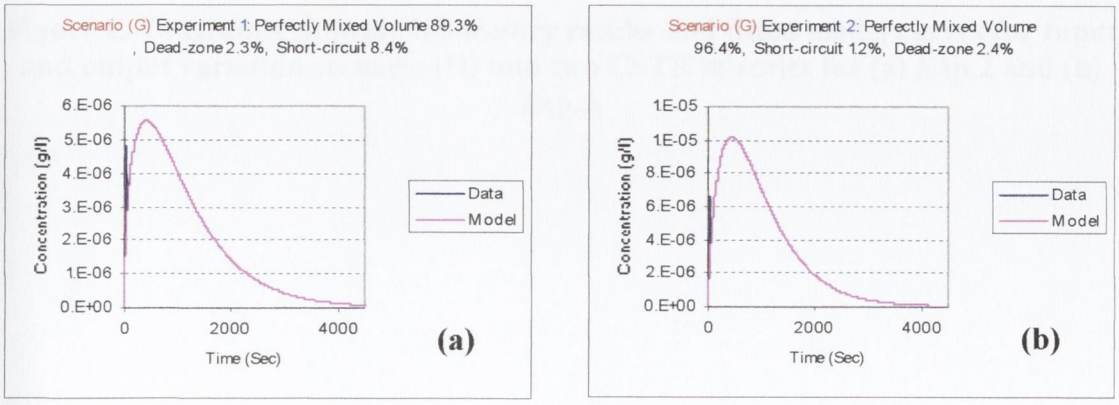

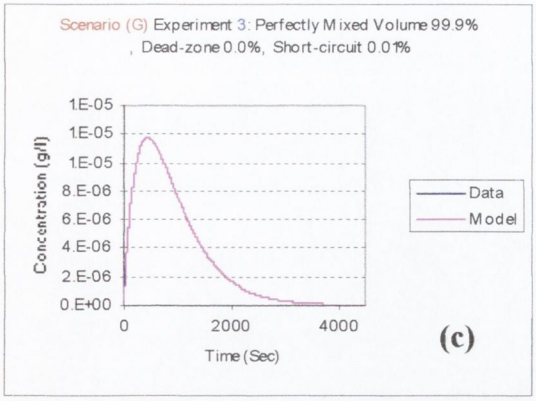

Figure E. 15 Graphs showing laboratory results and fitted model curves for Input and output variation scenario (G) into 2 CSTR in-series for (a) Exp.1, (b) Exp.2 and (c) Exp.3

E.9.8 Scenario (H)

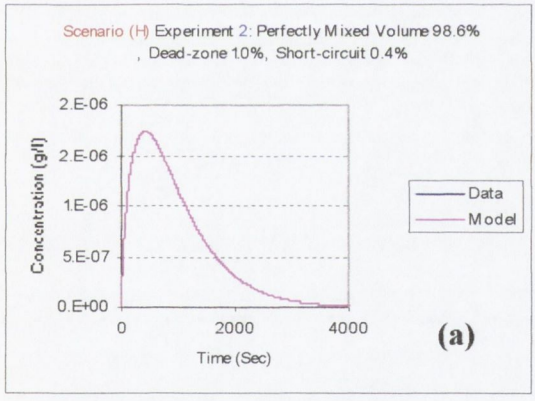

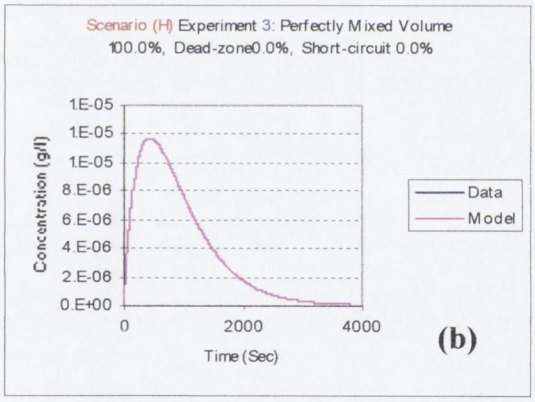

Figure E. 16 Graphs showing laboratory results and fitted model curves for Input and output variation scenario (H) into two CSTR in-series for (a) Exp.2 and (b) Exp.3.

Appendix F

Computer programme Codes

Appendix F

Computer programme Codes

F.1 Computer Programme 1

The following Computer programme using Basic language attached to Excel spreadsheet © has been employed to evaluate the tracer recovery at any time during the experiments run. The programme code is as following:

```
Function Recovery (teta, n, g)
Dim f As Double
Dim L As Double
Dim R As Double
Dim limit As Integer
f = 0
For limit = 1 To n Step 1
If limit = 1 Then
f1 = Exp (-n * teta)
Else
f1 = (n * teta ^ (limit - 1)) / factorial(limit - 1) * Exp(-n * teta)
End If
f = f + f1
Next
L = 1 - f
R = L * 100
Recovery = R
End Function
Function factorial (x)
Dim f1 As Double
If x <= 1 Then
f1 = 1
Else
f1 = x * factorial (x - 1)
End If
Factorial = f1
End Function
```

F.2 Computer Programme 2

Module-1

Computer programme placed into Visual Basic Editor to evaluate the fraction remaining in the system at any time (θ).

```
Function fraction (teta, n)
Dim f As Double
Dim limit As Integer
F = 0
For limit = 1 To n Step 1
If limit = 1 Then
Fl = Exp (-n * teta)
Else
Fl = (n * teta ^ (limit - 1)) / factorial (limit - 1) * Exp (-n * teta)
End If
F= f + fl
Next
Fraction = f
End Function
---------------------------------------------------------------------------
Function factorial (x)
Dim fl As Double
If x <= 1 Then
Fl = 1
Else
Fl = x * factorial (x - 1)
End If
Factorial = fl
End Function
```

F.3 Computer Programme 3

This programme was used to evaluate the amount of tracer that has been in the reactor for less than time (θ).

Module-2

```
Function Fcurve (teta, n)
Dim f As Double
Dim L As Double
Dim limit As Integer
F = 0
For limit = 1 To n Step 1
If limit = 1 Then
Fl = Exp (-n * teta)
Else
Fl = (n * teta ^ (limit - 1)) / factorial (limit - 1) * Exp (-n * teta)
End If
F = f + fl
Next
L = 1 - f
Fcurve = L
End Function
```

```
Function factorial (x)
Dim fl As Double
If x <= 1 Then
Fl = 1
Else
Fl = x * factorial (x - 1)
End If
Factorial = fl
End Function
```

Appendix G

Graphs for Reactor Diagnosis Experiments

(Rectangular CSTR)

Appendix G

Graphs for Reactor Diagnosis Experiments (Rectangular CSTR)

G.1 Trial-2 (Two CSTR-in-Series Fitted Model Curves)

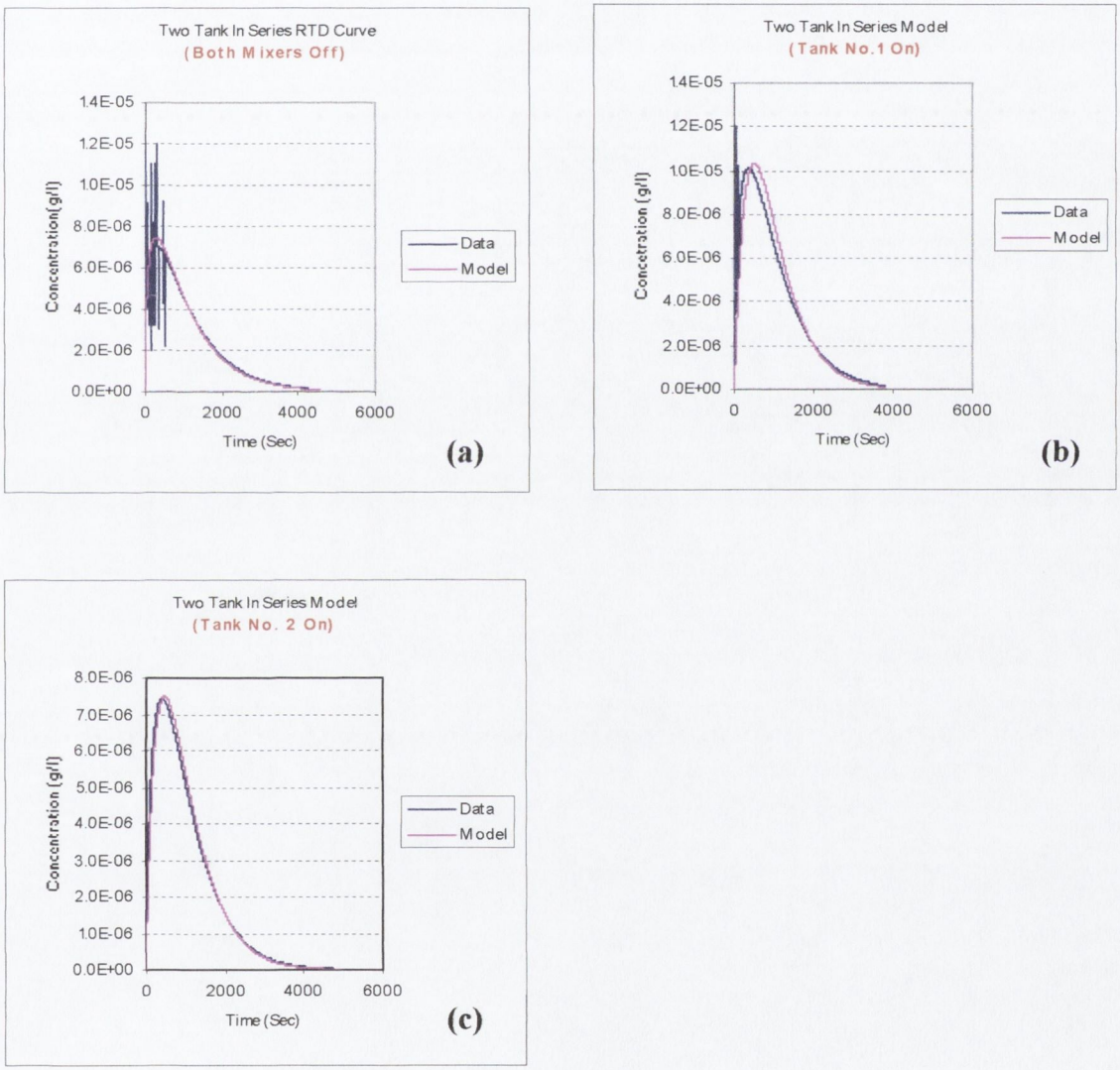

Figure G. 1 Graphs showing laboratory results and fitted model curves for Trial-2 scenarios into two CSTR-in-series for (a) Scenario B, (b) Scenario C and (c) Scenario D.

G.1.1 Trial-2 (Effluent Concentration Results Curves)

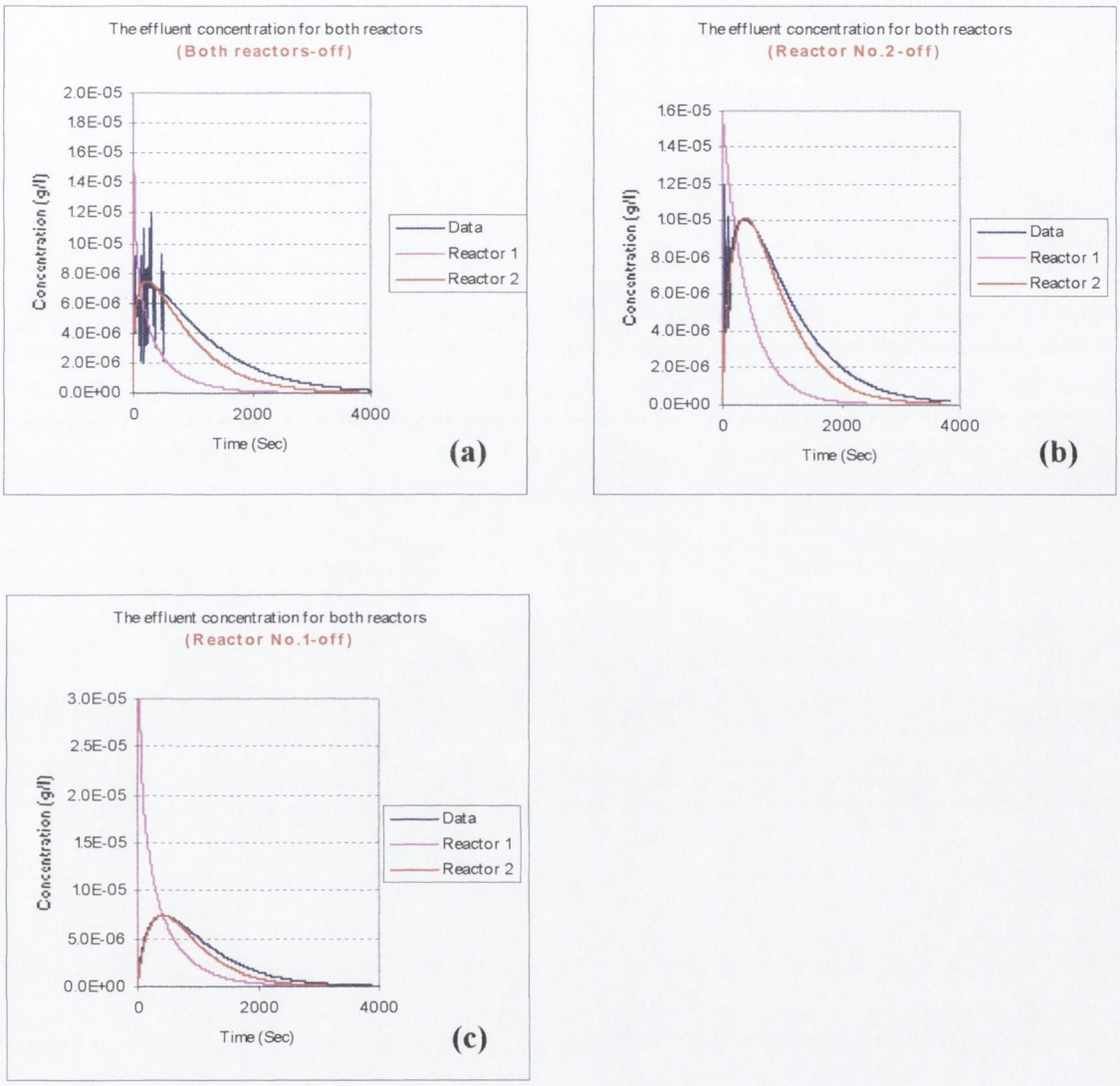

Figure G. 2 Graphs showing laboratory effluent concentration results and fitted model curves from each reactor for Trial-2 scenarios into two CSTR-in-series for (a) Scenario B, (b) Scenario C and (c) Scenario D.

G.2 Trial-3 (Three CSTR in-Series Fitted Model Curves)

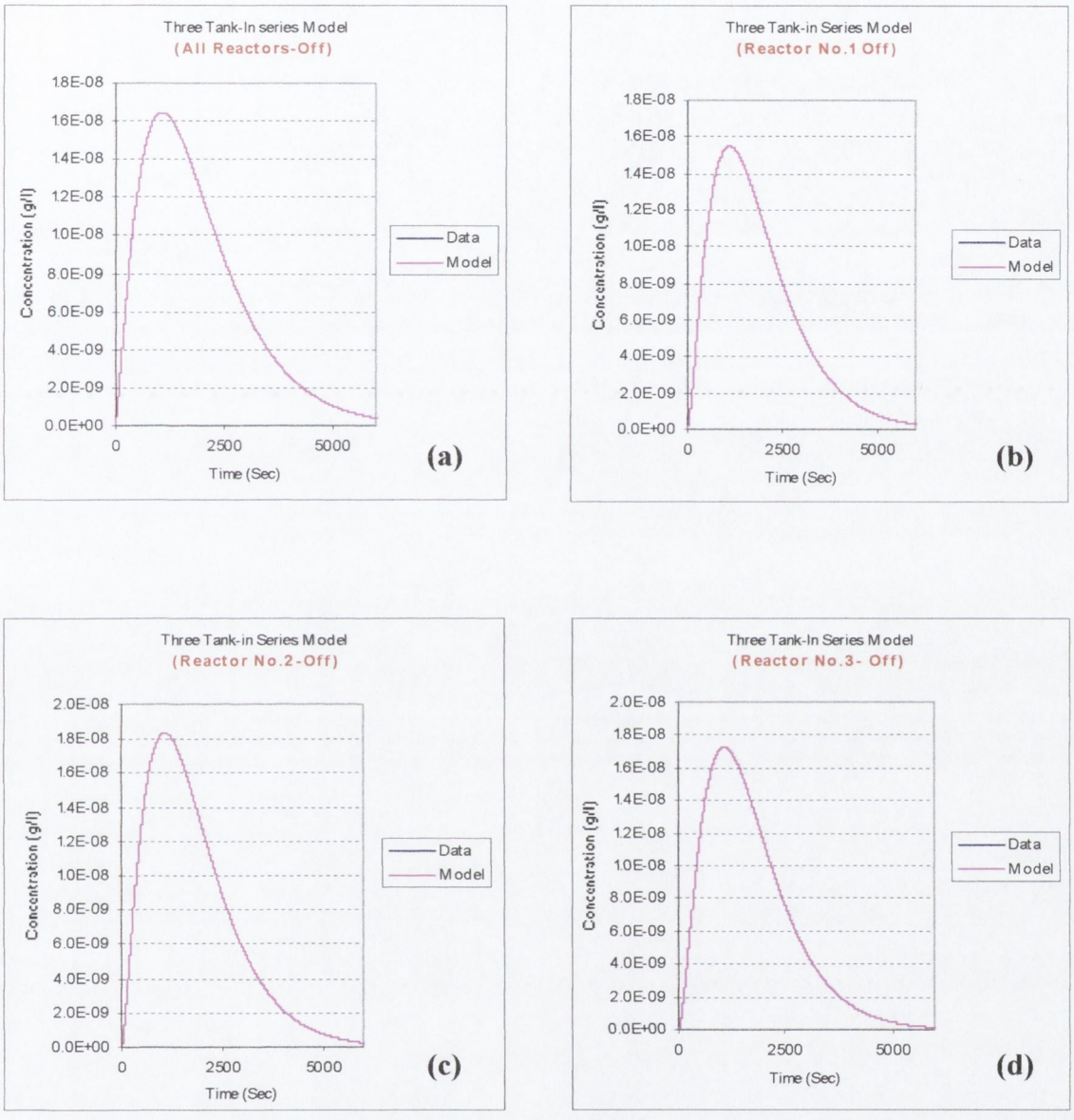

Figure G. 3 Graphs showing laboratory results and fitted model curves for Trial-3 scenarios into three CSTR-in-series for (a) Scenario B, (b) Scenario C, (c) Scenario D and (d) Scenario E.

G.2.1 Trial-3 (Effluent Concentration Results Curves)

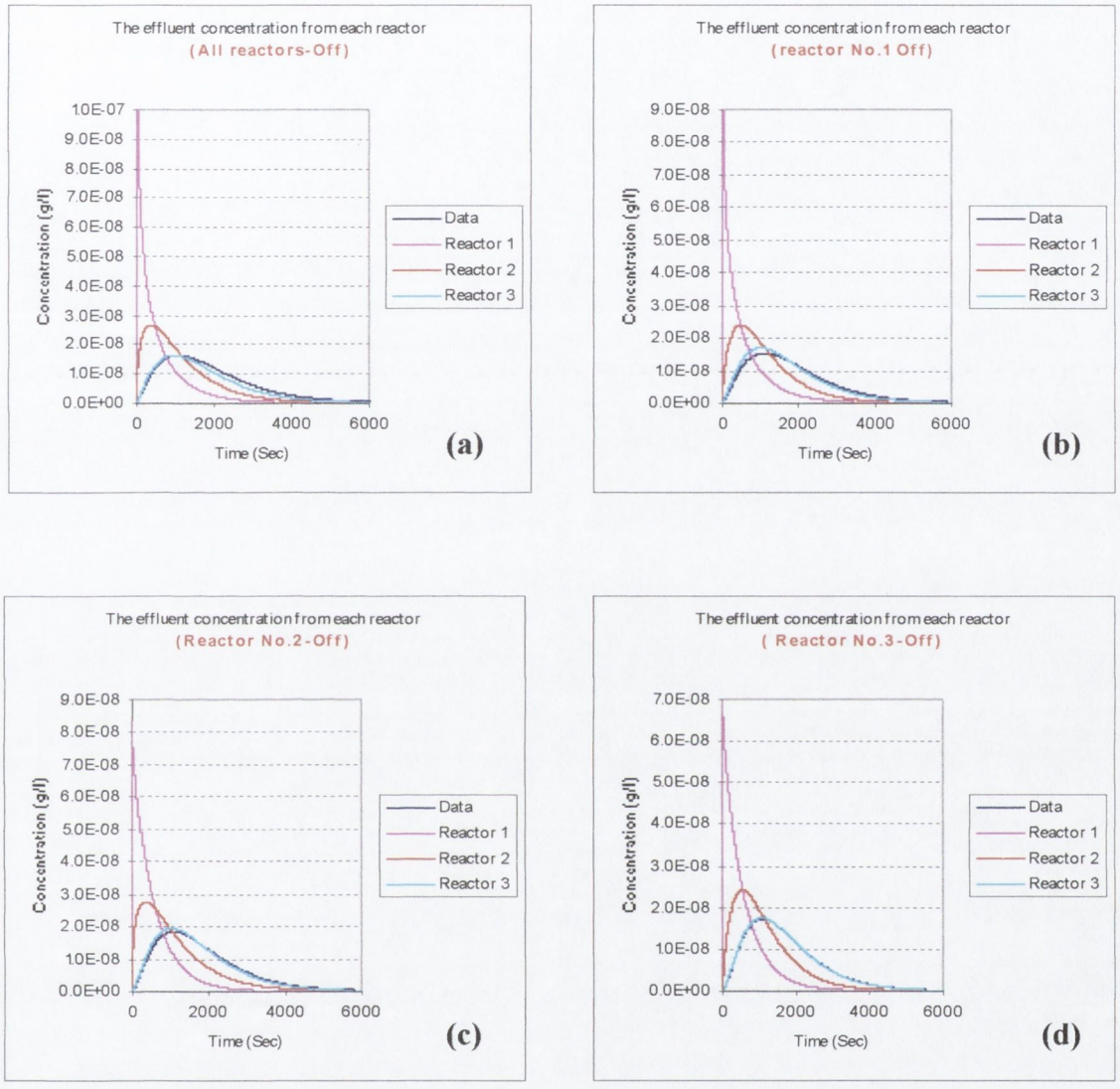

Figure G. 4 Graphs showing laboratory effluent concentration results and fitted model curves from each reactor for Trial-3 scenarios into three CSTR-in-series for (a) Scenario B, (b) Scenario C, (c) Scenario D and (d) Scenario E

G.3 Trial-4 (Four CSTR in-Series)

G.3.1 Overall Flow Direction Fitted Model Curves

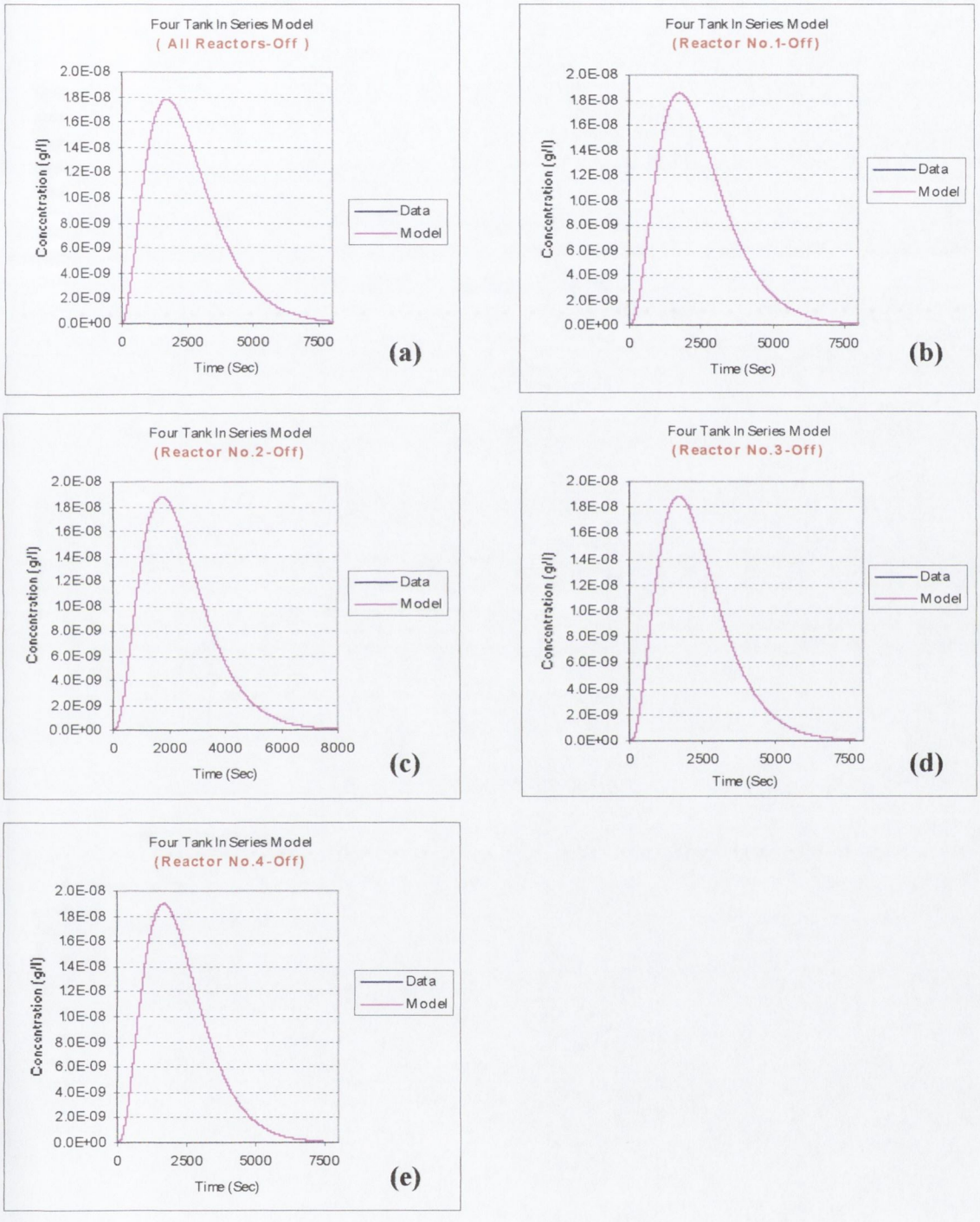

Figure G. 5 Graphs showing laboratory results and fitted model curves for Trial-4 scenarios into four CSTR-in-series (overall flow direction) for (a) Scenario B, (b) Scenario C, (c) Scenario D, (d) Scenario E and (e) Scenario F.

G.3.1.1 Overall Flow Direction (Effluent Concentration Results Curves)

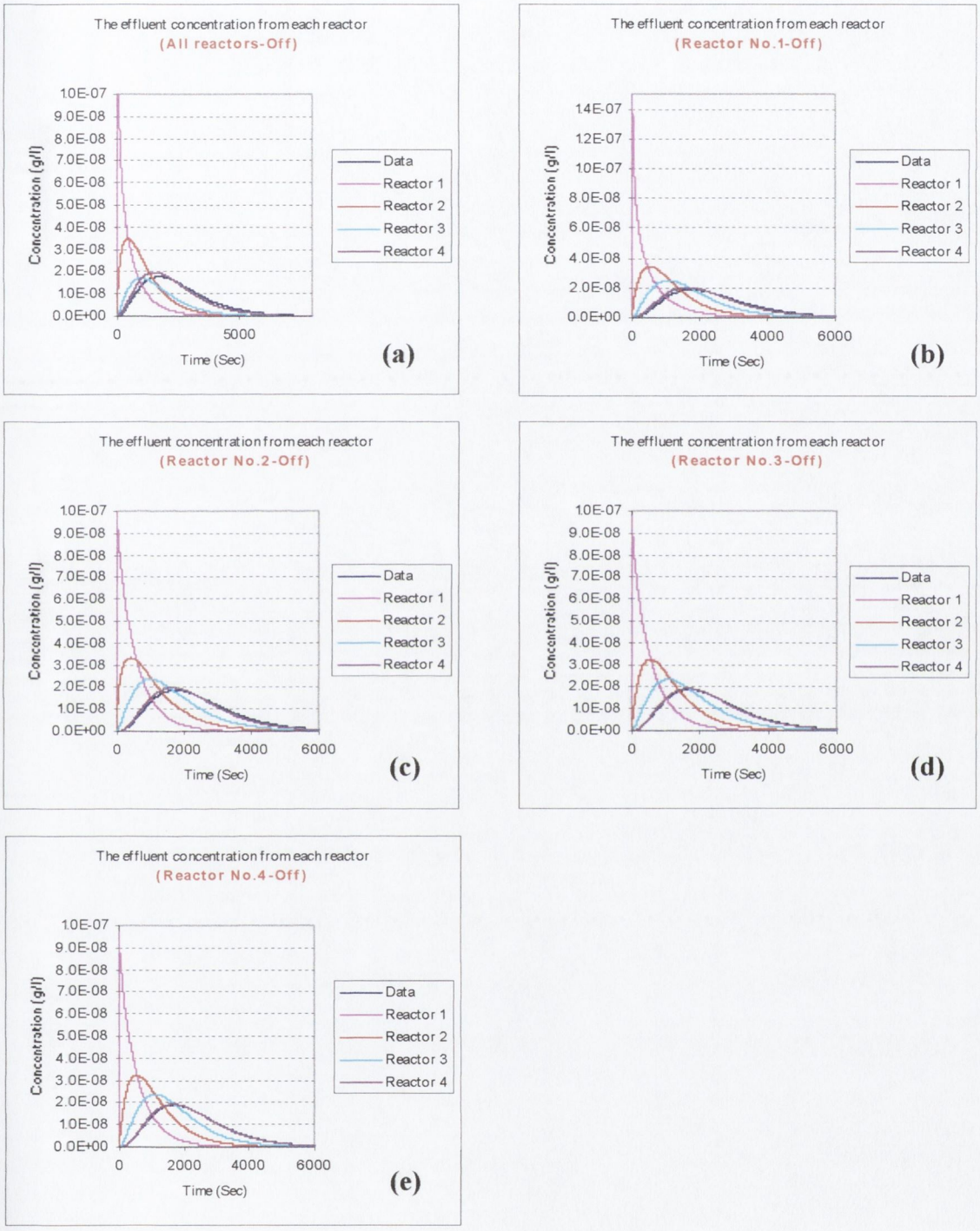

Figure G. 6 Graphs showing laboratory effluent concentration results and fitted model curves from each reactor for Trial-4 scenarios into four CSTR –in-series (overall flow direction) for (a) Scenario B, (b) Scenario C, (c) Scenario D, (d) Scenario E and (e) Scenario F

G.3.2 Vertical Flow Direction Fitted Model Curves

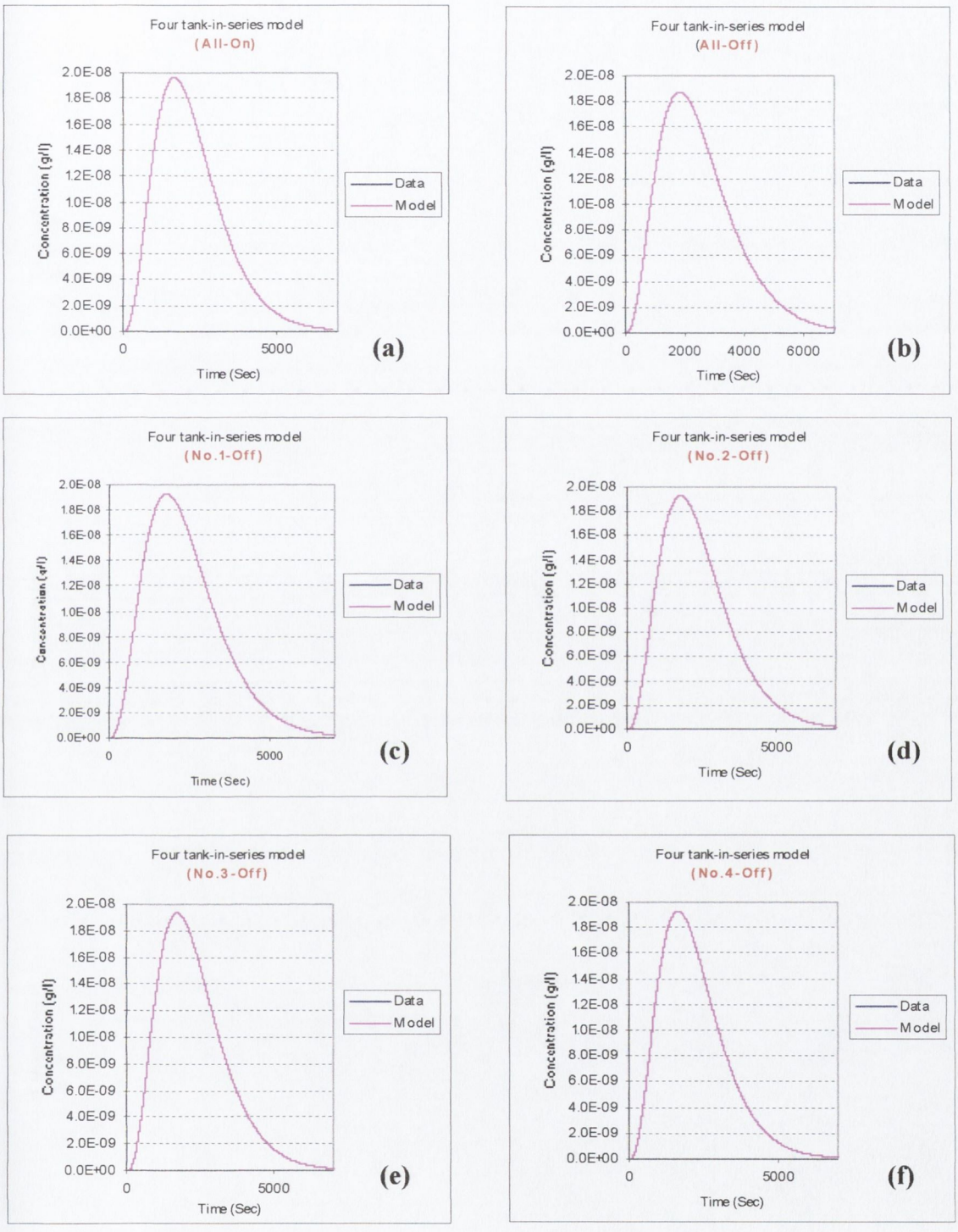

Figure G. 7 Graphs showing laboratory results and fitted model curves for Trial-4 scenarios into four CSTR-in-series (vertical flow direction) for (a) Scenario A, (b) Scenario B, (c) Scenario C, (d) Scenario D, (e) Scenario E and (f) Scenario F.

G.3.2.1 Vertical Flow Direction (Effluent Concentration Results Curves)

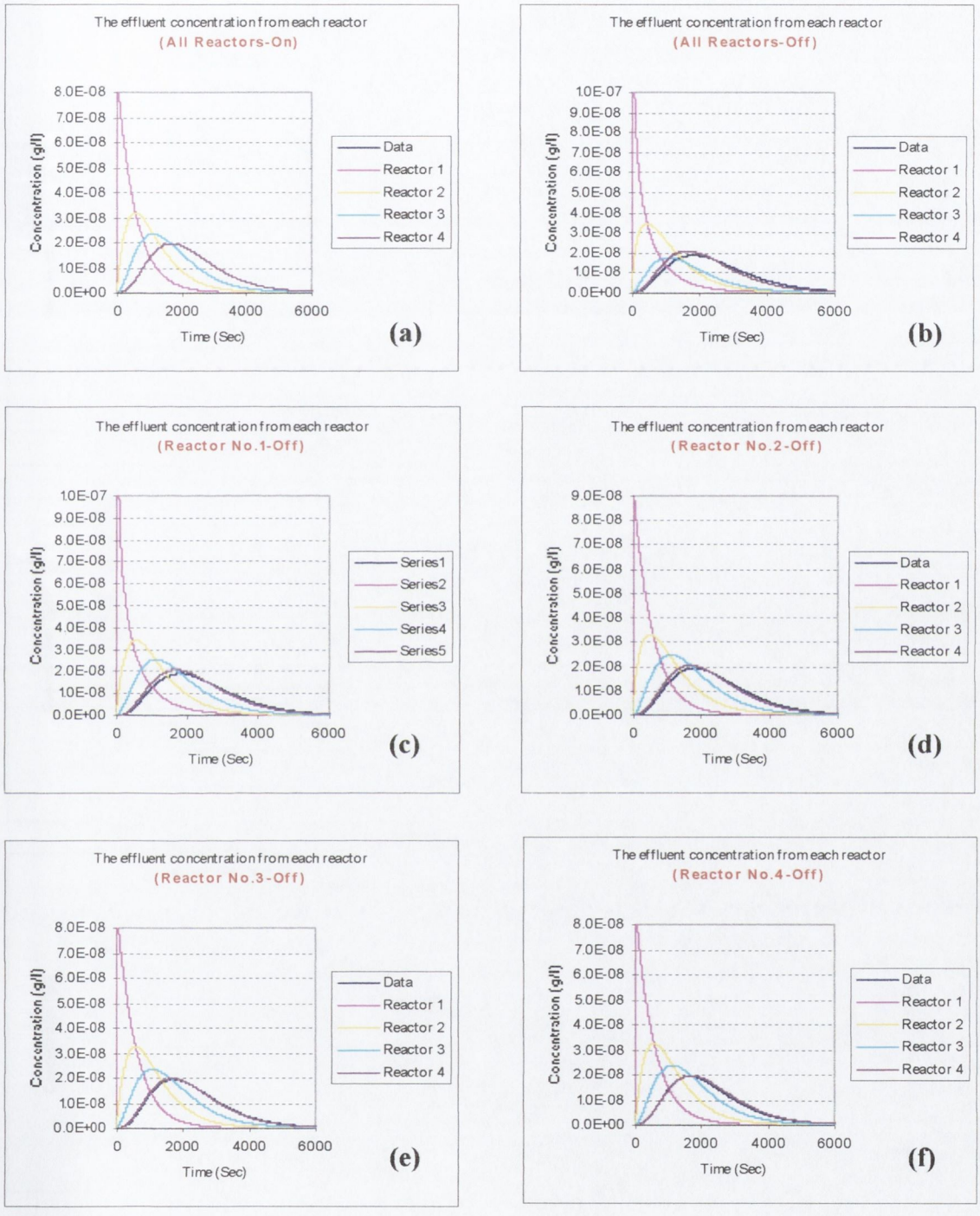

Figure G. 8 Graphs showing laboratory effluent concentration results and fitted model curves from each reactor for Trial-4 scenarios into four CSTR-in-series (vertical flow direction) for (a) Scenario A, (b) Scenario B, (c) Scenario C, (d) Scenario D, (e) Scenario E and (f) Scenario F

G.3.3 Horizontal Flow Direction Fitted Model Curves

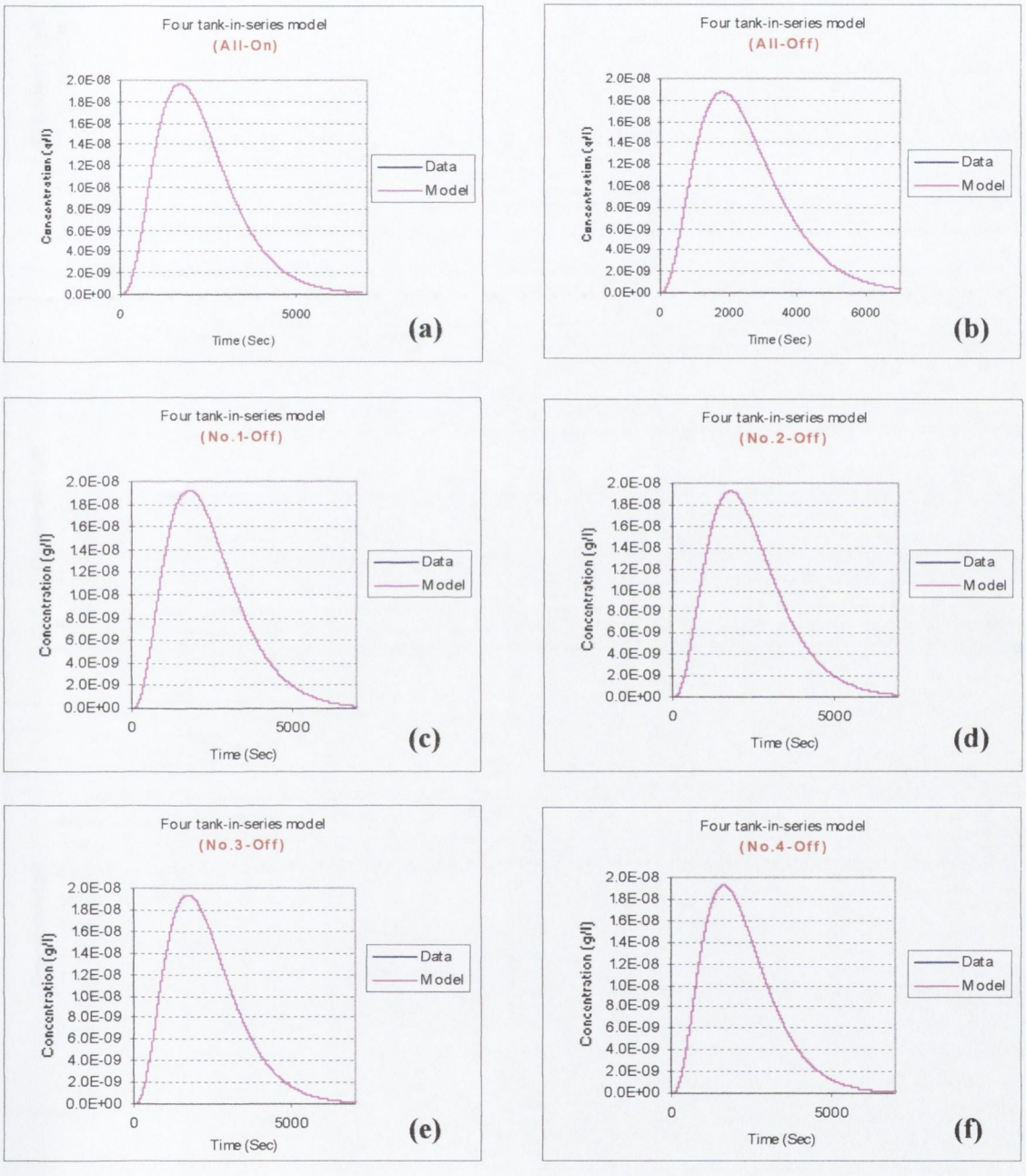

Figure G. 9 Graphs showing laboratory results and model curves for Trial-4 scenarios into rectangular CSTR for (a) Scenario A, (b) Scenario B, (c) Scenario C, (d) Scenario D, (e) Scenario E and (f) Scenario F.

G.3.3.1 Horizontal Flow Direction (Effluent Concentration Results Curves)

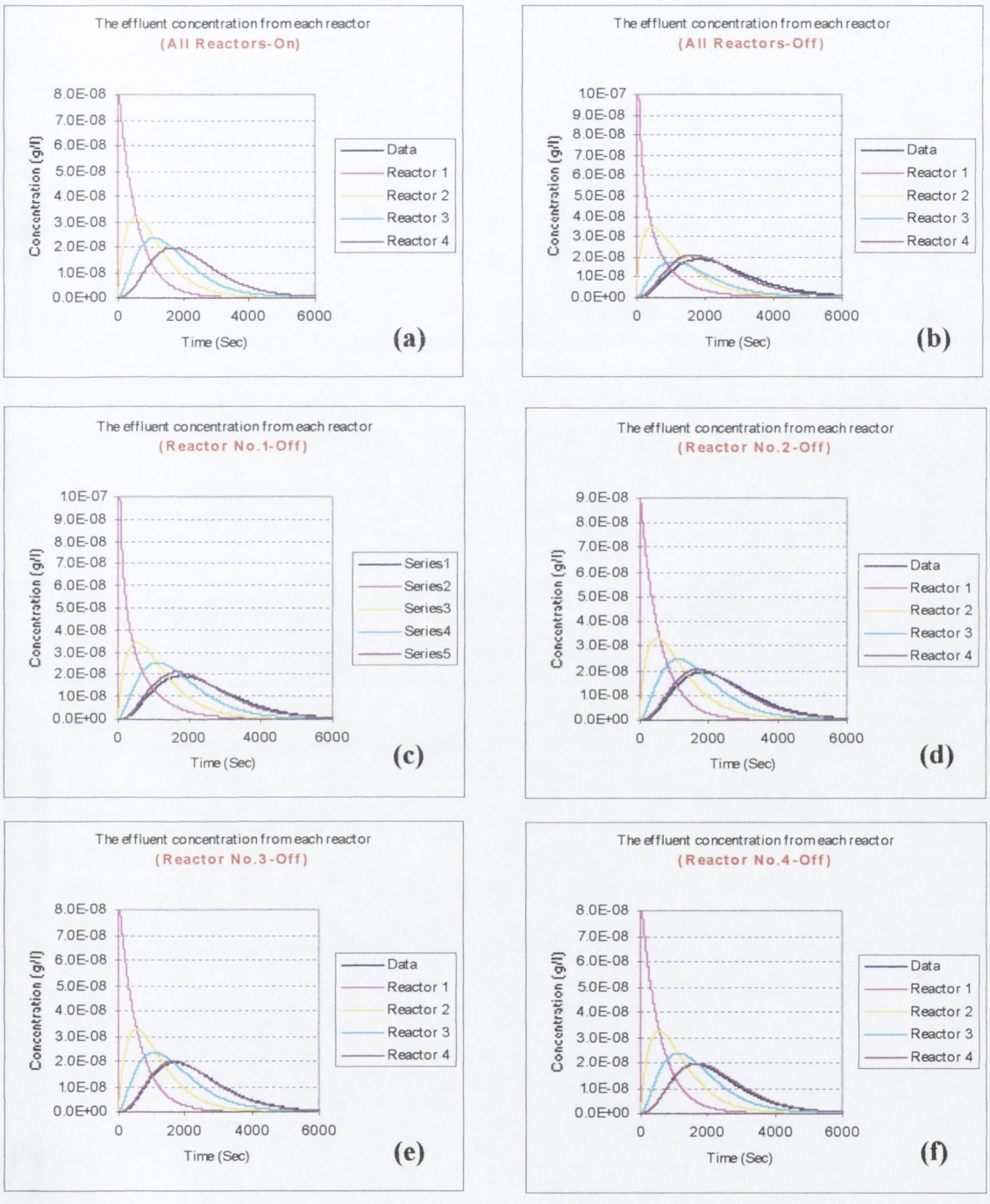

Figure G. 10 Graphs showing laboratory effluent concentration results and fitted model curves from each reactor for Trial-4 scenarios into four CSTR-in-series (horizontal flow direction) for (a) Scenario A, (b) Scenario B, (c) Scenario C, (d) Scenario D, (e) Scenario E and (f) Scenario F

G.4 Input and Output Variation Fitted Model Curves

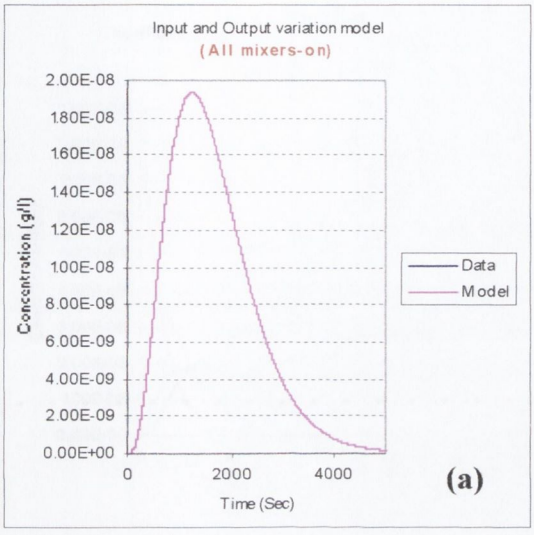

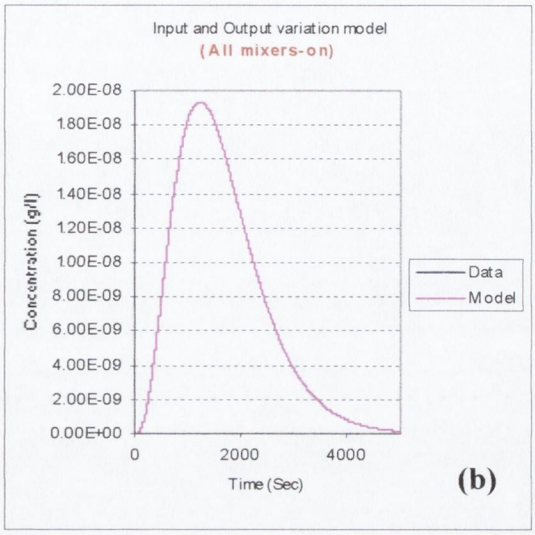

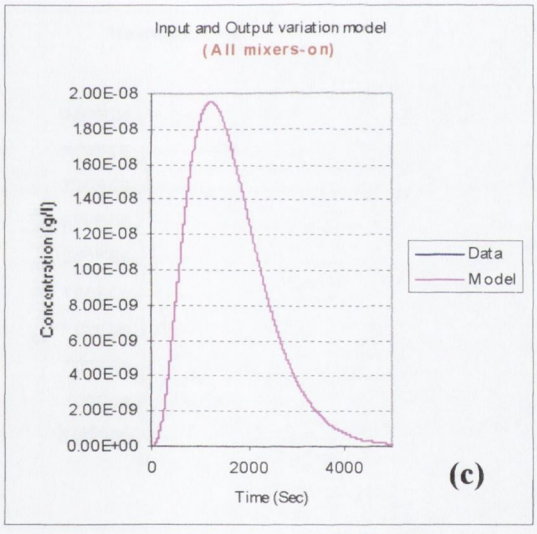

Figure G. 11 Graphs showing laboratory results and fitted model curves for input and output variation scenarios into four CSTR-in-series for (a) Scenario B, (b) Scenario C and (c) Scenario D

G.4.1 Input and Output Variation (Effluent Concentration Results Curves)

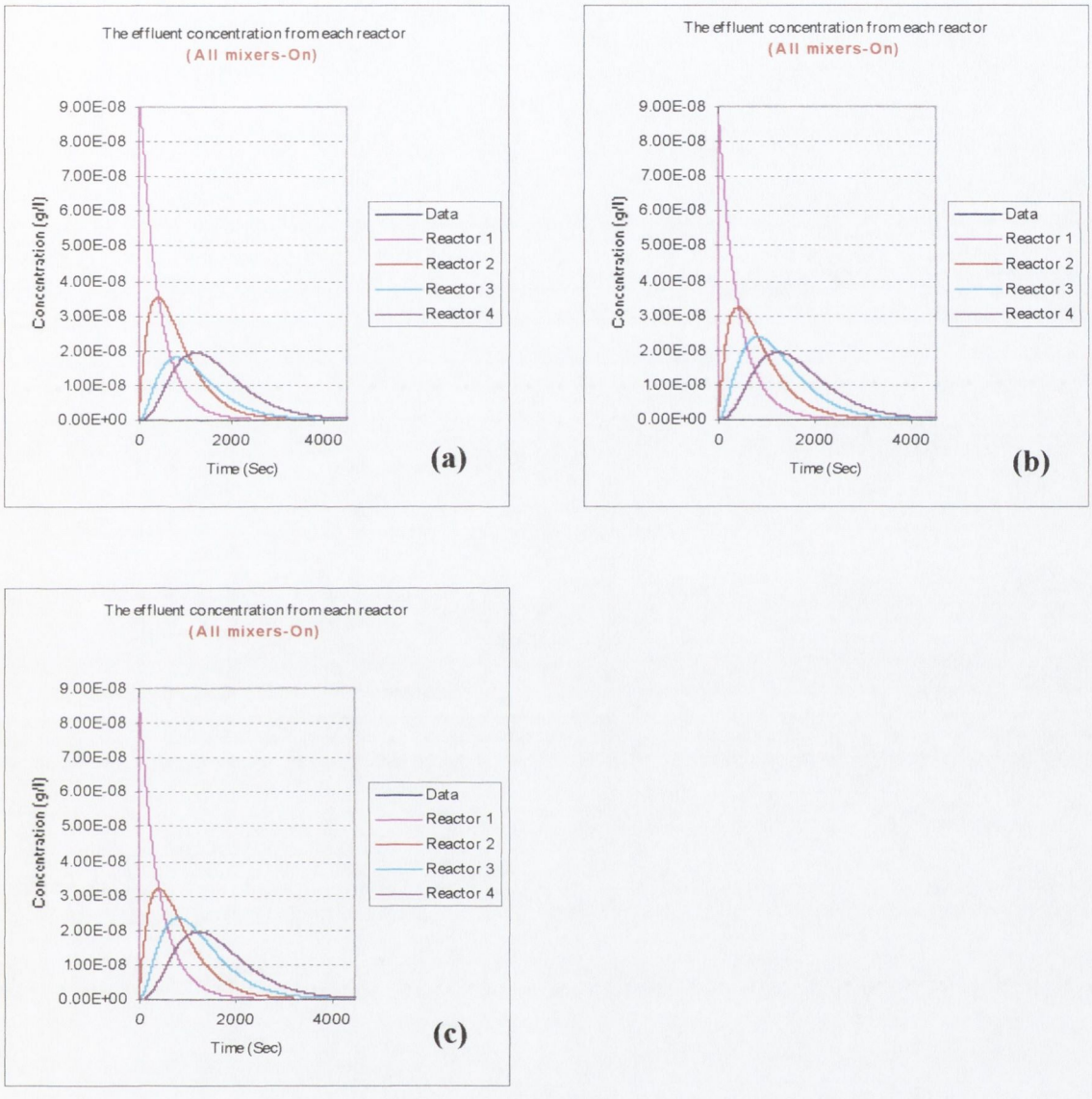

Figure G. 12 Graphs showing laboratory effluent concentration results and fitted model curves from each reactor for input and output variation scenarios into four CSTR-in-series for (a) Scenario B, (b) Scenario C and (c) Scenario D

Appendix H

Physical Properties of Water and Air

Appendix H

Physical Properties of Water

H.1 Velocity Gradient (G)

The velocity gradient is known as the rate of shear, which represents the differences in velocity between the layers of fluid. It is this speed variation (or velocity gradient dv/dy) that causes viscosity and is responsible for shearing the fluid internally; therefore, the magnitude of the shear stress depends on the velocity gradient from layer to layer. The mathematical relationship of velocity gradient, shear stress and dynamic viscosity is given as:

$$\mu = \frac{\tau_s}{dv/dy} \qquad \text{----------(H.1)}$$

where,

μ= dynamic viscosity of fluid (Ns/ m^2) or (kg /ms)
τs= shear stress of fluid (N/m^2)
dv/dy= the velocity gradient (S^{-1})

The velocity gradient is also known as (G) (see Chapter 8) which itself depends on the power input per unit volume, volumetric flow rate, reactor volume and the dynamic viscosity.

H.2 Shear stress (τ_s) & shear strain (∅)

Consider ABCD as shown in Figure H.1 represents an element in a fluid with thickness (L) perpendicular to the diagram, then the force F will act over an area (A) equal to (AB × L).

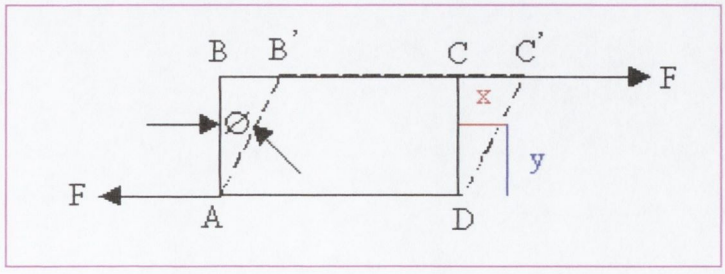

Figure H. 1 Deformation caused by shearing forces

The force per unit area is known as shear stress (τ_s) is given as:

$$Shear\ stress, \tau_s = \frac{F}{A} \qquad ----------(H.2)$$

The deformation measured by the angle ($\varnothing$) is known as shear strain is given as:

$$Shear\ strain, \Phi = \frac{x}{y} \qquad ----------(H.3)$$

where,

F= force (N)
A= area (m^2)
τs=shear stress of fluid (N/m^2)
$\varnothing$=shear strain of fluid (unit less)
X= distance in x-direction (m)
Y= distance in y-direction (m)

H.2 Dynamic Viscosity (μ)

Viscosity is an important property that affects the behaviour of hydraulic systems. The coefficient of dynamic viscosity μ can be defined as the shear force per unit area (or shear stress) required to drag one layer of fluid with velocity past another layer a unit distance away from it in the fluid. The unit of dynamic viscosity is (kg/ms) or ($N\ s\ m^{-2}$), and is easily to be found by using the chart Figure H.2 below or by using the Table H.1 as shown below.

$$\mu = \frac{Force \times Time}{Area} \quad \text{or} \frac{Mass}{Length \times Time} \qquad -------(H.4)$$

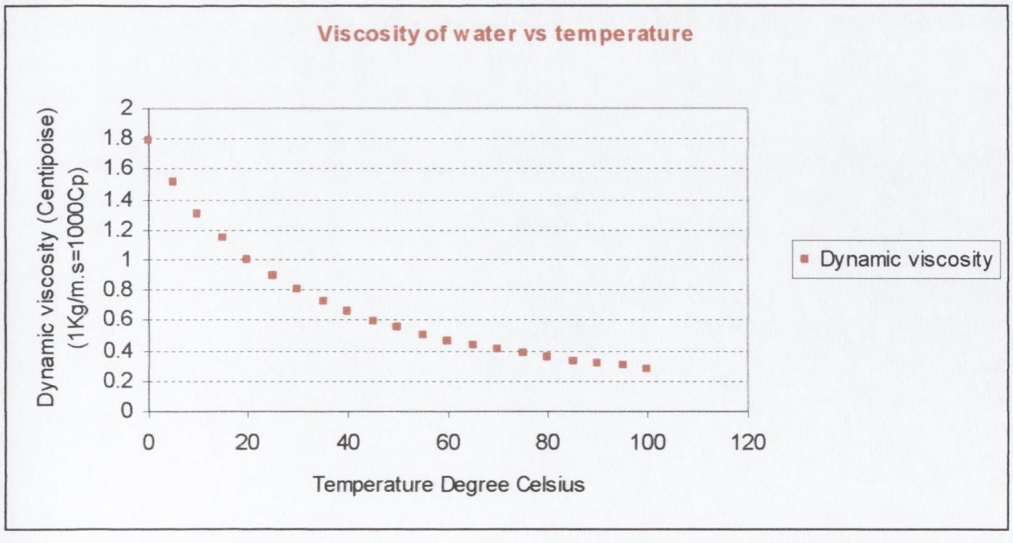

Figure H. 2 Viscosity of water versus temperature

Temperature (Celsius)	Dynamic Viscosity (Centipoise)
0	1.787
5	1.519
10	1.307
15	1.139
20	1.002
25	0.8904
30	0.7975
35	0.7194
40	0.6529
45	0.596
50	0.5468
55	0.504
60	0.4665
65	0.4335
70	0.4042
75	0.3781
80	0.3547
85	0.3337
90	0.3147
95	0.2975
100	0.2818

Table H. 1 Dynamic viscosity vs. temperature

H.3 Density of Water (ρ)

The density of wastewater ρ_w is defined as its mass per unit volume expressed as kg/m^3. Density is an important physical characteristic of wastewater because of the potential for the formation of density currents in the treatment units such as aeration system, sediments tanks and chlorine contact tanks. For water, ρ is 1000 kg/m^3 at 4°C. There is a slight decrease in density with increasing temperature; this can be seen graphically as shown in Figure H.3 and numerically as shown in Table H.2.

Temperature C°	Density (Kg/m^3)
0	999.8
5	1000.0
10	999.7
15	999.1
20	998.2
25	997.0
30	995.7
40	992.2
50	988.0
60	983.2
70	977.8
80	971.8
90	965.3
100	958.4

Table H. 2 Density of water vs. temperature

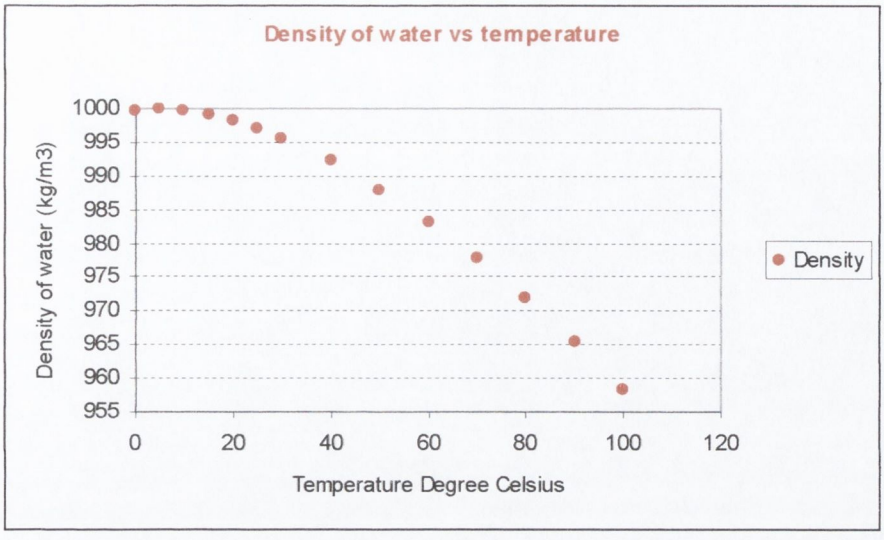

Figure H. 3 Density of water versus temperature

H.4 Kinematic Viscosity (ν)

In many problems concerning the fluid motion, the viscosity appears with the density in the form with single term (ν) is defined as the ratio of dynamic viscosity to mass density:

$$\nu = \frac{\mu}{\rho} \qquad \text{----------}(H.5)$$

where,

ν= kinematic Viscosity (m^2/s)
μ= dynamic Viscosity (Ns/m^2)
ρ= density of Water (mg/m^3)

The kinematic viscosity of a liquid diminishes with increasing temperature this can be seen numerically as shown in Table H.3 and graphically as shown in Figure H.4.

Temperature C^0	Kinematic viscosity x 10^6 (m^2/s)
0	1.785
5	1.519
10	1.306
15	1.139
20	1.003
25	0.893
30	0.800
40	0.658
50	0.553
60	0.474
70	0.413
80	0.364
90	0.326
100	0.294

Table H. 3 Kinematic viscosity vs. temperature

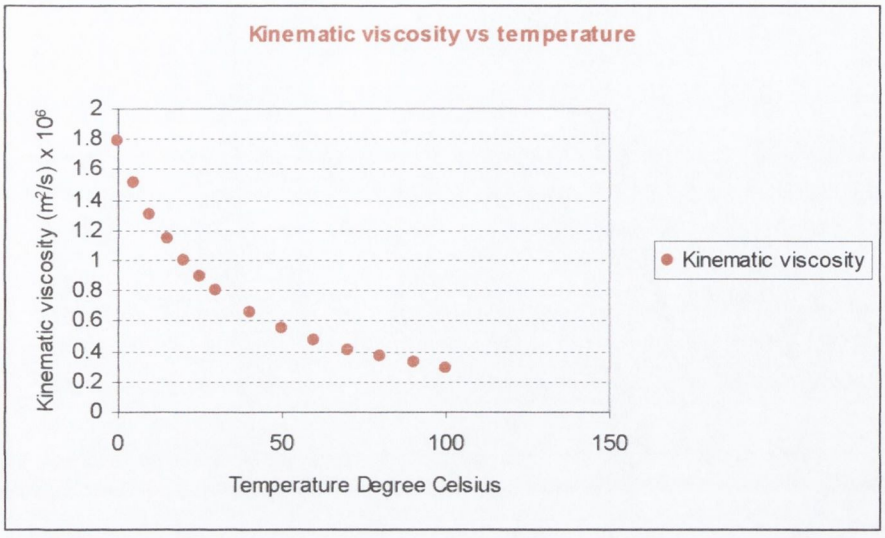

Figure H. 4 Kinematic viscosity of water versus temperature

H.5 Density of Air at Given Temperature

The following relationship has been used to compute the density of air ρ_a at a given temperature.

$$\rho_a = \frac{PM}{RT} \qquad ----------(H.6)$$

where,

P=atmospheric pressure = $1.01325 \times 10^5\ N/m^2$
M=mole of air = 28.97 kg/kg-mole
R=universal gas constant = 8314 N.m/kg-mole.K
T= temperature, K (Kelvin) = $273.15+C^0$

H.6 Weight of flow of air

The following relationship has been used to compute the weight of flow of air W at given temperature, density and air flow rate.

$$W = Q_{air} \times \rho_a \qquad ----------(H.7)$$

where,

W=weight of air per time at given temperature (g/s)
Q_{air}= air flow rate (m^3/s)
ρ_a= Density of air (g/m^3)

Appendix I

Graphs for Full-scale Implementation Trials

Appendix I

Graphs for Full-scale Implementation Trials

I.1 Approximated Scaled-down Version [Trial-1]

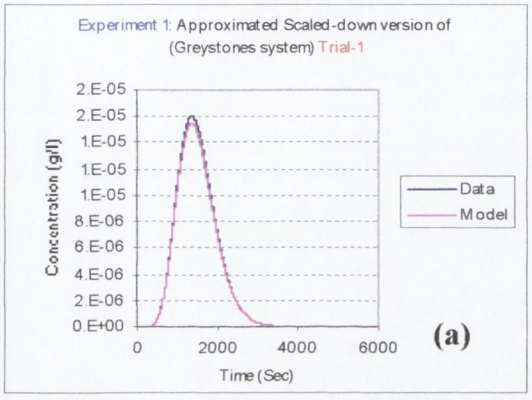

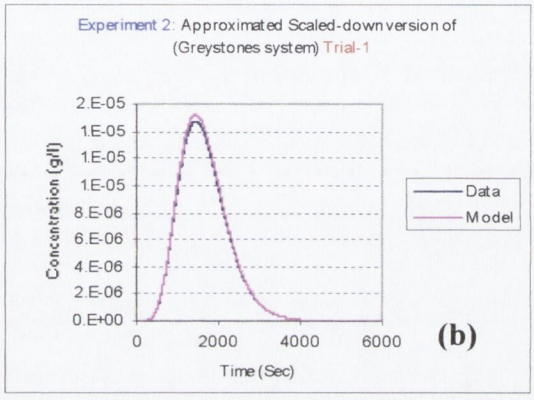

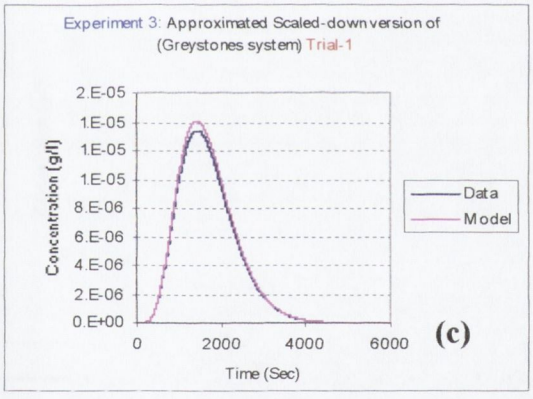

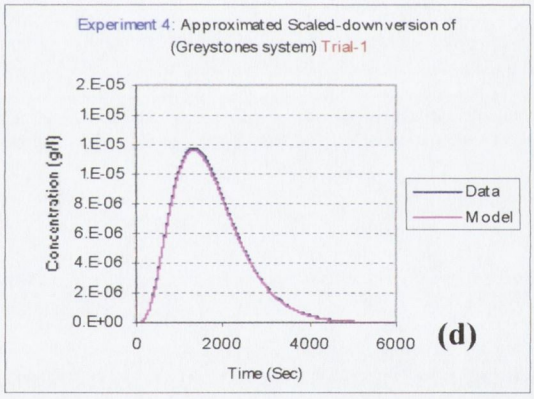

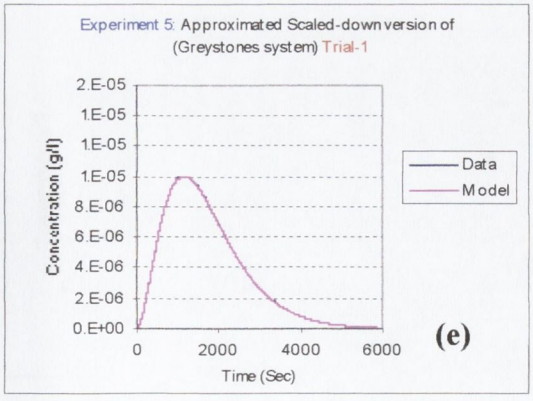

Figure I. 1 Graphs showing laboratory results and fitted model curves for approximated scaled-down version Trial-1 for (a) Exp.1, (b) Exp.2, (c) Exp. 3, (d) Exp. 4, and (e) Exp. 5

I.1.1 Effluent Concentration Result Curves for [Trial-1]

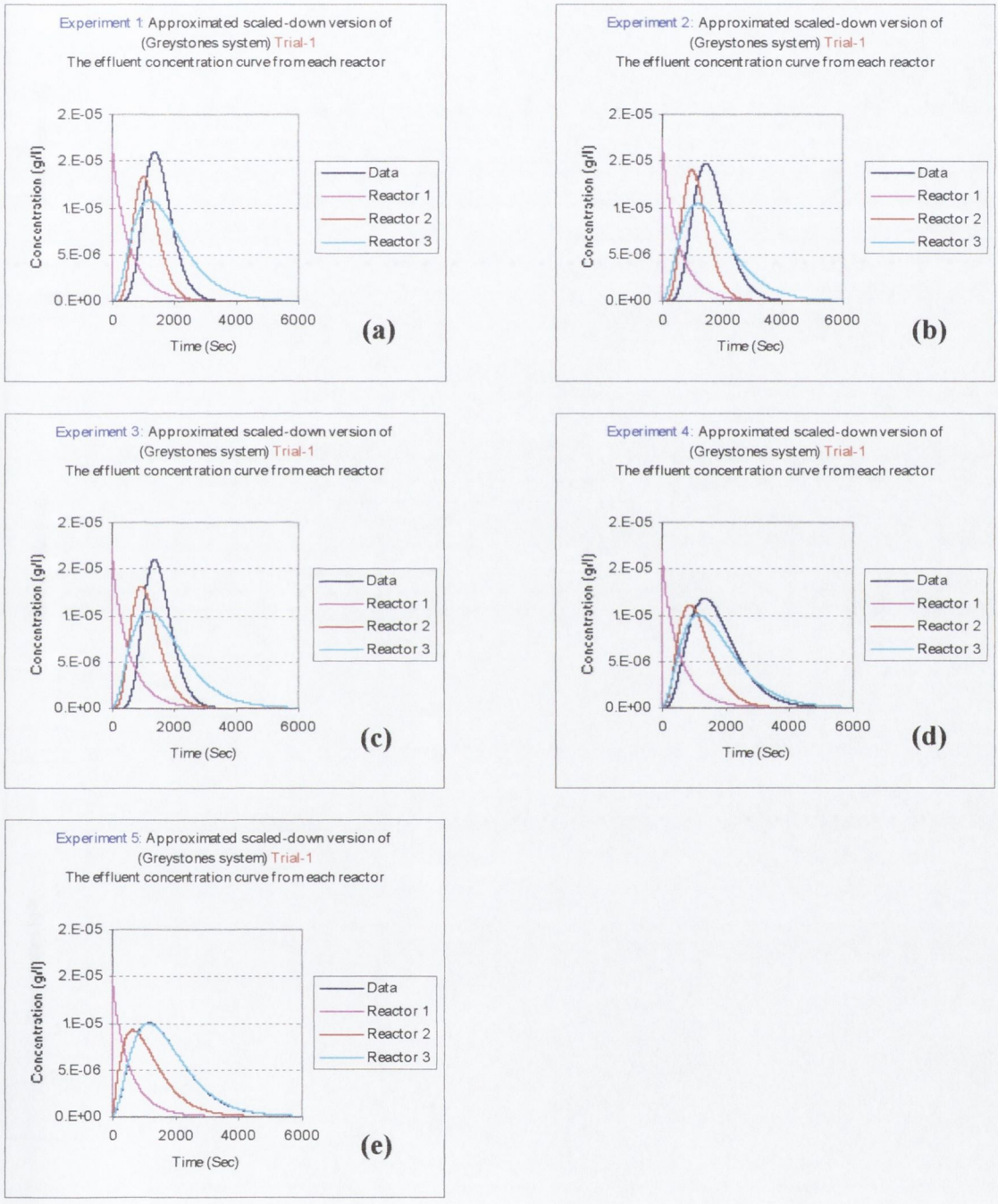

Figure I. 2 Graphs showing laboratory effluent concentration results and fitted model curves from each reactor for approximated scaled-down version Trial-1 for (a) Exp.1, (b) Exp.2, (c) Exp. 3, (d) Exp. 4, and (e) Exp. 5

I.2 Approximated Scaled-down Version [Trial-2]

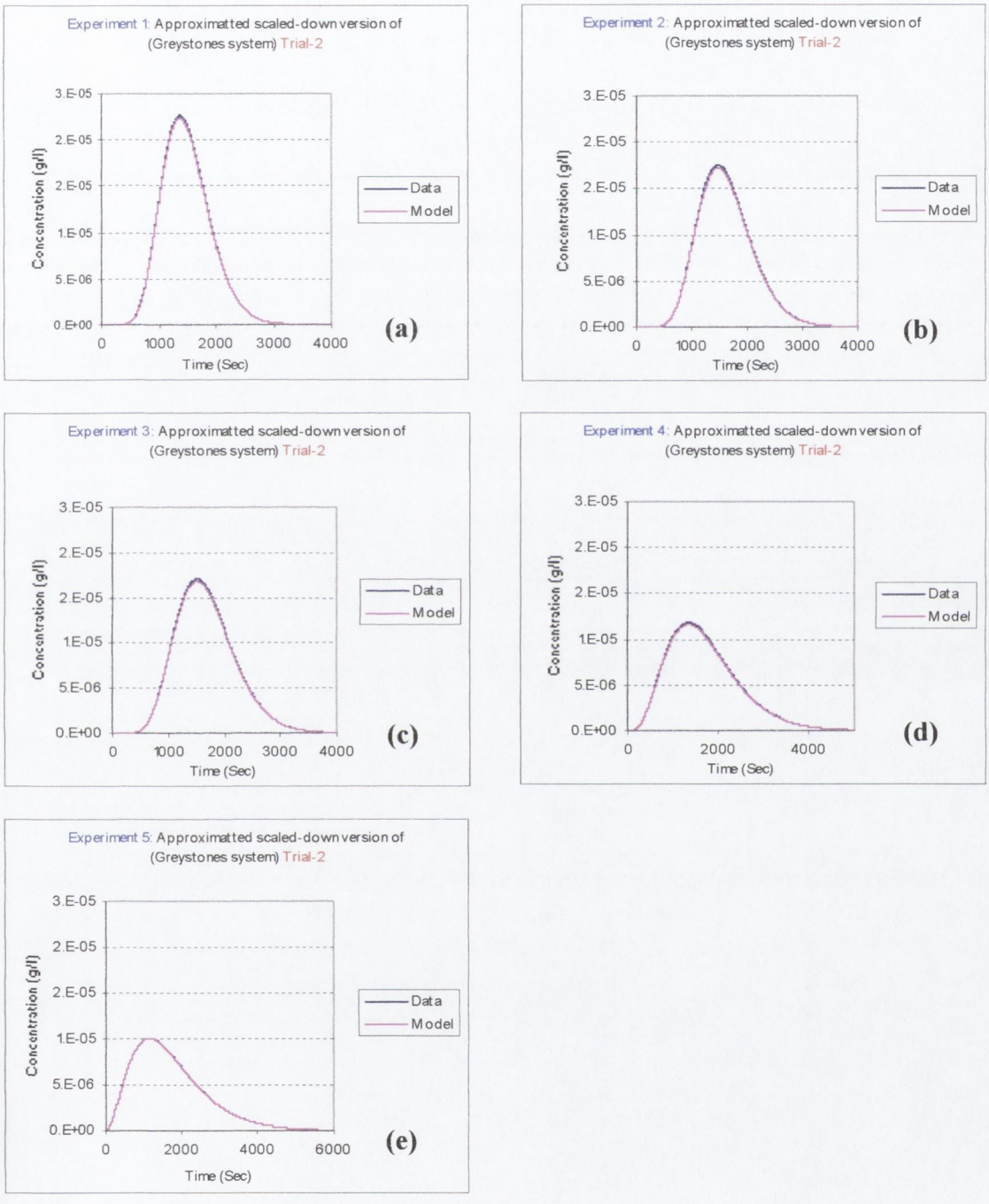

Figure I. 3 Graphs showing laboratory results and fitted model curves for approximated scaled-down version Trial-2 for (a) Exp.1, (b) Exp.2, (c) Exp. 3, (d) Exp. 4, and (e) Exp. 5

I.2.1 Effluent Concentration Result Curves for [Trial-2]

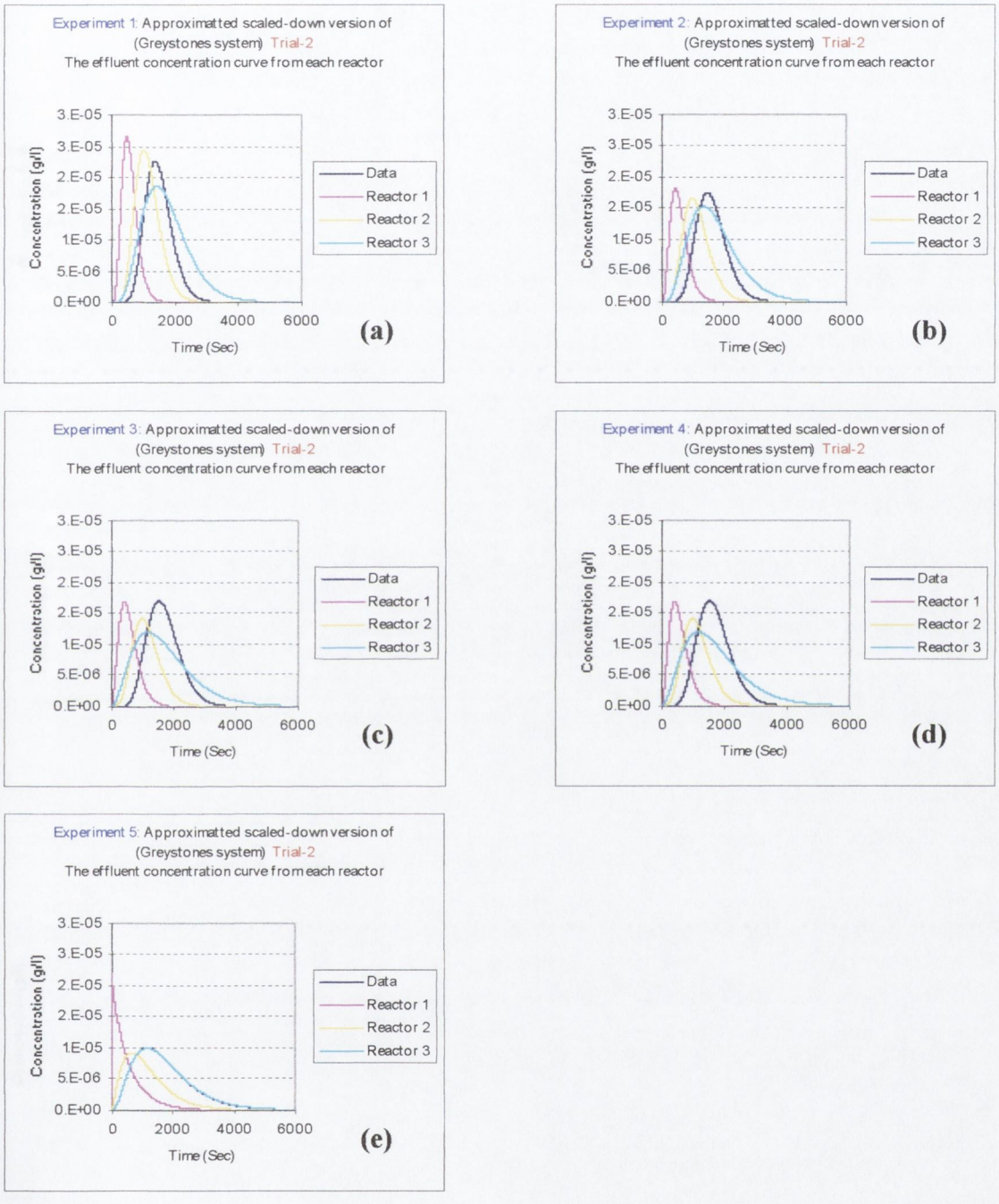

Figure I. 4 Graphs showing laboratory effluent concentration results and fitted model curves from each reactor for approximated scaled-down version Trial-2 for (a) Exp.1, (b) Exp.2, (c) Exp. 3, (d) Exp. 4, and (e) Exp. 5

I.3 Modification Version [Trial-1]

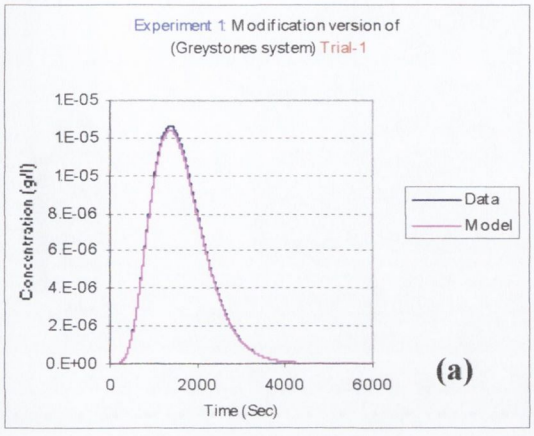

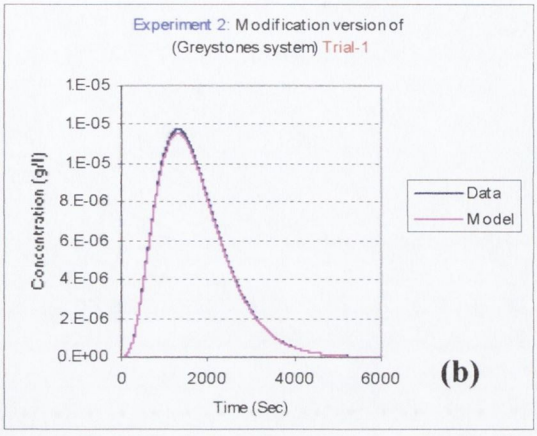

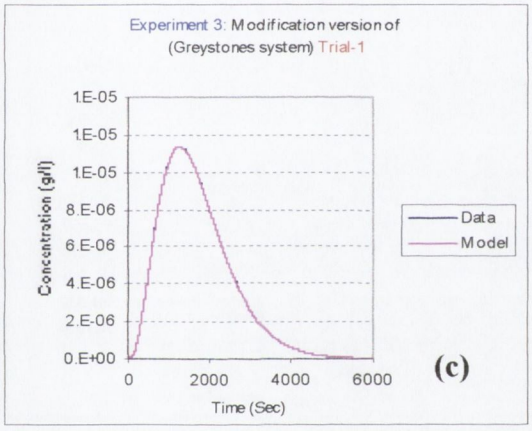

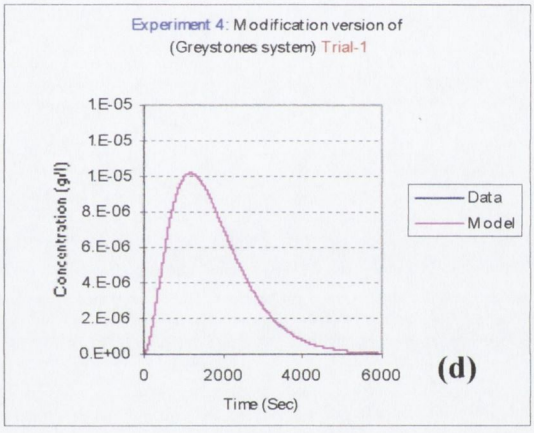

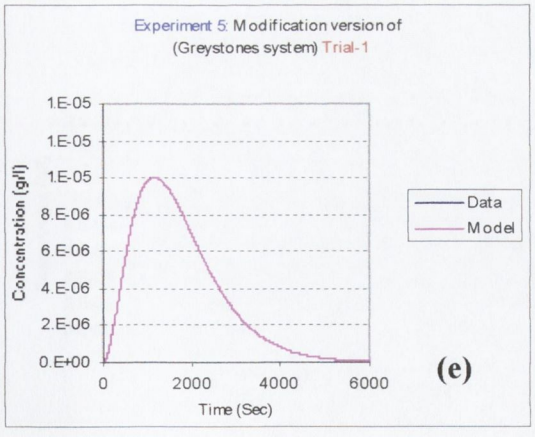

Figure I. 5 Graphs showing laboratory results and fitted model curves for modification version Trial-1 for (a) Exp.1, (b) Exp.2, (c) Exp. 3, (d) Exp. 4, and (e) Exp. 5

I.3.1 Effluent Concentration Result Curves for [Trial-1]

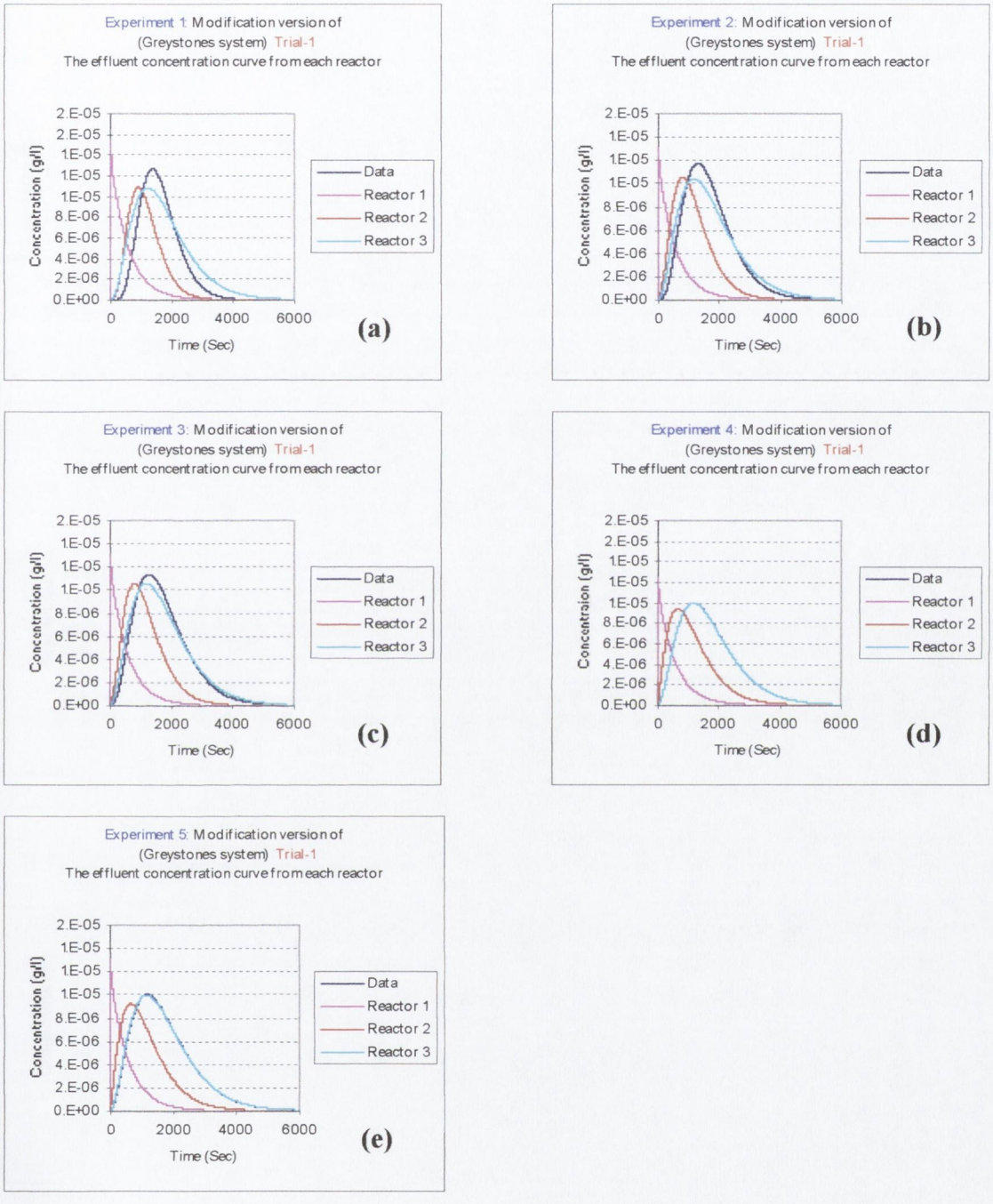

Figure I. 6 Graphs showing laboratory effluent concentration results and fitted model curves from each reactor for modification version Trial-1 for (a) Exp.1, (b) Exp.2, (c) Exp. 3, (d) Exp. 4, and (e) Exp. 5

I.4 Modification Version [Trial-2]

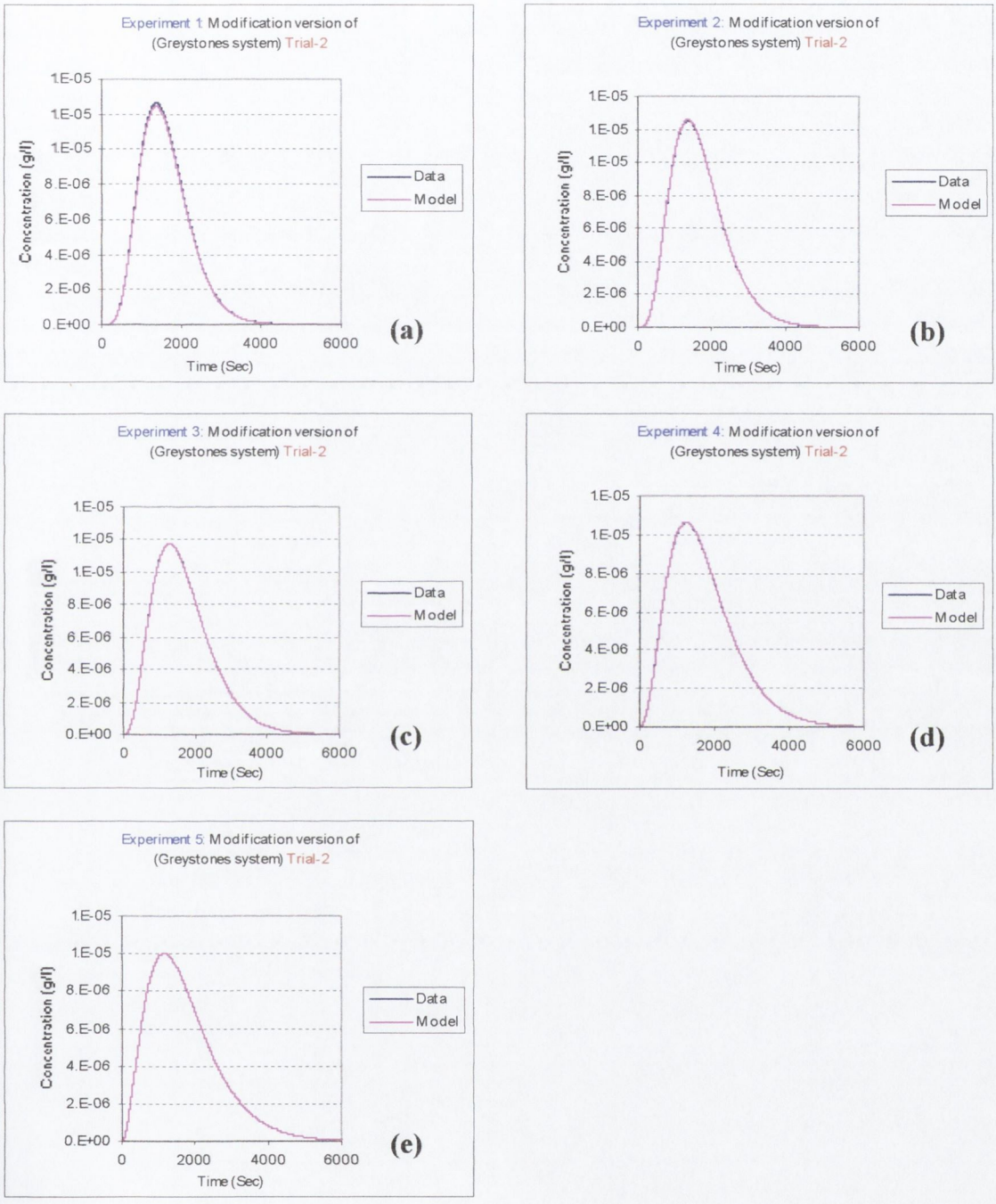

Figure I. 7 Graphs showing laboratory results and fitted model curves for modification version Trial-2 for (a) Exp.1, (b) Exp.2, (c) Exp. 3, (d) Exp. 4, and (e) Exp. 5

I.4.1 Effluent Concentration Result Curves for [Trial-2]

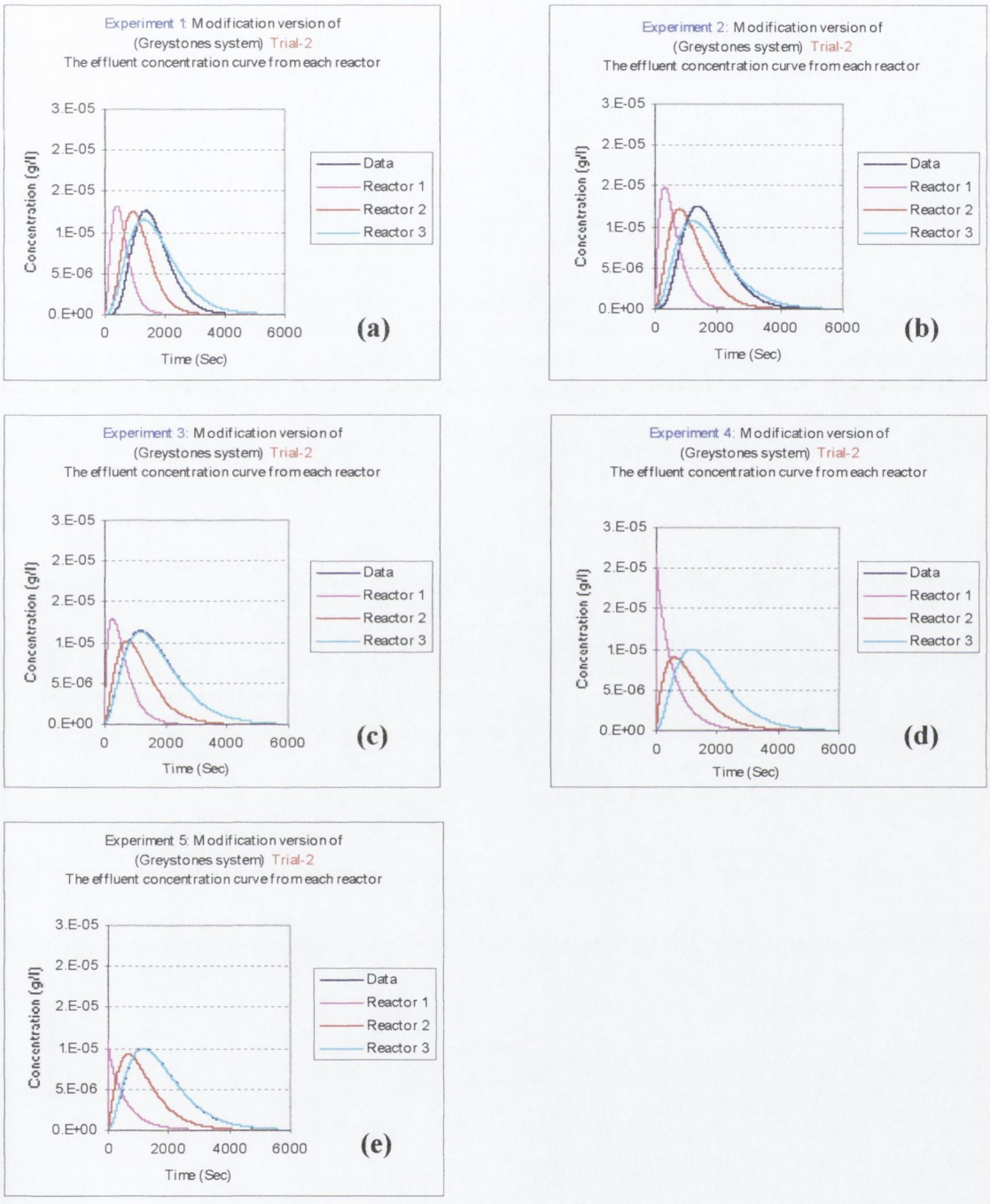

Figure I. 8 Graphs showing laboratory effluent concentration results and fitted model curves from each reactor for modification version Trial-2 for (a) Exp.1, (b) Exp.2, (c) Exp. 3, (d) Exp. 4, and (e) Exp. 5

I.5 Scaled-down Version [Trial-1]

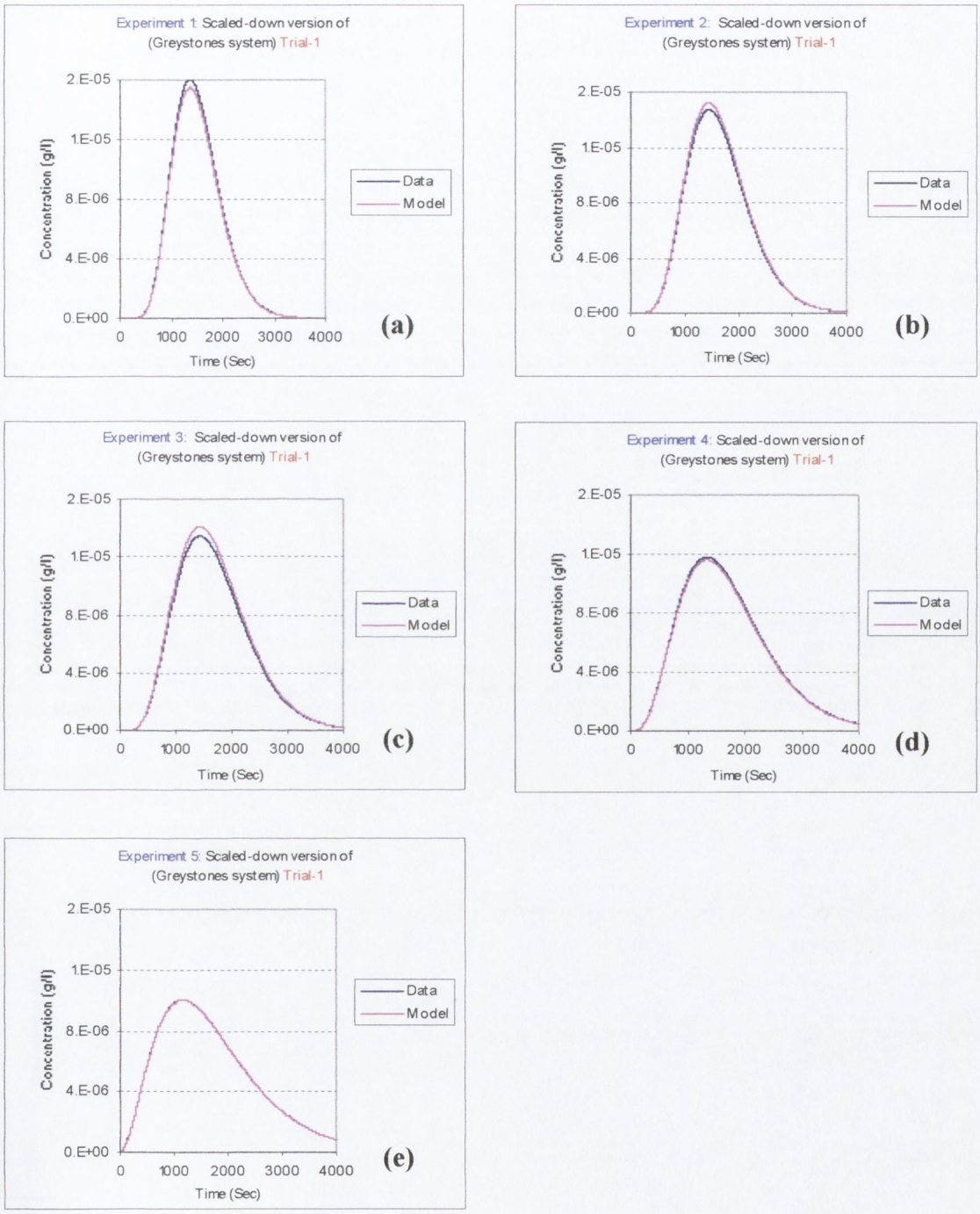

Figure I. 9 Graphs showing laboratory results and fitted model curves for scaled-down version Trial-1 for (a) Exp.1, (b) Exp.2, (c) Exp. 3, (d) Exp. 4, and (e) Exp. 5

I.5.1 Effluent Concentration Result Curves for [Trial-1]

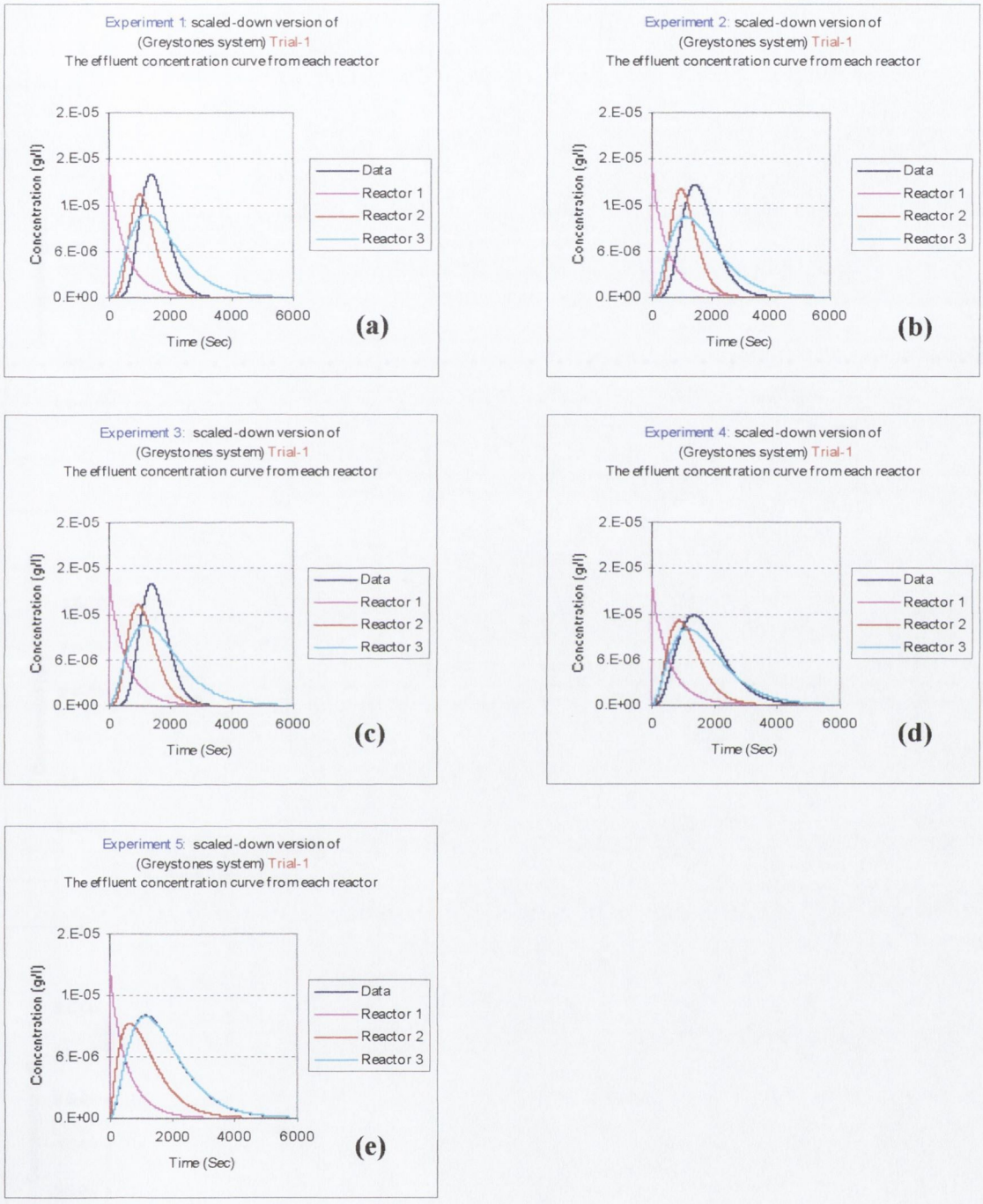

Figure I. 10 Graphs showing laboratory effluent concentration results and fitted model curves from each reactor for scaled-down version Trial-1 for (a) Exp.1, (b) Exp.2, (c) Exp. 3, (d) Exp. 4, and (e) Exp. 5

I.6 Scaled-down Version [Trial-2]

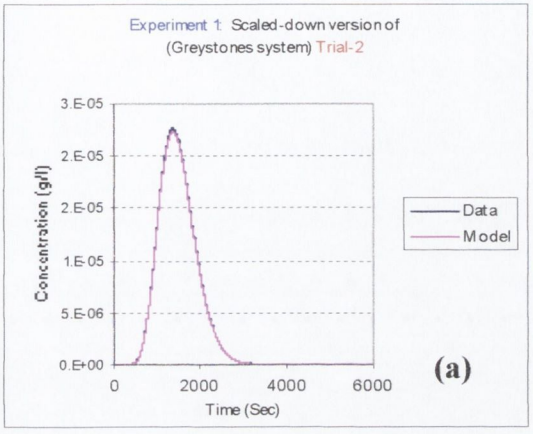

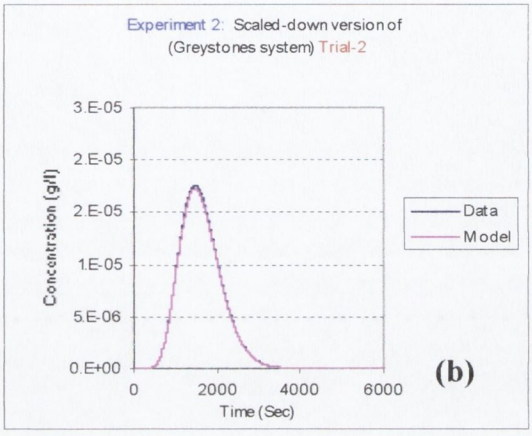

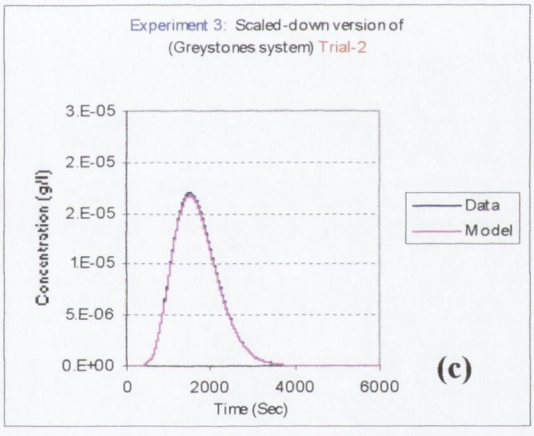

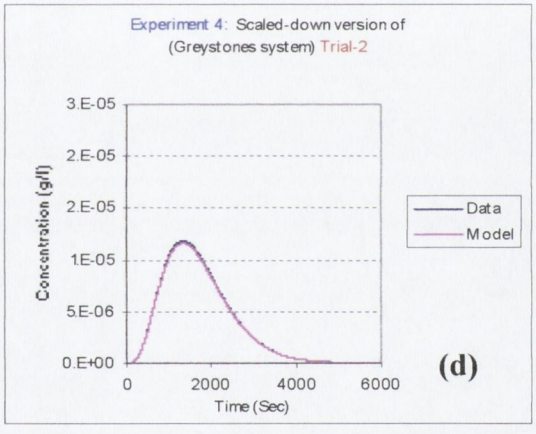

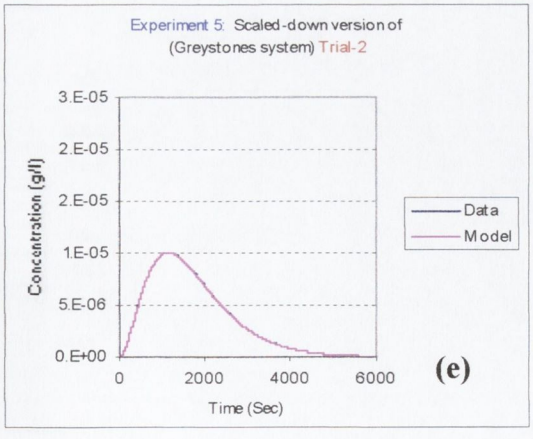

Figure I. 11 Graphs showing laboratory results and fitted model curves for scaled-down version Trial-2 for (a) Exp.1, (b) Exp.2, (c) Exp. 3, (d) Exp. 4, and (e) Exp. 5

I.6.1 Effluent Concentration Result Curves for [Trial-2]

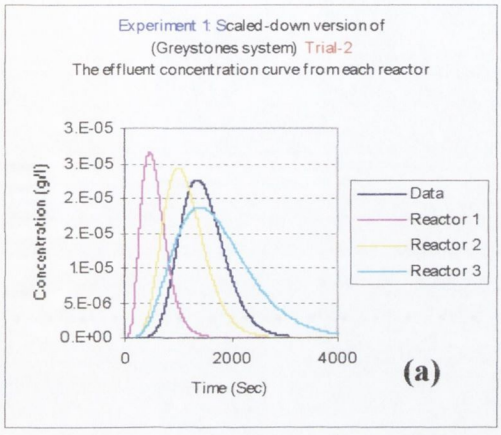

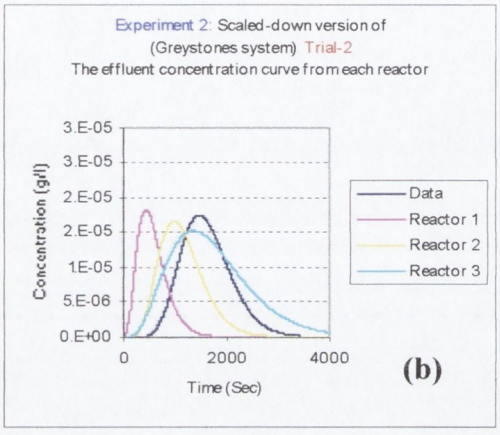

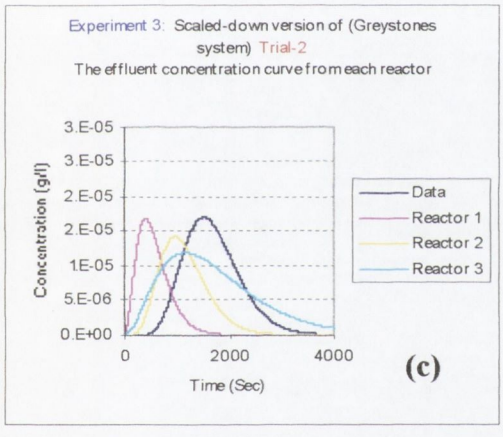

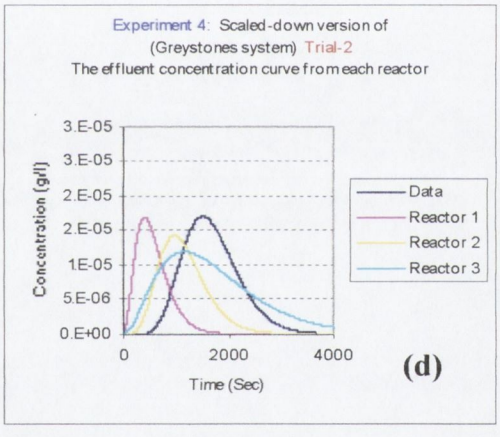

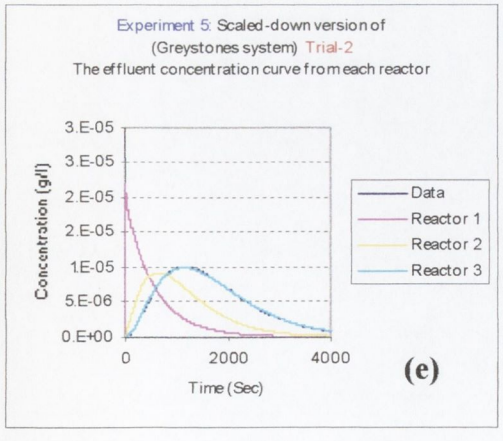

Figure I. 12 Graphs showing laboratory effluent concentration results and fitted model curves from each reactor for scaled-down version Trial-2 for (a) Exp.1, (b) Exp.2, (c) Exp. 3, (d) Exp. 4, and (e) Exp. 5

Appendix J

Full Set of Experimental Data with the Spreadsheet Model

Appendix J

Full Set of Experimental Data with the Spreadsheet Model

J.1 Pulse Input: Circular CSTR: Experiment 1

Mixer Speed	0	rev/min							
	Theoretical Retention Time			342.8571	Sec				
						Gamma Parameters			
				Retention time		505.18			
Flow	3.5	L/min		$1/\sigma^2$ (alpha)	=N	0.7237			
RAS flow	0	L/min		σ^2 (beta)		1.3818			
Volume	20	L		Pe		0.9			
				fraction		0.0085			Σ(Difference^2)
Total mass of Rhodamine			0.002	g					4.83728E-12
Background concentration			0	ug/l					

Sample No.	Time (Sec)	Return (ug/l)	Rhodamine mass (g)	Exit (ug/l)	θ	C(θ)	C(θ) fract	Difference squared
1	0	0	0.002	0	0	0	0	0
2	5	0	0	3.8773E-05	0.009897	0.004457	3.78845E-05	7.89348E-13
3	10	0	0	3.17872E-05	0.019795	0.003654	3.10582E-05	5.31377E-13
4	15	0	0	2.82158E-05	0.029692	0.003243	2.75684E-05	4.19064E-13
5	20	0	0	2.5874E-05	0.03959	0.002974	2.52802E-05	3.52618E-13
6	25	0	0	2.41535E-05	0.049487	0.002776	2.3599E-05	3.07432E-13
7	30	0	0	2.28031E-05	0.059385	0.002621	2.22795E-05	2.74126E-13
8	35	0	0	2.16963E-05	0.069282	0.002494	2.11981E-05	2.48246E-13
9	40	0	0	2.07613E-05	0.07918	0.002386	2.02844E-05	2.27374E-13
10	45	0	0	1.99531E-05	0.089077	0.002294	1.94948E-05	2.1007E-13
11	50	0	0	1.92424E-05	0.098975	0.002212	1.88003E-05	1.95414E-13
12	55	0	0	1.86085E-05	0.108872	0.002139	1.8181E-05	1.82788E-13
13	60	0	0	1.80369E-05	0.11877	0.002073	1.76224E-05	1.71761E-13
14	65	0	0	1.75165E-05	0.128667	0.002013	1.7114E-05	1.62019E-13
15	70	0	0	1.7039E-05	0.138564	0.001959	1.66474E-05	1.53329E-13
16	75	0	0	1.6598E-05	0.148462	0.001908	1.62165E-05	1.45514E-13
17	80	0	0	1.61883E-05	0.158359	0.001861	1.58162E-05	1.38437E-13
18	85	0	0	1.58058E-05	0.168257	0.001817	1.54425E-05	1.31988E-13
19	90	0	0	1.54471E-05	0.178154	0.001776	1.5092E-05	1.26079E-13
20	95	0	0	1.51095E-05	0.188052	0.001737	1.47621E-05	1.2064E-13
21	100	0	0	1.47905E-05	0.197949	0.0017	1.44505E-05	1.15612E-13
22	105	0	0	1.44883E-05	0.207847	0.001665	1.41553E-05	1.10946E-13
23	110	0	0	1.42012E-05	0.217744	0.001632	1.38747E-05	1.06601E-13
24	115	0	0	1.39278E-05	0.227642	0.001601	1.36075E-05	1.02544E-13
25	120	0	0	1.36667E-05	0.237539	0.001571	1.33525E-05	9.87432E-14

26	125	0	0	1.34E-05		0.247437	0.001542	1.31085E-05	9.51745E-14
27	130	0	0	1.32E-05		0.257334	0.001515	1.28747E-05	9.18156E-14
28	135	0	0	1.29E-05		0.267231	0.001488	1.26502E-05	8.86475E-14
29	140	0	0	1.27E-05		0.277129	0.001463	1.24343E-05	8.56533E-14
30	145	0	0	1.25E-05		0.287026	0.001438	1.22264E-05	8.28184E-14
31	150	0	0	1.23E-05		0.296924	0.001415	1.2026E-05	8.01298E-14
32	155	0	0	1.21E-05		0.306821	0.001392	1.18325E-05	7.75759E-14
33	160	0	0	1.19E-05		0.316719	0.00137	1.16454E-05	7.51464E-14
34	165	0	0	1.17E-05		0.326616	0.001349	1.14644E-05	7.28322E-14
35	170	0	0	1.16E-05		0.336514	0.001328	1.12891E-05	7.06249E-14
36	175	0	0	1.14E-05		0.346411	0.001308	1.11191E-05	6.85171E-14
37	180	0	0	1.12E-05		0.356309	0.001289	1.09542E-05	6.65021E-14
38	185	0	0	1.1E-05		0.366206	0.00127	1.0794E-05	6.45738E-14
39	190	0	0	1.09E-05		0.376104	0.001252	1.06382E-05	6.27266E-14
40	195	0	0	1.07E-05		0.386001	0.001234	1.04868E-05	6.09555E-14
41	200	0	0	1.06E-05		0.395898	0.001216	1.03393E-05	5.92559E-14
42	205	0	0	1.04E-05		0.405796	0.0012	1.01958E-05	5.76234E-14
43	210	0	0	1.03E-05		0.415693	0.001183	1.00558E-05	5.60543E-14
44	215	0	0	1.02E-05		0.425591	0.001167	9.91934E-06	5.45449E-14
45	220	0	0	1E-05		0.435488	0.001151	9.78618E-06	5.3092E-14
46	225	0	0	9.88E-06		0.445386	0.001136	9.65619E-06	5.16924E-14
47	230	0	0	9.75E-06		0.455283	0.001121	9.52923E-06	5.03435E-14
48	235	0	0	9.63E-06		0.465181	0.001106	9.40516E-06	4.90425E-14
49	240	0	0	9.5E-06		0.475078	0.001092	9.28388E-06	4.7787E-14
50	245	0	0	9.38E-06		0.484976	0.001078	9.16525E-06	4.65748E-14
51	250	0	0	9.26E-06		0.494873	0.001065	9.04918E-06	4.54037E-14
52	255	0	0	9.15E-06		0.504771	0.001051	8.93557E-06	4.42718E-14
53	260	0	0	9.03E-06		0.514668	0.001038	8.82433E-06	4.31773E-14
54	265	0	0	8.92E-06		0.524566	0.001025	8.71535E-06	4.21184E-14
55	270	0	0	8.81E-06		0.534463	0.001013	8.60858E-06	4.10935E-14
56	275	0	0	8.7E-06		0.54436	0.001	8.50391E-06	4.01012E-14
57	280	0	0	8.6E-06		0.554258	0.000988	8.40129E-06	3.91399E-14
58	285	0	0	8.5E-06		0.564155	0.000977	8.30063E-06	3.82084E-14
59	290	0	0	8.4E-06		0.574053	0.000965	8.20188E-06	3.73053E-14
60	295	0	0	8.3E-06		0.58395	0.000954	8.10497E-06	3.64296E-14
61	300	0	0	8.2E-06		0.593848	0.000942	8.00984E-06	3.558E-14
62	305	0	0	8.1E-06		0.603745	0.000931	7.91644E-06	3.47556E-14
63	310	0	0	8.01E-06		0.613643	0.000921	7.8247E-06	3.39553E-14
64	315	0	0	7.92E-06		0.62354	0.00091	7.73459E-06	3.31781E-14
65	320	0	0	7.83E-06		0.633438	0.0009	7.64604E-06	3.24233E-14
66	325	0	0	7.74E-06		0.643335	0.000889	7.55902E-06	3.16899E-14
67	330	0	0	7.65E-06		0.653233	0.000879	7.47347E-06	3.09771E-14
68	335	0	0	7.56E-06		0.66313	0.000869	7.38937E-06	3.02841E-14
69	340	0	0	7.48E-06		0.673027	0.00086	7.30666E-06	2.96103E-14
70	345	0	0	7.4E-06		0.682925	0.00085	7.22531E-06	2.8955E-14
71	350	0	0	7.31E-06		0.692822	0.000841	7.14527E-06	2.83174E-14
72	355	0	0	7.23E-06		0.70272	0.000831	7.06653E-06	2.76969E-14
73	360	0	0	7.15E-06		0.712617	0.000822	6.98903E-06	2.7093E-14
74	365	0	0	7.08E-06		0.722515	0.000813	6.91275E-06	2.65051E-14
75	370	0	0	7E-06		0.732412	0.000804	6.83766E-06	2.59326E-14

76	375	0	0	6.92E-06	0.74231	0.000796	6.76373E-06	2.53751E-14
77	380	0	0	6.85E-06	0.752207	0.000787	6.69092E-06	2.48319E-14
78	385	0	0	6.78E-06	0.762105	0.000779	6.61922E-06	2.43027E-14
79	390	0	0	6.7E-06	0.772002	0.00077	6.54859E-06	2.3787E-14
80	395	0	0	6.63E-06	0.7819	0.000762	6.479E-06	2.32844E-14
81	400	0	0	6.56E-06	0.791797	0.000754	6.41044E-06	2.27943E-14
82	405	0	0	6.49E-06	0.801694	0.000746	6.34288E-06	2.23165E-14
83	410	0	0	6.42E-06	0.811592	0.000738	6.2763E-06	2.18506E-14
84	415	0	0	6.36E-06	0.821489	0.000731	6.21067E-06	2.13961E-14
85	420	0	0	6.29E-06	0.831387	0.000723	6.14597E-06	2.09527E-14
86	425	0	0	6.23E-06	0.841284	0.000716	6.08219E-06	2.05202E-14
87	430	0	0	6.16E-06	0.851182	0.000708	6.01929E-06	2.00981E-14
88	435	0	0	6.1E-06	0.861079	0.000701	5.95727E-06	1.96861E-14
89	440	0	0	6.03E-06	0.870977	0.000694	5.89611E-06	1.9284E-14
90	445	0	0	5.97E-06	0.880874	0.000687	5.83578E-06	1.88915E-14
91	450	0	0	5.91E-06	0.890772	0.00068	5.77626E-06	1.85082E-14
92	455	0	0	5.85E-06	0.900669	0.000673	5.71756E-06	1.81339E-14
93	460	0	0	5.79E-06	0.910567	0.000666	5.65963E-06	1.77684E-14
94	465	0	0	5.73E-06	0.920464	0.000659	5.60248E-06	1.74114E-14
95	470	0	0	5.68E-06	0.930361	0.000652	5.54608E-06	1.70626E-14
96	475	0	0	5.62E-06	0.940259	0.000646	5.49042E-06	1.67219E-14
97	480	0	0	5.56E-06	0.950156	0.000639	5.43548E-06	1.6389E-14
98	485	0	0	5.51E-06	0.960054	0.000633	5.38126E-06	1.60636E-14
99	490	0	0	5.45E-06	0.969951	0.000627	5.32773E-06	1.57457E-14
100	495	0	0	5.4E-06	0.979849	0.000621	5.27489E-06	1.54349E-14
101	500	0	0	5.35E-06	0.989746	0.000614	5.22272E-06	1.51311E-14
102	505	0	0	5.29E-06	0.999644	0.000608	5.17121E-06	1.48341E-14
103	510	0	0	5.24E-06	1.009541	0.000602	5.12034E-06	1.45437E-14
104	515	0	0	5.19E-06	1.019439	0.000596	5.07011E-06	1.42597E-14
105	520	0	0	5.14E-06	1.029336	0.000591	5.0205E-06	1.3982E-14
106	525	0	0	5.09E-06	1.039234	0.000585	4.97151E-06	1.37105E-14
107	530	0	0	5.04E-06	1.049131	0.000579	4.92312E-06	1.34448E-14
108	535	0	0	4.99E-06	1.059028	0.000574	4.87531E-06	1.3185E-14
109	540	0	0	4.94E-06	1.068926	0.000568	4.82809E-06	1.29308E-14
110	545	0	0	4.89E-06	1.078823	0.000563	4.78144E-06	1.26821E-14
111	550	0	0	4.85E-06	1.088721	0.000557	4.73535E-06	1.24388E-14
112	555	0	0	4.8E-06	1.098618	0.000552	4.68981E-06	1.22006E-14
113	560	0	0	4.75E-06	1.108516	0.000546	4.64482E-06	1.19676E-14
114	565	0	0	4.71E-06	1.118413	0.000541	4.60035E-06	1.17396E-14
115	570	0	0	4.66E-06	1.128311	0.000536	4.55641E-06	1.15164E-14
116	575	0	0	4.62E-06	1.138208	0.000531	4.51299E-06	1.12979E-14
117	580	0	0	4.58E-06	1.148106	0.000526	4.47007E-06	1.1084E-14
118	585	0	0	4.53E-06	1.158003	0.000521	4.42766E-06	1.08746E-14
119	590	0	0	4.49E-06	1.167901	0.000516	4.38573E-06	1.06696E-14
120	595	0	0	4.45E-06	1.177798	0.000511	4.34429E-06	1.04689E-14
121	600	0	0	4.4E-06	1.187695	0.000506	4.30332E-06	1.02723E-14
122	605	0	0	4.36E-06	1.197593	0.000502	4.26282E-06	1.00798E-14
123	610	0	0	4.32E-06	1.20749	0.000497	4.22278E-06	9.89132E-15
124	615	0	0	4.28E-06	1.217388	0.000492	4.1832E-06	9.70671E-15
125	620	0	0	4.24E-06	1.227285	0.000488	4.14406E-06	9.52588E-15

126	625	0	0	4.2E-06		1.237183	0.000483	4.10536E-06	9.34876E-15
127	630	0	0	4.16E-06		1.24708	0.000478	4.0671E-06	9.17526E-15
128	635	0	0	4.12E-06		1.256978	0.000474	4.02926E-06	9.00529E-15
129	640	0	0	4.09E-06		1.266875	0.00047	3.99184E-06	8.83877E-15
130	645	0	0	4.05E-06		1.276773	0.000465	3.95484E-06	8.67562E-15
131	650	0	0	4.01E-06		1.28667	0.000461	3.91824E-06	8.51576E-15
132	655	0	0	3.97E-06		1.296568	0.000457	3.88205E-06	8.35912E-15
133	660	0	0	3.94E-06		1.306465	0.000453	3.84625E-06	8.20562E-15
134	665	0	0	3.9E-06		1.316362	0.000448	3.81085E-06	8.0552E-15
135	670	0	0	3.86E-06		1.32626	0.000444	3.77582E-06	7.90778E-15
136	675	0	0	3.83E-06		1.336157	0.00044	3.74118E-06	7.7633E-15
137	680	0	0	3.79E-06		1.346055	0.000436	3.70691E-06	7.62169E-15
138	685	0	0	3.76E-06		1.355952	0.000432	3.67301E-06	7.48288E-15
139	690	0	0	3.73E-06		1.36585	0.000428	3.63948E-06	7.34682E-15
140	695	0	0	3.69E-06		1.375747	0.000424	3.6063E-06	7.21343E-15
141	700	0	0	3.66E-06		1.385645	0.00042	3.57348E-06	7.08268E-15
142	705	0	0	3.62E-06		1.395542	0.000417	3.541E-06	6.95448E-15
143	710	0	0	3.59E-06		1.40544	0.000413	3.50887E-06	6.8288E-15
144	715	0	0	3.56E-06		1.415337	0.000409	3.47708E-06	6.70557E-15
145	720	0	0	3.53E-06		1.425235	0.000405	3.44562E-06	6.58474E-15
146	725	0	0	3.49E-06		1.435132	0.000402	3.41449E-06	6.46626E-15
147	730	0	0	3.46E-06		1.445029	0.000398	3.38369E-06	6.35008E-15
148	735	0	0	3.43E-06		1.454927	0.000394	3.35321E-06	6.23615E-15
149	740	0	0	3.4E-06		1.464824	0.000391	3.32305E-06	6.12442E-15
150	745	0	0	3.37E-06		1.474722	0.000387	3.2932E-06	6.01484E-15
151	750	0	0	3.34E-06		1.484619	0.000384	3.26366E-06	5.90736E-15
152	755	0	0	3.31E-06		1.494517	0.000381	3.23442E-06	5.80195E-15
153	760	0	0	3.28E-06		1.504414	0.000377	3.20548E-06	5.69856E-15
154	765	0	0	3.25E-06		1.514312	0.000374	3.17685E-06	5.59714E-15
155	770	0	0	3.22E-06		1.524209	0.00037	3.1485E-06	5.49766E-15
156	775	0	0	3.19E-06		1.534107	0.000367	3.12044E-06	5.40007E-15
157	780	0	0	3.17E-06		1.544004	0.000364	3.09267E-06	5.30434E-15
158	785	0	0	3.14E-06		1.553902	0.000361	3.06518E-06	5.21042E-15
159	790	0	0	3.11E-06		1.563799	0.000357	3.03797E-06	5.11827E-15
160	795	0	0	3.08E-06		1.573697	0.000354	3.01103E-06	5.02787E-15
161	800	0	0	3.05E-06		1.583594	0.000351	2.98437E-06	4.93917E-15
162	805	0	0	3.03E-06		1.593491	0.000348	2.95797E-06	4.85215E-15
163	810	0	0	3E-06		1.603389	0.000345	2.93184E-06	4.76675E-15
164	815	0	0	2.97E-06		1.613286	0.000342	2.90597E-06	4.68296E-15
165	820	0	0	2.95E-06		1.623184	0.000339	2.88036E-06	4.60073E-15
166	825	0	0	2.92E-06		1.633081	0.000336	2.855E-06	4.52004E-15
167	830	0	0	2.9E-06		1.642979	0.000333	2.8299E-06	4.44086E-15
168	835	0	0	2.87E-06		1.652876	0.00033	2.80504E-06	4.36315E-15
169	840	0	0	2.85E-06		1.662774	0.000327	2.78043E-06	4.28688E-15
170	845	0	0	2.82E-06		1.672671	0.000324	2.75606E-06	4.21203E-15
171	850	0	0	2.8E-06		1.682569	0.000321	2.73193E-06	4.13857E-15
172	855	0	0	2.77E-06		1.692466	0.000319	2.70804E-06	4.06647E-15
173	860	0	0	2.75E-06		1.702364	0.000316	2.68439E-06	3.99569E-15
174	865	0	0	2.72E-06		1.712261	0.000313	2.66096E-06	3.92622E-15
									4.83728E-12

J.2 Pulse Input: Circular CSTR: Experiment 5

Mixer Speed	120	rev/m

Theoretical Retention Time	342.8571	Sec

			Gamma Parameters
		Retention time	380.58
Flow	3.5 L/min	$1/\sigma^2$ (alpha) =N	0.8404985
RAS flow	0 L/min	σ^2 (beta)	1.1897702
Volume	20 L	Pe	0.5
		fraction	0.00652

Total mass of Rhodamine	0.002	g

Background concentration	0	g/l

Σ(Difference^2)
7.72347E-13

Sample No.	Time (Sec)	Return (ug/l)	Rhodamine mass (g)	Exit (g/l)	θ	C(θ)	C(θ) fract	Difference squared
1	0	0	0.002	0	0	0	0	0
2	5	0	0	2.00414E-05	0.013138	0.003041178	1.98285E-05	4.53189E-14
3	10	0	0	1.77467E-05	0.026276	0.00269297	1.75582E-05	3.55352E-14
4	15	0	0	1.64526E-05	0.039414	0.0024966	1.62778E-05	3.05418E-14
5	20	0	0	1.55421E-05	0.052551	0.002358443	1.53771E-05	2.72551E-14
6	25	0	0	1.4834E-05	0.065689	0.002250985	1.46764E-05	2.4828E-14
7	30	0	0	1.42506E-05	0.078827	0.002162457	1.40992E-05	2.29135E-14
8	35	0	0	1.37518E-05	0.091965	0.002086766	1.36057E-05	2.13375E-14
9	40	0	0	1.33142E-05	0.105103	0.002020357	1.31727E-05	2.0001E-14
10	45	0	0	1.29229E-05	0.118241	0.001960982	1.27856E-05	1.88427E-14
11	50	0	0	1.2568E-05	0.131378	0.001907127	1.24345E-05	1.7822E-14
12	55	0	0	1.22424E-05	0.144516	0.001857727	1.21124E-05	1.69106E-14
13	60	0	0	1.19411E-05	0.157654	0.001812003	1.18143E-05	1.60884E-14
14	65	0	0	1.16601E-05	0.170792	0.00176937	1.15363E-05	1.53403E-14
15	70	0	0	1.13966E-05	0.18393	0.001729376	1.12755E-05	1.46546E-14
16	75	0	0	1.11481E-05	0.197068	0.001691666	1.10297E-05	1.40225E-14
17	80	0	0	1.09127E-05	0.210205	0.001655955	1.07968E-05	1.34367E-14
18	85	0	0	1.0689E-05	0.223343	0.001622009	1.05755E-05	1.28915E-14
19	90	0	0	1.04757E-05	0.236481	0.001589638	1.03644E-05	1.23821E-14
20	95	0	0	1.02717E-05	0.249619	0.001558682	1.01626E-05	1.19045E-14
21	100	0	0	1.00761E-05	0.262757	0.001529004	9.96911E-06	1.14555E-14
22	105	0	0	9.88823E-06	0.275895	0.001500491	9.7832E-06	1.10322E-14
23	110	0	0	9.70735E-06	0.289033	0.001473042	9.60424E-06	1.06323E-14
24	115	0	0	9.53292E-06	0.30217	0.001446573	9.43166E-06	1.02536E-14
25	120	0	0	9.36445E-06	0.315308	0.001421008	9.26497E-06	9.8944E-15
26	125	0	0	9.2015E-06	0.328446	0.001396282	9.10376E-06	9.55306E-15
27	130	0	0	9.0437E-06	0.341584	0.001372337	8.94764E-06	9.22821E-15
28	135	0	0	8.89071E-06	0.354722	0.001349121	8.79627E-06	8.91862E-15
29	140	0	0	8.74221E-06	0.36786	0.001326588	8.64935E-06	8.62319E-15
30	145	0	0	8.59795E-06	0.380997	0.001304697	8.50662E-06	8.34095E-15
31	150	0	0	8.45768E-06	0.394135	0.001283411	8.36784E-06	8.071E-15
32	155	0	0	8.32116E-06	0.407273	0.001262695	8.23277E-06	7.81256E-15
33	160	0	0	8.18821E-06	0.420411	0.001242521	8.10124E-06	7.56491E-15
34	165	0	0	8.05864E-06	0.433549	0.001222859	7.97304E-06	7.32739E-15
35	170	0	0	7.93229E-06	0.446687	0.001203685	7.84803E-06	7.09941E-15

36	175	0	0	7.8E-06	0.459824	0.001184975	7.72604E-06	6.88042E-15
37	180	0	0	7.7E-06	0.472962	0.001166708	7.60694E-06	6.66992E-15
38	185	0	0	7.6E-06	0.4861	0.001148864	7.4906E-06	6.46746E-15
39	190	0	0	7.5E-06	0.499238	0.001131425	7.37689E-06	6.2726E-15
40	195	0	0	7.3E-06	0.512376	0.001114374	7.26572E-06	6.08496E-15
41	200	0	0	7.2E-06	0.525514	0.001097694	7.15697E-06	5.90417E-15
42	205	0	0	7.1E-06	0.538652	0.001081372	7.05055E-06	5.7299E-15
43	210	0	0	7E-06	0.551789	0.001065394	6.94637E-06	5.56182E-15
44	215	0	0	6.9E-06	0.564927	0.001049747	6.84435E-06	5.39965E-15
45	220	0	0	6.8E-06	0.578065	0.00103442	6.74442E-06	5.24312E-15
46	225	0	0	6.7E-06	0.591203	0.001019399	6.64648E-06	5.09196E-15
47	230	0	0	6.6E-06	0.604341	0.001004677	6.55049E-06	4.94594E-15
48	235	0	0	6.5E-06	0.617479	0.000990241	6.45637E-06	4.80483E-15
49	240	0	0	6.4E-06	0.630616	0.000976083	6.36406E-06	4.66842E-15
50	245	0	0	6.3E-06	0.643754	0.000962195	6.27351E-06	4.53651E-15
51	250	0	0	6.3E-06	0.656892	0.000948567	6.18465E-06	4.40892E-15
52	255	0	0	6.2E-06	0.67003	0.000935191	6.09745E-06	4.28546E-15
53	260	0	0	6.1E-06	0.683168	0.000922061	6.01184E-06	4.16596E-15
54	265	0	0	6E-06	0.696306	0.000909169	5.92778E-06	4.05028E-15
55	270	0	0	5.9E-06	0.709443	0.000896508	5.84523E-06	3.93826E-15
56	275	0	0	5.8E-06	0.722581	0.000884072	5.76415E-06	3.82976E-15
57	280	0	0	5.7E-06	0.735719	0.000871854	5.68449E-06	3.72463E-15
58	285	0	0	5.7E-06	0.748857	0.000859849	5.60621E-06	3.62277E-15
59	290	0	0	5.6E-06	0.761995	0.00084805	5.52929E-06	3.52403E-15
60	295	0	0	5.5E-06	0.775133	0.000836454	5.45368E-06	3.42831E-15
61	300	0	0	5.4E-06	0.788271	0.000825053	5.37935E-06	3.33549E-15
62	305	0	0	5.4E-06	0.801408	0.000813845	5.30627E-06	3.24548E-15
63	310	0	0	5.3E-06	0.814546	0.000802822	5.2344E-06	3.15817E-15
64	315	0	0	5.2E-06	0.827684	0.000791982	5.16372E-06	3.07346E-15
65	320	0	0	5.1E-06	0.840822	0.00078132	5.09421E-06	2.99126E-15
66	325	0	0	5.1E-06	0.85396	0.000770831	5.02582E-06	2.91149E-15
67	330	0	0	5E-06	0.867098	0.000760512	4.95854E-06	2.83406E-15
68	335	0	0	4.9E-06	0.880235	0.000750359	4.89234E-06	2.75889E-15
69	340	0	0	4.9E-06	0.893373	0.000740367	4.82719E-06	2.6859E-15
70	345	0	0	4.8E-06	0.906511	0.000730533	4.76308E-06	2.61503E-15
71	350	0	0	4.8E-06	0.919649	0.000720855	4.69997E-06	2.54619E-15
72	355	0	0	4.7E-06	0.932787	0.000711327	4.63785E-06	2.47933E-15
73	360	0	0	4.6E-06	0.945925	0.000701948	4.5767E-06	2.41438E-15
74	365	0	0	4.6E-06	0.959062	0.000692714	4.51649E-06	2.35128E-15
75	370	0	0	4.5E-06	0.9722	0.000683622	4.45721E-06	2.28996E-15
76	375	0	0	4.4E-06	0.985338	0.000674668	4.39884E-06	2.23037E-15
77	380	0	0	4.4E-06	0.998476	0.000665851	4.34135E-06	2.17245E-15
78	385	0	0	4.3E-06	1.011614	0.000657168	4.28473E-06	2.11616E-15
79	390	0	0	4.3E-06	1.024752	0.000648615	4.22897E-06	2.06143E-15
80	395	0	0	4.2E-06	1.03789	0.00064019	4.17404E-06	2.00823E-15
81	400	0	0	4.2E-06	1.051027	0.00063189	4.11992E-06	1.9565E-15
82	405	0	0	4.1E-06	1.064165	0.000623714	4.06662E-06	1.90619E-15
83	410	0	0	4.1E-06	1.077303	0.000615659	4.01409E-06	1.85727E-15
84	415	0	0	4E-06	1.090441	0.000607722	3.96234E-06	1.80969E-15
85	420	0	0	4E-06	1.103579	0.000599901	3.91135E-06	1.76342E-15

86	425	0	0	3.9E-06	1.116717	0.000592194	3.8611E-06	1.7184E-15
87	430	0	0	3.9E-06	1.129854	0.000584599	3.81159E-06	1.67461E-15
88	435	0	0	3.8E-06	1.142992	0.000577114	3.76278E-06	1.632E-15
89	440	0	0	3.8E-06	1.15613	0.000569737	3.71469E-06	1.59054E-15
90	445	0	0	3.7E-06	1.169268	0.000562466	3.66728E-06	1.5502E-15
91	450	0	0	3.7E-06	1.182406	0.000555298	3.62055E-06	1.51095E-15
92	455	0	0	3.6E-06	1.195544	0.000548233	3.57448E-06	1.47274E-15
93	460	0	0	3.6E-06	1.208681	0.000541268	3.52907E-06	1.43556E-15
94	465	0	0	3.5E-06	1.221819	0.000534402	3.4843E-06	1.39937E-15
95	470	0	0	3.5E-06	1.234957	0.000527633	3.44017E-06	1.36414E-15
96	475	0	0	3.4E-06	1.248095	0.000520958	3.39665E-06	1.32985E-15
97	480	0	0	3.4E-06	1.261233	0.000514378	3.35374E-06	1.29646E-15
98	485	0	0	3.3E-06	1.274371	0.000507889	3.31143E-06	1.26396E-15
99	490	0	0	3.3E-06	1.287509	0.00050149	3.26972E-06	1.23231E-15
100	495	0	0	3.3E-06	1.300646	0.000495181	3.22858E-06	1.2015E-15
101	500	0	0	3.2E-06	1.313784	0.000488958	3.18801E-06	1.17149E-15
102	505	0	0	3.2E-06	1.326922	0.000482822	3.148E-06	1.14227E-15
103	510	0	0	3.1E-06	1.34006	0.00047677	3.10854E-06	1.11382E-15
104	515	0	0	3.1E-06	1.353198	0.000470801	3.06962E-06	1.0861E-15
105	520	0	0	3.1E-06	1.366336	0.000464914	3.03124E-06	1.05911E-15
106	525	0	0	3E-06	1.379473	0.000459107	2.99338E-06	1.03282E-15
107	530	0	0	3E-06	1.392611	0.000453379	2.95603E-06	1.00721E-15
108	535	0	0	3E-06	1.405749	0.000447729	2.9192E-06	9.82262E-16
109	540	0	0	2.9E-06	1.418887	0.000442156	2.88286E-06	9.5796E-16
110	545	0	0	2.9E-06	1.432025	0.000436658	2.84701E-06	9.34285E-16
111	550	0	0	2.8E-06	1.445163	0.000431234	2.81165E-06	9.11219E-16
112	555	0	0	2.8E-06	1.4583	0.000425884	2.77676E-06	8.88746E-16
113	560	0	0	2.8E-06	1.471438	0.000420605	2.74234E-06	8.6685E-16
114	565	0	0	2.7E-06	1.484576	0.000415396	2.70838E-06	8.45515E-16
115	570	0	0	2.7E-06	1.497714	0.000410258	2.67488E-06	8.24725E-16
116	575	0	0	2.7E-06	1.510852	0.000405188	2.64182E-06	8.04467E-16
117	580	0	0	2.6E-06	1.52399	0.000400185	2.60921E-06	7.84725E-16
118	585	0	0	2.6E-06	1.537128	0.000395249	2.57702E-06	7.65485E-16
119	590	0	0	2.6E-06	1.550265	0.000390378	2.54526E-06	7.46735E-16
120	595	0	0	2.5E-06	1.563403	0.000385572	2.51393E-06	7.28461E-16
121	600	0	0	2.5E-06	1.576541	0.000380829	2.483E-06	7.1065E-16
122	605	0	0	2.5E-06	1.589679	0.000376148	2.45249E-06	6.9329E-16
123	610	0	0	2.4E-06	1.602817	0.00037153	2.42237E-06	6.76368E-16
124	615	0	0	2.4E-06	1.615955	0.000366972	2.39265E-06	6.59874E-16
125	620	0	0	2.4E-06	1.629092	0.000362473	2.36333E-06	6.43795E-16
126	625	0	0	2.4E-06	1.64223	0.000358034	2.33438E-06	6.28122E-16
127	630	0	0	2.3E-06	1.655368	0.000353652	2.30581E-06	6.12842E-16
128	635	0	0	2.3E-06	1.668506	0.000349328	2.27762E-06	5.97946E-16
129	640	0	0	2.3E-06	1.681644	0.00034506	2.24979E-06	5.83424E-16
130	645	0	0	2.2E-06	1.694782	0.000340847	2.22232E-06	5.69266E-16
131	650	0	0	2.2E-06	1.707919	0.000336689	2.19521E-06	5.55461E-16
132	655	0	0	2.2E-06	1.721057	0.000332585	2.16845E-06	5.42002E-16
133	660	0	0	2.2E-06	1.734195	0.000328534	2.14204E-06	5.28879E-16
134	665	0	0	2.1E-06	1.747333	0.000324535	2.11597E-06	5.16083E-16
135	670	0	0	2.1E-06	1.760471	0.000320588	2.09023E-06	5.03605E-16

136	675	0	0	2.1E-06		1.773609	0.000316692	2.06483E-06	4.91438E-16
137	680	0	0	2.1E-06		1.786747	0.000312845	2.03975E-06	4.79574E-16
138	685	0	0	2E-06		1.799884	0.000309048	2.015E-06	4.68004E-16
139	690	0	0	2E-06		1.813022	0.0003053	1.99056E-06	4.5672E-16
140	695	0	0	2E-06		1.82616	0.0003016	1.96643E-06	4.45717E-16
141	700	0	0	2E-06		1.839298	0.000297947	1.94262E-06	4.34985E-16
142	705	0	0	1.9E-06		1.852436	0.000294341	1.9191E-06	4.24519E-16
143	710	0	0	1.9E-06		1.865574	0.000290781	1.89589E-06	4.14311E-16
144	715	0	0	1.9E-06		1.878711	0.000287266	1.87297E-06	4.04355E-16
145	720	0	0	1.9E-06		1.891849	0.000283795	1.85035E-06	3.94645E-16
146	725	0	0	1.8E-06		1.904987	0.000280369	1.82801E-06	3.85174E-16
147	730	0	0	1.8E-06		1.918125	0.000276986	1.80595E-06	3.75935E-16
148	735	0	0	1.8E-06		1.931263	0.000273647	1.78418E-06	3.66924E-16
149	740	0	0	1.8E-06		1.944401	0.000270349	1.76268E-06	3.58134E-16
150	745	0	0	1.8E-06		1.957538	0.000267093	1.74145E-06	3.4956E-16
151	750	0	0	1.7E-06		1.970676	0.000263878	1.72049E-06	3.41196E-16
152	755	0	0	1.7E-06		1.983814	0.000260704	1.69979E-06	3.33036E-16
153	760	0	0	1.7E-06		1.996952	0.00025757	1.67936E-06	3.25077E-16
154	765	0	0	1.7E-06		2.01009	0.000254475	1.65918E-06	3.17312E-16
155	770	0	0	1.7E-06		2.023228	0.000251419	1.63925E-06	3.09737E-16
156	775	0	0	1.6E-06		2.036366	0.000248402	1.61958E-06	3.02346E-16
157	780	0	0	1.6E-06		2.049503	0.000245422	1.60015E-06	2.95136E-16
158	785	0	0	1.6E-06		2.062641	0.000242479	1.58097E-06	2.88102E-16
159	790	0	0	1.6E-06		2.075779	0.000239574	1.56202E-06	2.81239E-16
160	795	0	0	1.6E-06		2.088917	0.000236705	1.54331E-06	2.74543E-16
161	800	0	0	1.5E-06		2.102055	0.000233871	1.52484E-06	2.68009E-16
162	805	0	0	1.5E-06		2.115193	0.000231073	1.5066E-06	2.61635E-16
163	810	0	0	1.5E-06		2.12833	0.00022831	1.48858E-06	2.55415E-16
164	815	0	0	1.5E-06		2.141468	0.000225581	1.47079E-06	2.49346E-16
									7.72347E-13

Appendix K

Graphs for Tank in-series Trials Showing the Delay Time

Appendix K

Graphs for Tank in-series Trials Showing the Delay Time

K.1 δ-Function

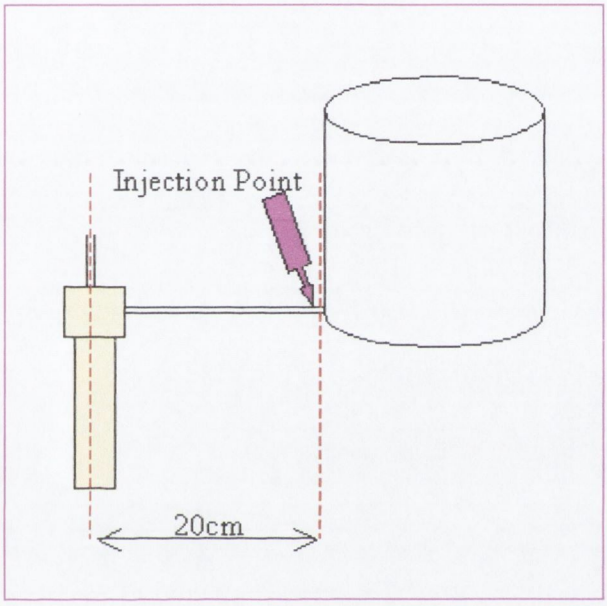

Figure K. 1 Schematic diagram showing the injection point for 20cm downstream connected to the SCUFA

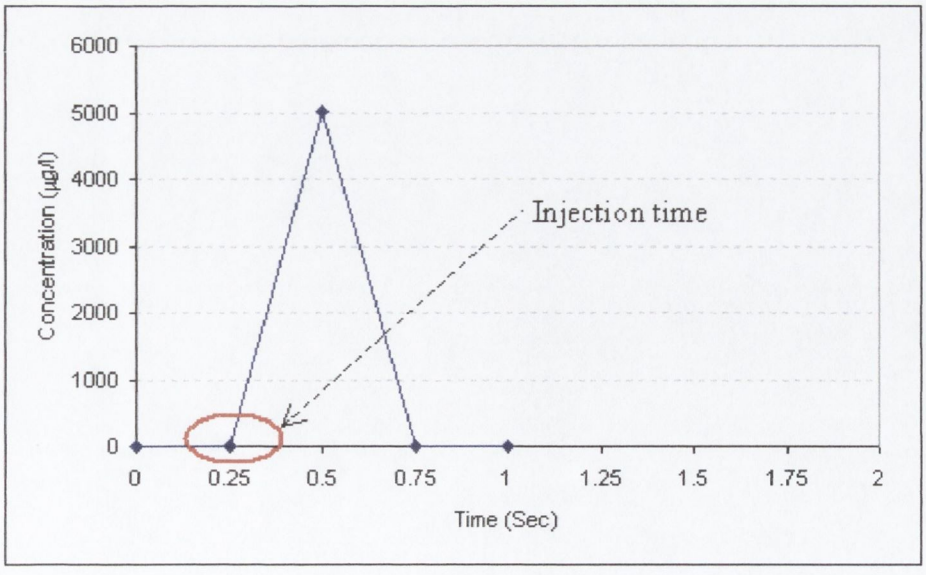

Figure K. 2 Graph showing δ-function for the injection of the tracer (pulse inputs) 20cm downstream connected to the SCUFA

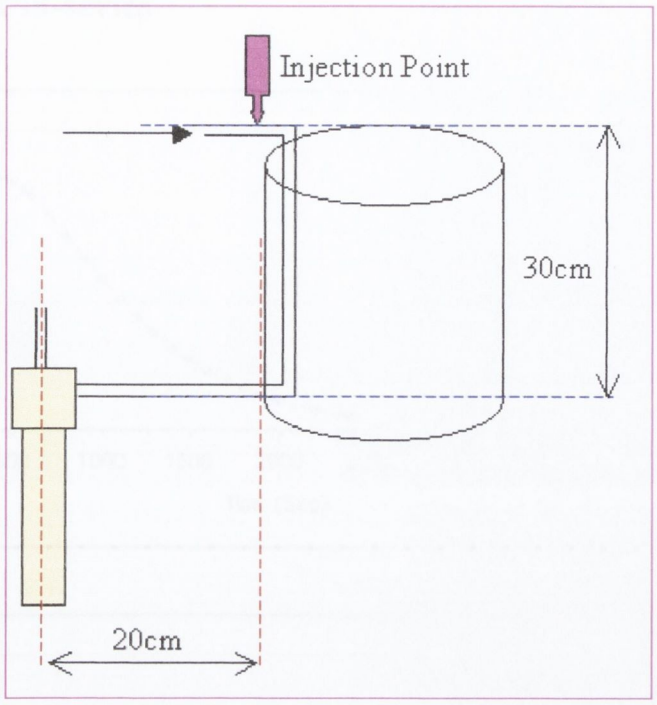

Figure K. 3 Schematic diagram showing the injection point for 50cm downstream connected to the SCUFA

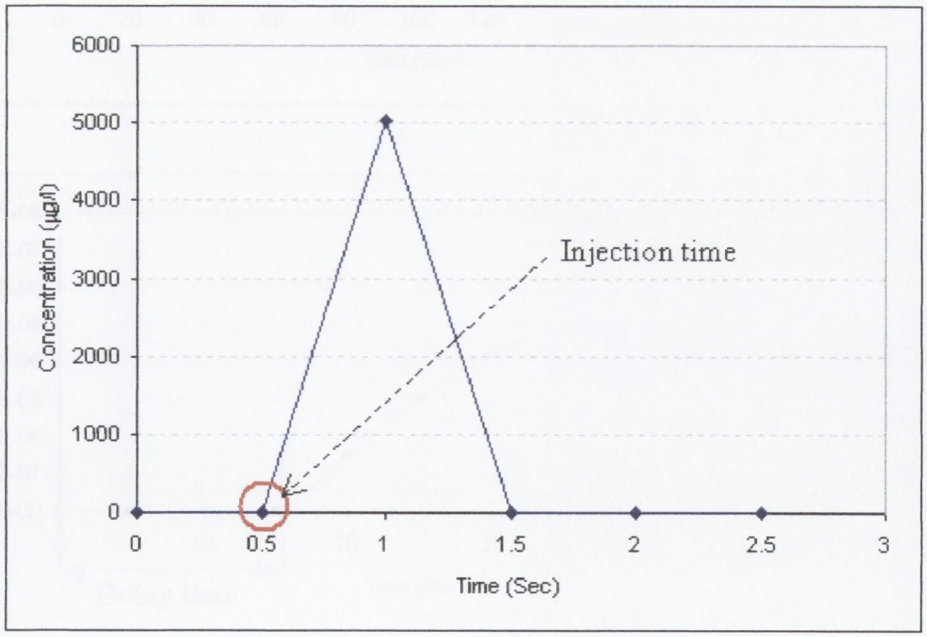

Figure K. 4 Graph showing δ-function for the injection of the tracer (pulse inputs) 50cm downstream connected to the SCUFA

K.2 Two CSTR in-series

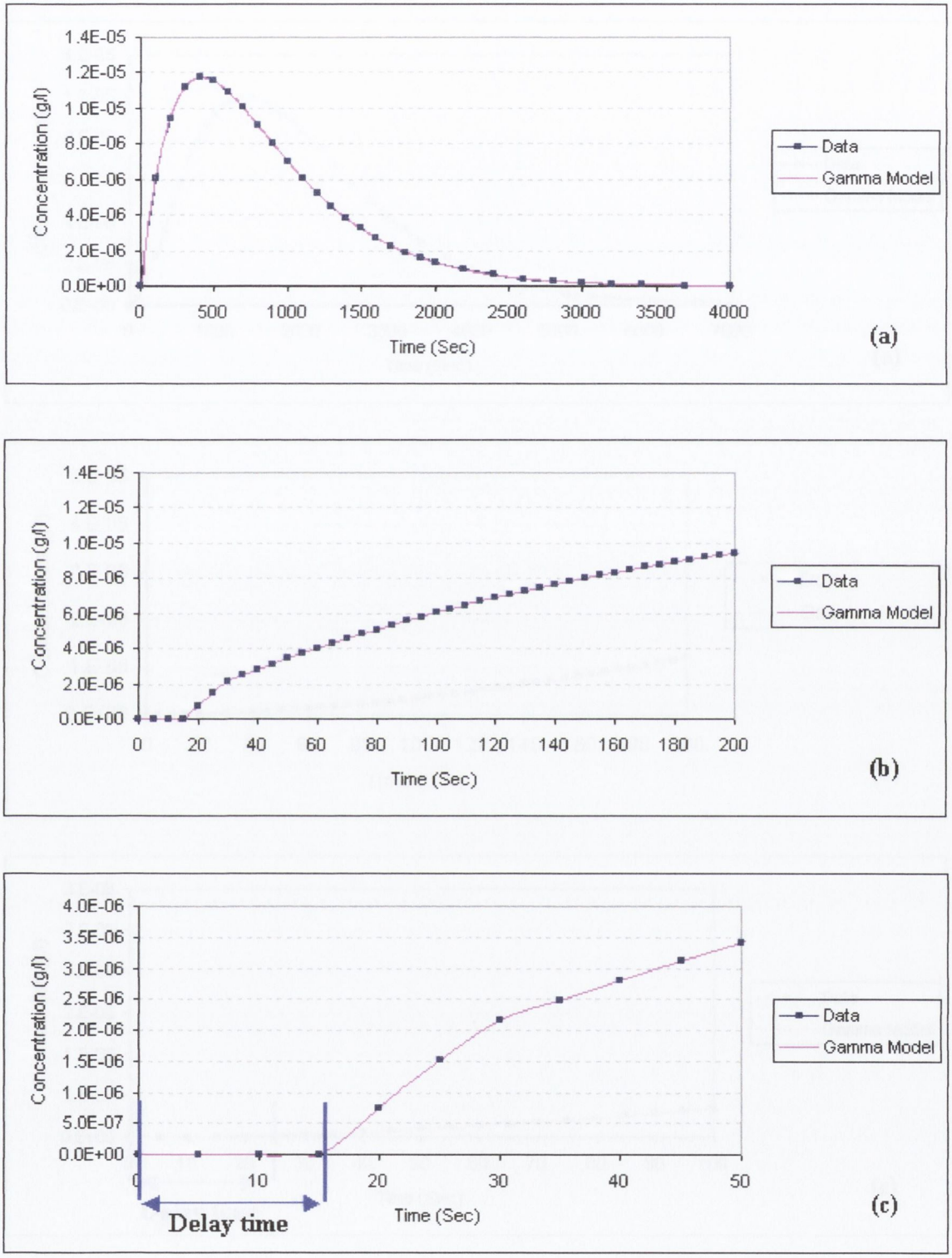

Figure K. 5 Graphs showing the delay time for 2 CSTR in-series (a) Full set of RTD's points, (b) 200 second resolution (c) 50 second resolution

K.3 Three CSTR in-series

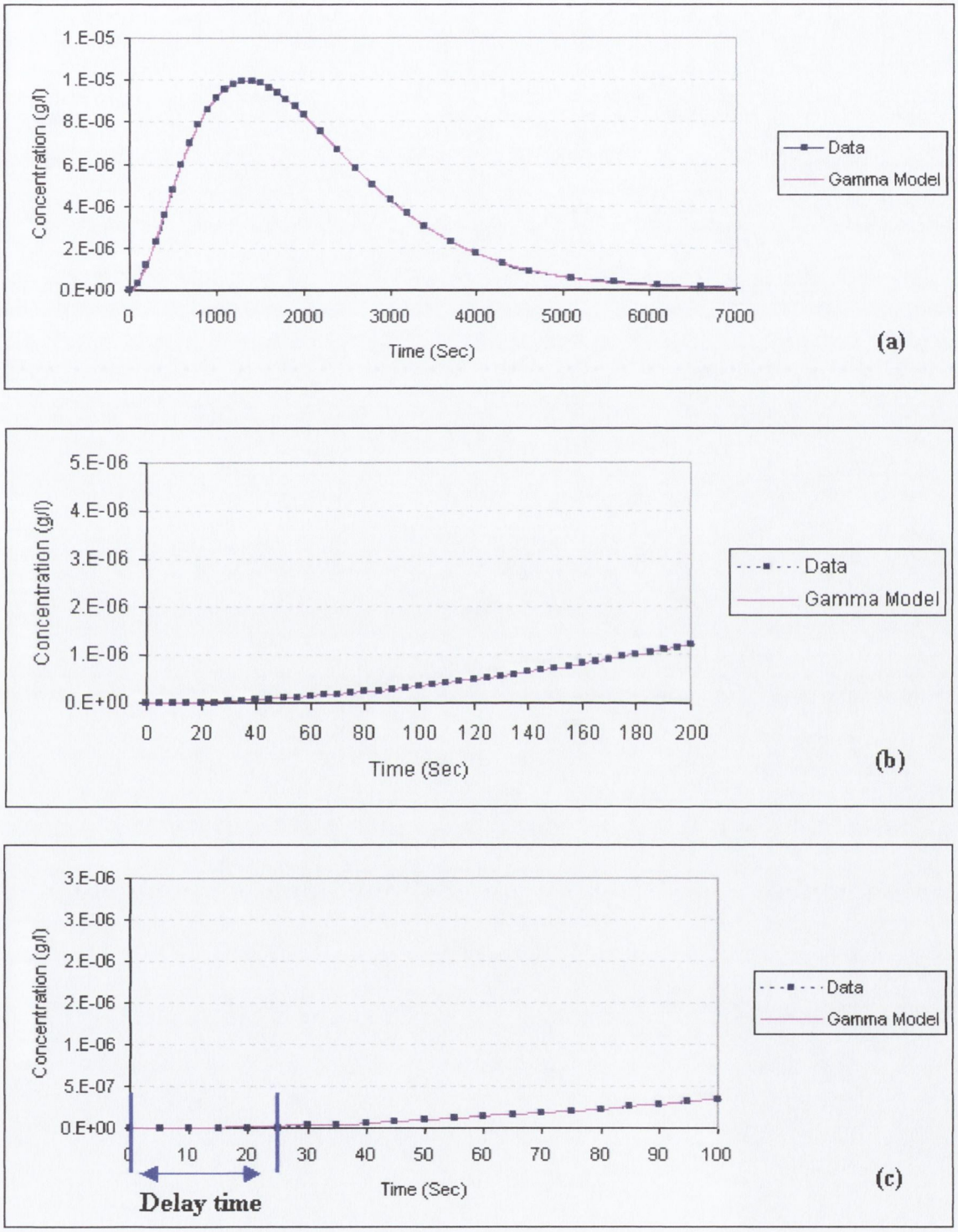

Figure K. 6 Graphs showing the delay time for 3 CSTR in-series (a) Full set of RTD's points, (b) 200 second resolution (c) 100 second resolution

K.4 Four CSTR in-series

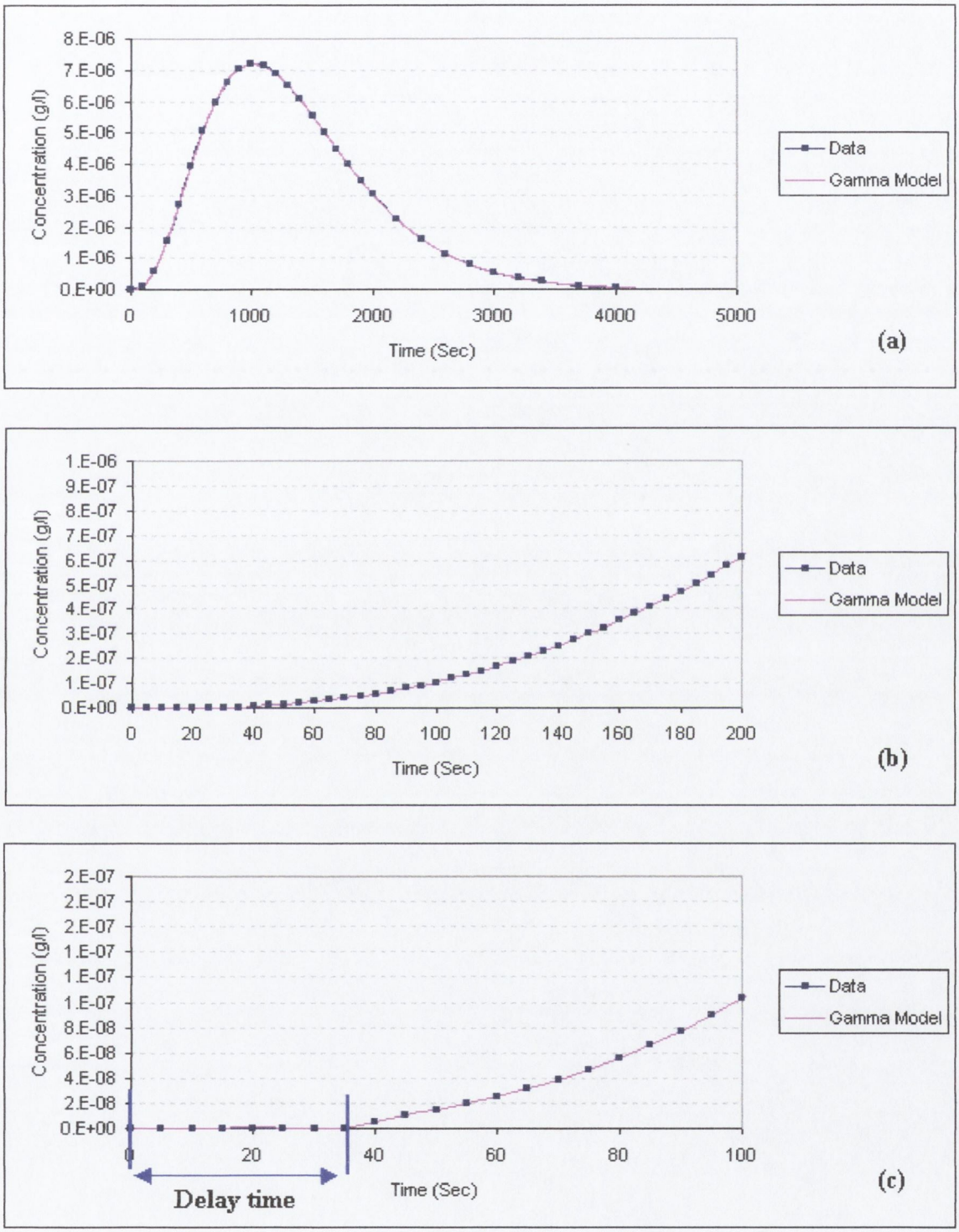

Figure K. 7 Graphs showing the delay time for 4 CSTR in-series (a) Full set of RTD's points, (b) 200 second resolution (c) 100 second resolution